

THE GEOLOGY OF THE LETSENG  
KIMBERLITES, LESOTHO

by

Norman Philip Lock

Submitted in fulfilment of the  
requirements for the  
Degree of Ph.D.

Department of Geology,  
University of Sheffield.

July, 1980

**CONTAINS**

**PULLOUTS**

## SUMMARY

Mining operations at the Letseng Diamond Mine in Lesotho have facilitated the study of the fresh kimberlite in the two diatremes (Main and Satellite pipes), and the included lower crustal and upper mantle nodules. The present day erosion level of these diatremes is close to the transition from diatreme to crater facies in the model of a kimberlite pipe.

The two pipes contain a variety of distinctive kimberlites. The zonation of large and dense xenoliths in the Main pipe garnetiferous kimberlite is believed to reflect the near-surface emplacement by a process of fluidisation. The geochemistry, xenolith and diamond contents of the two pipes indicate diverse origins despite their close proximity. REE abundances together with strontium and neodymium isotopic evidence indicates kimberlite genesis by a small degree of partial melting of slightly depleted chondritic mantle. Kimberlite dykes, both older and younger than the pipes, indicate some chemical and mineralogical evolution of the parent magma.

The peridotites are chromite and/or garnet bearing lherzolites and harzburgites similar to those from other Lesotho kimberlites. Textures vary from coarse to mosaic porphyroclastic and extreme fluidal and LAD varieties. All garnet-bearing xenoliths display coronas on the garnets resulting from retrograde reaction to spinel facies. In some cases reaction has gone to completion. Granuloblastic aluminous spinel lherzolites and garnet/spinel lherzolites are interpreted to derive from normal garnet lherzolite by a process of reaction, deformation, chemical homogenisation and re-equilibration during diapiric upwelling. Several peridotites are interpreted to show chemical disequilibrium and do not plot on a smoothly curving 'fossil geotherm'. This disequilibrium is believed to result from readjustment of primary phase compositions during diapiric upwell.

A synthesis is presented of the kimberlite genesis in the upper mantle, the subsequent diapiric ascent and the surface emplacement.

## ACKNOWLEDGEMENTS

This research project was undertaken with the financial support of a NERC Research Studentship, during the period January, 1977 to December, 1979. The grant covered both my study in Britain, a return field trip to Lesotho and visits to other Universities to attend a postgraduate course in thermodynamics and to utilise their analytical facilities.

The majority of my field work and sample collection was undertaken while I was employed by the Anglo-American Corporation of South Africa. During two periods of secondment to De Beers, Lesotho, I received much encouragement and advice, in particular from Mr. J.B. Hawthorne and Mr. C.R. Clement, for which I warmly thank them. I also acknowledge the permission of the Company to undertake this research. De Beers very generously arranged all of my sample transport from South Africa, and have also contributed to my support since the expiry of the NERC grant at the end of 1979. I should also take this opportunity to thank the staff at the Letseng Diamond Mine, and in particular the Manager - Mr. T.K. Whitelock - who enabled my stay in Lesotho to be not only rewarding but also enjoyable.

Professor J.B. Dawson received my initial enquiry for supervision with a reference to the 1st International Kimberlite Conference to establish my credentials! I trust that this first tenuous contact is now more firmly rooted. Since moving to St. Andrews (and latterly Sheffield) University, I have found his guidance both abounding in useful practical comparisons, and brimming with enthusiasm often more youthful than my own. I am also grateful for access to his personal collection of Letseng xenoliths (samples with BD prefix).

At St. Andrews University, I received considerable direction and assistance in computer programming from Dr. W.E. Stephens to whom I extend thanks. I acknowledge also the help offered by the technical staff, and in particular Mr. R.E. Bachelor who analysed many peridotite samples.

During my final year I moved to Sheffield University, where Mr. V. Somogyi gave me direction in the wet chemistry laboratory and completed a number of sodium analyses for me. XRF analyses were made by Miss S. Burley and Dr. R. Kanaris-Sotiriou.

In 1979, I also spent several weeks using the mass spectrometer at Leeds University. Dr. J. Kramers gave me enthusiastic direction and assistance with the instrumental analyses for isotopic compositions and REE abundances.

The many microprobe analyses reported in this thesis were made at four different Universities on five separate machines. There were no doubt some analytical disadvantages to this, but I believe the personal experience was invaluable. I wish to thank Drs P.G. Hill (Edinburgh), T. Hopkins (Manchester), F.G.F. Gibb (Sheffield) and P. Treloar (Cambridge) for their direction of this work. I am also grateful to Drs F.G.F. Gibb and D.A. Carswell for permission to use their presently unpublished NODMINS computer program for T and P calculations.

Finally I wish to express my appreciation to Miss Pat Mellor for the typing of this thesis and for smiling even on the darkest of days.

## CONTENTS

	<u>Page</u>
INTRODUCTION	1
PART I: THE KIMBERLITES	
<u>CHAPTER 1:</u> <u>Field Relations: Main and Satellite Pipes</u>	10
1. Main Pipe	10
2. Satellite Pipe	20
3. Dykes	22
<u>CHAPTER 2:</u> <u>Petrography and Phase Chemistry</u>	24
1. Main Pipe	24
2. Satellite Pipe	29
3. Dykes	30
4. Phase Chemistry	35
<u>CHAPTER 3:</u> <u>Bulk Rock Chemistry</u>	41
Analytical Techniques	41
Major Element Chemistry	42
Trace Elements	45
Summary	46
<u>CHAPTER 4:</u> <u>Kimberlite REE, Rb, Sr, <math>^{87}\text{Sr}/^{86}\text{Sr}</math> and <math>^{143}\text{Nd}/^{144}\text{Nd}</math></u>	48
Introduction	48
Analytical Techniques	49
Rb and Sr Isotopes	51
REE Patterns	54
$^{143}\text{Nd}/^{144}\text{Nd}$	57
Covariation of $^{143}\text{Nd}/^{144}\text{Nd}$ and $^{87}\text{Sr}/^{86}\text{Sr}$	58
Mantle Depletion	58
Partial Melting	59
Summary	61
<u>CHAPTER 5:</u> <u>Megacrysts and Xenocrysts</u>	63
Phase Chemistry	65

Temperature of Megacryst Crystallisation	69
Summary	71

## PART II: THE XENOLITHS

<u>CHAPTER 6:</u>	<u>Peridotites and Related Rocks: Petrography</u>	73
	1. Coarse Textured Rocks	75
	2. Porphyroclastic Textured Rocks	81
	3. Annealed Rocks	83
	4. Pyroxenites	86
	5. Metasomatism and Kimberlite Veining	87
	Summary	88
<u>CHAPTER 7:</u>	<u>Peridotites: Phase Chemistry</u>	90
	1. Primary Phases	91
	2. Chemistry of Reaction Corona Phases	95
	3. Annealed Rocks	97
	Summary	103
<u>CHAPTER 8:</u>	<u>Peridotites: Bulk Rock Compositions</u>	104
<u>CHAPTER 9:</u>	<u>Peridotite: Equilibration Temperature and Pressures</u>	109
	1. The 'Geotherm'	111
	2. Chemical Equilibrium	114
	3. Spinel and Garnet/Spinel Lherzolites	119
	Summary	120
<u>CHAPTER 10:</u>	<u>Granulites</u>	122
	Introduction	122
	Petrography	123
	Bulk Rock Chemistry	127
	Phase Chemistry	131
	Estimates of Equilibration P/T Conditions	134
	Summary	138

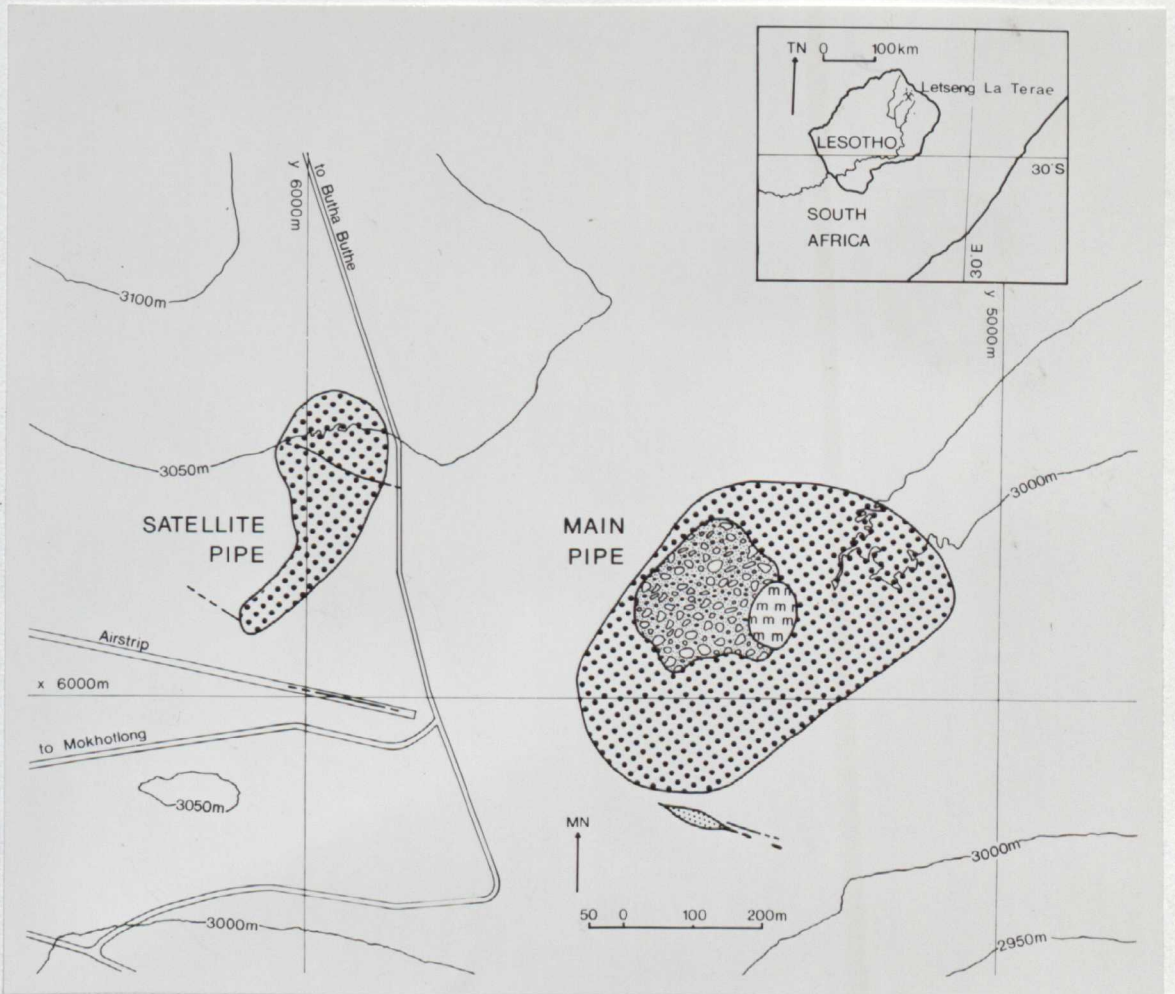
PART III: SYNOPSIS

<u>CHAPTER 11:</u>	<u>Synopsis of Geological History</u>	140
	1. The Genesis of the Kimberlite	140
	2. The Ascent of the Kimberlite	142
	3. The Emplacement of the Kimberlite	147
	4. The Structure of the Sub-Letseng Crust and Upper Mantle	149
<u>REFERENCES</u>		153
<u>APPENDICES:</u>	1. Underground Mapping Technique	
	2. Brief Description of Thin Sections: Main Pipe	
	3. Brief Description of Thin Sections; Satellite Pipe	
	4. Analyses of Minerals from Main Pipe Peridotites	
	5. Analyses of Minerals from Satellite Pipe Peridotites	



Plate 1.1: Aerial view of the Letseng Mine looking north-east. Satellite Pipe left foreground, Main Pipe right foreground.

Plate 1.2: Locality map showing the position of the Main and Satellite Pipes and the surface distribution of the major kimberlite types.



## INTRODUCTION

The two kimberlite pipes at Letseng-la-Terae (hereafter referred to as Letseng) lie in the heart of the Maluti Mountains of northern Lesotho (lat. 29°00'S; long. 28°43'E) at an altitude of 3000 m (see Plates 1.1 and 1.2). These mountains form a high rolling plateau, are deeply dissected by southward flowing rivers and truncated to east, north and west by breathtaking shear escarpments. The eastern escarpment forms the border with neighbouring South Africa and in places is vertical for 1500 m. In the west the escarpment is less steep but the undulating lowlands of Lesotho are similar, if less well watered, to the area to the east of the escarpment in Natal.

The mountain climate is harsh with cool, wet summers and cold, dry winters. Rainfall may exceed 1000 mm near the eastern escarpment and temperatures only rarely exceed 25°C on the high plateau. The weather is unpredictable with, often, several changes from sunny to windy, rainy, sleet and snow in a single day. Winters are usually dry, but any precipitation occurs as snow which may lie on southward facing slopes for several months. Winter night-time temperatures may drop as low as -20°C.

The Letseng kimberlites are part of a major kimberlite province in northern Lesotho which probably contains the greatest concentration of kimberlites, per unit area, of any country in the world. Both of the kimberlites are now being mined for their diamonds. However, the history of diamond mining in Lesotho (formerly Basutoland) is long and checkered, and the Letseng mine represents a considerable achievement for the efficacy of human endeavour and risk capital.

The first mining of kimberlite 'blueground' for diamonds began in 1870 at Jagersfontein in South Africa. In the following years many kimber-

lite pipes were discovered and worked by prospectors for diamonds. Indeed the name kimberlite derives from the city of Kimberley which grew up around four important mines in South Africa. By the turn of the century most of the mining was amalgamated under the control of a few large companies. Wagner (1914) has recorded this history in his classical monogram. One discovery in the eastern Orange Free State of South Africa (Monastery Mine) revealed that 'modern man' was not the first miner of these kimberlite pipes: here several pits of earlier workings were found. These early miners, however, were more interested in the ilmenite enclosed in the kimberlite; indeed in the Basutoland lowlands many of the early kimberlite discoveries were the result of tracing 'sekama' (ilmenite) deposits which had sometimes been worked for more than a century. The ilmenite was used as a base for cosmetics.

Apart from the few 'barren' kimberlites, known in the Basutoland lowlands, Stockley (1947) considered that "the outlook for diamond prospecting cannot be considered promising", although the basis for this reasoning is obscure. Up to this time, no diamonds of verifiable Basutoland source had been found, and it was not until 1954 that the Kao kimberlite in the Maluti Mountains was discovered and exploited by the local people. This diamond discovery heralded the new era of exploration, led by Colonel J. Scott, which over the next five years revealed the extent of the kimberlite province. Further prospecting, during the late 1960's and 1970's, by a United Nations team did not add any significant discoveries to those found in the late 1950's.

In 1957, Peter Nixon, who was employed by Colonel Scott while studying for a Ph.D. at Leeds University, discovered the Letseng-la-Terae Main Pipe. He was returning to Kao from the Orange River valley, along the Namahali bridle track and had camped at Letseng-la-Terae, or "the turn by the swamp" as the crossroads had long been known locally. All such swamps or sponges

were routinely examined because several kimberlites were known to occupy such depressions, and local information proved Letseng to be no exception. Pits and trenches (Nixon, 1960), gave the first indications of the size of the pipe and allowed some preliminary petrographic, mineralogical and geochemical study (Nixon, 1960; Dawson, 1960; 1962; Nixon et al., 1963). However, the exposure was poor and because of the low diamond grade the mining company relinquished its interest.

The surface of the two pipes was divided into small 'claims' and worked by local 'diggers' much as in the early days at Kimberley. In the period 1960-1967, 62,000 carats of diamonds - including the 601.25 Lesotho Brown - were extracted. The size and quality of some of the stones attracted considerable interest and the government of the newly independent Kingdom of Lesotho negotiated with the RTZ Mining Company, to re-evaluate the economic potential of the two pipes.

Over the next five years, RTZ carried out an ambitious sampling programme which, while unsuccessful in proving a viable mine, enabled considerable detailed geological study to proceed. More than 2,000 m of diamond drill core was recovered and over 80,000 tons of kimberlite processed through a small diamond treatment plant. RTZ demonstrated the low grade (3.5 carat/100 ton) of the Letseng kimberlites, but confirmed the presence of large, high quality, stones. Their negotiations with the government however, were unsuccessful and the mining lease was allowed to lapse.

The De Beers Mining Company were at this stage invited by the Lesotho government to carry out a further limited feasibility study, mainly on the basis of the RTZ data. I was seconded to Lesotho to assist in the geological aspects of the study. An agreement to mine was signed in March, 1975, between De Beers and the Lesotho government, and the mine was finally commissioned a few months after I left Lesotho in December, 1976.

### Local Geology

The rocks exposed in Lesotho, belong mainly to the upper part of the Karoo System (Carboniferous-Jurassic) which covers vast areas of south and central Africa (see Haughton, 1969). This widespread series of rocks consist of flat-lying conformable sandstones and shales extensively intruded by dolerite dykes and sheets, and overlain by vast outpourings of basaltic lavas.

In Lesotho most of these rocks have been assigned to the Stormberg series (Stockley, 1940) and comprise the Molteno beds, the Red beds, the Cave sandstone and the Drakensberg beds. The Molteno beds are composed of massive white grits and sandstones with occasional shaly layers (rarely carbonaceous). The Red beds are composed of varicoloured sandstones, alternating with red, green and purple shales, and mudstones. Carbonaceous beds are absent and reptile fossils are abundant. The Cave sandstone is composed of a massive, fine grained, aeolian sandstones. The Drakensberg (Stormberg) beds comprise the full sequence of basaltic rocks (>1600 m) and dolerite intrusions. These lavas are tholeiitic in composition and are chemically comparable to the dolerites (Cox and Hornung, 1966). Potassium/Argon whole rocks ages obtained from samples collected over the Bushman's Pass in the west (Fitch and Miller, 1971) indicate an age range from 187-155 m.y. These samples come from altitudes of less than 3000 m so the final basaltic outpourings perhaps represented by the 3500 m high tops in Lesotho (Dempster, 1973) may be considerably younger.

### The Kimberlite Intrusions

The kimberlite intrusions in Lesotho post-date the Karoo System rocks and have been generally accepted as of Cretaceous age (Haughton, 1969). However, the oldest age of a post-Karoo kimberlite in southern Africa (150 m.y. Swartruggens - Allsop and Kramers, 1977), is very close in age to the youngest Karoo basalt. In Lesotho an isotopic age of 87.1 m.y.

was obtained for the Mothae kimberlite, about 7 km north of Letseng (Davis, 1977) and other South African kimberlites group in the range 82-96 m.y. (Allsopp and Barrett, 1975; Davis, 1977; Allsopp and Kramers, 1977) although some older ages have been obtained for individual samples from certain pipes.

The Lesotho kimberlite pipes contain abundant inclusions of the Karoo System lavas and sediments, as well as fragments of unexposed basement terrain and mantle-derived nodules. Near-surface structural control has imposed a pronounced WNW trend on the kimberlite emplacement. This trend is displayed by fractures along which dolerite and kimberlite dykes have been intruded. The kimberlite pipes lie on the same WNW trend and often occur associated with a pre-existing dyke (Dempster, 1973). However the position of the pipes along these dykes does not usually relate to any obvious cross-cutting structural control and may reflect the location of deep seated fractures.

At Letseng the smaller Satellite pipe truncates an early micaceous kimberlite dyke and is itself cut by a late calcite-rich kimberlite dyke. Both dykes trend WNW as do the other dykes in the area. However the long axis of the Satellite pipe (and to a lesser extent the Main pipe) lies nearly perpendicular to this dyke trend and no cross-cutting structure has been recognised to explain the localisation of the kimberlite pipe emplacement.

As indicated above, the emplacement of the kimberlite dykes brackets the major phase of kimberlite diatreme formation. In the Satellite pipe, diatreme formation may have been simple with only one diatreme phase kimberlite exposed. Kimberlite inclusions in the kimberlite suggest this is a simplistic model and the Main pipe with five varieties of kimberlite and two or three varieties of kimberlite inclusions demonstrates that diatreme formation was a long and complicated process. In each pipe, late

calcite-rich kimberlite dykes indicate that differentiation towards a carbonate-rich (not carbonatitic) fraction has occurred.

The post-kimberlite gravel deposits have been largely disturbed by 'diggers'. These gravels have washed into the depression which is the geomorphic expression of the Main pipe and to a lesser extent the Satellite pipe. The gravels tend to thin towards the pipe centre but are nowhere thicker than 5 m (on the Satellite pipe) and usually less than 2 m on the Main pipe. The gravels overlies about 50 cm of oxidised kimberlite (yellow ground) and are overlain by up to 1 m of peat or 'black cotton' soil. The undisturbed surface expression was a swamp or sponge with lush grass and other vegetation which contrasts sharply with the surrounding basalt where the soil cover is usually poor and thin.

#### Previous Research

The first detailed account of the geology at Letseng was given by Bloomer and Nixon (1973) but earlier minor references were made to the Qaqa pipe (as it was then called) by Nixon (1960), Nixon et al. (1963) and Dawson (1960, 1962). The paper by Bloomer and Nixon was made possible by the considerable exposure of fresh kimberlite revealed during the RTZ sampling operation and its publication in the book 'Lesotho Kimberlites' coincided with the first International Kimberlite Conference held in South Africa. The resurgence of interest in kimberlites and their mantle xenoliths may have been spurred on by the failure of the Moho project, but improved experimental techniques undoubtedly allowed for more detailed estimation of geothermometry and geobarometry as applied to garnet peridotites.

Boyd (1973b) outlined the concept of a pyroxene geotherm using data from Lesotho peridotites, including some Letseng data (Boyd, 1973a). Many succeeding papers by Boyd and Nixon (e.g. Nixon and Boyd, 1973; Boyd and Nixon, 1975) refer to this 'Lesotho geotherm'. Mercier and Carter



(1975) using this same data, interpret this perturbed geotherm as an artifact reflecting the degree of depletion with depth. Nixon et al. (1973) indicate that Letseng's position close to the Kaapvaal craton edge results in sheared mantle nodules from shallower depth than Thaba Putsoa.

Nixon and Boyd (1973) discuss the petrogenesis of the discrete nodule association, including sub-calcic diopside from Letseng, and conclude these megacrysts are derived from a crystal mush in the low velocity zone. McCallister (1979) has investigated unmixing in these and other sub-calcic diopside megacrysts as a clue to the kimberlite emplacement rate.

A chrome-rich garnet-clinopyroxene rock analysed by Boyd (1973a) was compared to the knorringite-rich garnets from Kao (Hornung and Nixon, 1973). Haggerty (1973) and Boyd and Nixon (1972) discuss chromite compositions and referred to data from Qaqa in Nixon et al. (1963). Chromite compositions in xenoliths from Letseng and elsewhere are discussed in Smith and Dawson (1975), and the chromite/silicate intergrowths (fingerprint spinel) in Dawson and Smith (1975). Some data on other Letseng mantle xenoliths appear in a study of peridotite phlogopite (Smith et al, 1979) and in Bishop et al. (1978) who investigated Na, K, P and Ti in peridotite silicates.

Research on some granulites from Letseng is reported in the paper by Griffin et al. (1979) and alteration effects in these rocks have been studied by Ferguson et al. (1973) and Kruger (1978, 1980).

The geophysical expression of the two pipes has been investigated by Burley and Greenwood (1972) and the pipe structure is incorporated in Hawthorne's (1975) model of a kimberlite pipe. Petrographic research on the kimberlites is mainly contained in unpublished company reports but modal analysis of one fresh dyke is reported by Skinner and Clement (1979). Kruger (1978) gave a crude outline of the petrography, but description of the kimberlite is mainly limited to megascopic features

(Bloomer and Nixon, 1973). Kresten (1973) has identified saponite using DTA. The geochemistry of some dykes and diatreme-facies rocks has been investigated by Gurney and Ebrahim (1973) and Kruger (1978), but the altered nature of the samples and the high xenolith content do not give confidence in the results. The studies of autolith chemistry by Danchin et al. (1975) may give a better estimate of the kimberlite magma composition.

Isotope studies have been carried out by Kramers (1977, 1979) incorporating some Letseng data, and Allsopp et al. (1979) explain some anomalous radio-isotope ages in relation to different mica types.

The Letseng diamonds have been briefly described by Harris (1973) and studied in more detail by Harris et al. (1979). Their conclusions are important in view of the large differences in the diamonds between the two pipes. Whitelock (1979) has produced a detailed popular history of the Letseng Mine development up to 1978.

### Outline of Present Study

The research reported in this thesis began while the writer was employed by De Beers Lesotho Mining Company. The thesis is in three parts: Part 1 deals with the kimberlites, their field relations, petrography, geochemistry, isotope geochemistry, and also the included megacrysts; Part 2 deals with the accidental inclusions of mantle-derived peridotites and lower crustal granulites, their petrography, geochemistry and mineral chemistry; and Part 3 is a concluding chapter drawing together the many lines of study into an overall synthesis of the geological history.

The kimberlite exposures at Letseng are important because the kimberlite is relatively unaltered and probably represents the best exposures at an erosion level close to the transition between crater and diatreme facies and because the mining activity has allowed the detailed study of the marked zoning features observed in the Main pipe.

The petrography of the dykes and autoliths demonstrates the very fresh nature of these rocks and their suitability therefore for geochemical study. The K/Rb ratios are among the lowest recorded in kimberlites which lends considerable confidence to the interpretation of the isotope geochemistry reported in Chapter 4.

The garnet peridotites display many of the features seen in other xenolith populations in petrography, chemistry and mineral chemistry. However significant differences are noted between the xenolith populations from the Main and Satellite pipes, which is most significant in view of their close proximity. The Letseng garnet peridotites also display well preserved garnet reaction coronas illustrative of re-equilibration to spinel facies conditions. Textural and chemical evidence is presented linking the garnet peridotites with a small group of spinel and garnet/spinel peridotites. Examination of the primary mineral compositions reveals that the two kimberlite pipes have sampled distinctly different parts of the mantle during their ascent from depth. Some specimens do not plot on a simple 'fossil geotherm' but these samples are not interpreted as part of a perturbed geotherm.

The concluding discussion attempts to draw on all the known evidence to present a simple model explaining all the important features observed in both the kimberlite and the xenoliths from Letseng.

PART I

THE KIMBERLITES

CHAPTER 1Field Relations: Main and Satellite Pipes1. Main Pipe

(a) Pipe Structure: The Main Pipe is an elliptical, downward tapering cone-shaped body, with surface dimensions of 540 m x 365 m and area of 15.9 hectares. The outline of the body and the distribution of the various kimberlites within the body have been established from natural exposures and pits (Nixon, 1960); surface trenches, diamond drilling and subsurface mining development by the RTZ Mining Company (reported by Bloomer and Nixon, 1973), and further drilling, remapping underground and mapping of the open pit during the pre-production stage of mining development (Lock, 1975, 1976). The present geological interpretation is shown in the 1:1000 scale maps (see inside back cover).

Bloomer and Nixon observed that the pipe/wallrock contact dips inwards at a fairly constant  $83^{\circ}$  and calculated that coning downwards at this angle gives a point of origin for the pipe 1350 m below the present erosion surface, and close to the assumed base of the Stormberg lavas. The contacts are generally sharp, as they describe, with no upwarp or chemical alteration of the adjacent country rock. Narrow zones (1-2 m) of shattering, mylonitisation and calcite veining of the kimberlite often lie on these sharp contacts.

The contact exposed in the south-west of the pipe is exceptional in that the hanging wall contact is some 30 m nearer the pipe centre than the footwall. No shattering of mylonitisation is present and the country-rock lava has undergone some alteration as evidenced by slight colour changes. Beneath this hanging wall contact, a very large (> 25 m) angular block of basalt may be observed partially dislodged from the wallrock and

dipping  $20^{\circ}$  towards the pipe centre. Further from the contact are many large (2-4 m) angular blocks of basalt, considerably larger than generally found in this kimberlite.

In the north-east part of the pipe the kimberlite shows a rapid transition to a kimberlite/basalt breccia composed of about 80% basalt showing considerable alteration to a red-brown colour. The true wallrock contact was not intersected underground, but would appear to roughly parallel the surface contact.

Rudimentary flow banding is present in kimberlite containing few xenoliths at the north-west contact of the pipe. The flow orientation dips steeply towards the contact.

If the assumption of pipe origin 1350 m below the present surface is accepted, the present level of erosion at Letseng corresponds to the + 850m level in the kimberlite pipe model of Hawthorne (1975) which is 200 m lower than the level proposed by this author. While the stratigraphy of the intruded countryrock, as presented in the Hawthorne model, is obviously wrong for both these proposals, the wallrock features observed are compatible with either model. +850 m marks the transition from smooth walls to highly irregular stepped contacts and zones of wallrock/kimberlite breccia, features which are all visible at Letseng. It can be deduced from the model that the original surface was 400-500 m above the present erosion level. This would imply an original surface at Letseng of 3500 m O.D. (present surface 3000 m O.D.) which approximates the highest point in Lesotho that may represent the final outpouring of the Stormberg lavas (Dempster and Richard, 1973).

Bloomer and Nixon have attempted a structural analysis of fractures and joints within the Main Pipe. The most prominent peak on the joint distribution projection plot consists of near vertical joints striking  $240^{\circ}$  which they relate to the regional joint pattern shown in the lavas (Richard, 1972);

other peaks were attributed to relation to emplacement of dyke-like bodies of K2, K4 and K5 intrusions. However, the K2 kimberlite is now recognised as being the result of metasomatic alteration of the K1 and K3 kimberlites, along joints and fractures. The K4 and K5 intrusions are not interpreted as having a dyke-like shape in the present study.

Much of the earlier structural analysis is therefore considered invalid; and the joints and fractures are now attributed to differential settling within the pipe. A regional stress field may also have exercised a controlling influence as is suggested by present of post-pipe diatreme formation dykes along the same general E-W trend.

(b) The Kimberlites: One of the writer's tasks while employed by the De Beers Lesotho Mining Company at Letseng was to examine the relationship of the economic K6 (garnetiferous) kimberlites to the surrounding kimberlites; and to characterise this kimberlite for ease of identification during mining operations. Consequently considerable time was spent in delineating these field relations and macroscopic characteristics. It soon became apparent first that the number of kimberlites previously mapped was an unnecessary complication; and second, that although typical K6 and non-K6 descriptions could be applied to the two major kimberlites, the marginal zone between the two was often blurred.

The kimberlites mapped as K1, K2, K3, K7 and K8 by Bloomer and other geologists of the RTZ Company (Bloomer and Nixon, 1973) are here grouped as the autolithic kimberlite (the non-K6 of the De Beers geologists) and the K6 type is here termed the garnetiferous kimberlite. K4 and K5 are both distinctive micaceous kimberlites and are referred to here by their original names. No genetic inference is implied by these names: their use is purely descriptive. The use of the term 'autolith' follows that of Ferguson et al. (1973) and is distinct from the views of Clement and Skinner (1979) who

define a 'segregation' texture. The term autolith is reserved by these authors to describe cognate xenoliths.

Mapping Technique: In addition to normal mapping procedures at surface and underground, a technique was developed to describe in detail the kimberlite at a series of locations in the underground (55 m level) workings (see Plate 1.10). At each locality one square metre of sidewall was cleaned and a series of observations and measurements were made. The detailed procedure together with a specimen logsheet is presented in Appendix 1. In addition to in-situ observations, hand specimens were removed for further study which in some cases included point counting on polished slabs and in selected thin sections (the thin section study was conducted by Clement (1975)).

This technique allowed not only the characterisation of the kimberlite but also areal plots of the variations in size and abundance of minerals and xenoliths in the kimberlites. Many observations proved relatively valueless or rather obvious and others, while suggesting variations, could not be presented diagrammatically.

Other samples were collected for crushing and heavy mineral separation. The garnets extracted were examined under the binocular microscope. Abundance, colour and type of garnet were recorded and the kimberlite identified accordingly (see below). This procedure has more recently been used with considerable success in the soft kimberlite of the mine's open pit, to delineate the economic ore body.

Autolithic Kimberlite: The bulk of the pipe is filled by the autolithic kimberlite which is considered the oldest of those presently exposed. Inclusions of micaceous kimberlite similar to some of the dyke kimberlites and, more significantly, of epiclastic or pyroclastic kimberlite of the crater facies (cf. Edwards and Hawkins, 1966; Hawthorne, 1975; Hepworth et al. 1976) suggest that a pipe structure was well established before the intrusion of this kimberlite.



This kimberlite type encompasses the K1, K2, K3, K7 and K8 varieties of Bloomer and Nixon (1973). Late deuteric alteration processes distinguishing K1 and K3 are not considered sufficient grounds for separation within such a heterogeneous rock. K2 was also mapped as a separate body but it was observed that 'apophyses' of K2 in K1 (RTZ map of surface geology, 1970) are colour changes due to (late stage) metasomatism along veins and fractures which are sometimes calcite filled.

The autolithic kimberlite is generally a moderately hard blue-grey or grey tuffisitic kimberlite breccia (classification of Clement and Skinner, 1979) characterised by the virtual absence of kimberlitic (pyrope) garnet and by the very often well developed autolithic texture (Plate 1.3). Autoliths, recognisable by eye, locally compose up to 10% of the rock and are always present. The autoliths have cores of altered olivine or rock fragments as nuclei and often show a concentric growth structure which distinguishes them from kimberlite xenoliths of angular habit and different texture (cognate xenoliths - see Chapter 2). Olivine xenocrysts and phenocrysts are invariably pseudomorphed by serpentine and other secondary minerals. The rounded olivine pseudomorphs average 7 mm in size and compose some 15-20% of the rock. Small phlogopite xenocrysts (~ 1 mm) are locally moderately common as rounded flakes.

Accidental inclusions of Karoo System lavas and sediments, basement gneisses and granulites and various peridotites compose <20% of the rock. All these inclusions are usually angular, <<1 m size and highly altered. Inclusions of pre-existing kimberlite have already been noted although they are not abundant as a macroscopic feature.

The remainder of the rock is composed of a fine grained matrix of serpentine and other minerals (see Chapter 2).

The generally harder, more compact, nature of this rock is testified to by the weathering characteristics of fresh exposures. In contrast to

the garnetiferous and other kimberlites which crumble rapidly on exposure to air, this kimberlite often maintains its tough character for a considerable time.

Another feature of note, only observed in this kimberlite, is the flow structure which are seen at several widely separated localities. This flow texture is in contrast to that previously noted in the north-west of the pipe. All such examples lie on near-vertical fault planes showing considerable vertical slickensiding. No regular orientation of these planes is apparent, although a very crude parallelism with the pipe contact may be suggested. The presence of flow is usually interpreted from a narrow selvedge of fine grain kimberlite lying on the fault plane; the faulting is considered to have removed the evidence of more extensive flow banding. One locality in the south-west of the pipe however, shows a one metre wide zone of alternating coarse and fine bands of kimberlite (Plate 1.11). The fine grey kimberlite has the appearance of the matrix of the coarse kimberlite and is similar to the autolithic material (see Chapter 2).

Garnetiferous Kimberlite: This kimberlite is a soft grey-green tuffisitic kimberlite breccia characterised by abundant kimberlitic (pyrope) garnet large phlogopite xenocrysts and the virtual absence of recognisable macroscopic autoliths (Plate 14). The garnet xenocrysts and megacrysts average 4 mm in size, but range up to 2 cm. Their colour varies from orange to pink, red and lilac. They are often rimmed by kelyphite; the red garnet megacrysts have a thin black kelyphite rind in contrast to the considerably thicker grey-brown kelyphite seen on the lilac garnets. Red garnets often have a crude cubic shape and larger size, in contrast to the rounded lilac garnets. Phlogopite xenocrysts and megacrysts of dark brown-bronze colour are common and range up to as large as 5 cm, although the average is only about 2 mm. Olivine xenocrysts and phenocrysts are entirely altered

to serpentine and clay minerals. They compose 15-20% of the rock but are slightly smaller on average than in the autolithic kimberlite.

The suite of accidental inclusions is similar to that in the autolithic kimberlite except that Karoo system sediments are virtually absent. There are fewer basement xenoliths but their size is considerably larger (cf. Plate 10A 'Lesotho Kimberlites' p.36, 1973). The basalt inclusions also are considerably larger (up to 3 m or more), fresher and more abundant (up to 40% of the rock). Similarly, ultramafic xenoliths are larger and more abundant.

A significant feature displayed in the garnetiferous kimberlite is the zonation resulting from the increasing abundance or size of the characteristic xenoliths and megacrysts towards the centre of this kimberlite. In particular, garnet and phlogopite megacrysts and basalt xenoliths are more abundant and larger towards the centre of the garnetiferous kimberlite (see below).

Three kimberlite dykes are exposed in this kimberlite which were interpreted as a ring dyke by Bloomer and Nixon (1973). One of these dykes is a carbonate-rich rock with abundant fresh olivine and showing sharp contacts (NL379 see description below). This dyke is in contrast to the other two dykes which show gradational contacts and lack fresh olivine. Their character is similar to that of the host garnetiferous kimberlite but lacking accidental inclusions. No dykes were encountered in drill holes located between these exposures. These dykes are not considered as part of a ring dyke, but may represent a magmatic segregation from the bulk of the garnetiferous kimberlite, i.e. they may represent the hypabyssal variety of this intrusion.

Contacts between the garnetiferous and autolithic kimberlites are rarely sharp and usually transitional over a distance of 2 or 3 m. Although the form of the intrusion would tend to suggest the younger age of the garnet-

iferous kimberlite it is important to note that, since the autolithic kimberlite was probably not fully consolidated at the time, the time separation of the two intrusions may have been quite small.

K4 Kimberlite: This kimberlite shows some sharp contacts and cross-cutting relations to the previous two varieties and is interpreted as being younger. It is a fine grained, mottled, green hypabyssal (?) kimberlite. It has a distinctive weathering appearance as a result of flaky exfoliation. Olivine xenocrysts and phenocrysts up to 4 mm are always serpentinitised and the rock contains some rare lilac garnets. These components are set in a highly micaceous groundmass together with well rounded xenoliths of altered lava and sediment; the xenoliths are rarely > 1 cm and compose only 5-10% of the rock.

K5 Kimberlite: The relationship between this kimberlite and the K4 is uncertain but the K5 is here interpreted as the younger of the two. The relations of the other kimberlites suggests a younging towards the centre of the diatreme where the K5 is found. The intrusion shows well developed horizontal joints which terminate abruptly at the contact with the K4 kimberlite. The kimberlite is characterised by fresh olivine phenocrysts and xenocrysts up to 4 mm in size. Apart from the dykes, this is the only kimberlite in either of the pipes at Letseng in which fresh olivine has been found. Xenoliths of highly altered lava and sediment composed 10-15% of the rock; they vary in size up to 15 cm. Some smaller xenoliths have been strung out in a magmatic flow texture observed close to the contact. The xenoliths also act as a locus for serpentinitisation giving rise to local bleached areas of the kimberlite groundmass.

(c) Distribution of Xenoliths and Megacrysts: As indicated in the previous sections there are considerable variations in the xenolith and megacryst

abundances and sizes within the Main Pipe kimberlites. The major variations occur within and between the garnetiferous and autolithic kimberlites. Xenolith abundances are low in both K4 and K5 kimberlites.

Orange-red and lilac pyrope garnets are characteristic of the garnetiferous kimberlite in contrast to the predominant pink, orange-brown and red-brown almandine garnets in the autolithic kimberlite. These different abundances partly reflect the greater abundance of ultramafic xenoliths in the garnetiferous kimberlite and of garnet bearing basement rocks in the autolithic kimberlite. Plate 1.5 shows the increasing size of garnet towards the centre of the garnetiferous kimberlite. This kimberlite is clearly demarcated by the 2 mm size contour and the autolithic kimberlite shows a uniformly small garnet size. Garnets in the garnetiferous kimberlite also display a much thicker kelyphite rind. It should be noted that the true zonation in size is probably only of the red garnet megacrysts and not of lilac pyrope which is rarely larger than 4 mm in the ultramafic xenoliths from which it is probably derived by disaggregation. This zonal size variation is also largely matched by a similar abundance variation with garnet most abundant at the centre of the garnetiferous kimberlite.

Plate 1.6 demonstrates that the size of phlogopite xenocrysts may also be used to delineate the garnetiferous kimberlite. The zonation within this kimberlite is not so marked as with garnet but the relative abundance between the two major kimberlites is similar to that for the pyrope garnet.

As already mentioned, ultramafic xenoliths are noticeably larger and more abundant in the garnetiferous kimberlite. Only two xenoliths of >10 cm size have been found in the autolithic kimberlite whereas xenoliths from the garnetiferous kimberlite are often >20 cm.

The distribution of almandine garnet described above is related to the abundance of basement xenoliths. In the autolithic kimberlite this

varies considerably across the pipe from some localities with a 'snowstorm' appearance as a result of myriads of small (<5 cm) basement xenoliths, to other areas less well endowed. The garnetiferous kimberlite has a uniformly low concentration of basement xenoliths in number, but individual inclusions are usually considerably larger (up to 30 cm) than in the autolithic kimberlite.

The average lava xenolith size (Plate 1.7) for + 10 cm inclusions shows a marked zonation towards and within the garnetiferous kimberlite. The large xenoliths in the south-west and north-east are explained by the proximity of the unusual contacts there (described in Chapter 1). While the moving average plot used to display the data tends to smooth over any sharp distinction between the two kimberlites it would not alter the zonation observed within the garnetiferous kimberlite.

Plates 1.8 and 1.9 show the abundance of lava xenoliths measured in-situ and on polished slabs and indicate an essentially similar variation to that shown by the lava xenolith size.

Lava xenoliths, at least of larger size, show considerably less alteration within the garnetiferous kimberlite and often appear as fresh as in-situ lava exposed in the underground drives outside the pipe.

Autoliths and kimberlite inclusions are not common in the garnetiferous kimberlite. In contrast the autolithic kimberlite always contains more than 2% of autoliths and sometimes as much as 10%. Recent petrographic examination by E.M. Skinner (personal communication) indicates that autoliths are more common in the garnetiferous kimberlite than previously believed, but these poorly developed autoliths are only visible under the microscope.

Nixon (1960) noted a zonation of heavy minerals in the Kao Main Pipe and Kresten and Kempster (1973) have recorded variations in heavy minerals and xenoliths from Pipe 200 but neither study shows a regular zonation as

displayed by the garnetiferous kimberlite at Letseng. The increasing abundance of larger and denser minerals and xenoliths towards the centre of the garnetiferous kimberlite may have a profound bearing on the emplacement history of this kimberlite. It is worth noting here that the orientations of xenolith long axes (especially well developed in discoidal and ovoidal ultramafic inclusions) recorded (see geological field logsheet. Appendix 1) indicate a tendency towards the vertical.

## 2. Satellite Pipe

(a) Pipe Structure: The Satellite Pipe is a tadpole-shaped body of dimensions 425 m x 130 m and surface area of 4.7 hectares. The pipe/wallrock contacts vary in orientation from  $83^{\circ}\text{W}$  in the east to almost vertical in the north and south, and  $60^{\circ}$ - $70^{\circ}\text{W}$  in the west. Contacts encountered in the underground development are similar to those found at surface and implied from diamond drilling by the RTZ Company. The pipe increases in cross-sectional area, at least to the depths of present exploration.

The pipe contacts are generally very sharp with only minor shattering and slickensiding evidenced in the east. The western contact is outward dipping with some irregularities and small scale stoping features suggesting that the country rock in this area was undergoing large scale undercutting and stoping when the present relationships were 'frozen in'.

At the southern end of the pipe, a large mass of kimberlite/basalt breccia, similar to that in the north-east of the Main Pipe, was encountered. This mass occurs partly on the wallrock contact (exposed in RTZ borehole core) and partly separated from it by a narrow zone of normal kimberlite.

It is not possible to accurately estimate the point of origin of the pipe, as for the Main Pipe, but the relative abundance of inclusions of Karoo System sediments may imply that the pipe structure is well developed below the base of the Stormberg lavas.

(b) The Kimberlite: The RTZ geologists mapped nine varieties of kimberlite of unknown relative age (reported in Bloomer and Nixon, 1973). The mapped differences were apparently due mainly to varying accidental inclusion content and rock colour. Remapping of the surface exposures and mapping in the new underground workings has shown that the dominant autolithic character of the kimberlite (only sporadically mapped as 'pseudopisolitic' texture by the RTZ geologists) extends throughout the pipe. The pipe is now considered to contain only one major kimberlite intrusion here referred to simply as the Satellite Pipe kimberlite and classified as a tuffisitc kimberlite breccia.

This tuffisitc kimberlite breccia is characterised by an often well developed autolithic texture. The autolith content may in places be as high as 30%. This widespread presence of macro- and microscopic autoliths is considered of greater genetic significance than slight changes in colour or inclusion content and, in the absence of well defined contacts, is considered to represent a single intrusive phase. However, the occurrence of kimberlite inclusions of hypabyssal character, as in the Main Pipe kimberlites, is evidence for earlier intrusive episodes.

The autoliths are set in a serpentinous matrix containing serpentinised olivine pseudomorphs and accidental inclusions in a texture very similar to the Main Pipe autolithic kimberlite.

It has already been noted that sedimentary inclusions are more abundant than in the Main Pipe kimberlites. These, together with lava xenoliths, compose up to 25% of the rock. The inclusions are generally well rounded, highly altered and less than 50 cm in size. Peridotite nodules are rarer even than in the Main Pipe autolithic kimberlite and are mainly encountered in heavy mineral concentrates discarded during the diamond recovery process. These ultramafic nodules appear slightly more abundant towards the north end of the pipe.



A dyke-like body of fine grain micaceous kimberlite with few xenoliths and containing abundant fresh olivine, occurs near the centre of the pipe at surface and underground. Its contacts with the surrounding tuffisitic kimberlite breccia are rather diffuse and its dimensions rather small (1.5 m width, length unknown but <50 m). The long axis of the exposure appears to coincide with that of the pipe. This rock is discussed in more detail in the next section and in succeeding chapters.

### 3. Dykes

Bloomer and Nixon (1973) have described a number of dykes in the vicinity of Letseng and have grouped them according to the dominant heavy minerals. The northern group near the Mothae kimberlite are characterised by ilmenite and olivine; the central group by ilmenite and garnet; and the southern group (including the dykes at Letseng) by olivine only.

Several dykes and small blows in the vicinity of the Letseng pipes have been mapped at surface. One exposed during the excavation of the airstrip is a friable greenish micaceous kimberlite with olivine pseudomorphs. The rock is highly altered but a heavy mineral separate may yield some fresh olivine. The other dykes of the southern area described by Bloomer and Nixon (1973) were not recorded as micaceous but were probably also highly altered obscuring their true mineralogy.

Dykes, occurring within the two pipes and exposed underground where the original mineralogy is preserved, belong to at least two and possibly three or more different intrusive events. At the south-west tip of the Satellite Pipe, a closely packed group of kimberlite dykelets in a one metre wide zone, are cut by the diatreme facies kimberlite of the Satellite Pipe. The strike is approximately south-east and the dip  $70^{\circ}$  to the north-east. The kimberlite is highly micaceous, dark brown in colour and contains some large rounded olivine xenocrysts (up to 2 cm) which are sometimes fresh, but often partially

or wholly serpentinitised. Country rock xenoliths are rare. Sample NL380 from this dyke is discussed in some detail in succeeding chapters.

A dyke in the surface trenches of the Satellite Pipe is encountered again underground in several tunnels on a strike of  $092^{\circ}\text{C}$ . The orientation is vertical and the dyke cuts the pipe/wallrock contact in the east. The kimberlite is fine grained, black in colour, lacking xenoliths and containing abundant small ( $\ll \frac{1}{2}$  cm) fresh olivine phenocrysts. The glistening matrix suggests the presence of mica. The dyke in the Main Pipe may possibly represent an eastward extension of this dyke. Samples of these two dykes, NL379 and NL416 respectively, are described in the following chapters.

Several other dykes within the Main and Satellite pipes have already been mentioned. Those in the Main Pipe are highly altered and resemble the matrix of the host diatreme facies kimberlite. Similarly, the micaceous kimberlite within the Satellite Pipe previously mentioned may bear a close relationship to its host kimberlite. The lack of sharp contacts for these dykes in contrast to those for the demonstrably early and late dykes suggests to the writer that these dykes closely followed the major kimberlite intrusions in time and may be genetically related (the hypabyssal equivalent of the diatreme facies?)

The interesting and unusual chronology of early and late dykes, not previously recorded in Lesotho (Dempster and Richard, 1973) affords a unique opportunity to investigate in some detail the evolution of kimberlite magma in this area. The petrography of these dykes is discussed in more detail in the next chapter and the chemistry in Chapters 3 and 4.

Plate 1.3: Mined block of autolithic kimberlite showing the general texture. An autolith is shown arrowed in the bottom right corner.

Plate 1.4: View of south-east wall of the Main Pipe open pit showing the micaceous (K4) kimberlite on the left, the garnetiferous kimberlite in the centre, and the autolithic kimberlite at the right. The arrows mark the approximate positions of the contacts.



Plate 1.5:Size distribution of pyrope garnet in the Main Pipe (contour interval 2mm).

Plate 1.6:Size distribution of phlogopite xenocrysts in the Main Pipe (contour interval 2mm).

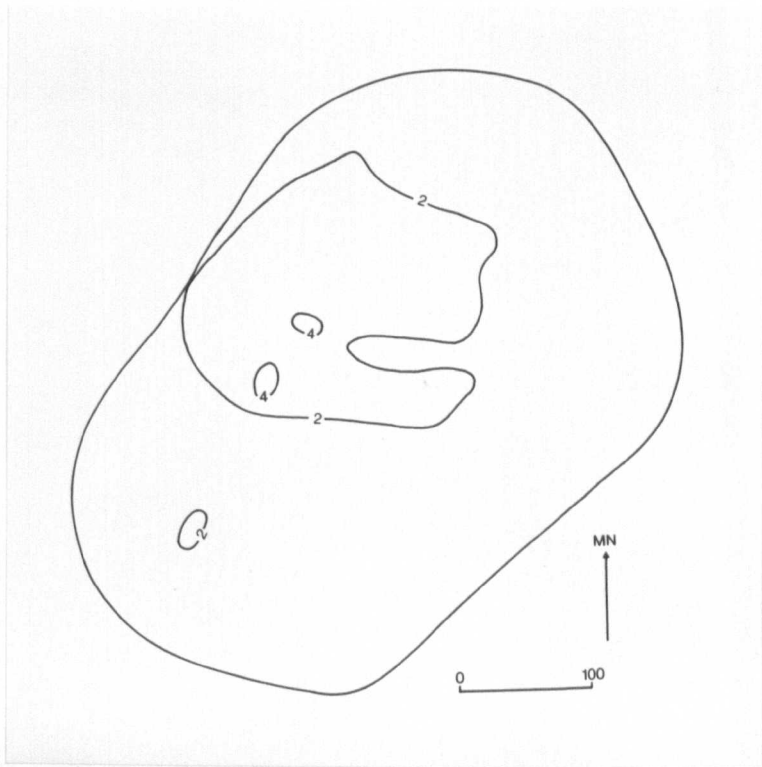
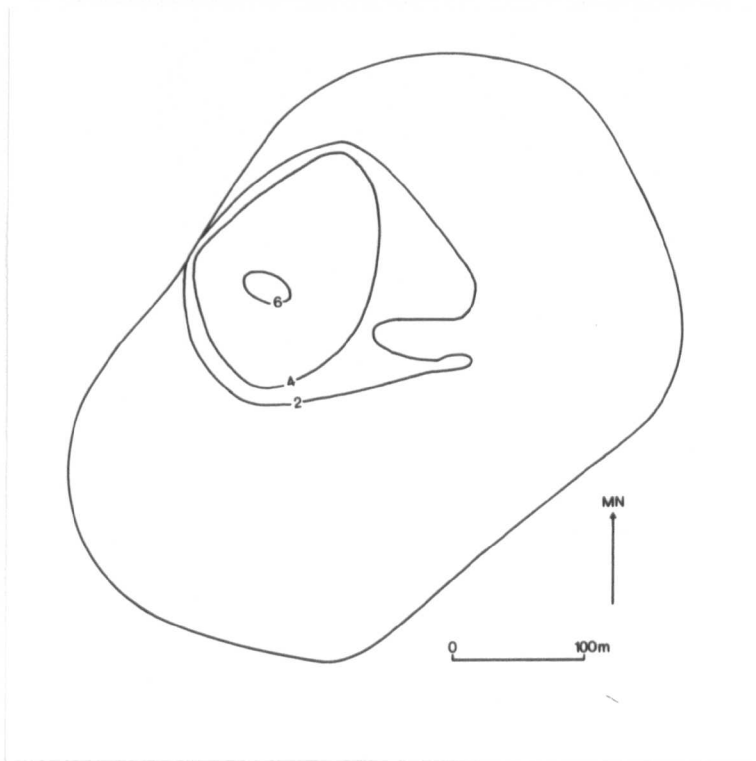


Plate 1.7: Size distribution of +10cm lava xenoliths in the Main Pipe (contour interval 10cm).

Plate 1.8: Abundance of lava xenoliths in the Main Pipe. (measured in situ, contour interval 5%).

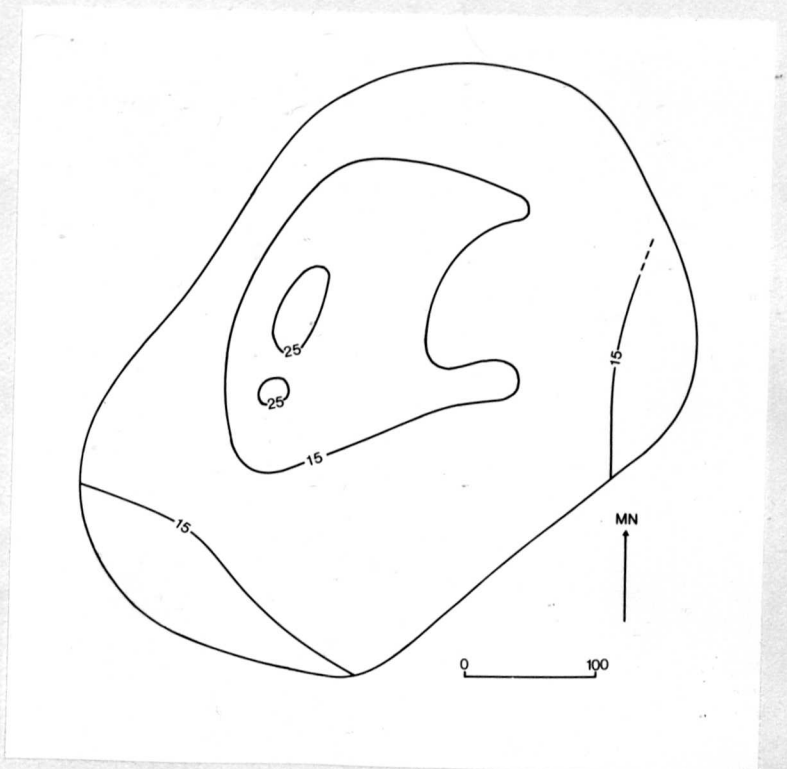
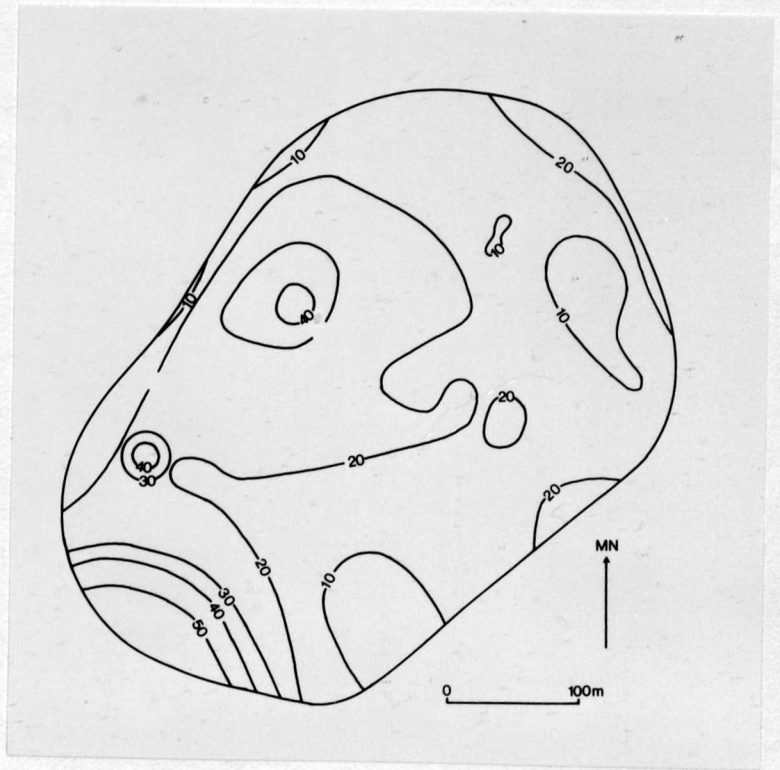




Plate 1.9: Abundance of lava xenoliths in the Main Pipe.  
(measured on polished slabs, contour interval 5%).

Plate 1.10: Underground (55m level) sample localities.

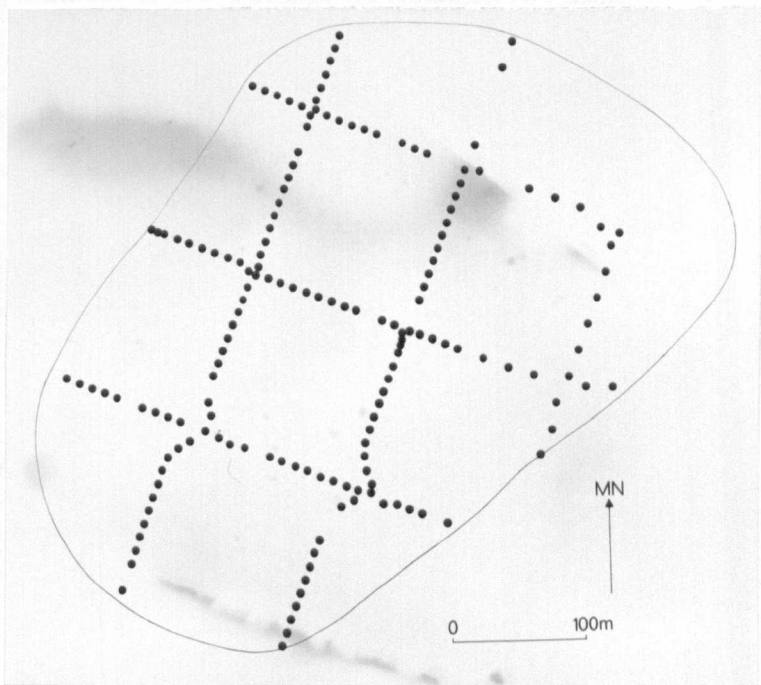
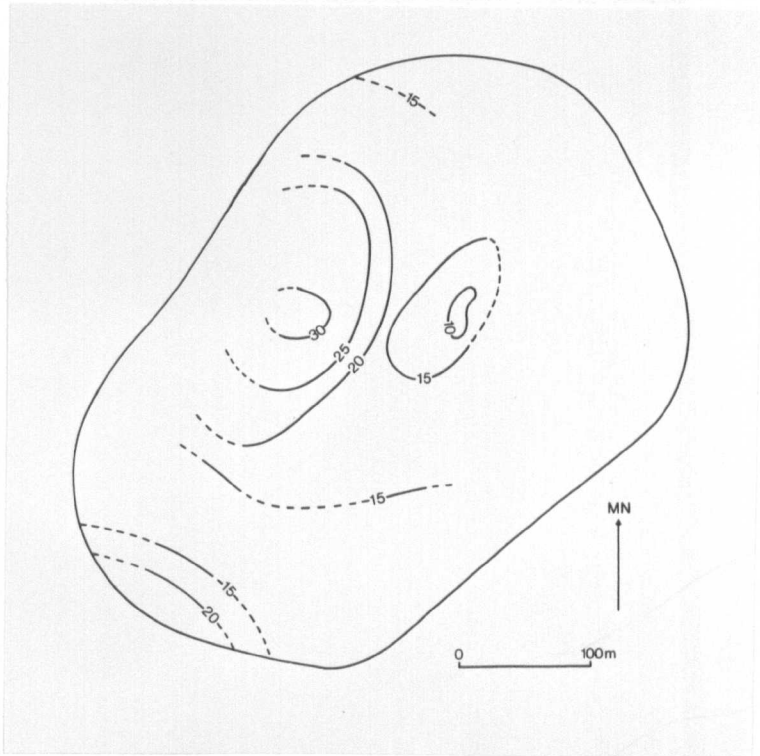


Plate 1.11: Flow-banded kimberlite from the autolith  
kimberlite, Main Pipe. Photograph shows coarse and fine  
bands, alternating from bottom to top.



## CHAPTER 2

### Petrography and Phase Chemistry

The petrography of the diatrema facies kimberlites of both the Main and Satellite pipes is being studied in some detail by E.M. Skinner of De Beers Consolidated Mines, who has examined a large number of thin sections prepared from samples collected by the present author and other geologists employed by De Beers. The following descriptions of the diatrema-facies rocks are abridged from his preliminary, unpublished reports. The petrography of the dyke kimberlites is described by the present author.

Electron microprobe analyses of selected olivines and phlogopites from the dyke kimberlites have been made at Sheffield University, using a Cambridge Instruments Microscan IX and at Cambridge University using the departmental developed Miniscan (E.D.S. System). Accelerating voltages were 15K and 20 Kv respectively, and sample currents  $3-4 \times 10^{-8}$  A.

#### 1. Main Pipe

(a) Autolithic Kimberlite: All the specimens are classified according to the scheme of Clement and Skinner (1979) as microlitic tuffisitic kimberlite breccia. Mineralogically it is a diopside kimberlite.

This kimberlite is characterised by the presence of abundant inclusions of mainly basalt and early generation kimberlite as well as abundant fine grained diopside and serpentine in the groundmass. The thin sections contain > 15 vol.% of xenolithic material larger than 4 mm. Larger sized components include country rock basalt xenoliths, xenocrysts derived therefrom, inclusions of earlier generation kimberlite and altered olivine grains. Macrocrysts of phlogopite, orthopyroxene, chrome diopside, garnet, ilmenite and spinel are rare.

Microplitic late-stage groundmass diopside and serpentine are unevently distributed and segregation (= autolithic) textures are well developed. In some specimens the groundmass diopside and serpentine are more uniformly distributed. Olivine is always pseudomorphed by serpentine and groundmass serpentine is often replaced by very fine grained phyllosilicates.

Some of the early generation kimberlite inclusions appear to be genetically related to the segregations but others are demonstrably different with a mineralogy containing melilite (?) or moticellite.

The average modal abundances of twenty one samples of autolithic kimberlite (based on 500 point counts over single thin sections from Skinner and Clement, 1979) are:

Basalt xenoliths and derived xenocrysts	30
Other xenoliths and xenocrysts	4
Kimberlite inclusions	<u>19</u>
	<u>53</u>
Olivine pseudomorphs	21
Matrix phlogopite	1
Matrix diopside	14
Serpentine and clay	9
Calcite	trace
Opaque minerals	1
Perovskite	trace

The flow banding illustrated in Plate 1.9 is well exhibited in thin section. Differentiation into coarse and fine bands and mineralogical banding is evident, although the overall mineralogy is as described above.

(b) K2 Kimberlite: The naming of this kimberlite by Skinner is confusing as it does not refer to the K2 variety originally mapped by the RTZ geologists (see Chapter 1), but embraces a small area to the east of the garnetiferous kimberlite, adjacent to the K4 and K5 kimberlites. No field evidence is

presented for its recognition, but microscopic examination reveals an unusual segregatory texture.

The segregations are similar in appearance to those in the autolithic and garnetiferous kimberlites, however the matrix is relatively coarse-grained and the minerals more varied. The groundmass of the segregations consists of perovskite, spinels, diopside, phlogopite, apatite, calcite and serpentine whereas the late stage interstices include all these minerals with the exception of perovskite and spinel. The interstitial minerals are extensively replaced by a variety of secondary minerals and subhedral olivine is always pseudomorphed by a similar variety of minerals.

Xenoliths consists almost exclusively of altered basalt but rare ultramafic nodules also occur. Phlogopite is present in at least four modes from mica-rich nodules and xenocrysts to phenocrysts and bleached groundmass grains.

The average modal abundances of minerals and xenoliths for three samples of the K2 tuffisitic kimberlite breccia are:

Xenoliths and xenocrysts	20
Kimberlite inclusions	trace
Olivine pseudomorphs	34
Phlogopite	11
Diopside	7
Apatite	2
Perovskite	1
Opaque minerals	2
Calcite	3
Serpentine and fine grained phyllosilicate	20

Mineralogically this is classified as a phlogopite rich serpentine kimberlite.

(c) Garnetiferous Kimberlite: Like the autolithic kimberlite this is a microlitic tuffisitic kimberlite breccia, which is characterised by an abundance of xenolithic basalt and very fine grained diopside and

serpentine. It is distinguished from the earlier kimberlite, however, by containing fewer inclusions of early generation kimberlite and by being more highly altered. In addition it contains more olivine pseudomorphs, garnet xenocrysts, serpentine, calcite and perovskite but less diopside. All the specimens exhibit microscopic segregation textures but these are generally smaller and much less evident than in the autolithic kimberlite.

Inclusions of early generation kimberlite are melilite (?) and monticellite varieties, similar to those in the autolithic kimberlite but an unusual amphibole bearing variety has also been recorded (Skinner, 1980).

The average modal abundances for seventeen samples of the garnetiferous kimberlite are:

Basalt xenoliths and derived xenocrysts	27
Other xenoliths and derived xenocrysts	3
Kimberlite inclusions	<u>1</u>
Total inclusions	<u>31</u>
Olivine pseudomorphs	38
Matrix phlogopite	trace
Matrix diopside	8
Groundmass serpentine and clay	18
Calcite	3
Opaque minerals	1
Perovskite	1

The mineralogical classification of this kimberlite is a diopside-rich serpentine kimberlite.

(d) K4 Kimberlite: This is characterised in thin section by being highly altered and by a relative abundance of matrix phlogopite. Alteration products include serpentine carbonate and 'clay minerals'. The dominant texture is porphyritic with abundant olivine pseudomorphs of two generations (up to 4 mm), occasional phlogopite grains (up to 1 mm), rare inclusions of early generation kimberlite and variable amounts (up to 10%) of altered



basalt xenoliths in a fine grained matrix. Scattered small xenocrysts (?) of ilmenite occur but no garnet was observed.

The fine grained matrix contains abundant but variable proportions of 'bleached' phlogopite, serpentine, carbonate and clay minerals together with accessory groundmass spinel, perovskite, apatite and relict diopside.

The average modal abundances for five K4 kimberlite samples are:

Xenoliths	5
Olivine pseudomorphs	46
Phlogopite (macrocrysts and matrix)	15
Diopside	1
Apatite	2
Perovskite	1
Opaque minerals	4
Calcite (+ dolomite)	8
Serpentine + clay	18

Mineralogically this is a phlogopite serpentine kimberlite. Texturally this may be a kimberlite (sensu stricto) of the hypabyssal facies.

(e) K5 Kimberlite: This is characterised by the relative abundance of (macroscopic) fresh olivine and microscopic monticellite and is highly distinctive since no fresh olivine has been found in any of the other massive kimberlites at Letseng. The texture is that of a typically macro-porphyritic-kimberlite (sensu stricto) of the hypabyssal facies. Two generations of olivine and rare xenoliths are set in a finer grained matrix. Olivine occurs as anhedral grains (up to 5 mm) and subhedral to euhedral grains (up to 1 mm). Monticellite is the most abundant matrix mineral as equidimensional grains <0.01 mm size. It is commonly enclosed in poikilitic grains of interstitial irregular shaped phlogopite (up to 1 mm). This phlogopite exhibits reverse pleochroism. Perovskite is relatively abundant and shows a large size range from anhedral crystals of 2 mm size to later crystallising small euhedral grains. The coarse

crystals are commonly found as partial mantles to the olivine (cf. dykes NL379 and NL416). Calcite occurs as discrete euhedral grains and as ragged rafts in serpentinous segregations.

The modal abundances for two samples of K5 kimberlite are:

Xenoliths	trace
Olivine	45
Phlogopite	11
Diopside	1
Monticellite	23
Apatite	1
Perovskite	3
Opaque minerals	3
Calcite	2
Serpentine + clay	10

Mineralogically, this is a serpentine and phlogopite-rich monticellite kimberlite.

## 2 Satellite Pipe

The tuffisitic kimberlite breccia of the Satellite pipe has not been described in great detail. Skinner (1976) has outlined a texture very similar to the Main pipe autolithitic kimberlite. The rock contains altered country rock xenoliths, early generation kimberlite inclusions and olivine pseudomorphs which together with autoliths compose a major portion of the rock. The interautolithitic matrix consists of serpentine and minor calcite. Pseudo-octahedral apophyllite, originally claimed to be diamond (!) by Basotho miners, was identified by XRD (Gurney, pers. comm.) on rare  $\frac{1}{2}$  cm. crystals. Other minerals recognised in the autoliths include phlogopite, perovskite, spinel and opaque phases. Diopside was not mentioned in Skinner's report but by analogy with more recent studies the autoliths are possibly diopside segregations. Mineralogically this rock therefore is probably a serpentine-rich diopside kimberlite.

### 3. Dykes

(a) Early Dyke NL380: This rock in hand specimen has a macroporphyritic texture, olivine macrocrysts (up to 2 cm) being set in a finer grained micaceous matrix. Xenoliths of country rock are rare: one xenolith found in thin section is basaltic. The olivine appears to occur in two generations. The larger olivines are anhedral xenocrysts and the smaller (<0.3 cm) olivine phenocrysts are euhedral. Only the larger grains have relict cores of fresh olivine and even these are extensively serpentinised.

In thin section a microporphyritic texture of euhedral phlogopite is seen in a groundmass of serpentine and calcite. Hexagonal crystals of pale brown phlogopite are of uniform size (<0.1 mm). Cleavage sections often show bending. The rims are commonly a deep red-brown with a strong reverse pleochroism and some exhibit marginal chloritisation and serpentinisation. Rare grains of subhedral phlogopite (up to 1 mm) have a dark brown strongly pleochroic core mantled by a pale brown rim (similar to the phlogopite microphenocrysts) (Plate 2.1). This pale rim may rarely also be rimmed by the red-brown phlogopite.

The groundmass of this rock is peppered with subhedral perovskite and euhedral to subhedral opaque spinel (magnetite?) (Plate 2.2). Rare larger (<0.05 mm) red-brown chromite is always mantled by magnetite or perovskite (Plate 2.4). Fine grain acicular apatite and anhedral calcite is locally abundant interstitial to the phlogopite microphenocrysts.

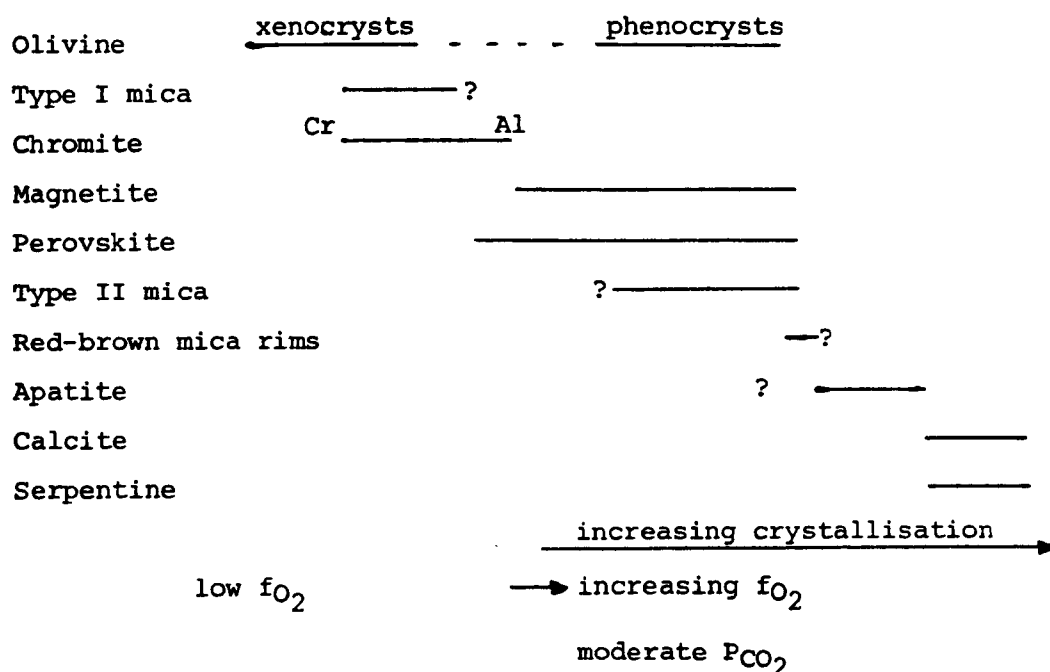
Plate 2.3 shows a micaceous segregation which contains abundant euhedral green to brown pleochroic phlogopite and subhedral magnetite in a serpentine matrix (+ minor calcite). The contact between the segregation and the surrounding kimberlite is usually marked by a dense cluster of opaque oxide but elsewhere the contact is gradational.

The phlogopite of this kimberlite accords with the petrographic distinctions between type I mica (dark brown cores of larger grains) and

type II mica (microphenocrysts of pale brown phlogopite) made by Smith et al. (1978). These authors also observed red-brown reversely pleochroic rims on type II micas, a feature previously recorded in south-west Greenland kimberlites by Emeleus and Andrews (1975).

No point counting was undertaken but the abundance of phlogopite readily defines this rock as a phlogopite kimberlite. It is very similar in texture to the Sydney-on-Vaal dyke in South Africa (Skinner and Clements, 1979).

A simple diagrammatic crystallisation sequence is as follows:



(b) Intermediate Dyke NL381: This rock has been interpreted in Chapter 1 as possibly related to the diatreme facies kimberlite of the Satellite pipe, because of the gradational contacts between the two rocks. The texture is macro-porphyrific with two generations of olivine in a matrix of phlogopite, diopside, serpentine, perovskite, opaque minerals and minor calcite.

The olivine macrocrysts are rounded grains up to 1 cm size. The smaller olivine grains (< 2mm) are subhedral to euhedral. Some of the larger grains are in fact aggregates of anhedral or subhedral crystals which may represent an early cumulate fraction. The olivine is usually only partially altered

along the grain margins to a greenish serpentine similar to that in the groundmass.

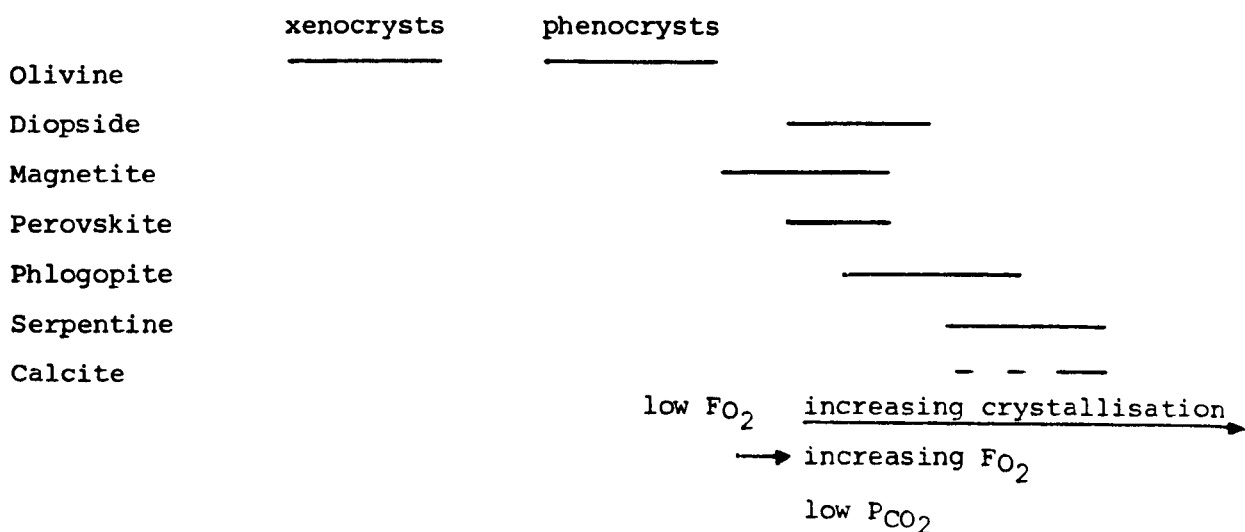
Red-brown reversely pleochroic phlogopite occurs interstitial to the olivine and poikilitically encloses diopside, perovskite and opaque oxides. Diopside microlites occur throughout the groundmass but are best seen in serpentinous areas often as radiation acicular laths (Plate 2.6) up to 0.2 mm long. Perovskite is a paler yellow brown than in NL380 and shows a greater range in size from 0.02 mm to submicroscopic inclusions in phlogopite. Some of the larger grains form partial rims to olivine phenocrysts. Opaque oxides (magnetite?) are distributed in a similar fashion to perovskite, although one grain rimmed by perovskite (Plate 2.5) indicates it may occur slightly earlier in the paragenesis. Reflected light study (Plate 2.7) indicates that perovskite is zoned to more reflective rims of opaque material (?magnetite).

Serpentine in the groundmass occurs as irregular pools which are largely separate from all the other minerals and often altered to hydromica (?). Rare calcite appears as small anhedral grains adjacent to these areas.

Skinner (1976) has described unusual circular structures (up to 2.5 mm) containing all the groundmass minerals in a peculiar radiate texture. He suggests that they may represent areas of remelting and recrystallisation.

The mineral mode for this rock was reported in Skinner and Clement (1979) who classify it as a diopside-phlogopite kimberlite.

A simplified paragenetic sequence is:



(c) Late Dyke NL379: This rock, which is shown to post-date the Satellite pipe kimberlite, is a fine grained block porphyritic rock with abundant small olivine phenocrysts in hand specimen. In thin section only one generation of olivine is present. The phenocrysts which are rarely larger than 1 mm often have perfect euhedral shapes which are emphasised by the almost complete lack of serpentinisation and the common adherence of phlogopite flakes (Plate 2.8). Some other olivine grains are more rounded and some aggregates of anhedral and weakly strained grains are seen. The euhedral phenocrysts are often rimmed by perovskite and opaque oxides (Plate 2.10) in addition to mica (largely chloritised).

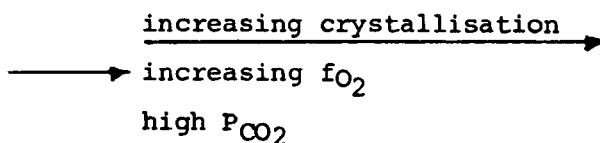
The matrix is dominated by calcite and serpentine. Calcite occurs as euhedral rhombs (often with a fibrous calcite margin) as 'rafts' within clear serpentine areas or bordering such areas (Plate 2.9). Serpentine is usually free of other minerals, but occasional stumpy diopside crystals (0.02 mm) may be present.

Elsewhere the matrix is composed of a pale reddish-brown reversely pleochroic phlogopite which poikilitically enclosed myriads of small sub-hedral perovskite and opaque oxide grains. Larger (0.5 mm) subhedral perovskite and opaque oxide (magnetite?) occur sporadically within this groundmass or rimming olivine phenocrysts. The larger perovskites show a faint 'atoll' texture with a marginal over-growth of an opaque mineral where the grain is not in contact with olivine (Plate 2.10).

The mineralogical classification of this rock is a serpentine-calcite kimberlite. The paragenetic sequence is:

Olivine	_____ - - _____
Perovskite	_____ - - _____
Magnetite	_____ - - _____
Phlogopite	_____
Diopside	_____

Calcite  
Serpentine



(d) Late Dyke NL416: This dyke cuts sharply through the Main pipe garnetiferous kimberlite on a strike which might suggest it is an extension of the late dyke (NL379) cutting the Satellite pipe. In hand specimen, this rock is very similar in appearance to NL379 with abundant small fresh olivine phenocrysts set in a fine grained black matrix. However, some olivines are slightly larger and more suggestive of a second generation. In addition, there is abundant (?) hydrogrossular not present in NL379.

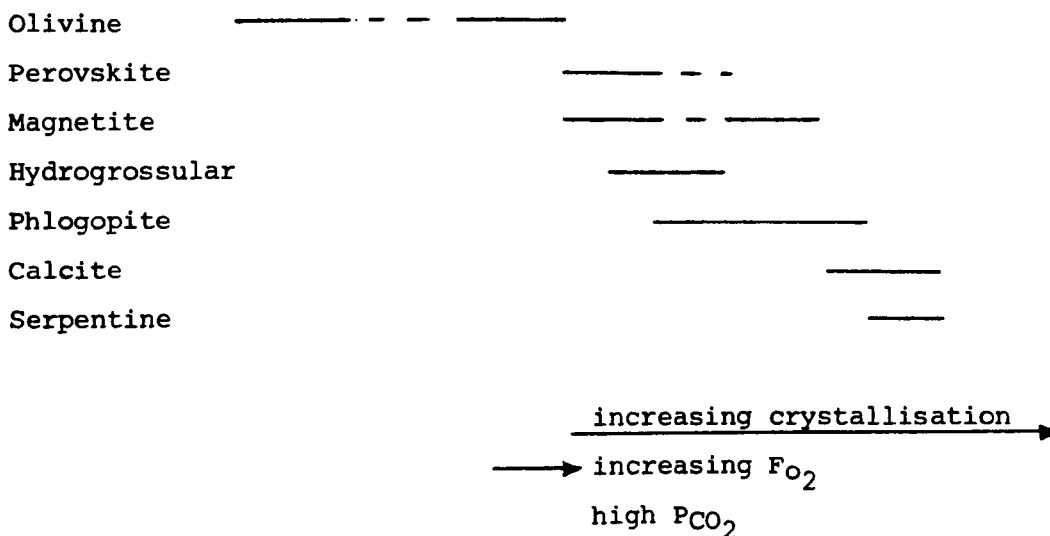
The olivine phenocrysts have suffered less serpentinitisation than any others at Letseng. Some larger subhedral and anhedral grains and aggregates may represent an early generation of crystallisation. As with NL379 the olivines are often rimmed by perovskite and opaque oxide (magnetite ?) although not phlogopite.

The matrix is dominated by calcite, phlogopite and poikilitically enclosed opaque oxides (Plate 2.11) and hydrogrossular (?) (Plate 2.14a). The carbonate and silicate fractions are separate and may indicate liquid immiscibility. The pale brown phlogopite is reversely pleochroic and large (up to 0.5 mm) grains poikilitically enclose the small opaques and hydrogrossular. The larger opaques may occur as subhedral to euhedral crystals up to 0.05mm size, often skeletal or showing 'atoll' texture (Plate 2.12). In other areas the opaque oxide is very fine grained and shows a weak radiating acicular texture (Plate 2.13). The hydrogrossular is a major groundmass phase occurring sporadically mainly as dense aggregates in the silicate areas but sometimes marginally in calcite. The hexagonal outline and probably isotropic character are very similar to hydrogrossular identified in the carbonate dykes at Premier Mine (J.B. Dawson, pers. comm). These tiny (0.02 mm) equant

crystals are typically hollow and reflected light observation reveals a faint zoning (Plate 2.14b).

The carbonate is mainly calcite occurring as large irregular grains crystallised between the silicate minerals. Staining suggests the presence of a small amount of dolomite. Colourless (bleached?) inclusion free phlogopite is often intergrown with the calcite, but is optically continuous with the pale brown poikilitic phlogopite.

Phlogopite is more abundant in this rock than is apparent at first, and the mineralogical classification would probably be a phlogopite-calcite kimberlite. The mineral paragenesis is:



#### 4. Phase Chemistry

The analyses and structural formulae of the kimberlites, olivines, phlogopites and other minerals are present in Tables 2.1, 2.2 and 2.3.

Olivine: Olivine compositions show a considerable variation between the three specimens analysed. Within the two samples NL379 and NL416, there is also a noticeable spread in composition despite analysing only euhedral phenocrysts.

The early dyke NL280 only contains xenocrysts of fresh olivine (the smaller phenocrysts are all serpentinised). Surprisingly these are the most iron rich of all the olivines analysed ( $F_{O_{86}}$ ). Each of the xeno-



TABLE 2.1: Microprobe Analyses of Olivine in Kimberlite Dykes

	NL380 (early)		NL381 (intermediate)				NL416 (late)		
SiO <sub>2</sub>	40.51	40.64	40.13	40.80	40.65	40.13	41.26	40.91	40.08
FeO	13.02	13.11	13.79	10.62	11.89	12.30	8.50	11.04	12.86
MnO	-	0.16	-	-	-	-	0.12	-	-
MgO	46.51	46.76	46.08	48.50	47.56	46.54	50.39	48.17	46.96
CaO	-	-	-	0.02	0.10	0.09	0.08	0.13	0.10
NiO	0.24	0.17	0.18	0.36	0.38	0.35	0.27	0.31	0.29
Total	100.28	100.83	100.18	100.30	100.58	99.41	100.71	100.56	100.29
Si	1.00	1.00	1.00	1.00	1.00	1.00	1.00	1.00	0.99
Fe	0.27	0.27	0.29	0.22	0.25	0.26	0.17	0.23	0.27
Mn	-	0.00	-	-	-	-	0.00	-	-
Mg	1.72	1.72	1.71	1.77	1.74	1.73	1.81	1.75	1.73
Ca	-	-	-	0.00	0.00	0.00	0.00	0.00	0.00
Ni	0.01	0.00	0.00	0.01	0.01	0.01	0.01	0.01	0.01
Total	3.00	2.99	3.00	3.00	3.00	3.00	2.99	2.99	3.00
%FO	86.4	86.4	85.6	89.0	87.7	87.1	91.3	88.6	86.7

Analyses in specimen NL381 made at Sheffield University. Other analyses made at Cambridge University

TABLE 2.2: Microprobe Analysis of Phlogopite in Kimberlite Dykes

	NL380 (early)				NL381 (intermediate)						
	Type I		Type II		Type II		Type II				
	Core	Rim	Core*	Rim*	(Normal pleochroism)	(Reversely pleochroic)	(Reversely pleochroic)	(Reversely pleochroic)			
SiO <sub>2</sub>	37.72	38.63	37.02	38.26	39.90	39.04	39.32	38.30	39.78	40.00	38.24
TiO <sub>2</sub>	2.50	3.04	2.47	3.03	2.52	2.12	2.69	2.54	1.20	3.27	2.64
Al <sub>2</sub> O <sub>3</sub>	15.64	13.89	14.69	12.82	11.80	12.32	12.56	10.89	10.92	9.28	8.73
Cr <sub>2</sub> O <sub>3</sub>	0.03	0.02	-	-	0.19	0.10	0.09	0.01	0.02	0.02	0.00
FeO	16.98	7.02	17.13	8.22	6.67	6.89	6.87	4.94	6.69	8.31	9.01
MnO	-	-	0.22	-	-	-	-	-	-	-	-
NiO	0.03	0.02	-	-	0.06	0.00	0.00	0.02	0.05	0.02	0.02
MgO	12.43	22.03	12.90	21.07	24.10	24.77	23.10	25.93	25.56	24.02	23.88
CaO	-	-	0.12	0.13	-	-	-	-	-	-	-
Na <sub>2</sub> O	0.05	0.00	-	-	0.00	0.00	0.00	0.11	0.16	0.38	0.29
K <sub>2</sub> O	9.69	9.58	9.57	9.67	8.89	7.94	9.21	9.80	10.02	9.95	10.09
Total	95.07	94.23	94.39	93.20	94.13	93.18	93.84	92.54	94.40	92.25	92.90
Si	5.69	5.62	5.65	5.66	5.78	5.69	5.73	5.66	5.80	5.84	5.77
Ti	0.28	0.33	0.28	0.34	0.28	0.23	0.29	0.28	0.13	0.36	0.30
Al	2.78	2.38	2.69	2.24	2.01	2.12	2.16	1.90	1.88	1.60	1.55
Cr	0.00	0.00	-	-	0.02	0.01	0.01	0.00	0.00	0.00	0.00
Fe	2.14	0.85	2.19	1.02	0.81	0.84	0.84	0.61	0.82	1.01	1.14
Mn	-	-	0.03	-	-	-	-	-	-	-	-
Ni	0.00	0.00	-	-	0.00	0.00	0.00	0.00	0.01	0.00	0.00
Mg	2.80	4.78	2.93	4.65	5.20	5.38	5.02	5.71	5.55	5.22	5.38
Ca	-	-	0.02	0.02	-	-	-	-	-	-	-
Na	0.01	0.00	-	-	0.00	0.00	0.00	0.03	0.05	0.11	0.09
K	1.86	1.78	1.86	1.82	1.64	1.48	1.71	1.85	1.86	1.85	1.94
Total	15.56	15.74	15.65	15.75	15.75	15.75	15.76	16.04	16.10	15.99	16.17
8-Al-Si	-0.469	-0.001	-0.339	+0.106	+0.207	+0.192	+0.117	+0.441	+0.328	+0.569	+0.675
Mg/(Mg+Fe)	0.566	0.848	0.573	0.820	0.866	0.865	0.857	0.903	0.872	0.837	0.825
Na <sub>2</sub> O/(Na <sub>2</sub> O+K <sub>2</sub> O)	0.005	-	-	-	-	-	-	0.011	0.016	0.035	0.028

Analyses marked \* made at Cambridge University. Other Analyses made at Sheffield University

**TABLE 2.3: Microprobe Analyses of Chromite and Clinopyroxene in Kimberlite Dykes**

	NL380 SP	NL381 CP
SiO <sub>2</sub>	0.00	52.05
TiO <sub>2</sub>	0.05	1.78
Al <sub>2</sub> O <sub>3</sub>	30.98	0.58
Cr <sub>2</sub> O <sub>3</sub>	40.23	0.00
Fe <sub>2</sub> O <sub>3</sub>	0.00	-
FeO	13.04	6.61
MnO	-	0.24
MgO	15.37	15.35
CaO	-	22.84
Na <sub>2</sub> O	-	1.70
NiO	0.06	0.00
<b>Total</b>	<b>99.73</b>	<b>101.15</b>
Si	0.00	1.92
Ti	0.00	0.05
Al	1.07	0.03
Cr <sub>3+</sub>	0.93	0.00
Fe <sup>3+</sup>	0.00	-
Fe <sup>2+</sup>	0.32	0.20
Mn	-	0.01
Mg	0.67	0.85
Ca	-	0.90
Na	-	0.12
Ni	0.00	0.00
<b>Total</b>	<b>2.99</b>	<b>4.08</b>
Mg/(Mg+Fe)	0.677	0.806
Ca/(Ca+Mg)		0.517
Cr/(Cr+Al)	0.466	
Ca%		46.3
Mg%		43.3
Fe%		10.5

Analyses made at Sheffield University

crysts analysed show remarkably similar compositions.

The olivines from the intermediate (NL381) and late dykes (NL416) show progressively more magnesian compositions with some overlap at  $FO_{87}$  but ranging to  $FO_{91}$ . The morphology precludes derivation of this olivine from ultramafic xenoliths but the compositions are less magnesian anyway.

Phlogopite: In specimen NL380 the cores of petrographically described type I micas conform to the chemical definition of Smith et al. (1978).  $Mg/(Mg+Fe) = 0.57$  and  $Al_2O_3 > 14$  wt.%.  $Na_2O$  was not detected in one grain, but Dawson (pers. comm.) has suggested that the high  $Na_2O/(Na_2O + K_2O)$  ratio may not be significant. Importantly no  $Fe^{3+}$  is required to fill the tetrahedral site (8-Al-Si is negative).

The rims of these grains are, in contrast much more magnesian ( $Mg/(Mg+Fe) = 0.82-0.85$ ),  $Al_2O_3 < 14$  wt.% and some  $Fe^{3+}$  may be required to fill the tetrahedral site for one rim composition (8-Al-Si is positive). These rim compositions are similar to the type II groundmass micas in the same rock. Type II mica (Smith et al. op. cit.) has  $Mg/(Mg+Fe) = 0.86$  and slightly lower  $Al_2O_3$  wt.% implying the necessity for  $Fe^{3+}$  in the tetrahedral sites for all these grains (8-Al-Si = 0.1-0.2). The red-brown reversely pleochroic rims to these type II micas could not be analysed but similar phlogopite in the intermediate dyke NL381 is notable for the much higher  $Fe^{3+}$  required (8-Al-Si = 0.3-0.7) and is nearly comparable to compositions for tetraferriphlogopites discussed by Smith et al. (op.cit.).  $Mg/(Mg+Fe)$  varies from 0.82 to 0.90, possibly reflecting local microscopic variations in the bulk Mg/Fe ratio, possibly resulting from coprecipitation of Fe-oxide due to increased  $fO_2$ .

It was not possible to analyse the phlogopite of the two late dykes (NL379 and NL416), but their petrographic appearance suggests they may be similar in composition to the mica of NL381.

When attempting to make comparisons with earlier published data, comparison was attempted with analyses published by Allsopp et al. (1979) who have formulated a chemical discrimination plot to differentiate type I and type II micas, in connection with anomalous isotope ages obtained from some kimberlites (see Chapter 4). These new data from Letseng are plotted in Figure 2.1 and compared to the points plotted by Allsopp et al. (op.cit.). It is apparent that the micas from NL380 do show some conformity to their grouping of type II micas. However, it was not possible to plot some other analyses because Na and/or Cr (elements used in the construction of the plot) were not detected during analysis. This plot is particularly susceptible to serious error at low  $\text{Cr}_2\text{O}_3$  concentrations, and I do not believe these discrimination indices to be either effective or necessary.

Chromite: The perovskite-mantled chromite in the early dyke NL380 is aluminous ( $\text{Cr}/(\text{Cr}+\text{Al}) = 0.466$ ) compared to chromite in peridotite (see Chapter 7). However, the spinel colour in different grains in this rock varies from red-brown to pale brown and suggests a range in composition from Cr-rich to Al-rich similar to the trend described by Haggerty (1975) and Pasteris (1979). The extension of this trend is described by these authors as towards Fe-enrichment. This feature is illustrated by the opaque (magnetite) mantles described above.

Diopside: The groundmass clinopyroxene is a high Ca diopside ( $\text{Ca}/(\text{Ca}+\text{Mg}) = 0.517$ ), it plots close to the diopside-hedenbergite join in the pyroxene quadrilateral, showing very little solid solution towards enstatite. In this system it is striking that it plots at the low temperature extension of the trend displayed by sub-calcic diopside megacrysts (see Chapter 5, Figure 5.3a). Like the lower temperature sub-calcic diopside megacrysts it requires some  $\text{Fe}^{3+}$  to balance Na in acmite. The low Al content indicates low jadeitic content, suggesting low pressure during crystallisation.

Dawson et al. (1977) have analysed groundmass diopside from various kimberlites. These diopsides all plot close to the diopside-hedenbergite join, have low Al, Cr and Na and have  $Na > Al^{IV} + Cr$  (implying presence of  $Fe^{3+}$ ). The only significant difference observed in this Letseng diopside is that it is more Fe rich, although Na and hence  $Fe^{3+}$ , is also appreciably higher.

## 6. Discussion

The earliest kimberlite to crystallise (NL380) has precipitated early crystals of iron rich olivine and phlogopite. This probably occurred prior to emplacement and Smith et al. (1978) have suggested that Fe rich type I micas may have crystallised from a carbonatitic precursor to the kimberlite. The Fe rich olivine in this early dyke may also suggest a more Fe-rich liquid but the reaction of the type I micas with the more magnesian liquid crystallising the type II micas in the groundmass implies a xenocrystic origin for these Fe rich components. As crystallisation proceeded, possibly at relatively high level, the  $f_{O_2}$  increased markedly so that early crystallised cores of aluminous chromite were mantled by magnetite and groundmass type II micas were mantled by  $Fe^{3+}$  enriched phlogopite. This trend towards iron enrichment is exemplified by the segregation of green mica and magnetite. The final stages of crystallisation involved the volatile portions and both calcite and serpentine were precipitated. In addition some olivine and the margins of some phlogopite phenocrysts suffered serpentinisation.

The early stages of diatreme formation are only represented by inclusions in the later tuffisitic kimberlite breccias of the main fluidisation stage. These kimberlite inclusions indicate an early phase of the diatreme facies having a different mineralogy reflecting different emplacement conditions. The presence of monticellite and melilite in these

rocks suggests crystallisation at low pressure (but variable temperature) (Janse, 1971) in a system with only H<sub>2</sub>O as the volatile phase. Yoder (1975) has shown that in the presence of high  $f_{\text{CO}_2}$  the monticellite field is condensed to even lower pressure (< 100 bars) at temperatures of < 685°C.

The crystallisation of the diatreme facies tuffisitic kimberlite breccias may be considered together with that of the intermediate dyke NL381. This rock has some of the features of the hypabyssal facies but the very low CO<sub>2</sub> content attests to its degassed nature which is characteristic of the diatreme facies. Both have crystallised abundant diopside and both have  $P_{\text{H}_2\text{O}} \gg P_{\text{CO}_2}$ : Serpentine is abundant in both rocks and calcite rare. Dawson et al. (1977) suggest diopside-bearing kimberlites have crystallised at a late stage (after emplacement) at low pressure and temperature (T = 400–500°C) and  $P_{\text{H}_2\text{O}}/P_{\text{CO}_2} > 20$ . Early crystallised perovskite sometimes adheres to olivine phenocrysts but perovskite has also crystallised after magnetite and is poikilitically enclosed in Fe<sup>3+</sup> enriched phlogopite. These diatreme facies rocks represent the fluidisation phase of kimberlite intrusion in which breakthrough to the surface involves rapid outgassing of the volatile phase, and consequent drop in pressure and temperature. The fine grain size in the groundmass of these rocks owes much to this rapid quenching. Diopside microlites occurring in autoliths (segregations) have nucleated on mineral grains or rock fragments some of which may have promoted crystallisation by being relatively cool. I infer that the greater abundance of such segregations in the autolithic kimberlite of the Main pipe, and the Satellite pipe, results from a slightly slower intrusion rate which allowed almost complete outgassing of CO<sub>2</sub> but also promoted crystallisation. The later garnetiferous kimberlite, I interpret as having a much more rapid emplacement history thus preventing complete outgassing and quenching the kimberlite in the early stages of autolith formation.

The late kimberlite dykes are enriched in carbonate component possibly as a result of differentiation and/or liquid immiscibility (Dawson and Hawthorne, 1973; Clement, 1975; Mitchell, 1979). Early crystallised perovskite and opaque minerals adhere to olivine phenocrysts suggesting crystal cumulates but magnetite has crystallised later on the perovskite and in the silicate groundmass. The presence of a small amount of diopside in NL379 suggests a similar low temperature crystallisation to NL381 but in this rock  $P_{CO_2}$  is high and the diopside crystallisation may only have occurred at a very late stage in the serpentine after the removal of  $CO_2$  as calcite. The hydrogrossular in NL416 may have crystallised at about  $500^{\circ}C$  at low pressures as indicated by experimental studies (Deer et al., 1966).



Plate 2.1: Type I mica showing marginal alteration to type II mica. Matrix consists of type II mica, opaques, apatite, serpentine & calcite. Early kimberlite dyke NL380. (scale bar 0.2mm)

Plate 2.2: Groundmass type II mica, perovskite, opaques, apatite, serpentine & calcite. Early kimberlite dyke NL380. (scale bar 0.2mm)

Plate 2.3: Part of segregation containing green mica and opaques with minor serpentine and calcite. Early kimberlite dyke NL380. (scale bar 0.5mm)

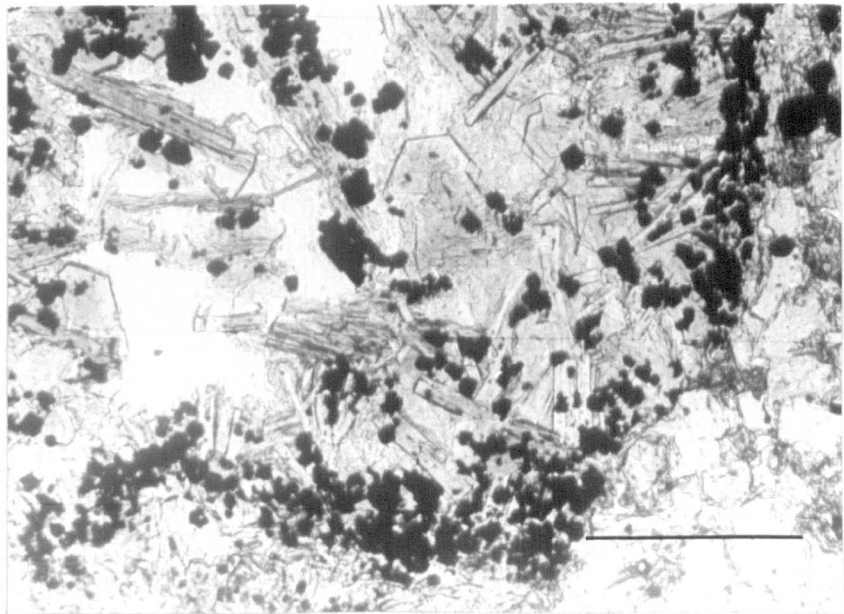
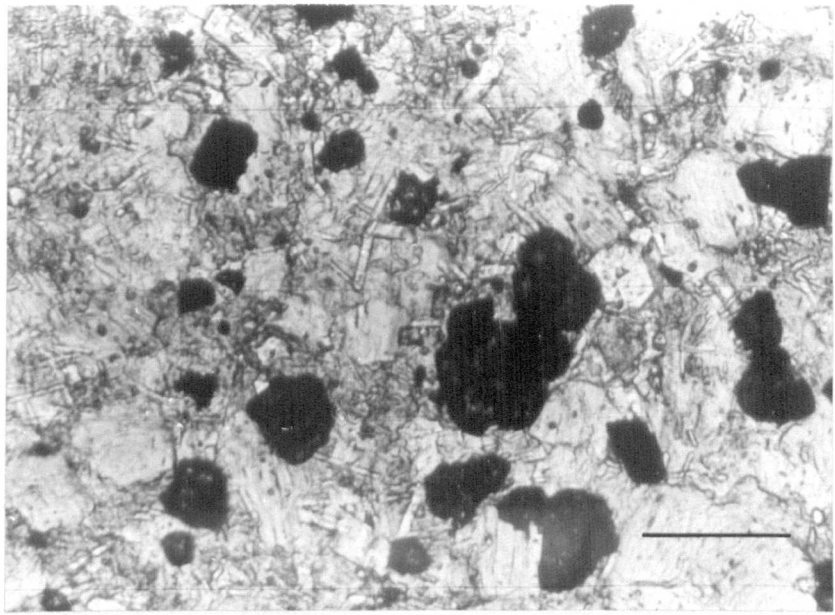
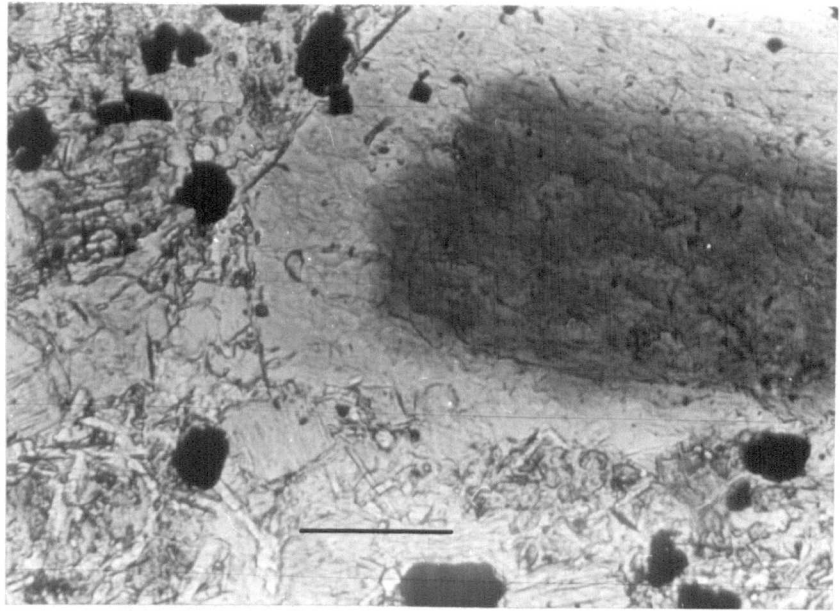


Plate 2.4:Perovskite-mantled spinel(?) viewed in reflected light.Early kimberlite dyke NL380.(scale bar 0.1mm)

Plate 2.5:Perovskite-mantled spinel(?) viewed in transmitted light.Intermediate dyke NL381.(scale bar 0.5mm)

Plate 2.6:Fan of acicular diopside in finely fibrous hydromica(?).Large colourless crystals are olivine and the non-fibrous grey groundmass is mica.High relief and black grains are perovskite and opaques respectively. Intermediate kimberlite dyke NL381.(scale bar 0.2mm)

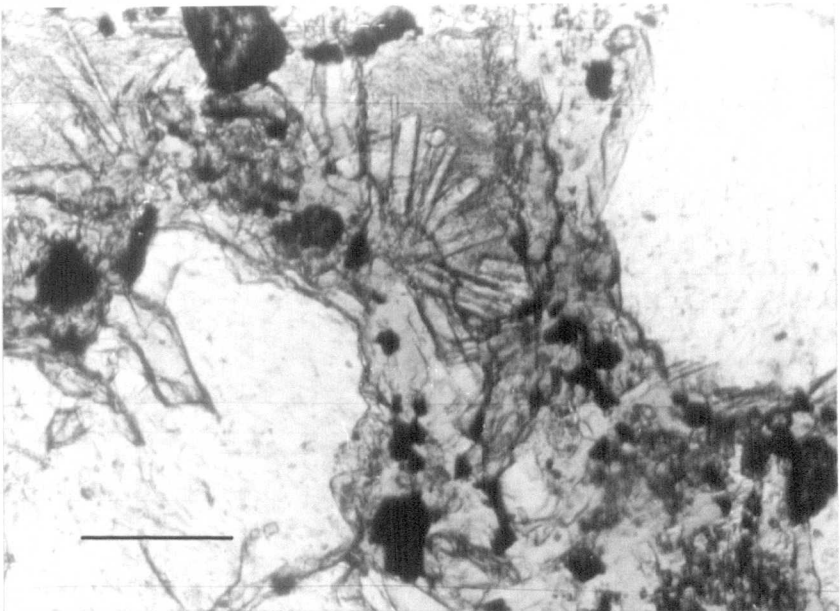
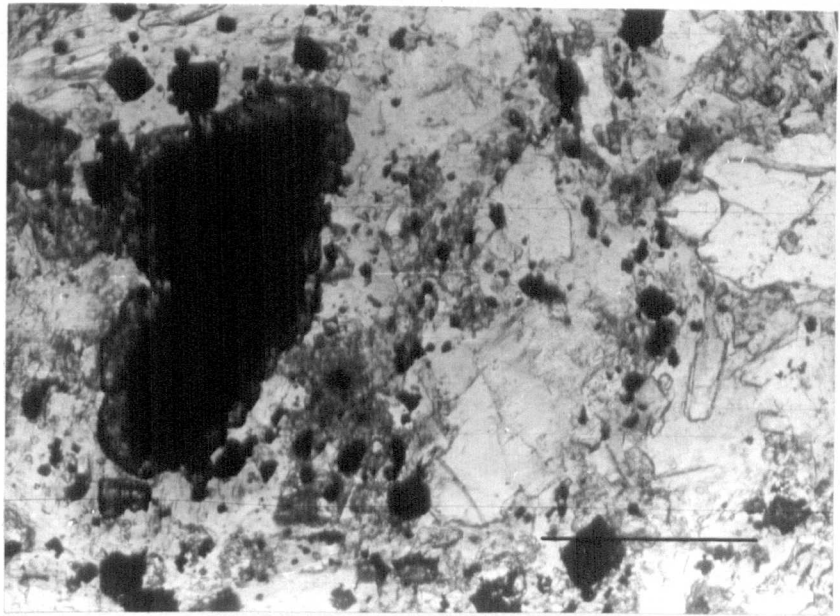
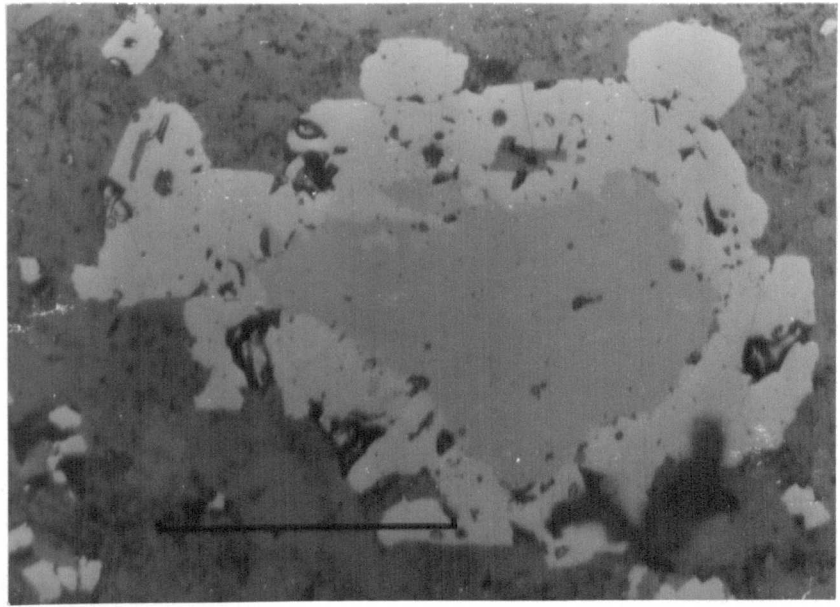


Plate 2.7: Reflected light photomicrograph showing faintly zoned perovskite (more reflective rims) and weak 'atoll' structure. Irregular shaped areas of slightly darker grey may be diopside. Intermediate dyke NL381. Barscale 0.1mm.

Plate 2.8: View of late kimberlite dyke showing the abundance of small unserpentinised euhedral olivine in a matrix of high relief calcite, serpentine, opaques and perovskite. NL379. Bar scale 2.0mm.

Plate 2.9: Rafts of calcite with fibrous calcite margins in serpentinous patches. Note that the margin of the olivine grain in the bottom left corner is mantled by altered mica. Late kimberlite dyke NL379. Bar scale 0.5mm.

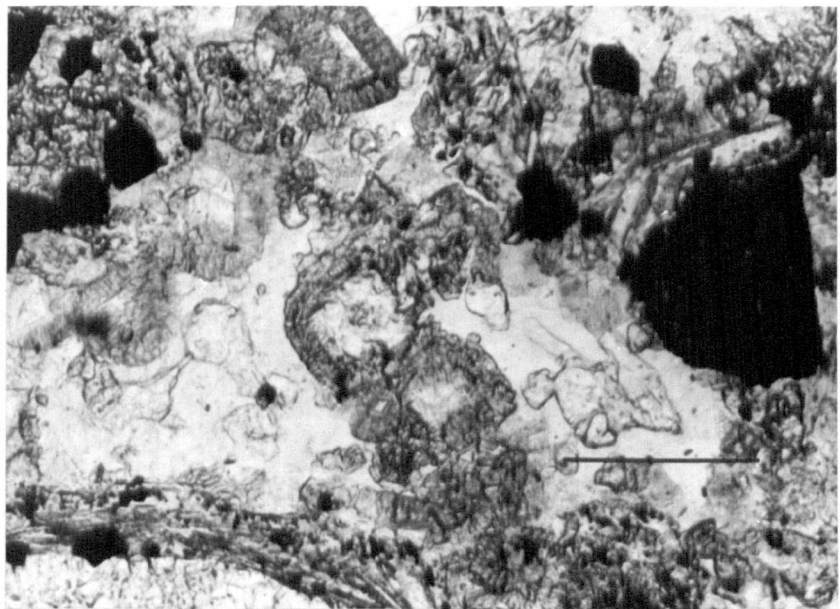
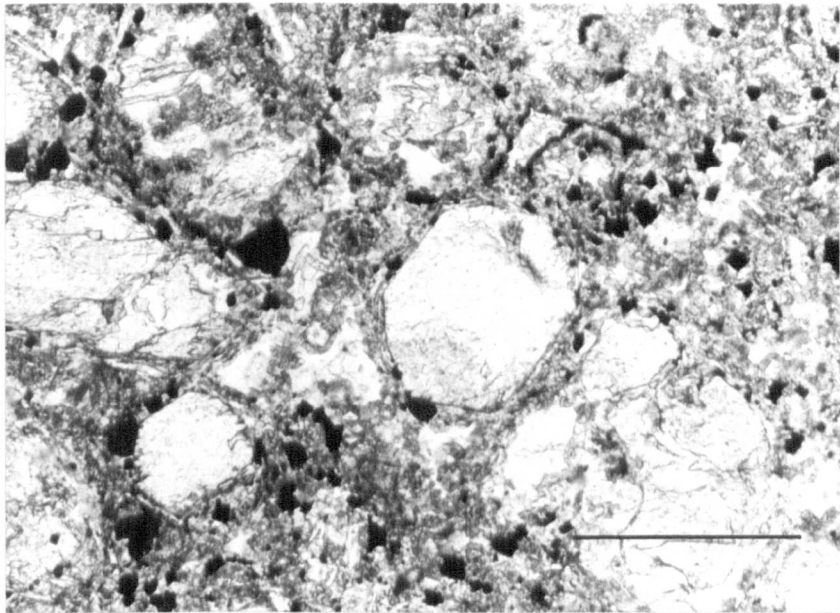
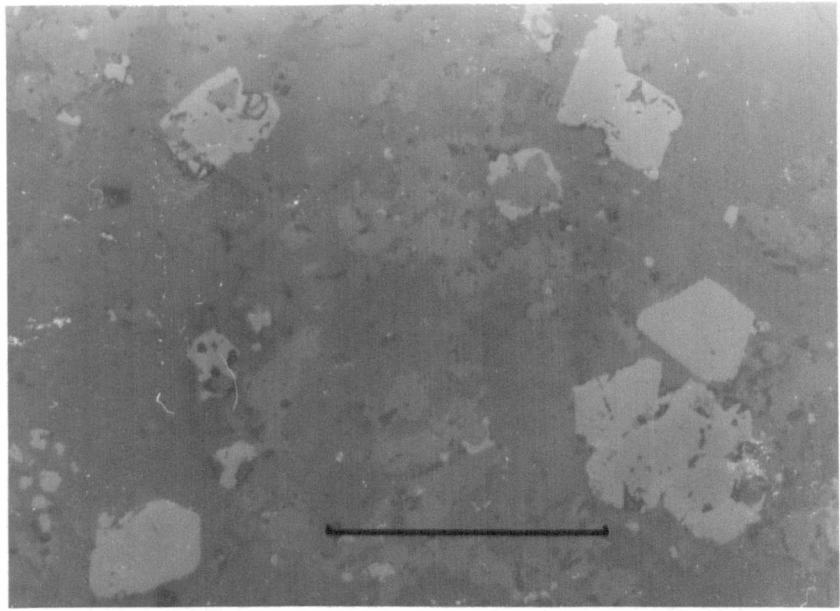


Plate 2.10: Reflected light photomicrograph of olivine grain (bottom right) rimmed by euhedral magnetite(?) and rounded perovskite. The perovskite shows a marginal 'atoll' of an opaque mineral where not in contact with the olivine. Late kimberlite dyke NL379. Bar scale 0.1mm.

Plate 2.11: Calcite (light grey area) interfingering with pale mica which in the dark areas poikilitically encloses perovskite and opaques. The large grain at bottom right is a partly serpentinised olivine. Late kimberlite dyke NL416. Bar scale 0.5mm.

Plate 2.12 Reflected light photomicrograph of weakly zoned opaque minerals with possibly perovskite cores. Some crystals are skeletal. Late kimberlite dyke NL416. Bar scale 0.05mm.

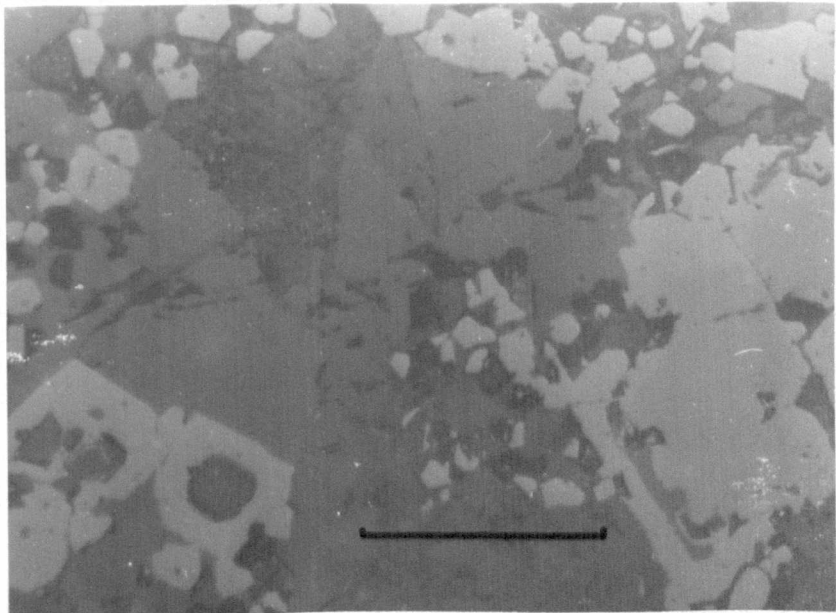
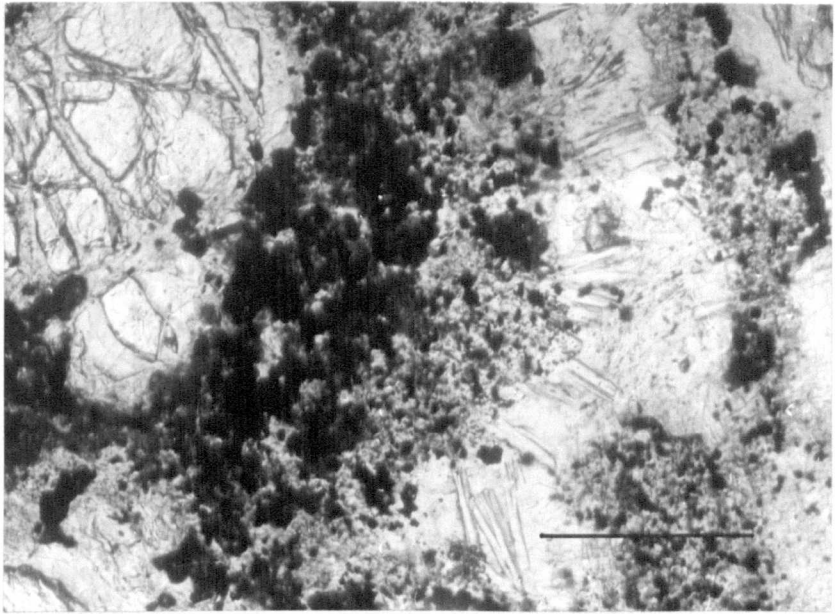
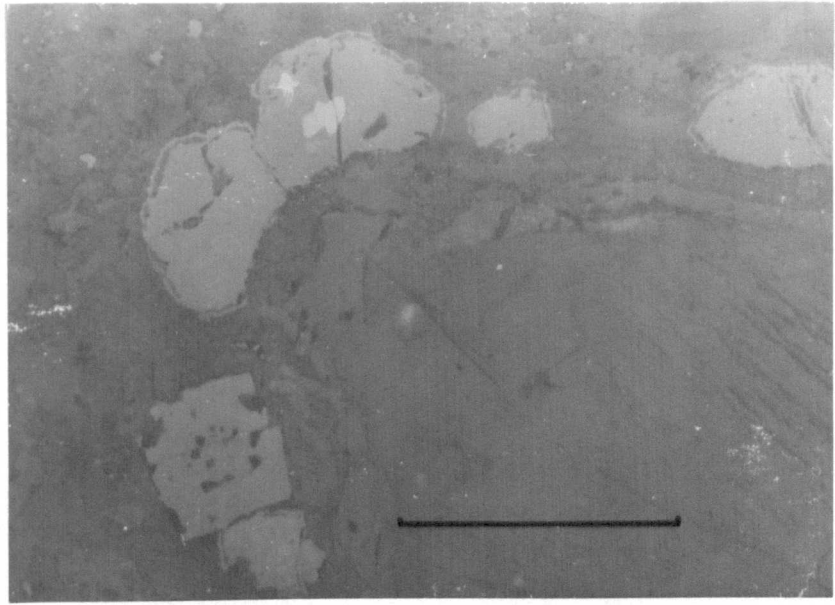




Plate 2.13: Very fine grained groundmass of acicular opaque minerals shown in reflected light. Weakly developed radiate structure. Late kimberlite dyke NL416. Bar scale 0.1mm

Plate 2.14a: Euhedral crystals of hydrogrossular(?) in a serpentine groundmass. Late kimberlite dyke NL416. Bar scale 0.1mm.

Plate 2.14b: Reflected light photomicrograph of the hydrogrossular in plate 2.14a showing central voids and weak zonation. Bar scale 0.1mm.

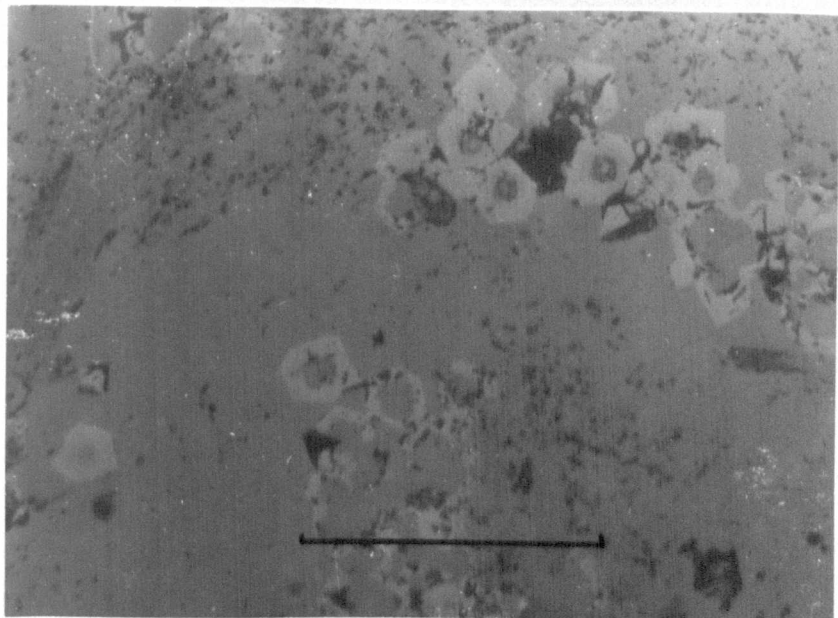
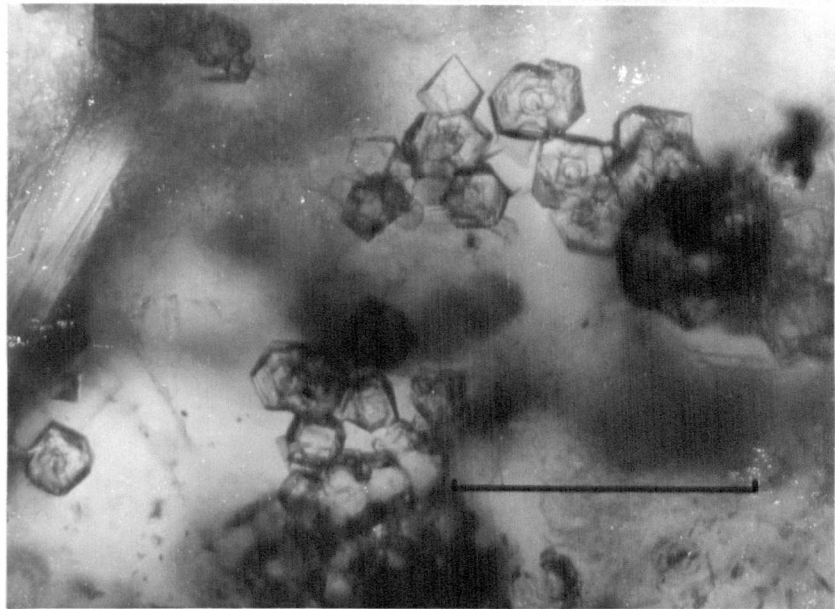
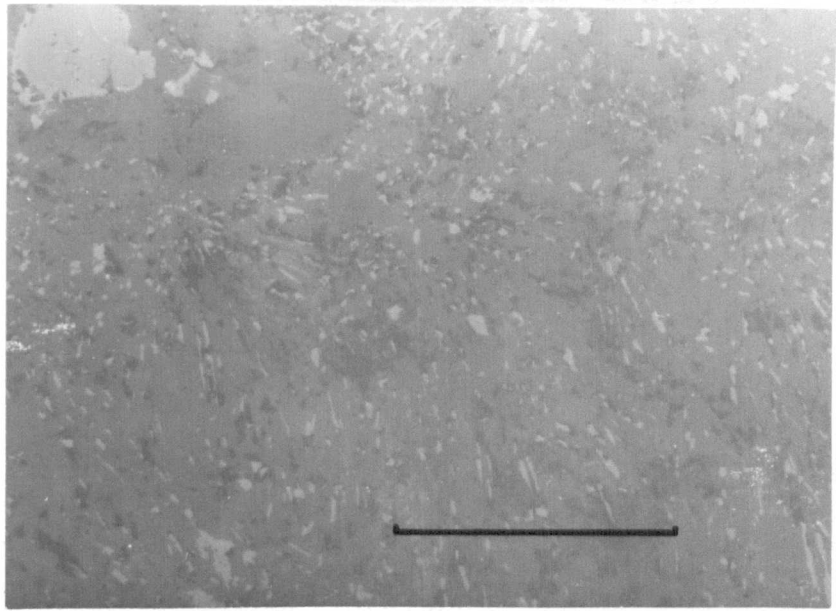
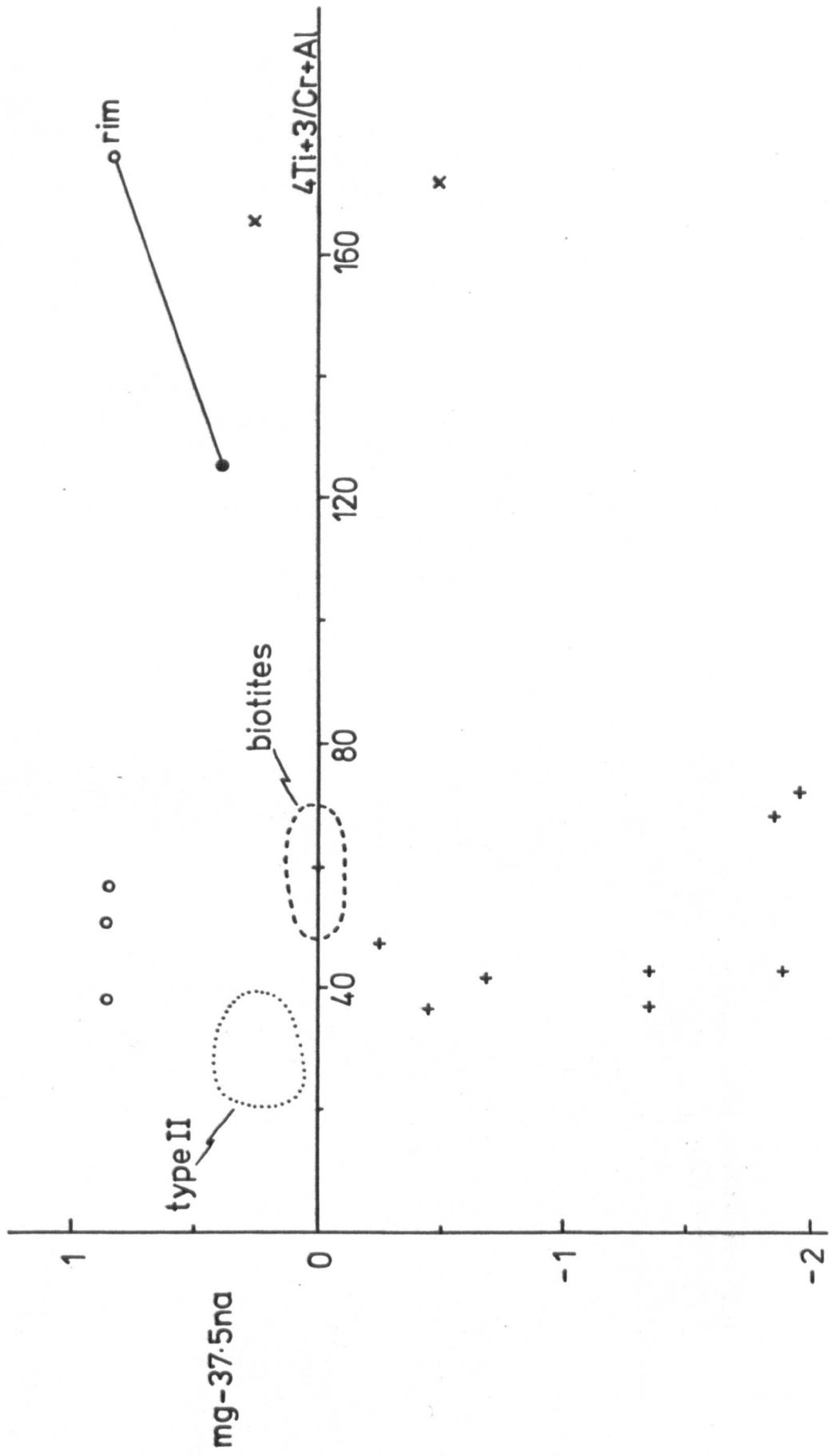


Figure 2.1: Chemical discrimination diagram for type I & II phlogopite from kimberlite (Allsopp et al 1979). Closed circle: type I mica this study, open circle: type II mica and rim to type I mica (connected to core by tie line) this study (early dyke NL380). Inclined crosses: type II mica this study (intermediate dyke NL381). Vertical crosses: type I mica Allsopp et al (1979), dotted field: type II mica Allsopp et al (1979).



## CHAPTER 3

### Bulk Rock Chemistry

To gain some insight into the geochemistry of these kimberlites, fifteen autoliths from the Main and Satellite pipes were analysed for major and trace element composition. The chemistry of autoliths is thought to more nearly reflect the chemistry of the kimberlite magma (Ferguson et al., 1973) being less contaminated by accidental inclusions than the highly altered and contaminated diatrema facies rock. In addition analyses of the four fresh dyke kimberlites described earlier are included.

#### Analytical Techniques

The autoliths were carefully selected for freshness and macroscopic similarity. They are distinct from the early generation kimberlite inclusions. Individual autoliths were removed from hand specimens using a dentist's drill and the xenocryst or xenolith nucleus removed before crushing by hand in an agate mortar. The dyke rocks were prepared by conventional techniques but care was taken to remove any visible xenolithic material. All the powdered samples were dried at 110°C before analysis.

FeO was determined by titration of a sample solution (prepared by dissolving the powder in 50% v/v H<sub>2</sub>SO<sub>4</sub> and 40% HF) against a standard potassium dichromate solution using a sodium diphenylamine sulphonate/orthophosphoric acid mix indicator.

Na<sub>2</sub>O was determined by atomic absorption spectrometry on a sample solution prepared by dissolving the powder in 40% HF and 60% H<sub>3</sub>PO<sub>4</sub> acid.

CO<sub>2</sub> was determined by conventional wet chemical analysis and total H<sub>2</sub>O was measured by the Penfield method.



**TABLE 3.1: Kimberlite Geochemistry - Comparison of XRF Analyses with Classical Wet Chemical Analyses**

Specimen	BD1072		BD1075B		BD1092	
	Classical	XRF	Classical	XRF	Classical	XRF
SiO <sub>2</sub>	27.00	27.08	24.99	25.56	36.27	36.42
TiO <sub>2</sub>	1.84	1.95	2.69	3.09	0.94	1.06
Al <sub>2</sub> O <sub>3</sub>	1.80	2.07	4.28	3.88	3.45	2.66
Fe <sub>2</sub> O <sub>3</sub>	5.29	9.07	7.12	10.08	6.60	9.28
FeO	3.89	-	3.01	-	2.92	-
MnO	0.18	0.21	0.24	0.27	0.28	0.30
MgO	28.91	28.86	24.76	25.16	25.24	25.32
CaO	13.03	13.05	15.63	15.50	7.32	7.13
Na <sub>2</sub> O	0.24	-	0.87	-	0.39	-
K <sub>2</sub> O	0.83	0.90	1.08	1.21	2.61	2.67
P <sub>2</sub> O <sub>5</sub>	2.22	1.93	1.30	1.31	0.42	0.99
CO <sub>2</sub>	7.90		5.87		4.44	
H <sub>2</sub> O <sup>+</sup>	6.01		6.47		7.15	
H <sub>2</sub> O <sup>-</sup>	0.66		1.30		1.69	
SO <sub>3</sub>		0.94		0.07		0.31
F			0.14			
Cr <sub>2</sub> O <sub>3</sub>			0.41			
O ≡ F			0.06			
L.O.I.		13.67		12.87		12.33
Total	99.60	99.73	100.10	99.00	99.72	98.47
Total Fe as Fe <sub>2</sub> O <sub>3</sub>	9.61		10.47		9.84	

TABLE 3.2: Kimberlite Geochemistry - Dykes

	NL380	NL381	NL379	NL416
SiO <sub>2</sub>	32.49	37.28	28.60	31.83
TiO <sub>2</sub>	2.85	2.72	2.44	2.05
Al <sub>2</sub> O <sub>3</sub>	4.24	3.61	2.31	2.61
Cr <sub>2</sub> O <sub>3</sub>	0.14	0.17	0.14	0.18
Fe <sub>2</sub> O <sub>3</sub>	7.56	6.83	5.11	6.01
FeO	4.73	4.85	5.11	3.92
MnO	0.21	0.20	0.15	0.17
MgO	22.56	28.75	24.76	28.89
CaO	10.29	7.32	14.23	9.60
Na <sub>2</sub> O <sub>3</sub>	0.31	0.24	0.30	0.10
K <sub>2</sub> O	1.92	2.05	1.07	1.42
P <sub>2</sub> O <sub>5</sub>	1.15	0.64	0.64	0.63
CO <sub>2</sub>	4.49	0.54	11.29	6.42
H <sub>2</sub> O <sup>±</sup>	5.61	4.58	3.32	6.39
SO <sub>3</sub>	0.18	0.07	0.20	0.08
Total	98.73	100.85	99.67	100.30
Mg/(Mg+Fe) %	.65	.71	.71	.74

TABLE 3.3: Kimberlite Geochemistry - Main Pipe Autoliths Kimberlite

	Autoliths							Fine Flow Kimberlite
	NL254	NL540a	NL540b	NL540d	NL540e	NL540f	NL540g	
SiO <sub>2</sub>	38.83	36.25	38.19	41.28	39.73	42.26	39.76	39.61
TiO <sub>2</sub>	2.85	2.39	2.89	2.25	2.59	2.42	2.76	1.24
Al <sub>2</sub> O <sub>3</sub>	7.58	2.94	4.55	5.95	4.81	6.52	4.92	6.61
Cr <sub>2</sub> O <sub>3</sub>	N.D.	0.26	N.D.	N.D.	0.18	N.D.	0.17	0.10
Fe <sub>2</sub> O <sub>3</sub>	6.93	8.75	8.17	7.34	8.50	5.95	8.61	5.95
FeO	3.65	2.19	3.45	4.15	3.44	3.97	3.70	4.22
MnO	0.16	0.18	0.21	0.18	0.16	0.16	0.17	0.14
MgO	21.87	29.42	23.27	18.09	21.69	20.10	21.71	23.16
CaO	8.84	6.70	7.29	10.90	10.55	9.41	8.69	8.45
Na <sub>2</sub> O	0.43	0.04	0.29	1.67	0.45	0.75	0.48	0.27
K <sub>2</sub> O	1.81	1.18	1.90	1.67	1.12	2.51	1.47	1.35
P <sub>2</sub> O <sub>5</sub>	0.72	0.68	0.75	0.57	0.78	0.35	0.76	0.37
CO <sub>2</sub>	0.26	0.32	1.28	0.67	1.25	0.79	0.60	2.61
H <sub>2</sub> O <sup>±</sup>	5.72	8.78	6.47	5.08	5.88	3.97	4.32	6.41
SO <sub>3</sub>	0.08	0.17	0.12	0.12	0.12	0.13	0.13	0.07
Total	99.73	100.27	98.83	99.92	101.25	99.29	98.25	100.56
Mg/(Mg+Fe)	.67	.73	.67	.61	.65	.67	.64	.71



TABLE 3.4: Kimberlite Geochemistry - Satellite Pipe

	Autoliths						
	NL382	NL386	NL387	NL388	NL389	NL393	NL397
SiO <sub>2</sub>	36.32	37.61	37.89	37.00	36.20	37.10	36.28
TiO <sub>2</sub>	3.56	3.38	3.26	3.41	3.49	3.68	3.53
Al <sub>2</sub> O <sub>3</sub>	7.92	6.95	7.79	7.58	5.99	6.24	6.13
Cr <sub>2</sub> O <sub>3</sub>	N.D.	N.D.	N.D.	N.D.	N.D.	N.D.	N.D.
Fe <sub>2</sub> O <sub>3</sub>	6.74	8.74	7.60	7.91	8.71	9.11	8.44
FeO	3.66	3.57	3.86	4.00	3.27	3.40	3.43
MnO	0.14	0.23	0.27	0.15	0.19	0.22	0.16
MgO	21.32	20.12	21.22	22.69	20.45	19.08	20.12
CaO	9.31	10.41	9.53	8.10	11.08	10.39	11.45
Na <sub>2</sub> O	0.38	0.56	0.49	0.32	0.29	0.33	0.39
K <sub>2</sub> O	1.54	0.81	1.35	1.23	1.51	1.62	1.18
P <sub>2</sub> O <sub>5</sub>	1.02	0.81	0.82	0.80	0.85	0.80	0.82
CO <sub>2</sub>	0.63	1.26	0.62	0.34	2.15	0.70	2.14
H <sub>2</sub> O <sup>+</sup>	7.05	6.89	6.20	7.10	5.28	6.11	6.21
SO <sub>3</sub>	0.07	0.06	0.06	0.11	0.16	0.16	0.15
Total	99.66	101.40	100.96	100.74	99.62	98.94	100.43
Mg/ (Mg+Fe) %	.69	.64	.67	.66	.63	.60	.63

The remaining major elements and total Fe as Fe<sub>2</sub>O<sub>3</sub> were determined by XRF in fused glass discs using a commercially available flux (Spectroflux 105) and NaNO<sub>3</sub> as an oxidising agent. Loss on ignition was measured for each sample and compared to the values of H<sub>2</sub>O + CO<sub>2</sub> measured independently. The procedure followed is that described by Norrish and Hutton (1969).

Cr<sub>2</sub>O<sub>3</sub> was determined by XRF together with the other trace elements (Ni, Co, Mn, V, Zn, Cu, Rb, Sr, Y, Zr) on pressed powder pellets.

Major element analyses for three kimberlites of similar composition, from the collection of J.B. Dawson, were made using the XRF technique and compared in Table 3.1 with analyses made elsewhere by classical wet chemical techniques. The analyses by the two techniques show very good agreement for SiO<sub>2</sub>, FeO, MgO, CaO and total alkalis, but show slight differences for Al<sub>2</sub>O<sub>3</sub>, TiO<sub>2</sub> and P<sub>2</sub>O<sub>5</sub>. These latter three oxides were probably the least accurately determined by the classical techniques (Dawson, pers. comm.) because of difficulties inherent in the method.

Major Element Chemistry

The autoliths from the Main Pipe (autolithic kimberlite) (Table 3.3) show a considerable range in composition: SiO<sub>2</sub> 36.25-42.26 wt.%; MgO 18.09-29.42 wt.%; CaO 6.70-10.90 wt.%; Na<sub>2</sub>O 0.04-1.67 wt.%; K<sub>2</sub>O 1.12-2.51 wt.%; P<sub>2</sub>O<sub>5</sub> 0.35-0.78 wt.%; CO<sub>2</sub> 0.26-2.61 wt.%. TiO<sub>2</sub> and Al<sub>2</sub>O<sub>3</sub> are roughly constant. The fine grained flow banded kimberlite (NL 370) described in Chapters 1 and 2 has a very similar chemistry apart from the low TiO<sub>2</sub>.

In contrast the autoliths from the Satellite Pipe (Table 3.4) show remarkably constant compositions: SiO<sub>2</sub> 36.20-37.89 wt.%; MgO 19.08-22.69 wt.%; CaO 8.10-11.45 wt.%; Na<sub>2</sub>O 0.29-0.56 wt.%; K<sub>2</sub>O 0.81-1.62 wt.%; P<sub>2</sub>O<sub>5</sub> 0.80-1.02 wt.%; CO<sub>2</sub> 0.34-2.15 wt.%. Other components are also constant.

In comparison with the Main Pipe autoliths these analyses show lower  $\text{SiO}_2$ ,  $\text{FeO}$ ,  $\text{Na}_2\text{O}$  and  $\text{K}_2\text{O}$  wt.% but higher  $\text{TiO}_2$ ,  $\text{Al}_2\text{O}_3$ ,  $\text{Fe}_2\text{O}_3$ ,  $\text{CO}_2$  and  $\text{H}_2\text{O}$  wt.%. Some of these differences may be seen in Figures 3.1, 3.3, 3.4 and 3.6. Figure 3.1 shows the wt.% of various oxides plotted against  $\text{MgO}$  wt.%. The plots for  $\text{SiO}_2$  and  $\text{TiO}_2$  demonstrate the clear separation of compositions for the two pipes although the other components show considerable overlap. Figure 3.3 is a conventional discrimination diagram for kimberlites and carbonatites (Dawson, 1967). Note the close grouping for the Satellite Pipe autoliths and the partial compositional separation from the Main Pipe autoliths. Note also that most of the autoliths together with the low  $\text{CO}_2$  dyke kimberlite (NL381) plot outside the main kimberlite field due to their low volatile content. Figure 3.4 shows the spread of the partial kimberlite compositions within plot of  $\text{MgO-FeO-Al}_2\text{O}_3$ . The variation is along the axis of the kimberlite field (Cornellissen and Verwoerd, 1975), and probably mainly reflects varying olivine content. Figure 3.5 shows the high  $\text{TiO}_2$  and  $\text{P}_2\text{O}_5$  character of the Satellite Pipe autoliths. The linear trend is similar to that of Kable et al. (1975) for Premier and Koffyfontein kimberlites, although at higher  $\text{TiO}_2$  wt.%.

The major element compositions of the dykes (Table 3.2) show considerable differences to the autolith compositions, probably reflecting abundant xenocrystic olivine and in the early and late dykes considerable amounts of carbonate. The low  $\text{CO}_2$  dyke (NL381) is closest in composition to the autoliths and may represent a devolatilised hypabyssal variety of the same magma. The highly micaceous early dyke and highly calcitic late dykes have chemistries which may reflect profoundly on the evolution of the parent kimberlite magma. Noticeable trends of  $\text{TiO}_2$ ,  $\text{Al}_2\text{O}_3$ ,  $\text{Fe}_2\text{O}_3$  and  $\text{P}_2\text{O}_5$  depletion are apparent between early and late intrusion and the carbonate component is considerably enriched in the late dyke NL379. These trends appear not to reflect on processes operating in the

TABLE 3.5: Kimberlite Geochemistry (from Gurney and Ebrahim, 1973)

	LLT1	LLT2	AD78	LLT3	LLT13	S4B	S3
SiO <sub>2</sub>	23.17	28.10	32.34	37.36	36.18	40.20	38.12
TiO <sub>2</sub>	2.77	2.11	2.66	1.19	0.92	1.70	1.88
Al <sub>2</sub> O <sub>3</sub>	2.88	5.26	3.04	5.84	5.41	7.30	6.34
Cr <sub>2</sub> O <sub>3</sub>	0.15	0.17	0.19	0.12	0.14	0.67	0.13
Fe <sub>2</sub> O <sub>3</sub>	8.35	8.57	6.72	4.46	3.87	5.26	4.70
FeO	2.16	2.52	4.72	4.46	4.44	4.88	5.24
MnO	0.26	0.19	0.18	0.14	0.12	0.16	0.15
MgO	12.56	16.46	26.80	21.53	21.22	19.86	22.77
CaO	21.69	14.95	9.37	6.95	7.86	8.75	8.46
Na <sub>2</sub> O	0.09	(0.004)	0.13	0.94	0.32	0.67	0.37
K <sub>2</sub> O	0.33	0.17	1.73	1.13	0.51	0.53	0.58
P <sub>2</sub> O <sub>5</sub>	1.15	0.88	0.70	0.38	0.23	0.40	0.43
CO <sub>2</sub>	13.79	7.93	2.49	3.61	3.78	0.37	0.35
H <sub>2</sub> O <sup>-</sup>	3.95	4.47	0.46	4.51	6.09	2.91	1.51
H <sub>2</sub> O <sup>+</sup>	7.03	8.23	7.26	6.88	7.98	6.66	7.96
S <sub>2</sub> <sup>-</sup>	0.02	0.04	0.33	0.27	0.25	0.09	0.22
Less O=S	0.01	0.02	0.16	0.13	0.12	0.04	0.11
Total	100.34	100.03	98.96	99.64	99.20	100.37	99.10
Mg/ (Mg/Fe)	.50	.56	.66	.66	.67	.62	.67

LLT1 Blow 151 Letseng la Terae  
 LLT2 Dyke 145 Letseng la Terae  
 AD78 Duke 158 Khubelu  
 LLT3 Autolithic kimberlite, Main Pipe, Letseng la Terae  
 LLT13 Garnetiferous Kimberlite, Main Pipe, Letseng la Terae  
 S4B Tuffisitic kimberlite breccia, Satellite Pipe, Letseng la Terae  
 S3 Tuffisitic kimberlite breccia, Satellite Pipe, Letseng la Terae

TABLE 3.6: Kimberlite Geochemistry (from Kruger, 1978)

	AVE NK6	AVE K6	AVE K5	AVE K4
SiO <sub>2</sub>	39.43	37.91	34.82	35.96
TiO <sub>2</sub>	1.33	1.36	1.82	1.68
Al <sub>2</sub> O <sub>3</sub>	4.95	4.49	3.22	3.67
Fe <sub>2</sub> O <sub>3</sub> <sup>T</sup>	10.75	10.44	10.34	10.00
MnO	0.17	0.16	0.17	0.17
MgO	27.10	27.47	29.48	29.54
CaO	7.94	7.69	9.12	8.07
Na <sub>2</sub> O	0.60	0.69	0.47	0.70
K <sub>2</sub> O	0.77	0.93	1.71	1.50
P <sub>2</sub> O <sub>5</sub>	0.37	0.38	0.59	0.54
CO <sub>2</sub>	2.52	2.77	6.69	7.28
H <sub>2</sub> O	4.54	6.48	2.32	1.64
} LOI				
Total	100.47	100.77	100.75	100.75
Mg/(Mg+Fe)	0.68	0.69	0.71	0.72
Sr	389	505	781	459
Rb	38	43	72	50
Y	14	11	14	11
Zr	132	117	183	156
Nb	54	59	107	93
Zn	69	62	74	71
Cu	51	46	56	47
Co	86	89	87	94
Ni	1347	1441	1352	1443
V	128	107	125	129
Cr	666	836	1008	982
Th	5	5	7	5
La	28	28	53	53
Ce	57	53	94	94
Nd	27	22	47	47
Rb/Sr	.098	.085	.092	.109
K/Rb	84.1	89.8	98.6	124.5
Ni/Co	15.7	16.2	15.5	15.4
Cr/Ni	0.49	0.58	0.75	0.68
Ca/Sr	145.9	108.8	83.5	125.7

TABLE 3.7: Kimberlite Geochemistry - Averages and Comparisons

	i				b	c
	Ave Autolith Main Pipe	Ave Autolith Satellite Pipe	Ave Lesotho Kimberlite	Ave Autolith Group 6		
SiO <sub>2</sub>	39.68	36.91	33.21	33.71	27.47	32.09
TiO <sub>2</sub>	2.61	3.47	1.97	2.27	3.07	3.14
Al <sub>2</sub> O <sub>3</sub>	5.35	6.94	4.45	4.09	3.15	3.32
Cr <sub>2</sub> O <sub>3</sub>	7.50	8.18	6.78	6.81	8.56	0.30
Fe <sub>2</sub> O <sub>3</sub>	3.81	3.60	3.43	2.04	3.60	11.51*
FeO	0.18	0.19	0.17	0.20	0.26	0.20
MnO	20.95	20.71	22.78	22.03	20.27	21.77
MgO	10.24	10.04	9.36	5.11	13.20	8.79
CaO	0.71	0.39	0.19	0.20	0.24	0.27
Na <sub>2</sub> O	1.53	1.32	0.79	0.67	1.60	1.15
K <sub>2</sub> O	0.74	0.85	0.65	0.46	1.21	0.73
P <sub>2</sub> O <sub>5</sub>	0.95	1.12	4.58	1.40	8.38	4.33
CO <sub>2</sub>	5.22	6.41	10.70	20.02	7.44	8.88
H <sub>2</sub> O <sup>±</sup>	0.16	0.11	0.20 (s <sup>2-</sup> )			
Total	99.63	100.24	99.51	99.28	98.66	96.48
Mg/(Mg+Fe)	0.66	0.65	0.71	0.73	0.64	0.62

(a) Gurney and Ebrahim (1973)  
 (b) Ferguson et al. (1973)  
 (c) Danchin et al. (1975)

\* Fe total expressed as Fe<sub>2</sub>O<sub>3</sub>

source region (see Chapter 4 for discussion of REE) or on contamination (see Chapter 4 for discussion of isotopic data) and are therefore inferred to reflect magma evolution as a result of crystallisation under changing physical conditions.

Tables 3.5 and 3.6 give analyses for Letseng kimberlites from Gurney and Ebrahim (1973) and Kruger (1978). These analyses are mainly for highly contaminated diatreme facies rocks whose chemistry, even after correction for contaminating components (Kruger, 1978) bear little relation to those of the present study. The three dyke rocks of Gurney and Ebrahim (1973) display some similarity to the dyke compositions presented here although the low  $K_2O$  and high  $H_2O^+$  contents of two dykes suggests these samples were considerably altered or weathered.

The Letseng autoliths show considerable differences to the average Lesotho kimberlite of Gurney and Ebrahim (1973) which partially reflect the freshness of the samples analysed (low  $H_2O$ ) but the higher  $TiO_2$ ,  $Al_2O_3$ ,  $Fe_2O_3$  and  $K_2O$  are probably real differences. Compared to the average kimberlite of Wedepohl and Muramatsu (1979), compiled from a wide variety of geographic localities, the Letseng kimberlites (Figure 3.2) show a normal spread about the mean apart from high  $TiO_2$ ,  $Fe^T$ ,  $MnO$ , and low  $Na_2O$ ,  $K_2O$ . In view of the almost complete absence of ilmenite from the Letseng kimberlites this  $TiO_2$  must be accommodated mainly in perovskite, the most important Ti-bearing mineral found at Letseng although the early micaceous kimberlite (NL380) may have 0.5-1.0%  $TiO_2$  in phlogopite. The late dykes (NL379, NL416) have considerably lower  $TiO_2$  but this cannot be entirely explained by the relative scarcity of phlogopite.

Compared to the autoliths of groups 6 and 8 (Ferguson et al., 1973) in Table 3.7, the Letseng autoliths are noticeably enriched in  $SiO_2$  and  $Al_2O_3$  but other significant variations include higher  $K_2O$  than group 6, lower  $CO_2$  than group 8, and significantly lower  $H_2O$  than group 6.

TABLE 3.8: Kimberlite Trace Elements (ppm)

	Dykes						Autoliths			
	NL370	NL379	NL380	NL381	NL416	NL540a	NL540e	NL540g		
Ni	1005	1076	852	1311	1292	1358	1239	1310		
Co	97	105	106	128	107	116	116	124		
Mn	1091	1314	1650	1451	1326	1472	1537	1464		
V	170	143	165	166	81	108	158	162		
Cr	717	989	962	1180	1256	1782	1231	1168		
Zn	74	75	90	82	64	73	81	82		
Cu	78	67	87	77	67	78	84	88		
Rb	43	64	95	110	63	56	56	66		
Sr	488	932	977	342	836	351	491	533		
Y	22	17	43	17	19	19	24	23		
Zr	143	232	353	208	220	211	245	260		
K	5603	4441	7969	8509	5894	4898	4649	6102		
K/Rb	130	67	86	94	95	89	83	88		
Ni/Co	10.4	10.2	8.0	10.2	12.1	11.7	10.7	10.6		
Cr/Ni	0.71	0.92	1.13	0.90	0.97	1.31	0.99	0.89		
Ca/Sr	123.8	109.3	75.3	153.0	82.1	136.4	153.6	116.5		
Zr/P	0.089	0.083	0.071	0.075	0.080	0.071	0.072	0.077		
Ti/Cr	10.4	14.7	17.8	13.8	9.8	8.0	12.6	14.2		
La/P		0.028	0.034		0.037	0.030				



Very similar differences to the average Lesotho autolith of Danchin et al. (1975) (Table 3.7) are also observed. The high  $\text{Al}_2\text{O}_3$  and  $\text{K}_2\text{O}$  in the Letseng autoliths may reflect higher modal phlogopite abundance, but the lower  $\text{CO}_2$  and  $\text{H}_2\text{O}$  may be either of genetic significance or merely reflect on the degree of alteration. The low  $\text{CO}_2$  and relatively high CaO suggests that the balance of CaO not accommodated in perovskite must have crystallised as diopside (or monticellite).

### Trace Elements

The trace element abundances in some of these samples have been measured (Table 3.8) and the values are compared with the average kimberlite values of Wedepohl and Muramatsu (1979) in Figure 3.2. The Letseng values cluster about their means, with the exception of a slight enrichment in Co and Zr.

The K/Rb ratios are very low compared to measured values in other kimberlites (Fesq et al., 1975a; Barrett and Berg, 1975; Barrett, 1975; Kramers, 1977) from southern Africa and more nearly match the ratios measured in diamonds (Fesq et al., 1957b) of 20-130. The Letseng kimberlites (Table 3.8 and Figure 3.5) have K/Rb values of <100 for both the autoliths and the dykes. The values of Kruger (1978) for Letseng diatreme facies rocks are not surprisingly slightly higher due to their altered and contaminated nature.

Other trace element ratios shown in Table 3.8 are similar to values given by Dawson (1967), Kable et al. (1975) and Fesq et al. (1975a).

Of importance in the understanding of these kimberlites is the linear relationship between Sr ppm and  $\text{CO}_2$  wt.%(Figure 3.7) which demonstrates the co-relationship of these two components. Figure 3.8 shows some element abundances normalised to mantle values (given in Hawkesworth et al., 1979). The generally coherent pattern of trace element abundances for these

different samples suggests a similar history, but the wide fluctuations of Sr concentrations is related to  $\text{CO}_2$  wt.% and is attributed to variations in the amount of devolatilisation of fundamentally similar rocks. It is not possible to estimate the expected Sr abundances but if carbonate does accumulate as a late differentiate of kimberlite (see for example Dawson and Hawthorne, 1973) or as an immiscible liquid (e.g. Clement, 1975), then these Sr abundances may reflect both enrichment or depletion of the carbonate component. If the early dyke NL380 is taken as a standard (i.e. assumed primitive carbonate abundance unaffected by devolatilisation or differentiation) then the plot (Figure 3.8) shows that the autoliths (representing the diatreme facies) are depleted in carbonate (low Sr) and the late dykes (NL379 and NL416) are enriched in carbonate (high Sr). The intermediate age dyke which has an inferred relation to the diatreme facies, is like the autoliths depleted in carbonate.

### Summary

- (1) Autoliths from the Main Pipe autolithic kimberlite show a range in composition, notably in  $\text{SiO}_2$ ,  $\text{MgO}$ ,  $\text{CaO}$ ,  $\text{Na}_2\text{O}$ ,  $\text{K}_2\text{O}$ ,  $\text{P}_2\text{O}_5$  and  $\text{CO}_2$ . In contrast the autoliths from the Satellite Pipe display a remarkably constant composition.
- (2) Satellite Pipe autoliths differ from Main Pipe autoliths. They display lower  $\text{SiO}_2$ ,  $\text{FeO}$ ,  $\text{Na}_2\text{O}$ , and  $\text{K}_2\text{O}$ , but higher  $\text{TiO}_2$ ,  $\text{Al}_2\text{O}_3$ ,  $\text{Fe}_2\text{O}_3$ ,  $\text{CO}_2$  and  $\text{H}_2\text{O}$ .
- (3) Kimberlite dyke compositions show major differences to those of the autoliths, probably largely reflecting abundant xenocrystic olivine and, in the early and late dykes, abundant carbonate.
- (4) Kimberlite dykes show trends of  $\text{TiO}_2$ ,  $\text{Al}_2\text{O}_3$ ,  $\text{Fe}_2\text{O}_3$  and  $\text{P}_2\text{O}_5$  depletion with younger age.

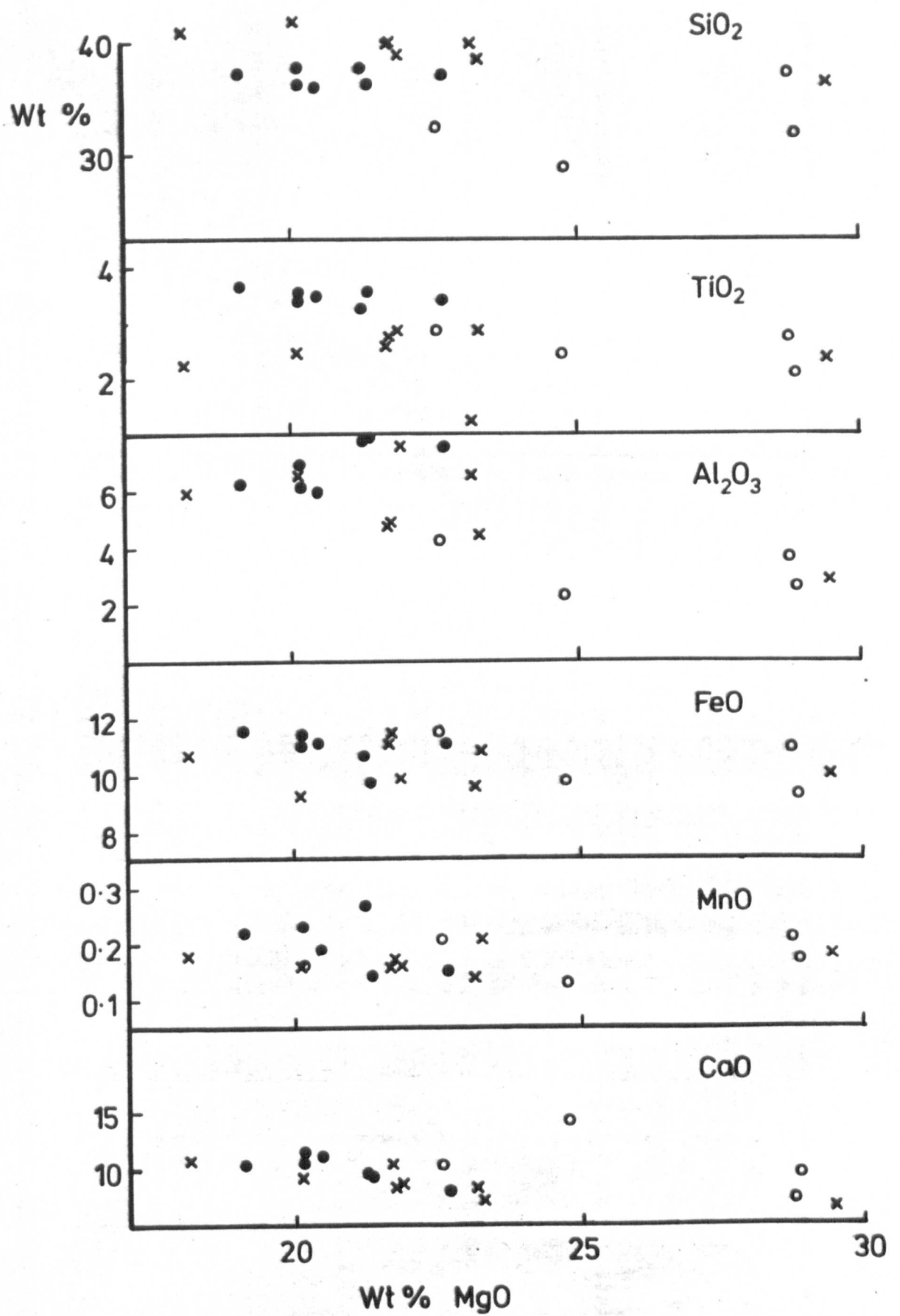
- (5) The intermediate age dyke may represent a devolatilised hypabyssal variety of the diatreme facies tuffisitic kimberlite breccia.
- (6) Compared to published analyses for Lesotho and other kimberlites, the Letseng samples are notably enriched in  $\text{TiO}_2$  and  $\text{Al}_2\text{O}_3$ .
- (7) Trace element abundances are normal for kimberlite.
- (8) K/Rb ratios are very low (<100) and match the ratios measured in diamonds.
- (9) Sr and  $\text{CO}_2$  show a linear correlation and an immiscible carbonate liquid is inferred from the lack of coherence between the Sr and other trace element abundances.
- (10) The autoliths are interpreted as depleted in carbonate component as a result of devolatilisation and the late dykes enriched in carbonate through differentiation.

Figure 3.1: Kimberlite major element variation diagram. Oxide  
Wt% v. MgO Wt%.

Solid circles: Satellite Pipe autoliths.

Inclined crosses: Main Pipe autoliths.

Open circles: Dykes.



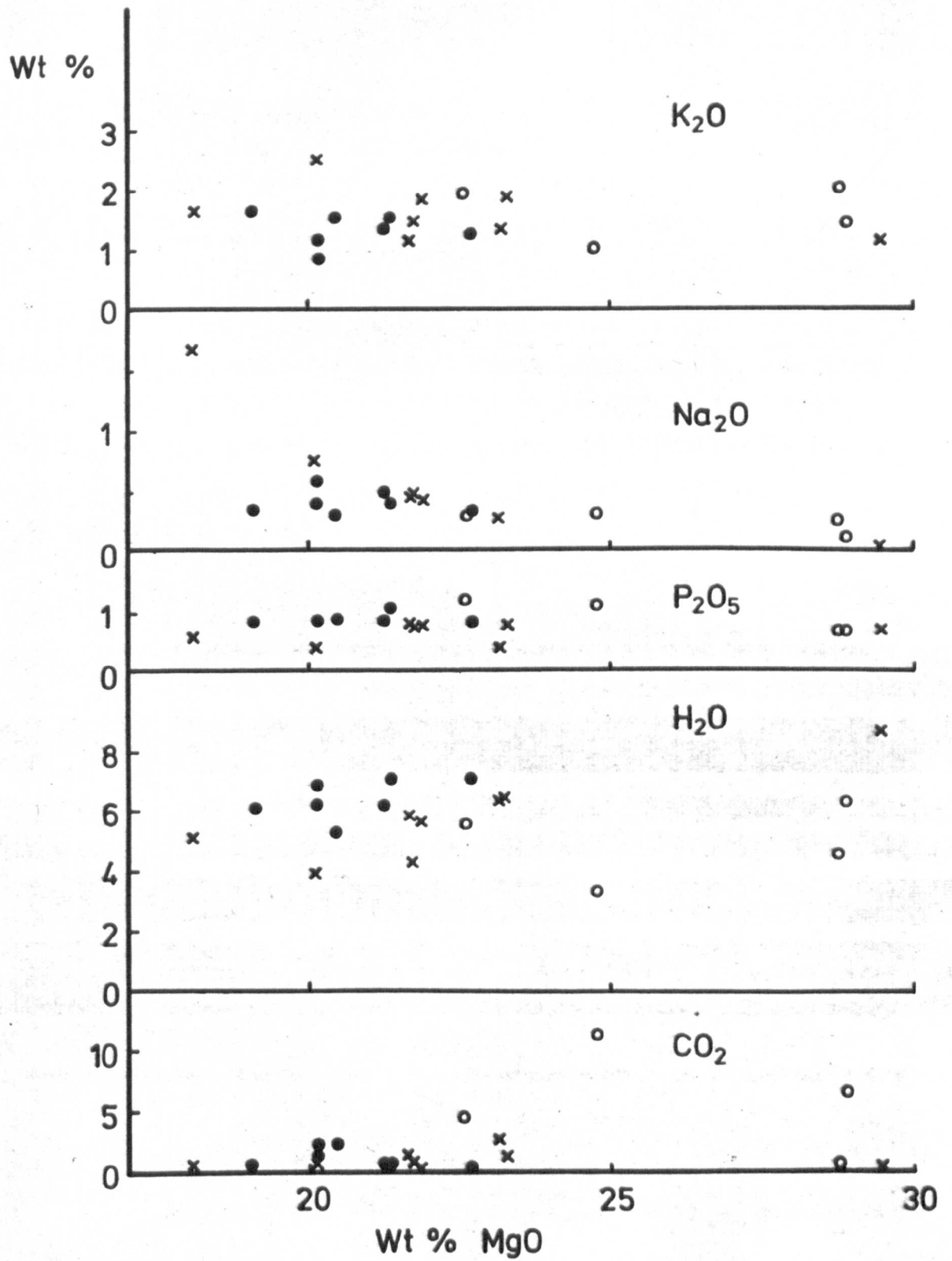
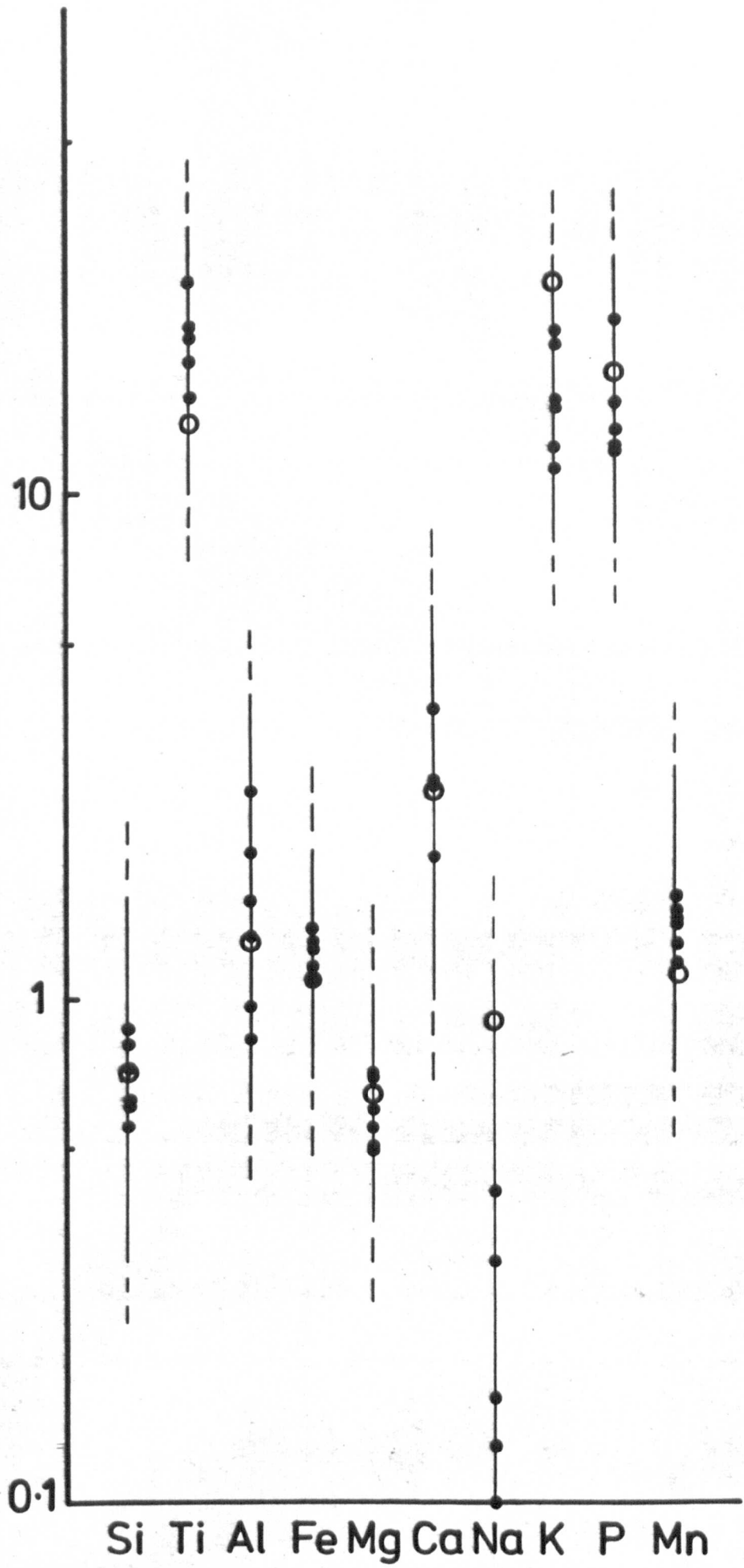


Figure 3.2: Kimberlite major and trace element abundances normalised to an ultramafic rock (Wedepohl 1975).  
Closed circles: Letseng kimberlite samples (autoliths and dykes).  
Large open circle: average kimberlite of Wedepohl & Marumatsu (1979).

KIMBERLITE / ULTRAMAFIC ROCK





KIMBERLITE/ULTRAMAFIC ROCK

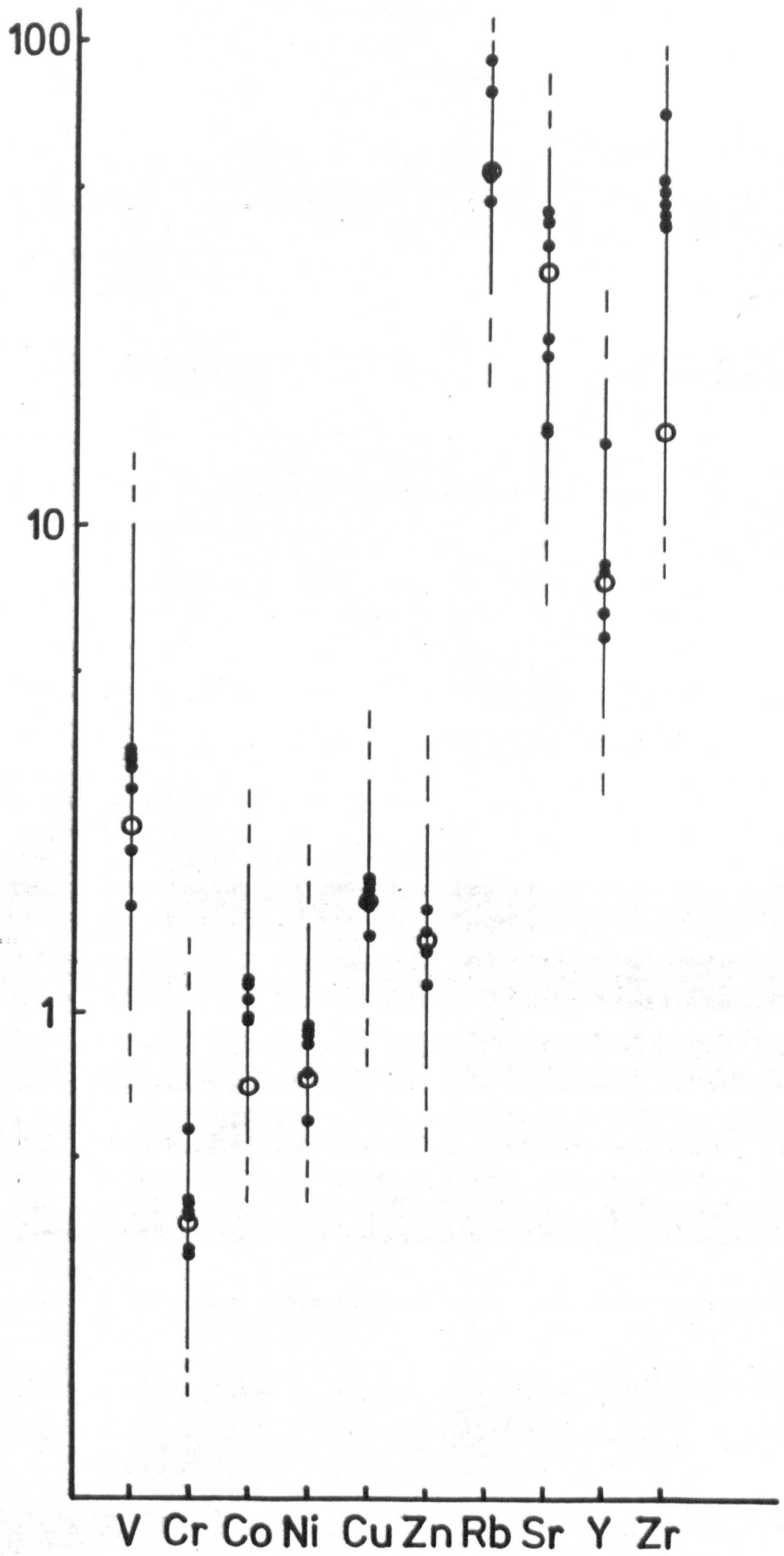


Figure 3.3: Major element variation diagram for Letseng kimberlites.  $\text{SiO}_2 + \text{Al}_2\text{O}_3 + \text{Na}_2\text{O} + \text{K}_2\text{O}$  v.  $\text{CaO} + \text{MgO} + \text{FeO} + \text{Fe}_2\text{O}_3 + \text{TiO}_2$   
v.  $\text{CO}_2 + \text{H}_2\text{O}$

Symbols as for figure 3.1

Dotted line demarcates the field of kimberlite and dashed line the field of carbonatite (Dawson 1967).

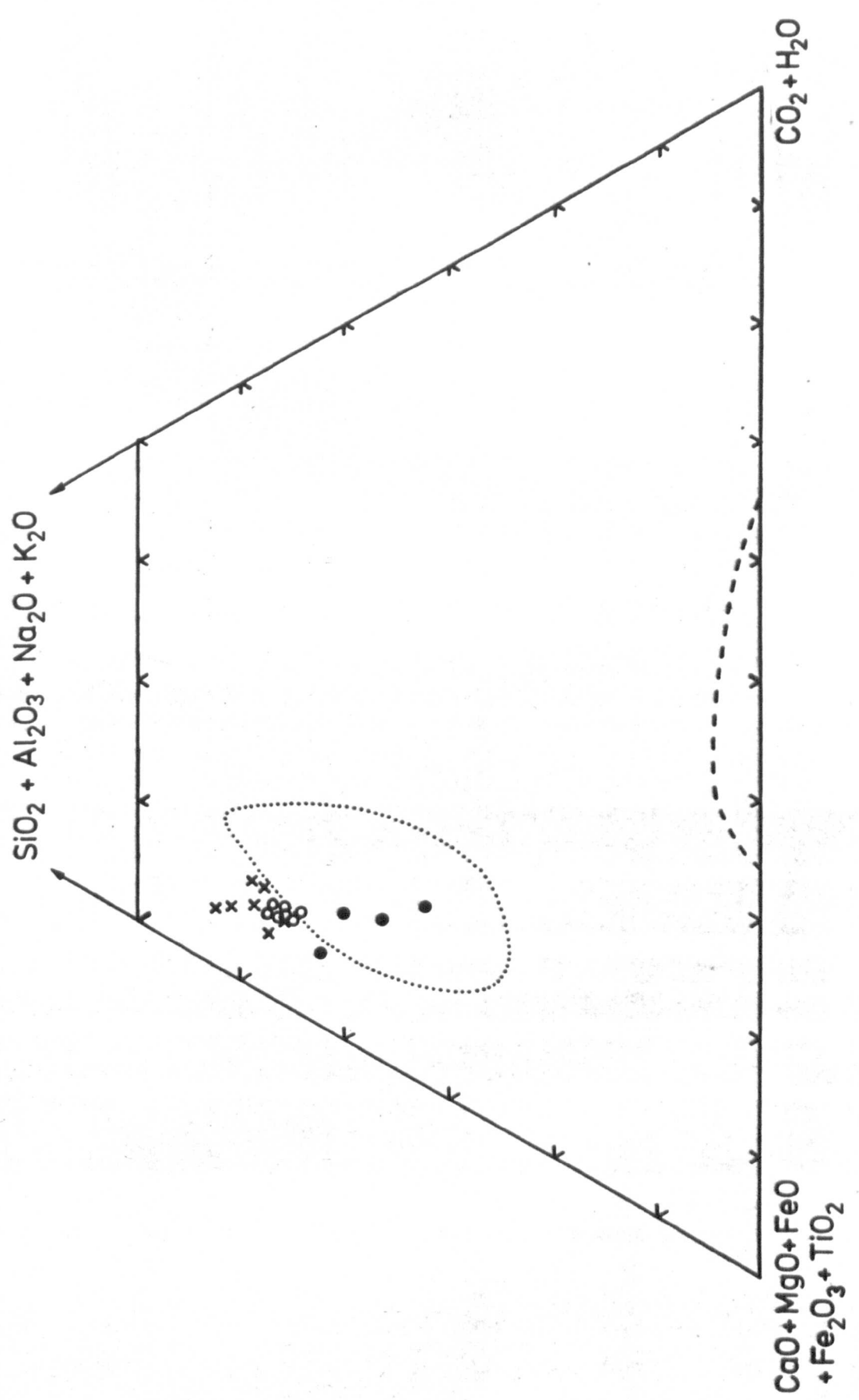


Figure 3.4: Major element variation diagram for Letseng kimberlites.  $\text{Al}_2\text{O}_3$  v.  $\text{MgO}$  v.  $\text{FeO}$   
Symbols as for figure 3.1  
Dotted line demarcates the field of kimberlite (Cornellisen & Verwoerd 1975).

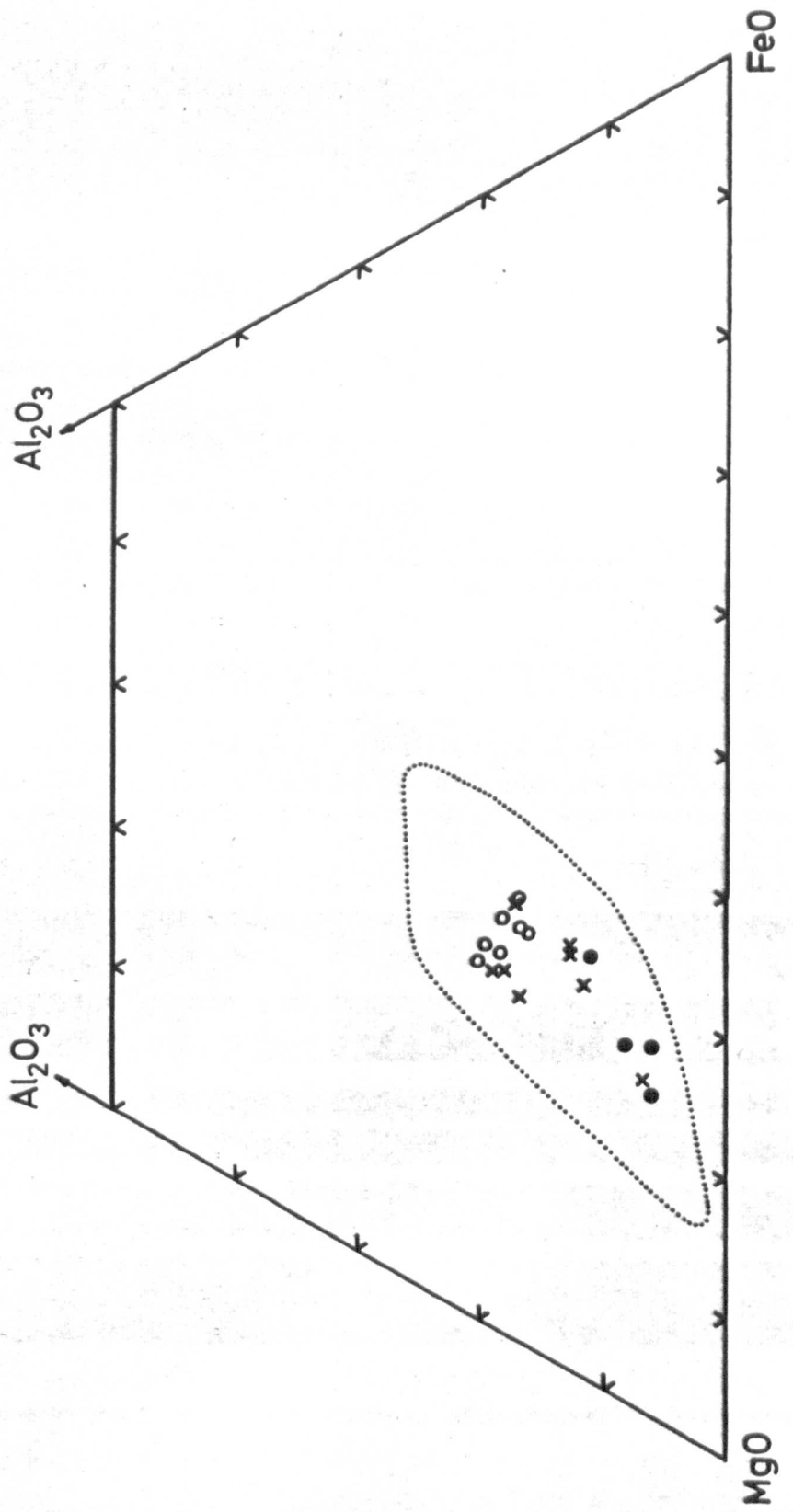


Figure 3.5: Potassium and rubidium variation in Letseng kimberlites.

Closed circles: dykes.

Inclined crosses: autoliths

Vertical crosses: from Kruger (1978).

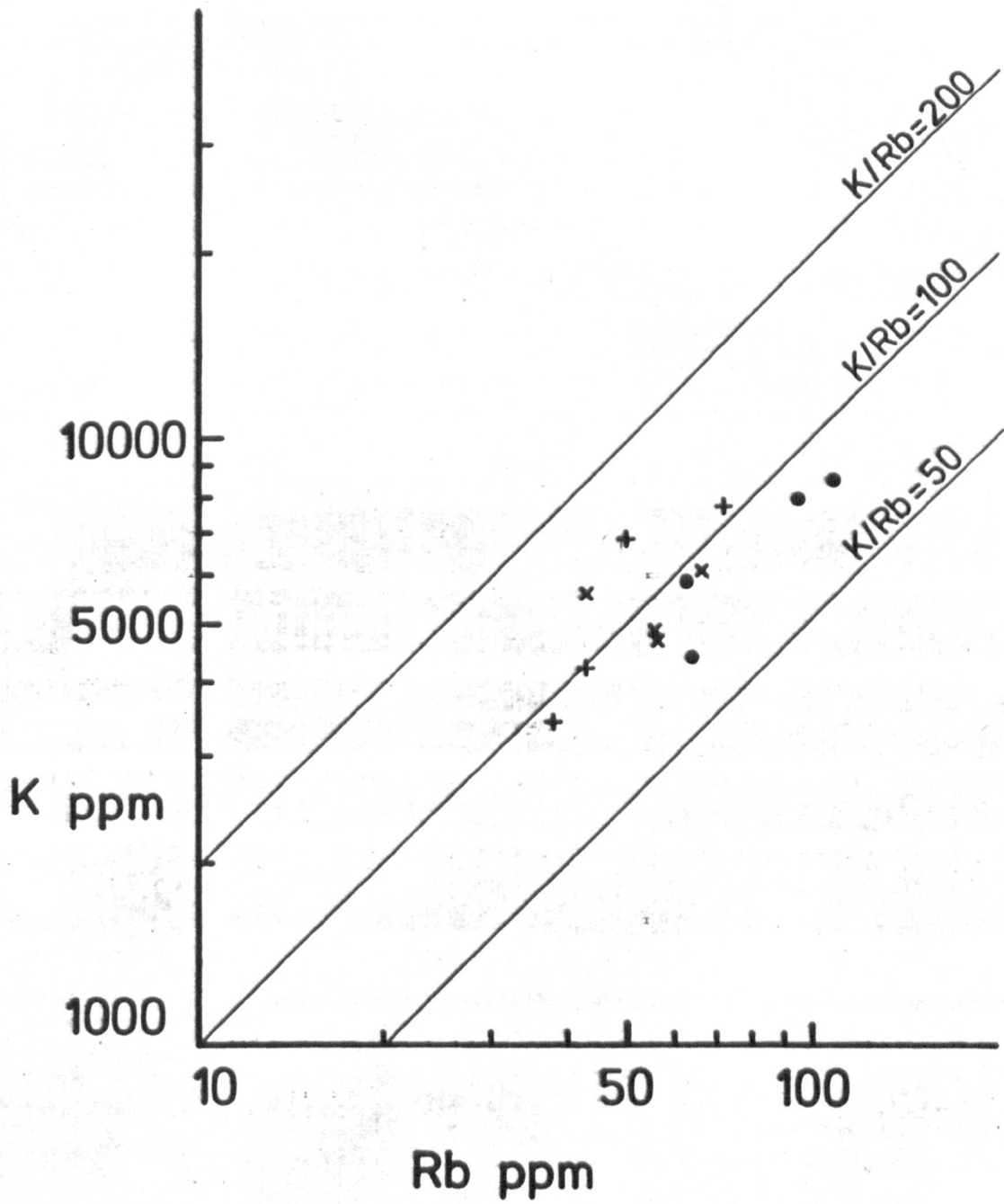


Figure 3.6a:TiO<sub>2</sub> Wt% v. P ppm for Letseng kimberlites.  
symbols as for figure 3.1.

Figure 3.6b:Zr ppm v. P ppm for Letseng kimberlites.  
symbols as for figure 3.1.



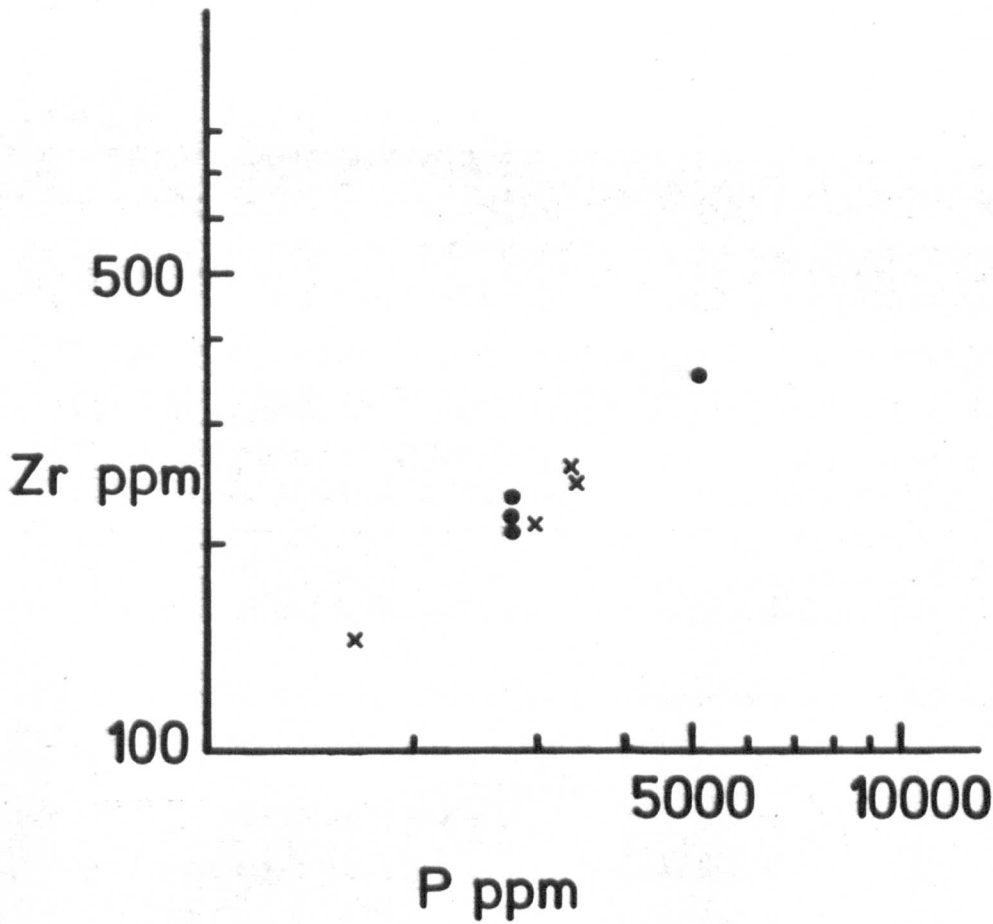
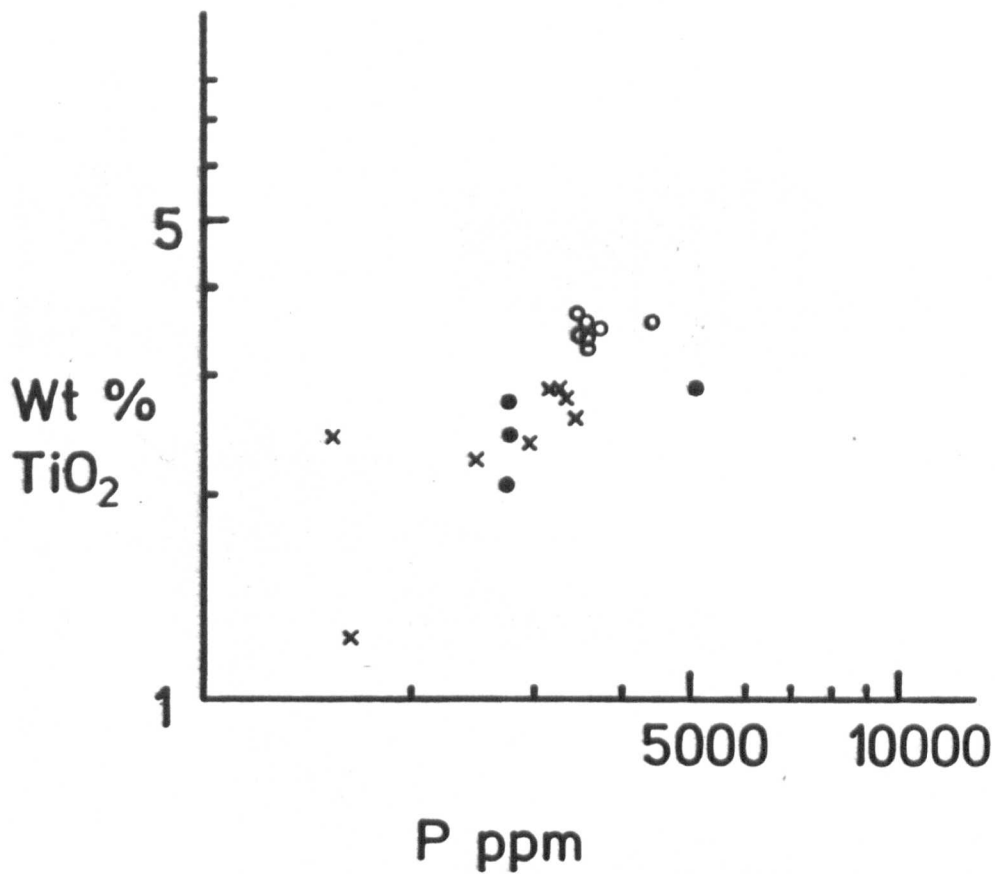


Figure 3.7:CO<sub>2</sub> Wt% v. Sr ppm for Letseng kimberlites.

Closed circles: Sr abundances measured by isotope dilution.

Inclined crosses: Sr abundances measured by XRF.

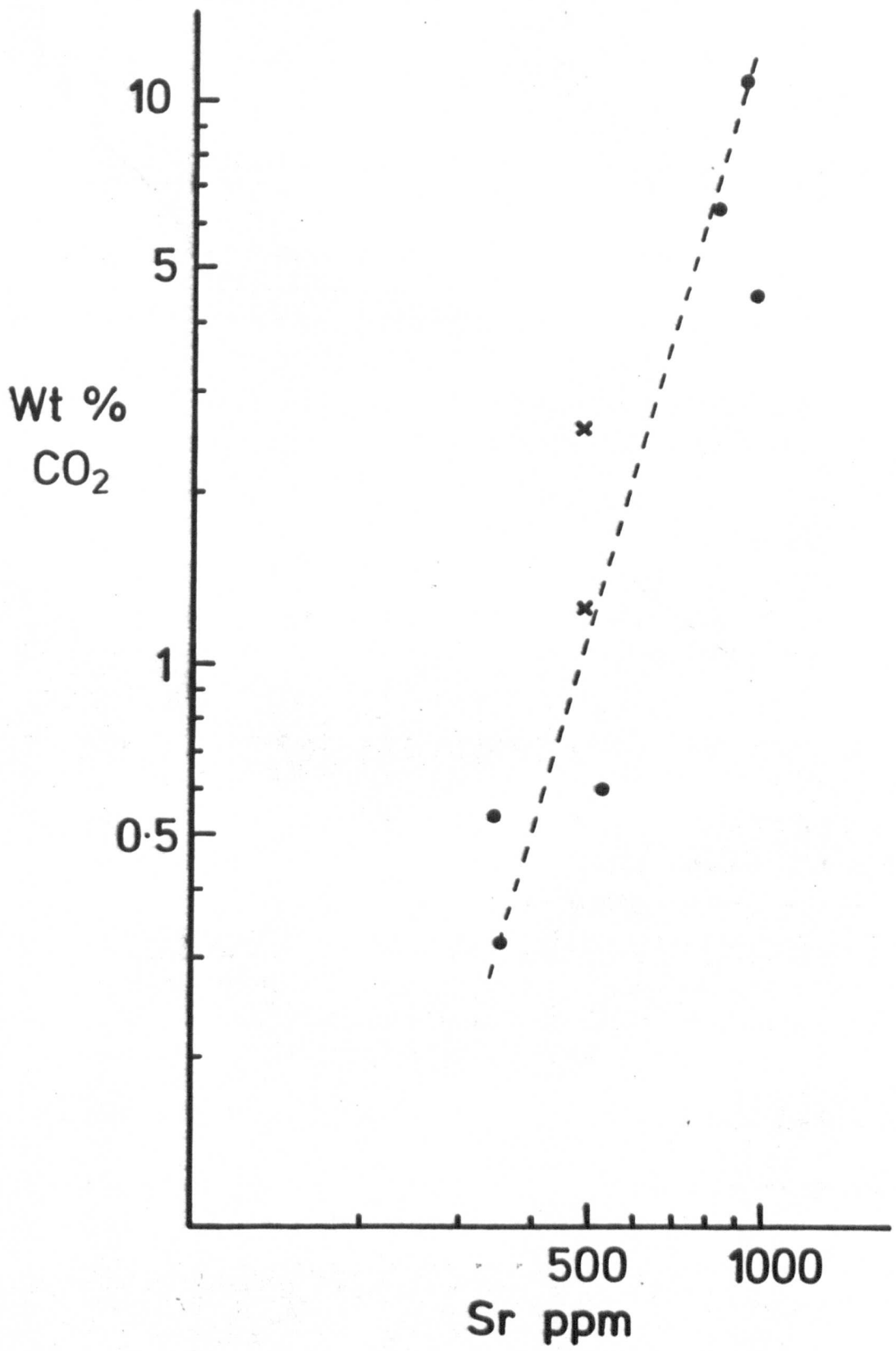
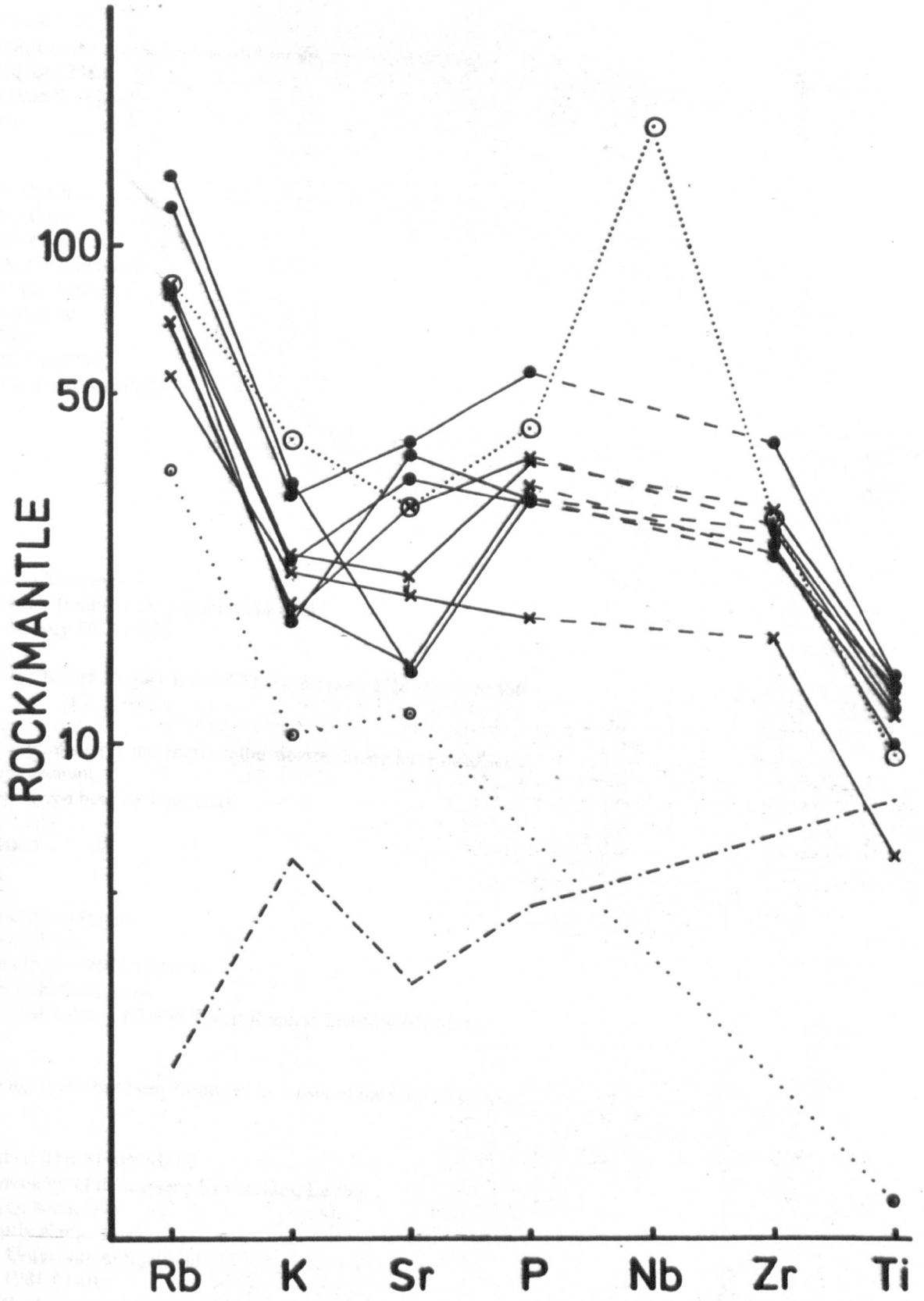


Figure 3.8: Mantle normalised trace element abundances for Letseng kimberlites.  
Symbols as for figure 3.1.  
Mantle values from Norry (in Hawkesworth et al 1979).  
For comparison the diagram shows plots of average kimberlite (Wedepohl & Marumatsu 1979), diamond (Fesq et al 1975), and an average oceanic tholeiite (Reykjanes Ridge -- O'Nions & Pankhurst 1974).



CHAPTER 4

Kimberlite REE, Rb, Sr,  $^{87}\text{Sr}/^{86}\text{Sr}$   
and  $^{143}\text{Nd}/^{144}\text{Nd}$

Introduction

Tight geological/geochronological constraints exist for the maximum possible age of kimberlites in the Lesotho province, but geological constraint on a minimum age is very poor. At Letseng the unaltered state of the dykes and the interesting and unusual chronology of early and late dykes affords an ideal opportunity for geochronological study. Mica from the two younger dykes is, however, impossible to extract in sufficient quantity due to the textural complexity and relative scarcity. Mica from the oldest dyke NL380 is easily extracted but the petrographic evidence for two mica generations explained the reason for the anomalous high ages obtained.

The extremely fresh nature of these kimberlite samples makes them particularly suitable for trace element isotopic analysis and REE analysis. REE analyses are particularly useful for petrogenetic interpretation and the present study concentrates mainly on analyses of the dyke kimberlites; a single analysis for an autolith affords a comparison with the diatreme facies kimberlites. Sr isotopes have been shown to be particularly useful in elucidating petrogenetic problems and more recently instrumental advances have allowed analyses of the low concentrations of Nd isotopes in oceanic volcanics and other rocks. Nd isotopes are much less sensitive to contamination and their joint interpretation with Sr isotopes has facilitated the development of petrogenetic models of mantle derived magmas. The present study reports the first combined Sr and Nd isotope analyses in kimberlite from Lesotho.

## Analytical Techniques

(1) Chemical Separations: All the chemical and instrumental techniques described below are those currently employed in the geochronology laboratory at Leeds University. The rare earth elements (REE) were separated in three groups by a mixed solvent ion exchange technique similar to that outlined by Hooker et al. (1975). This involves dissolution of the spiked sample powder in conc.  $\text{HNO}_3$  and 40% HF in a heated Teflon 'bomb'. The solution is passed through two anion exchange columns: in the first column the solution is loaded in a mixture of 75%  $\text{CH}_3\text{COOH}$ , 25% 5M  $\text{HNO}_3$  and the REE fraction collected in 0.05M  $\text{HNO}_3$ ; in the second column the sample is loaded in a mixture of 90% methanol, 10% 5M  $\text{HNO}_3$  and the REE collected in three groups - the heavy REE (Dy, Er, Yb) in the same methanol/ $\text{HNO}_3$  mixture; the light REE (Nd, Sm, Eu, Gd) in a mixture of 90% methanol, 10% 0.01M  $\text{HNO}_3$ ; and Ce and La in 1M  $\text{HNO}_3$ .

Rb and Sr were separated by standard cation exchange techniques similar to that outlined by Pankhurst and O'Nions (1973). The spiked sample is dissolved in conc.  $\text{HNO}_3$  and 40% HF and loaded in the exchange column in 2.5M HCl. The Rb and Sr portions are both collected in 2.5M HCl. The REE portion is collected in 6M HCl for Nd separation on anion exchange columns.

Nd is separated from this REE fraction by a two-column mixed-solvent anion exchange technique outlined by O'Nions et al. (1977). The REE are separated as a group using a procedure similar to that described above, but using a mixture of 90%  $\text{CH}_3\text{COOH}$ , 10% 5M  $\text{HNO}_3$  to load the sample. The Nd portion is separated on a second temperature-controlled anion exchange column using a  $\text{CH}_3\text{COOH-CH}_3\text{OH-HNO}_3$  mixture.

(2) Mass Spectrometry: REE and Rb analyses were made on a modified AEI MS5 mass spectrometer with digital readout and on-line data processing and Sr and Nd analyses on a Vacuum Generators Micromass 30.

REE samples are loaded in phosphoric acid on single tantalum filaments. About 100 scans are made for various masses for each element and an on-line computer calculates the element abundances and chondrite-normalised values (using the chondrite REE abundances of Nakamura, 1974). The measured isotopic ratios were usually accurate to better than  $\pm 1\%$  ( $2\sigma$ ).

Rb samples are loaded as the metal species on the tantalum side filaments of Ta/Re triple filaments. The Rb spectrum is measured at masses 87 and 85 and the background monitored at mass 84.5. 120-250 scans are made for each sample and the on-line computer corrected for fractionation effects before calculating the isotope ratio and element concentration. The measured isotope ratios were accurate to better than  $\pm 1\%$  ( $2\sigma$ ) and usually better than  $\pm 0.5\%$  ( $2\sigma$ ).

Sr samples are loaded in phosphoric acid on single tantalum filaments. The Sr spectrum is measured at masses 88, 87, 86 and 84, and the background and Rb at masses 87.5, 85 and 84.5. 150-300 measurements are made for each sample and the computer corrected for fractionation effects and normalised the isotope ratios to  $^{88}\text{Sr}/^{86}\text{Sr} = 8.364$  before calculation of the isotope ratios and element concentration. Measured  $^{87}\text{Sr}/^{86}\text{Sr}$  ratios were accurate to better than  $\pm 0.00004$  ( $2\sigma$ ) for whole rock samples and  $\pm 0.00012$  ( $2\sigma$ ) for mica separates.

Nd samples are loaded in phosphoric acid on the tantalum side filaments of Ta/Re triple filaments. The Nd spectrum is measured at masses 146, 144 and 143. Sm is monitored at mass 147 and the background at 146.5. Elemental Ba and Nd oxides are monitored initially until their



TABLE 4.1: Sr and Rb Isotopic Abundances in Kimberlites

Sample	K/Rb	Rb ppm	Sr ppm	$^{87}\text{Rb}/^{86}\text{Sr}$	$^{87}\text{Sr}/^{86}\text{Sr}_N^*$	$^{87}\text{Sr}/^{86}\text{Sr}_I$	$\Delta\text{Sr} \%$	$\delta\text{Sr} \%$
<u>Dyke</u>								
NL379	69.4	63.99	932.2	0.1985	$0.70407 \pm 4$	0.70382	-191	+1650
NL380	84.0	94.9	977.1	0.2810	$0.70439 \pm 3$	0.70403	-156	+2596
NL381	77.3	110.1	342.0	0.9313	$0.70474 \pm 3$	0.70355	-236	+12170
NL416	93.7	62.9	835.8	0.2176	$0.70386 \pm 2$	0.70358	-231	+2057
<u>Autolith</u>								
NL540a	88.1	55.6	350.9	0.4583	$0.70399 \pm 2$	0.70340	-261	+5700
NL540g	92.1	66.3	533.3	0.3993	$0.70489 \pm 3$	0.70443	-89	+3260
<u>Mica</u>								
NL380 3		296.2	92.4	9.3165	$0.75494 \pm 12$			
NL380 4		248.2	49.9	15.4071	$0.72767 \pm 11$			

\*  $^{87}\text{Sr}/^{86}\text{Sr}$  value normalised to  $^{88}\text{Sr}/^{86}\text{Sr} = 8.364$

$\Delta\text{Sr}$  as defined by Carter et al. (1978)

$$\Delta\text{Sr} = \frac{(\text{Rb}/\text{Sr})_{\text{Single Stage}} - (\text{Rb}/\text{Sr})_{\text{Bulk Earth}}}{(\text{Rb}/\text{Sr})_{\text{Bulk Earth}}} \times 10$$

where  $(^{87}\text{Rb}/^{86}\text{Sr})_{\text{Single Stage}} = \frac{(^{87}\text{Sr}/^{87}\text{Sr})_{\text{Measured}} - (^{87}\text{Sr}/^{86}\text{Sr})_{\text{BABI}}}{(e^{\lambda 87.t} - 1)}$

$(^{87}\text{Sr}/^{86}\text{Sr})_{\text{BABI}} = 0.69898$  assumed initial ratio for the earth

t = time from earth formation to kimberlite emplacement 4410 m.y.

$\delta\text{Sr}$  as defined by O'Nions et al. (1977)

$$\delta\text{Sr} = \frac{(^{87}\text{Sr}/^{86}\text{Sr})_{\text{Measured}} - (^{87}\text{Rb}/^{86}\text{Sr})_{\text{Single Stage}}}{(^{86}\text{Rb}/^{86}\text{Sr})_{\text{Single Stage}}}$$

where  $(^{87}\text{Rb}/^{86}\text{Sr})_{\text{Single Stage}}$  is as above

ion beam size is very much smaller than the Nd metal beam size. The beam intensity is gradually increased in the range  $2-3 \times 10^{-12}$  A during the course of measurement. 530 and 1000 measurements were made for the two samples. Fractionation effects are corrected by the on-line computer and the  $^{146}\text{Nd}/^{144}\text{Nd}$  ratio normalised to 0.7219. The measured isotope ratios were accurate to  $\pm 0.00004$  ( $2\sigma$ ) and  $\pm 0.00003$  ( $2\sigma$ ).

(3) Initial Ratio Correction: Initial ratios are calculated using an assumed kimberlite emplacement age of 90 m.y. Other kimberlites in a similar geological environment and in close geographic proximity give ages by different methods in the range 82-96 m.y. (Allsopp and Barrett, 1975; Davis, 1977). Mothae, a kimberlite about 7 km from Letseng, has an age of 87.1 m.y. using the zircon U/Pb method (Davis, 1977). The Sm/Nd ratios are obtained from the REE concentration data and the  $^{147}\text{Sm}/^{144}\text{Nd}$  ratio calculated from the natural abundances of Sm isotopes (Russ III, et al., 1971) and Nd isotopes (based on Hamilton et al., 1977; and  $^{143}\text{Nd}/^{144}\text{Nd} = 0.51116$  measured at Leeds on Johnson-Mathey  $\text{Nd}_2\text{O}_3$ ).

#### Rb and Sr Isotopes

Analyses for Rb, Sr,  $^{87}\text{Rb}/^{86}\text{Sr}$  and  $^{87}\text{Sr}/^{86}\text{Sr}$  were made for samples from four fresh dyke kimberlites, two kimberlite autoliths and two mica separates from one of the dykes (Table 4.1). The field relations previously discussed indicate the relative chronology of the kimberlite dykes. Only one dyke (NL 380) contained sufficient separable mica for analysis but no reliable age was found from mineral-whole rock isochrons. The autoliths allow some comparison between the diatreme facies and dyke kimberlites.

(1) Anomalous Ages: Whole rock-mica separate isochron plots for sample NL380 (Figure 4.2) give calculated ages of 116 and 393 m.y. These ages cannot be considered representative of the true kimberlite emplacement age

and are similar to the results of Allsopp and Kramers (1977) of 380, 580 and 660 m.y. They suggested that the mica may be contaminated by more ancient mica or by non-radiogenic  $^{86}\text{Sr}$ . The latter possibility seems unlikely as the extremely fresh Letseng samples show only a very small range in initial  $^{87}\text{Sr}/^{86}\text{Sr}$  ratios and no correlation with carbonate content. NL540a has the lowest initial ratio of 0.70340 and the lowest  $\text{CO}_2$  content of 0.32 wt.%. Thus it seems unlikely that there is a significant difference between the 'micaceous whole rock' initial ratios and the 'leachable carbonate component' initial ratios and therefore no scope existed for cross-contamination on a scale great enough to cause these anomalous ages.

The former possibility has now been confirmed by microprobe analysis of various micas (Allsopp et al., 1979). Smith et al. (1978) have defined type I and type II mica in the kimberlite groundmass on the strength of petrographic and chemical differences. Allsopp et al. (1979) have shown that kimberlites giving anomalously high Rb/Sr ages contain type I mica. Their data include an analysis for a Letseng mica (analysis 2, Table 1, Allsopp et al., 1979) and their Figure 1 shows a plot of  $\text{Mg} - 37.5 \text{ na}$  ( $\text{mg} = \text{Mg}/(\text{Mg}+\text{Fe})$ ,  $\text{na} = \text{Na}_2\text{O}/(\text{Na}_2\text{O} + \text{K}_2\text{O})$ ) against  $4\text{Ti} + 3/\text{Cr} + \text{Al}$  and since this plot separates the two types of mica from several localities, the separation appears to be real. Their Letseng samples plot well away from the tightly clustered type II micas.

Petrographic examination of NL380 shows that it too contains type I mica (in addition to more abundant type II mica) (see Chapter 2). Microprobe analysis (Table 2.1) shows that chemically these micas conform to the definitions of type I and type II micas. Figure 2.1 shows their plot, relative to the data from other pipes, in the chemical discrimination diagram described above. Clearly this diagram is inadequate to differentiate these phlogopites.

(2) Initial Ratios: Initial  $^{87}\text{Sr}/^{86}\text{Sr}$  ratios for both dyke kimberlites and kimberlite autoliths group closely in the range 0.70340-0.70443 (Figure 4.3). Excluding the values obtained from the autoliths the grouping is even closer: 0.70355-0.70403. These values show less spread than the kimberlites analysed by Barrett and Berg (1975), Allsopp and Barrett (1975) and Barrett (1975) or the autoliths analysed by Kramers (1977). They are also lower than the early strontium isotope analyses from kimberlite of Mitchell and Crockett (1971) and Berg and Allsopp (1972).

In contrast to the conclusion of Barrett and Berg (1975) these 'micaceous' kimberlites have initial ratios less than 0.705. It is important to note the low K/Rb ratios (Figure 3.5) in the rocks of this study especially in relation to the relative mobility of K and Rb as discussed by Fesq et al. (1975a). These low K/Rb ratios are comparable to the values (20-130) found in diamonds by Fesq et al. (1975b). It may be inferred that these rocks have K/Rb and  $^{87}\text{Sr}/^{86}\text{Sr}$  ratios more nearly representative of the values for southern African Cretaceous kimberlites at depth and unaffected by either contamination or late stage deuteric or meteoric alteration.

It is noted above that there is no correlation between carbonate content and strontium initial ratio. There is, however, a crude positive correlation between  $\text{CO}_2$  wt.% and Sr ppm (Figure 3.7) because strontium resides mainly in the carbonates. As these low  $\text{CO}_2$  and Sr samples have the closest temporal relation to the diatreme facies it is important to consider the possible effects on the strontium initial ratio of volatile outgassing during diatreme formation. The higher  $^{87}\text{Rb}/^{86}\text{Sr}$  values and the tendency for the measured  $^{87}\text{Sr}/^{86}\text{Sr}$  values to be higher in the autoliths from the diatreme facies kimberlite, suggests that if any strontium has been lost during volatile outgassing this loss has had no significant

**TABLE 4.2: REE in Kimberlite (ppm)**

	Dykes			Autolith
	NL379	NL380	NL416	NL540a
La	79.6	168.3	101*	90.0
Ce	154.4	324.1	192.9	173.4
Nd	62.0	124.9	74.7	69.0
Sm	9.83	19.32	11.32	10.82
Eu	2.65	4.95	2.88	2.53
Gd	6.61	12.37	7.04	6.87
Dy	3.50	6.77	3.51	3.52
Er	1.21	2.53	1.23	1.20
Yb	0.74	1.91	0.75	0.78
Sm/Nd	0.1586	0.1548	0.1515	0.1569
La/Yb	108	88	~136	115
La <sub>N</sub> /Yb <sub>N</sub>	72	59	~ 90	77
La <sub>N</sub> /Eu <sub>N</sub>	7.0	7.9	~ 8.2	8.3
La <sub>N</sub> /Sm <sub>N</sub>	5.0	5.3	~ 5.5	5.1

\* Value estimated by extrapolation

effect on the strontium initial ratio. This adds some confidence to the interpretation of strontium isotopic data because it is apparent from other trace element data (Table 3.8, Figure 3.8) that whereas the other trace elements follow a coherent pattern, the strontium analyses demonstrate considerable scatter possibly as a result of varying amounts of volatile loss. It may also be relevant to considerable strontium and volatile enrichment as a result of differentiation as observed in the Benfontein sills (Dawson and Hawthorne, 1973).

It may be concluded that these values are compatible with kimberlite derivation from an uncontaminated mantle source as has been proposed for other rocks with low  $^{87}\text{Sr}/^{86}\text{Sr}$  ratios (e.g. basalts - Hurley, 1967; carbonatites - Powell et al., 1966; Hutchison and Dawson, 1970). Variations in strontium concentration may be the result of volatile outgassing or differentiation processes during or prior to emplacement but these variations do not affect the  $^{87}\text{Sr}/^{86}\text{Sr}$  initial ratio.

### REE Patterns

The measured REE abundances are given in Table 4.2. Figure 4.1 shows the chondrite normalised REE distribution patterns for these Letseng kimberlites. These patterns are essentially linear with no Eu anomaly and strong LREE enrichment ( $\text{La}_N/\text{Yb}_N = 60-90$ ).

There is a marked separation of the early dyke NL380 from the grouping of the autolith NL540a and the two late dykes NL379 and NL416.  $\text{La}_N/\text{Yb}_N$  for NL380 is the lowest for any of these samples but this should be viewed with caution as its Yb value was only poorly determined. It is more likely that the subparallel nature of the REE distribution patterns is the result of differing modal abundances of REE bearing minerals. Mitchell and Brunfelt (1975) have discussed this with reference to apatite, perovskite and carbonate. In the present study the coincidence of three patterns for

rocks with very different  $\text{CO}_2$  contents (0.32-11.29 wt.%) but very similar  $\text{P}_2\text{O}_5$  contents (0.63-0.68 wt.%) (see Tables 3.2 and 3.3) suggests that apatite (which is visible under the microscope in NL380 where  $\text{P}_2\text{O}_5 = 1.15$  wt.%) may be the important host for the REE.  $\text{TiO}_2$  is also appreciably higher in NL380 although the variation between the other three samples is much greater than for  $\text{P}_2\text{O}_5$ . However, if the  $\text{TiO}_2$  is considered only to reside in perovskite in these rocks this may be a further reason for the higher REE content of NL380. Ilmenite has not been identified in the kimberlite and is very rare in the heavy mineral concentrates.

A number of other studies have analysed kimberlite REE patterns from a wide range of geographic locations (e.g. South Africa - Haskin et al., 1966, Frey et al., 1971, Mitchell and Brunfelt, 1975, Fesq et al., 1975; Canada - Mitchell and Brunfelt, 1975; India - Paul et al., 1975; Australia - Frey et al., 1977; U.S.S.R. - Burkov and Podporina, 1966; U.S.A. - Smith et al., 1977). It is immediately apparent that all kimberlites are LREE enriched although with a wide range of  $\text{La}_N/\text{Yb}_N$  ratios (20 at Premier - 150 at Bellsbank).

Negative Eu anomalies have been reported from kimberlites in the U.S.S.R. (Burkov and Podporina, 1966) and at Bellsbank (Fesq, et al., 1975a). Fesq and co-workers attributed this anomaly to the highly micaceous nature of the kimberlite: they analysed the REE from a peridotite phlogopite and suggested that the Eu anomaly observed in this mica may be imposed on the kimberlite REE pattern if the mica is abundant enough. At Letseng however, NL380 and NL381 show no Eu anomaly despite having a considerable phlogopite component. This point requires further investigation as the REE patterns in the various phlogopites from kimberlite (type I and II) may be entirely different from that observed in phlogopite from peridotite.

Mitchell and Brunfelt (1975) have discussed the possibility of the preferential exclusion of Eu from perovskite causing anomalous whole rock patterns if the perovskite is abundant enough. However, the high  $\text{TiO}_2$  content of the Letseng kimberlites (higher than the Lesotho average of Gurney and Ebrahim, 1973 or Dawson, 1968; the Yakutian average of Ilupin and Lutz, 1971; or the South African average of Gurney and Ebrahim, 1973) suggests that this may not be the case if this  $\text{TiO}_2$  is contained in perovskite. Modal perovskite is common in the Letseng kimberlite dykes but no Eu anomalies are apparent in the whole rock REE patterns.

Thus it seems that Eu anomalies in phlogopite and perovskite may be invoked to explain the whole rock Eu anomalies observed in some kimberlites. However, it would seem that in the Letseng rocks phlogopite and perovskite have no Eu anomaly because, despite their abundance, they have imposed no anomaly on the whole rock pattern. Investigation of the REE patterns of kimberlite minerals would be required to resolve this discussion.

Discussion of the origin of the highly fractionated REE patterns observed in kimberlites has concentrated on processes involving small degrees of partial melting of peridotitic material (e.g. Frey et al., 1971; Mitchell and Brunfelt, 1975; Fesq et al. 1975a; Paul et al, 1975) although Mitchell and Brunfelt (1975) re-examined the possibility of eclogite fractionation. Frey et al. (1977) have proposed a mantle model with LREE enrichment which is attractive as it overcomes the La-dilemma discussed by Fesq et al. (1975a). This dilemma results from the impossibility of obtaining the kimberlite LREE enrichment ( $\text{La/Ce} > 1$ ) from partial melting of phlogopite-bearing garnet peridotite, with constituent phlogopite and clinopyroxene  $\text{La/Ce} < 1$ . However, Rogers (1979) has investigated the REE patterns for various garnet peridotites and suggests that the LREE



TABLE 4.3: Sm and Nd Isotopic Abundances in Kimberlite

Sample	Sm ppm	Nd ppm	Sm/Nd	$^{147}\text{Sm}/^{144}\text{Nd}$	$^{143}\text{Nd}/^{144}\text{Nd}_N^*$	$^{143}\text{Nd}/^{144}\text{Nd}_I$	$\Delta\text{Nd} \%$	$\delta\text{Nd} \%$
<u>Dyke</u>								
NL380	19.33	128.87	0.1548	0.0936	$0.51278 \pm 4$	0.51272	92	-540
NL416	11.32	74.71	0.1515	0.0916	$0.51274 \pm 3$	0.51269	87	-547

\*  $^{143}\text{Nd}/^{144}\text{Nd}$  value normalised to  $^{146}\text{Nd}/^{144}\text{Nd} = 0.7219$

$\Delta\text{Nd}$  as defined by Carter et al. (1978)

$$\Delta\text{Nd} = \frac{(\text{Sm}/\text{Nd})_{\text{Single Stage}} - (\text{Sm}/\text{Nd})_{\text{Bulk Earth}}}{(\text{Sm}/\text{Nd})_{\text{Bulk Earth}}} \times 10^3$$

where  $(^{147}\text{Sm}/^{144}\text{Nd})_{\text{Single Stage}} = \frac{(^{143}\text{Nd}/^{144}\text{Nd})_{\text{Measured}} - (^{143}\text{Nd}/^{144}\text{Nd})_{\text{JUV}}}{(e^{\lambda 147.t} - 1)}$

$(^{143}\text{Nd}/^{144}\text{Nd})_{\text{JUV}} = 0.50677$  assumed initial ratio for the earth

t = time from earth formation to kimberlite emplacement 4410 m.y.

Nd as defined by O'Nions et al. (1977)

$$\text{Nd} = \frac{(^{147}\text{Sm}/^{144}\text{Nd})_{\text{Measured}} - (^{147}\text{Sm}/^{144}\text{Nd})_{\text{Single Stage}}}{(^{147}\text{Sm}/^{144}\text{Nd})_{\text{Single Stage}}}$$

where  $(^{147}\text{Sm}/^{144}\text{Nd})_{\text{Single Stage}}$  is as above

enriched peridotites have had their REE patterns imposed on them by a metasomatic event with 'kimberlitic' trace element abundances.

The volatile transfer model for the control of REE abundances (e.g. Mitchell and Bell, 1976) seems even less attractive in the present instance. As already mentioned the carbonate does not seem to be the major host for the REE and as the carbonate crystallised later than the perovskite (and perhaps apatite) it is difficult to envisage how a volatile-REE complex could on crystallising transfer the REE to perovskite and apatite.

It is apparent that much further work still requires to be done to elucidate the possible petrogenetic history of kimberlites. The analyses of the present study confirm the similarity of the Letseng rocks to other kimberlites but do not cast any new light on the problem. Neodymium isotopes can give information about the long-term fractionation pattern of REE in the (mantle) source region for kimberlites and the combined study with strontium isotopes allows quantitative modelling of source region fractionation and partial melting. The following sections report these models for the Letseng kimberlites as compared to mantle-derived oceanic volcanics and hypothetical peridotitic mantle.

#### $^{143}\text{Nd}/^{144}\text{Nd}$

Analyses of the whole rock  $^{143}\text{Nd}/^{144}\text{Nd}$  ratio were made for two kimberlite dyke samples NL380 and NL416 representing early and late kimberlite intrusion relative to the diatreme phase (Table 4.3, Figure 4.4). The initial  $^{143}\text{Nd}/^{144}\text{Nd}$  ratios compare favourably with the results of Basu and Tatsumoto (1979) measured on kimberlites of similar age from Kimberley. These workers also measured the  $^{143}\text{Nd}/^{144}\text{Nd}$  ratio for other kimberlites of different ages and geographical location. These results demonstrate a linear relation with time which is coincident with the time-integrated evolution line for  $^{143}\text{Nd}/^{144}\text{Nd}$  measured in the Juvinas

chondritic meteorite. This coincident relationship is inferred to imply the genesis of kimberlite from a chondritic mantle source.

#### Covariation of $^{143}\text{Nd}/^{144}\text{Nd}$ and $^{87}\text{Sr}/^{86}\text{Sr}$

Several recent studies of neodymium isotopes from oceanic basalts (Richard et al., 1976; De Paolo and Wasserburg, 1976; and O'Nions et al., 1977) indicate a clear negative correlation between  $^{143}\text{Nd}/^{144}\text{Nd}$  and  $^{87}\text{Sr}/^{86}\text{Sr}$  ratios (Figure 4.5) which is of great importance because of the improbability of contamination of these mantle derived rocks by crustal material. This covariation demonstrates that Rb/Sr and Sm/Nd have fractionated coherently in the sub-oceanic mantle through earth history: localised depletion in Rb/Sr is accompanied by a complementary enrichment in Sm/Nd and vice-versa. It may be inferred that the sub-oceanic mantle is heterogeneous relative to a chondritic bulk earth composition.

In the present study the kimberlite samples are seen to plot close to this line of covariation (account must be taken of the kimberlite age) indicating that the (deep) sub-continental mantle has followed the same coherent fractionation pattern as the sub-oceanic mantle.

#### Mantle Depletion

De Paolo and Wasserburg (1976) and O'Nions et al. (1977) have argued that the earth has an approximately chondritic Sm/Nd ratio (= 0.308). Consequently the present day bulk earth  $^{143}\text{Nd}/^{144}\text{Nd}$  ratio should be 0.51264 which implies, from the line of covariation of  $^{143}\text{Nd}/^{144}\text{Nd}$  and  $^{87}\text{Sr}/^{86}\text{Sr}$ , that the present day bulk earth  $^{87}\text{Sr}/^{86}\text{Sr}$  ratio is  $\sim 0.705$  and the bulk earth Rb/Sr ratio is 0.032. From this it can be inferred that rocks with  $^{87}\text{Sr}/^{86}\text{Sr} > 0.705$  and  $^{143}\text{Nd}/^{144}\text{Nd} < 0.51264$  are generated from source areas enriched in Rb/Sr and depleted in Sm/Nd relative to the bulk earth. Conversely rocks with  $^{87}\text{Sr}/^{86}\text{Sr} < 0.705$  and  $^{143}\text{Nd}/^{144}\text{Nd} >$

0.51264 are generated from source areas depleted in Rb/Sr and enriched in Sm/Nd (LREE depleted) relative to the bulk earth. This enrichment or depletion can be conveniently expressed in terms of  $\Delta Nd$  and  $\Delta Sr$  parameters as defined by Carter et al. (1978) (see Tables 4.1 and 4.3). In Figure 4.6 it can be seen that  $\Delta Sr = \Delta Nd = 0$  corresponds to unmodified mantle with bulk earth Rb/Sr and Sm/Nd ratios. Most of the oceanic basalts together with the Letseng kimberlites plot in the  $-\Delta Sr + \Delta Nd$  quadrant which corresponds to source regions with Rb/Sr and LREE depletion. These variations may reflect regional or local inhomogeneities in the mantle or real depletion events. The  $^{143}Nd/^{144}Nd$  ratios of Basu and Tatsumoto (1979) for Kimberley area kimberlites suggest that there the sub-continental mantle may be nearer to the bulk earth composition than the slightly depleted Letseng rocks, implying sub-continental mantle heterogeneity. However the sub-southern African mantle has possibly suffered depletion on a number of occasions during the last 3500 m.y. Basic volcanic rocks of the Onverwacht system (3400 m.y.), Dominion Reef system (2820 m.y.), Ventersdorp system (2300 m.y.), Bushveld complex (1950 m.y.) and Karoo system (200 m.y.) (see for example 'African Magmatism and Tectonics', 1970) derived from the mantle may have left that part of the mantle relatively depleted.

#### Partial Melting

The possibility of partial melting being a mechanism responsible for kimberlite magma genesis has already been discussed in relation to the highly fractionated REE patterns. An alternative approach is to compare the measured Rb/Sr and Sm/Nd ratios from the whole rock samples with those calculated to exist in the source region. These ratios may be altered by later fractional crystallisation and/or crustal contamination but it is useful to model the element partitioning between liquid and solid during partial melting assuming no such late stage processes.

Carter et al. (1978) and O'Nions et al. (1977) have defined the parameters  $\delta'Nd$  and  $\delta'Sr$ , and  $\delta Nd$  and  $\delta Sr$  (see Tables 4.1 and 4.3) to investigate the results of model partial melting of a peridotitic mantle. These parameters measure the deviation of the measured parent/daughter ratios from the respective bulk earth and single stage parent/daughter ratios. These deviations can be clearly seen in the conventional isochron diagrams for the Rb-Sr and Sm-Nd systems (Figures 4.3 and 4.4). In these diagrams the measured  $^{87}Rb/^{86}Sr$  and  $^{147}Sm/^{144}Nd$  values for the Letseng rocks falls considerably to the right and left respectively of a 4500 m.y. isochron for the bulk earth. In the  $\delta Nd$  and  $\delta Sr$  diagram, the samples plot in the  $-\delta Nd + \delta Sr$  quadrant together with some oceanic basalts (Figure 4.7). This figure also shows a model partial melting trajectory for peridotitic source rocks (see Carter et al., 1978) and it is clearly demonstrated that rocks originating by partial melting of mantle peridotite will plot in the  $-\delta Nd + \delta Sr$  quadrant. Rocks originating by 100% melting will plot at  $\delta Nd = \delta Sr = 0$  and the residues in the  $+\delta Nd - \delta Sr$  quadrant. The oceanic basalts do not follow a simple pattern and it is possible that a more complicated evolution perhaps involving fractional crystallisation has subsequently affected the Rb/Sr and Sm/Nd fractionation.

The Letseng kimberlites plot well into the  $-\delta Nd + \delta Sr$  quadrant and it is possible that fractional crystallisation had had a minimal effect on any subsequent evolution. If phlogopite were a fractionating phase the  $\delta Sr$  value would have been decreased from the original partial melt value but the REE pattern for mica (Fesq et al., 1975) suggests that the  $\delta Nd$  value may not have been appreciably altered. A  $\delta Sr$  value larger than that already measured might imply an unreasonably small amount of partial melting or a degree of volatile loss (as in the diatreme facies autoliths and the dyke NL381 - see Table 4.1) as discussed above. Also if the

unlikely possibility of apatite or perovskite fractionation were operative the  $\delta Nd$  value would be reduced without any change to the  $\delta Sr$  value. The Letseng rocks plot close to the modelled values for 1% partial melting. It is concluded that the kimberlite has been generated by a small degree of partial melting of peridotitic mantle. This mantle was of chondritic character but some slight LIL and LREE depletion relative to the bulk earth demonstrates a similarity to the heterogeneous sub-oceanic mantle. Subsequent fractionation (at least of Rb-Sr and REE-bearing minerals) has not appreciably altered the Rb-Sr and Sm-Nd systematics in the rock.

#### Summary

1. The paucity of extractable mica and presence of two different types of mica (type I and type II) has precluded attempts to obtain Rb/Sr dates on the dyke kimberlites.
2. Low initial  $^{87}Sr/^{86}Sr$  ratios, characteristic of uncontaminated mantle derived rocks, were obtained for all rocks. Autoliths representative of the diatreme facies rocks gave initial ratios bracketing those from the fresh dykes, suggesting a similar origin. Whole rock carbonate content varies sympathetically with total Sr, although there is no significant change in the initial Sr isotope ratio; this suggests that the carbonate and silicate sub-systems have a common origin.
3. REE patterns are strongly LREE enriched and near linear with no Eu anomaly. An autolith from the diatreme facies has a REE pattern identical to those for the two late dykes which despite differences in major element chemistry might suggest a common history. The early dyke has significant total REE enrichment compared to the other samples, probably due only to a greater abundance of REE-bearing minerals such as perovskite or apatite.

Carbonate does not seem to be an important REE host mineral. The REE patterns may reflect a small degree of partial melting of a peridotitic mantle.

4. The line of covariation of Nd and Sr isotopes established for oceanic basalts passes through the data for the Letseng kimberlites. This establishes that coherent fractionation of Rb/Sr and Sm/Nd has occurred not only in the sub-oceanic mantle but also in the sub-continental mantle.

5. The application of  $\Delta Nd$  and  $\Delta Sr$  parameters to the Letseng kimberlite data demonstrates the depleted nature of this kimberlite source region, although other kimberlites may be derived from enriched source regions.

6. Comparison of  $\delta Nd$  and  $\delta Sr$  parameters with those for an ideal partial melting model indicate the possible origin of kimberlite magma by about 1% partial melting of a peridotitic mantle.

Figure 4.1: Chondrite normalised REE patterns for Letseng kimberlites.

Closed circles: dykes.

Vertical crosses: Main Pipe autolith.

REE abundances normalised to the chondrite values of Nakamura(1974).



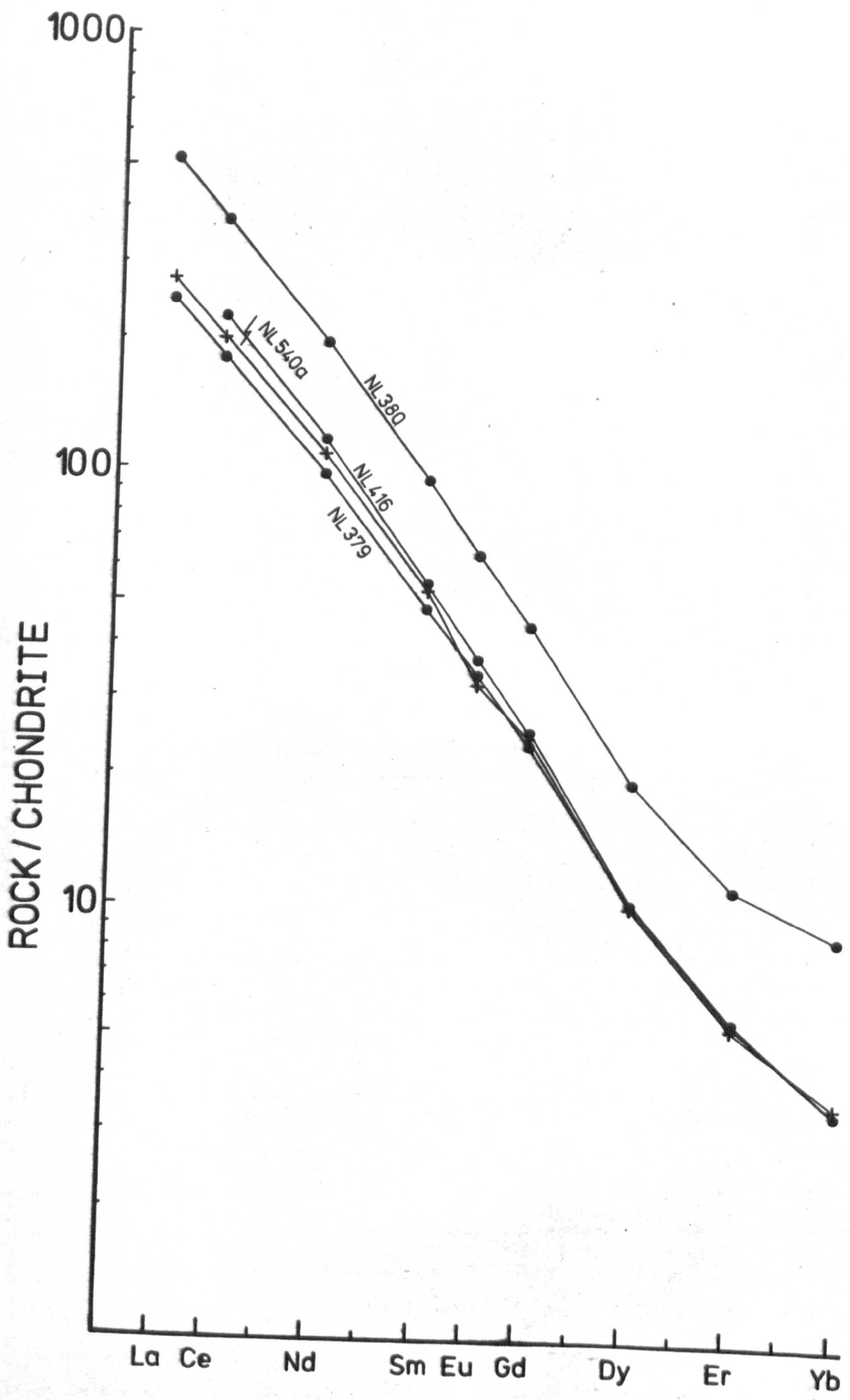


Figure 4.2:  $^{87}\text{Sr}/^{86}\text{Sr}$  v.  $^{87}\text{Rb}/^{86}\text{Sr}$  isochron diagram for Letseng kimberlites.

Closed circles: dyke whole rock.

Open circles: dyke mica separate.

Crosses: Main Pipe autoliths.

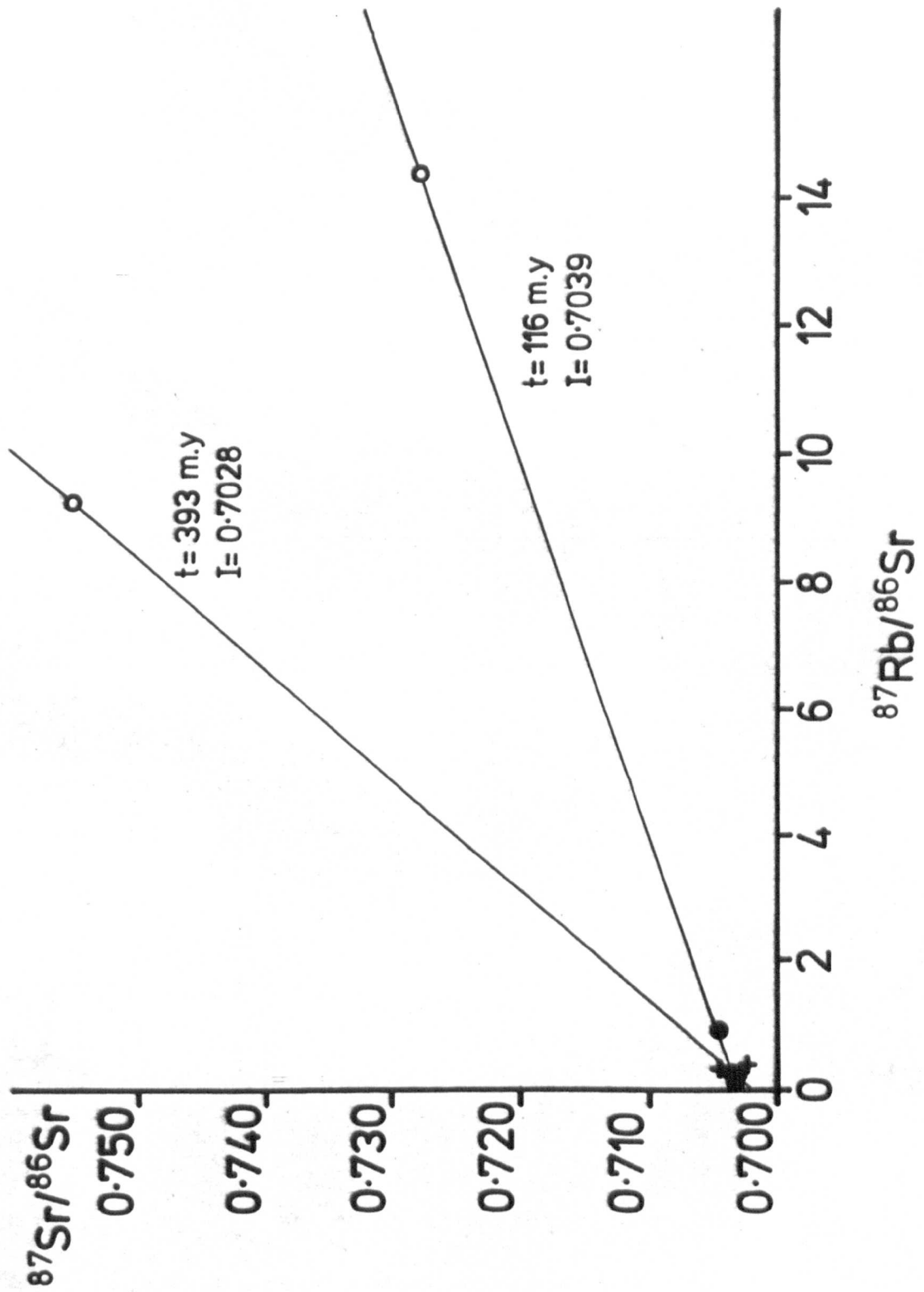


Figure 4.3: Initial  $^{87}\text{Sr}/^{86}\text{Sr}$  ratios for Letseng kimberlites.  
Assumed age of 90m.y.  
Symbols as for figure 4.2.

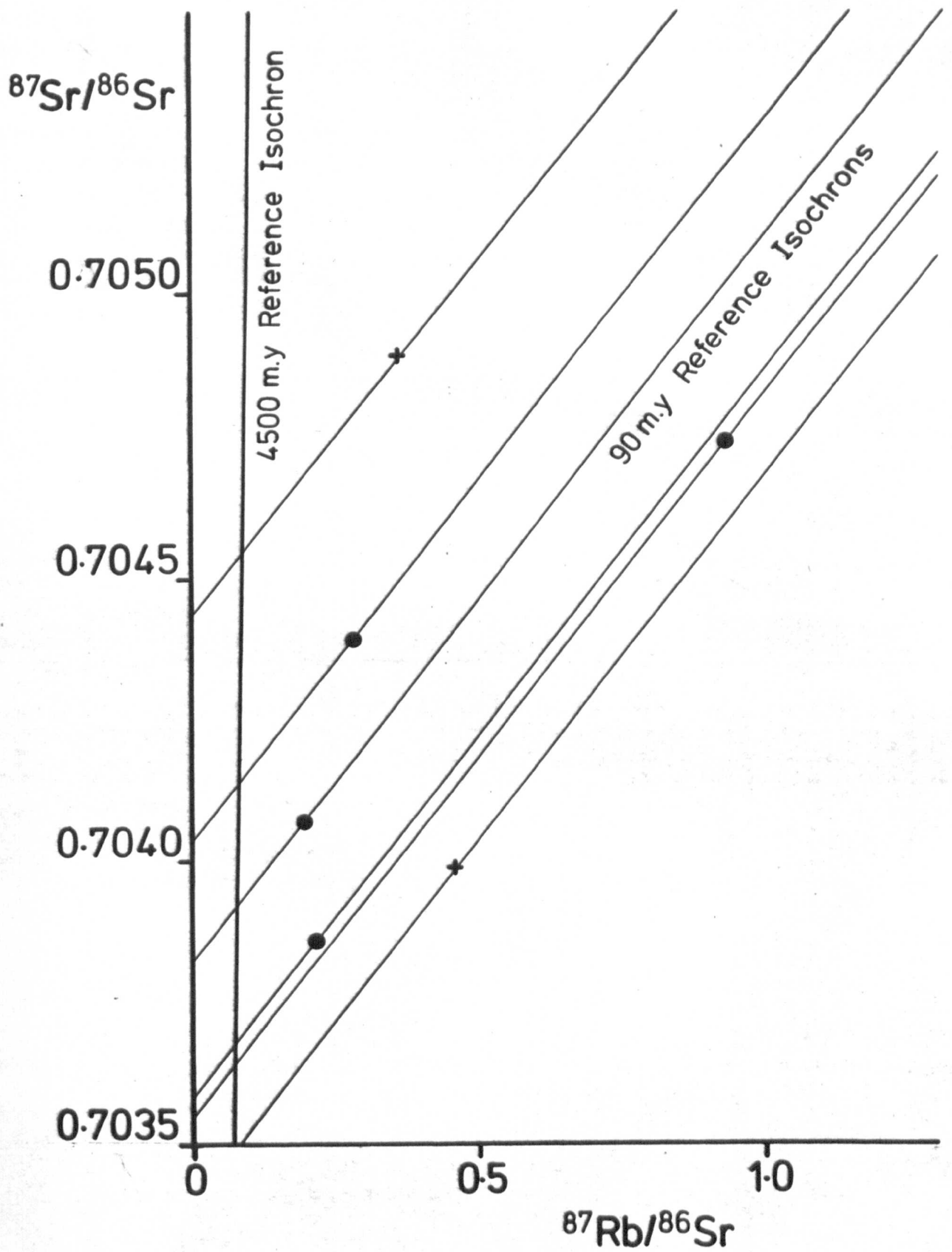


Figure 4.4: Initial  $^{143}\text{Nd}/^{144}\text{Nd}$  ratios for Letseng kimberlites.

Assumed age of 90m.y.

Symbols as for figure 4.2.

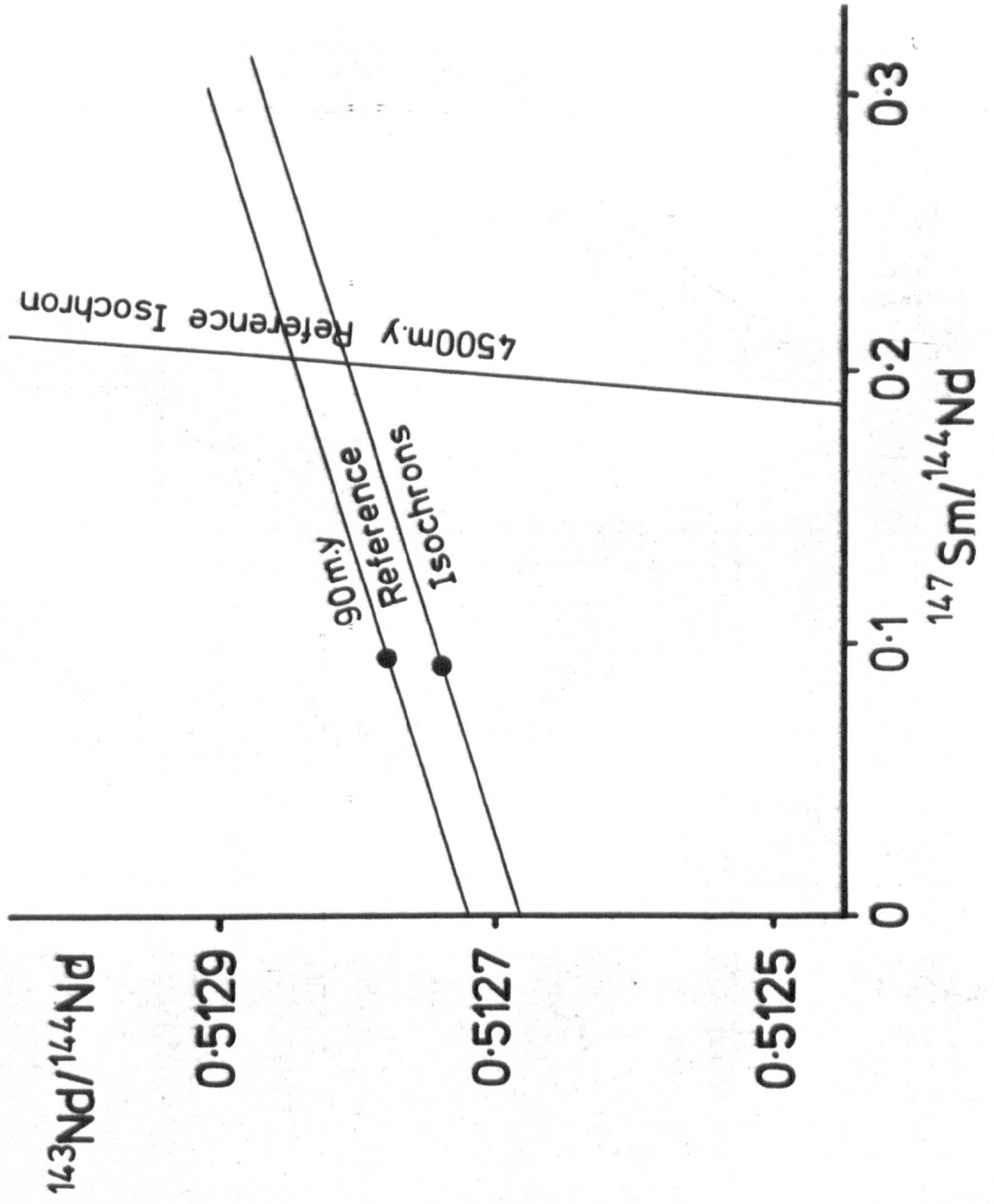


Figure 4.5: Covariation diagram for  $^{87}\text{Sr}/^{86}\text{Sr}$  &  $^{143}\text{Nd}/^{144}\text{Nd}$   
for Letseng kimberlites and oceanic rocks (for comparison)  
Data for oceanic rocks from Richard et al (1976), De Paolo  
& Wasserburg (1976), and O'Nions et al (1977).  
See figure for explanation of symbols.



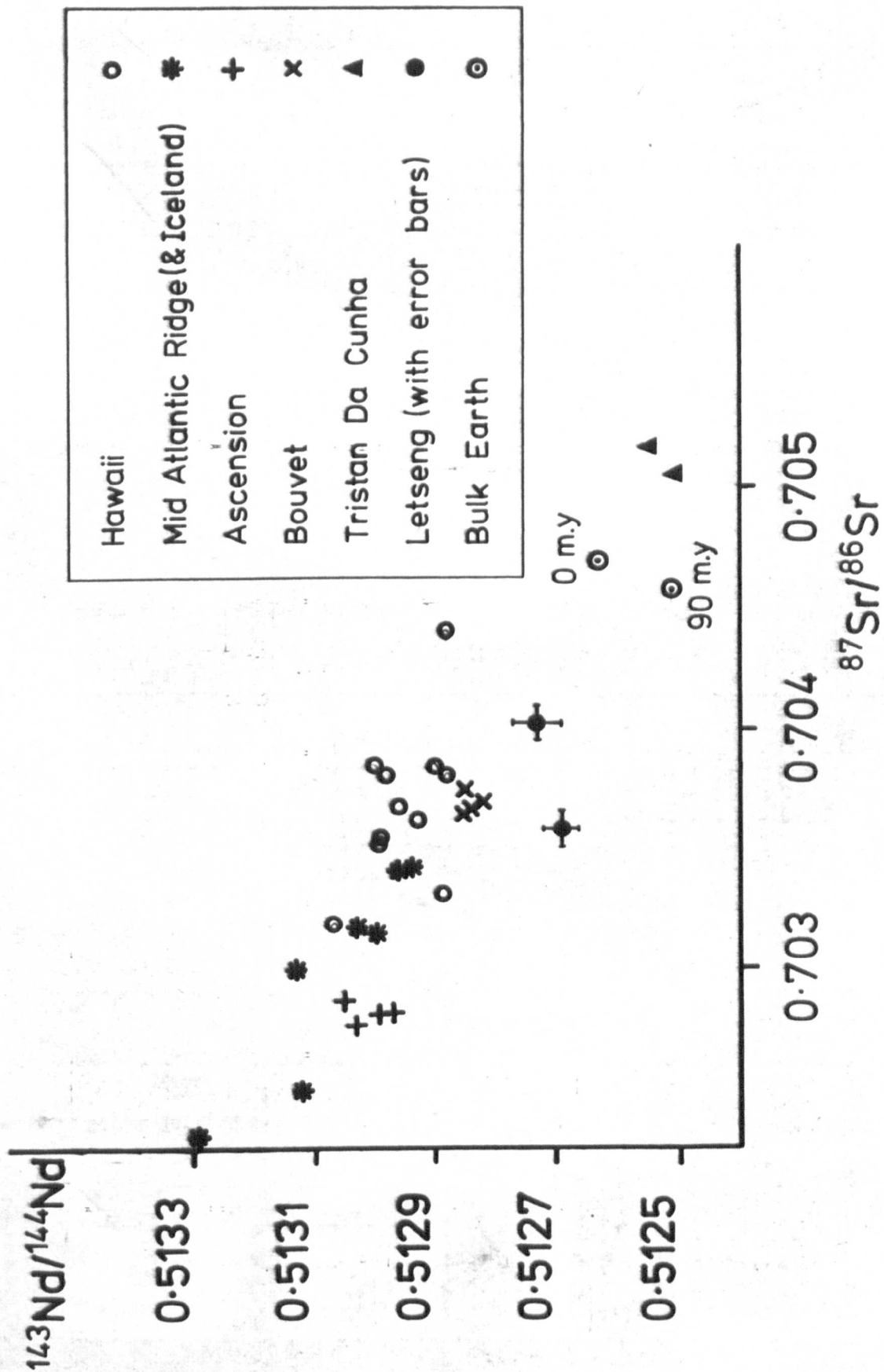


Figure 4.6:  $\Delta Nd$  and  $\Delta Sr$  plots for Letseng kimberlites and oceanic rocks.

$\Delta$  values as defined by Carter et al (1978). See text.  
Symbols and data sources as for figure 4.5

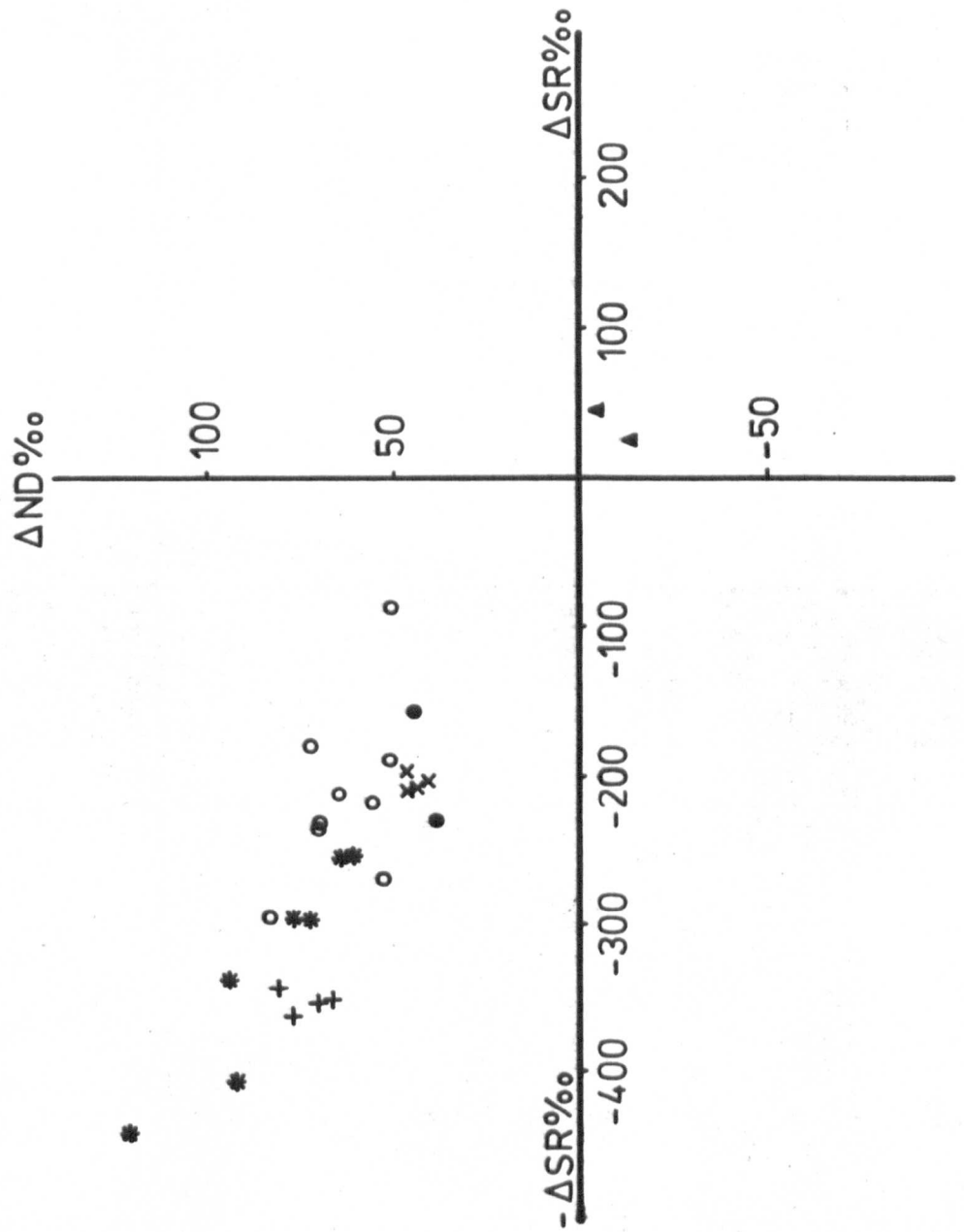
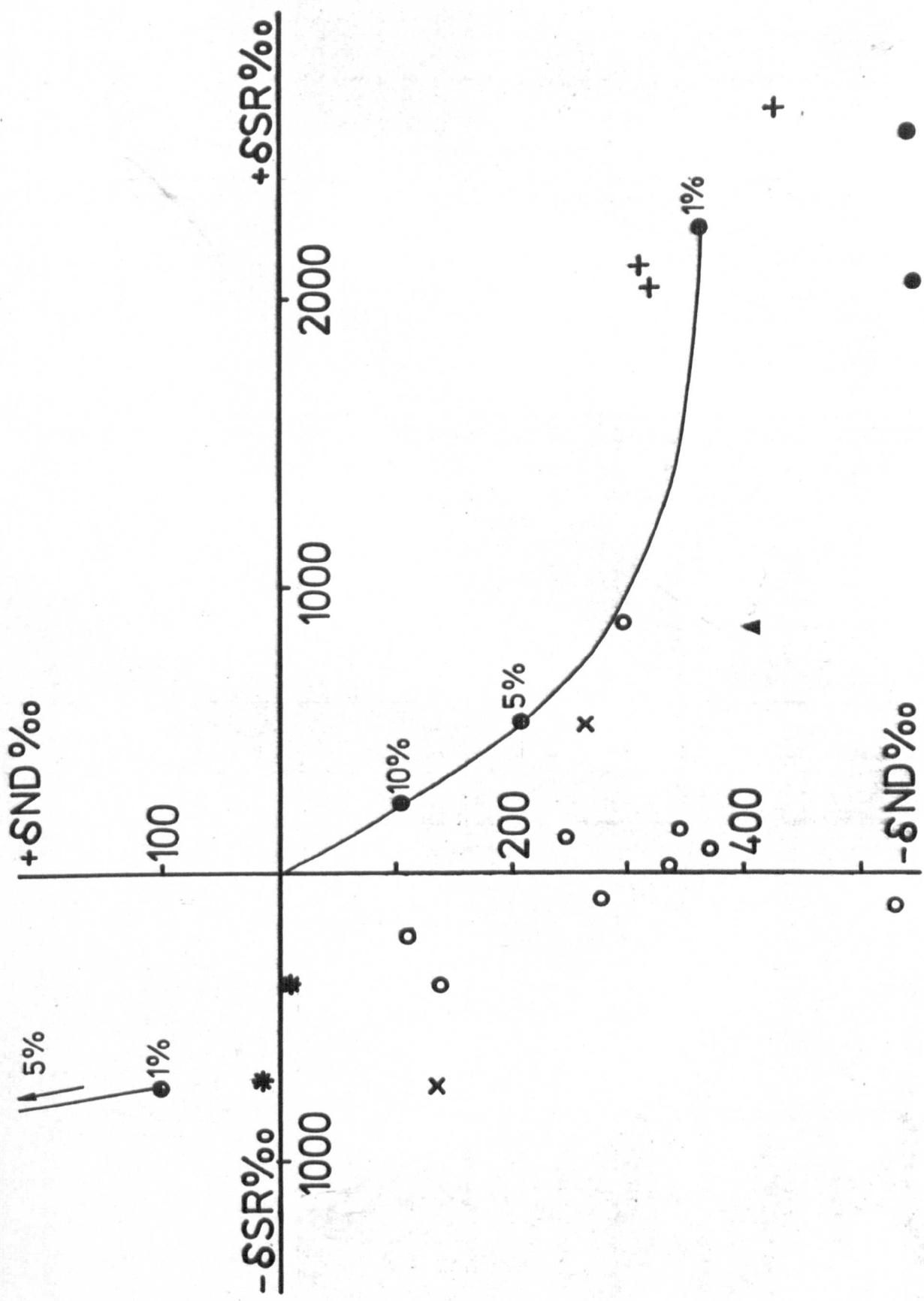


Figure 4.7:  $\delta\text{Nd}$  and  $\delta\text{Sr}$  plots for Letseng kimberlites and oceanic rocks.

$\delta$  values as defined by O'Nions et al (1977).

Symbols and data sources as for figure 4.5.

The lines connecting circled crosses are theoretical partial melting trajectories for liquid ( $+\delta\text{Sr} -\delta\text{Nd}$  quadrant) and residue ( $-\delta\text{Sr} +\delta\text{Nd}$  quadrant) in a model mantle (see O'Nions et al 1977).



CHAPTER 5Megacrysts and Xenocrysts

Considerable interest has been generated in the study of megacrysts in kimberlite, and in particular has centred on the pyroxene-ilmenite intergrowths so common at the Monastery Mine (e.g. Nixon and Boyd, 1973; Boyd and Nixon, 1973; Gurney et al., 1979). However, these studies and those on megacrysts from other kimberlites (e.g. North America - Egger et al. 1979; Botswana - Shee 1979; Frank Smith (South Africa) - Pasteris et al., 1979) treat these intergrowths as one part of a megacryst suite composed of garnets, sub-calcic diopside, enstatite and olivine, in addition to ilmenite, ilmenite-silicate intergrowths and silicate inclusions in silicate.

It is now generally agreed that these megacrysts are the early phenocrysts crystallised from a liquid undergoing cooling and Fe enrichment. Argument continues as to the extent and composition of the differentiating liquid, but present evidence suggests this may be kimberlitic.

Discrete monomineralic nodules from the Letseng kimberlites have been described earlier by Bloomer and Nixon (1973). The nodules described here are found in +1 cm concentrate from the diamond recovery plant. They consist of reddish-brown pyrope, grey-green clinopyroxene, pale grass-green enstatite and smoky brown bronzite together with olivine, chromite and rare ilmenite. The pyrope often has a rounded boxlike shape with numerous sub-parallel internal fractures and a thin black kelyphite rind. The clinopyroxenes were shown by Boyd (1973) to be sub-calcic diopside. These rounded cleavage-free megacrysts sometimes attain a size of 10 cm and rarely may show a porphyroclastic texture (Plate 5.1. See Chapter 6 for a description of this texture). Another group of very similar sub-calcic diopsides have now been found in concentrate from the Main Pipe

garnetiferous kimberlite. These nodules are characterised by scattered garnets protruding from the worn surface. The garnets are a bright orange colour. Coexisting orthopyroxene has been found in one nodule. The enstatite and bronzite grains are usually much smaller (< 1 cm) but still generally larger than orthopyroxenes of similar composition in peridotite nodules. These pyroxene grains show the results of natural etching with ridges developed parallel to the cleavage (Plate 10c in 'Lesotho Kimberlites' 1973). In addition some notable textures are seen: cross-cutting pyrope veinlets (Plate 5.2); exsolved lamellar clinopyroxene (Plate 5.3) and intergrown rods of pyrope, chrome diopside and chromite.

Heavy mineral concentrates indicate that most of these megacrysts are present in both the Main and Satellite Pipes. The sub-calcic diopside and the larger pyrope megacrysts are only found in the Main Pipe garnetiferous kimberlite. This may be the result of selective concentration by the host kimberlite as was shown to be the case with large and dense xenoliths (see Chapter 4). However in view of the fact that ultrabasic xenoliths from the two pipes show some definite petrographic and chemical differences (see Part II) the absence of sub-calcic diopside (and pyrope) megacrysts from the Satellite Pipe may be a real phenomenon.

Investigation of the heavy mineral concentrates has revealed another group of clinopyroxene grains. These clinopyroxenes often have irregular grain margins similar to chrome diopsides presumed to derive from disaggregated ultrabasic nodules. By analogy these diopsidic-salitic clinopyroxenes may also derive from some disaggregated rock. These xenocrysts are never larger than 1 cm, but sometimes consist of an aggregate of smaller grains. Biotite is rarely a minor intergrown or included phase and opaque oxides (ilmenite) are also found. The clinopyroxene is coloured various shades of green to dark green (related to Fe content) and is usually strongly pleochroic to brown. Schiller structures are also common. The unusual

TABLE 5.1: Mail Pipe. Sub-Calcic Diopside Suite Mineral Analyses

Sub-Calcic Diopside Suite											GT	OP
	*	56.01	54.72	55.69	55.62	55.50	55.91	55.09	GT	OP		
SiO <sub>2</sub>	55.48	56.01	54.72	55.69	55.62	55.50	55.91	55.09	42.83	57.30		
TiO <sub>2</sub>	0.22	0.32	0.35	0.32	0.30	0.30	0.37	0.33	0.82	0.19		
Al <sub>2</sub> O <sub>3</sub>	2.13	2.56	2.48	2.48	2.70	2.59	2.59	2.65	20.77	1.05		
Cr <sub>2</sub> O <sub>3</sub>	0.50	0.31	0.28	0.38	0.24	0.23	0.24	0.17	1.72	0.27		
FeO	4.64	5.64	5.56	5.72	5.80	5.73	5.81	6.40	7.47	6.17		
MnO	0.14	0.11	0.14	0.13	0.16	0.14	0.14	0.16	0.19	0.13		
MgO	21.51	20.29	19.90	20.42	20.18	19.61	19.16	16.10	21.83	33.47		
CaO	13.47	13.91	13.96	14.06	13.93	14.51	15.03	17.77	4.68	1.73		
Na <sub>2</sub> O	1.34	1.77	1.74	1.64	1.75	1.74	1.80	2.07	-	0.63		
NiO	0.15	0.06	0.08	0.08	0.06	0.06	0.06	0.03	-	0.16		
Total	99.61	100.98	99.21	100.92	100.74	100.44	101.11	100.77	100.31	101.10		
Si	1.99	1.99	1.98	1.98	1.98	1.99	1.99	1.99	3.03	1.97		
Ti	0.01	0.01	0.01	0.01	0.01	0.01	0.01	0.01	0.04	0.00		
Al	0.09	0.11	0.11	0.10	0.11	0.11	0.11	0.11	1.73	0.04		
Cr	0.01	0.01	0.01	0.01	0.01	0.01	0.01	0.01	0.10	0.01		
Fe	0.14	0.17	0.17	0.17	0.17	0.17	0.17	0.19	0.44	0.18		
Mn	0.00	0.00	0.00	0.01	0.00	0.00	0.00	0.01	0.01	0.00		
Mg	1.15	1.07	1.07	1.08	1.07	1.05	1.02	0.87	2.30	1.71		
Ca	0.52	0.53	0.54	0.54	0.53	0.56	0.57	0.69	0.35	0.06		
Na	0.09	0.12	0.12	0.11	0.12	0.12	0.12	0.15	-	0.04		
Ni	0.00	0.00	0.00	0.00	0.00	0.00	0.00	0.00	-	0.00		
Total	4.00	4.01	4.01	4.02	4.01	4.02	4.00	4.03	8.00	4.01		
Ca/(Ca+Mg)	0.310	0.330	0.335	0.331	0.332	0.347	0.360	0.442	0.839	0.906		
Mg/(Mg+Fe)	0.892	0.865	0.864	0.864	0.861	0.859	0.855	0.818				
Ca%	28.65	29.9	30.3	30.0	29.9	31.4	32.5	39.3	11.45	3.26		
Fe%	7.71	9.5	9.4	9.5	9.7	9.7	9.8	11.0	14.26	9.07		
Mg%	63.64	60.7	60.2	60.5	60.3	59.0	57.7	49.6	74.28	87.67		

\* N.B. This sub-calcic diopside nodule (NL506) contains coexisting garnet and orthopyroxene shown in the last two columns of the Table.



TABLE 5.2: Satellite Pipe. Discrete Mineral Analyses - Pyroxenes

	Orthopyroxene										Chrome Diopside										Diopside-Salite #2																						
SiO <sub>2</sub>	56.06	56.10	56.63	56.18	56.86	56.97	56.82	57.63	57.61	54.01	53.46	53.73	53.94	54.09	54.72	53.59	52.24	51.75	51.28	49.96	54.01	53.46	53.73	53.94	54.09	54.72	53.59	52.24	51.75	51.28	49.96	54.01	53.46	53.73	53.94	54.09	54.72	53.59	52.24	51.75	51.28	49.96	
TiO <sub>2</sub>	0.27	0.19	0.21	0.17	0.13	0.12	0.21	0.00	0.05	0.32	0.33	0.32	0.10	0.03	0.00	0.01	0.07	0.06	0.24	0.00	0.32	0.33	0.32	0.10	0.03	0.00	0.01	0.07	0.06	0.24	0.00	0.32	0.33	0.32	0.10	0.03	0.00	0.01	0.07	0.06	0.24	0.00	
Al <sub>2</sub> O <sub>3</sub>	1.01	0.82	1.24	1.34	1.34	1.31	1.20	0.80	0.81	2.63	3.09	3.46	1.78	2.09	1.76	1.32	2.01	1.53	1.83	0.28	2.63	3.09	3.46	1.78	2.09	1.76	1.32	2.01	1.53	1.83	0.28	2.63	3.09	3.46	1.78	2.09	1.76	1.32	2.01	1.53	1.83	0.28	
Cr <sub>2</sub> O <sub>3</sub>	0.00	0.00	0.05	0.05	0.17	0.18	0.33	0.34	0.34	1.27	1.82	2.32	1.38	2.07	1.39	0.14	0.06	0.03	0.00	0.00	1.27	1.82	2.32	1.38	2.07	1.39	0.14	0.06	0.03	0.00	0.00	1.27	1.82	2.32	1.38	2.07	1.39	0.14	0.06	0.03	0.00	0.00	
FeO	10.22	10.26	7.91	7.38	6.30	5.50	5.15	4.45	4.28	3.92	2.19	1.72	1.87	1.71	1.30	6.13	9.35	12.09	13.01	21.61	3.92	2.19	1.72	1.87	1.71	1.30	6.13	9.35	12.09	13.01	21.61	3.92	2.19	1.72	1.87	1.71	1.30	6.13	9.35	12.09	13.01	21.61	
MnO	0.16	0.16	0.11	0.10	0.14	0.13	0.13	0.14	0.10	0.11	0.09	0.06	0.08	0.06	0.07	0.27	0.45	0.17	0.25	0.25	0.11	0.09	0.06	0.08	0.06	0.07	0.27	0.45	0.17	0.25	0.25	0.11	0.09	0.06	0.08	0.06	0.07	0.27	0.45	0.17	0.25	0.25	
MgO	31.03	31.37	31.90	32.41	33.06	33.51	34.58	35.79	36.25	15.83	15.20	15.30	16.82	16.26	16.58	15.45	13.25	12.05	10.83	6.37	15.83	15.20	15.30	16.82	16.26	16.58	15.45	13.25	12.05	10.83	6.37	15.83	15.20	15.30	16.82	16.26	16.58	15.45	13.25	12.05	10.83	6.37	
CaO	1.00	0.79	1.26	1.66	1.48	1.38	0.95	0.31	0.29	18.68	20.03	20.09	21.44	20.90	22.65	22.48	22.16	20.78	22.36	21.25	18.68	20.03	20.09	21.44	20.90	22.65	22.48	22.16	20.78	22.36	21.25	18.68	20.03	20.09	21.44	20.90	22.65	22.48	22.16	20.78	22.36	21.25	
Mn <sub>2</sub> O	0.25	0.19	0.32	0.34	0.32	0.24	0.20	0.06	0.06	2.33	2.27	2.45	1.43	2.04	1.24	0.62	0.59	0.81	0.68	0.58	2.33	2.27	2.45	1.43	2.04	1.24	0.62	0.59	0.81	0.68	0.58	2.33	2.27	2.45	1.43	2.04	1.24	0.62	0.59	0.81	0.68	0.58	
NiO	0.05	0.05	0.13	0.19	0.07	0.10	0.06	0.03	0.03	0.07	0.07	0.08	0.04	0.09	0.01	0.05	0.00	0.01	0.02	0.03	0.07	0.07	0.08	0.04	0.09	0.01	0.05	0.00	0.01	0.02	0.03	0.07	0.07	0.08	0.04	0.09	0.01	0.05	0.00	0.01	0.02	0.03	
Total	100.05	99.93	99.76	99.82	99.87	99.24	99.63	99.55	99.82	99.17	98.55	99.53	98.88	99.34	99.72	100.06	100.00	99.56	100.42	100.29	99.17	98.55	99.53	98.88	99.34	99.72	100.06	100.00	99.56	100.42	100.29	99.17	98.55	99.53	98.88	99.34	99.72	100.06	100.00	99.56	100.42	100.29	
Si	1.97	1.97	1.98	1.96	1.97	1.98	1.96	1.98	1.97	1.98	1.96	1.95	1.97	1.97	1.98	1.98	1.96	1.97	1.95	1.98	1.98	1.96	1.95	1.97	1.97	1.98	1.98	1.96	1.97	1.95	1.98	1.98	1.96	1.95	1.97	1.97	1.98	1.98	1.96	1.97	1.95	1.98	
Ti	0.01	0.01	0.01	0.00	0.00	0.00	0.01	0.00	0.00	0.01	0.01	0.01	0.00	0.00	0.00	0.00	0.00	0.00	0.01	0.00	0.01	0.01	0.01	0.00	0.00	0.00	0.00	0.00	0.00	0.01	0.00	0.01	0.01	0.01	0.00	0.00	0.00	0.00	0.00	0.00	0.01	0.00	
Al	0.04	0.03	0.05	0.06	0.05	0.05	0.05	0.03	0.03	0.11	0.13	0.15	0.08	0.09	0.08	0.06	0.09	0.07	0.08	0.01	0.11	0.13	0.15	0.08	0.09	0.08	0.06	0.09	0.07	0.08	0.01	0.11	0.13	0.15	0.08	0.09	0.08	0.06	0.09	0.07	0.08	0.01	
Cr	0.00	0.00	0.00	0.00	0.00	0.00	0.01	0.01	0.01	0.04	0.05	0.07	0.04	0.06	0.04	0.00	0.00	0.00	0.00	0.00	0.04	0.05	0.07	0.04	0.06	0.04	0.00	0.00	0.00	0.00	0.00	0.04	0.05	0.07	0.04	0.06	0.04	0.00	0.00	0.00	0.00	0.00	
Fe	0.30	0.30	0.23	0.22	0.18	0.16	0.15	0.13	0.12	0.12	0.07	0.05	0.06	0.05	0.04	0.19	0.29	0.38	0.41	0.72	0.12	0.07	0.05	0.06	0.05	0.04	0.19	0.29	0.38	0.41	0.72	0.12	0.07	0.05	0.06	0.05	0.04	0.19	0.29	0.38	0.41	0.72	
Mn	0.00	0.00	0.00	0.00	0.00	0.00	0.00	0.00	0.00	0.00	0.00	0.00	0.00	0.00	0.00	0.00	0.00	0.01	0.01	0.01	0.00	0.00	0.00	0.00	0.00	0.00	0.00	0.00	0.00	0.01	0.01	0.00	0.00	0.00	0.00	0.00	0.00	0.00	0.00	0.00	0.01	0.01	
Mg	1.63	1.64	1.66	1.69	1.71	1.73	1.78	1.83	1.85	0.86	0.83	0.83	0.92	0.88	0.90	0.85	0.74	0.68	0.61	0.38	0.86	0.83	0.83	0.92	0.88	0.90	0.85	0.74	0.68	0.61	0.38	0.86	0.83	0.83	0.92	0.88	0.90	0.85	0.74	0.68	0.61	0.38	
Ca	0.04	0.03	0.05	0.06	0.05	0.05	0.04	0.01	0.01	0.73	0.79	0.78	0.84	0.82	0.88	0.89	0.89	0.85	0.91	0.90	0.73	0.79	0.78	0.84	0.82	0.88	0.89	0.89	0.85	0.91	0.90	0.73	0.79	0.78	0.84	0.82	0.88	0.89	0.89	0.85	0.91	0.90	
Na	0.02	0.01	0.02	0.02	0.02	0.02	0.01	0.00	0.00	0.16	0.16	0.17	0.10	0.14	0.09	0.04	0.04	0.06	0.05	0.04	0.16	0.16	0.17	0.10	0.14	0.09	0.04	0.04	0.06	0.05	0.04	0.16	0.16	0.17	0.10	0.14	0.09	0.04	0.04	0.06	0.05	0.04	
Ni	0.00	0.00	0.00	0.01	0.00	0.00	0.00	0.00	0.00	0.00	0.00	0.00	0.00	0.00	0.00	0.00	0.00	0.00	0.00	0.00	0.00	0.00	0.00	0.00	0.00	0.00	0.00	0.00	0.00	0.00	0.00	0.00	0.00	0.00	0.00	0.00	0.00	0.00	0.00	0.00	0.00	0.00	
Total	4.01	3.99	4.00	4.02	3.98	3.99	4.01	3.99	3.99	4.01	4.00	4.01	4.01	4.01	4.01	4.02	4.02	4.02	4.03	4.04	4.01	4.00	4.01	4.01	4.01	4.01	4.01	4.02	4.02	4.02	4.03	4.04	4.01	4.00	4.01	4.01	4.01	4.01	4.01	4.02	4.02	4.03	4.04
Ca/(Ca+Mg)	0.023	0.017	0.028	0.036	0.031	0.029	0.019	0.006	0.006	0.459	0.487	0.486	0.478	0.480	0.496	0.511	0.546	0.554	0.597	0.706	0.459	0.487	0.486	0.478	0.480	0.496	0.511	0.546	0.554	0.597	0.706	0.459	0.487	0.486	0.478	0.480	0.496	0.511	0.546	0.554	0.597	0.706	
Mg/(Mg+Fe)	0.844	0.845	0.878	0.887	0.903	0.916	0.923	0.935	0.938	0.878	0.925	0.941	0.941	0.944	0.958	0.812	0.716	0.640	0.597	0.344	0.878	0.925	0.941	0.941	0.944	0.958	0.812	0.716	0.640	0.597	0.344	0.878	0.925	0.941	0.941	0.944	0.958	0.812	0.716	0.640	0.597	0.344	
Ca#	1.9	1.5	2.4	3.2	2.8	2.6	1.8	0.6	0.5	42.6	46.6	47.0	46.3	46.5	48.4	45.9	46.1	43.9	46.9	45.0	42.6	46.6	47.0	46.3	46.5	48.4	45.9	46.1	43.9	46.9	45.0	42.6	46.6	47.0	46.3	46.5	48.4	45.9	46.1	43.9	46.9	45.0	
Fe#	15.5	15.5	12.1	11.1	9.6	8.4	7.7	6.7	6.3	7.2	4.1	3.3	3.3	3.1	2.3	10.2	15.6	20.7	21.6	36.2	7.2	4.1	3.3	3.3	3.1	2.3	10.2	15.6	20.7	21.6	36.2	7.2	4.1	3.3	3.3	3.1	2.3	10.2	15.6	20.7	21.6	36.2	
Mg#	82.6	83.0	85.5	85.7	87.6	89.0	90.5	92.7	93.2	50.2	49.2	49.7	50.4	50.4	49.3	43.9	38.3	35.4	31.6	18.8	50.2	49.2	49.7	50.4	50.4	49.3	43.9	38.3	35.4	31.6	18.8	50.2	49.2	49.7	50.4	50.4	49.3	43.9	38.3	35.4	31.6	18.8	

\*1 Contains chromite inclusion (see Table 5.4)

\*2 Contains ilmenite inclusion (see Table 5.4)

TABLE 5.3: Satellite Pipe. Discrete Mineral Analyses - Garnet

	Granulitic										Peridotitic																									
SiO <sub>2</sub>	38.71	39.67	39.80	40.29	39.99	40.19	40.30	40.13	40.54	40.50	41.42	41.89	41.83	42.59	42.44	42.55	42.69	42.36	42.31	42.45	41.89	42.95	41.74	42.68	41.93	41.95	41.90	42.85	42.20	42.32	42.95	42.74	42.64			
TiO <sub>2</sub>	0.03	0.06	0.08	0.03	0.01	0.07	0.09	0.05	0.05	0.02	0.27	0.22	1.02	0.83	0.94	0.10	0.40	0.10	0.71	0.31	0.03	0.35	0.02	0.03	0.01	0.05	0.06	0.52	0.25	0.25	0.00	0.03	0.11			
Al <sub>2</sub> O <sub>3</sub>	22.22	22.54	22.47	22.60	22.42	22.62	22.41	22.83	22.75	22.87	22.87	22.47	21.46	21.52	21.11	23.82	23.45	21.42	20.97	20.55	18.44	21.28	19.04	22.38	19.10	20.62	19.31	21.09	20.81	19.55	21.71	21.93	21.21			
Cr <sub>2</sub> O <sub>3</sub>	0.04	0.06	0.06	0.06	0.10	0.12	0.05	0.04	0.08	0.07	0.09	0.85	0.59	0.83	1.04	0.38	0.28	3.27	3.04	4.12	7.02	2.38	6.77	2.21	6.44	4.44	6.03	1.92	3.72	5.11	3.45	3.06	3.61			
FeO	30.04	24.67	20.90	23.52	20.36	19.51	19.40	16.21	16.76	19.40	14.48	11.31	10.65	8.96	8.74	8.45	8.49	7.55	7.30	6.86	6.64	6.95	6.56	6.88	6.58	6.57	6.44	6.94	6.59	6.31	6.30	6.11	5.61			
MnO	0.61	0.90	1.08	0.43	0.84	0.63	0.51	0.46	0.43	0.56	0.34	0.39	0.29	0.24	0.22	0.39	0.31	0.35	0.30	0.34	0.39	0.24	0.43	0.30	0.38	0.37	0.37	0.26	0.32	0.29	0.31	0.28	0.27			
MgO	7.83	10.21	10.50	12.13	10.76	10.94	11.12	10.74	11.85	14.17	16.52	18.94	19.78	21.14	21.30	20.81	21.18	20.81	21.51	21.25	20.86	21.93	20.72	21.78	21.04	21.16	20.77	22.52	21.53	21.37	23.20	23.75	23.26			
CaO	1.99	3.06	5.97	1.88	6.40	7.25	6.76	9.74	8.07	2.85	4.96	4.41	4.50	4.45	4.39	4.30	4.02	4.91	4.64	4.94	5.47	4.42	5.23	4.42	4.71	5.40	5.42	4.52	4.69	5.14	2.52	2.44	3.61			
Na <sub>2</sub> O	0.04	0.04	0.03	0.04	0.02	0.03	0.04	0.03	0.01	0.03	0.09	0.07	0.16	0.09	0.13	0.07	0.11	0.05	0.09	0.06	0.04	0.08	0.05	0.02	0.02	0.04	0.05	0.09	0.07	0.05	0.03	0.05	0.04			
NiO	0.05	0.03	0.02	0.04	0.02	0.04	0.03	0.03	0.02	0.03	0.00	0.01	0.04	0.01	0.03	0.01	0.01	0.00	0.01	0.01	0.01	0.00	0.02	0.00	0.00	0.02	0.01	0.01	0.01	0.01	0.00	0.01	0.00	0.01		
<b>Total</b>	101.56	100.94	100.91	101.02	100.92	101.40	100.71	100.26	100.56	100.49	101.04	100.56	100.32	100.52	100.34	100.88	100.94	100.82	100.88	100.89	100.78	100.60	100.56	100.70	100.23	100.61	100.36	100.72	100.19	100.39	100.48	100.39	100.37			
Si	2.97	2.99	2.99	3.01	2.99	2.98	3.01	2.99	3.00	2.99	2.99	3.00	3.00	3.02	3.02	2.99	2.99	3.00	2.99	3.00	3.00	3.03	2.99	3.00	3.00	2.98	3.00	3.02	3.00	3.01	3.01	2.99	3.00			
Ti	0.00	0.00	0.00	0.00	0.00	0.00	0.01	0.00	0.00	0.00	0.01	0.01	0.05	0.04	0.05	0.01	0.02	0.01	0.04	0.02	0.00	0.02	0.00	0.00	0.00	0.00	0.03	0.01	0.01	0.00	0.00	0.01				
Al	2.01	2.00	1.99	1.99	1.98	1.98	1.97	2.00	1.98	1.99	1.95	1.90	1.81	1.80	1.77	1.97	1.94	1.79	1.75	1.71	1.56	1.77	1.61	1.85	1.61	1.73	1.63	1.75	1.74	1.64	1.79	1.81	1.76			
Cr	0.00	0.00	0.00	0.00	0.01	0.01	0.00	0.00	0.00	0.00	0.00	0.05	0.03	0.05	0.06	0.02	0.02	0.18	0.17	0.23	0.40	0.13	0.38	0.12	0.36	0.25	0.34	0.11	0.21	0.29	0.19	0.17	0.20			
Fe	1.93	1.55	1.31	1.47	1.27	1.21	1.21	1.01	1.04	1.20	0.87	0.68	0.64	0.53	0.52	0.50	0.50	0.45	0.43	0.41	0.40	0.41	0.39	0.40	0.39	0.39	0.39	0.41	0.39	0.38	0.37	0.36	0.33			
Mn	0.04	0.06	0.07	0.03	0.05	0.04	0.03	0.03	0.03	0.03	0.02	0.02	0.02	0.01	0.01	0.02	0.02	0.02	0.02	0.02	0.02	0.01	0.03	0.02	0.02	0.02	0.02	0.02	0.02	0.02	0.02	0.02	0.02			
Mg	0.90	1.16	1.17	1.35	1.20	1.21	1.24	1.19	1.31	1.56	1.78	2.02	2.11	2.23	2.25	2.18	2.21	2.19	2.26	2.24	2.22	2.30	2.21	2.28	2.24	2.24	2.21	2.36	2.28	2.27	2.42	2.48	2.44			
Ca	0.16	0.25	0.48	0.15	0.51	0.58	0.54	0.78	0.64	0.22	0.38	0.34	0.35	0.34	0.33	0.32	0.30	0.37	0.35	0.37	0.42	0.33	0.40	0.33	0.36	0.41	0.42	0.34	0.36	0.39	0.19	0.18	0.27			
Na	0.01	0.01	0.00	0.01	0.00	0.00	0.01	0.00	0.00	0.00	0.01	0.01	0.02	0.01	0.02	0.01	0.01	0.01	0.01	0.01	0.01	0.00	0.01	0.01	0.00	0.01	0.01	0.01	0.01	0.01	0.01	0.01				
Ni	0.00	0.00	0.00	0.00	0.00	0.00	0.00	0.00	0.00	0.00	0.00	0.00	0.00	0.00	0.00	0.00	0.00	0.00	0.00	0.00	0.00	0.00	0.00	0.00	0.00	0.00	0.00	0.00	0.00	0.00	0.00	0.00				
<b>Total</b>	8.02	8.02	8.01	8.01	8.01	8.01	8.02	8.00	8.00	7.99	8.01	8.03	8.03	8.03	8.03	8.02	8.01	8.02	8.02	8.01	8.02	8.01	8.02	8.00	7.98	8.03	8.02	8.05	8.02	8.02	7.99	8.02	8.04			
Mg/(Mg+Fe)	0.317	0.425	0.472	0.478	0.485	0.500	0.505	0.541	0.557	0.565	0.670	0.749	0.768	0.808	0.813	0.814	0.816	0.831	0.840	0.847	0.849	0.849	0.849	0.849	0.851	0.852	0.852	0.853	0.854	0.858	0.868	0.874	0.881			
Cr/(Cr+Al)	0.001	0.002	0.002	0.002	0.003	0.004	0.002	0.001	0.002	0.002	0.003	0.025	0.018	0.025	0.032	0.011	0.008	0.093	0.089	0.118	0.203	0.070	0.192	0.062	0.184	0.126	0.173	0.058	0.107	0.149	0.096	0.085	0.103			
Ca#	5.4	8.2	15.8	5.0	16.9	19.0	17.9	25.8	21.2	7.5	12.6	11.1	11.1	10.8	10.7	10.7	10.0	12.3	11.5	12.3	13.7	10.9	13.3	11.0	11.9	13.4	13.7	10.9	11.7	12.8	6.3	6.0	8.9			
Fe#	65.0	53.6	45.5	49.9	43.7	41.2	41.1	34.5	35.4	40.9	29.3	22.9	21.1	17.5	17.1	17.2	17.0	15.4	14.7	14.0	13.7	13.9	13.8	13.9	13.8	13.5	13.4	13.6	13.5	12.9	12.9	12.3	11.3			
Mg#	29.6	38.2	38.7	45.1	39.4	39.8	41.0	39.7	43.4	51.7	58.1	66.0	67.8	71.7	72.2	72.1	73.0	72.3	73.8	73.7	72.6	75.2	72.9	75.1	74.3	73.1	72.9	75.5	74.8	74.3	80.8	81.6	79.8			

TABLE 5.4: Satellite Pipe Discrete Mineral Grains - Chromite and Ilmenite

	Chromite				*1	Ilmenite			*2
SiO <sub>2</sub>	0.02	0.03	0.02	0.97		0.02	0.03	0.04	
TiO <sub>2</sub>	0.32	0.93	1.23	0.03		55.11	47.14	52.81	
Al <sub>2</sub> O <sub>3</sub>	12.98	13.16	9.92	16.60		0.42	0.21	0.04	
Cr <sub>2</sub> O <sub>3</sub>	52.22	48.85	55.78	53.04		2.13	0.46	0.03	
Fe <sub>2</sub> O <sub>3</sub>	5.76	8.71	7.01	3.56		4.08	14.39	1.58	
FeO	13.69	13.17	13.22	11.81		25.15	31.88	46.17	
MnO	0.64	0.61	0.64	0.57		0.24	0.24	0.33	
MgO	12.49	12.89	13.06	14.66		13.40	6.21	0.52	
CaO	0.00	0.00	0.00	0.43		0.00	0.00	0.01	
Na <sub>2</sub> O	0.00	0.02	0.01	0.02		0.04	0.02	0.04	
NiO	0.16	0.20	0.17	0.02		0.16	0.03	0.00	
Total	98.28	98.47	101.06	101.71		100.76	100.61	101.57	
Si	0.00	0.00	0.00	0.03		0.00	0.00	0.00	
Ti	0.01	0.02	0.03	0.00		0.94	0.85	0.98	
Al	0.50	0.50	0.37	0.60		0.01	0.01	0.00	
Cr	1.34	1.25	1.41	1.28		0.04	0.01	0.00	
Fe <sup>3+</sup>	0.15	0.23	0.18	0.09		0.07	0.26	0.03	
Fe <sup>2+</sup>	0.37	0.36	0.35	0.30		0.48	0.64	0.96	
Mn	0.02	0.02	0.02	0.01		0.00	0.00	0.01	
Mg	0.60	0.62	0.62	0.67		0.45	0.22	0.02	
Ca	0.00	0.00	0.00	0.01		0.00	0.00	0.00	
Na	0.00	0.00	0.00	0.00		0.02	0.00	0.00	
Ni	0.00	0.01	0.00	0.00		0.03	0.00	0.00	
Total	2.99	3.01	2.98	2.99		2.04	1.99	2.00	
Mg/(Mg+Fe)	0.619	0.636	0.638	0.689					
Al%	25.0	25.4	19.0	30.4	FeTiO <sub>3</sub>	49.5	64.6	96.0	
Cr%	67.4	63.2	71.8	65.2	MgTiO <sub>3</sub>	46.4	22.2	2.0	
Fe <sup>3+</sup> %	7.6	11.4	9.2	4.4	Fe <sub>2</sub> O <sub>3</sub>	4.1	13.1	2.0	

\*<sup>1</sup> included in chrome diopside (see Table 5.2)

\*<sup>2</sup> included in salite (see Table 5.2)

composition of these diopsidic-salitic pyroxenes differs from that of pyroxene xenocrysts from other kimberlites. They are not considered to be of cognate origin but from the disaggregation of some unknown rock-type not represented as xenoliths in the kimberlite or recognised from the strata known to exist beneath Lesotho.

### Phase Chemistry

Electron microprobe analyses of selected grains from heavy mineral concentrates were made at Edinburgh University using a Cambridge Instruments Microscan V. Accelerating voltages were 20 Kv and specimen currents  $4 \times 10^{-8}$  A. Analyses of sub-calcic diopside megacrysts were made at Sheffield University using a Cambridge Instruments Microscan IX. Accelerating voltages were 15 Kv and  $3 \times 10^{-8}$  A. Analyses of the garnet and orthopyroxene bearing sub-calcic diopside megacryst (Table 5.3) were made at Cambridge University using the energy dispersive system Miniscan, developed within that department. Accelerating voltages and specimen currents were similar to those employed at Edinburgh University. Analyses are presented in Tables 5.1, 5.2, 5.3 and 5.4.

### Clinopyroxenes

Clinopyroxenes show a variety of compositions reflecting the petrographic differences described above. Two groups of clinopyroxenes of xenocrystic origin are shown in Figure 5.1. Green chrome diopsides almost exactly match diopside in Letseng ultramafic nodules (shown in the figure for comparison). One diopside xenocryst has a chromite inclusion whose composition (Table 5.4) is very similar to the chromites in peridotite (see Chapter 7).

The second group of xenocrystic clinopyroxene appears to be of unknown exotic origin. These pyroxenes (Figure 5.1) show a compositional trend from diopside towards ferrosalite ( $Mg/(Mg+Fe) = 0.812 - 0.344$ ).

The Ca/(Ca+Mg) ratio is nearly constant at 0.46; TiO<sub>2</sub> is low and usually <0.1 wt.%; Cr<sub>2</sub>O<sub>3</sub> is consistently low (<0.14 wt.%) and is less than the detection limits in two grains; and Na<sub>2</sub>O is low (although relatively constant. 0.58-0.81 wt.%). The structural formulae indicate that the most Fe-rich compositions contain a considerable amount of acmite component.

This Fe-enrichment trend suggests an igneous fractionation sequence but the pyroxenes do not compare with those from intrusive bodies like the Bushveld complex or the Skaergaard intrusion, which typically are more aluminous and less calcic. One pyroxene xenocryst has an inclusion of ilmenite (Table 5.4) whose composition (Figure 5.7) plots well outside the kimberlite ilmenite field (Haggerty, 1975). It is characterised by low MgO, Fe<sub>2</sub>O<sub>3</sub> and Cr<sub>2</sub>O<sub>3</sub> wt.% and plots close to FeTiO<sub>3</sub> which is the field for basaltic ilmenites (Haggerty, op.cit.). In the absence of further evidence these xenocrysts are inferred to derive from rocks of basaltic composition crystallised under low temperature plutonic conditions involving fractionation and Fe-enrichment.

The sub-calcic diopside megacrysts from this study and Boyd (1973) (Figures 5.2 and 5.3a) display a trend of Fe-enrichment (Mg/(Mg+Fe) = 0.88-0.82) and increasing Ca/(Ca+Mg) ratio (0.31-0.44). Although the Ca/(Ca+Mg) ratio matches that in some diopsides from peridotites, the Mg/(Mg+Fe) ratio is consistently lower. It is worthy of note that compositions at the Fe-rich end of this sequence probably require small amounts of ferric iron to balance Na in acmite. Phlogopite in kimberlite shows a similar trend towards higher fO<sub>2</sub> (Chapter 2) and ilmenites in other megacryst studies already mentioned trend from MgTiO<sub>3</sub> towards FeTiO<sub>2</sub> and Fe<sub>2</sub>O<sub>3</sub> (with decreasing Mg/(Mg+Fe) in coexisting silicate).

Two nodules plot to the more Mg-rich side of this trend: one represents the garnet-sub-calcic diopside megacrysts at the low Ca/(Ca+Mg) end of the trend; the other from Boyd (1973) at intermediate Ca/(Ca+Mg). These analyses may possibly represent analytical error but the possibility exists that they are relicts of a second parallel more magnesian fractionation trend.

A linear trend between Mg/(Mg+Fe) and Ca/(Ca+Mg) was shown by Nixon and Boyd (1973) and is confirmed and extended by analyses from the present study (Figure 5.3b). This trend was related by these workers to an igneous fractionation sequence with progressive enrichment in Fe as crystallisation proceeds to lower temperature (higher Ca/(Ca+Mg)). The two points mentioned above deviate from this linear relationship and may lie on a parallel but more magnesian trend.

In view of the rarity of ilmenite at Letseng it is interesting to note that no sub-calcic diopside with Ca/(Ca+Mg) between 0.36 and 0.44 has been found at Letseng. Nixon and Boyd (1973) state that this is the range of diopside composition more often associated with ilmenite. Comparison with the megacryst association at Monastery (Gurney et al., 1979) and elsewhere (op.cit.) confirms this conclusion.

### Orthopyroxene

These compositions reflect the petrographic grouping into pale brown bronzites (Mg/(Mg+Fe) = 0.84-0.90) and pale green enstatites (Mg/(Mg+Fe) > 0.90). The enstatites may in some cases be derived from ultrabasic nodules, but the bronzites are distinct (except for two rare Fe-rich nodules) and their slightly more Ca-rich (> 1 wt.%) composition implies different conditions of equilibration or crystallisation.

## Garnet

Grains from the mineral concentrates have widely varying compositions (Figure 5.4 and 5.5) reflecting several different modes of origin. The compositions have been plotted to show the variations in relation to colour (Figure 5.4) and classification, according to the scheme of Dawson and Stephens (1975, 1977) (Figure 5.5). The colour classification was loosely constrained due to personal bias and variation in grain size, but is similar to that used by De Beers to identify kimberlitic (pyrope) and non-kimberlitic (almandine) garnets in kimberlite. Apart from some orange garnets and a single pink (= pale lilac?) garnet, this plot demonstrates the clear distinction between almandine garnets derived from the disaggregation of basement granulites (see Chapter 10) and the pyrope garnets of the kimberlite association. The statistical classification of Dawson and Stephens (op.cit.) does not clearly distinguish between these two groups as the granulite garnets classify as type 3 - calcic pyrope-almandine, which is found in many xenoliths of the kimberlite association. The type 5 magnesian almandine is however, not found in ultrabasic nodules, but does occur in eclogites. The classification does not account for MnO which in the granulite garnets is up to twice that in the peridotite garnets (0.2-0.4 wt.%). The grouping previously noted is again apparent if MnO is considered. It is also worth remarking that no eclogites are known from Letseng.

Among the garnets of the kimberlite association many of the compositions correspond to garnets in peridotites from Letseng (cf. Chapter 7) but one group show more Mg-rich compositions and another group trend towards more Fe-rich compositions (at constant Ca). The first group are of lilac colour and in the plot of  $\text{Cr}_2\text{O}_3$  v CaO wt.% these garnets fall to the low side of CaO trend of Hornung and Nixon (1973). This compositional variation

agrees very well with the deep lilac colour development (Figure 5.6).

These writers attributed the origin of these knorringitic garnets to disaggregated ultradepleted mantle xenoliths. The lilac garnets in contrast fall off the CaO trend and are similar in composition to the CaO-poor garnets included in diamonds (Gurney and Switzer, 1973; Meyer and Svisero, 1975; Prinz et al. 1975; Gurney et al. 1979).

The garnets trending towards Fe-enriched compositions may correspond with Fe-rich peridotite garnets such as those at Matsoku (Cox et al. 1973) and are also found at Letseng (see Chapter 7) but the relatively high  $TiO_2$  (sometimes <0.5 wt.%) indicates that these garnets may be similar to garnet megacrysts from other kimberlites (Nixon and Boyd, 1973; Shee, 1979; Gurney et al., 1979; Robey, 1979) from southern Africa.

#### Ilmenite

Only two ilmenite xenocrysts have been analysed. These indicate similar compositions to other kimberlitic ilmenites (e.g. Haggerty, 1975) with  $Fe_2O_3 < 15$  wt.%,  $Cr_2O_3 < 2.2$  wt.%, and  $MgO > 6$  wt.% (Figure 5.7). It is not possible on such limited data to suggest any trends but these results are compatible with the interpretation of other megacryst studies already mentioned. The trend is from  $MgTiO_3$  towards  $FeTiO_3$  and  $Fe_2O_3$  with decreasing  $Mg/(Mg+Fe)$  in coexisting silicate (Gurney et al., 1979).  $Cr_2O_3$  has a minimum value at  $MgO = 8$  wt.% (Haggerty, 1975) or 9 wt.% (Shee, 1979) but increases at both lower and higher MgO concentrations. The Letseng ilmenites more nearly fit the hyperbolic curve of Haggerty (op.cit.).

#### Temperatures of Megacryst Crystallisation

The sub-calcic diopside megacrysts display a considerable range in  $Ca/(Ca+Mg)$  ratio which may be related, assuming equilibrium with orthopyroxene, to the temperature of crystallisation by comparing with the experimental results of Davis and Boyd (1966) for the diopside solvus. This range of



Ca/(Ca+Mg) of 0.31-0.44 indicates crystallisation over the temperature range 1400°C-1050°C. It is possible in the case of the single nodule containing coexisting garnet and orthopyroxene to obtain a more accurate temperature estimate using the geothermometers of Wells (1977) or Mori and Green (1977) (see Chapter 9). These geothermometers give estimates of 1246°C and 1451°C respectively (see Chapter 9 for comparison of the two methods).

Boyd and Nixon (1973) have devised a method for estimating the equilibration temperature of orthopyroxene megacrysts which were assumed to have crystallised with clinopyroxene and garnet. An empirical curve fit was made for the temperature of orthopyroxenes in lherzolites (estimated from the Ca/(Ca+Mg) ratio of coexisting diopside) and its Ca/(Ca+Mg) ratio (Figure 5.8). This curve can then be used to interpolate the temperature of formation of single orthopyroxene grains. The plot indicates that the Letseng megacryst orthopyroxene (bronzites) have equilibrated in the temperature range 1450°C-1150°C which is in good agreement with the estimates for sub-calcic diopside megacrysts from Letseng and other studies (op.cit.).

Unlike the clinopyroxene data (Figure 5.3b) there is no linear relationship between Ca/(Ca+Mg) and Mg/(Mg+Fe) for these orthopyroxenes which might have been expected if these pyroxenes had crystallised together. However, the considerable reaction that these orthopyroxenes have had with the enclosing kimberlite magma (etched surfaces) may have caused variable amounts of re-equilibration of early formed crystals. The linear trend seen in the clinopyroxenes may thus have been partially destroyed in the orthopyroxenes. The temperature estimates obtained from the orthopyroxene megacrysts should therefore be viewed with suspicion.

It is worth noting that two groups of orthopyroxene megacrysts of differing Mg/(Mg+Fe) ratio have been described. This would accord with the observation of a possible second clinopyroxene trend.

### Summary

- (1) Xenocrysts of orthopyroxene, clinopyroxene, and garnet of peridotitic composition, and garnet of granulitic composition, are abundant.
- (2) Exotic xenocrysts of diopside-salite are of unknown origin, but coexisting ilmenites indicate a basaltic association.
- (3) CaO-poor pyrope garnet xenocrysts are similar to garnets only found as diamond inclusions.
- (4) Pyrope garnets, sub-calcic diopsides, bronzites and enstatites display similar compositional trends to megacrysts in other kimberlites.
- (5) Rare ilmenites are compositionally similar to those of the megacryst association found in other kimberlites.
- (6) The megacryst pyroxene indicate crystallisation over the temperature range 1450°-1050°C.
- (7) The sub-calcic diopsides may display a composition gap normally associated with pyroxene-ilmenite intergrowths.
- (8) There may be two parallel trends of sub-calcic diopside (and orthopyroxene) crystallisation.
- (9) Ilmenite is rare, which may be very significant in view of the TiO<sub>2</sub> rich character of the host kimberlite.

It is concluded that the megacryst suite of minerals from Letseng crystallised as early phenocrysts in the kimberlite magma as proposed for other similar suites (e.g. Nixon and Boyd, 1973; Gurney et al. 1979) but no new evidence is available in favour of a restricted magma chamber (Gurney et al., 1979) or more widespread mixture of megacrysts and interstitial liquids (Pasteris et al., 1979). The absence of ilmenite and

ilmenite-silicate intergrowths may result from resorption by the host magma, although such selective resorption seems unlikely. Alternatively the kimberlite emplacement may have occurred before the magma had cooled to the temperatures at which ilmenite and lower temperature silicates would crystallise. In any event the high  $\text{TiO}_2$  kimberlite compositions suggest that this component is now largely crystallised as groundmass perovskite.

The evidence for the possibility of two parallel clinopyroxene crystallisation trends is important because they may represent separate pulses of kimberlite.

Plate 5.1: Porphyroclastic sub-calcic diopside megacryst.  
NL563. Bar scale 1.0mm.

Plate 5.2: Crosscutting pyrope veinlet in orthopyroxene megacryst. NL529. Bar scale 0.5mm.

J

Plate 5.3: Clinopyroxene exsolution lamellae in orthopyroxene megacryst. NL537. Bar scale 0.5mm.

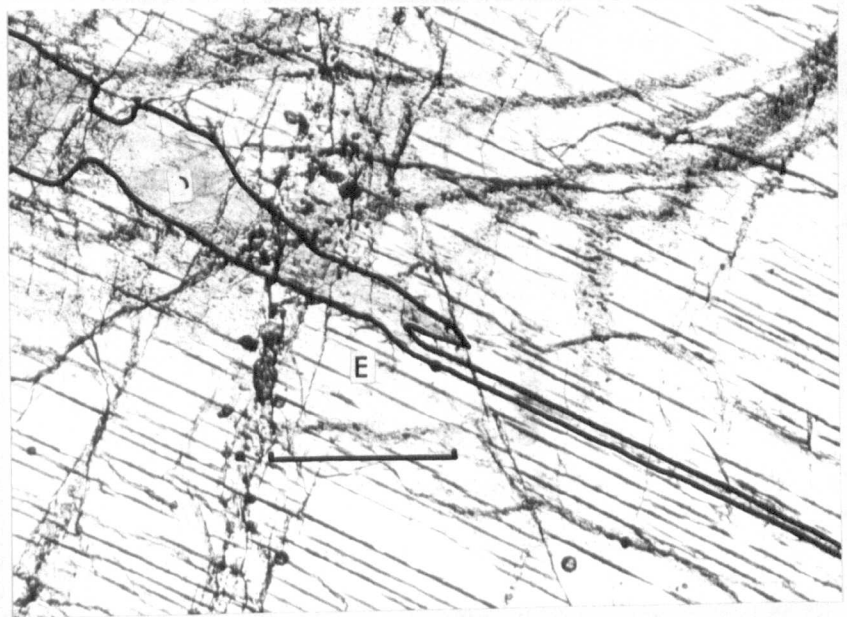
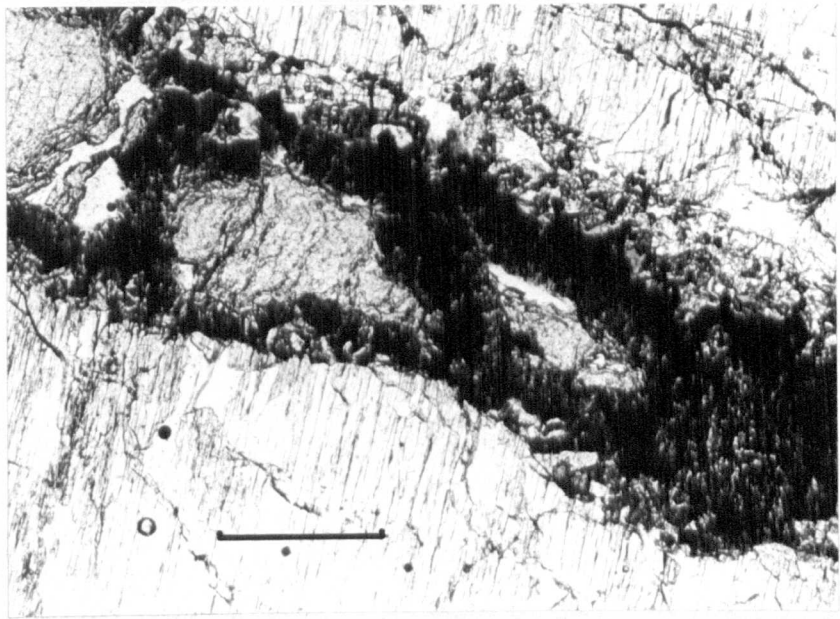
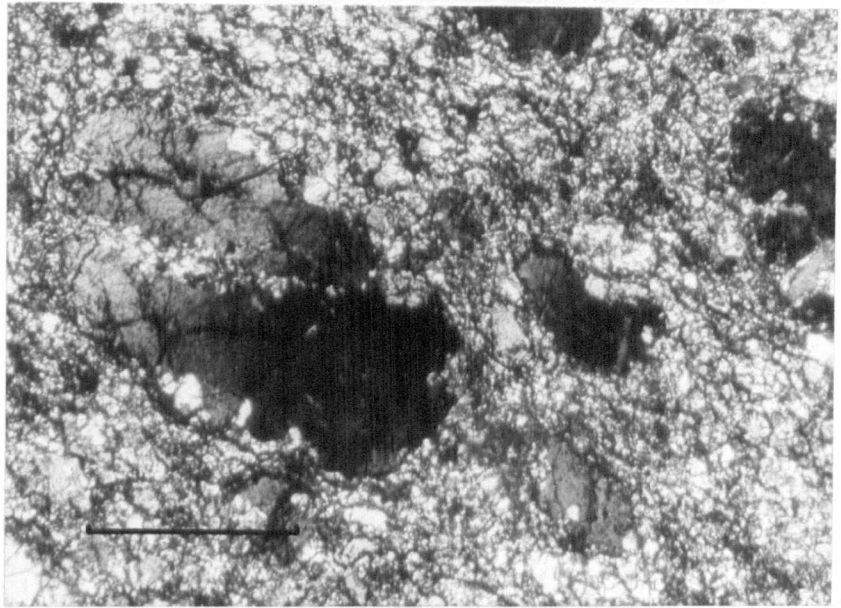


Figure 5.1:Ca - Mg - Fe plot of Cr-diopside and diopside-salite  
-ferrosalite xenocrysts in the Satellite Pipe kimberlite.  
Closed circles:Cr-diopside.  
Open circles:rims of Cr-diopside.  
Vertical crosses:salitic pyroxenes.  
Inclined crosses:rims of salitic pyroxenes.  
Dashed line demarcates the compositions of clinopyroxenes  
in peridotite xenoliths (see chapter 7).

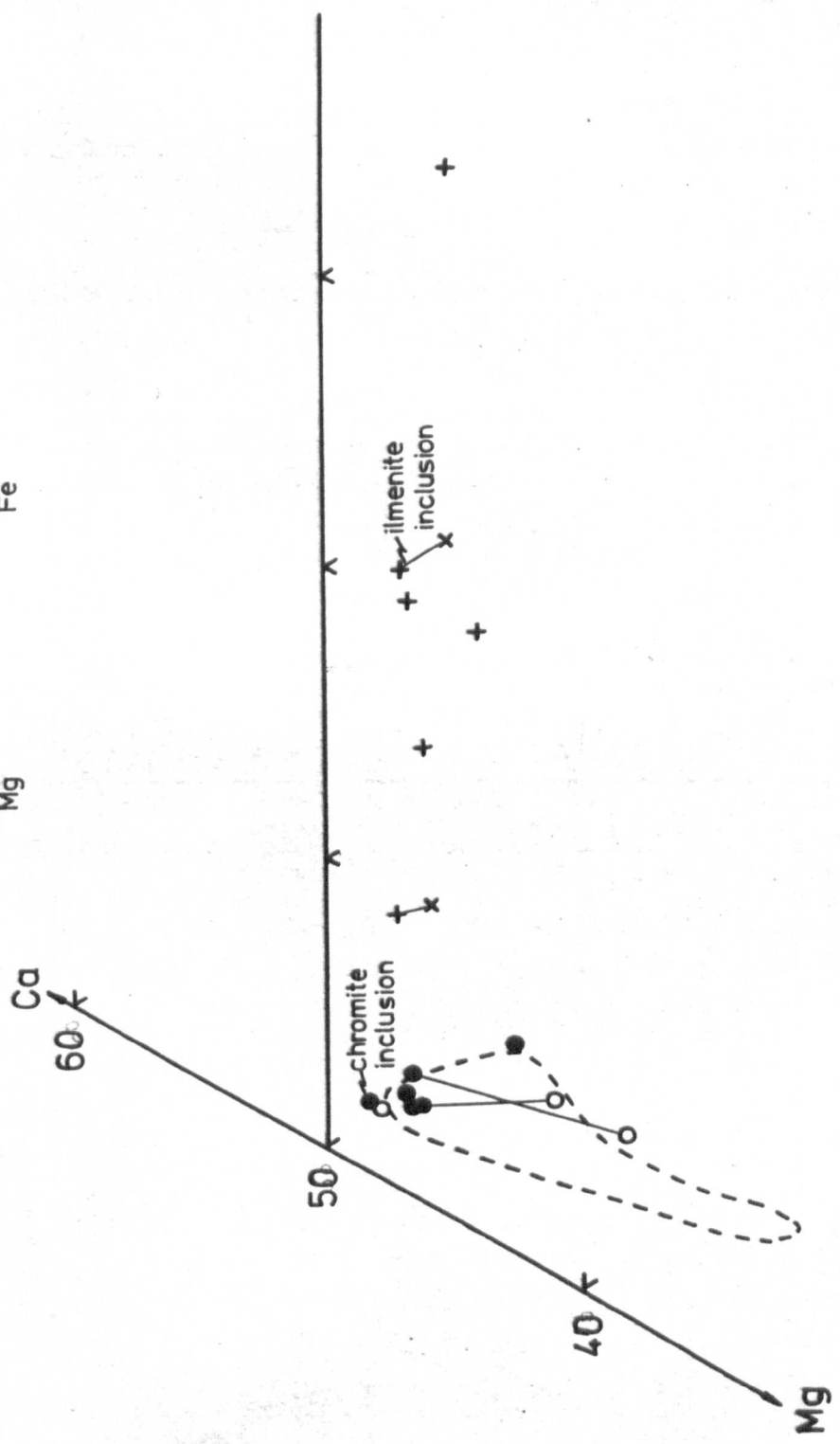
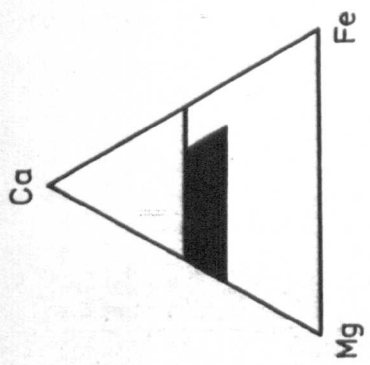


Figure 5.2:Ca - Mg - Fe plot of sub-calcic diopside and orthopyroxene xenocrysts from Letseng kimberlites.

Closed circles:orthopyroxene (this study-Satellite Pipe)

Open circles:Orthopyroxene rims.

Crosses:orthopyroxene and sub-calcic diopside (Boyd1973)

Dotted lines demarcate the areas of pyroxene compositions in peridotite xenoliths (see chapter 7).



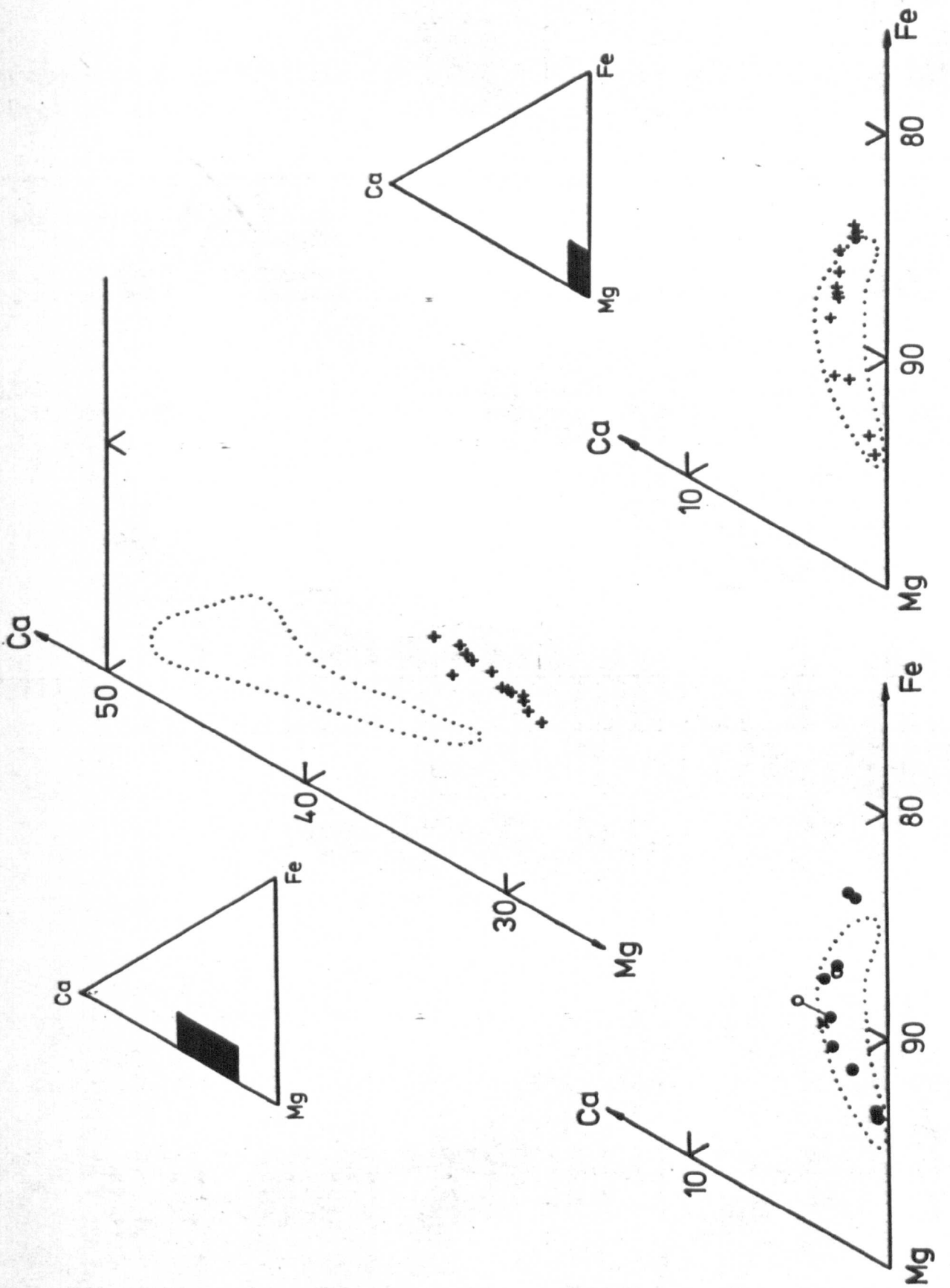


Figure 5.3a:Ca - Mg - Fe plot of sub-calcic diopside megacrysts from the Main Pipe kimberlite compared to those of Boyd (1973).

Closed circles:this study.

Dotted open circle:this study,coexisting with garnet and orthopyroxene.

Crosses:Boyd(1973).

Figure 5.3b:Mg/(Mg+Fe) v. Ca/(Ca+Mg) for sub-calcic diopside megacrysts from the Main Pipe kimberlite.  
Symbols as for figure 5.3a.

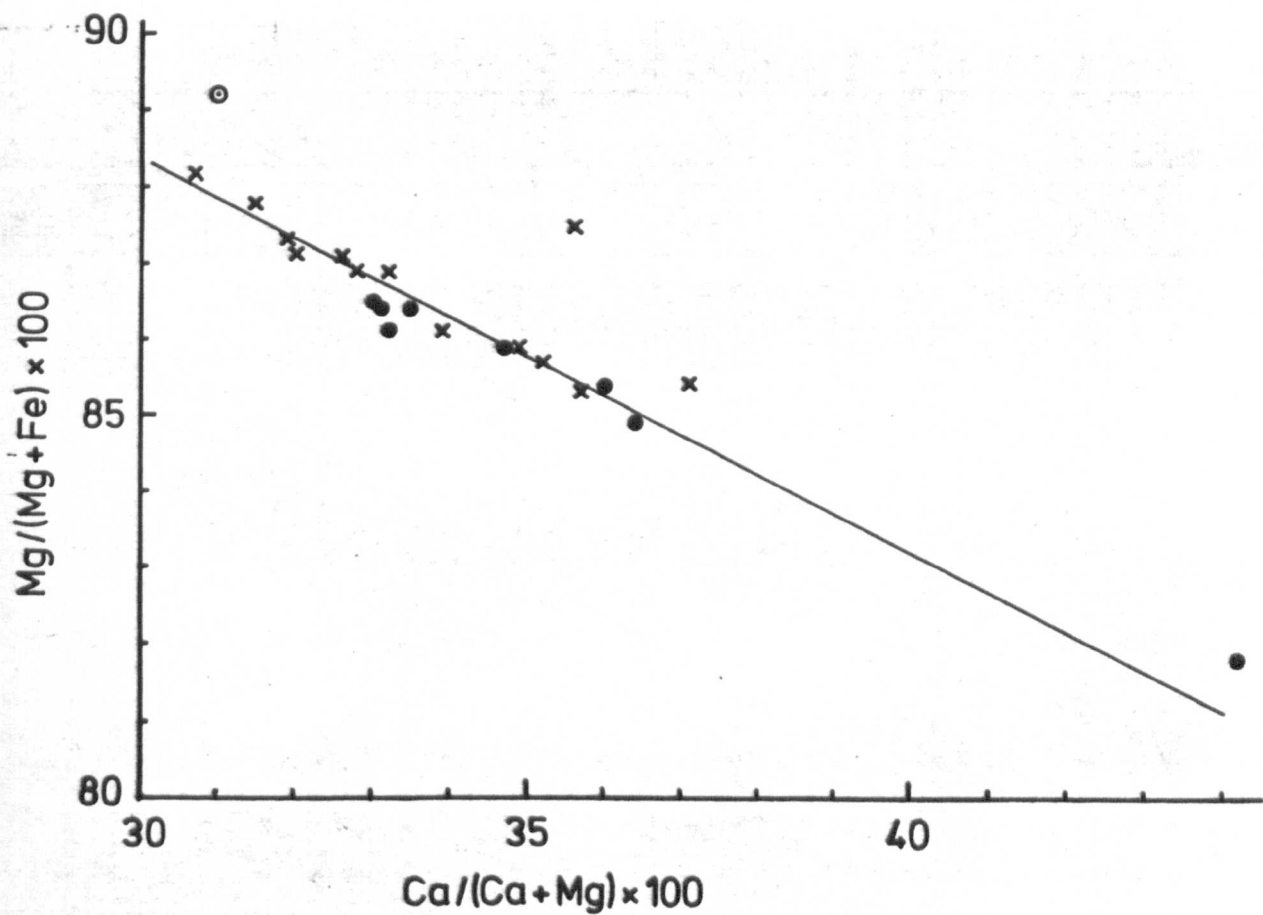
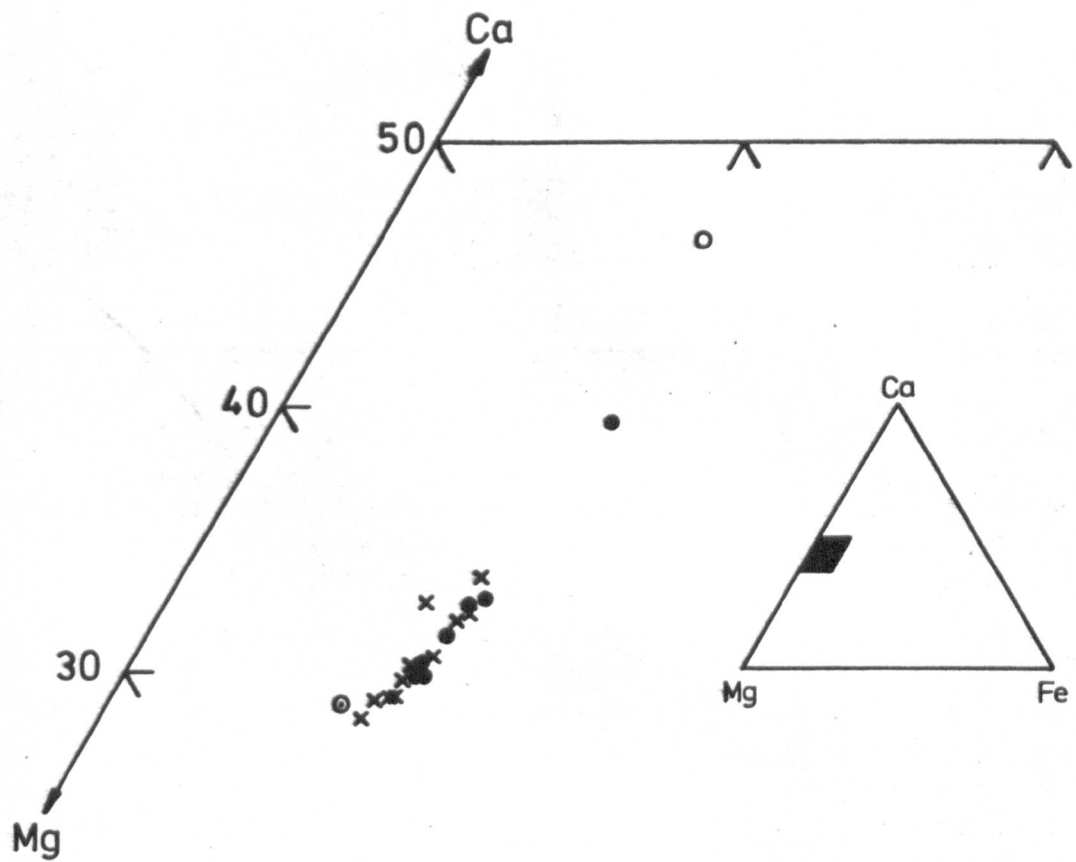


Figure 5.4:Ca - Mg - Fe plot of garnet xenocrysts in the  
Satellite Pipe kimberlite.

D:Deep lilac;W:Red lilac;L:Lilac;R:Red;O:Orange;@:Pale  
orange;P:Pink.

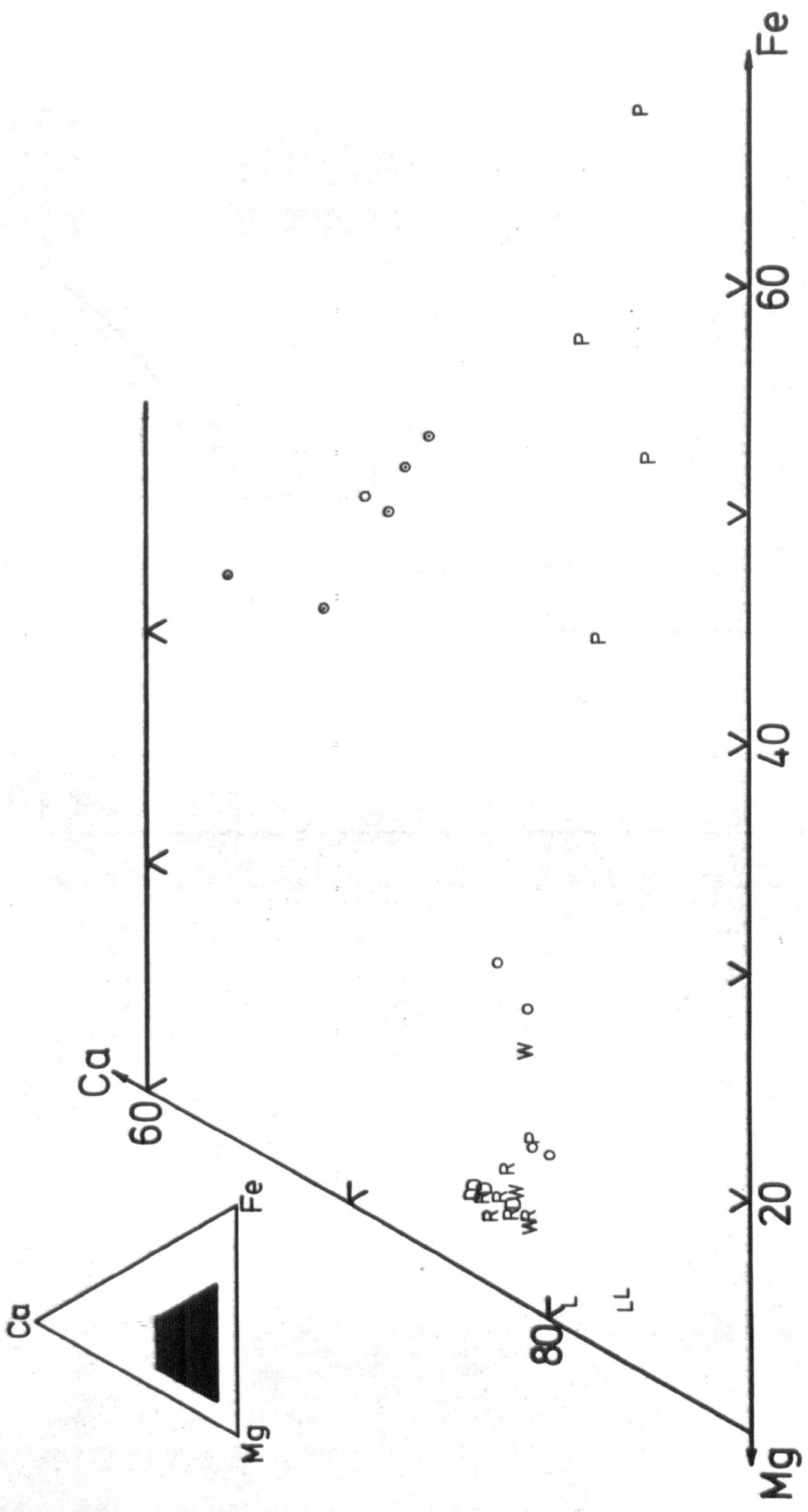


Figure 5.5:Ca - Mg - Fe plot of garnet xenocrysts in the  
Satellite Pipe kimberlite.

Closed circle:type 1 Dawson & stephens (1976)

Open circle:type 2

Vertical cross:type 3

Inclined cross:type 5

Asterisk:type 9

Triangle:type 10

Dashed line demarcates the area of granulite garnet  
compositions (see chapter 10).

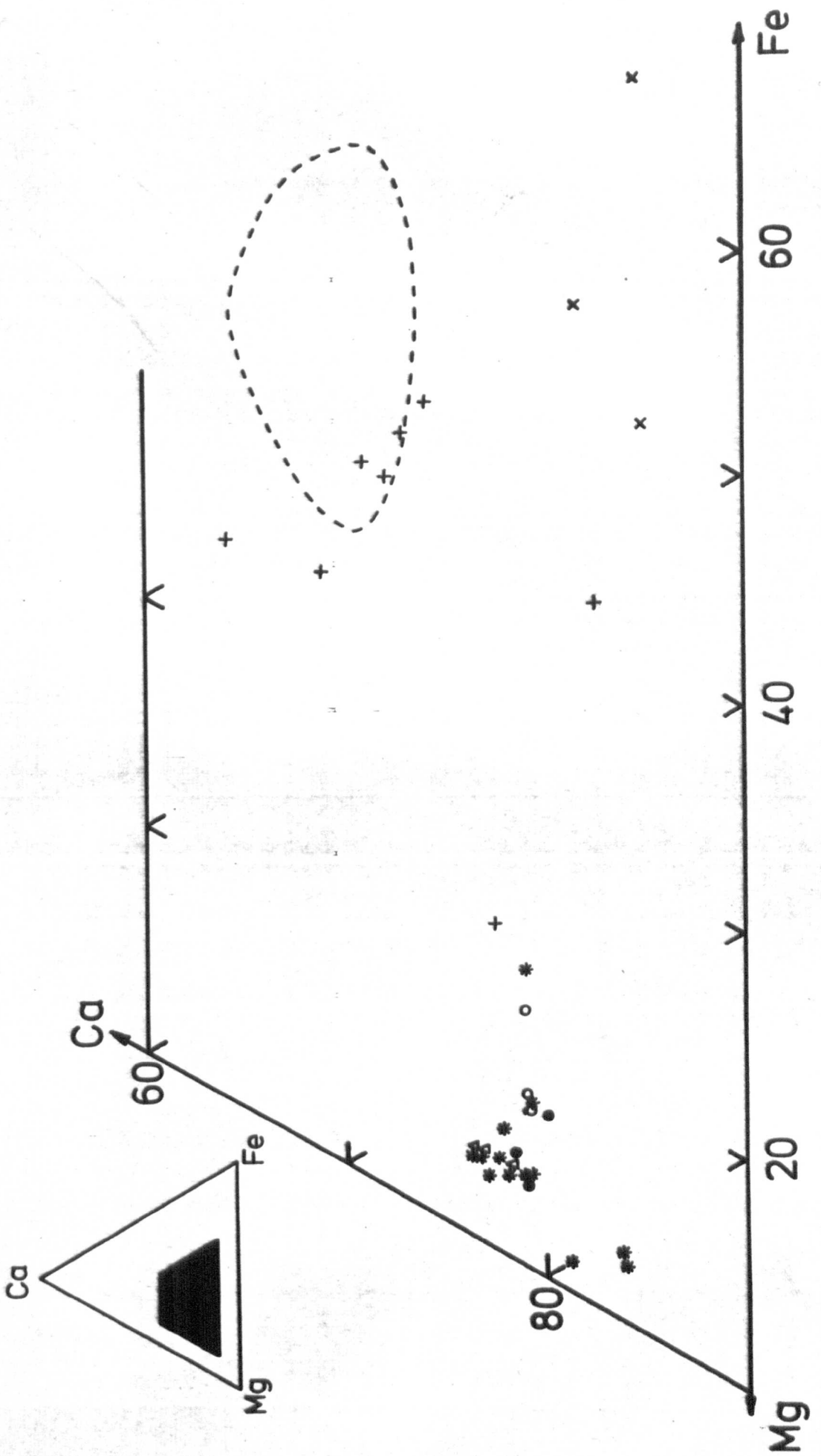


Figure 5.6:Cr<sub>2</sub>O<sub>3</sub> Wt% v. CaO Wt% & Al<sub>2</sub>O<sub>3</sub> Wt% for garnet xenocrysts in the Satellite Pipe kimberlite.  
Symbols as for figure 5.4.



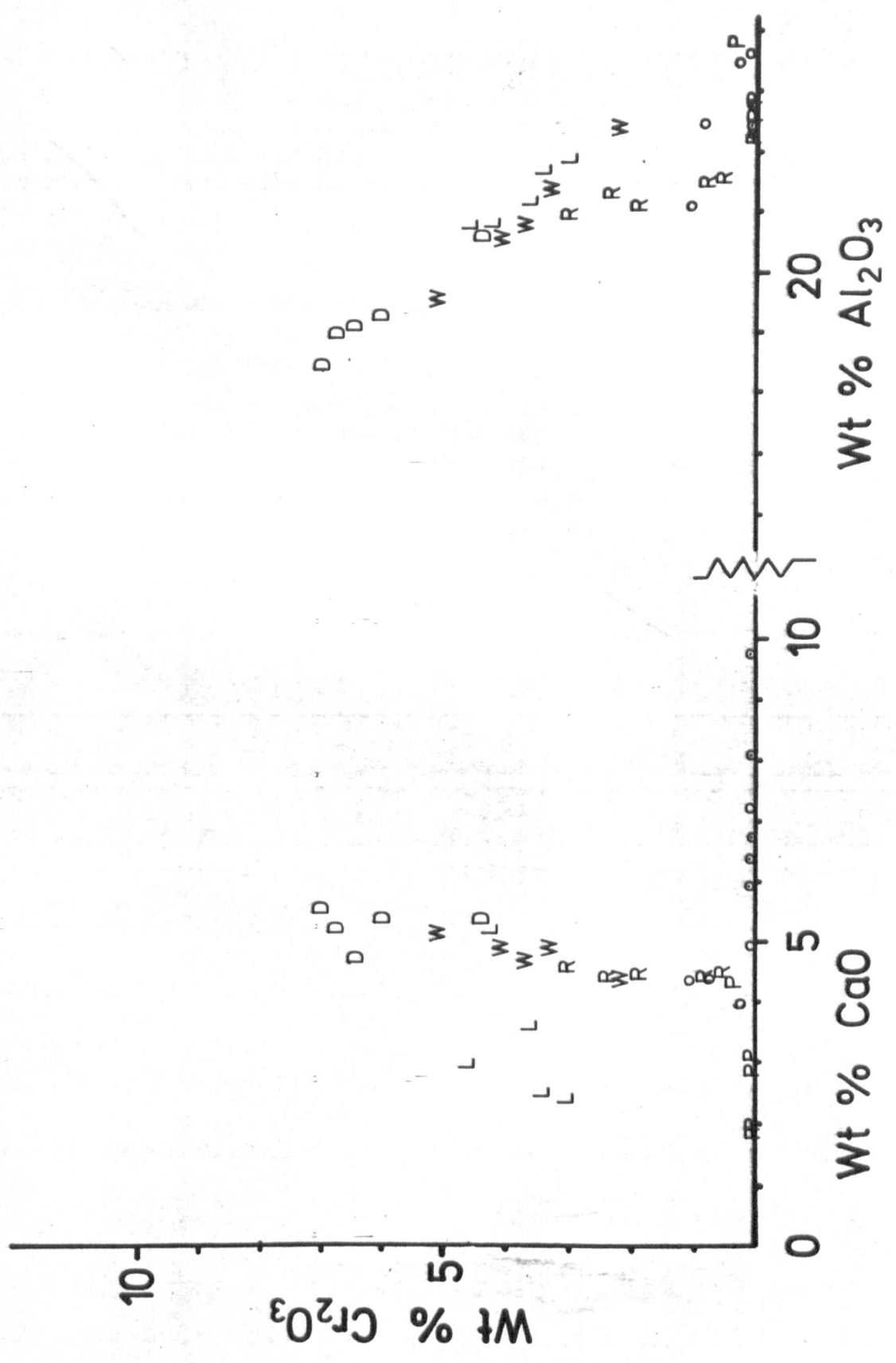


Figure 5.7:  $\text{FeTiO}_3$  -  $\text{MgTiO}_3$  -  $\text{Fe}_2\text{O}_3$  plot for ilmenite xenocrysts in the Satellite Pipe kimberlite.

Closed circles: xenocrysts in kimberlite.

Cross: inclusion in salitic pyroxene xenocryst.

Dashed line demarcates the field of kimberlitic ilmenites (Boyd & Nixon 1973).

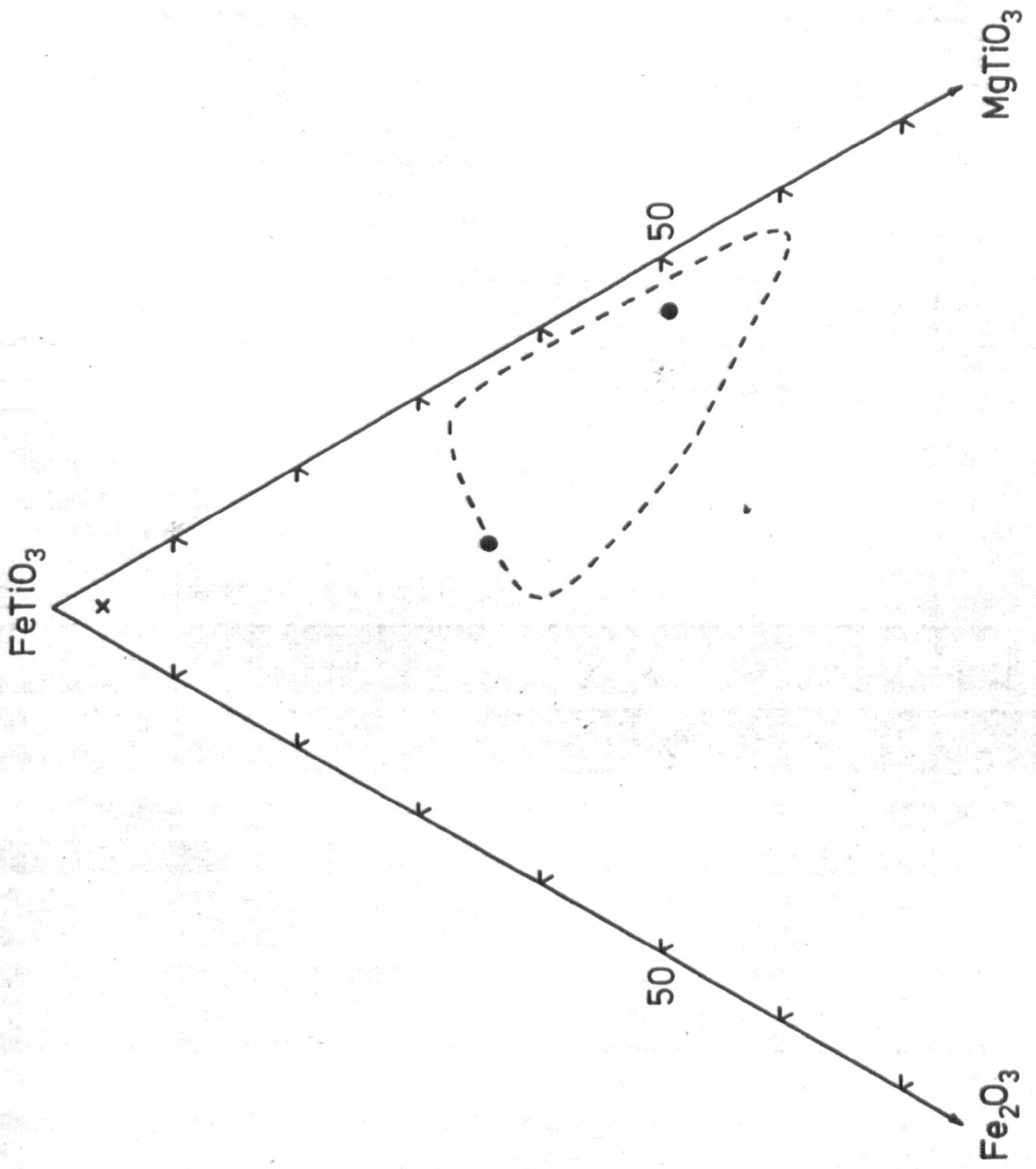
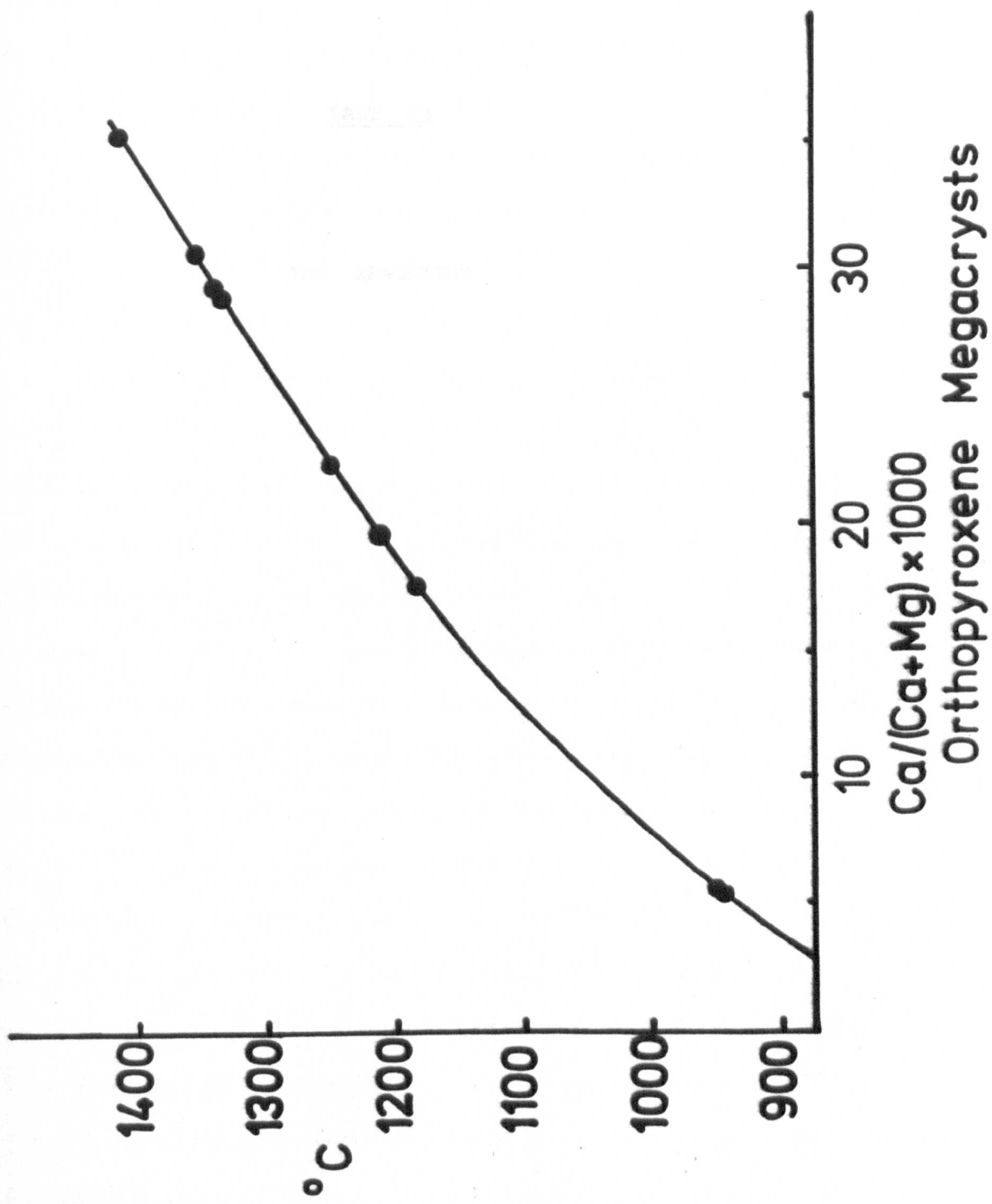


Figure 5.8:  $\text{Ca}/(\text{Ca}+\text{Mg})\times 100$  v.  $T^{\circ}\text{C}$  for orthopyroxene xenocrysts from the Satellite Pipe kimberlite.

The curve is from Boyd & Nixon (1973) and may be used to interpret xenocryst crystallisation temperatures.



Orthopyroxene Megacrysts

PART II

THE XENOLITHS

CHAPTER 6

Peridotites and Related Rocks: Petrography

The peridotite xenoliths are composed of varying proportions of the mineral assemblage olivine + orthopyroxene ± clinopyroxene ± garnet ± chromite ± phlogopite. One xenolith contains possibly primary amphibole.

Bloomer and Nixon (1973, Table 8) report the varying proportions of these peridotite xenoliths and other accidental inclusions as recorded in heavy mineral concentrates from the diamond recovery process at Letseng; however no indication is given as to whether the proportions are the same for the populations from the two pipes. Later estimates by Dawson (pers. comm.) of xenoliths in fresh concentrate from the Satellite pipe and a separate count by the writer are presented in Table 6.1 and are in broad agreement. The proportions measured indicate that coarse-textured, garnet-free, peridotite > porphyroclastic textured garnet peridotite > coarse textured garnet peridotite > megacrysts. This is in contrast to the proportions found in the Main pipe peridotites and suggests that the count of Bloomer and Nixon was probably biased in favour of the Satellite pipe; they noted that coarse textured garnet peridotites, which are common in the Main pipe kimberlite exposed underground and at surface, are strangely absent from the concentrate. They suggest this may be due to its friable nature. This may be true for some nodules, but the rarity of these nodules in the Satellite pipe and the relative abundance of deformed peridotites strongly suggests a bias in their counting towards the Satellite pipe, probably as a result of mixing of concentrates.

My collection of the largest and freshest peridotites exposed in the underground workings demonstrates a considerable difference in the proportions and nature of the various xenoliths from the two pipes. The histograms (Figures 6.1 and 6.2) show the variations of rock types for which thin

**TABLE 6.1: Proportion of Xenolithic Material in Satellite Pipe Concentrate**

	This Study	Dawson, 1979
Garnet { lherzolite harzburgite }	(coarse) 9.2	4 (18)
Garnet { lherzolite harzburgite } (porphyroclastic)	24.8	
Garnet websterite	N.D.	2 (9)
Chromite { lherzolite harzburgite }	(coarse) 51.6	15 (68)
Spinel lherzolite (granuloblastic)	6.5	N.D.
Megacrysts	7.8 (olivine)	8 (all) (5 olivine)
Granulites	N.D.	33
Basalt	N.D.	38

The figures in brackets for the proportions measured by J.B. Dawson are recalculated after ignoring the granulites and basalts



TABLE 6.2: Modal Proportions of Some Selected Peridotite Xenoliths from the Main Pipe

Sample	GT	OPX	CPX	OL	SP	PH	Textures and Comments
NLO01	4.5	25.4	0.9	68.3			Coarse
NLO07	2.3	22.1	10.3	58.1		7.3	Porphyroclastic
NLO12	14.2	31.1	0.3	54.7			Coarse. Fe-rich assemblage
NLO14	3.2	27.4		69.4			Coarse
NLO69	4.1	28.8		67.1			Coarse
NLO80	14.5	31.2	1.0	53.3			Coarse. Tabular OPX
NLO82	2.5	37.4		60.1			LAD. Mosaic porphyroclastic
NLO83	4.5	36.0		59.5		+	Coarse
NL124	0.7	24.8	0.9	72.7	0.9		Coarse. Chromite
NL125	7.5	17.9	1.1	72.2		1.2	Coarse
NL148		14.0	8.8	75.2	2.0		Granuloblastic. Altered olivine
NL196	5.4	30.9		63.7			Coarse
NL197	5.7	13.2	1.4	79.7			Coarse
NL424	4.9	36.4	+	58.8			Coarse
NL426	4.3	40.3	+	55.4			LAD. Mosaic porphyroclastic
NL441	10.3	30.6	+	59.3			Porphyroclastic
NL451	2.0	19.5		78.5			Fluidal Mosaic porphyroclastic
NL492	1.7	35.0	8.7	54.2		0.5	Coarse
NL494	4.2	18.4	0.1	77.3			Fluidal Mosaic porphyroclastic
NL495	3.1	11.5	2.3	83.1			Fluidal Mosaic porphyroclastic

GT = Garnet; OPX = Orthopyroxene; CPX = Clinopyroxene; OL = Olivine; SP = Spinel (or chromite); PH = Phlogopite

Area counted = 300-550 mm<sup>2</sup> (except NL148 = 175 mm<sup>2</sup>)

Number of points = 2000-17000 (mainly ~ 3500)

sections were made (brief descriptions are presented in Appendices 2 and 3). It is immediately apparent that the Satellite pipe shows a marked deficiency of coarse-textured garnet peridotites. This low proportion is more marked than it appears because while all the Satellite pipe samples have been sectioned this is not so for the Main pipe. Also the peridotites are generally <5 cm in size in the Satellite pipe, but are far more massive (up to 40 cm) in the Main pipe (see Plate 9c in 'Lesotho Kimberlites', 1973). These differences in the xenolith populations are further emphasised by the phase chemistry which indicates that the two pipes have sampled the upper mantle selectively at different levels. Certain textural features also indicate that these separate suites have had different deformation histories.

The mineral chemistry (see Chapter 7) shows some mainly subtle variations between the xenoliths which are not readily appreciated from the petrography. The pyrope garnet shows some slight colour variations from peridotite to peridotite, notably from red-lilac to deep purple (Cr enrichment) and brownish-red (Fe enrichment). Clinopyroxene may also reflect Cr enrichment (bright green colour) and Fe enrichment (weak pleochroism).

The modal proportions of the primary phases in several selected specimens from the Main pipe are presented in Table 6.2. This data shows these xenoliths are of the 'Common Peridotite' type (Cox et al., 1973) in which the ranges of modes are:

garnet	0-15%
orthopyroxene	10-40%
clinopyroxene	0-10%
olivine	50-85%
chromite	0- 1%
phlogopite	0- 7%

Rocks intermediate between dunite and websterite are rare but the presence of a few garnet websterites may suggest a continuous modal variation.

When chromite is the alumina-bearing phase there is a suggestion that the modal proportions of chromite and clinopyroxene are less than in the garnet bearing CP. This may imply the depletion in lower melting components in the chromite bearing rocks. However, the mineral compositions are unknown and it is possible that these components are held in the orthopyroxene.

Peridotites from both paper have suffered varying degrees of deformation which is described here using the textural classification of Harte (1977). All the textures described by Harte are represented in the Letseng peridotites and are discussed here under the headings coarse textured rocks, porphyroclastic textured rocks, and annealed rocks.

The primary phases generally show textural equilibrium but retrograde reaction of garnet with adjacent olivine or pyroxene is often well developed. Textural evidence suggests this reaction may have occurred before or during deformation (Lock and Dawson, 1980). Post-reaction and post-deformation metasomatism mainly involves the development of phlogopite but the phlogopite may also relate to late stage kimberlitic(?) veinlets which penetrate some rocks.

Other rocks such as websterites and orthopyroxenites have not been studied in detail.

## 1. Coarse Textured Rocks

(a) General Description: These rocks are characterised by mineral grains of 2-6 mm size. Smaller grains of all the anhydrous silicates except garnet occur but larger grains are rare in rocks other than dunite. The coarse texture (Harte, 1977) is an aggregate of interlocking crystals of generally irregular outline but often showing quite straight or smoothly

curving grain boundaries and occasional  $120^\circ$  triple points (Plate 6.1). Some xenoliths show a weak mineral lineation displayed by tabular orthopyroxene, but no crystallographic fabric is evident. Grain boundaries are often obscured by extensive serpentinisation of olivine. Sometimes serpentinised fractures within olivine show a persistent subparallel orientation across a xenolith.

Olivine and Orthopyroxene: These two minerals are the most abundant in these rocks as discussed above. They occur as grains in the size range indicated above, and there is no marked tendency for one mineral to be larger than the other. Olivine sometimes displays a weak pseudo-cleavage and orthopyroxene may be colourless in contrast to its more usual neutral colour.

The coarse grains are invariably anhedral although some fine recrystallised olivine grains may be euhedral (see below). Grain boundaries may be straight or smoothly curving, but are more often less regular, sometimes serrate and occasionally highly irregular. Dihedral angles at triple junctions are variable but where the grain boundaries are most regular, angles of  $120^\circ$  are found.

In rocks with tabular orthopyroxene, the orthopyroxene may display weakly rational faces with long axis grain boundaries roughly paralleling the cleavage.

Garnets: The garnets are often crudely spherical in outline but the characteristic reaction corona (described below) and alteration rim (= kelyphite) have generally obscured the grain boundaries. Nevertheless, grains do not appear to have been euhedral or even to show changes in boundary orientation at triple junctions. Some rare exceptions have been noted where dihedral angles in garnet at triple junctions are  $<180^\circ$ .

In hand specimen, slight colour changes from red to deep lilac and brownish red are apparent, but most grains appear colourless to pink in thin sections. A Cr-rich garnet in specimen NL145 (see Chapter 7) has a greenish tinge in thick section.

Clinopyroxene is by far the most common inclusion in garnet, but olivine, orthopyroxene and chromite are all seen. In one specimen (NL128) the garnet has strange rod-like inclusions of chromite which are sometimes only partially enclosed within the garnet. There is no evidence for any compositional difference between the normal primary phases and the inclusions.

Clinopyroxene: Clinopyroxene grains show a wide range in size from < 1 mm to 4 or 5 mm even within a single xenolith. Small (< 2 mm) clinopyroxene grains are found intergranular to the larger olivine and orthopyroxene grains and are consequently of highly irregular shape. Larger grains usually assume a habit similar to orthopyroxenes. Commonly, clinopyroxene occurs in close association with garnet which it may sometimes partially mantle.

Grains are usually pale green, but may be a bright green (especially in hand specimen) reflecting a high chrome content. Sometimes a faint pleochroism in shades of green may be seen, especially in thick sections, which may relate to iron content. Some clinopyroxene grains occurring as porphyroclasts in deformed Satellite pipe peridotites show lamellar twinning (Plate 6.11). Other grains in Satellite pipe peridotite (in both undeformed and deformed rocks) display a 'spongy' margin similar to those described by Carswell (1975) and Donaldson (1977).

Chromite: Chromite is a dark red-brown colour often with almost opaque rims. It varies in size from 0.1 to 4 mm and is usually anhedral. Some larger grains may be subhedral. The larger grains are intergranular to the silicates but smaller grains are more often poikilitically

enclosed in the other phases. Rare 'fingerprint' textures of vermicular chromite (Plate 6.2 ) intergrown with orthopyroxene or olivine are similar to those described by Dawson and Smith (1975). Some unusual rod-like inclusions in garnet have already been mentioned.

Chromite only rarely occurs in the same rock as garnet but an aluminous chromite is common in garnet-free xenoliths.

Phlogopite: Coarse (up to 5 mm) flakes of reddish brown strongly pleochroic phlogopite are difficult to interpret as 'primary' because of the inherent anisotropy of the crystal lattice. Plate 6.3 shows a garnet with an imposed planar boundary where it has grown against previously crystallised phlogopite. This mica is interpreted as 'primary' and is in contrast to typical 'secondary' phlogopite which replaces the silicate minerals in garnet reaction coronas (Plate 6.4), and along grain boundaries. This secondary phlogopite is a darker colour and more strongly pleochroic but both primary and secondary phlogopite show normal pleochroism unlike the tetraferriphlogopite of similar colour in the kimberlite groundmass.

(b) Deformation Effects: All the xenoliths show the effects of varying amounts of deformation as described by Boullier and Nicolas (1973), Harte et al. (1975), Boullier and Nicolas (1975), Pike and Scharzman (1977), Harte (1977) and others for nodule suites from southern Africa and America. These authors have described the various textures and show how the different minerals respond to differing strain rates.

In the coarse textured rocks most olivine grains show undulose extinction although many grains are strain-free. Diffuse deformation bands and fine deformation lamellae (Plates 6.5 and 6.6) are not uncommon. More rarely the olivine may recrystallise as strain free neoblasts along grain margins and internal features (Plate 6.7). These

neoblasts are usually  $< 0.01$  mm and of equant shape but larger neoblasts indicate progressive annealing. Strained olivine grains and sometimes unstrained neoblasts may be replaced by tabular euhedral neoblasts up to 0.5 mm in size.

Orthopyroxene also commonly shows undulose extinctions but, whereas olivine readily recrystallised to equant neoblasts, in the orthopyroxene continued deformation is more commonly accommodated by polygonsiation textures. Very sharp kink band boundaries develop between deformation bands with considerable angles of misorientation. This mode of accommodation to the prevailing strain allows new relatively strain-free sub-grain development without recrystallisation. Recrystallisation of orthopyroxene occurs only rarely in the coarse textured rocks and when seen it is usually along kink band boundaries (KBB). The recrystallised strain-free neoblasts are similar in size and shape to the equant olivine neoblasts.

Clinopyroxene very rarely exhibits undulose extinction and recrystallised neoblasts are not seen in the coarse textured rocks.

Phlogopite when present as a primary phase is very susceptible to strain and often shows considerable undulose extinctions and diffuse kink bands.

Similar deformation features to these are much rarer in the coarse textured chromite peridotites, although it should be noted that some chrome spinel peridotites (see below) may be completely annealed rocks rather than undeformed.

(c) Retrograde Reaction: In common with garnet peridotites from other kimberlites (e.g. Carswell, 1975; Carswell et al., 1979) the garnets in these Letseng rocks show the development of a considerable rind of 'kelyphite'. However, in contrast to most other localities the mineralogy of these rims is relatively unaffected by late stage metasomatic

alteration. The complex textural relations of intergrown spinel and pyroxene are usually well preserved although the pyroxene is often partially or wholly replaced by phlogopite (Plate 6.4) as in the kelyphite observed on garnet in other xenolith suites.

This reaction corona may be seen in various stages of development from very little to complete reaction and replacement of the original garnet (Plate 6.8a and b). These reaction coronas are very similar to those found in peridotites from the Lashaine volcano, Tanzania (Reid and Dawson, 1972) where there is a zonal development. Immediately adjacent to the garnet (Zone 1) is a microcrystalline aggregate that is unresolvable under the microscope; this zone is succeeded outwards by a fine grain zone of acicular pyroxene and spinel, the grains being arranged approximately normal to the garnet margin (Zone 2); the outermost Zone 3 contains relatively coarse equant spinel set in a matrix of orthopyroxene and clinopyroxene (Plate 6.9a). These zoned coronas are found most commonly between garnet and olivine but also occur between garnet and orthopyroxene, and garnet and clinopyroxene; where the primary phase involved in the reaction was pyroxene, the reaction corona pyroxene has grown in optical continuity with the earlier primary pyroxene (Plate 6.9b).

The corona assemblage suggests garnet breakdown according to the reaction:



This reaction represents the transition from garnet to spinel facies within the upper mantle which has been investigated experimentally by many authors (e.g. Green and Ringwood, 1967; O'Hara et al., 1971; Ringwood, 1975) and consequently is of some importance in elucidating the history of these rocks, especially in relation to the deformation which many of these peridotites have suffered (see below).



## 2. Porphyroclastic Textured Rocks

Included in this group of rocks are examples of porphyroclastic and mosaic porphyroclastic textures, together with subordinate variations such as fluidal and LAD (laminated and disrupted) (Harte, 1977). The group contains only garnet peridotites, although the rare evidence of deformation in chromite peridotites suggests some samples do follow a similar textural development. It may only imply that these chromite bearing rocks did not suffer a similar strain, or more simply that such rocks have not yet been found.

The texture is characterised by the development of abundant small equant olivine neoblasts surrounding unrecrystallised, strained porphyroclasts of olivine, pyroxene and garnet. Harte (op.cit.) defines the porphyroclastic texture (Plate 6.7) as that rock in which unstrained olivine neoblasts completely surround one or more strained porphyroclasts. When more than 90% of the olivine has recrystallised to equant neoblasts the texture is described as mosaic porphyroclastic. (This transition is displayed in Plates 6.10, 6.11, and 6.12). The textural transition is essentially gradational from the relatively unstrained coarse to the strongly deformed mosaic porphyroclastic textured rocks and there is no textural evidence of a separate origin for the deformed and undeformed rocks as suggested by Nixon and Boyd (1973) and Boyd and Nixon (1975).

The recrystallisation of olivine follows the pattern described in the previous section but with the further development of neoblasts at the expense of porphyroclasts. Orthopyroxene (and to a lesser extent clinopyroxene) remain largely as porphyroclasts in the mosaic olivine but show progressively more recrystallisation with increasing deformation. Kink bands in orthopyroxene become well developed with a fanned extinction pattern (Plate 6.11) being quite common.

A variant of these two textures occurs when a superimposed shear causes the development of a fluidal texture (Boullier and Nicolas, 1973) where tiny olivine and orthopyroxene neoblasts are strung out along evenly spaced shear planes (Plate 6.13a). This may give rise to a laminated and disrupted texture in which bands of olivine and orthopyroxene have segregated as a result of shearing and the deformation has been intense enough to physically disrupt garnet (Plate 6.13a). Note in Plate 6.13b, that the reaction corona minerals developed at the expense of garnet described above are strung out in the fluidal texture.

At the upper mantle temperatures in the source regions of these rocks, the mosaic olivine should rapidly anneal to generate a 'secondary' coarse texture as discussed by Harte et al. (1975). However, incorporation in rapidly ascending kimberlite magma, allows the 'freezing-in' of these disequilibrium textures. Plates 6.14 and 6.15 show rocks in which locally considerable grain growth has occurred perhaps indicating that annealing of early formed neoblasts proceeds even while deformation and recrystallisation continued. Plate 6.8a shows a rock in which the mosaic olivine is evenly annealed to about  $\frac{1}{4}$  mm size.

Chromite is only found in coarse textured rocks, but phlogopite is also present in low temperature deformed rocks. In all other respects the mineralogy of the undeformed and deformed rocks is identical. A few xenoliths containing more abundant and smaller ( $\sim 3$  mm) garnet grains have no equivalent among the undeformed rocks but no chemical differences have been found. NLO71 is the only chromite bearing peridotite which approaches a porphyroclastic texture.

Porphyroclastic textured rocks from the Satellite pipe have a distinctive mineral chemistry (see Chapter 7) and also show two petrographic differences from the Main pipe porphyroclastites. First, there is indication that the primary undeformed mineral assemblage may have been con-

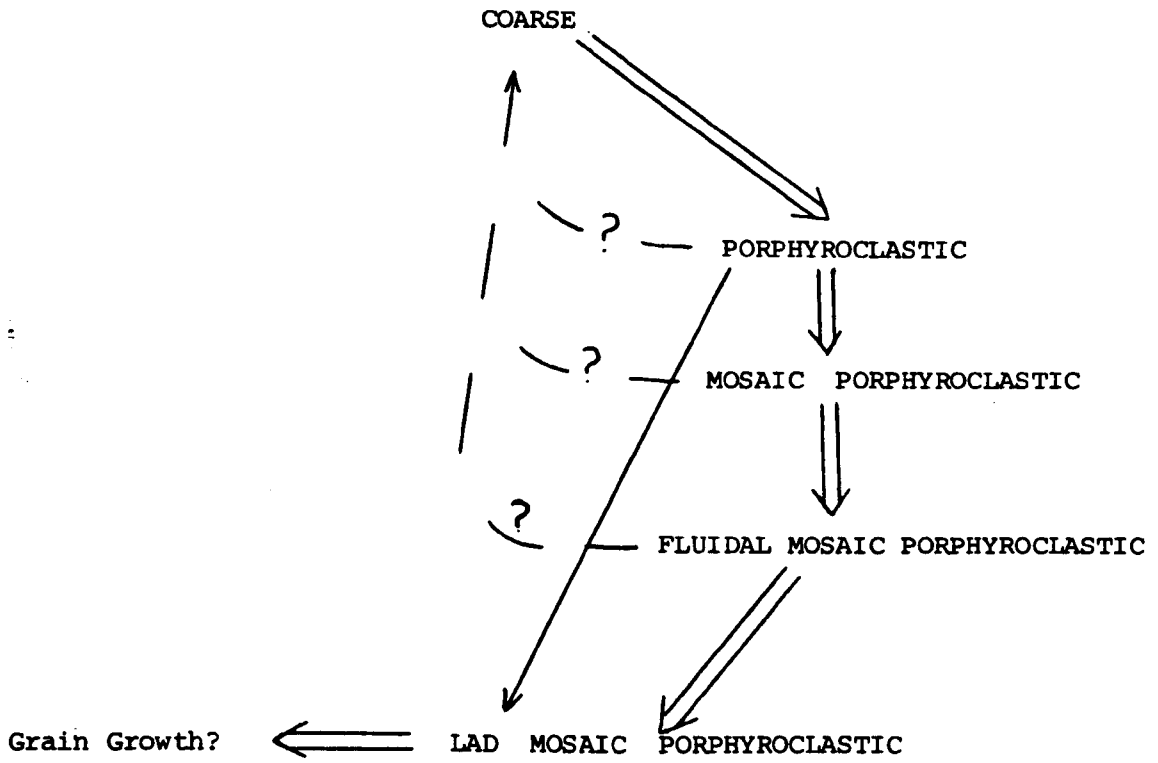
siderably coarser grained. NLO28 for example, contains olivine porphyroclasts of > 8 mm. Other rocks with more olivine neoblasts also suggest, from the porphyroclast size, a slightly coarser grained primary assemblage. Second, the clinopyroxenes in some Satellite pipe xenoliths have 'spongy' margins as mentioned above. These 'spongy' margins occur mainly in the deformed rocks, but have also been observed in coarse textured rocks. No similar feature has been observed in any peridotite xenolith from the Main pipe. It may also be significant that no fluidal textures are found in Satellite pipe xenoliths whereas more than half of the Main pipe deformed xenoliths display fluidal or LAD textures.

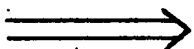
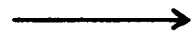
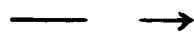
Petrographic examination of the xenolith suites from Letseng demonstrates the progressive development of porphyroclastic and mosaic porphyroclastic textured rocks from 'parental' coarse textured rocks. Further deformation to fluidal and LAD textural varieties is also apparent. Annealing and grain growth features may be seen in rocks at all stages of textural development. These observations accord with part of the deformation cycle interpreted by Harte et al. (1975) for xenoliths from the Matsoku kimberlite (see diagram overleaf).

Some of the lines of development are rather uncertain. The LAD texture may in some cases develop from a porphyroclastite rather than a fluidal mosaic porphyroclastite if the super plastic flow was imposed before the extensive development of olivine neoblasts. Some of the Letseng LAD textured xenoliths contain more olivine as porphyroclasts than would be compatible with their development from mosaic porphyroclastites.

### 3. Annealed Rocks

A small group of xenoliths characterised by the presence of aluminous spinel has been recognised in both the Main and Satellite pipes. The spinel is brown in colour and similar in appearance to those in the garnet reaction coronas described previously. These rocks are composed



-  - Major deformation cycle
-  - Minor deformation cycle
-  - Grain growth

of the assemblage spinel-orthopyroxene-clinopyroxene-olivine although a few rare garnet bearing xenoliths have also been found. Although most of the rocks display equilibrium textures, they are not coarse grained, and are different from xenoliths of similar character described by Ferguson et al. (1977) from south-east Australia and Nixon and Boyd (1979) in alnöite from Malaita, south-west Pacific.

Using the terminology of Harte (1977) the spinel peridotites would be described as granuloblastic (Plate 6.16) or tabular granuloblastic (Plate 6.17) but in the absence of garnet it may be more appropriate to use the classification of Mercier and Nicolas (1975) established for spinel peridotites from basalts. In this scheme the rocks would be described as equigranulaire.

This even-grained texture consists of a mosaic of generally unstrained, <2 mm sized grains of olivine and pyroxene with often perfect  $120^{\circ}$  triple junctions; it is interpreted as arising by extensive recrystallisation and grain growth from porphyroclastites (Harte et al., 1975; Mercier and Nicolas, 1975). Spinel assumes an intergranular texture often with 'holly leaf' shapes, but sometimes as small rounded inclusions in the other phases. Some rocks show a strong mineral fabric and elongation.

At first sight there appears to be a problem in interpreting the history of these rocks, in relation to the established deformation cycles discussed above, because no coarse textured or porphyroclastic spinel peridotites have been found in the Letseng kimberlites. However, there is some textural evidence, afforded by the study of the garnet-bearing spinel peridotites, to suggest a genetic link between the annealed spinel peridotites and the mosaic porphyroclastic garnet peridotites.

Garnet-bearing spinel peridotites contain rather small and grossly irregular shaped garnet porphyroclasts in an otherwise typical granuloblastic texture (Plate 6.18). The silicate grain size may be a little

coarser than normally associated with this texture in the spinel peridotites, but the polygonal grain shapes and the strong fabric (displayed in NL535) are more consistent with the definition of granuloblastic rather than coarse texture. In addition in NL528 (Plate 6.19) and other rocks where the garnet has variable amounts of marginal reaction corona, there are 'pools' of reaction corona minerals showing no obvious association with parental garnet. These 'pools' are too common to be attributed to coincidence from sectioning. Usually the spinels in these 'pools' match those in normal coronas surrounding garnet and as discrete grains with 'primary' textural relations to other silicates. Some have a distinct greenish tinge due to unusually high Fe and Al (see Chapter 7) and are similar to 'primary' spinels in xenoliths from alnöite at Malaita (Nixon and Boyd, 1979).

NL108 is a unique rock in the present xenolith suite. It exhibits a grossly inequigranular texture resulting from the association of granoblastic aggregates of orthopyroxene and olivine, together with orthopyroxene porphyroclasts (see Plate 6.20a). One such porphyroclast (Plate 6.20b) shows misoriented strain free segments reminiscent of porphyroclasts normally seen in mosaic porphyroclastites (cf. fanned extinction in orthopyroxene - Plate 6.11). The rock shows considerable modal variation on a thin section scale, from orthopyroxene-rich to olivine rich areas, which may relate to a gross mineral banding (the specimen size is too small to know for sure). Brown aluminous spinel is abundant as intergranular and holly leaf textured grains up to 1 mm size, but garnet is very rare as irregular shaped < 0.5 mm grains with a microcrystalline orthopyroxene corona.

This rock shows elements of both the mosaic porphyroclastic and granuloblastic textures and in addition contains aluminous spinel together with garnet remnants. This rocks is interpreted as providing the link in the

deformation cycle between the deformed garnet peridotites and the annealing spinel peridotites. It is envisaged that garnet in peridotite reacted to give a spinel-bearing assemblage; accompanying deformation (not necessarily genetically related) stripped the reaction corona minerals from the garnet, strung them out during the formation of fluidal textures (Plate 6.13b) and physically and chemically homogenised the phases; later annealing and grain growth produced the texturally equilibrated spinel peridotites. In some instances the garnet breakdown reaction has not gone to completion at the culmination of the deformation thus giving rise to peridotites containing both garnet and aluminous spinel. In other cases the deformation was not intense enough to completely homogenise the primary and secondary phases, so that 'pools' of corona minerals are preserved in the annealed texture. These xenoliths have then been incorporated in the rapidly ascending kimberlite magma thus preserving these unique textures.

Some coarse textured rocks may contain aluminous spinel (although no analyses are available) and hence might be interpreted as the culmination of the deformation cycle. These rocks show exsolution of clinopyroxene and spinel (Plate 6.21 and 6.22) from orthopyroxene, usually along kink band boundaries. This may result from readjustment to the chemical disequilibrium inherent in the solution of garnet in the orthopyroxene during garnet breakdown.

#### 4. Pyroxenites

A range of pyroxenites and garnet pyroxenites of ultrabasic character have been identified in heavy mineral concentrates at Letseng. Orthopyroxenites have a distinctive sugary texture due to the presence of coarse polygonal crystals (Plate 6.23). Minor green clinopyroxene occurs at some triple junctions. These orthopyroxenites possibly grade into garnet clinopyroxenites in which orthopyroxene is subordinate to typical pyrope garnet and bright green chrome diopside. The equilibrium texture

is not as well displayed in the coarse rocks.

These pyroxenites are difficult to distinguish from basic garnet pyroxenites of the granulite association, but in the absence of mineral chemical data they are separated on the basis of probable chrome rich clinopyroxene and garnet in the former and presence of rutile in the later (cf. Chapter 10).

##### 5. Metasomatism and Kimberlite Veining

Many rocks, especially from the Main pipe peridotites (see figure 6.2) contain small but significant amounts of strongly pleochroic dark red-brown phlogopite. This phlogopite is often seen rimming garnets and replacing minerals in the reaction corona as already described. Elsewhere in the peridotites it occurs along grain boundaries as small (< 0.5mm) often euhedral grains and aggregates. In this mode it usually occurs as the sole replacement mineral (apart from ubiquitous serpentine). Sometimes however, it may be associated along grain boundaries with a very pale green clinopyroxene of stumpy euhedral habit (< 1 mm) and often showing a perfect basal section.

This association leads to comparisons with textures seen in cross-cutting veinlets of kimberlitic (?) origin. In two deformed rocks (NLO82, NL427), these veinlets occur sub-parallel to the mineral banding. The veinlets are composed mainly of fine to coarse aggregates of phlogopite, but also contain some coarse, euhedral clinopyroxene as well as fine-grained acicular clinopyroxene (Plate 6.24). Serpentine is an abundant phase, both within the veinlet and as the alteration product of adjacent silicates.

Some other textures only rarely observed may result from partial melting of xenolith minerals. These textures show fine acicular clinopyroxene in areas of possibly quenched glass. In one specimen (NLO15) the preferential corrosion of orthopyroxene relative to olivine (Plate



6.25) is seen and elsewhere in the same rock twinned euhedral clinopyroxene has crystallised along the margin of a corroded primary orthopyroxene (Plate 6.26 a and b). The abundance of fine grained phlogopite in these veins testifies to the introduction of hydrous K-bearing fluids, but the 'calved-off' fragment of orthopyroxene separated from the vein wall by massive clinopyroxene crystallisation (Plate 6.27) indicates that physical disaggregation, as well as metasomatism, was an operative process.

Some melting of the primary peridotite minerals is evident, but it is concluded that this is the result of introduced kimberlitic liquids and not of any upper mantle process operating prior to incorporation of the peridotite fragments in the kimberlite.

#### Summary

1. Peridotite xenoliths are lherzolites and harzburgites containing garnet and/or chromite. Primary phlogopite is sometimes present.
2. Coarse textured garnet lherzolites are rare in the Satellite pipe.
3. Modal proportions show these rocks to be common peridotites (CP) but garnet websterites, pyroxenites and dunites are also found.
4. Textures vary from coarse to porphyroclastic and mosaic porphyroclastic. Fluidal and LAD varieties of the deformed rocks are only found in garnet peridotites from the Main pipe. Chromite peridotites only show coarse textures.
5. All garnets show reaction with adjacent olivine (and pyroxene). The reaction coronas contain the assemblages spinel-orthopyroxene-clinopyroxene.
6. Aluminous spinel peridotites and garnet/aluminous spinel peridotites of granuloblastic texture are interpreted to derive from normal garnet peridotite by a process involving garnet breakdown, deformation and physical homogenisation of the phases, and annealing, and accompanying chemical re-equilibration.

7. Many rocks contain minor amounts of 'secondary' phlogopite of metasomatic origin. In a few rocks kimberlitic (?) veinlets are found which sometimes show reaction with the host peridotite.

Figure 6.1: Histogram showing the rock type and texture of peridotite xenoliths from the Main and Satellite Pipe kimberlites.

Unornamented: coarse texture.

Cross ornament: porphyroclastic texture.

Diagonally ruled ornament: mosaic porphyroclastic texture.

Dotted ornament: granuloblastic texture.

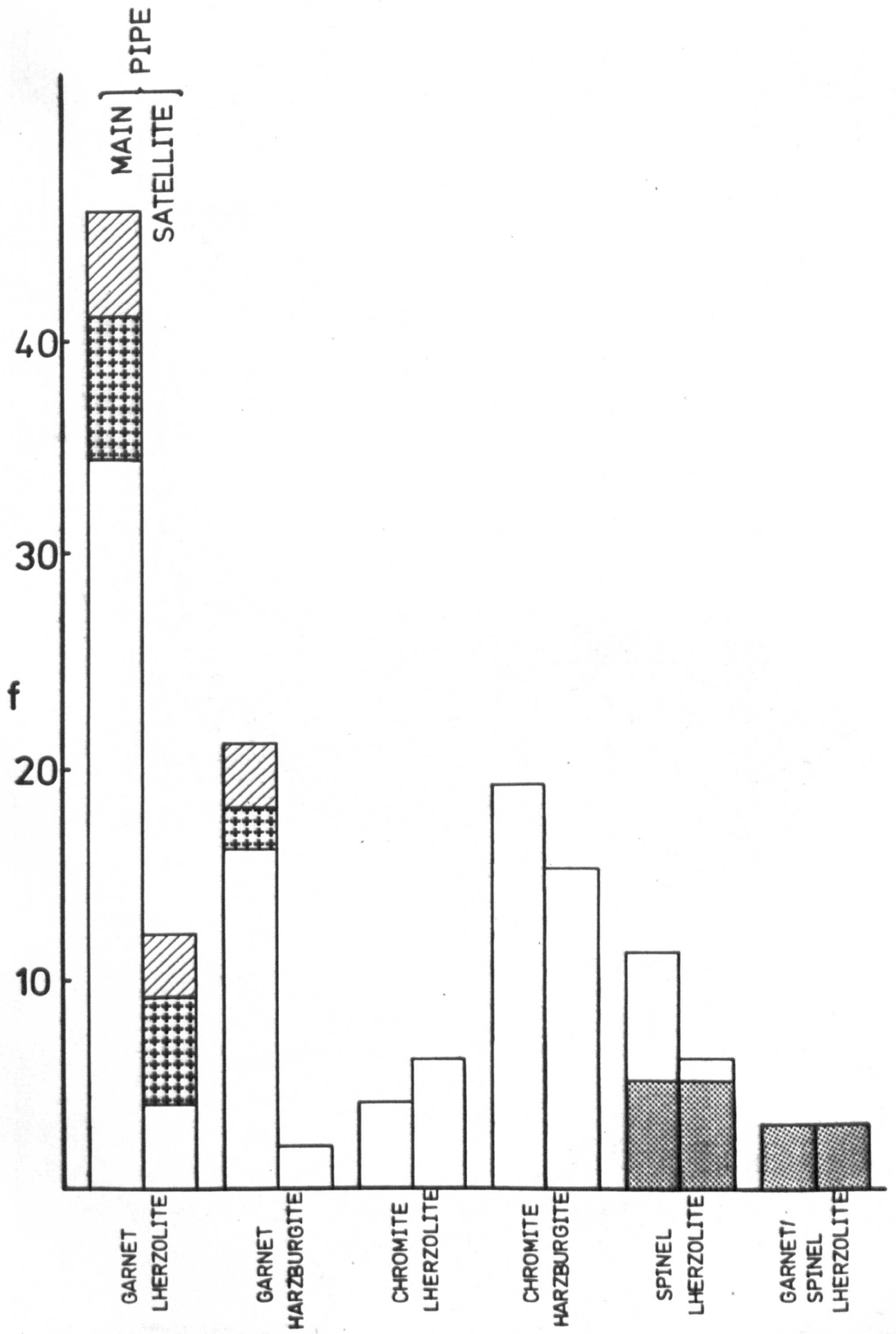


Figure 6.2: Histogram showing the phlogopite content of the peridotites from the Main and Satellite Pipe kimberlites. Unornamented: phlogopite free rocks. Dotted ornament: primary phlogopite-bearing rocks. Diagonally ruled ornament: secondary phlogopite-bearing rocks.

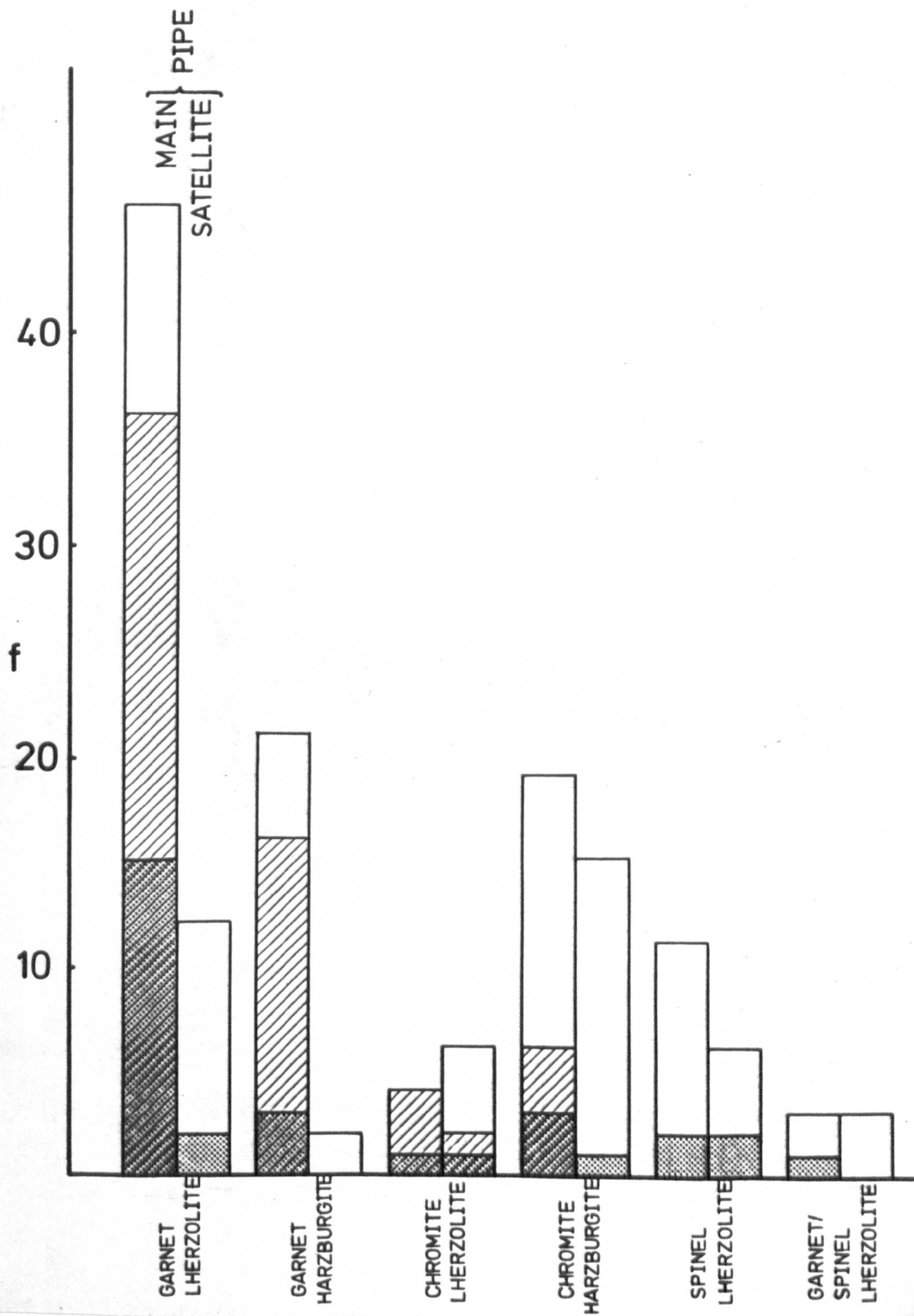


Plate 6.1: Coarse textured garnet lherzolite. Garnet (isotropic) at top left. The other minerals are olivine and orthopyroxene. NL144. Bar scale 2mm. Crossed polars.

Plate 6.2: Fingerprint spinel in coarse textured peridotite. BD1881. Bar scale 1mm.

Plate 6.3: Primary phlogopite (top) predates the reaction surrounding the garnet (bottom). NL492. Bar scale 0.5mm.

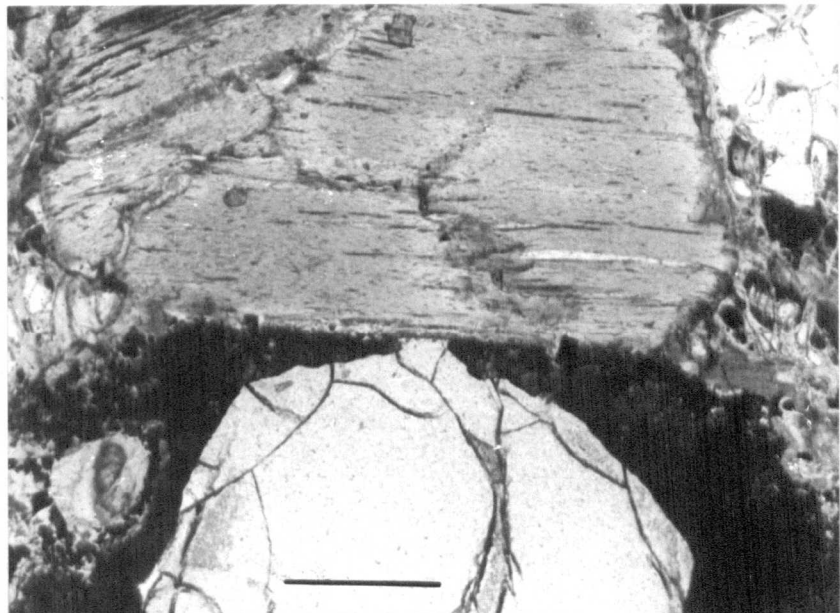
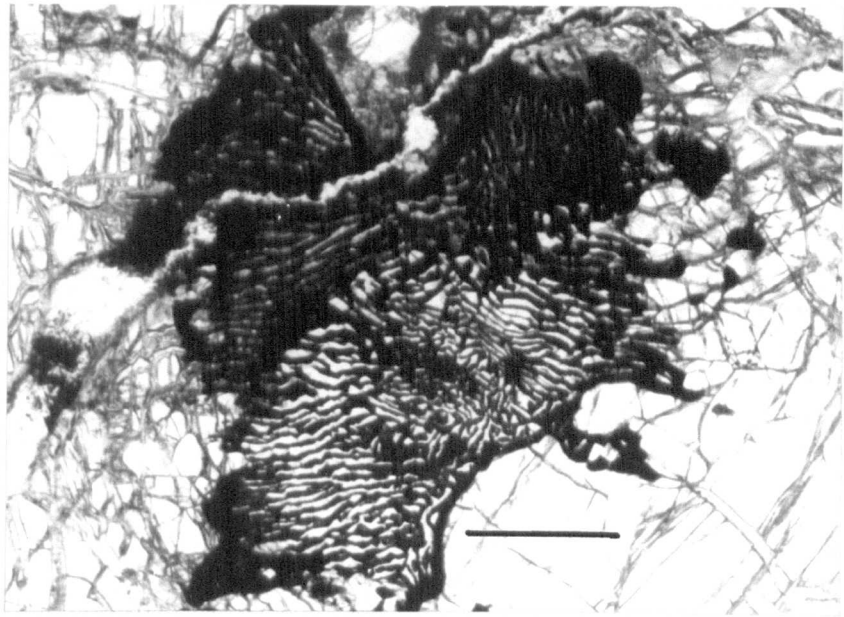
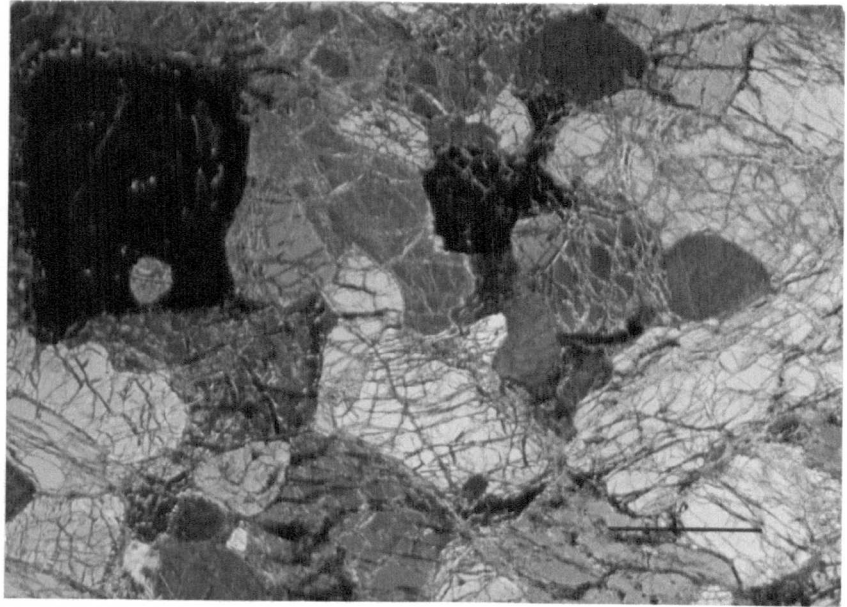




Plate 6.4:Secondary phlogopite with euhedral hexagonal outlines replacing the minerals in the garnet reaction corona (top right) and penetrating along grain boundaries (bottom left).NLO08.Bar scale 0.2mm.

Plate 6.5:Diffuse deformation bands and linear deformation lamellae in olivine porphyroclast in peridotite.NLO82.  
Bar scale 0.5mm.

Plate 6.6:Diffuse deformation bands and sub-linear deformation lamellae in olivine porphyroclast in peridotite.NL441.  
Bar scale 0.5mm.

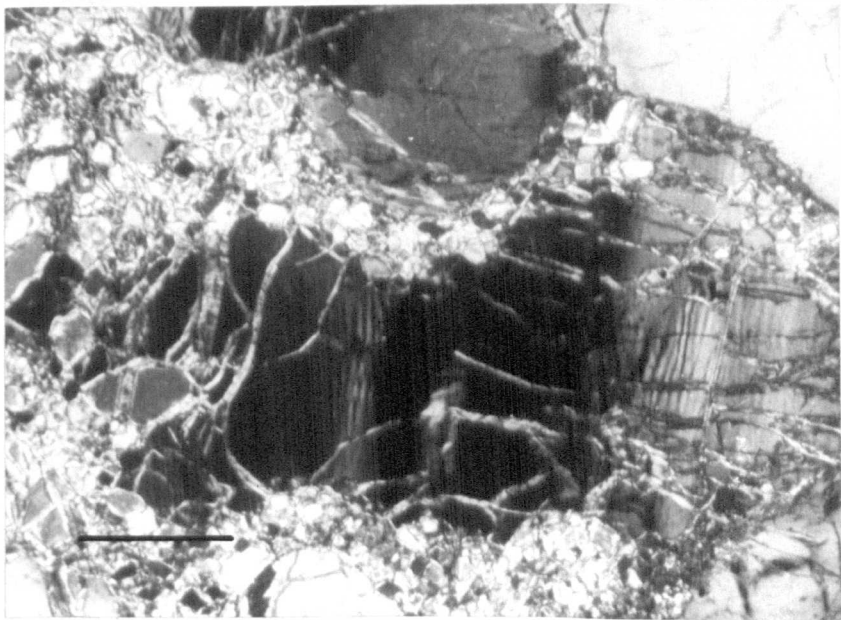
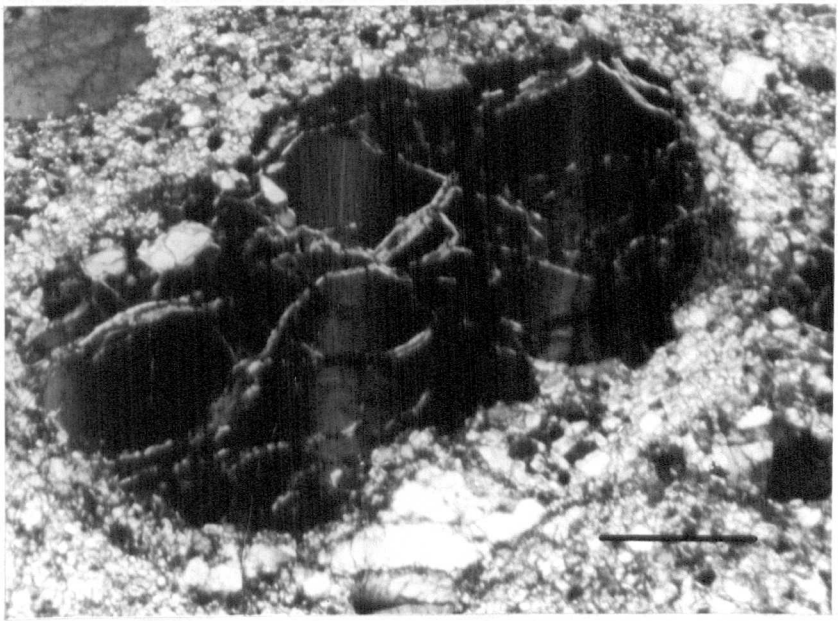
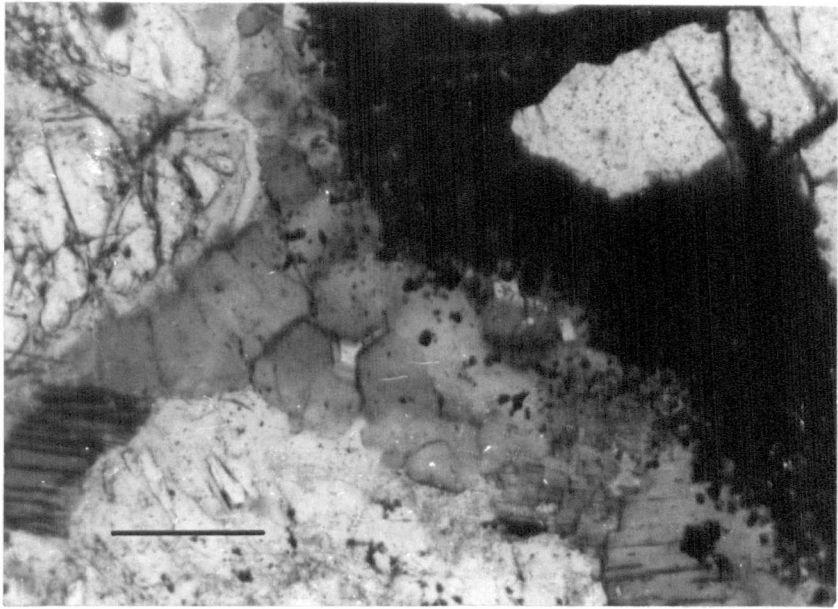


Plate 6.7: Recrystallised strain-free olivine neoblasts (top and bottom right) in garnet (bottom left) lherzolite. NL141. Bar scale 2mm.

Plate 6.8a: Complex symplectic texture of spinel (dark grey) and pyroxene (pale grey) replacing garnet. Large grain at left is orthopyroxene with mosaic olivine at bottom. BD1895. Bar scale 0.5mm.

Plate 6.8b: As for plate 6.8a but with crossed polars to show the mosaic olivine.

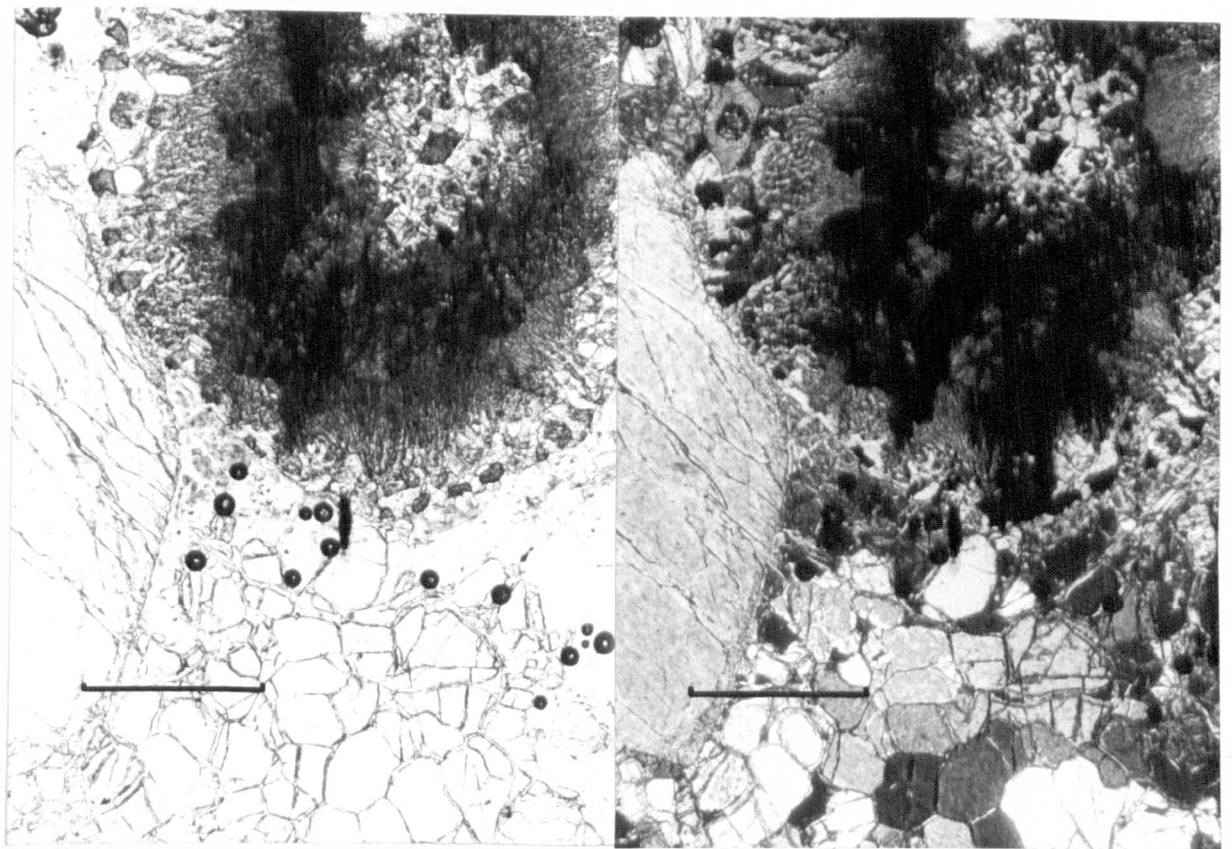
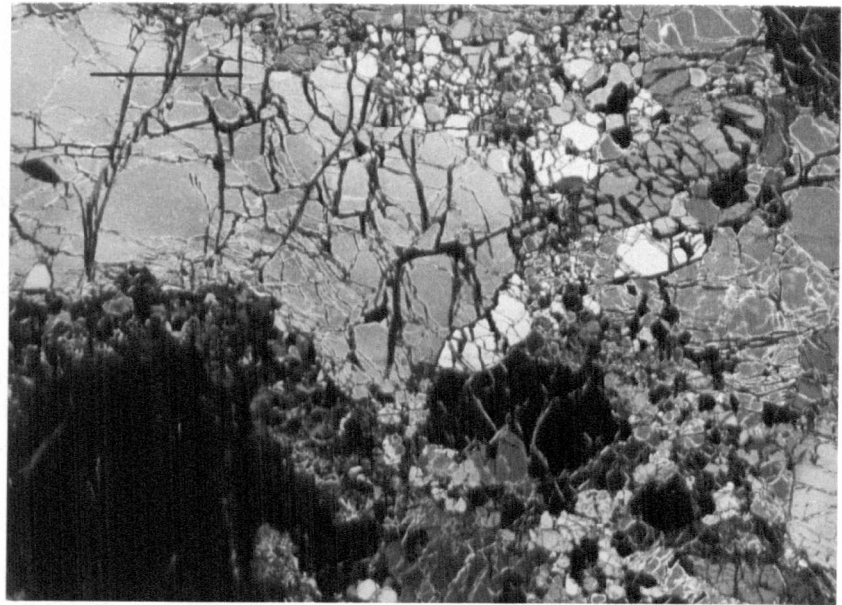


Plate 6.9a: Zonal development of garnet reaction corona.

Garnet (top right) and orthopyroxene (bottom left) with spinel (black grains) demarcating the outer margin of the reaction corona and intergrown with pyroxene. NL141. Bar scale 1mm.

Plate 6.9b: Optical continuity of primary (P) and reaction corona (R) orthopyroxene in plate 6.9a. NL141. Bar scale 1mm. Crossed polars.

Plate 6.10: Porphyroclastic garnet lherzolite. NL441. Bar scale 2mm. Crossed polars.

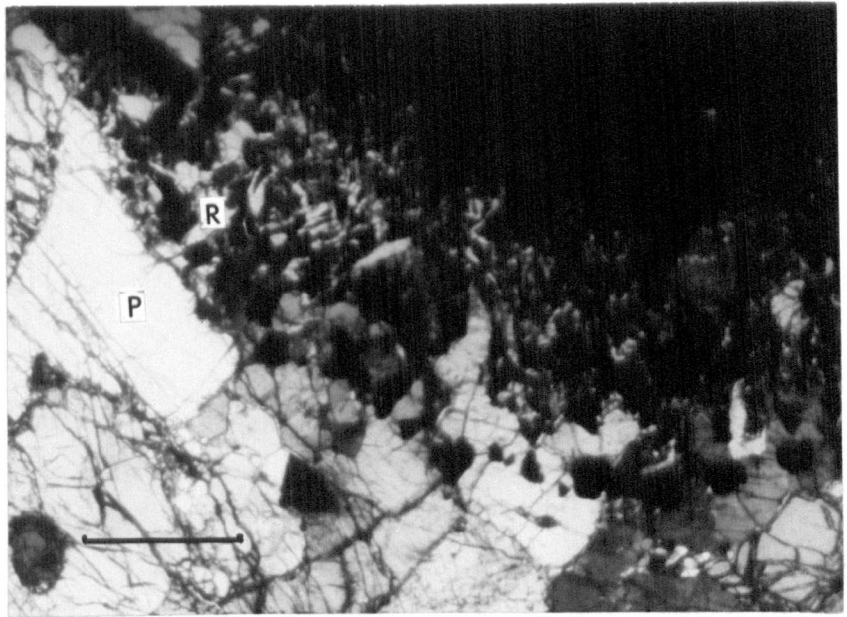
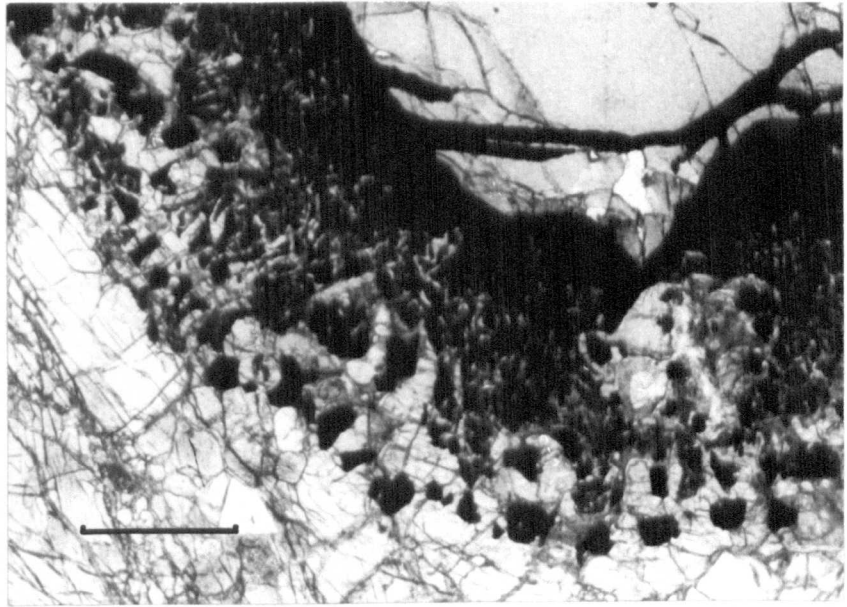


Plate 6.11: Porphyroclastic garnet lherzolite. NL021. Note the 'spongy' margin of the clinopyroxene grain in the centre (grey with lamella twinning). Bar scale 2mm. Crossed polars.

Plate 6.12: Mosaic porphyroclastic garnet lherzolite. NL495. Note some regrowth of olivine neoblasts. Bar scale 2mm. Crossed polars.

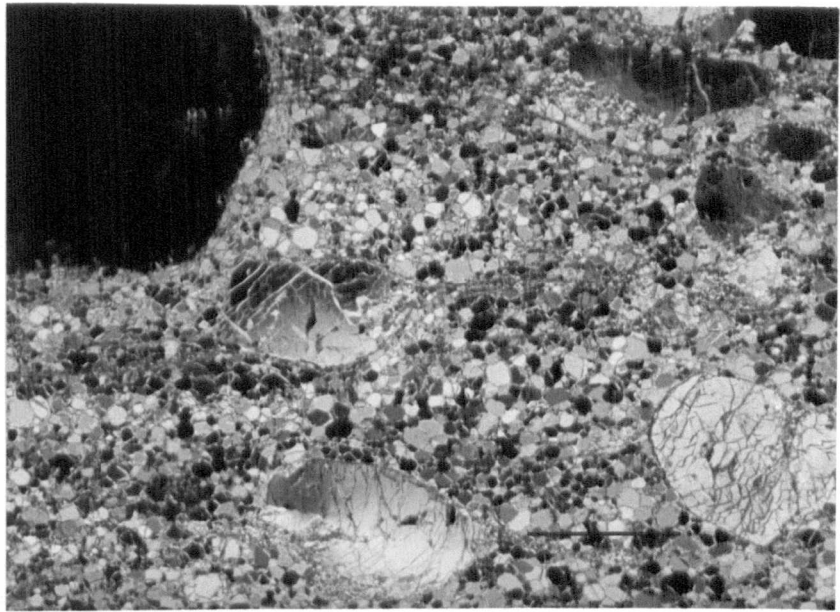
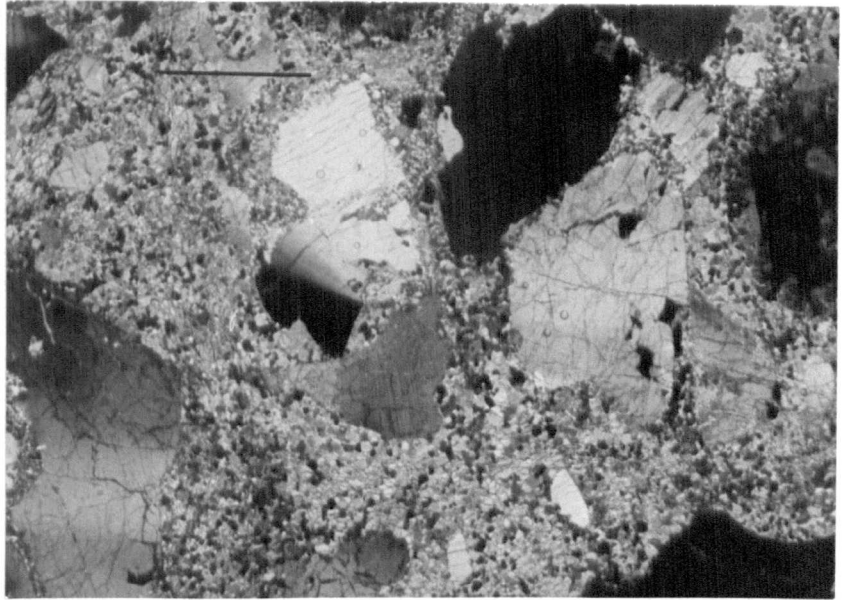




Plate 6.13a:LAD mosaic porphyroclastic garnet harzburgite.  
Note disrupted garnet at top right and fluidal texture of  
olivine (and orthopyroxene) neoblasts. Some olivine  
porphyroclasts (bottom) still present. NLO82. Bar scale  
2mm.

Plate 6.13b:Detail of completely reacted garnet at bottom  
left of plate 6.13a showing the reaction products strung  
out in the fluidal texture. Bar scale 0.5mm.

Plate 6.14:Mosaic porphyroclastic garnet lherzolite. Note  
the variable amounts of olivine neoblasts grain growth.  
NL503. Bar scale 2mm. Crossed polars.

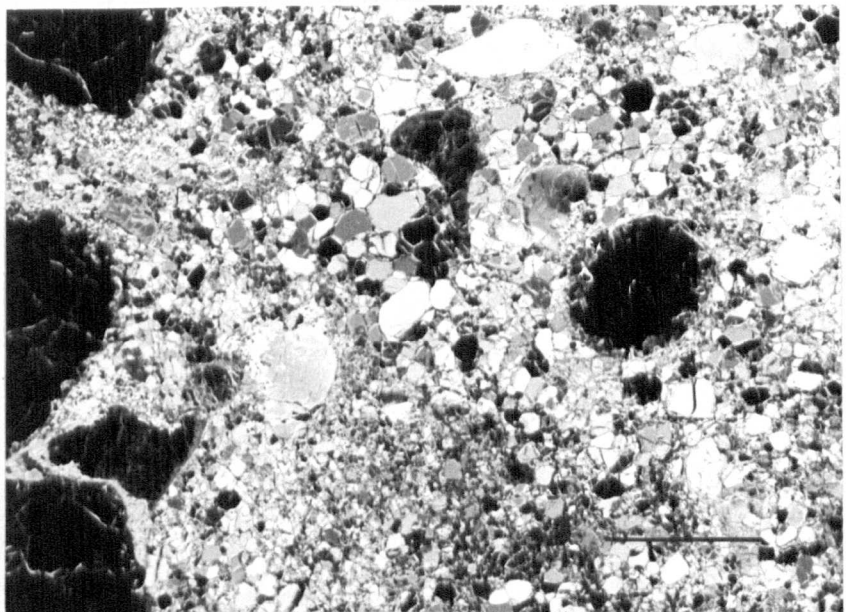
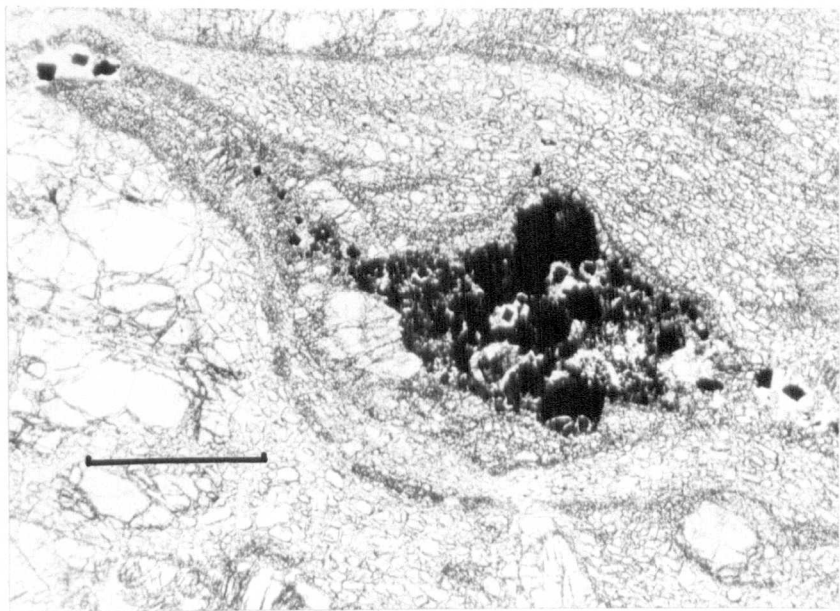
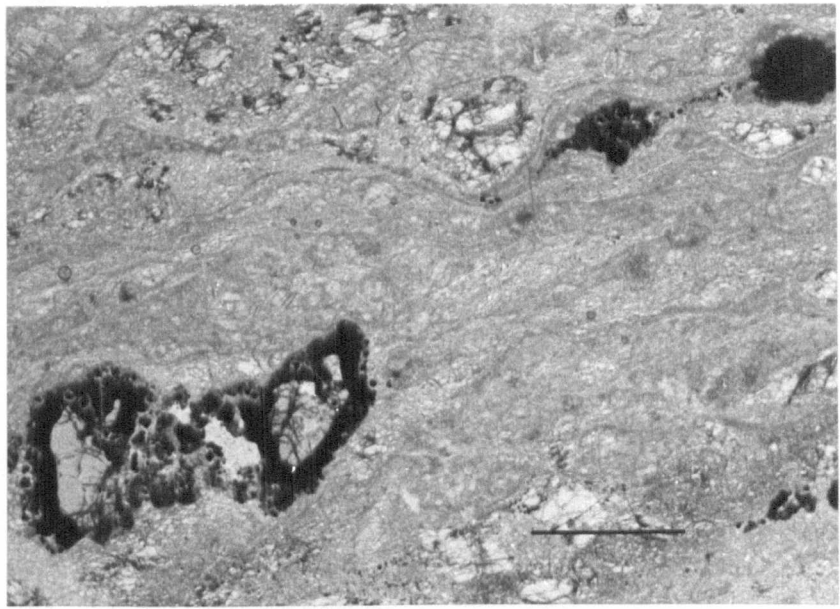


Plate 6.15: Fluidal mosaic porphyroclastic garnet lherzolite.  
Note the variable amounts of olivine neoblast grain  
growth. Dark lenticular grain at left centre is an olivine  
porphyroclast. NL494. Bar scale 2mm. Crossed polars.

Plate 6.16: Granuloblastic spinel lherzolite. NL171. Black grains  
are spinel. Bar scale 2mm. Crossed polars.

Plate 6.17: Tabular granuloblastic spinel lherzolite. BD1876.  
Black grains are spinel. Bar scale 2mm. Crossed polars.

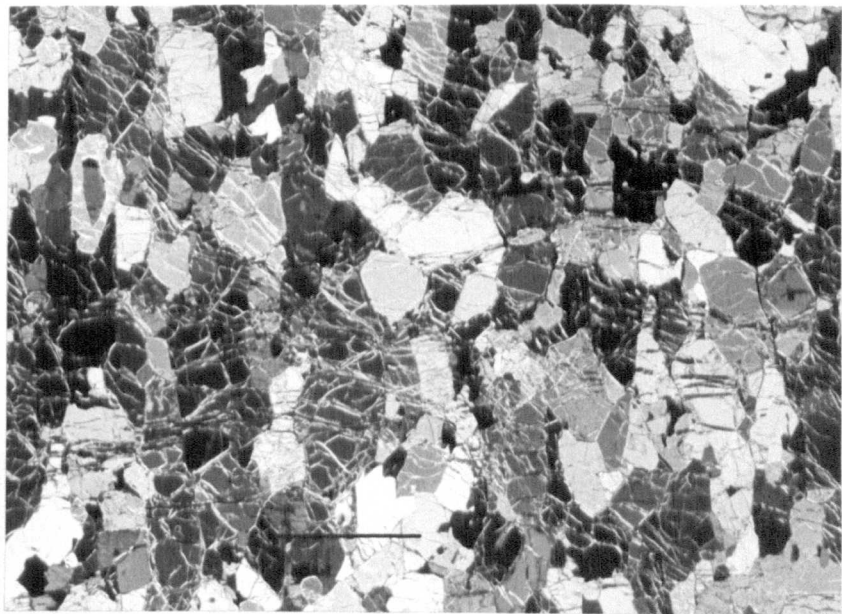
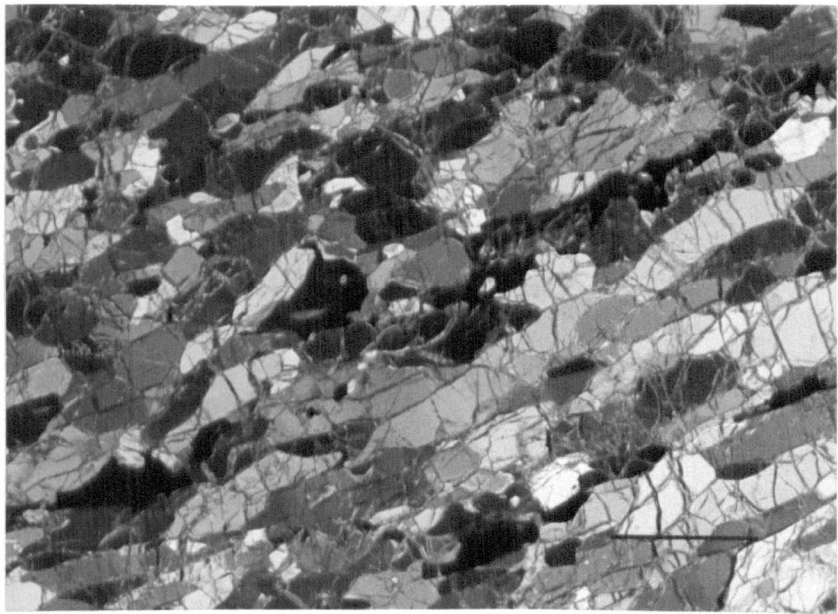
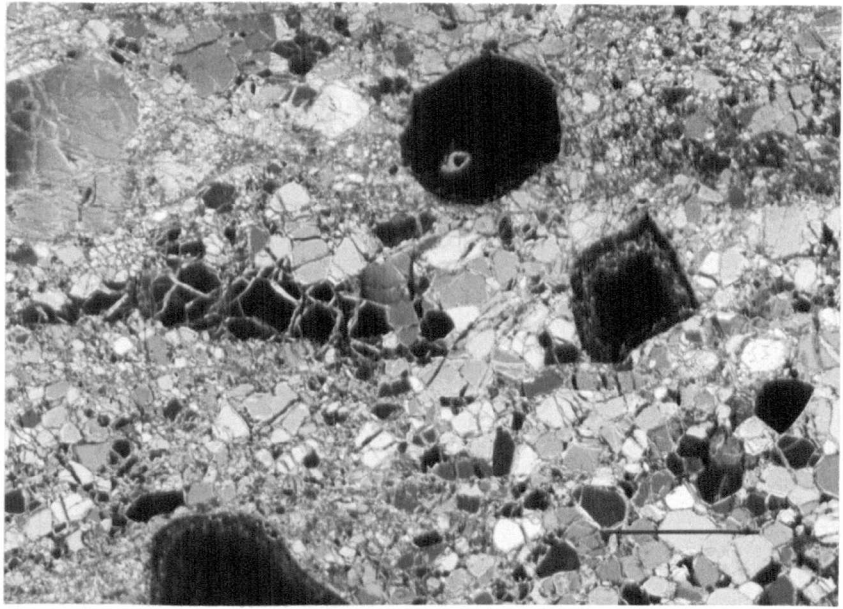


Plate 6.18:Granuloblastic garnet/spinel lherzolite with a strong fabric.The two large black grains are garnet porphyroclasts (see also figure 6. Lock & Dawson(1980)) NL535.Bar scale 2mm.Crossed polars.

Plate 6.19:Garnet/spinel lherzolite with 'pools' of corona minerals (top left).Black grains are spinel and garnet displays a typical corona.NL528.Bar scale 2mm.

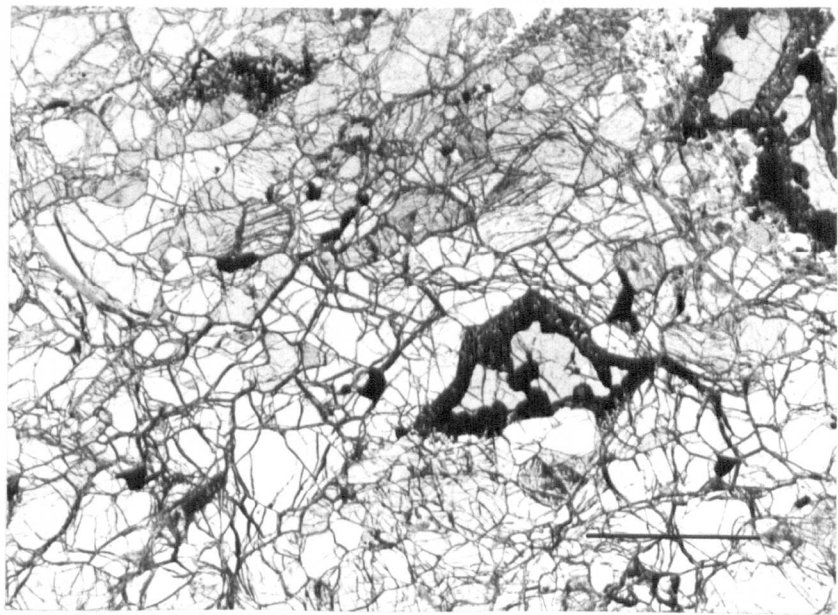
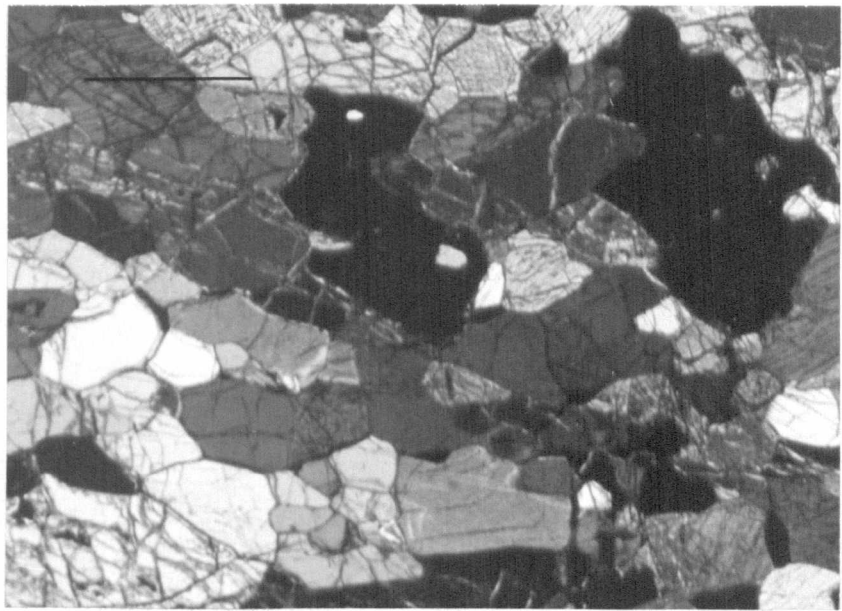


Plate 6.20a: Inequigranular texture of granoblastic aggregates and orthopyroxene porphyroclasts. Small black grains are spinel. NL108. Bar scale 2mm. Crossed polars.

Plate 6.20b: Detail of orthopyroxene porphyroclast at the bottom left of plate 6.20a. Bar scale 0.5mm. Crossed polars.

Plate 6.20: Clinopyroxene exsolution lamellae in orthopyroxene in coarse (recovered granuloblastic) spinel lherzolite. BD1863. Bar scale 0.2mm. Crossed polars.

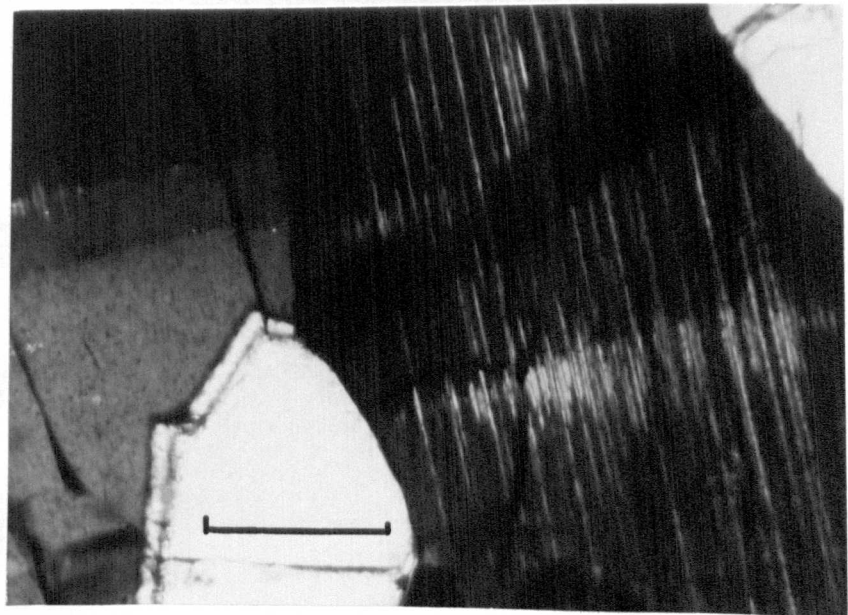
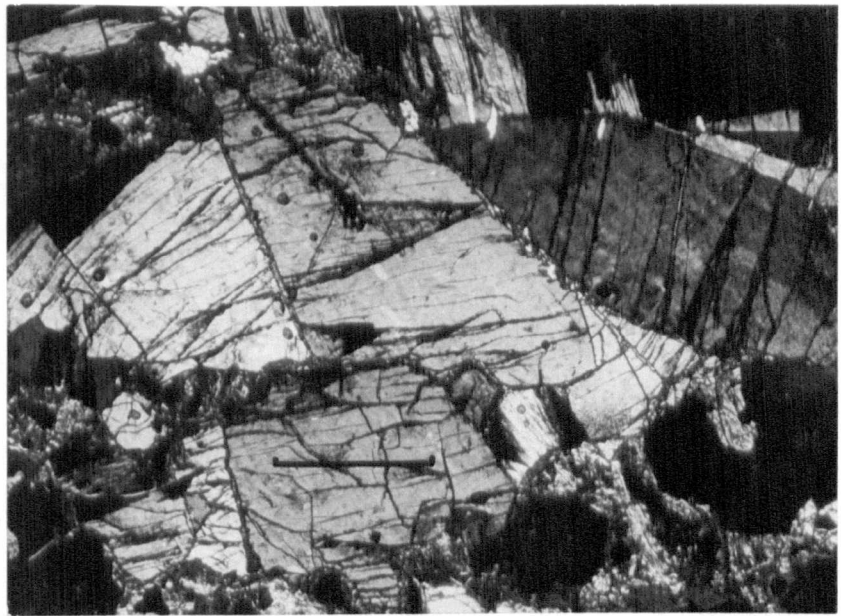
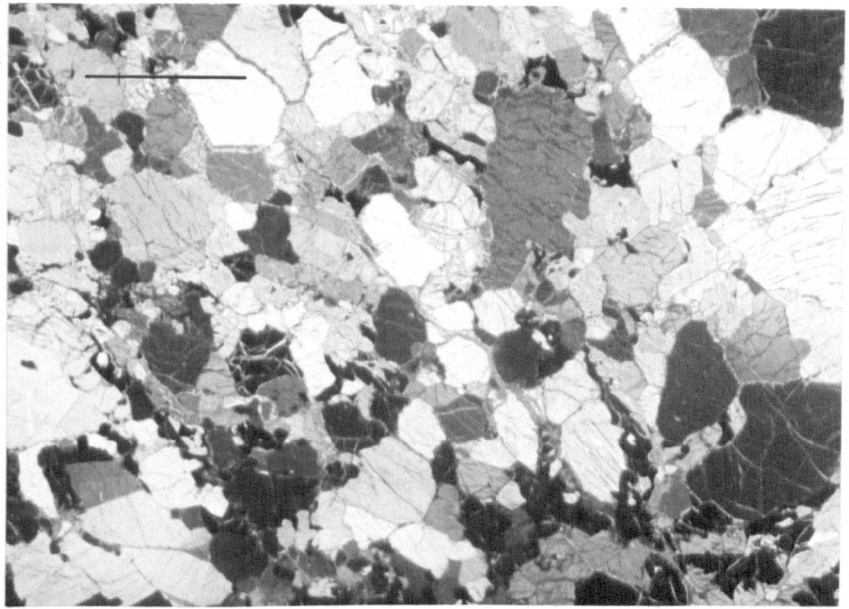




Plate 6.22: Spinel exsolution blebs along KBB in orthopyroxene in coarse chromite harzburgite. BD1884. Bar scale 0.5mm. Crossed polars.

Plate 6.23: 'Sugary' textured orthopyroxenite. Note extremely well equilibrated texture. NL520. Bar scale 2mm. Crossed polars.

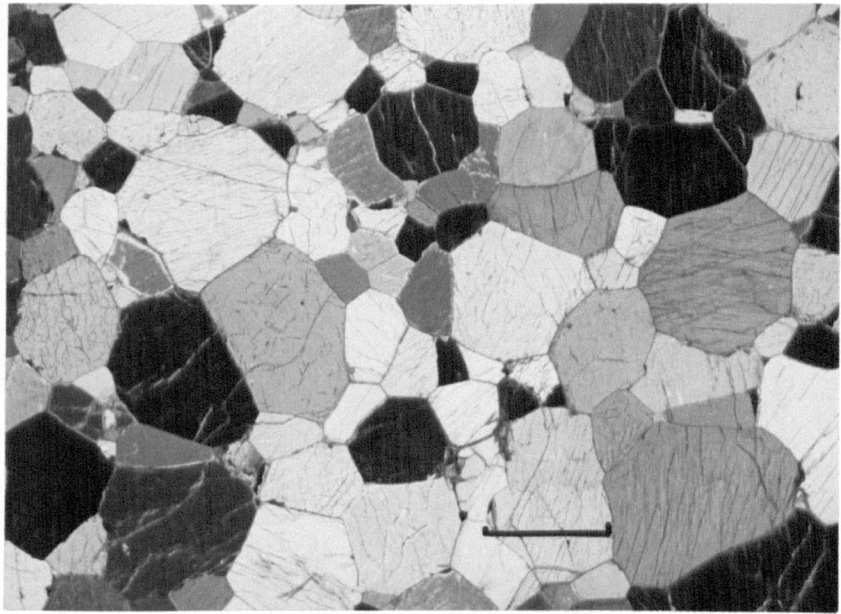
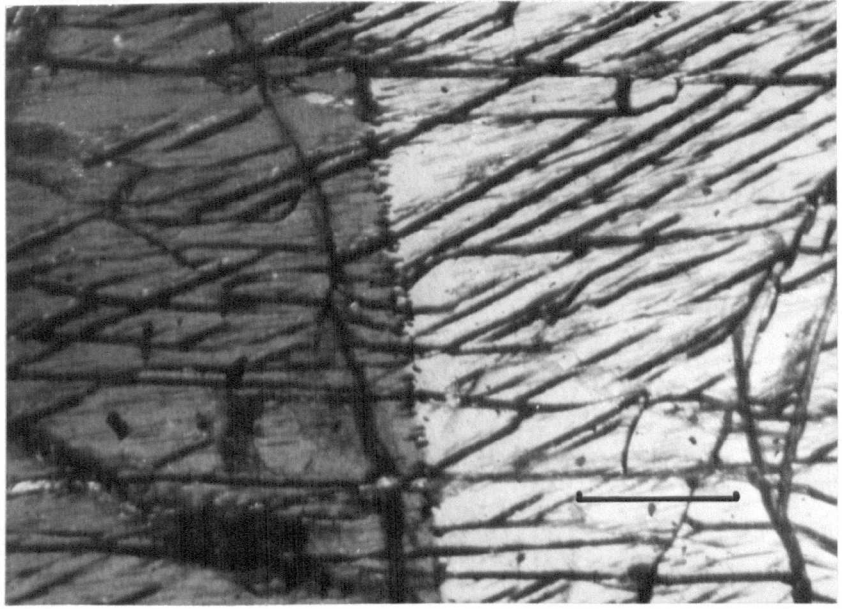


Plate 6.24:Acicular clinopyroxene in serpentine.Kimberlite veinlet in peridotite.NL108.Bar scale 0.1mm.

Plate 6.25:Acicular clinopyroxene,opaque oxides and phlogopite in kimberlite veinlet in peridotite.Note the preferential corrosion of primary orthopyroxene (top left) rather than olivine (bottom left).NL015.Bar scale 0.5mm.

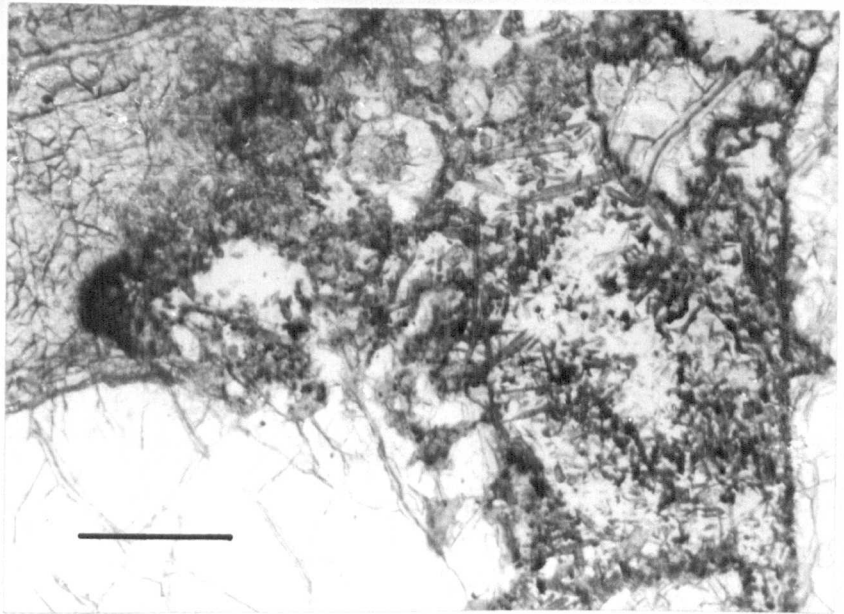
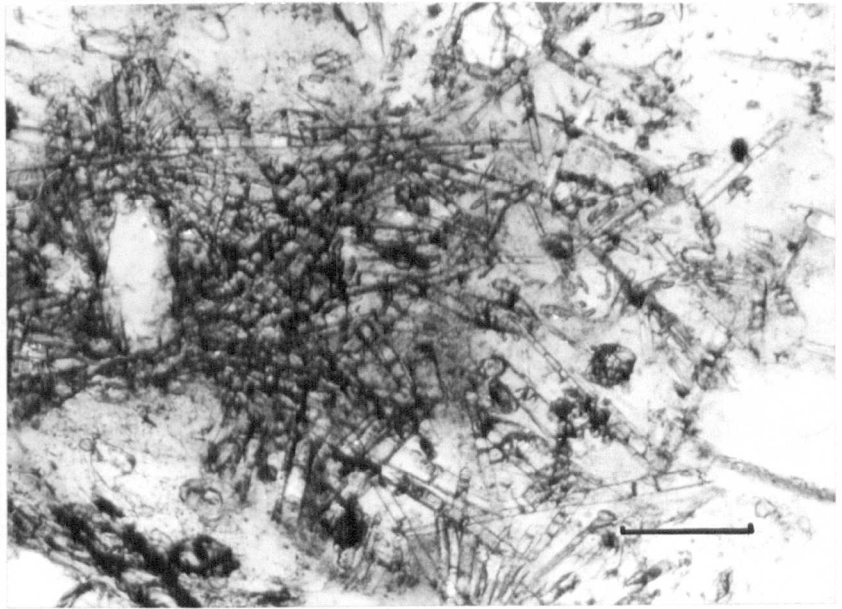
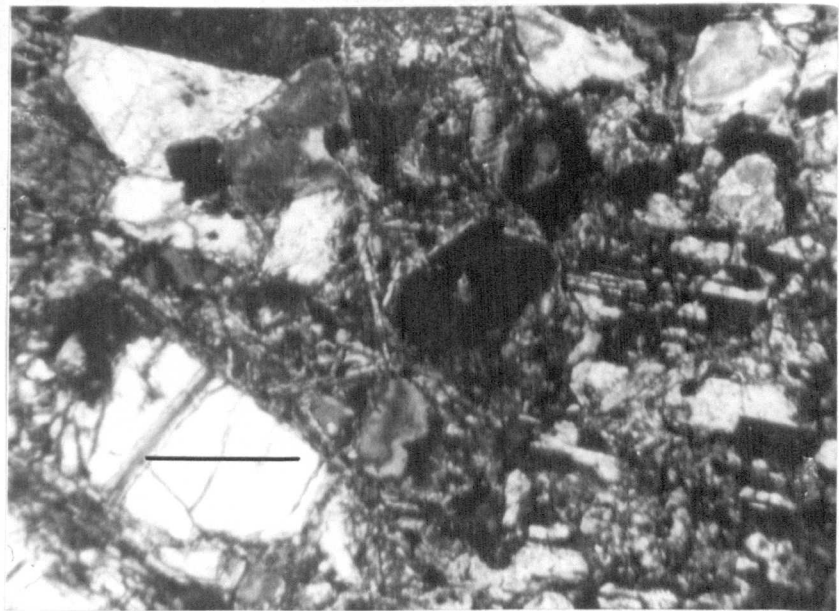
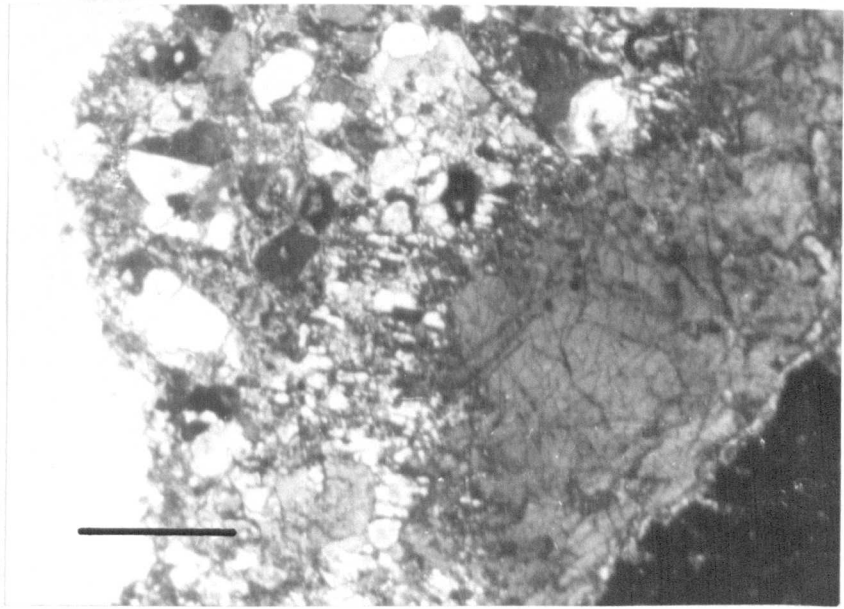


Plate 6.26a: Euhedral clinopyroxene in kimberlite veinlet. Groundmass of the vein contains very fine acicular clinopyroxene, phlogopite and serpentine. Note twinned clinopyroxene (top left). NL015. Bar scale 0.5mm. Crossed polars.

Plate 6.26b: Detail of plate 6.26a showing twinned euhedral clinopyroxene (top left). On the right are a group of small euhedral clinopyroxene crystals showing parallel alignment of twin planes. Bar scale 0.2mm. Crossed polars.

Plate 6.27: Kimberlite veinlet. 'Calved-off' fragment of primary orthopyroxene (centre) separated from the vein wall by massive secondary clinopyroxene (dark grey). NL015. Bar scale 0.5mm. Crossed polars.



CHAPTER 7Peridotites: Phase Chemistry

Phase compositions in peridotite xenoliths from both the Main and Satellite pipes were analysed by conventional microprobe techniques at Edinburgh, Manchester and Cambridge Universities, using both the wavelength (WDS) and energy dispersive (EDS) methods. Instrumental conditions have been described in earlier chapters. Analyses for sodium and aluminium in orthopyroxene by EDS are generally not of high precision because of interference with the large Mg and Si peaks. In rocks from the Satellite pipe where it was intended to make geothermometric and geobarometric calculations these two elements were analysed by WDS on an early Cambridge Instruments Geoscan. The ZAF corrections were recalculated from these apparent concentrations to give the true element abundances. Na and Al were compared to a jadeite standard which proved to be unfortunate in the case of alumina. Calculation using the jadeite standard gave high  $\text{Al}_2\text{O}_3$  values compared to otherwise identical rocks analysed by Boyd (1973). Al was also monitored in a corundum standard: calculation using this standard would have yielded alumina values ~15% lower than those actually recorded here and within the range of Boyd's values. This discrepancy does not affect much of the following discussion but does have serious repercussions when making geobarometric calculations (see Chapter 9).

The analyses of the primary silicate phases (garnet, orthopyroxene, clinopyroxene and olivine) and oxides (chromite and spinel) are given in Appendices 4 and 5 for Main and Satellite pipe peridotites respectively. Each analysis generally represents the average of three grain compositions for that phase within a single section and demonstrates considerable within-specimen homogeneity (cf. Boyd and Finger, 1975). Garnet, orthopyroxene and clinopyroxene compositions are displayed in the Ca-Mg-Fe

system (Figures 7.1, 7.2 and 7.3) for Main pipe, Satellite pipe and published peridotite mineral analyses respectively. The individual phase compositions will be discussed in more detail below but note that the clinopyroxene from Satellite pipe rocks trend to more sub-calcic compositions and are absent in the range  $\text{Ca}/(\text{Ca}+\text{Mg}) = 0.45-0.64$  which is so common among Main pipe xenoliths. Also note that the garnets display two composition trends, one of which is reflected also in more Fe-rich pyroxene compositions (e.g. NLO12).

### 1. Primary Phases

Garnet: The compositions show considerable variety in both range in  $\text{Mg}/(\text{Mg}+\text{Fe})$  ratio (0.779-0.864) and chrome content ( $\text{Cr}_2\text{O}_3 = 2.77-11.10$  wt.%). All analyses fall on the 'CaO trend' of Hornung and Nixon (1973) (Figure 7.4). No xenoliths contain garnet similar to the low CaO pyrope found as xenocrysts in the kimberlite (see Chapter 5) and interpreted as equivalent to garnet included in diamond. The 'CaO trend' relates to garnets showing a slowly decreasing  $\text{Mg}/(\text{Mg}+\text{Fe})$  ratio with increasing CaO and  $\text{Cr}_2\text{O}_3$  wt.%. One garnet in NL145 has 11.10 wt.%  $\text{Cr}_2\text{O}_3$  which is among the most chrome-rich of any found in fresh garnet peridotite from southern African kimberlites (although not in xenocrysts, e.g. Kao, Lesotho - Hornung and Nixon op.cit. - Finsch, South Africa - Gurney and Switzer, 1973). Sobolev et al. (1973) have found garnets of similar high chrome content in kimberlites from Yakutia, USSR, both as part of the peridotite paragenesis and as xenocrysts. The general trend however is similar to that for other garnet lherzolites in Lesotho (Nixon and Boyd, 1972; Carswell et al., 1979), and South Africa (Gurney and Switzer op.cit.; Danchin, 1979).

The majority of these garnets classify as chrome pyrope (Group 9) in the statistical classification of Dawson and Stephens (1975, 1976) but the high-chrome garnets in NL145 is a knorringitic uvarovite-pyrope



(Group 12). Carswell et al. (1979) have suggested that these two groups should be amalgamated because of the similar paragenesis. However, it should be remembered that this is a purely statistical classification scheme and is not intended to differentiate such detailed paragenetic groupings. It seems pedantic to suggest such a change.

This drawback is further illustrated by the second group of garnets which trend towards high iron composition (e.g. NLO12 FeO = 9.78 wt.%). Such garnets are group 9 chrome pyrope but their paragenesis is distinct from others on the 'CaO trend'. These garnets, coexisting with Fe-rich pyroxenes and olivines are very similar to those in Matsoku xenoliths investigated by Cox et al. (1973) who have concluded that these rocks represent a series of compositions reflecting equilibration of crystal and liquid cumulates under upper mantle conditions (Gurney et al. 1975). The Fe-rich Letseng xenoliths (e.g. NLO12) also derive from similar mantle depths (see Chapter 9) and are interpreted to have originated in a similar way.

There are no chemical differences between garnets from deformed and undeformed rocks as described by Nixon and Boyd (1973). A slight tendency towards higher TiO<sub>2</sub> wt.% in some deformed higher temperature rocks (e.g. NL141, NL495) is matched by contrary examples (NL494).

Clinopyroxene: The range in Ca/(Ca+Mg) ratios (0.351-0.489) and chrome content (Cr<sub>2</sub>O<sub>3</sub> = 0.75-3.66 wt.%) is reflected in their grouping as ureyitic and chrome diopsides as well as diopside and sub-calcic diopside (classification of Stephens and Dawson, 1977). These authors provisionally define sub-calcic diopside as clinopyroxene with Ca/(Ca+Mg) < 0.40 of which there are several in Letseng xenoliths (see Figures 7.1, 7.2 and 7.3) and notably in the Satellite pipe peridotites. This ratio, illustrating the solubility of enstatite in diopside, is indicative of the equilibration temperature in the peridotite paragenesis (e.g. Davis and Boyd,

1966; see chapter 9) and demonstrates the wide equilibration temperature range in the Letseng peridotites.

Figure 7.5 illustrates the considerable range in jadeite and ureyite ( $\text{NaCrSi}_2\text{O}_6$ ) content of these clinopyroxenes. The close relationship to the ideal slope ( $\text{Na} = \text{Al} + \text{Cr}$ ) demonstrates that these clinopyroxenes contain little if any tschermakite molecule, and do not require any  $\text{Fe}^{3+}$  for an acmite molecule.

Orthopyroxene: This mineral shows a range in  $\text{Mg}/(\text{Mg} + \text{Fe})$  ratio (0.898-0.938) and  $\text{CaO}$  content (0.20-1.59 wt.%) reflecting coexistence with other silicates of varying iron content and clinopyroxene of varying  $\text{Ca}/(\text{Ca} + \text{Mg})$  ratio. High  $\text{Mg}/(\text{Mg} + \text{Fe})$  orthopyroxenes coexists with magnesium rich silicates and high  $\text{CaO}$  orthopyroxene coexists with low  $\text{Ca}/(\text{Ca} + \text{Mg})$  clinopyroxene.

All these enstatites contain appreciable alumina ( $\text{Al}_2\text{O}_3 = 0.69-1.29$  wt.% or higher in some specimens as previously described), which is mainly accounted for as tschermakite molecule. Figure 7.6 shows atomic  $\text{Na} \text{ v } \text{Al} + \text{Cr}$  where the tendency towards a linear correlation is not a real feature disturbed by analytical inaccuracy, but does indicate some solubility of jadeite and ureyite. Such a linear relationship would imply identical tschermakite contents in orthopyroxenes from rocks with widely divergent equilibration temperatures; this is considered highly improbable.

Olivine: All the olivine are forsterites ( $\text{Fo}_{87}-\text{Fo}_{94}$ ) which, like the Matsoku suite of xenoliths (Cox et al., 1973), display a crude linear correlation between % $\text{Fo}$  and  $\text{Mg}/(\text{Mg} + \text{Fe})$  ratio of coexisting silicates. At Matsoku this correlation was inferred to relate to equilibration under similar physical conditions (demonstrated by the limited range of  $\text{Ca}/(\text{Ca} + \text{Mg})$  in clinopyroxene). The Letseng rocks however, do not show such a clear linear correlation (Figures 7.7 and 7.8) because of the much wider range in equilibration conditions discussed above. This is to be expected and

indeed the distribution of Fe/Mg between garnet and clinopyroxene varies with temperature (Råheim and Green, 1974). Mori and Green (1978) have investigated the distribution of Fe/Mg between various pairs of peridotite silicates, all of which are at least theoretically useful geothermometers. The point is that rocks equilibrated at similar temperatures will display linear trends similar to the Matsoku Suite. This is exemplified in Figure 7.8 for the Satellite pipe xenoliths where garnets in high temperature rocks plot above the Matsoku trend and garnets in low temperature rocks plot below it. Each group separately shows a sub-parallel trend to that of the Matsoku suite and shows that at high temperatures Fe is fractionated into olivine preferentially to Mg, and at low temperatures into garnet.

Similar, although much less well defined, correlations are shown between the Al/(Al+Cr) ratio of garnet and pyroxene with  $f_{O_2}$  in coexisting olivine (Figure 7.9). The most magnesian assemblages are the most chrome-rich, as was found in xenoliths from Premier Mine (Danchin, 1979).

Chromite: Figure 7.10 shows the compositions of chromites and spinels (see below) from Letseng lherzolites in the expanded spinel prism (Smith and Dawson, 1975). The chromite compositions are for phases coexisting with garnet and demonstrate that chrome fractionates preferentially into chromite ( $(Cr/Al)_{CHR} > (Cr/Al)_{Gt}$ ) which is not surprising, as Smith and Dawson (1975) have already demonstrated that Cr favours spinel over pyroxene. The coexistence of chromite and garnet in these compositions is compatible with the experimental work of MacGregor (1970) who showed that the reaction boundary between spinel and garnet peridotites moves to higher pressure with increasing Cr/Al. Because of variations in the bulk Cr/Al ratio, garnet and spinel may coexist over a considerable upper mantle depth range.

Specimen	NL141					NL197					NL108	NL102				
	OP	±	CP	±	SP	±	OP	±	CP	±		OP	CP	OP	SP	
Mineral Number of Analyses	8		5		9		5		5		5		1	2	2	2
SiO2	52.10	1.94	50.14	2.00	0.08	0.02	51.69	0.91	0.04	1.52	0.04	52.53	52.08	50.33	0.00	
TiO2	0.46	0.10	1.49	0.45	0.69	0.12	0.08	0.01	0.02	0.05	0.02	-	0.23	0.56	0.32	
Al2O3	7.52	2.24	8.25	1.88	50.23	1.69	7.77	0.90	1.30	1.81	1.30	8.72	6.91	7.88	45.67	
Cr2O3	1.40	0.40	1.70	0.43	16.92	1.65	1.24	0.44	1.36	0.66	1.36	0.67	0.71	0.65	19.05	
Fe2O3	-	-	-	-	3.48	0.50	-	-	-	-	-	-	-	-	6.38	
FeO	6.15	0.52	4.30	0.45	8.26	0.03	6.52	0.13	0.55	0.25	0.55	7.35	9.16	5.49	7.68	
MnO	0.27	0.06	0.22	0.05	0.28	0.03	0.38	0.01	0.02	0.30	0.02	0.43	0.14	0.10	0.39	
MgO	30.36	1.43	19.53	2.58	20.62	0.40	29.81	0.60	0.40	1.73	0.40	29.18	28.20	16.29	20.36	
CaO	1.44	0.17	14.20	1.76	0.01	0.01	1.39	0.30	0.02	0.82	0.02	2.20	2.19	17.03	0.00	
Na2O	0.15	0.02	1.14	0.20	0.01	0.01	0.12	0.02	0.01	0.23	0.01	0.26	0.19	1.05	0.00	
NiO	0.01	0.01	0.03	0.02	0.03	0.03	0.00	0.00	0.02	0.02	0.02	-	0.14	0.08	0.04	
Total	99.86		100.81		100.61		99.00			97.88		101.34	99.95	99.46	99.89	
Si	1.82		1.79		0.00		1.82			0.00		1.81	1.84	1.84	-	
Ti	0.01		0.04		0.01		0.00			0.00		-	0.01	0.02	0.01	
Al	0.31		0.35		1.56		0.32			1.59		0.35	0.29	0.34	1.45	
Cr	0.04		0.05		0.35		0.03			0.35		0.02	0.02	0.02	0.41	
Fe3+	-		-		0.07		-			0.05		-	-	-	0.13	
Fe2+	0.18		0.13		0.18		0.19			0.22		0.21	0.27	0.17	0.17	
Mn	0.01		0.01		0.01		0.01			0.01		0.01	0.00	0.00	0.01	
Mg	1.58		1.04		0.81		1.56			0.77		1.50	1.48	0.89	0.82	
Ca	0.05		0.54		0.00		0.05			0.00		0.08	0.08	0.67	-	
Na	0.01		0.08		0.00		0.01			0.00		0.02	0.01	0.07	-	
Ni	0.00		0.00		0.00		0.00			0.00		-	0.00	0.00	0.00	
Total	4.01		4.03		2.99		3.99			2.99		4.01	4.00	4.02	3.00	
Mg/(Mg+Fe)	0.90		0.89		0.81		0.89			0.77		0.88	0.85	0.84	0.83	
Ca/(Ca+Mg)			0.34		0.18					0.18				0.43	0.22	
Cr/(Cr+Al)																
Ca*	2.96		31.35				2.87			38.16		4.47	4.52	38.74		
Mg*	86.75		60.75				85.95			54.66		83.80	80.77	51.54		
Fe*	10.29		7.90				11.17			7.18		11.73	14.71	9.72		

Microprobe analyses for NL108 carried out at Manchester University using the EDS mode.  
Other analyses were made at Edinburgh University using the WDS mode.

## 2. Chemistry of Reaction Corona Phases

Two specimens with well developed reaction coronas and significantly different primary equilibration temperatures, were selected for a detailed study of the chemistry of the reaction-corona pyroxenes and spinels. Microprobe analyses of several grains from zone 3 (see Chapter 6) of the corona are presented in Table 7.1 for these two specimens. NL141 and NL197. Additional analyses for two other rocks are shown for comparison.

These reaction corona minerals are characterised by being highly aluminous. The orthopyroxenes contain between 6 and 8.7 wt.%  $\text{Al}_2\text{O}_3$  and much of this alumina must be in four-fold co-ordination; nonetheless on the basis of the structural formulae a considerable proportion of the alumina in the six-fold site must be regarded as magnesium tschermakite molecule. The clinopyroxenes likewise are highly aluminous and must contain calcium tschermakite molecule, and together with the orthopyroxenes show appreciable  $\text{Cr}_2\text{O}_3$  content. Both the ortho- and clinopyroxenes show a very constant  $\text{Mg}/(\text{Mg}+\text{Fe})$  ratio of 0.89-0.91, but are more Mg- and Fe-rich than the primary pyroxenes in the same rock (Figure 7.11). The orthopyroxenes are more calcic and the clinopyroxenes less calcic than the equivalent primary phases. The spinels are magnesian aluminous spinels unlike the chromites described in the last section (see Figure 7.10) and found in the groundmass of many peridotites (Smith and Dawson, 1975). In their high magnesia and alumina content they resemble other spinels reported from reaction coronas around garnets in peridotites (Reid and Dawson, 1972; Haggerty, 1975; Carswell et al., 1979).

As in the corona minerals in the Lashaine peridotites (Reid and Dawson, op.cit.) most of the chemical features of the pyroxenes and spinels are compatible with their being developed by reaction between garnet and olivine, their overall chemical composition being a reflection

of the chemical gradient between these two minerals. An exception is the imbalance in the sodium and titanium contents of the corona pyroxenes which are not matched by similar values in either parental garnet or olivine. The present data concur with the suggestion of Reid and Dawson (op.cit.) that small quantities of sodium may have been introduced during or after an otherwise isochemical reaction. By contrast, nickel, which is present in significant quantities in the parent olivine, only appears in trace amounts in the corona minerals. This component may be preferentially retained in primary olivine by intragrain diffusion.

It should be noted that these two different samples show that different proportions of corona minerals developed, presumably as some reflection of difference in primary phase composition. For example in NL141 (the more Ti- and Fe-rich rock) a balanced equation for the elements Si, Al, Cr, Mg and Ca, based on the structural formulae of the primary and corona phases, gives the reaction:

187 garnet + 108 olivine → 270 orthopyroxene + 100 clinopyroxene + 111 spinel

By contrast the corresponding reaction for NL197 is:

212 garnet + 135 olivine → 390 orthopyroxene + 100 clinopyroxene + 137 spinel

These reactions show that, compared to the Lashaine samples, the Letseng samples have more reaction corona clinopyroxene. A further difference between these two sets of samples is that, whereas the pyroxenes of the Lashaine coronas attain values of 12-14 wt.%  $Al_2O_3$  those at Letseng never exceed 10 wt.%

Theoretically the transition from the garnet lherzolite assemblage to the spinel lherzolite assemblage of the corona could take place by a rise in temperature to over  $1300^{\circ}C$ , by a fall in pressure or a combination of the two (MacGregor, 1965, 1970, 1974; Green and Ringwood, 1967; O'Hara et al.,

TABLE 7.2: Compositions of Primary Minerals in Specimen NL108

	GT	OP	CORE→RIM	CP	OL	SP	CORE→RIM	SP	SP
SiO2	41.98	57.16	56.89	55.28	54.31	41.38	-	-	-
TiO2	-	-	-	-	-	-	-	-	-
Al2O3	22.39	1.48	2.39	3.58	2.15	-	45.25	47.25	49.91
Cr2O3	1.37	0.35	0.41	0.57	0.35	-	23.19	21.33	18.88
Fe2O3	-	-	-	-	-	-	-	-	-
FeO	7.62	4.24	4.39	4.09	1.07	5.84	9.39	9.13	8.30
MnO	0.52	-	-	-	-	-	-	-	-
MgO	19.55	36.25	35.78	34.70	17.30	51.84	19.76	19.90	20.91
CaO	5.94	0.20	0.22	0.18	24.04	-	-	-	-
Na2O	-	0.28	0.26	-	0.57	-	-	-	0.27
NiO	-	-	-	-	-	0.44	-	0.39	0.32
Total	99.37	99.96	100.33	98.40	99.79	99.37	97.57	98.00	98.67
Si	3.01	1.96	1.94	1.92	1.97	1.00	-	-	-
Ti	-	-	-	-	-	-	-	-	-
Al	1.89	0.06	0.10	0.15	0.09	-	1.47	1.52	1.58
Cr	0.08	0.01	0.01	0.02	0.01	-	0.51	0.46	0.40
Fe3+	-	-	-	-	-	-	-	-	-
Fe2+	0.46	0.12	0.13	0.12	0.03	0.12	0.22	0.21	0.19
Mn	0.03	-	-	-	-	-	-	-	-
Mg	2.09	1.85	1.82	1.80	0.93	1.87	0.81	0.81	0.84
Ca	0.46	0.01	0.01	0.01	0.93	-	-	-	-
Na	-	0.02	0.02	-	0.04	-	-	-	0.02
Ni	-	-	-	-	-	0.01	-	0.01	0.01
Total	8.01	4.03	4.02	4.00	4.01	3.00	3.01	3.01	3.02
Mg/(Mg+Fe)	0.82	0.94	0.94	0.94	0.97	0.94	0.79	0.80	0.82
Ca/(Ca+Mg)					0.50				
Cr/(Cr+Al)					49.21				
Ca%	15.28	0.50	0.51	0.52	49.21				
Mg%	69.44	93.43	92.86	93.26	49.21				
Fe%	15.28	6.06	6.63	6.22	1.59				

Microprobe analyses made at Manchester University using the EDS mode

TABLE 7.3: Compositions of Minerals in Garnet/Spinel Lherzolite, Specimen NL528

	GT	OP	CP	OL	SP	Reaction Corona		Pool	
						OP	SP	OP	SP
SiO <sub>2</sub>	41.80	56.04	52.84	40.27	0.23	49.49	0.59	51.28	0.87
TiO <sub>2</sub>	0.13	0.13	0.69	-	0.12	-	0.20	-	0.13
Al <sub>2</sub> O <sub>2</sub>	21.52	2.01	5.66	-	43.54	9.51	59.15	7.37	57.55
Cr <sub>2</sub> O <sub>3</sub>	2.13	0.22	1.43	-	21.96	0.97	5.85	0.49	5.67
Fe <sub>2</sub> O <sub>3</sub>	-	-	-	-	3.88	-	2.26	-	2.30
FeO	11.15	7.02	2.70	10.72	13.52	10.74	13.09	10.61	13.59
MnO	0.44	0.12	0.13	-	0.21	0.51	0.35	0.49	0.36
MgO	17.96	33.51	13.82	48.35	16.65	25.16	18.83	27.02	18.25
CaO	5.08	0.22	19.78	-	-	2.39	0.08	1.74	0.09
Na <sub>2</sub> O	-	-	2.86	-	-	-	-	0.51	-
Ni	-	-	-	0.39	0.24	-	0.15	-	-
Total	100.21	99.27	99.91	99.73	100.32	98.77	100.55	99.51	98.81
Si	3.02	1.95	1.92	1.00	0.01	1.78	0.02	1.83	0.02
Ti	0.01	0.00	0.02	-	0.00	-	0.00	-	0.00
Al	1.83	0.08	0.24	-	1.42	0.40	1.80	0.31	1.79
Cr	0.12	0.01	0.04	-	0.48	0.03	0.12	0.01	0.12
Fe <sup>3+</sup>	-	-	-	-	0.08	-	0.04	-	0.05
Fe <sup>2+</sup>	0.67	0.20	0.08	0.22	0.31	0.32	0.28	0.32	0.30
Mn	0.03	0.00	0.00	-	0.05	0.02	0.01	0.02	0.01
Mg	1.93	1.74	0.75	1.78	0.69	1.35	0.72	1.44	0.72
Ca	0.39	0.01	0.77	-	-	0.09	0.00	0.07	0.00
Na	-	-	0.20	-	-	-	-	0.04	-
Ni	-	-	-	0.01	0.01	-	0.00	-	-
Total	8.00	3.99	4.02	3.01	3.05	3.99	2.99	4.04	3.01
Mg/(Mg+Fe)	0.742	0.895	0.901		0.687	0.807	0.719	0.820	0.705
Ca/(Ca+Mg)			0.507						
Cr/(Cr+Al)					0.253		0.062		0.062
Ca%	13.11	0.42	48.12			5.22		3.66	
Mg%	64.44	89.11	46.76			76.47		78.95	
Fe%	22.45	10.47	5.12			18.31		17.39	
%Fo				88.9					

Microprobe analyses made at Cambridge University using the EDS mode



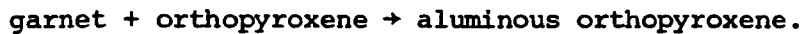
**TABLE 7.4:** Compositions of Minerals in Garnet/  
Spinel Lherzolites, Specimen NL535

	GT	OP	CP	OL	SP	AM	PH
SiO <sub>2</sub>	41.62	56.07	52.38	40.76	0.47	42.61	38.30
TiO <sub>2</sub>	-	0.12	0.39	-	0.18	1.33	2.68
Al <sub>2</sub> O <sub>3</sub>	22.12	2.04	3.69	-	38.72	13.28	14.77
Cr <sub>2</sub> O <sub>3</sub>	1.51	0.35	1.10	-	24.87	1.06	0.44
Fe <sub>2</sub> O <sub>3</sub>	-	-	-	-	5.45	-	-
FeO	10.18	6.55	2.81	9.57	14.94	3.94	3.40
MnO	0.48	0.14	-	-	0.22	-	-
MgO	18.16	33.72	15.12	48.78	15.50	17.71	23.02
CaO	5.54	0.25	22.08	-	-	11.79	-
Na <sub>2</sub> O	-	-	1.34	-	-	3.27	0.55
K <sub>2</sub> O	-	-	-	-	-	0.95	9.41
NiO	-	-	-	0.34	0.17	0.14	0.16
<b>Total</b>	<b>99.61</b>	<b>99.24</b>	<b>98.91</b>	<b>99.45</b>	<b>100.52</b>	<b>96.08</b>	<b>92.73</b>
Si	3.01	1.95	1.93	1.00	0.01	6.20	5.58
Ti	-	0.00	0.01	-	0.00	0.15	0.29
Al	1.88	0.08	0.16	-	1.29	2.28	2.54
Cr	0.09	0.01	0.03	-	0.56	0.12	0.05
Fe <sup>3+</sup>	-	-	-	-	0.12	-	-
Fe <sup>2+</sup>	0.62	0.19	0.09	0.20	0.35	0.48	0.41
Mn	0.03	0.00	-	-	0.01	-	-
Mg	1.96	1.75	0.83	1.79	0.65	3.84	5.00
Ca	0.43	0.01	0.87	-	-	1.84	-
Na	-	-	0.10	-	-	0.92	0.16
K	-	-	-	-	-	0.18	1.75
Ni	-	-	-	0.01	0.00	0.02	0.02
<b>Total</b>	<b>8.02</b>	<b>3.99</b>	<b>4.02</b>	<b>3.00</b>	<b>2.99</b>	<b>16.03</b>	<b>15.80</b>
Mg/(Mg+Fe)	0.761	0.902	0.906		0.649	0.889	0.923
Ca/(Ca+Mg)			0.512			0.324	
Cr/(Cr+Al)					0.301		
Ca%	14.30	0.48	48.74				
Mg%	65.19	89.74	46.42				
Fe%	20.51	9.78	4.84				
%Fo				90.1			

Microprobe analyses made at Cambridge University  
using the EDS mode

1971; Jenkins and Newton, 1979). Other studies of this phase transformation in natural systems (Kuno, 1967; Reid and Dawson, 1972; Smith, 1977) have attributed the reaction to decrease in pressure and Kuno (op.cit.) suggested this decrease was due to diapiric upwelling. He investigated assemblages which had partially transformed to plagioclase peridotite while still retaining relict garnet. Such phase transformations would be almost impossible solely as a result of increased temperature and as the Letseng samples have primary equilibration temperatures of  $> 1000^{\circ}\text{C}$  (see Chapter 9) it is more feasible that the phase change is largely the result of a pressure decrease.

The corona in specimen NL108 consists entirely of orthopyroxene (Table 7.1) and may represent the product of the reaction:



The corona minerals in specimen NL012 were not studied in detail, but are seen to reflect the Fe-rich character of the parent garnet and olivine. Note the slightly more chrome rich nature of the spinel despite the low chrome (2.77 wt.%  $\text{Cr}_2\text{O}_3$ ) in the primary garnet.

### 3) Annealed Rocks

The petrographic features of these rocks, described in Chapter 6, suggests some features unique among peridotite xenoliths in kimberlite. Their mineral phases also have compositions not previously recorded in xenoliths from kimberlite.

The phase compositions for three spinel lherzolites are given in Appendix 4 (NL148, NL162, and NL171 from the Main pipe) and those for garnet/spinel lherzolites in Tables 7.2, 7.3 and 7.4. The garnet and pyroxene compositions are shown in the system Ca-Mg-Fe in Figure 7.12.

The most striking feature of the spinel lherzolite is their aluminous character. The spinel is a magnesian aluminous spinel almost identical to the spinels found in the reaction coronas of the garnet lherzolites described in the previous section. The pyroxenes (both ortho- and clino-) show considerable solution of tschermakite molecule. The orthopyroxene contains 3.24-3.33 wt.%  $Al_2O_3$  and the clinopyroxenes 3.40-4.20 wt.%. Sodium is low even in the clinopyroxenes (<1 wt.%) so there is a considerable balance of atomic Al + Cr over Na. The Ca/(Ca+Mg) ratio in the clinopyroxene is very high, and on a Ca-Mg-Fe the diagram (Figure 7.12) plot closer to the diopside-hedenbergite join than any clinopyroxene from Letseng garnet peridotites. The low CaO in the coexisting orthopyroxene is compatible with the low temperature of equilibration of these rocks given by the clinopyroxene.

The Mg/(Mg+Fe) ratio in the orthopyroxene is lower than in the garnet peridotites, but the converse is true of the clinopyroxenes. The coexisting olivine in NL171 (no fresh olivine was found in NL148 or NL162) has a lower forsterite content ( $F_0$  90.7) than any of the Main pipe peridotites except the Fe rich NL012 but is similar to some of the olivines in the Satellite pipe xenoliths.

These rocks are texturally well equilibrated and chemically very homogeneous within a single section. This does not imply chemical equilibrium and the presence of clinopyroxene and spinel exsolution lamellae and blebs in the orthopyroxene suggests these assemblages are metastable. The exsolution is not related to any deformation feature. The clinopyroxene exsolution may imply re-equilibration to lower temperatures although this effect is likely to be very small in view of the already high Ca/(Ca+Mg) ratio of the clinopyroxene.

More important is the exsolution of spinel which suggests some adjustment to pressure change. The  $\text{Al}_2\text{O}_3$  isopleths of MacGregor (1974) show that this could only occur (at constant temperature) through an increase in pressure.

The texture of NL108 has already been described as intermediate between mosaic porphyroclastic and granuloblastic. The phase chemistry also shows some transitional features which relate to both the normal garnet lherzolites and the spinel lherzolites described above. The olivine (F0 94) is the most magnesian of any found in the Letseng peridotites although not greatly different from those in the Main pipe peridotites. The garnet is a chrome pyrope with low chrome (1.37 wt.%  $\text{Cr}_2\text{O}_3$ ). Clinopyroxene has rather low FeO and  $\text{Na}_2\text{O}$  contents (although within the Letseng peridotite range), but like the clinopyroxenes in the spinel lherzolites contains appreciable tschermakite molecule. The spinel is highly aluminous and of very similar composition to the reaction corona spinels described above.  $\text{Mg}/(\text{Mg}+\text{Fe})$  varies antipathetically with  $\text{Cr}/(\text{Cr}+\text{Al})$  although within narrow limits. This variation is similar to, although more restricted than, the trend noted by Nixon and Boyd (1973) and Carswell et al. (1979) in spinels in garnet kelyphite. Some slight zoning exists with alumina-enriched rims perhaps reflecting partial re-equilibration with orthopyroxene which shows the reverse of this zoning. The orthopyroxene shows a striking compositional variation:  $\text{Mg}/(\text{Mg}+\text{Fe})$  is a constant 0.94, but the alumina content varies between 1 wt.% and 3.5 wt.%; it is as high as 9.9 wt.% in the orthopyroxene corona around the garnet. This alumina is largely as magnesium tschermakite molecule.

This specimen (NL108) was described by Lock and Dawson (1980) and it was concluded that the phase chemistry resulted from the partial homogenisation and re-equilibration of an original garnet peridotite following extensive reaction between garnet and olivine, and subsequent deformation.

The orthopyroxene corona on the relict garnet is evidence that the reaction continued even after the culmination of the deformation and the preservation of garnet coronas in undeformed rocks is evidence of no direct relation between reaction and deformation. We also concluded that the spinel lherzolites were derived in a similar way from garnet lherzolites in which all the original garnet had been eliminated by reaction with olivine as a result of fall in pressure.

The two specimens NL528 and NL535 were referred to in Chapter 6 as further examples in which this textural and chemical transformation had been interrupted and 'frozen-in'. Analyses for phases in these two rocks (Tables 7.3 and 7.4) show the most striking features of both these rocks are the Fe-rich nature of the garnet ( $\text{FeO} > 10 \text{ wt.}\%$ ) and orthopyroxene ( $\text{FeO} > 6.5 \text{ wt.}\%$ ) and the aluminous pyroxenes. Compared to the Fe-rich rock NL012 these two specimens contain more magnesian olivine, however, this difference is quite small and may relate more to the partitioning of Fe and Mg between the various silicates rather than any bulk chemical differences. The  $\text{Ca}/(\text{Ca}+\text{Mg})$  ratio of 0.510 is considerably higher than in NL012 which, like the low temperature Satellite pipe peridotites, implies partitioning of Fe, preferentially to Mg, into garnet rather than olivine (see above).

The second important feature is that, like NL108, these specimens contain pyroxenes with appreciable tschermakite molecule, although within-specimen variation is not apparent from the few analysis carried out. The primary aluminous spinel, like those discussed above, has some similarity to the reaction corona spinels. It is, however, more chrome-rich (21.96 and 24.87 wt.%  $\text{Cr}_2\text{O}_3$ ) than the corona spinels or indeed than those in the spinel lherzolites; and in view of the low chrome in the coexisting garnet suggests a marked Cr partitioning into spinel at these equilibration temperatures.

The green spinel in the reaction corona of NL528 is considerably more aluminous (57.5-59.2 wt.%  $\text{Al}_2\text{O}_3$ ). Such compositions have recently been reported from garnet-free peridotites found in the Malaita alnoite, south-west Pacific (Nixon and Boyd, 1979) but these were a primary phase and not coexisting with garnet. In this rock, the spinel and orthopyroxene in the 'pools' described in Chapter 6 match the compositions of these minerals in the reaction corona (Table 7.3) and are therefore compatible with their deviation from the primary olivine and garnet in the reaction and deformation described above.

The major problem of the paragenesis of these rocks using the model presented by Lock and Dawson (1980) centres on explaining why the spinel 'primary' to the granuloblastic texture in the garnet/spinel peridotites, which our model implies derives from reworked reaction corona spinel, is consistently more chrome-rich than would be expected either from comparison with spinels in reaction coronas (e.g. NL528) or indeed by comparison with the low chrome nature of the coexisting garnet. The garnets in NL108, NL528 and NL535 plot at the low  $\text{Cr}_2\text{O}_3$  end of the 'CaO trend' referred to above (Figure 7.4) but show CaO contents of 5.5 to 6.0 wt.% which are more compatible with a chrome content of ~6.5 wt.%  $\text{Cr}_2\text{O}_3$ . The coupling between CaO and  $\text{Cr}_2\text{O}_3$  was illustrated by Wood (1977) as a linear correlation between  $K_D(\text{Cr}/\text{Al})_{\text{GT}} \cdot (\text{Al}/\text{Cr})_{\text{SP}}$  and  $X_{\text{Ca}}^{\text{GT}}$ . The present samples plot to the high  $K_D$  side of this line. I interpret that some re-equilibration of Cr and Al between garnet and spinel has occurred while the present CaO content reflects a previously more chrome rich garnet composition. Nixon and Boyd (1973) and Carswell et al. (1979) have already shown that reaction corona (kelyphite) aluminous spinels display a range of compositions towards typical chromite as found in other xenoliths. Dawson et al. (1978) have described multiple garnet-spinel transitions in a harzburgite from Liphobong, Lesotho. This garnet shows zoning from a Cr-rich core to Cr-poor rim and the groundmass spinel is an aluminous

spinel only slightly more chrome rich than some of the spinels in specimen NL108 from Letseng. If this explanation is true then the Lock and Dawson model (1980) may still be invoked to explain the mineral chemistry of these garnet/spinel peridotites.

Several garnet/spinel peridotites have been analysed from the Malaita alnoite (Nixon and Boyd, *op.cit.*) but these rocks display consistently more aluminous pyroxenes than those from Letseng. There is some similarity between the garnets and spinels, but the Letseng samples are usually more Fe-rich. Some of the Malaita garnets are low-chrome varieties with slightly higher CaO contents but others are consistent with the 'CaO trend'. It is tempting to speculate that the Malaita rocks, which sometimes contain orthopyroxene with cores of 'symplectite-like patches of yellow to red-brown spinel' may have formed in a similar way to that described above for Letseng garnet/spinel peridotites. One might then infer a much closer relationship between garnet and spinel facies rocks which may be continually modified by diapiric upwelling from the deeper mantle.

Specimen NL535 has equilibrated with both phlogopite and amphibole. The phlogopite is more alumina and iron rich than other primary upper mantle micas (e.g. Dawson and Smith, 1975; Carswell, 1975). This may reflect the lower equilibration temperatures and pressures, shown by the other silicates in this rock, relative to those in these other studies. Primary amphibole in upper mantle peridotites has only been reported from a relatively few localities (see Dawson and Smith, 1975; Nixon and Boyd, 1979). The texture and chemistry of the phases for this Letseng amphibole-bearing peridotite (NL535) compare closely with those reported by Nixon and Boyd (*op.cit.*) from a Malaita garnet peridotite and are distinct from the chromite intergrowths ('fingerprint spinel') of Dawson and Smith (*op.cit.*). The Letseng amphibole is a pargasite (terminology of Leake, 1978) with higher  $\text{Al}_2\text{O}_3$  wt.% and lower  $\text{Cr}_2\text{O}_3$  wt.% than the amphiboles occurring

as intergrowths with chromite. Although very similar to the Malaita amphibole, the Letseng amphibole shows slightly higher  $Mg/(Mg+Fe)$  and  $Ca/(Ca+Mg)$  ratios.

### Summary

1. Primary phases show similar composition trends to those seen in other xenolith suites.
2. Reaction corona phases are compatible with derivation during transformation from garnet to spinel facies peridotite.
3. Spinel and garnet/spinel rocks with annealed textures have phase compositions resulting from garnet breakdown, chemical homogenisation and re-equilibration.



Figure 7.1:Ca - Mg - Fe plot of garnets and pyroxenes from Main Pipe peridotites.

Closed circles:coarse textured rocks.

Crosses:porphyroclastic textured rocks.

Open circles:mosaic porphyroclastic textured rocks.

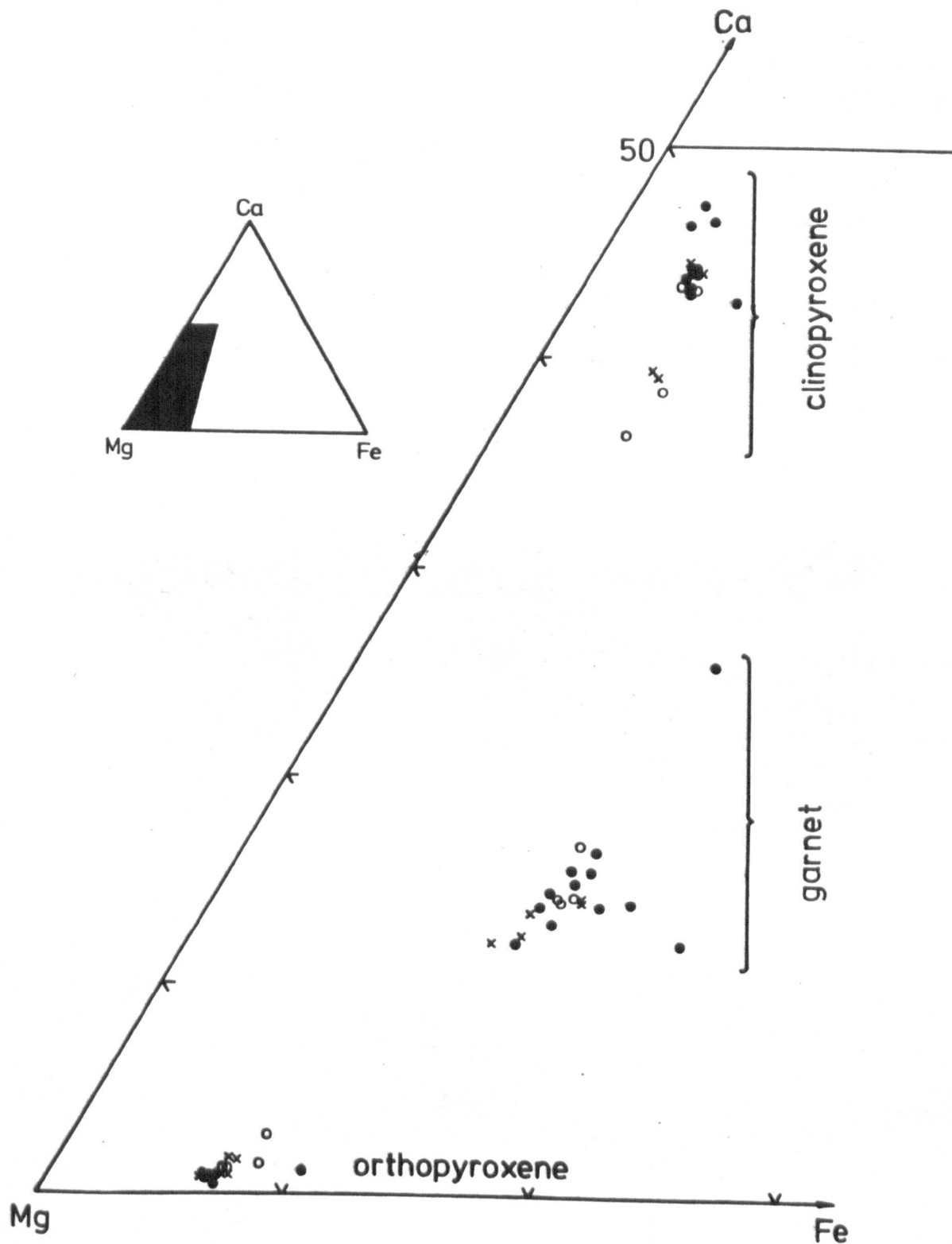


Figure 7.2:Ca - Mg - Fe plot of garnets and pyroxenes from  
Satellite Pipe peridotite.  
Symbols as for figure 7.1.

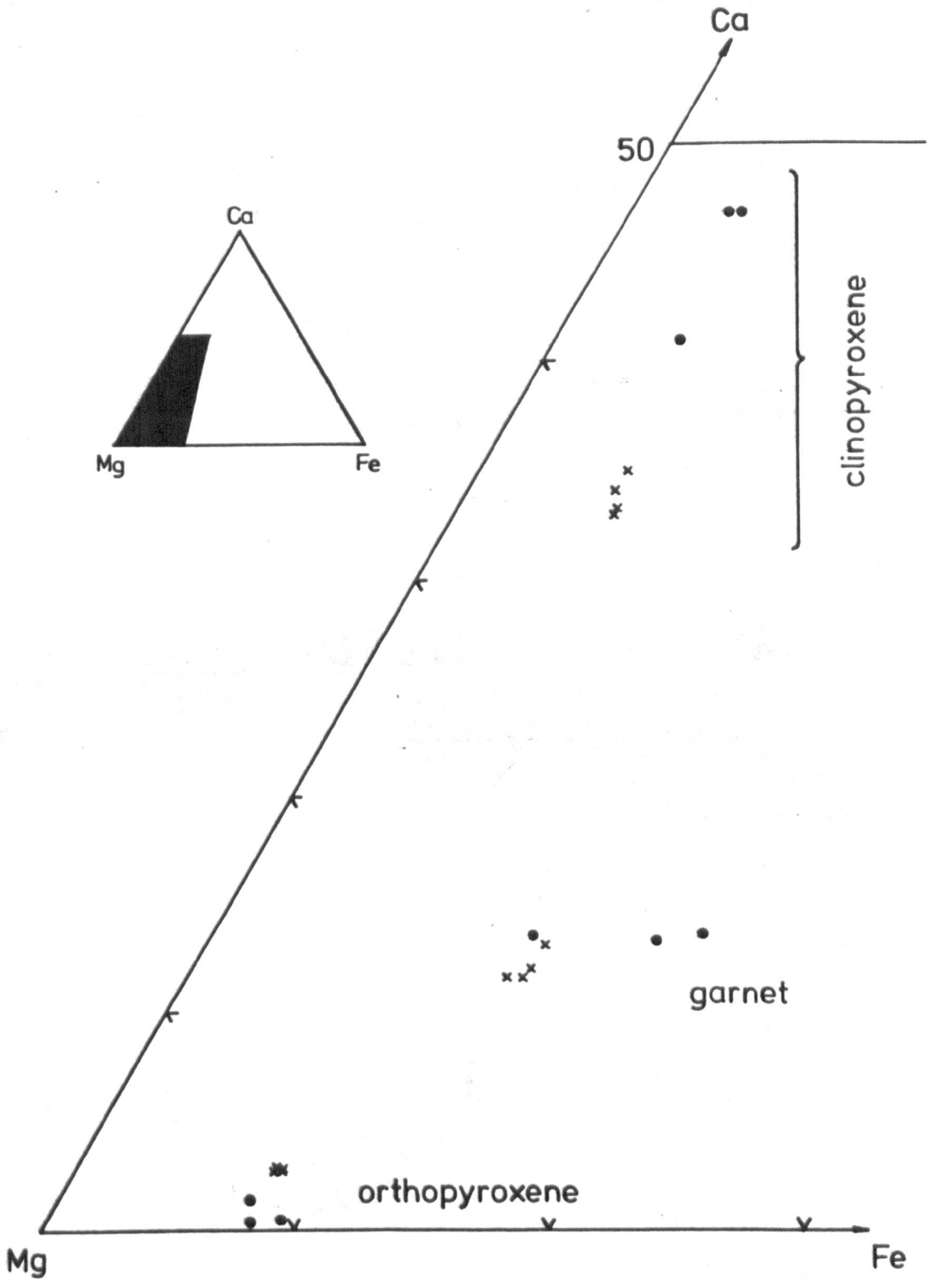


Figure 7.3:Ca - Mg - Fe plot of garnets and pyroxenes from Letseng peridotites (published data).

Closed circles:Boyd(1973).

Open circles:Bishop et al(1978).

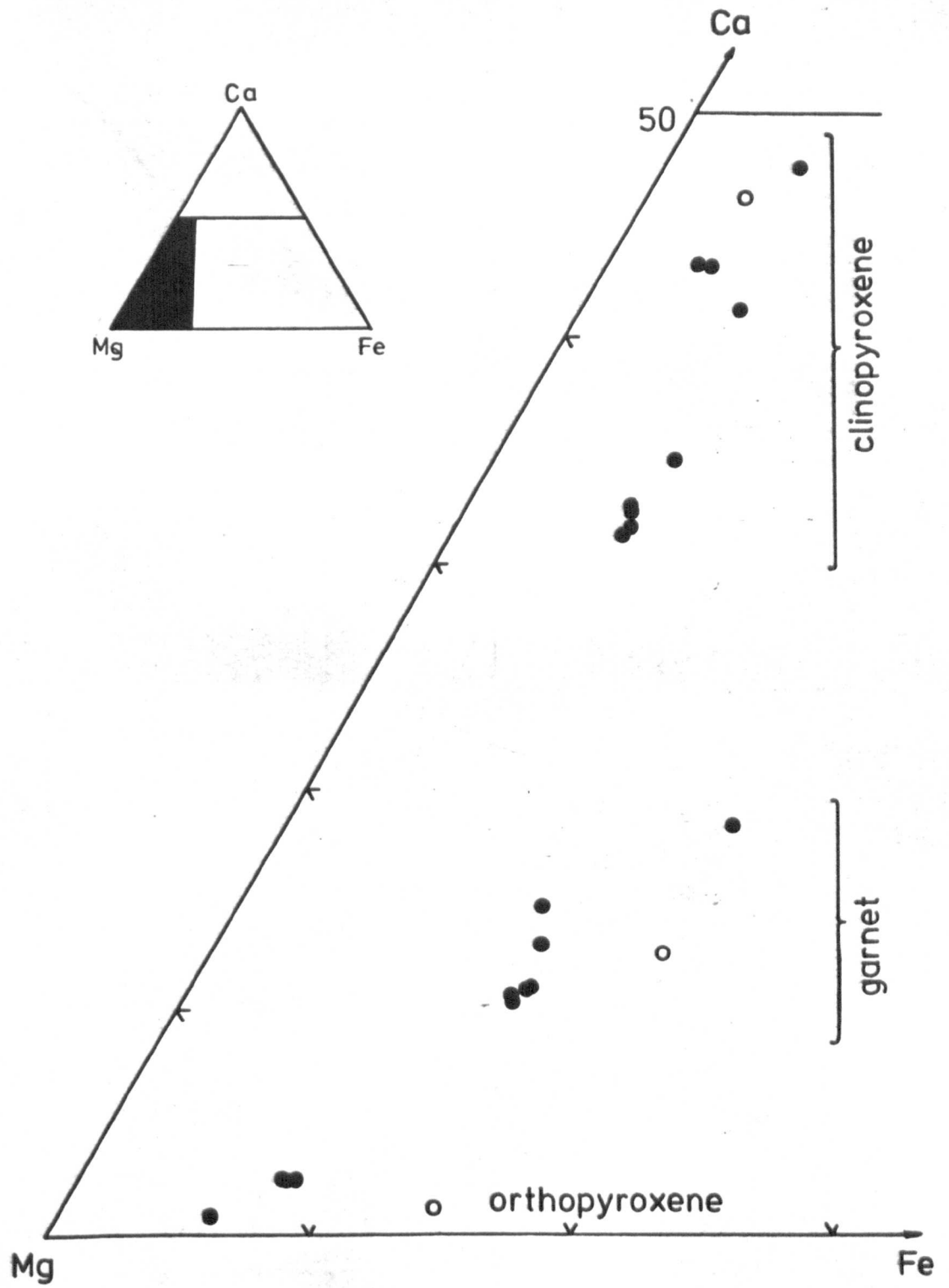


Figure 7.4: Garnets from Letseng peridotites.

Cr<sub>2</sub>O<sub>3</sub> Wt% v. CaO Wt% v. Al<sub>2</sub>O<sub>3</sub> Wt%.

Closed circles: this study.

Open circles: published analyses (see figure 7.3).

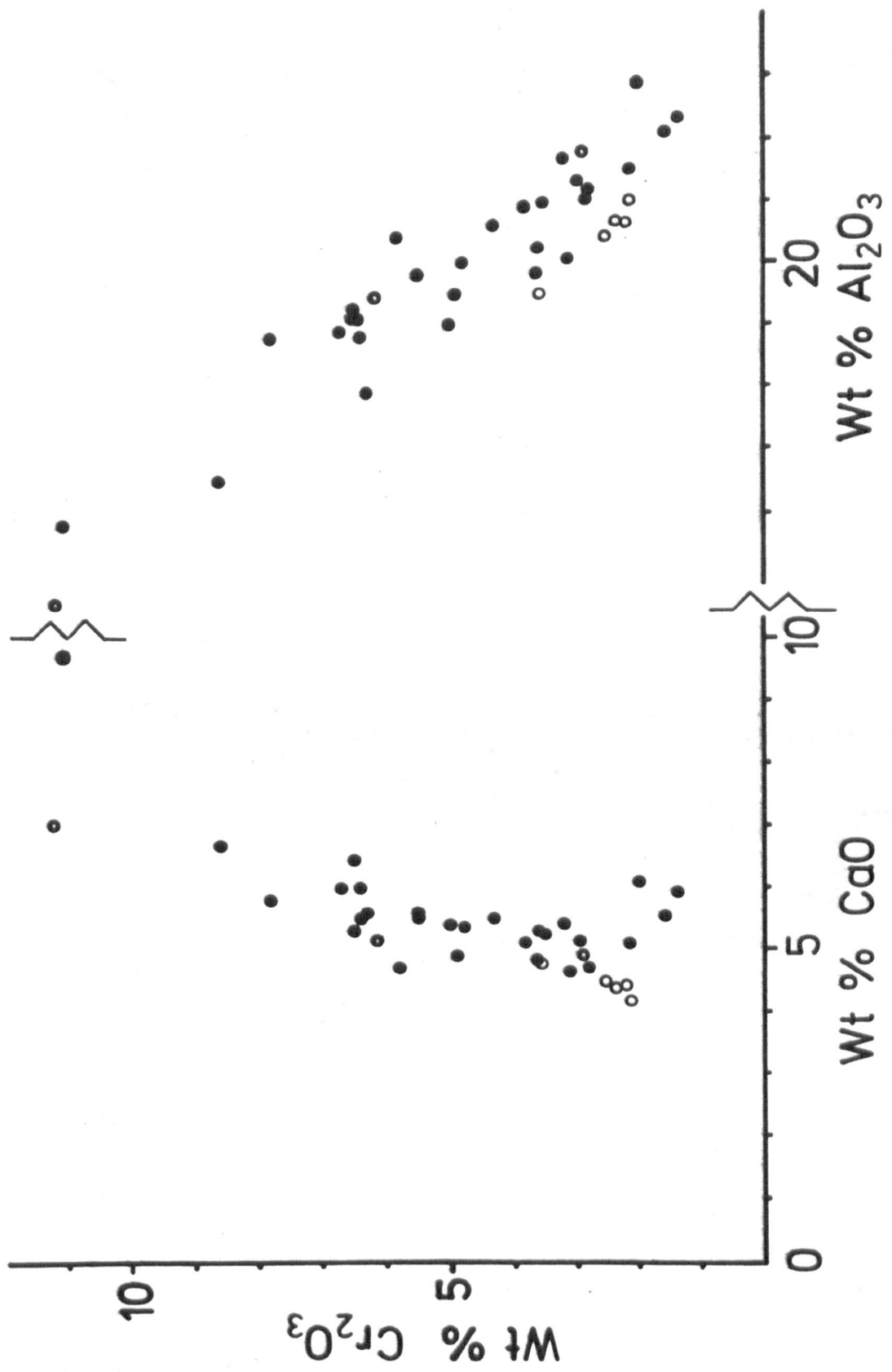




Figure 7.5: Clinopyroxenes from Letseng peridotites.  
Atomic Al+Cr v. Atomic Na.

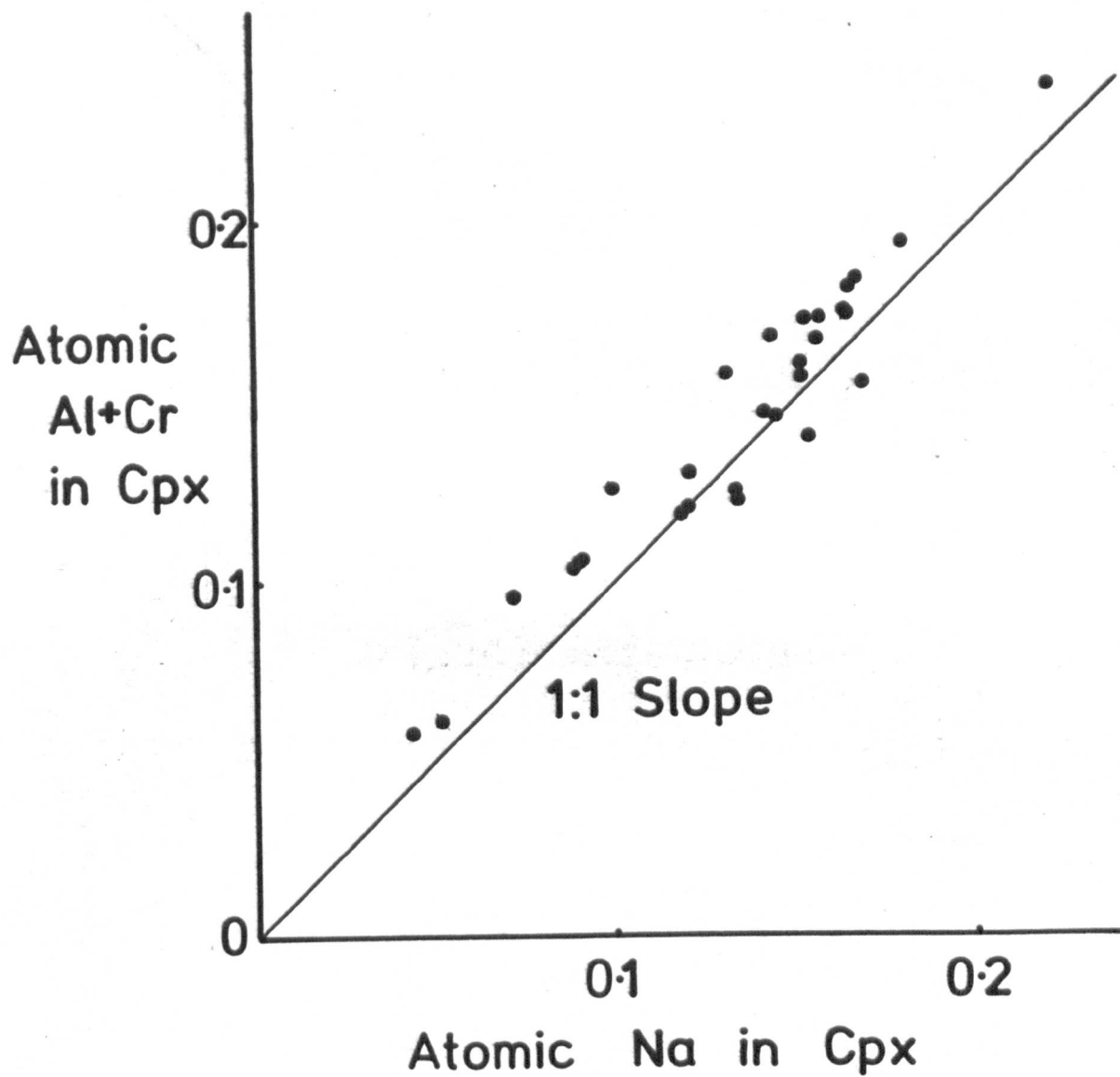


Figure 7.6: Orthopyroxenes from Letseng peridotites.  
Atomic Al+Cr v. Atomic Na.

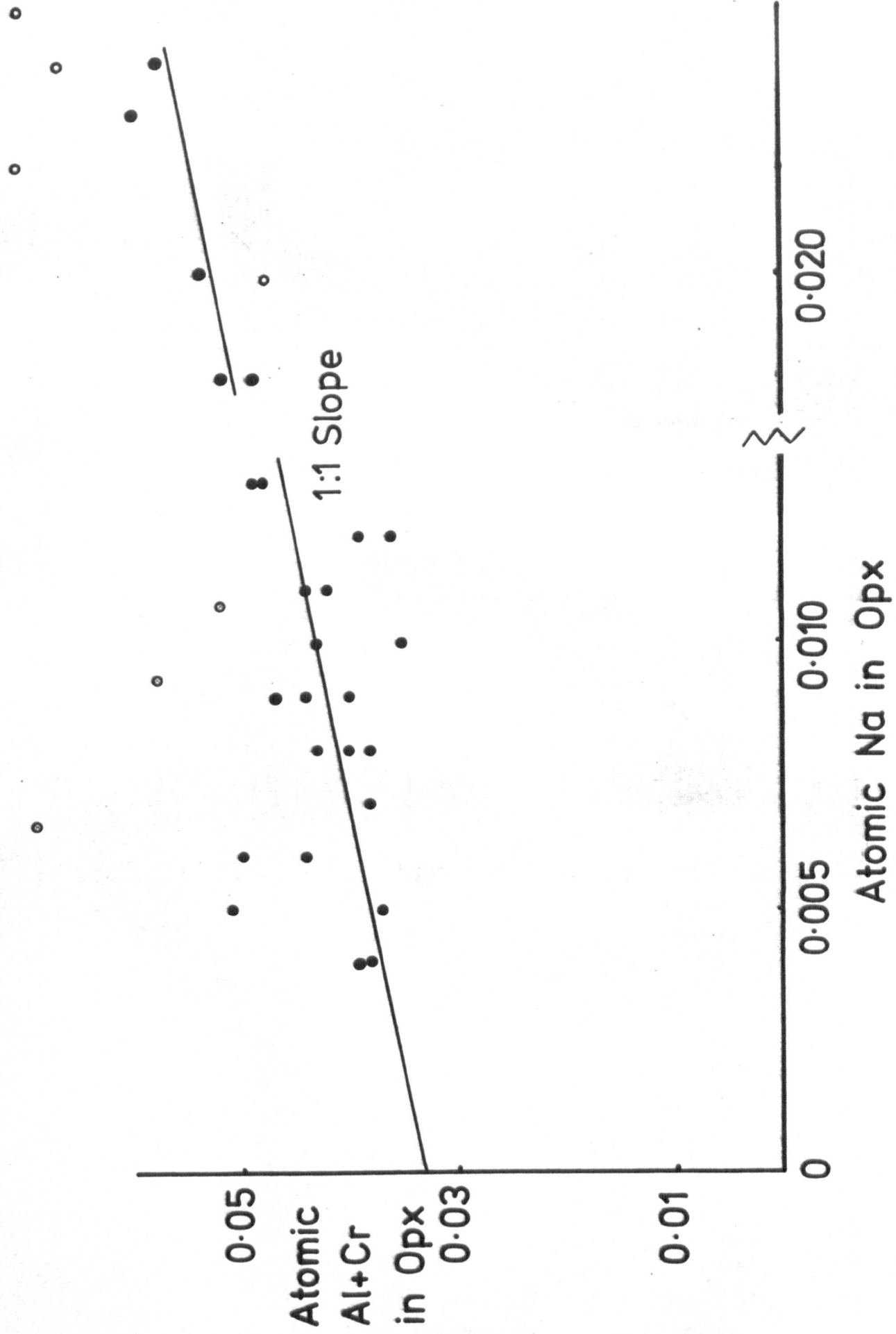


Figure 7.7: Silicate Mg/(Mg+Fe) ratio v. %Fo in coexisting olivine for Main Pipe peridotites.  
Closed circles: coarse textured rocks.  
Crosses: deformed rocks.

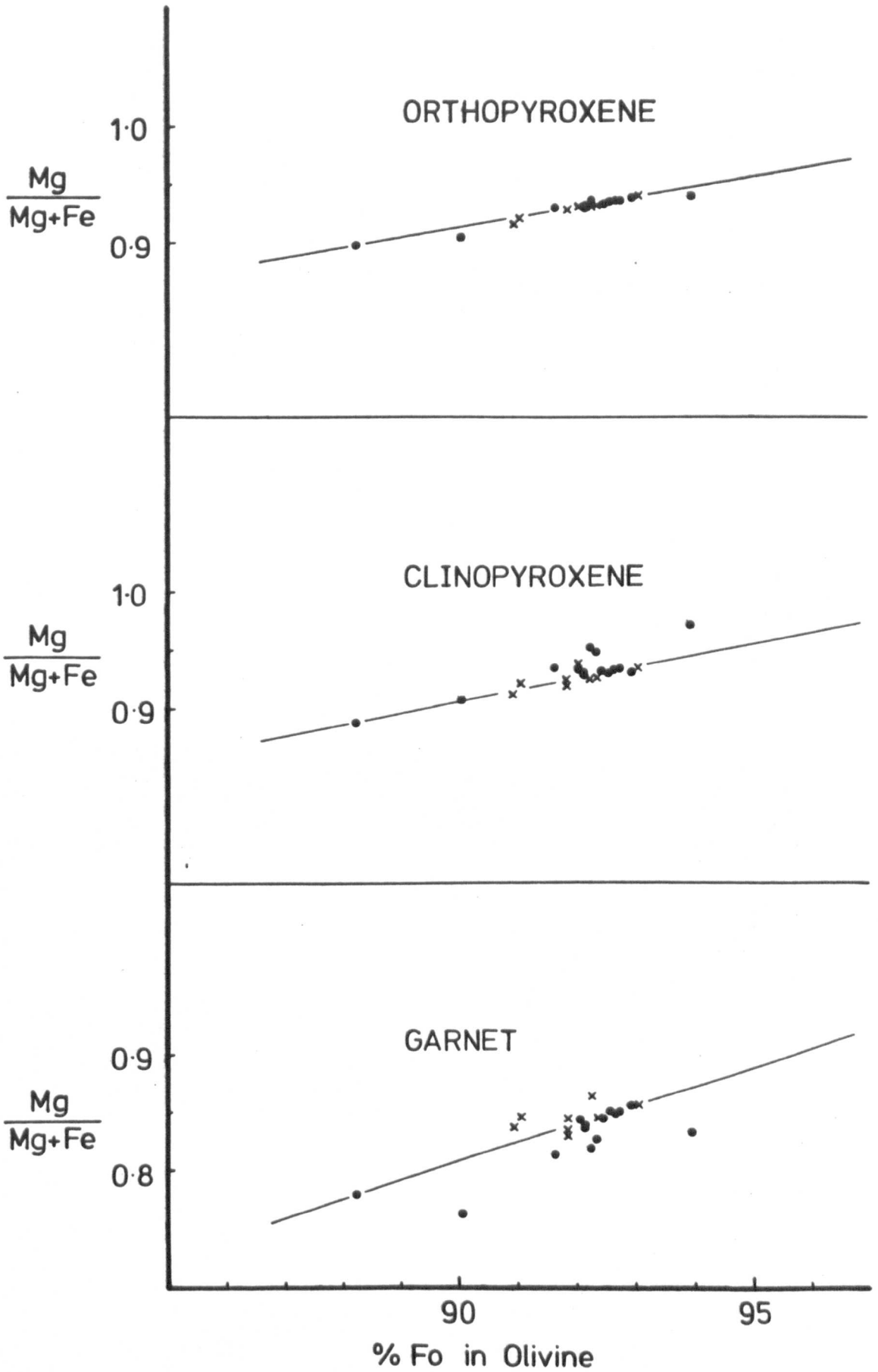


Figure 7.8: Silicate Mg/(Mg+Fe) ratio v. %Fo in coexisting olivine for Satellite Pipe peridotites.  
Symbols as for figure 7.7.

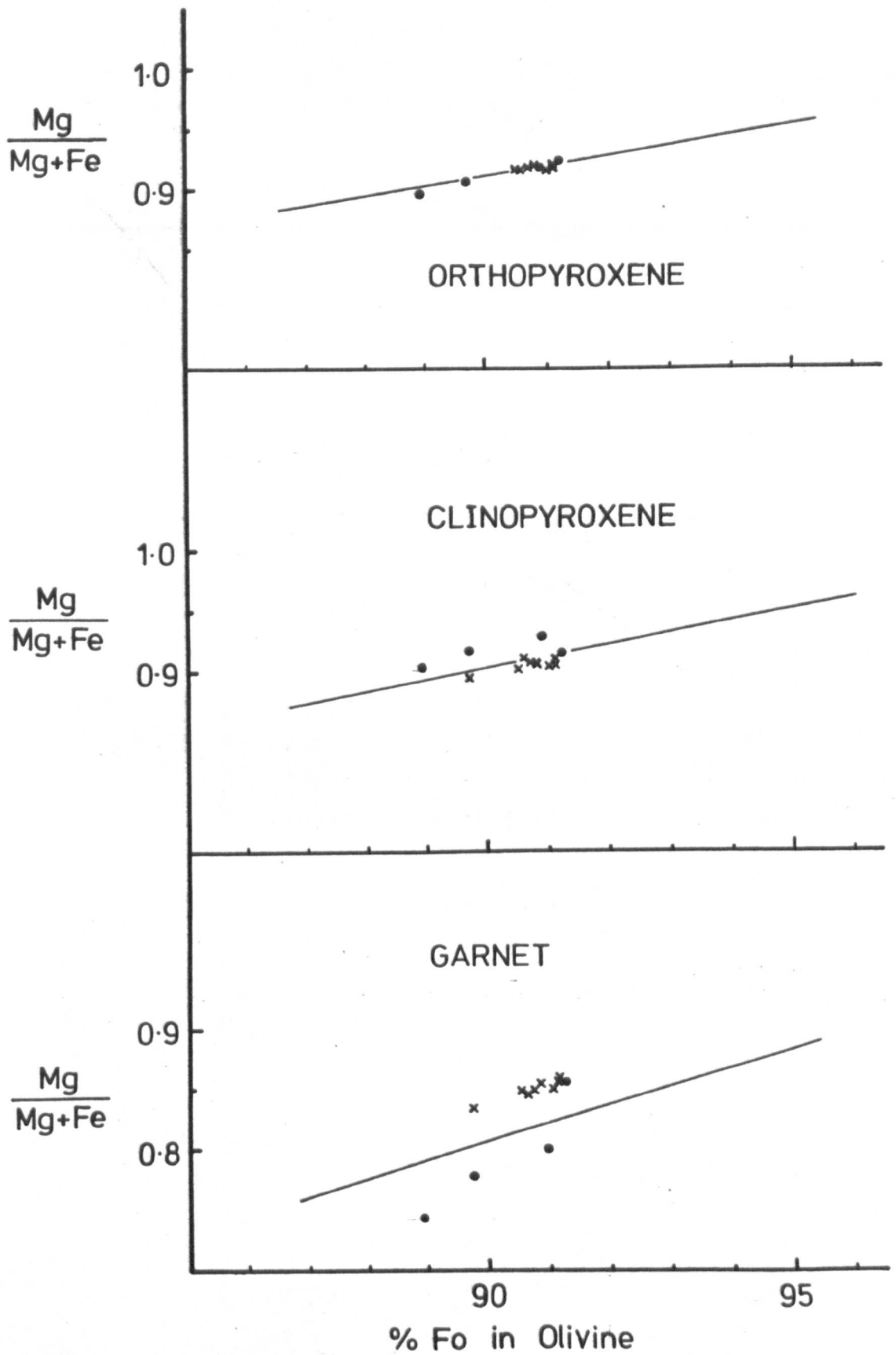




Figure 7.9: Silicate Al/(Al+Cr) ratio v. %Fo in coexisting  
olivine for Letseng peridotites.  
Symbols as for figure 7.7.

$$\frac{\text{Al}}{\text{Al}+\text{Cr}}$$

0.8  
0.7

ORTHOPYROXENE

$$\frac{\text{Al}}{\text{Al}+\text{Cr}}$$

0.8  
0.7  
0.6  
0.5

CLINOPYROXENE

$$\frac{\text{Al}}{\text{Al}+\text{Cr}}$$

0.9  
0.8

GARNET

% Fo in Olivine

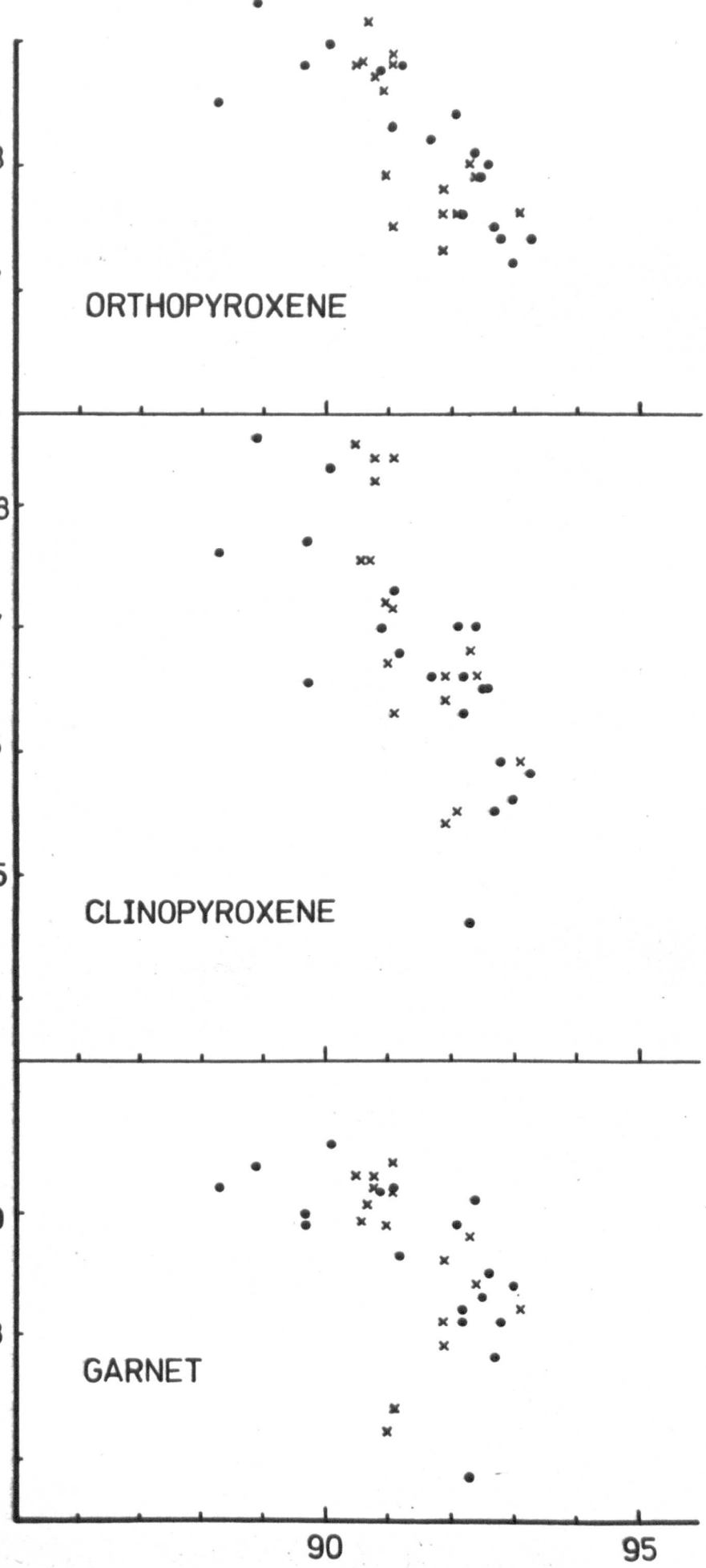


Figure 7.10: Compositions of spinels from peridotites and xenocrysts in Letseng kimberlites. Displayed in the expanded spinel prism (see Smith & Dawson 1975).

Closed circles: peridotites.

Open circles: peridotites (Boyd 1973, Smith & Dawson 1975)

Crosses: xenocrysts.

Enclosed crosses: xenocrysts (Boyd 1973).

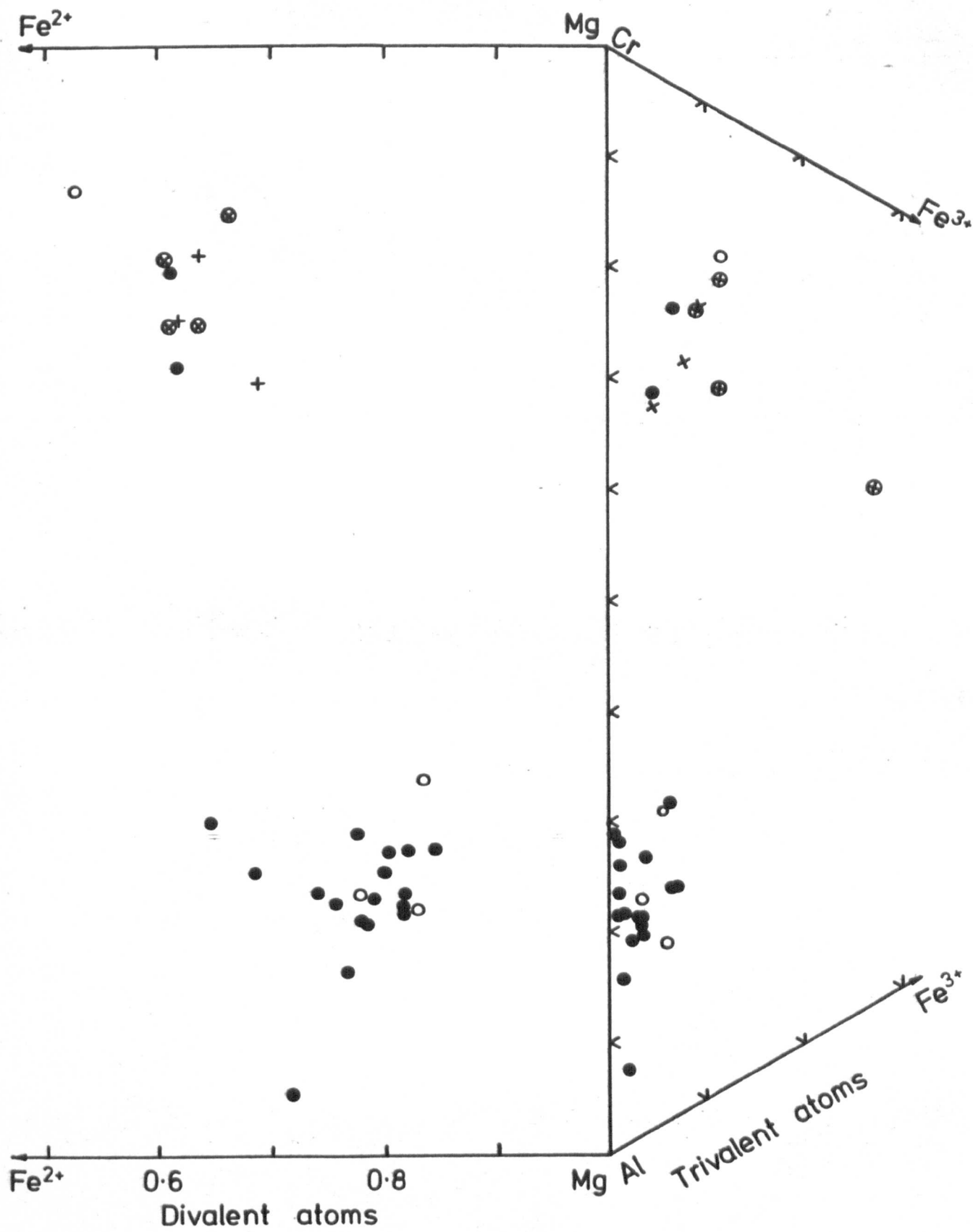


Figure 7.11: Comparison of compositions of primary and corona pyroxenes in Letseng peridotites showing garnet breakdown. Plot in Ca - Mg - Fe system.  
Closed circles: primary pyroxenes.  
Crosses: corona pyroxenes.

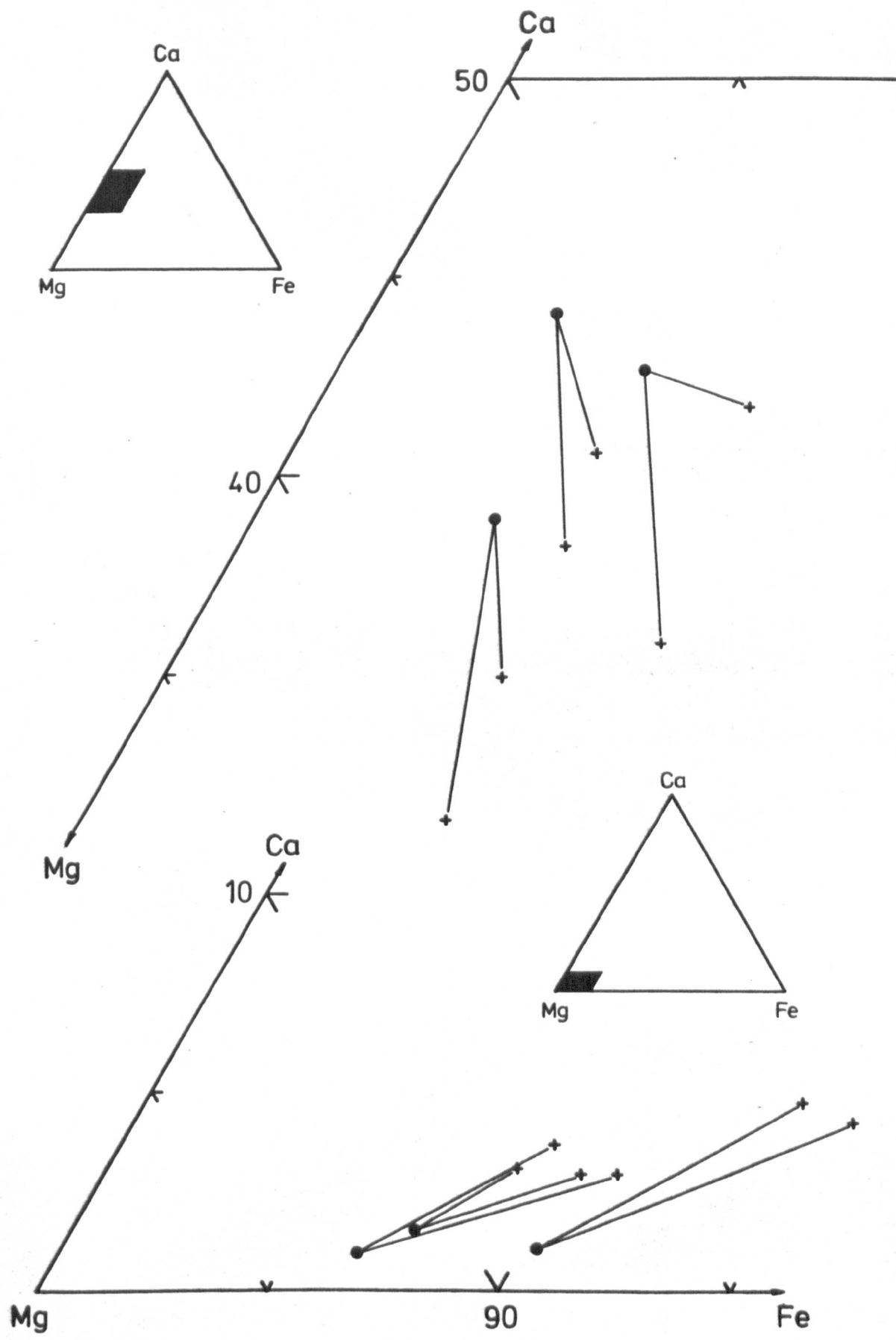
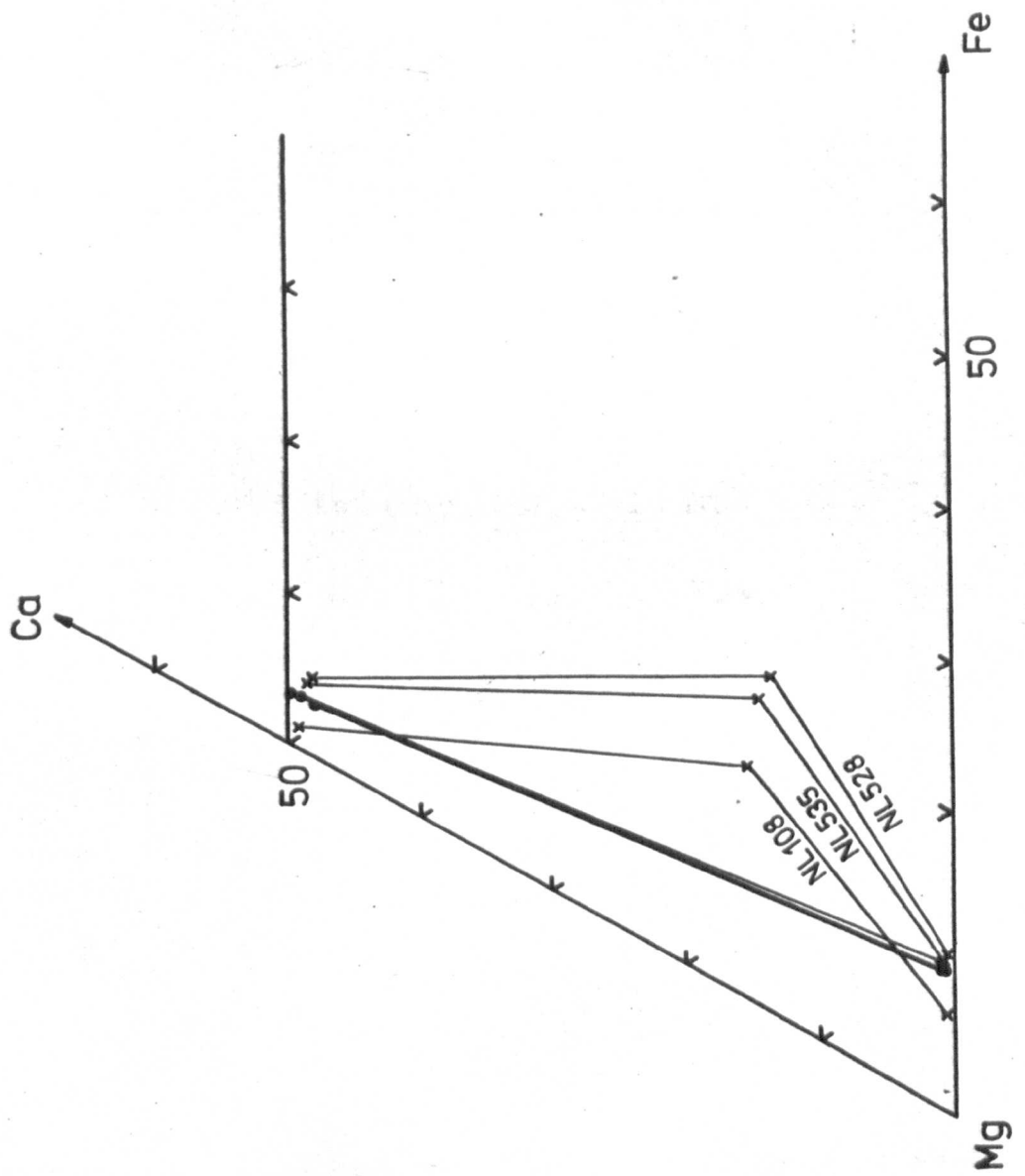


Figure 7.12:Ca - Mg- Fe plot of compositions of garnet and pyroxenes in spinel and garnet/spinel lherzolites.





CHAPTER 8Peridotites: Bulk Rock Chemistry

The bulk rock compositions of eighteen garnet and chromite/spinel peridotites of various textural types have been determined by atomic absorption spectrometry at St. Andrews University and X-ray fluorescence spectrometry at Sheffield University. The data are shown in Table 8.1.

At St. Andrews, the sample powders were dissolved in hydrofluoric and perchloric acids and the solution analysed by standard atomic absorption spectrometry techniques for the major elements, Cr and Ni. FeO and H<sub>2</sub>O were analysed by standard wet chemical techniques.

XRF analyses for major elements were made on the remaining samples as described in Chapter 3. Cr and Ni were measured as trace elements in powder pellets. Na<sub>2</sub>O, FeO and H<sub>2</sub>O were analysed as for the kimberlites (Chapter 3).

The FeO analyses made at Sheffield University by the writer give considerably lower values than analyses of similar rocks at St. Andrews University. The discrepancy is due to the presence of garnet for which special care is required to obtain accurate ferrous iron values. It is unlikely, considering the mineralogy, that these rocks should contain so large an amount of ferric iron as implied by the Sheffield analyses. However, in the following discussion all iron is considered to be in the ferrous state.

Table 8.2, shows some of these analyses recalculated volatile free, together with bulk rock compositions calculated from modal proportions and mineral compositions. This procedure allowed not only a comparison between the direct and indirect analyses but also the inclusion in the discussion of bulk rock chemistry of specimen NLO12. NLO12 was too small for meaningful bulk rock analysis but its Fe-rich character (revealed in

TABLE 8.1: Peridotite Bulk Rock Geochemistry\*

	NL495	NL494	NL451	NL427	NL141	NLO80	NL125	NL124	NL197
SiO <sub>2</sub>	41.98	42.44	41.28	42.60	42.20	43.90	43.40	42.80	41.70
TiO <sub>2</sub>	0.10	0.01	0.02	0.07	<0.10	<0.10	<0.10	<0.10	<0.10
Al <sub>2</sub> O <sub>3</sub>	0.75	0.85	0.45	0.87	0.80	1.28	1.23	0.49	0.60
Cr <sub>2</sub> O <sub>3</sub>	0.31	0.53	0.35	0.23	0.42	0.49	0.42	0.16	0.23
Fe <sub>2</sub> O <sub>3</sub>	4.35	4.05	4.26	4.34	2.41	1.77	1.88	1.62	2.30
FeO	4.74	4.65	3.93	3.41	5.25	5.06	4.96	5.69	4.80
MnO	0.10	0.14	0.14	0.13	0.11	0.11	0.11	0.11	0.09
MgO	42.90	42.52	44.50	41.80	45.25	43.50	44.25	44.00	46.75
CaO	0.68	0.70	0.27	0.47	0.69	0.61	0.48	0.62	0.50
Na <sub>2</sub> O	0.08	0.02	0.04	0.04	0.17	0.16	0.17	0.20	0.17
K <sub>2</sub> O	0.00	0.01	0.01	0.07	0.06	0.10	0.06	0.08	0.06
NiO	0.33	0.34	0.34	0.36	0.27	0.28	0.26	0.31	0.29
P <sub>2</sub> O <sub>5</sub>	0.02	0.01	0.02	0.02	0.02	0.01	0.01	0.01	0.01
SO <sub>3</sub>	0.05	0.08	0.06	0.08					
H <sub>2</sub> O <sup>T</sup>	4.08	4.07	5.08	5.83	4.04	3.64	4.66	5.50	4.66
Total	100.47	100.42	100.75	100.32	101.79	101.01	101.99	101.69	102.26
MgO/FeO <sup>T</sup>	5.0	5.1	5.7	5.7	6.1	6.5	6.7	6.7	6.8

XRF analyses (those including SO<sub>3</sub>) by R. Kanaris-Sotiriou and S. Burley

AA analyses (those not including SO<sub>3</sub>) by R. Bachelor

	NL441	NL196	NLO01	NL195	NL153	NL184	NL466	NL572	NL573
SiO <sub>2</sub>	45.00	44.40	43.10	45.00	44.50	43.80	45.20	42.01	45.19
TiO <sub>2</sub>	<0.10	<0.10	<0.10	<0.10	<0.10	<0.10	<0.10	0.01	0.01
Al <sub>2</sub> O <sub>3</sub>	1.00	1.23	0.86	0.80	0.83	0.71	0.33	0.68	1.93
Cr <sub>2</sub> O <sub>3</sub>	0.47	0.53	0.39	0.44	0.48	0.22	0.17	0.27	0.43
Fe <sub>2</sub> O <sub>3</sub>	2.15	1.66	1.64	1.42	1.45	1.47	1.35	3.59	2.89
FeO <sup>T</sup>	4.28	4.61	4.64	4.44	4.64	4.25	4.14	3.88	4.72
MnO	0.10	0.10	0.09	0.10	0.09	0.09	0.09	0.10	0.15
MgO	43.25	44.00	44.58	42.25	45.53	43.65	44.11	45.36	40.00
CaO	0.38	0.45	0.54	0.68	0.38	0.31	0.44	0.24	1.49
Na <sub>2</sub> O	0.17	0.17	0.25	0.19	0.22	0.22	0.22	0.02	0.07
K <sub>2</sub> O	0.06	0.08	0.02	0.10	0.02	0.03	<0.04	0.00	0.00
NiO	0.27	0.24	0.29	0.25	0.25	0.26	0.29	0.35	0.29
P <sub>2</sub> O <sub>5</sub>	0.01	0.01	0.01	0.03	0.01	0.01	0.02	0.02	0.01
SO <sub>3</sub>								0.03	0.04
H <sub>2</sub> O <sup>T</sup>	5.22	4.64	4.88	4.96	4.24	5.10	5.24	3.87	2.71
Total	102.46	102.22	101.39	100.76	102.74	100.22	101.74	100.42	99.93
MgO/FeO <sup>T</sup>	7.0	7.2	7.3	7.4	7.7	7.8	8.9	7.9	5.5

\*For modes and textures see Table 6.2 and below:

- NL451 Fluidal mosaic porphyroclastic garnet harzburgite
- NL427 LAD mosaic porphyroclastic garnet lherzolite
- NL141 Porphyroclastic garnet lherzolite
- NL195 Coarse garnet harzburgite
- NL153 Coarse garnet lherzolite
- NL184 Coarse chromite harzburgite
- NL466 Coarse chromite harzburgite
- NL572 Granuloblastic spinel lherzolite
- NL573 Granuloblastic spinel lherzolite

**TABLE 8.2: Peridotite Geochemistry - Bulk Rock Chemistry Recalculated from Mineral Chemistry and Modal Analysis Compared to those Recalculated Anhydrous from XRF**

	NL012	NL495	NL495*1	NL494	NL494*1	NL426	NL427*2	NL492	NL197	NL197*1	NL441	NL441*1	NL171
SiO <sub>2</sub>	46.06	42.50	43.81	43.72	44.40	47.65	45.33	47.99	42.88	43.87	46.43	46.20	44.57
TiO <sub>2</sub>	0.11	0.09	0.10	0.03	0.01	0.06	0.07	0.04	0.05	0.03	0.05	0.03	0.02
Al <sub>2</sub> O <sub>3</sub>	3.59	0.83	0.78	0.97	0.89	1.32	0.93	0.88	0.62	1.35	1.03	2.45	2.78
Cr <sub>2</sub> O <sub>3</sub>	0.51	0.35	0.32	0.56	0.55	0.42	0.24	0.29	0.24	0.39	0.48	0.88	0.81
Fe <sub>T</sub> <sup>T</sup>	9.75	8.26	9.04	7.98	8.69	6.69	7.79	6.19	7.06	6.79	6.42	5.98	7.89
MnO	0.18	0.11	0.10	0.13	0.15	0.12	0.14	0.09	0.09	0.08	0.10	0.13	0.13
MgO	39.32	46.44	44.77	45.84	44.49	43.19	44.48	42.11	48.07	46.68	44.63	43.41	42.28
CaO	0.98	0.72	0.71	0.67	0.73	0.50	0.50	2.02	0.51	0.69	0.39	0.77	1.54
Na <sub>2</sub> O	0.09	0.11	0.21	0.04	0.21	0.10	0.21	0.19	0.17	0.08	0.18	0.06	0.07
NiO	0.33	0.35	0.34	0.33	0.35	0.29	0.37	0.25	0.30	0.36	0.28	0.28	0.29
Total	100.92	99.76	100.18	100.27	100.47	100.34	100.06	100.05	99.99	100.32	99.99	100.19	100.38
MgO/FeO <sup>T</sup>	4.0	5.6	5.0	5.7	5.1	6.5	5.7	6.8	6.81	6.87	6.95	7.26	5.4

\*<sup>1</sup> XRF analyses recalculated, H<sub>2</sub>O, P<sub>2</sub>O<sub>5</sub> and SO<sub>3</sub> free

\*<sup>2</sup> Mineral chemistry and mode is almost identical to NL426

mineral compositions) is unique among the Letseng peridotites.

The garnet peridotites show a moderate spread of  $\text{MgO}/\text{FeO}^{\text{T}}$  ratios with most in the range 5-8. This variation in Fe content in no way correlates with the xenolith texture as suggested by Nixon and Boyd (1973) and Boyd and Nixon (1975). These authors showed that 'sheared' peridotites have  $\text{FeO}/(\text{FeO} + \text{MgO}) \times 100 > 0.12$ . Among the present data it is not possible to calculate this ratio for the reasons already discussed, but the  $\text{MgO}/\text{FeO}^{\text{T}}$  would demonstrate the same relationship. In this study there is a tendency to lower  $\text{MgO}/\text{FeO}^{\text{T}}$  in deformed rocks, (e.g. NL495, NL427, NL141) but the most Fe-rich sample, NLO12, is a coarse textured rock. Nixon and Boyd also correlated texture (and hence chemistry) with depth of origin, but the present data display a wide spread of equilibration temperatures and pressures (see Chapter 9) and demonstrate that more Fe-rich compositions do equilibrate to low temperature and pressure (NL427  $T = 976^{\circ}\text{C}$ ,  $P = 31.0 \text{ Kb}$ ; NLO12  $T = 964^{\circ}\text{C}$ ,  $P = 33.4 \text{ Kb}$ ).

This observation is in accord with the conclusions of Cox et al. (1973) and Gurney et al. (1975) for samples from Matsoku, Lesotho. Specimens with widely varying Mg/Fe ratios were shown to originate from a restricted shallow upper mantle source. Gurney et al. (1975) interpret their data in relation to an upper mantle igneous event with depleted Common Peridotites remaining as the residue of partial melting and Fe-enriched rocks representing liquid and/or crystal cumulates. Their data show variations of oxide abundances related to  $\text{MgO}/\text{FeO}^{\text{T}}$  ratio. In particular  $\text{Al}_2\text{O}_3$ ,  $\text{FeO}^{\text{T}}$ ,  $\text{CaO}$ ,  $\text{TiO}_2$ ,  $\text{MnO}$  and  $\text{Na}_2\text{O}$  increase with decreasing  $\text{MgO}/\text{FeO}^{\text{T}}$  whereas MgO shows a marked reciprocal relation and  $\text{SiO}_2$ ,  $\text{Cr}_2\text{O}_3$ ,  $\text{NiO}$  and  $\text{K}_2\text{O}$  do not show any recognisable trend.

The data presented here from Letseng peridotites is more difficult to interpret because of the spread of estimated equilibration temperatures and pressures. This precludes a complete explanation using the Matsoku model,

although the large number of rocks equilibrated under similar conditions to those at Matsoku may have a similar history. This group includes the specimen NLO12 which has a very similar mineral chemistry to some Matsoku rocks.

Figures 8.1 and 8.2 show the plots of oxide wt.% against  $\text{MgO}/\text{FeO}^{\text{T}}$  for the Letseng rocks using both the raw data and that calculated  $\text{H}_2\text{O}$ -free and from mineral analyses. Within the more limited range of  $\text{MgO}/\text{FeO}^{\text{T}}$  it is apparent that these rocks display similar trends to those from Matsoku.  $\text{Al}_2\text{O}_3$ ,  $\text{FeO}^{\text{T}}$ ,  $\text{CaO}$  and  $\text{MnO}$  increase with decreasing  $\text{MgO}/\text{FeO}^{\text{T}}$ ,  $\text{MgO}$  and  $\text{Na}_2\text{O}$  decrease and the other oxides show no recognisable trend. The  $\text{Na}_2\text{O}$  trend is the reverse of that seen at Matsoku, but as Carswell et al. (1979) have shown that the analyses of Cox et al. (1973) are in serious error for  $\text{Na}_2\text{O}$  values, it may be concluded that the Letseng rocks have a similar petrogenetic history to those from Matsoku. In particular it is important to note that the removal of the data for NL141, NL494, and NL495 (rocks with high equilibration temperatures and pressures - see Chapter 9) does not affect these observations.

These same high temperature rocks suggest that the deeper mantle may be less depleted in fusible components  $\text{FeO}^{\text{T}}$ ,  $\text{CaO}$  and  $\text{Al}_2\text{O}_3$  as concluded by Nixon and Boyd (1973), although these rocks seem to be strangely depleted in  $\text{Na}_2\text{O}$ . The sheared peridotites from Thaba Putsoa do not match these compositions and are even less depleted in fusible components.

Compared with peridotites in other kimberlites of similar age (Pipe 200, Lesotho - Carswell et al. (1979); Kimberley - Carswell et al. (op.cit.)) it is apparent that considerable upper mantle heterogeneity must have existed in the upper Cretaceous. Pipe 200 peridotites are very similar in most components but possibly contain a little more modal enstatite as reflected in higher  $\text{SiO}_2$  wt.% and lower  $\text{MgO}$  wt.%. Thaba Putsoa, Mothae and Liphobong coarse textured lherzolites are similar to Pipe 200 rocks, but the Kimberley garnet

lherzolites are considerably less depleted in  $\text{Al}_2\text{O}_3$ , CaO and  $\text{Na}_2\text{O}$ , as are the Matsoku common peridotites.

Peridotites from the Premier Mine (Danchin, 1979), a kimberlite of Pre-Cambrian age ( $1115 \pm 15$  m.y., Allsopp et al. 1967), show similar depth and texture related composition trends to the northern Lesotho rocks of Nixon and Boyd (op.cit.) but the coarse textured lower temperature rocks are considerably less depleted than the equivalent peridotites enclosed in upper Cretaceous kimberlites. This observation of a time related depletion giving a heterogeneous upper mantle by the time of kimberlite intrusion in the late Cretaceous would accord with the considerable volumes of mantle derived basaltic lava extruded over vast areas of southern Africa during the late Karoo period (Cox, 1969). Lesotho was a major volcanic centre during that period and such volcanism could have led to considerable depletion of the uppermost upper mantle. The deeper upper mantle sampled by the Premier kimberlite gives compositions much more similar to the high temperature, 'sheared', peridotites of northern Lesotho. This implies that the deeper parts of the stratified upper mantle suggested by Boyd and Nixon (1973) may not have evolved appreciably during about 1000m.y. Of course the plate tectonics model dictates that these kimberlites probably did not sample the same part of the asthenosphere but the isotopic evidence (see Chapter 4) shows that the source regions of kimberlites are near chondritic in character, i.e. undepleted relative to a chondritic model for the bulk earth.

In the analogous geological environment provided by studies of xenoliths in basalts and other basic volcanic rocks, Kuno and Aoki (1970) have demonstrated very similar chemical trends in their lherzolite xenoliths to those seen in Matsoku rocks. As at Matsoku these authors postulate partial melting and crystal fractionation processes as generating the observed rock compositions. These rocks were incorporated in the basaltic magma following extensive recrystallisation and sometimes deformation.

Kuno and Aoki (1970) also demonstrate the transformation of garnet lherzolite to spinel lherzolite and sometimes even to plagioclase lherzolite. They attribute these phase changes to pressure decrease as a result of convective overturn. In this context it is interesting to note that they found garnet lherzolite isochemical with garnet-free lherzolite. Table 8.1 shows two analyses for spinel lherzolites and Table 8.2 one analysis recalculated from mineral compositions. These three rocks have been interpreted as being derived from garnet lherzolite following garnet breakdown. Their bulk compositions are within the range of bulk compositions for Letseng garnet lherzolites (although high modal clinopyroxene has imposed some slight differences on NL573 and NL171).

Figure 8.1:Major element variation in Letseng peridotites.

Oxide Wt% v.  $\text{MgO}/\text{FeO}^*$

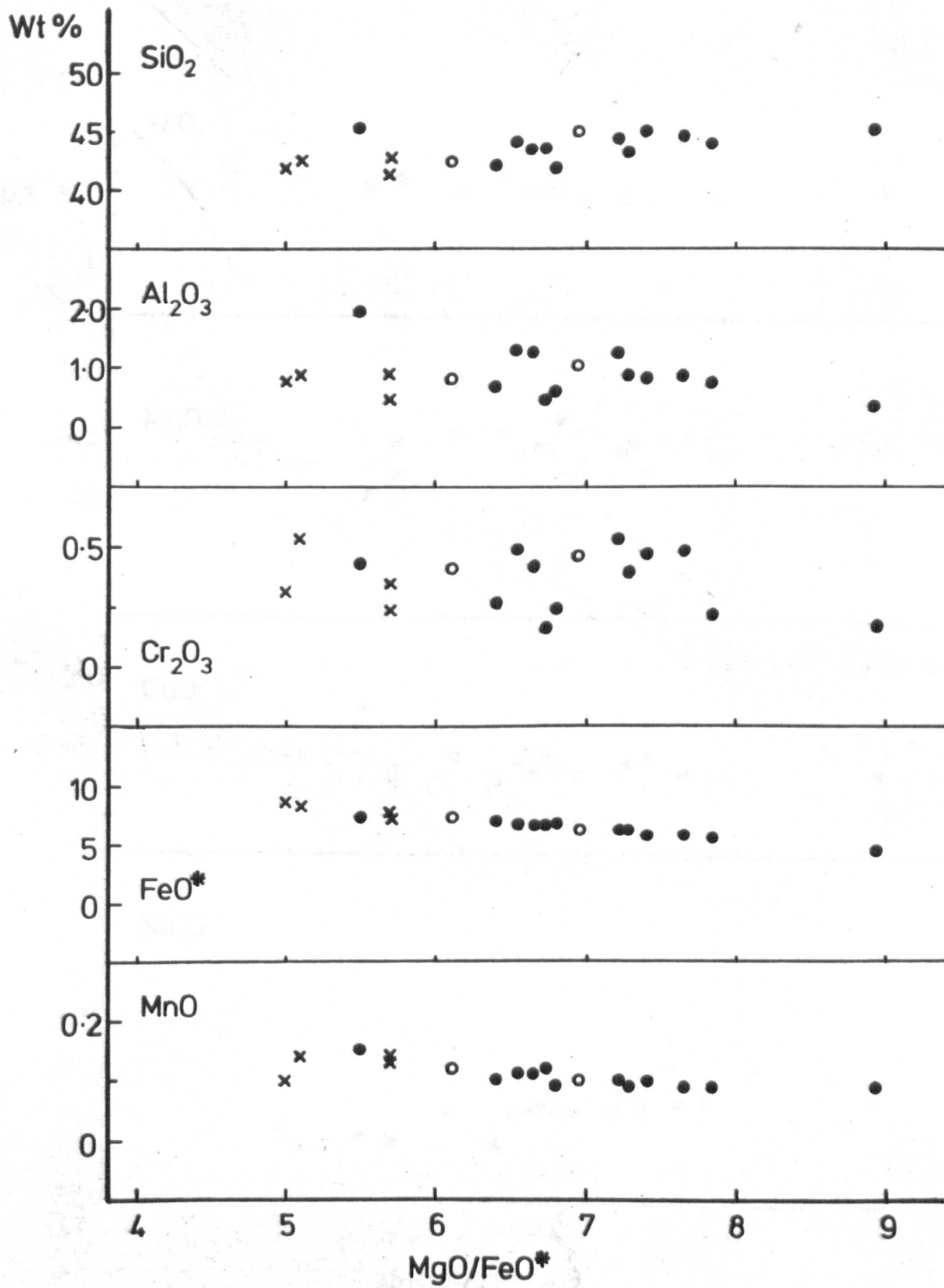
Closed circles:coarse textured rocks.

Crosses:porphyroclastic textured rocks.

Open circles:mosaic porphyroclastic textured rocks.

$\text{FeO}^*$  = total Fe as FeO.





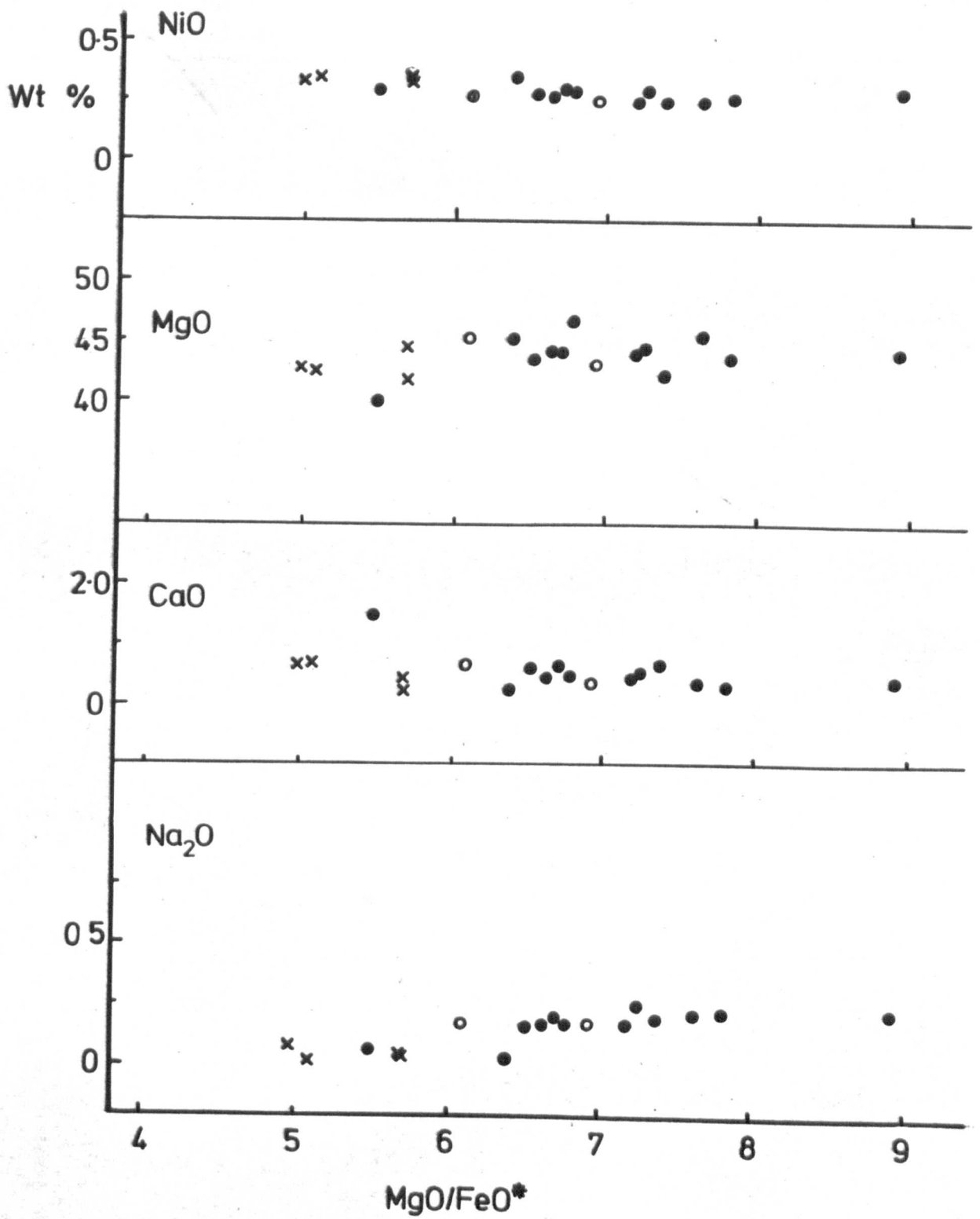
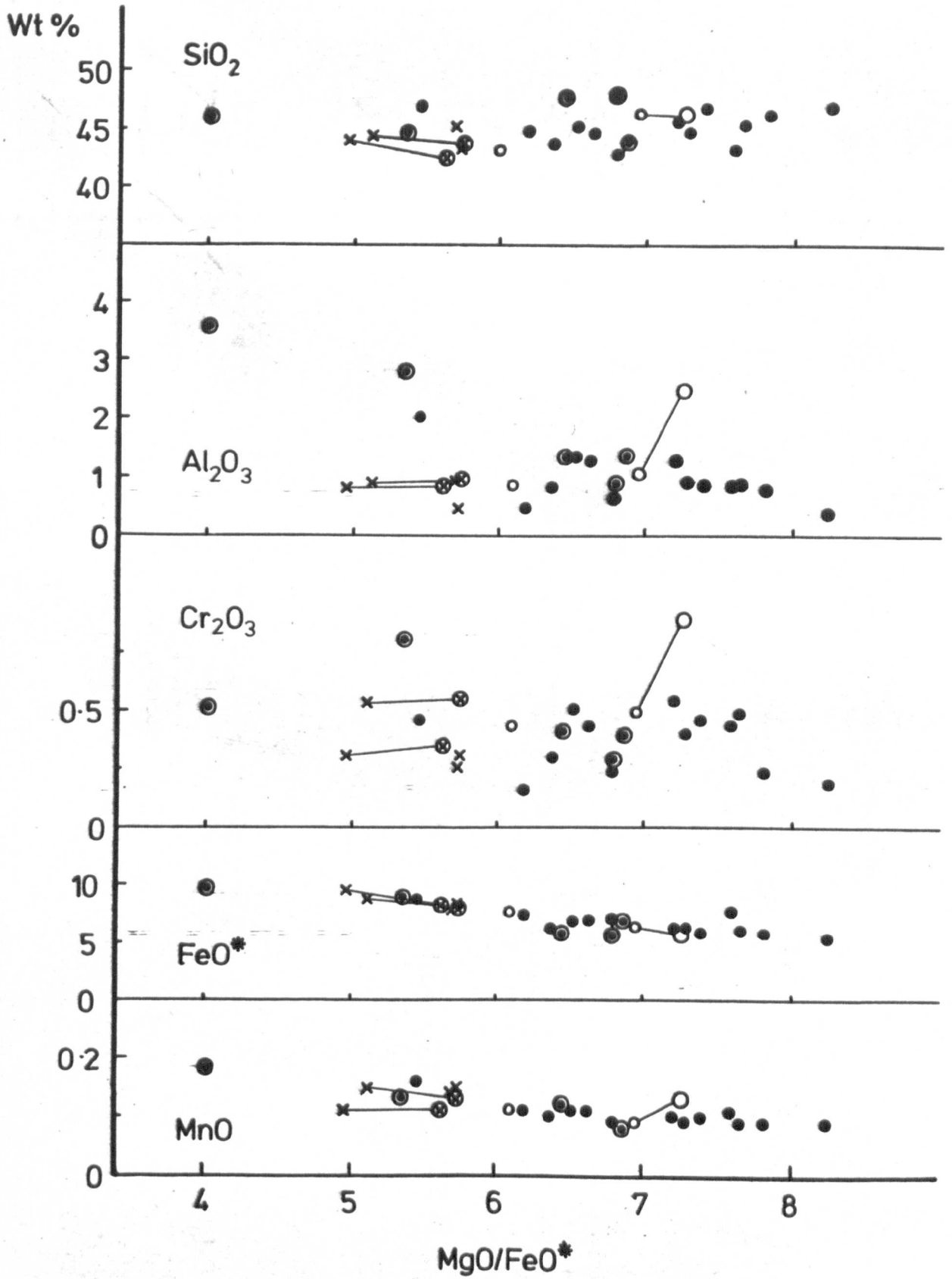


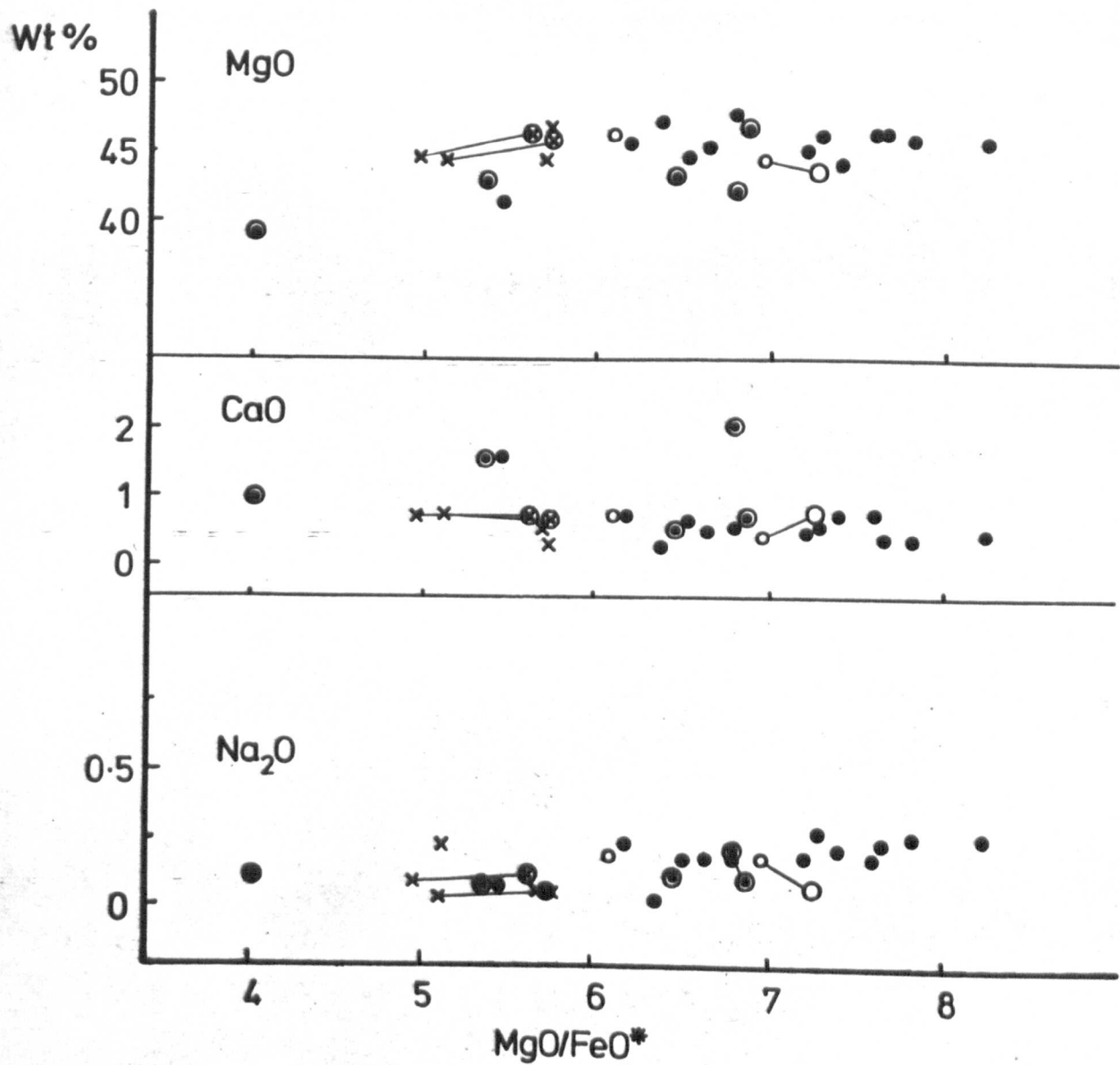
Figure 8.2: Major element variation in Letseng peridotites  
(H<sub>2</sub>O free).

Oxide Wt% v. MgO/FeO\*

Symbols as for figure 8.1.

Large circled symbols are analyses recalculated from phase compositions and mineral mode. Tie lines connect these analyses to those obtained by direct analysis.





CHAPTER 9

Peridotites: Equilibration Temperatures  
and Pressures

Many of the compositional variables discussed in Chapter 7 are sensitive functions of the temperature and pressure of crystallisation or sub-solidus equilibration. If the conclusions of experimental studies on simple synthetic systems can be extrapolated to the compositions recorded in natural multicomponent systems, it should be possible to establish the equilibration temperatures and pressures of these rocks.

In the simple system  $Mg_2Si_2O_6$ - $CaMgSi_2O_6$ , Davis and Boyd (1966) showed that the temperature may be estimated from the amount of solid solution of enstatite in diopside coexisting with orthopyroxene. This diopside solvus was thought to be relatively insensitive to pressure, but further experiments by Mori and Green (1975) and Lindsley and Dixon (1976) have confirmed the existence of a slight pressure effect. Wood and Banno (1973) have developed an empirical equation for temperature calculation, by the application of thermodynamic mixing models, with application in multicomponent systems which deviate from the simple system compositions. The most important additional component is  $FeSiO_3$ . Wells (1977) has further refined this empirical equation to account for  $X_{Fe}^{Opx} = 0 - 1.0$  and for aluminous pyroxenes. He showed that the model of Wood and Banno (op.cit.) was seriously in error for Mg-rich compositions. Mori and Green (1978) have also presented an empirical equation for temperature calculations based on more recently available experimental data and assuming a different intracrystalline partitioning of Mg/Fe between the M1 and M2 sites of the pyroxenes. They showed that the Wood and Banno equation yields low temperatures below  $1000^{\circ}C$  but high temperatures above  $1300^{\circ}C$ .

The relationship between the temperatures calculated using the three empirical geothermometers described above are shown in Figure 9.1 for co-

existing pyroxenes in the Letseng peridotites. This figure demonstrates for these natural assemblages the inaccuracy of the early empirical model of Wood and Banno and shows that temperatures calculated by the other two independent methods are in good agreement. At higher temperatures, the Mori and Green geothermometer gives slightly higher temperatures than those calculated by the Wells equation. However, the difference of about  $100^{\circ}\text{C}$  is only just greater than the estimated error in the calculations.

Another possible approach might be that of R  heim and Green (1974) who investigated the partitioning of Mg and Fe between coexisting garnet and clinopyroxenes. Their calibrations however were for rocks of basaltic composition, which leads to major over-estimates of temperature in rocks of peridotite composition. Mori and Green (1978) also investigated the partitioning of Mg and Fe between the various pairs of coexisting silicate phases in peridotites but their equation for the garnet/clinopyroxene pair gives widely varying (although usually high) temperatures compared with those calculated from the two-pyroxene geothermeters. The garnet/clinopyroxene pair was shown to be the most sensitive to changes in temperature and pressure: the other phase pairs show varying but less sensitivity to temperature and pressure changes as indicated in Chapter 7.

In rocks where garnet has crystallised in equilibrium with pyroxene, it is possible to estimate the equilibration pressure if the  $\text{Al}_2\text{O}_3$  content of the pyroxene and the equilibration temperature are known. With increasing pressure at constant temperature, there is decreasing solution of  $\text{Al}_2\text{O}_3$  in pyroxene and more garnet is formed. MacGregor (1974) has produced a phase diagram showing the isopleths of  $\text{Al}_2\text{O}_3$  wt.% in orthopyroxene for a range of temperatures and pressures applicable to upper mantle petrology. In natural diopside-bearing systems however, he stated that these pressures would be over-estimated. In systems that contain Ca and Fe, garnet is

stable with enstatites that are less aluminous than those in the equivalent pure system: a correction to account for these multi-component systems has been incorporated into the geobarometer of Wood and Banno (1973). Wood (1974) has further refined this geobarometer with new experimental data and has also devised a correction for the appreciable quantities of chromium found in the octahedral sites of most garnets from peridotites. These calculated pressures are accurate to within 2 or 3 Kbars.

### 1. The 'Geotherm'

Boyd (1973) proposed that calculation of the equilibration temperatures and pressures for suites of garnet lherzolite xenoliths from kimberlites and other rocks could be used to construct 'fossil geotherms'. This procedure contains the very basic assumption that these rocks from a high temperature and pressure regime have been transported rapidly to the earth's surface without chemical re-equilibration to the sudden temperature and pressure fall. Boyd outlined the procedure used to calculate this geotherm for a suite of xenoliths from northern Lesotho and the concept of a 'kinked' geotherm became established in the literature (e.g. Nixon and Boyd, 1973; Boyd and Nixon, 1975). Other geotherms from widely separated localities in southern Africa were soon established (MacGregor, 1975; Boyd and Nixon, 1978; Danchin, 1979). All these geotherms purported to show an inflected high temperature limb: a proposal which invoked considerable controversy not least because the high temperature rocks were apparently all deformed and the low temperature rocks undeformed. Dawson et al. (1975) and Gurney et al. (1975) have found highly deformed rocks with low equilibration temperatures from Bultfontein (South Africa) and Matsoku (Lesotho) respectively and similar examples are now known from Letseng (see Table 9.1). However, no undeformed high temperature rocks have yet been found.



**TABLE 9.1:** Calculated Equilibration Temperatures and Pressures for  
Main Pipe Garnet Iherzolites

Sample Number	Texture	Temperature and Pressure OC Wells		Temperature and Pressure Kb Wood		Temperature and Pressure OC Mori and Green		Temperature and Pressure Kb Wood	
		No OCT Cr in OPX	OCT CR in OPX	No OCT Cr in OPX	OCT CR in OPX	No OCT CR in OPX	OCT CR in OPX	No OCT CR in OPX	OCT CR in OPX
NL001	Coarse	943	34.0	34.0	30.3	96.2	35.1	31.4	
NL006	Coarse	948	34.8	34.8	29.9	969	36.1	31.1	
NL007	Porphyroclastic	932	33.2	33.2	28.7	954	34.5	30.0	
NL012	Coarse	964	35.6	35.6	33.4	1006	38.1	35.9	
NL103	Coarse	952	34.1	34.1	29.4	973	35.3	30.5	
NL104	Coarse	937	33.6	33.6	29.0	958	34.9	30.2	
NL128	Coarse	822	24.3	24.3	23.4	831	24.8	23.9	
NL141	Porphyroclastic	1115	42.8	42.8	38.2	1160	45.4	40.7	
NL144	Coarse	955	34.6	34.6	29.5	975	35.8	30.6	
NL145	Coarse	870	25.2	25.2	17.5	881	25.9	18.1	
NL148	Granuloblastic	793	-	-	-	812	-	-	
NL153	Coarse	916	32.3	32.3	28.2	931	33.2	29.1	
NL162	Granuloblastic	891	-	-	-	917	-	-	
NL163	Porphyroclastic	965	-	-	-	988	-	-	
NL166	Coarse	823	25.9	25.9	23.5	833	26.5	24.0	
NL169	Porphyroclastic	1107	42.3	42.3	38.6	1148	44.7	40.9	
NL171	Granuloblastic	741	-	-	-	752	-	-	
NL197	Coarse	944	36.4	36.4	32.2	963	37.6	33.3	
NL426	Mosaic Porphyroclastic	982	35.8	35.8	31.3	1009	37.4	32.8	
NL427	Mosaic Porphyroclastic	976	35.5	35.5	31.0	1000	37.0	32.4	
NL441	Porphyroclastic	964	35.3	35.3	30.5	983	36.5	31.6	
NL492	Coarse	952	35.3	35.3	32.3	974	36.7	33.6	
NL494	Mosaic Porphyroclastic	1251	48.1	48.1	41.6	1322	52.2	45.3	
NL495	Mosaic Porphyroclastic	1102	40.1	40.1	34.0	1153	43.0	36.6	
2011	Coarse	1010	-	-	-	1032	-	-	
2012	Coarse	977	35.3	35.3	31.0	996	36.4	32.0	
NL535	Granuloblastic	767	-	-	-	783	-	-	

2011 and 2012 from Boyd (1973) in 'Lesotho Kimberlites' of assumed Main pipe origin  
Temperatures and pressures are calculated using the computer program of F.G.F. Gibb (see text)

**TABLE 9.2: Calculated Equilibration Temperatures and Pressures for Satellite Pipe Garnet Lherzolites**

Sample Number	Texture	OC Wells		Temperature and Pressure Kb Wood		OC Mori and Green		Temperature and Pressure Kb Wood	
		No OCT CR on OPX	OCT CR in OPX	No OCT CR in OPX	OCT CR in OPX	No OCT CR in OPX	OCT CR in OPX	No OCT CR in OPX	OCT CR in OPX
NLO21	Porphyroclastic	1258	40.9	44.5	40.9	1336	48.7	44.8	44.8
NLO28	Porphyroclastic	1285	41.1	44.3	41.1	1365	48.5	45.2	45.2
NL503	Porphyroclastic	1268	41.1	43.9	41.1	1344	47.9	45.0	45.0
BD1870/1	Coarse	802	20.1	22.1	20.1	815	22.8	20.8	20.8
BD1894	Coarse	798	17.6	19.9	17.6	815	20.8	18.5	18.5
BD1899	Porphyroclastic	1265	42.4	46.1	42.4	1344	50.4	46.6	46.6
BD1910	Coarse	1055	32.7	36.9	32.7	1094	39.1	34.8	34.8
BD1870/2	Coarse	836	26.4	28.4	26.4	881	31.1	29.1	29.1
2573	Porphyroclastic	1270	45.6	47.9	45.6	1349	52.3	49.8	49.8
2575/2	Porphyroclastic	1279	46.9	49.5	46.9	1356	53.8	51.1	51.1
2575/3	Porphyroclastic	1274	45.7	47.8	45.7	1351	52.0	49.8	49.8
NL528	Granuloblastic	713				726			

BD1870/2 from Bishop et al. (1978)

2573, 2575/2, 2575/3 from Boyd (1973) in 'Lesotho Kimberlites' of assumed Satellite pipe origin

Temperatures and pressures are calculated using the computer program of F.G.F. Gibb (see text).

Boyd (1973) discussed and compared several methods of temperature and pressure calculation based on some of the geothermometers and geobarometers outlined above. His preferred and now established method is to calculate the temperature from the Ca/(Ca+Mg) ratio of the clinopyroxene using the diopside solvus data of Davis and Boyd (1966), and to estimate the pressure by the 'raw  $\text{Al}_2\text{O}_3$ ' method from the orthopyroxene isopleths of MacGregor (1974). He argued that while this method will not give accurate absolute values for a particular xenolith suite, the relative values should still be meaningful. This assumption seems to be fraught with difficulties: Howells and O'Hara (1978) suggested the perturbed upper limb of the geotherm may result from small errors in the calibration of the geobarometer thus giving 'spurious' kinks; Mercier and Carter (1975) believe the high temperature inflections may be artifacts of the degree of depletion with depth in the upper mantle; and Harte (1978) concluded that geotherms for single pipes do not show inflected high temperature limbs.

In the present study the equilibration temperatures and pressures for garnet lherzolites from both the Main and Satellite pipes have been calculated using the geothermometers of Wells (1977) and Mori and Green (1978) in conjunction with the geobarometer of Wood (1974) (see Tables 9.1 and 9.2). The calculations were made using a computer program developed by F.G.F. Gibb at Sheffield University, details of which have yet to be published. The pressure calculation followed the two alternatives of Wood (1974) in treating the alumina in orthopyroxene either as tschermakite or as tschermakite plus jadeite. The second method for allocating the alumina is preferred because of the correlation between sodium and aluminium, especially in the clinopyroxene (see Chapter 7). In this method chromium is also considered and subtracted as ureyite molecule ( $\text{NaCrSi}_2\text{O}_6$ ) before allocation of aluminium to jadeite. This

second method is considered the more accurate and yields a smooth curve from lherzolite values plotted on a P-T diagram (Figure 9.2). Note that the Satellite pipe xenoliths plot on the low pressure side of this curve because the measured  $\text{Al}_2\text{O}_3$  content is considered high (see Chapter 7). The calculations for the assumed Satellite pipe samples of Boyd (1973) however, plot on the same curve extrapolated from lower temperatures. Their similarity in most respects to my analyses suggests these would also plot on the curve if the  $\text{Al}_2\text{O}_3$  were reanalysed. Note also that three Main pipe xenoliths (NL145, NL494 and NL495) plot on the low pressure (or high temperature) side of the curve (see discussion below).

Figure 9.2 also shows the 'Lesotho Geotherm' of Nixon and Boyd (1973) for comparison although the Letseng data have not been calculated by Boyd's method for reasons already discussed. However, the plot of Letseng data for the first alternative of Wood (1974) shows the way in which a kinked geotherm might arise as a result of differences in the degree of depletion with depth (Mercier and Carter, 1975). If the high temperature rocks which are less depleted in alumina (Boyd and Nixon, 1973) are treated as containing only tschermakite molecule then the calculated pressure is necessarily too low as a disproportionate amount of alumina has been considered as solution of garnet in orthopyroxene.

The various textures are not displayed in the P-T diagram (Figure 9.2), but Table 9.1 shows that porphyroclastic and mosaic porphyroclastic rocks have equilibrated at temperatures  $<1000^\circ\text{C}$ . A single coarse textured rock (BD1910, Table 9.2) from the Satellite pipe has equilibrated at  $1055^\circ\text{C}$  and may be among the highest temperatures recorded in coarse rocks (cf. Danchin, 1979). The majority of the Main pipe garnet lherzolites, representing the vast bulk of the xenoliths from Letseng have equilibrated at temperatures of  $930^\circ\text{C}$ - $1000^\circ\text{C}$  and pressures of 33-36 Kbars. Within this

group some specimens plot a little to the high pressure side of the P-T curve. NL012, the Fe-rich assemblage, is one of these samples: in this instance the pressure recorded may be high because of slight inaccuracies in the geobarometer for high-Fe rocks (Wood, 1974).

The most startling result of the investigation of the two Letseng xenolith suites is the almost complete lack of overlap in the upper mantle rocks sampled by the kimberlites of the two pipes. The Satellite pipe xenoliths (with one exception) derive from the two extremes of the temperature range: 800°C and 1260-1285°C. The Main pipe specimens derive from the intermediate range 820°C-1250°C. From two kimberlite pipes in such close proximity this is a most surprising result and might suggest that a closer look be made of the xenolith suites from different kimberlites in the same pipe. Among the Letseng samples analysed a number were taken from both the Main pipe autolithic and garnetiferous kimberlites but no discernable petrographic or chemical differences were found. Thus in the case of Letseng at least I conclude that the kimberlites of the two pipes have divergent origins. The abundance of xenoliths and the greater range in temperatures observed in the Main pipe samples suggests that these kimberlites were intruded earlier than the Satellite pipe kimberlite which followed up the opened passage without further sampling of the conduit wall.

## 2. Chemical Equilibrium

An implicit assumption in the above discussion, is that both the experimental runs and the rocks to which the results have been applied are in chemical equilibrium. In order that these geothermometric and geobarometric calculations may be shown to have some validity in the natural systems studied, it is necessary to demonstrate that the individual phases are not only homogeneous within a single specimen, but also that the various critical elemental components have attained equilibrium with the coexisting



phases for the particular physical conditions pertaining at the moment of incorporation in the kimberlite. Boyd and Finger (1975) showed that the phases in some mantle xenoliths from northern Lesotho kimberlites are essentially homogeneous and that the compositional ranges within single specimens are not comparable to compositional ranges in xenolith suites. In Chapter 7, it was stated that the same is true for the Letseng xenolith suites, although the testing for homogeneity was less rigorous.

The deformed rocks display disequilibrium textures and extensive recrystallisation of olivine, orthopyroxene and clinopyroxene: it is certain that, had these rocks not been incorporated in the rapidly rising kimberlite, the textures would have evolved to produce an annealed coarse grained, even-textured rock. It is not unreasonable to suspect that such rocks might show chemical differences between the coarse-grained 'primary' porphyroclasts and the fine-grained 'secondary' neoblasts. Boyd (1975) examined this possibility in deformed rocks from Thaba Putsoa (Lesotho) and Bultfontein (South Africa). He noted slight increases in the  $\text{TiO}_2$  content of neoblasts which he concluded may relate to incorporation in the kimberlite. More importantly he found changes in the  $\text{CaO}$  and  $\text{Al}_2\text{O}_3$  content of neoblastic pyroxenes: higher  $\text{CaO}$  and  $\text{Al}_2\text{O}_3$  in orthopyroxene and lower  $\text{CaO}$  in clinopyroxene. He concluded these changes may reflect re-equilibration between garnet and pyroxenes and suggested the magnitude of the changes might be  $100^\circ\text{C}$  temperature increase and 20 km depth decrease. However, the neoblast compositions could not be considered representative of the new P-T conditions as the rate of reaction of enstatite with diopside and garnet may differ.

Table 9.3 shows compositions of clinopyroxene porphyroclasts and neoblasts from four Letseng mosaic porphyroclastites. Figure 9.3 indicates a tendency for neoblasts in the high temperature rocks (NL494, NL495) to equilibrate at lower temperatures and for neoblasts in low temperature rocks (NL426,

**TABLE 9.4:** Comparison of Compositions of primary and Neoblastic Orthopyroxene in Main Pipe Peridotites

	NL426						NL427					
	C	R	N	C	R	N	C	N	C	R	N	
SiO <sub>2</sub>	57.48	57.70	57.27	57.51	57.38	57.52	57.81	57.46	57.58	57.58	57.39	
TiO <sub>2</sub>	0.08	0.09	0.11	0.10	0.11	0.13	0.08	0.13	0.08	0.06	0.11	
Al <sub>2</sub> O <sub>3</sub>	0.81	0.90	1.09	0.83	0.82	1.10	0.86	0.85	0.83	0.79	1.07	
Cr <sub>2</sub> O <sub>3</sub>	0.33	0.39	0.51	0.33	0.39	0.42	0.36	0.35	0.30	0.31	0.38	
FeO	4.86	4.80	4.99	4.79	4.85	4.95	4.75	4.85	4.50	4.72	4.76	
MnO	0.10	0.12	0.13	0.14	0.13	0.12	0.11	0.11	0.12	0.12	0.12	
MgO	35.16	35.33	35.04	35.30	35.17	34.88	35.50	35.33	35.36	35.42	35.24	
CaO	0.48	0.60	0.63	0.55	0.55	0.60	0.56	0.66	0.57	0.61	0.59	
Na <sub>2</sub> O	0.19	0.12	0.16	0.14	0.19	0.12	0.13	0.15	0.20	0.16	0.14	
NiO	0.13	0.12	0.16	0.10	0.14	0.16	0.15	0.18	0.14	0.12	0.11	
<b>Total</b>	<b>99.62</b>	<b>100.17</b>	<b>100.09</b>	<b>99.79</b>	<b>99.73</b>	<b>100.00</b>	<b>100.33</b>	<b>100.07</b>	<b>99.68</b>	<b>99.89</b>	<b>99.91</b>	
Si	1.98	1.98	1.97	1.98	1.98	1.97	1.98	1.97	1.98	1.98	1.97	
Ti	0.00	0.00	0.00	0.00	0.00	0.00	0.00	0.00	0.00	0.00	0.00	
Al	0.03	0.04	0.04	0.03	0.03	0.04	0.03	0.03	0.03	0.03	0.04	
Cr	0.01	0.01	0.01	0.01	0.01	0.01	0.01	0.01	0.01	0.01	0.01	
Fe	0.14	0.14	0.14	0.14	0.14	0.14	0.14	0.14	0.13	0.14	0.14	
Mn	0.00	0.00	0.00	0.00	0.00	0.00	0.00	0.00	0.00	0.00	0.00	
Mg	1.80	1.80	1.79	1.81	1.80	1.78	1.81	1.81	1.81	1.81	1.80	
Ca	0.02	0.02	0.02	0.02	0.02	0.02	0.02	0.02	0.02	0.02	0.02	
Na	0.01	0.01	0.01	0.01	0.01	0.01	0.01	0.01	0.01	0.01	0.01	
Ni	0.00	0.00	0.00	0.00	0.00	0.00	0.00	0.00	0.00	0.00	0.00	
<b>Total</b>	<b>3.99</b>	<b>4.00</b>	<b>3.98</b>	<b>4.00</b>	<b>3.99</b>	<b>3.97</b>	<b>4.00</b>	<b>3.99</b>	<b>3.99</b>	<b>4.00</b>	<b>3.99</b>	
Ca/(Ca+Mg)	0.010	0.012	0.013	0.011	0.011	0.012	0.011	0.013	0.011	0.012	0.012	
Mg/(Mg+Fe)	0.928	0.929	0.926	0.929	0.928	0.926	0.930	0.929	0.933	0.930	0.930	
Ca%	0.9	1.1	1.2	1.0	1.0	1.1	1.0	1.2	1.1	1.1	1.1	
Fe%	7.3	7.2	7.5	7.2	7.3	7.5	7.1	7.2	6.8	7.0	7.1	
Mg%	91.8	91.7	91.3	91.8	91.7	91.4	91.9	91.6	92.1	91.9	91.8	
	NL441			NL494			NL495					
	C	N	N	C	N	N	C	N	N			
SiO <sub>2</sub>	57.84	57.62	56.50	57.25	56.84	57.29	56.36	56.92	56.73			
TiO <sub>2</sub>	0.01	0.02	0.11	0.01	0.01	0.00	0.20	0.24	0.20			
Al <sub>2</sub> O <sub>3</sub>	0.83	0.82	3.49	0.94	0.83	0.78	0.99	1.02	0.97			
Cr <sub>2</sub> O <sub>3</sub>	0.39	0.40	1.61	0.46	0.46	0.44	0.40	0.44	0.48			
FeO	4.20	4.12	4.42	5.22	5.13	5.24	5.55	5.32	5.22			
MnO	0.12	0.11	0.13	0.15	0.14	0.14	0.12	0.14	0.11			
MgO	35.81	35.85	34.16	34.32	34.39	34.24	34.22	34.42	34.28			
CaO	0.49	0.50	1.23	1.59	1.50	1.46	0.74	1.00	1.04			
Na <sub>2</sub> O	0.14	0.12	0.18	0.09	0.06	0.06	0.26	0.27	0.28			
NiO	0.09	0.08	0.09	0.17	0.14	0.14	0.12	0.16	0.14			
<b>Total</b>	<b>99.92</b>	<b>99.64</b>	<b>101.92</b>	<b>100.20</b>	<b>99.50</b>	<b>99.79</b>	<b>98.96</b>	<b>100.03</b>	<b>99.45</b>			
Si	1.98	1.98	1.91	1.97	1.97	1.98	1.96	1.96	1.97			
Ti	0.00	0.00	0.00	0.00	0.00	0.00	0.01	0.01	0.01			
Al	0.03	0.03	0.14	0.04	0.03	0.03	0.04	0.04	0.04			
Cr	0.01	0.01	0.04	0.01	0.01	0.01	0.01	0.01	0.01			
Fe	0.12	0.12	0.12	0.15	0.15	0.15	0.16	0.15	0.15			
Mn	0.00	0.00	0.00	0.00	0.00	0.00	0.00	0.00	0.00			
Mg	1.83	1.83	1.72	1.76	1.78	1.76	1.78	1.77	1.77			
Ca	0.02	0.02	0.04	0.06	0.06	0.05	0.03	0.04	0.04			
Na	0.01	0.01	0.01	0.01	0.00	0.00	0.02	0.02	0.02			
Ni	0.00	0.00	0.00	0.00	0.00	0.00	0.00	0.00	0.00			
<b>Total</b>	<b>4.00</b>	<b>4.00</b>	<b>3.98</b>	<b>4.00</b>	<b>4.00</b>	<b>3.98</b>	<b>4.01</b>	<b>4.00</b>	<b>4.01</b>			
Ca/(Ca+Mg)	0.010	0.010	0.025	0.032	0.030	0.030	0.015	0.020	0.021			
Mg/(Mg+Fe)	0.938	0.940	0.932	0.921	0.923	0.921	0.917	0.920	0.921			
Ca%	0.9	0.9	2.4	3.0	2.8	2.7	1.4	1.9	2.0			
Fe%	6.3	6.2	6.8	7.8	7.7	7.9	8.4	8.0	7.9			
Mg%	92.8	92.9	90.8	89.2	89.5	89.4	90.2	90.1	90.1			

C = Core of primary grain

R = Rim of same grain

N = Adjacent neoblast



**TABLE 9.5:** Comparison of Compositions of Primary and Neoblastic Olivine in Main Pipe Peridotites

	NL169			NL426		NL427	
	C	N	N	C	N	C	N
SiO <sub>2</sub>	41.20	41.14	41.24	41.09	42.32	40.84	41.38
TiO <sub>2</sub>	0.01	0.03	0.00	0.04	0.02	0.04	0.03
Al <sub>2</sub> O <sub>3</sub>	0.08	0.07	0.06	0.06	0.06	0.03	0.03
Cr <sub>2</sub> O <sub>3</sub>	0.06	0.04	0.06	0.03	0.05	0.02	0.02
FeO	7.64	7.54	7.61	8.02	7.88	7.44	7.68
MnO	0.10	0.08	0.08	0.10	0.11	0.11	0.11
MgO	51.07	50.86	50.86	50.85	49.68	50.86	50.77
CaO	0.06	0.10	0.09	0.04	0.08	0.04	0.08
Na <sub>2</sub> O	0.08	0.05	0.08	0.05	0.05	0.03	0.00
NiO	0.37	0.32	0.36	0.44	0.35	0.44	0.46
Total	100.67	100.23	100.44	100.72	100.60	99.85	100.56
Si	1.00	1.00	1.00	0.99	1.02	0.99	1.00
Ti	0.00	0.00	0.00	0.00	0.00	0.00	0.00
Al	0.00	0.00	0.00	0.00	0.00	0.00	0.00
Cr	0.00	0.00	0.00	0.00	0.00	0.00	0.00
Fe	0.15	0.15	0.15	0.16	0.16	0.15	0.16
Mn	0.00	0.00	0.00	0.00	0.00	0.00	0.00
Mg	1.84	1.84	1.83	1.83	1.78	1.84	1.83
Ca	0.00	0.00	0.00	0.00	0.00	0.00	0.00
Na	0.00	0.00	0.00	0.00	0.00	0.00	0.00
Ni	0.00	0.00	0.00	0.00	0.00	0.00	0.00
Total	3.99	3.99	3.98	2.98	2.96	2.98	2.99
Ca/(Ca+Mg) Mg/(Mg+Fe)	0.923	0.923	0.923	0.919	0.918	0.924	0.922
Ca%							
Fe%							
Mg%							

C = Core of primary grain

N = Adjacent neoblast

NL427) to equilibrate at higher temperature. Table 9.4 shows compositions of orthopyroxene porphyroclasts and neoblasts from five deformed rocks. The trend is not always consistent but most show higher CaO and  $Al_2O_3$  in the neoblasts as found by Boyd. An important factor not studied by Boyd (op.cit.) is the CaO content of olivine neoblasts (Table 9.5) which are consistently enriched in CaO relative to the olivine porphyroclasts. In view of the great abundance of olivine neoblasts in some of these rocks it is possible this is the host for CaO partitioned out of clinopyroxene under increased temperature.

The magnitude of the temperature and pressure changes indicated by these small chemical disequilibrium features is almost within the range of error for the geothermometers and geobarometers employed both in this study and by Boyd (1973). However, it may be that a continuous process of re-equilibration was operating so that at any moment in time the difference between the porphyroclasts and the neoblasts was quite small. If this is the case then the compositions of the porphyroclasts before deformation commenced remains unknown.

If homogeneity alone is used as a test for the precision of thermodynamic calculations it appears that the deviations from the idealised temperature/pressure curves (geothermal gradients, e.g. Clark and Ringwood, 1964) may be explained by such large scale geological processes as the shearing at the base of the lithosphere discussed by Boyd and Nixon (1975). But, as indicated above, the rate of reaction of enstatite with garnet and diopside, as a result of changing physical environment, may differ and their incorporation in the rapidly ascending kimberlite magma may preserve phase chemistries which show disequilibrium partitioning of the critical elements between the phases. The geothermometers employed here are all based on the diopside-enstatite solvus. In the simple system studied by Lindsley and Dixon (1976) the experimental data show a near

linear relationship between % Wo in enstatite and diopside (Figure 9.4). A similar plot for coexisting pyroxenes in the Letseng xenoliths (Figure 9.5) reveals a broad band of near-linear correlation for most of the garnet lherzolites. This trend lies a little to the right of the 20 Kbar values of Lindsley and Dixon (op.cit.) which is to be expected because of the influence of  $\text{FeSiO}_3$  in the natural systems. The small pressure effect these authors found is not significant in the following argument even though the Letseng xenoliths have equilibrated over a wide range of pressure. Figure 9.5 shows several rocks which deviate from this trend: a group at high  $[\text{Ca}] (= \text{Ca}/(\text{Ca}+\text{Mg}))$  represent the aluminous pyroxenes of the granuloblastic spinel-bearing rocks and demonstrate the effect of tschermakite solution (cf. Mercier and Carter (1975)  $f = 0.318$  for garnet lherzolites:  $f = 0.350$  for spinel lherzolites). Another two specimens at low  $[\text{Ca}]_{\text{Cpx}}$  however, contain very similar tschermakite content to the normal garnet lherzolites but plot to the high  $[\text{Ca}]_{\text{Opx}}$  side of the main trend. I believe that this diagram demonstrates these two rocks are in chemical disequilibrium and that the geothermometric calculations using these phase compositions do not relate to equilibration on the geotherm. The partitioning of Ca for these two rocks probably results from partial re-equilibration following temperature increase. The possibility of partial re-equilibration to falling temperature cannot be ignored, but in an isochemical system the partitioning of Ca between orthopyroxene and clinopyroxene would tend to move along a trajectory roughly parallel to the trend for equilibrated phases. It should be noted here that one of these rocks, NL494, does in fact plot to the high temperature side of the proposed geotherm.

The inflected limbs of the perturbed geotherms discussed above were originally suggested to result from stress-heating at the base of the lithosphere (Nixon and Boyd, 1973). Mercier and Carter (1975) have shown

that shear heating is not adequate to explain the inflexions observed; Green and Gueguen (1974) and Gurney et al. (1975) believe these inflexions may result from heating in the thermal aureole of a rising kimberlite diapir. The observation made above of [Ca] disequilibrium may result from such a heating episode. If diapiric upwelling can give rise to such thermal effects the possible results of pressure release should also be investigated. Certainly some material on the margins of such diapirs must move to shallower depths: the presence of extensive garnet breakdown is proof of this. It is therefore important, before accepting any geobarometric calculations, to investigate the partitioning of alumina between the garnet, clinopyroxene and orthopyroxene as a means of testing the equilibration to the prevailing pressure.

Figure 9.6 shows that the majority of the rocks equilibrated in the lower temperature range  $930^{\circ}$ - $1000^{\circ}$ C lie on a straight line relating atomic  $(Al+Cr)_{Opx}$  and  $(Al+Cr)_{Cpx}$ . Where the atomic  $(Al+Cr)_{Cpx} = 0$  we know that atomic Na is also zero (Figure 7.5) and  $(Al+Cr)_{Opx} = 0.03$  (Figure 7.6) at  $(Na)_{Opx} = 0$ . This straight line relationship therefore shows that coexisting ortho- and clinopyroxene have identical tschermakite components whatever the total  $Al_2O_3$  and  $Na_2O$  concentrations. (Note that for the few cases where  $Cr > Na$  the Cr has the same behaviour with respect to pressure as Al (MacGregor, 1970)). Rocks equilibrated at higher temperatures plot at a variety of points above this line, depending on tschermakite and jadeite (ureyite) content, and confirm in these natural systems the greater solubility of garnet in orthopyroxene at higher temperature (MacGregor, 1974). However, it is instructive to plot the partitioning of  $Al/(Al+Cr)$  between garnet, clinopyroxene and orthopyroxene as a test of whether these three have equilibrated to the prevailing P/T environment. If this ratio is a function of temperature (see Smith and Dawson, 1975) but not pressure (see above) then the

partitioning between these phases should show a linear relationship for various bulk compositions. Figure 9.7 demonstrates that for most of the specimens this is so (N.B. the Satellite pipe orthopyroxenes have slightly higher  $Al/(Al+Cr)$  due to analytical error - see Chapter 7). Three rocks (NL145, NL494 and NL495) do not display this simple correlation. In NL145, garnet and clinopyroxene plot on this linear trend, but orthopyroxene is enriched in alumina. In NL494 and NL495, orthopyroxene and clinopyroxene fall on the linear trend but garnet is depleted in alumina. In the case of the two latter samples this may be explained thus: movement to a lower pressure and/or higher temperature results in a primary reaction leading to greater solubility of garnet in pyroxene; since the garnet has a higher  $Al/(Al+Cr)$  ratio than coexisting pyroxene a secondary reaction is required to adjust the partitioning of these elements between the phases. This secondary reaction may not have been complete at the moment of incorporation. The case of the sample NL145 seems more difficult to explain unless the partitioning reaction between garnet and clinopyroxene is more rapid than between garnet and orthopyroxene.

In any event, these deviations suggest chemical disequilibrium between the phases in these rocks which may result in errors in the calculated pressures. In all three cases the rocks plot to the low-pressure and high-temperature side of the geotherm (Figure 9.2). This might be explained as part of a diapiric model in the case of the two higher temperature rocks, but it is more difficult to include the low temperature rock NL145 in this model because the effects of diapiric movement are not expected to be as great at shallower depths.

### 3. Spinel and Garnet/Spinel Lherzolites

Calculations of temperatures for these rocks using the two-pyroxene geothermometers indicate equilibration in the temperature range  $700^{\circ}-900^{\circ}C$ .

This seems to suggest considerable overlap with the low-temperature chromite-bearing depleted garnet lherzolites (NL128 and NL145); and if the chromite lherzolites and harzburgites are to be included in this part of the upper mantle stratigraphy (Nixon and Boyd, 1975) implies some unusual chemical and mineral combinations. However, in Chapter 7, I have discussed the origin of these spinel-bearing rocks in relation to diapiric upwelling and deformation of more deep-seated garnet lherzolites. If such an explanation is invoked then these temperatures must relate to the geothermal gradient and their origin from such levels does not relate to any unusual upper mantle stratigraphy.

Undoubtedly, if such a process has occurred it can account for mantle heterogeneity on either a regional or a local scale. However, caution must be exercised in interpreting these temperatures because some textural features already discussed indicate that despite considerable homogeneity, exsolution of clinopyroxene and spinel from orthopyroxene has occurred in response to decreasing temperature (?). The presence of primary amphibolite in one garnet/spinel lherzolite (NL535) is further testimony to the low temperature of equilibration (O'Hara, 1967).

#### Summary

- (1) Equilibration temperatures are estimated by application of empirical equations relating natural pyroxene phase compositions to the experimentally investigated diopside solvus.
- (2) Equilibration pressures are estimated by application of the geobarometer of Wood based on the solubility of garnet in pyroxene.
- (3) The Letseng 'geotherm' has been constructed after corrections for the jadeite (and ureyite) content of orthopyroxene.
- (4) The Letseng geotherm is a smooth curve devoid of 'kinks'.

- (5) Three rocks at different temperatures plot on the low-pressure/high-temperature side of the geotherm.
- (6) Highly deformed rocks are found at low temperature and pressure.
- (7) Main pipe garnet lherzolites derive from the temperature range 820-1250°C and group at 930°-1000°C. In contrast Satellite pipe garnet lherzolites derive mainly from ~800°C or >1250°C.
- (8) Recrystallised neoblasts of clinopyroxene, orthopyroxene and olivine indicate chemical re-equilibration in the deformed rocks.
- (9) Two rare examples of disequilibrium partitioning of Ca between orthopyroxene and clinopyroxene yield anomalous temperatures.
- (10) Three rocks have excess alumina in pyroxene, and calculated pressures are interpreted as anomalous.
- (11) These anomalous temperatures and pressures are related to changes occurring during diapiric upwelling and do not indicate steady-state conditions.
- (12) Spinel and garnet/spinel lherzolites, derived from normal garnet lherzolite by reaction and deformation, have equilibrated at temperatures in the range 700°-900°C.
- (13) The temperatures referred to in point (12) do not reflect a steady state conditions, as exsolution textures are commonly seen.

Figure 9.1: Correlation diagram for temperatures of equilibration calculated using the geothermometers of Wood & Banno (1973), Wells (1977), and Mori & Green (1978). See text for details.



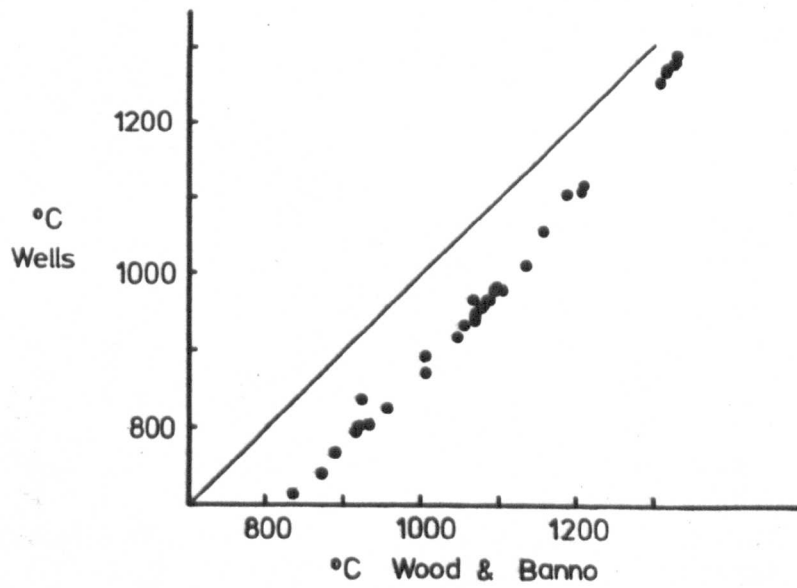
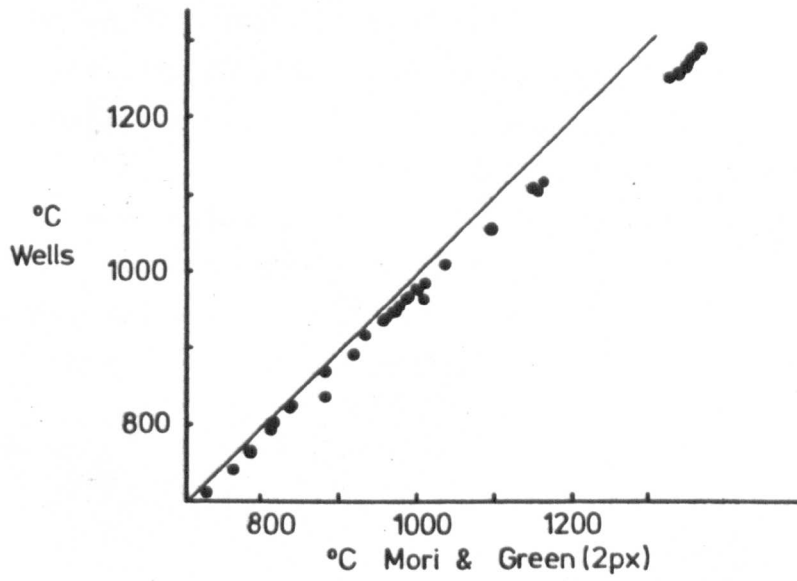
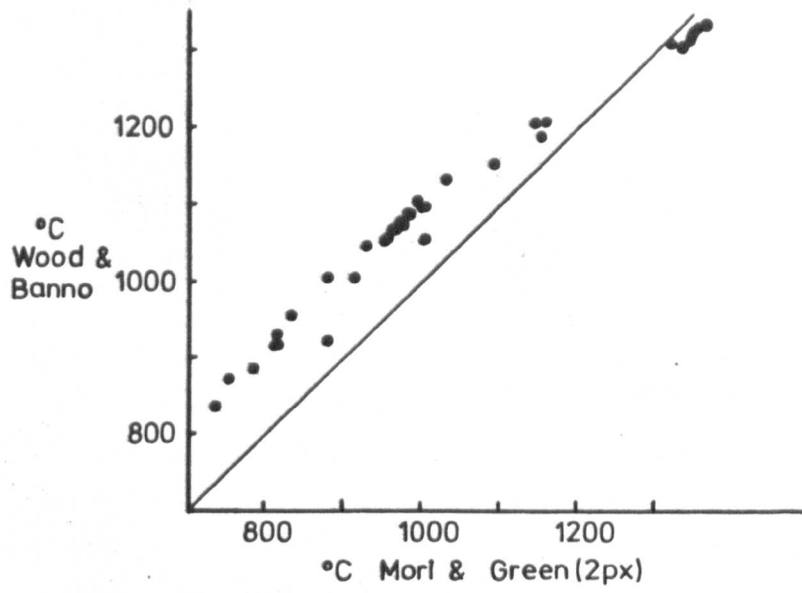


Figure 9.2: Pressure/temperature diagram showing the preferred geotherm estimated for the Letseng garnet lherzolites. The displayed temperatures are those calculated by the Wells geothermometer. The pressures are calculated by the geobarometer of Wood (1974). The upper plot uses the results of the calculation in which all alumina in orthopyroxene is treated as tschermakite molecule. The lower plot uses the results of the calculation in which Al and Cr are first allocated to jadeite and ureyite before estimation of tschermakite component.

Closed circles: Main Pipe peridotites.

Open circles: Satellite peridotites.

The dashed line shows the inflected geotherm of Boyd (1973) calculated by a different method (see text).

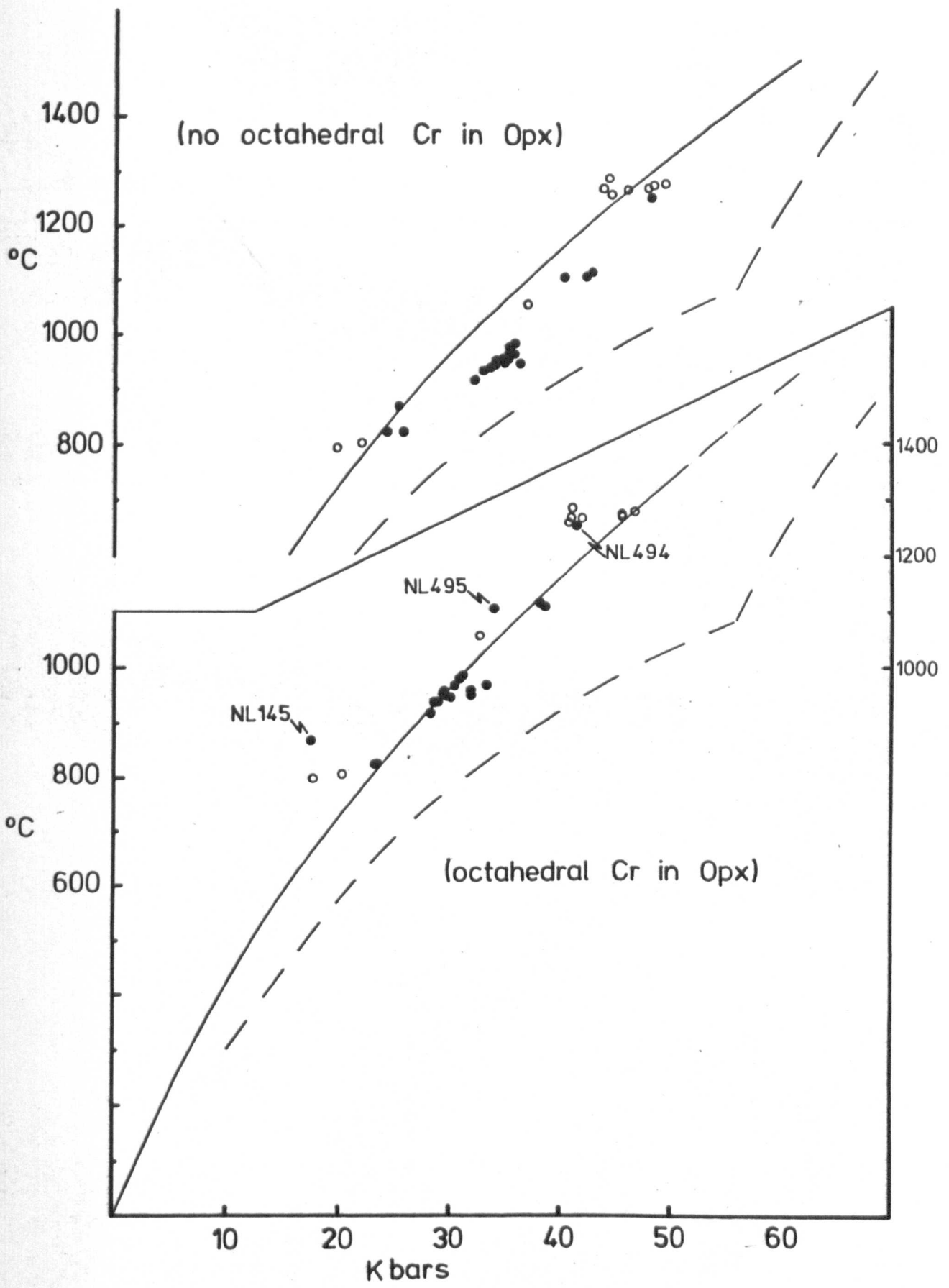


Figure 93: Compositional variation in clinopyroxene from Main  
Pipe mosaic porphyroclastic peridotites.  
Ca - Mg - Fe system.  
Closed circles: core of primary grain.  
Open circles: rim of primary grain.  
Crosses: adjacent recrystallised neoblast.  
Arrows connect related analyses.

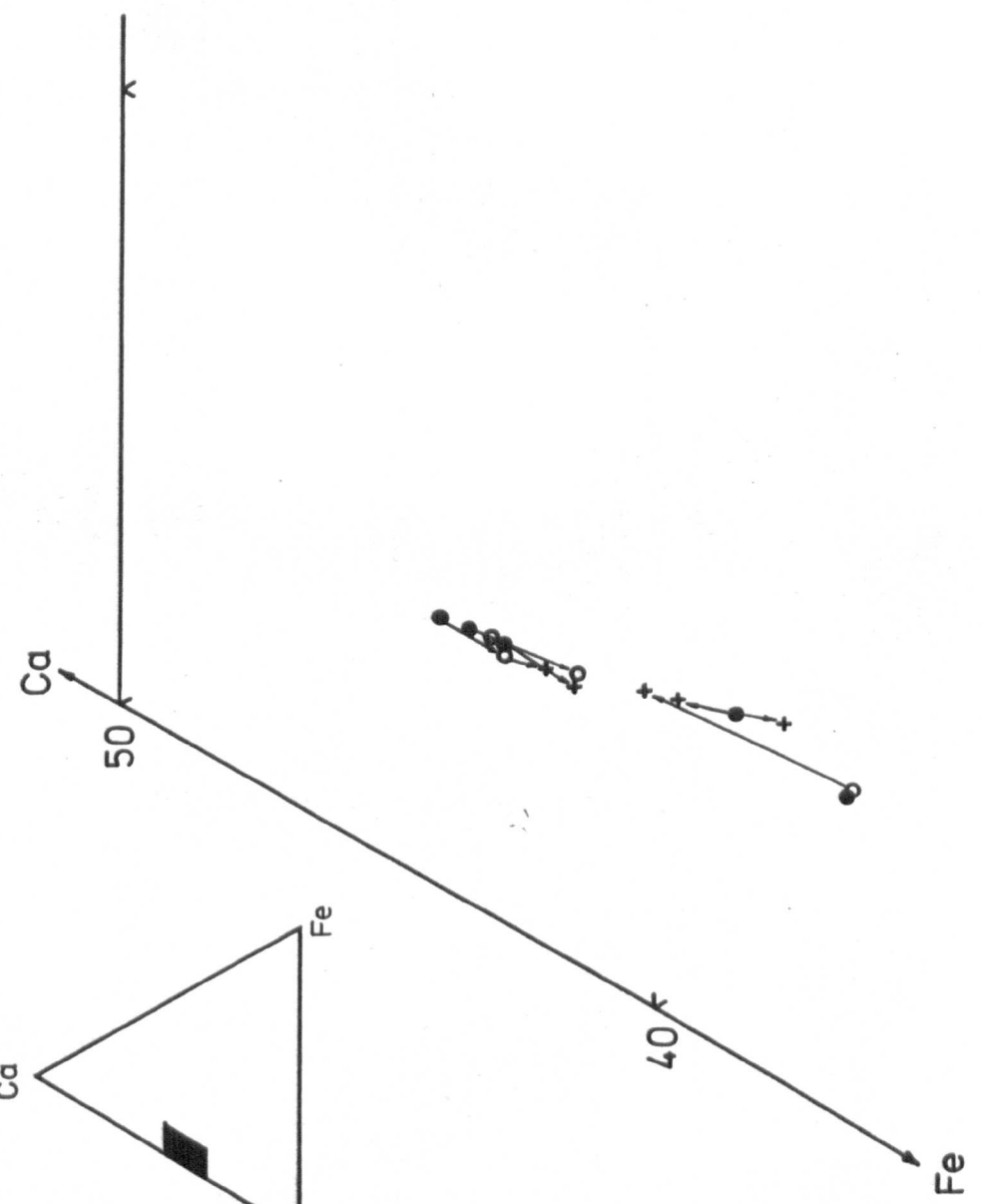
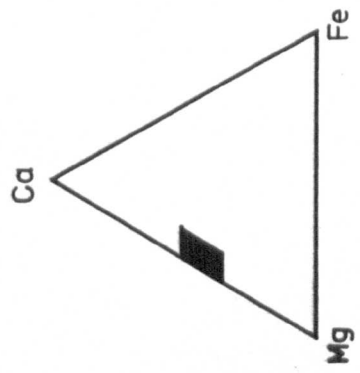


Figure 9.4:  $[Ca]_{\text{opx}}$  v.  $[Ca]_{\text{cpx}}$  for coexisting orthopyroxene and clinopyroxene in Letseng peridotites.

$[Ca] = Ca/(Ca+Mg)$ .

Closed circles: coarse textured rocks.

Inclined crosses: porphyroclastic textured rocks.

Open circles: mosaic porphyroclastic textured rocks.

Vertical crosses: granuloblastic textured rocks.

Large symbols are Main Pipe peridotites, and small symbols are Satellite Pipe peridotites.

G beside vertical cross denotes presence of garnet and spinel.

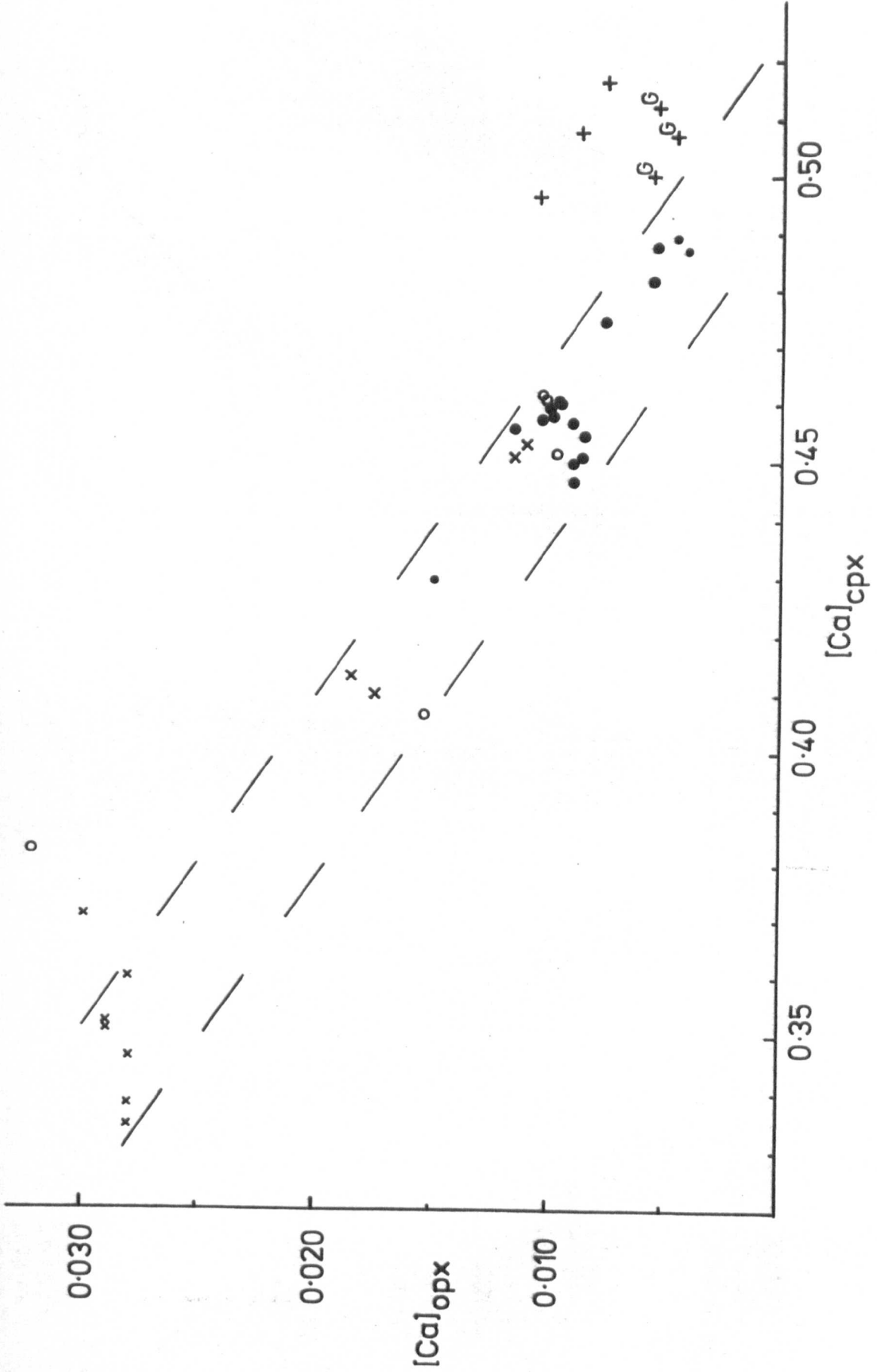


Figure 9.5: Plot of % Wo in Enss v. % Wo in Diss.

Data from the experimental results of Lindsley & Dixon (1976).

Measurements at 20Kb with error bars.



20Kb

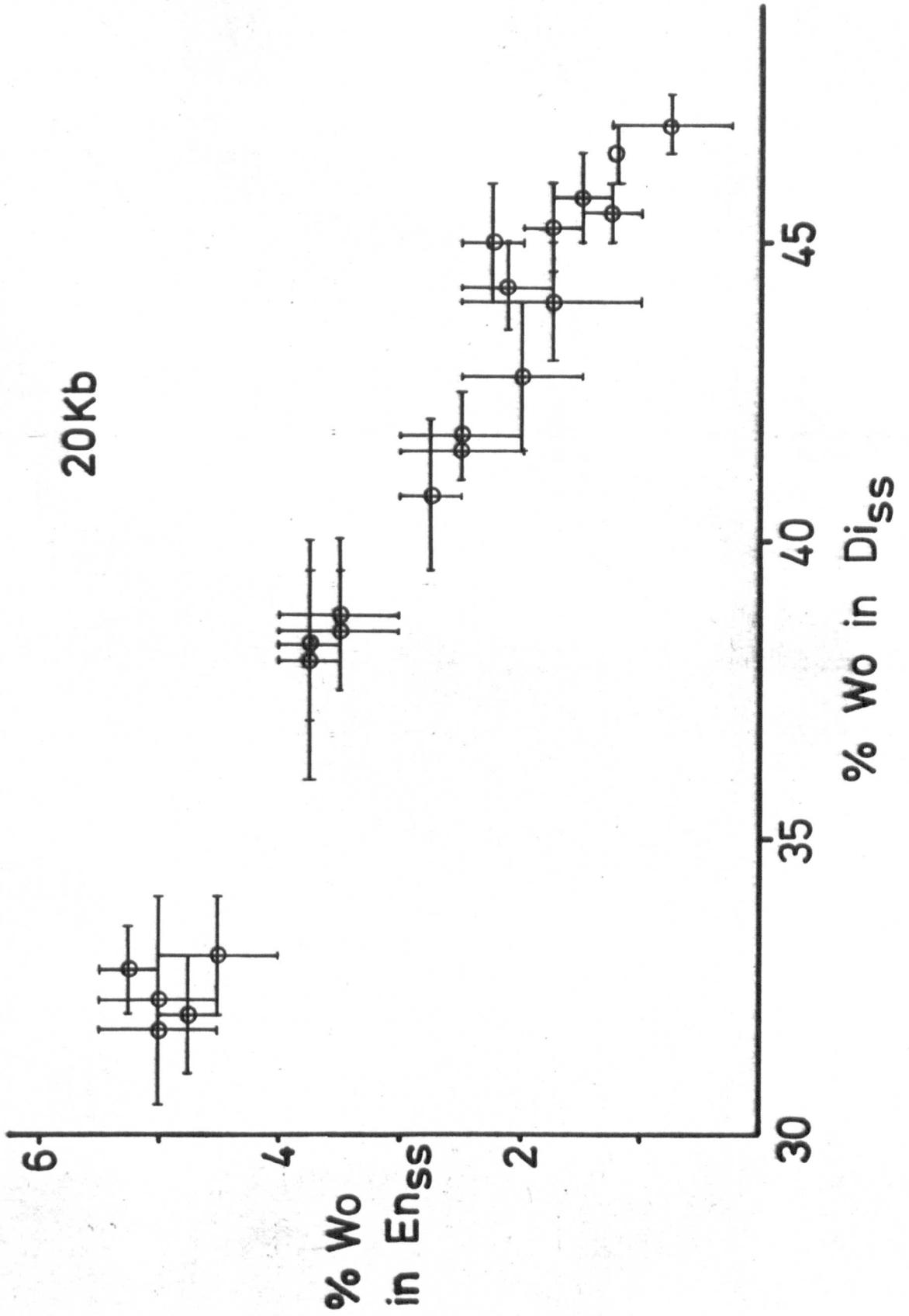


Figure 9.6: Atomic Al+Cr in OPX v. Atomic Al+Cr in CPX for coexisting orthopyroxene and clinopyroxene in Letseng peridotites.

Symbols as for figure 9.6.<sup>4</sup>

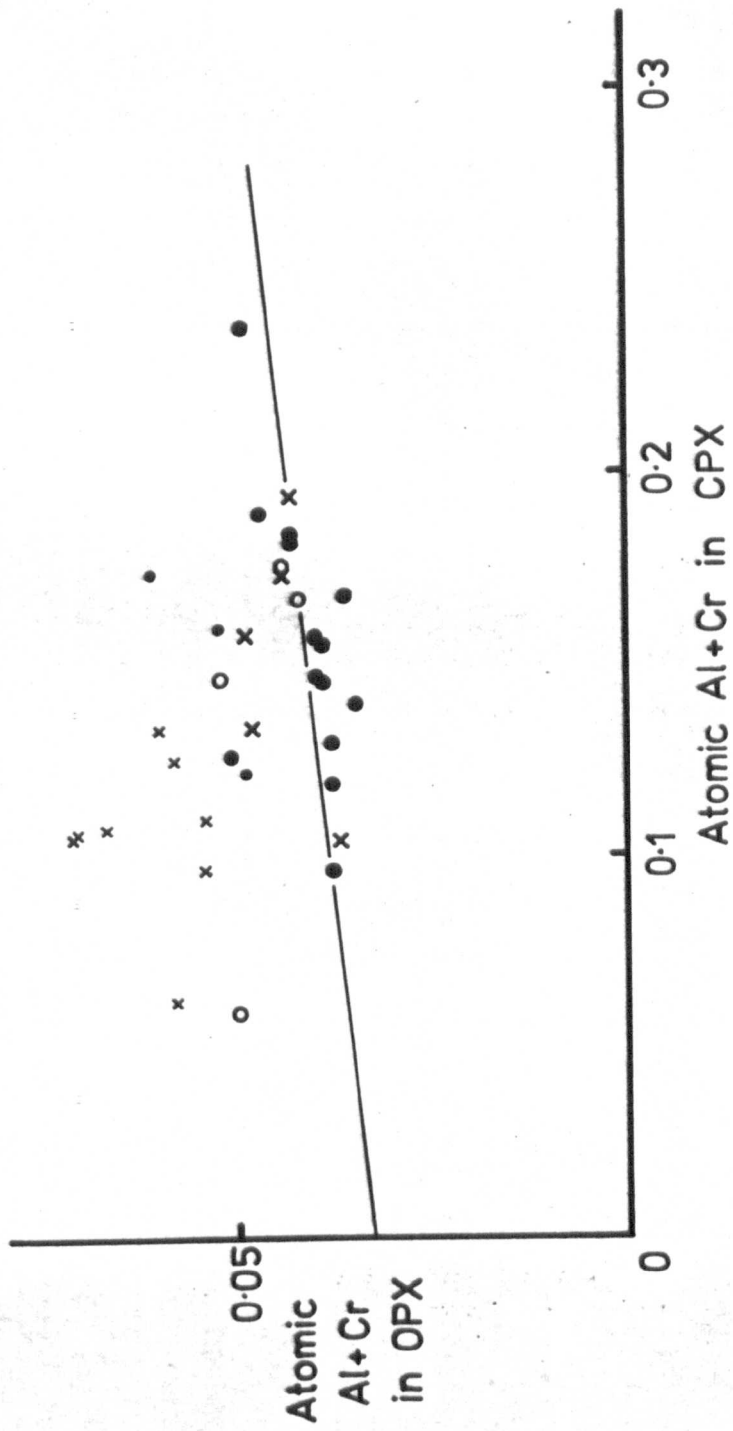


Figure 9.7:  $(Al/Al+Cr)_{GT}$  v.  $(Al/Al+Cr)_{Cpx}$  v.  $(Al/Al+Cr)_{Opx}$  for coexisting garnet, clinopyroxene, and orthopyroxene in Letseng peridotites.

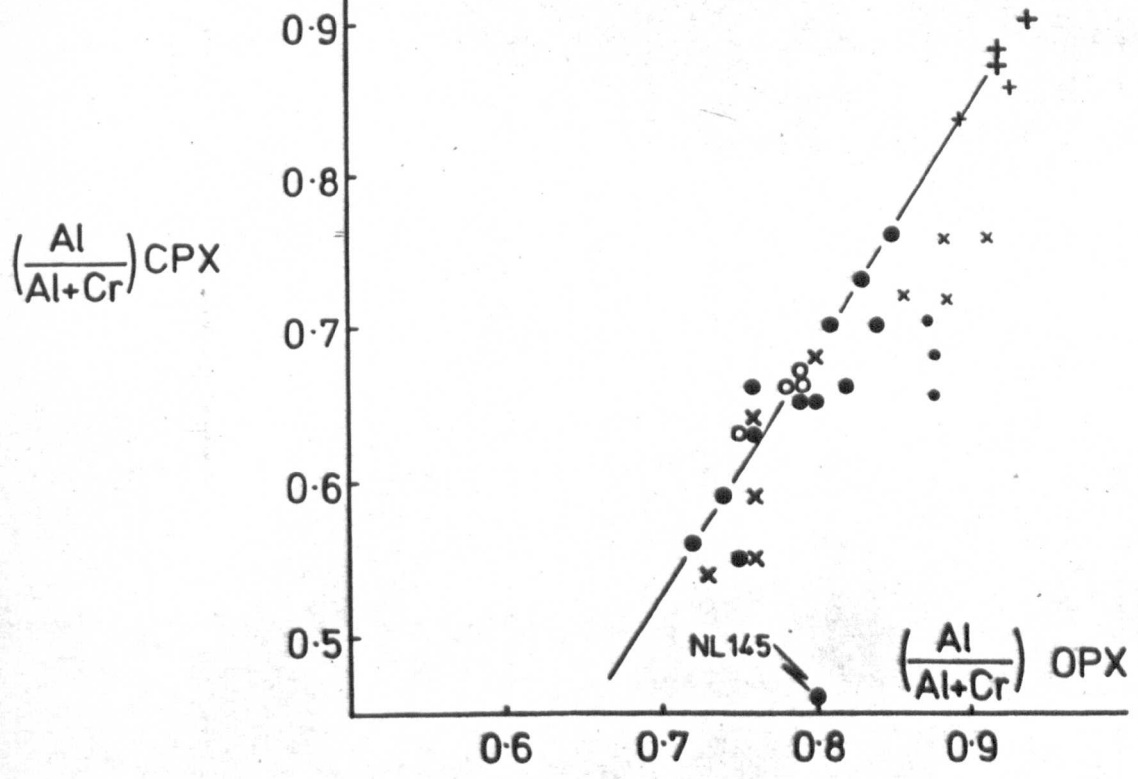
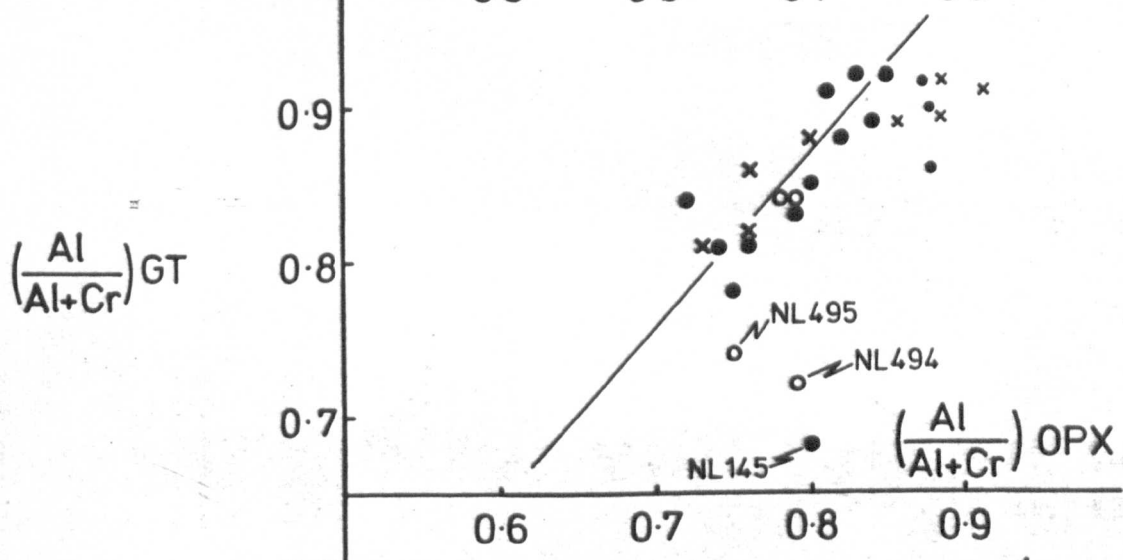
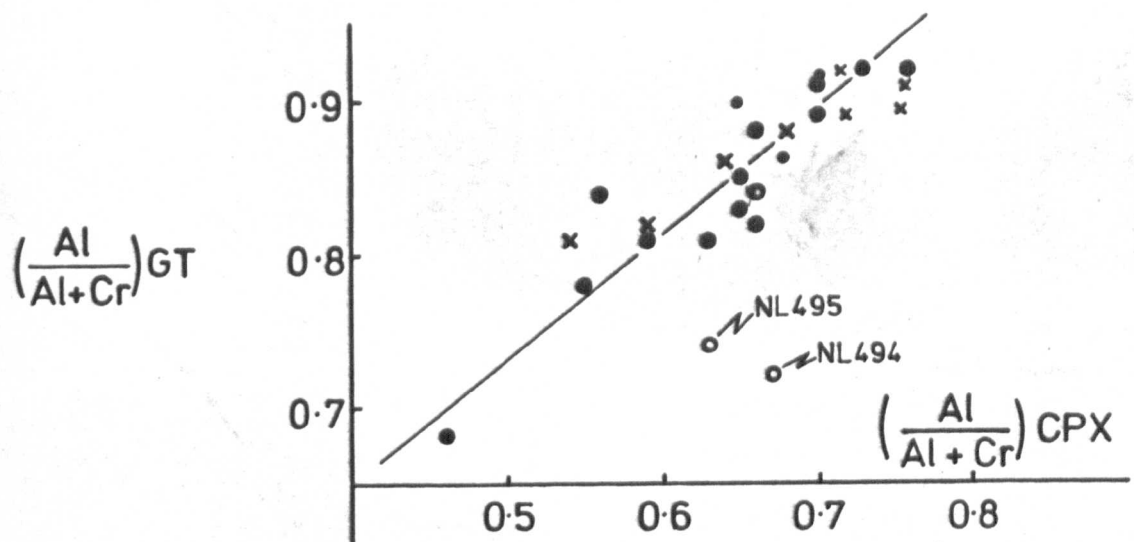
Closed circles: coarse textured rocks.

Inclined crosses: porphyroclastic textured rocks.

Open circles: mosaic porphyroclastic textured rocks.

Vertical crosses: granuloblastic textured rocks.

Large symbols are Main Pipe peridotites, and small symbols are Satellite Pipe peridotites.



## CHAPTER 10

### Granulites

#### Introduction

Kimberlites and similar mantle-derived volcanics offer the earth scientist a unique window to the unexposed rocks of the underlying basement terrain, as well as the eclogites and peridotites of mantle origin. These rocks, gneisses and granulites, are transported rapidly to the surface by the kimberlite allowing the preservation of the high temperature and pressure mineralogy. Hydrothermal alteration during transport is often extensive for the more acid rocks but the abundance of these basement rocks at Letseng and the scale of the mining operations has facilitated the sampling of fresh specimens. Xenolith suite studies have tended to concentrate on the more exotic mantle rocks while, until recently, ignoring the granulites. Amphibolite facies gneisses have received even less attention.

Griffin et al. (1979) have shown that in southern Africa granulite xenoliths in kimberlite seem to be restricted to the Kaapvall craton margin. Basement xenoliths in kimberlites within the craton are amphibolite facies gneisses. This outline completely ignores the presence of amphibolite facies gneisses in kimberlites along the craton margins (e.g. Bloomer and Nixon, 1973; Rolfe, 1973), thus giving a false impression about the distribution of these rock types. In his review of African granulites, Clifford (1974) records granulites in both the Rhodesian and Transvaal cratonic nuclei and Dawson (personal communication) has confirmed the presence of granulites in several within-craton kimberlites.

The Namaqualand belt may extend into Natal beneath Lesotho and zircon U/Pb ages (Davis, 1977) suggest that Lesotho kimberlites have penetrated this belt. If so it may be pertinent to observe that the lack of deformation

or fabric in these xenolithic granulites would accord with the suggestion of Joubert (1971) that the granulite facies rocks resulted at the culmination of a 'major regional thermal dome'. This is in contrast with rocks in the Limpopo belt (Wakefield, 1971) where granulites are associated with isoclinal folding and retrogressive amphibolites. The suggestion of relative movement of the Kaapvaal craton and the Namaqualand belt (Kröner, 1977) may explain the relative abundance of exposed granulites in the latter area but the relative absence of granulite xenoliths in within-craton kimberlites remains a problem.

The collection of granulites reported here is similar to that of Griffin et al. (1979) but including many more intermediate to acid garnet granulites. The amphibolite facies rocks reported by Bloomer and Nixon (1973) have not been studied here, although some comment is made on retrogressive features in the granulites.

#### Petrography

Many of the specimens were collected from coarse concentrate rejected during mining operations and consequently are rather small (< 6cm). However, the underground mine workings afforded considerable fresh exposure where a number of larger (and more siliceous) samples were collected. Plate 10A in 'Lesotho Kimberlites' (1973) shows the largest recorded basement xenolith from Letseng: a 30 cm biotite acid gneiss. Garnet bearing basement rocks are generally considerably smaller than this and often extremely friable due to the extensive feldspar alteration.

The xenoliths are usually well rounded but may be slightly ovoid in such rocks as the foliated gneisses. Other xenoliths may be more blocky in shape in relation to mineralogical banding present on a hand specimen scale. This banding is generally emphasised by discontinuous layers of garnet and, often, clinopyroxene. The term eclogite is not used here to

TABLE 10.1: Granulite Xenolith Modes

Sample	Gnt	Cpx	Opx	Plag	Scap	Perth	Qtz	Amph	Bio	Rutile	Ilm/ Magn	Apat	Sphene	Remarks
NLO52	✓			✓				✓	✓					Garnet rich bands. Badly altered. Trace calcite.
NLO61	8.3			68.5			30.9	✓	22.5	0.3	0.1	0.8		Weak foliation of biotite.
NLO65	11.1	9.9	+	47.5				✓	✓	✓	✓			Garnet/clinopyroxene rich bands.
NLO92	✓	✓		✓						+			+	Kelyphite.
NL110	14.3	5.6		40.2			39.9	+	✓	+	4 m			Coarse grained.
NL423	32	30	4	30					✓	+	1			Weak foliation.
NL544	35		64					✓	✓					Poikilitic Amphibole.
NL545	25	35	40	✓	+			✓	✓					Weak mineral banding.
NL550	✓	✓	✓	3				+	+					
NL551	40	55	2					✓	✓					
NL552	33	33	33					✓	✓	1	✓			
NL553	23	41	35					✓	✓	1	✓			
NL554	39	59	1	✓				✓	✓	1	✓			
NL556	✓	✓		✓				✓	✓	✓	✓			+Kyanite trace zircon. Very coarse grained
NL561	✓	✓		✓				✓	✓	✓	✓			Coarse grained.
NL562	✓	✓		✓				✓	✓	✓	✓			
BD1852	44.9	3.1		47.5										Garnet rich area.
BD1852	7.4	18.0	3.4	70.1							2.9m	1.6		Plagioclase rich area.
BD1853	27.7	11.1	0.8	57.8				0.1	+		0.2	0.9		Garnet,clinopyroxene,magnetite rich bands
BD1865	57.2	40.4						+	+	+	2.0	0.5		Coarse grained.
BD1867/A	18.7	25.5		52.0	3.9						2.4i			Amphibole mantled clinopyroxene.
BD1867/C	47.5	42.4		7.1				0.6	0.6	0.8	0.8		1.7	
BD1867/D	31.3	11.0		34.0				16.1	0.1	0.2	5.6i			Amphibole rimmed by clinopyroxene.
BD1867/E	34.3	17.9		43.6				0.4	0.4	0.2	4.0m			Very coarse grained
BD1867/E	54.2	19.3		20.2					0.6	0.7	8.2			
BD1867/F	8.9	8.9		3.6		77.4		✓	✓	✓				
BD1867/K	✓	✓		18.5				31.7	31.7	+				Poikilitic amphibole. Coarse kelyphite.
BD1867/L	25.8	24.0								+				

+ = Denotes trace amount of mineral

i = ilmenite

m = magnetite

} The majority of the opaque oxides are undifferentiated



describe these basic layers as the clinopyroxene is not of omphacitic composition.

The most basic rocks show a well developed polygonal granoblastic texture with an average and even grain size of 1-2 mm. The intermediate to acid rocks display a similar texture but the grain size is often much less even and polygonal grains less well defined with grain boundaries often interlocking or serrate. A few rocks have extremely coarse (5-10 mm) garnet grains. Elongation and/or orientation of mineral grains in a metamorphic fabric is rare, but most specimens display some undulose extinction in the feldspar (and pyroxene). Quartz in NL110 is strongly strained with considerable sub-grain growth.

Garnet, clinopyroxene and plagioclase are the three most abundant minerals in the majority of these rocks, often accounting for >90% of the mineral mode (Table 10.1). Figure 10.1 shows a fairly continuous variation in modal abundances from the acid garnet granulites to basic garnet pyroxenites with plagioclase varying from 55% to 0%. The pyroxenites likewise vary from garnet orthopyroxenites, through garnet websterites, to garnet clinopyroxenites with orthopyroxene varying from 64% to 0%. Orthopyroxene in plagioclase-bearing rocks is always <5%. It should be noted that these pyroxenites are superficially similar to rocks of the peridotite suite. The mineral compositions, however, differ markedly and the granulite pyroxenites usually contain rutile.

Other major phases include quartz (>30% in two samples) and perthitic K-feldspar (77% in one sample). One unusual rock contains abundant coarse laths of kyanite in roughly equal proportions with garnet and feldspar. This rock may correspond with E6 of Nixon (1960).

The hydrous phases amphibole and biotite usually occur in minor amounts in apparent textural equilibrium. In BD1867/A amphibole mantles remnant clinopyroxene in crystal continuity, and NL550 and BF1867/D show abundant poikilitic amphibole replacing pyroxene and feldspar. In contrast BD1867/L

displays abundant amphibole seemingly in textural equilibrium but often marginally replaced by a thin rim of pale green clinopyroxene.

Rutile is by far the most common accessory mineral occurring as discrete grains and as stumpy acicular inclusions in garnet, clinopyroxene and sphene. Ilmenite and magnetite are modally abundant (up to 8%) but do not coexist except where ilmenite-haematite solid solution appears as lens-shaped exsolution lamellae in magnetite-ülvospinel solid solution (see discussion below). Apatite commonly appears as subhedral inclusions in most other phases. Scapolite is rare and usually partly altered, but when present forms part of the granoblastic texture (Plate 10.1). Rare sphene is anhedral in form in contra-distinction to that expected from the idioblastic series of Becke. However, Turner and Verhoogen (p.594, 1960) noted the unusual droplike form of sphene in amphibolite. Pale yellow spherical zircon inclusions (<0.1 mm) are abundant in the minerals of NL556. Quartz in NL110 contains randomly oriented minute (0.2 x 0.001 mm) acicular crystals of an unidentified high relief mineral.

Many of these and other samples show the effects of considerable alteration due to hydrothermal or 'fenitising' fluids (Ferguson et al. 1973) associated with the kimberlite. Quartz (and feldspar) are replaced by sericite and to a lesser extent brown mica (Plate 58B 'Lesotho Kimberlites', 1973). Feldspar is replaced by natrolite (Nixon, 1960), cebolite (Kruger, 1978, 1980) and pectolite (Griffin et al., 1979) as well as calcite. The pyroxenes show no alteration but the garnets commonly have a green or brown kelyphite rim in which spinel, pyroxene and feldspar (?) may rarely be recognised. Zircon and monazite in a previously described specimen from Letseng (E6 of Nixon, 1960) were attributed to alteration by a gaseous phase, but the petrographic similarity between E6 and NL556, where all the minerals are fresh, may suggest a different origin, at least for the zircon. Some clinopyroxenes in rocks with little or no feldspar show spongy margins

(Plate 10.2), similar to those described by Carswell (1975) in garnet lherzolites and Donaldson (1977) in spinel lherzolites, and recorded by Griffin et al. (1979) in their granulite collection. This spongy margin is undoubtedly a secondary feature, but may not be the result of interaction with the host kimberlite as concluded by Griffin et al. (1979).

Most specimens display equilibrium textures. Some, as described above, show amphibole replacing pyroxene and/or poikilitically enclosing other phases. This texture suggests retrogressive metamorphism from pyroxene granulite to hornblende granulite, or possibly amphibolite facies conditions. In contrast, the clinopyroxene rimmed amphibole in BD1867/L may imply a prograde reaction to the pyroxene granulite facies.

A further example of disequilibrium is shown in NLO65 and BD1853, where clinopyroxene has replaced orthopyroxene. The replacing clinopyroxene has grown in crystallographic continuity with the orthopyroxene remnants (Plates 10.3 and 10.4). In NLO65 the orthopyroxene is entirely mantled by the clinopyroxene. The replacement may be represented by the reaction:



as suggested by Griffin et al. (1979) for LT2 from Letseng. It is worth noting the remarkable similarity between LT2 and NLO65, both in bulk rock and mineral composition. The modal differences may be the result of point counting different parts of these banded rocks.

The mineral assemblages are compatible with low pressure (orthopyroxene-plagioclase subfacies) and high pressure (clinopyroxene-almandine subfacies) granulite facies metamorphism (Winkler, 1967). The occasional presence of hydrous minerals suggests variable  $P_{H_2O}$  and sometimes more extensive retrograde reaction. Prograde reaction of anhydrous and hydrous minerals is also noted.

TABLE 10.2: Granulites - Whole Rock Chemistry

	NLO52	NLO65	NL110	BD1867/C	BD1867/E
SiO <sub>2</sub>	57.36	59.72	54.04	51.40	41.66
TiO <sub>2</sub>	0.15	0.60	0.17	0.42	1.78
Al <sub>2</sub> O <sub>3</sub>	13.90	12.92	13.88	18.65	14.32
Fe <sub>2</sub> O <sub>3</sub>	0.95	2.21	1.57	1.76	7.91
FeO	0.82	3.13	3.09	3.53	14.41
MnO	0.06	0.07	0.07	0.08	0.30
MgO	1.15	2.87	3.61	6.07	6.55
CaO	10.22	10.59	11.73	11.11	9.34
Na <sub>2</sub> O	5.55	4.40	6.38	4.56	1.75
K <sub>2</sub> O	3.22	0.99	0.69	0.47	0.41
P <sub>2</sub> O <sub>5</sub>	0.04	0.14	0.04	0.05	0.13
H <sub>2</sub> O	5.91	2.50	4.79	1.68	1.48
Total	99.33	100.14	100.06	99.78	100.04
Cr	5.5	24.7	32.1	81.7	19.5
Ni	4.2	6.7	9.1	40.2	52.4
Ba	2373.3	507.7	466.6	700.7	576.8
Sc	4.5	17.1	21.1	21.5	81.1
V	9.8	114.2	93.7	95.8	720.0
Cu	12.2	17.8	13.5	9.2	26.0
Nb	3.3	4.9	3.5	2.7	5.1
Rb	27.7	5.7	7.9	47.9	13.4
Sr	472.3	270.7	219.3	494.8	137.3
Y	7.7	13.9	7.7	8.9	38.3
Zr	60.6	64.9	31.5	13.5	33.1
La	12.5	26.2	2.2	4.3	19.2
Ce	26.6	51.8	4.6	8.8	35.0
Nd	15.3	23.0	4.4	5.9	14.9
Sm	2.0	6.6	1.3	3.1	7.5
100Mg/ (Mg+Fe <sup>2+</sup> )	71.4	62.0	67.6	75.4	44.8
Na/K	1.54	3.97	8.26	8.67	3.81
K/Rb	965.0	1441.8	725.1	81.5	254.0
Rb/Sr	0.059	0.021	0.036	0.097	0.098
K/Ba	11.3	16.2	12.3	4.8	5.9
Ba/Sr	5.01	1.88	2.13	1.42	4.20
Ca/Sr	154.32	279.59	382.28	160.50	486.96
Ba/Rb	85.7	89.1	59.1	14.6	43.0

TABLE 10.3: Granulites - CIPW Norms

	NLO52	NLO65	NLL10	BD1867/C	BD1867/E
Qtz	-	10.851	-	-	-
Or	19.029	5.851	4.078	2.778	2.423
Ab	45.153	37.233	38.654	31.338	14.809
An	3.506	12.580	7.198	29.033	30.009
Ne	0.981	-	8.307	3.927	-
Di	7.068	20.931	27.098	20.574	12.824
Wo	15.867	5.451	7.174	-	-
Hy	-	-	-	-	12.115
Ol	-	-	-	6.905	10.929
Mt	1.377	3.204	2.276	2.552	11.469
Il	0.285	1.140	0.323	0.798	3.381
Ap	0.093	0.325	0.093	0.116	0.302
Plag An	7.2	25.3	15.7	48.1	67.0
Ol Fo	-	-	-	76.0	46.6
Σfspr+Ne	68.7	55.7	58.2	67.1	47.2
ΣPyx+Ol	7.1	20.9	27.1	27.6	35.9

TABLE 10.4: Granulite REE Abundances (in ppm)

	N1065	BD1867/C
La	22.0	5.1
Ce	47.9	10.0
Nd	19.4	5.3
Sm	3.3	1.2
Eu	1.3	0.6
Gd	3.1	1.3
Dy	2.4	1.2
Er	1.3	0.6
Yb	1.2	0.5
$La_N/Yb_N$	12.0	6.2
Eu/Eu*	1.3	1.5

Values obtained by isotope dilution and mass spectrometry

## Bulk Rock Chemistry

Bulk rock analyses and CIPW norms for five xenoliths are presented in Tables 10.2 and 10.3. Samples were necessarily rather small although considerably more confidence may be had in the results for the less basic specimens where more material was available. Major (except for FeO and H<sub>2</sub>O) and trace elements were analysed at Edinburgh University by P. Jackson: major elements were analysed by XRF on fused glass discs and trace elements in pressed powder pellets. Analyses for FeO and H<sub>2</sub>O were carried out by N.P. Lock at Sheffield University, using standard wet chemical techniques. In addition two samples were analysed for REE (Table 10.4) by isotope dilution and mass spectrometry at Leeds University (see Chapter 4 for analytical technique).

It is immediately apparent that these analyses bear very little comparison with major element abundances in other granulites in Lesotho kimerlites (cf. Cox et al., 1973; Dawson, 1977; Rogers, 1977; Griffin et al., 1979) except for the remarkable similarity of NLO65 and LT2 mentioned above. This is not surprising for NLO65 and NL110 which both contain abundant modal quartz (>30%) and NLO65 which contains 11% normative quartz. BD1867/C and BD1867/E however are considerably more basic and might be expected to show some similarity to published results.

BD1876/C is near to alkali olivine basalt in composition with 4% nepheline and 7% olivine in the norm. However high SiO<sub>2</sub>, Al<sub>2</sub>O<sub>3</sub> and Na<sub>2</sub>O and low FeO<sup>T</sup> and MgO set this rock apart from other Lesotho granulites. A better comparison is obtained with the nepheline normative granulites from the Lashaine volcano in Tanzania (Dawson, 1977). The Letseng granulites display a meaningless scatter in a plot of Na<sub>2</sub>O + K<sub>2</sub>O v. SiO<sub>2</sub> except for BD1867/C which plots coincident with the Lashaine and Matsoku granulites of Dawson (1977).

BD1867/E contains 8% modal and 11.5% normative magnetite contributing to an unusual composition which bears a faint similarity to hortonolite ferrogabbro (Turner and Verhoogen, 1960, p.293) from the Skaergaard intrusion. In the AFM system (Figure 10.3a) this rock (BD1867/E) plots very close to the gabbro section of the Skaergaard differentiation line. The Rb, Sr, Cr and Ni abundances may be compatible with this comparison but Cu and Ba are too low and too high respectively.

The acid/intermediate rocks NLO52, NLO65 and NL110 do not correspond to any magma compositions and reference to the ACF diagram (Figure 10.2) demonstrates that these rocks are most likely metamorphosed calcareous sediments. Note that NLO52 is highly altered and has not been corrected for a minor carbonate content: hence it plots closer to the C apex of the diagram than it should. The remaining rocks plot at points reasonably compatible with their observed mineral assemblages. Note that the reaction observed in NLO65 and BD1853 implies the assemblage plagioclase-orthopyroxene is replaced by clinopyroxene-garnet.

Griffin et al. (1979) have shown a compositional control on the presence of modal plagioclase in their rocks which they infer annuls the necessity to postulate the origin of the 'eclogites' from greater depths than the granulites. The rocks of this study conform to this observation (Figure 10.3b) although no bulk analyses of plagioclase-free rocks was made and the possible effects of a sedimentary origin are ignored.

The trace element abundances, in accord with other xenolithic granulites show a wide scatter of values especially for LI elements. Rogers (1977) concludes that the presence of Eu anomalies in the REE distribution patterns is unlikely to result from kimberlite contamination (with essentially linear REE patterns) while suggesting that the Ba and Sr abundances may owe something to kimberlite contamination. This latter suggestion is not in accord with the observation of Griffin et al. (1979) that most Ba resides in K-



feldspar inclusions in textural equilibrium with the other phases. Kruger (1978) has shown that altered basement xenoliths from Letseng have a tendency to lower K/Rb ratios and higher Sr towards their margins. However, some of the trends are equivocal and were designed to analyse gradients from the fresh core to the altered surface of the xenoliths. Samples in this study, as no doubt in the others mentioned, were taken from the interior of the xenolith and the altered rim discarded. In the present study the lowest K/Rb ratios correspond to samples that appear petrographically fresher than those with high K/Rb ratios: this situation is unlikely to result from contamination by kimberlite with low K/Rb ratios (see Chapter 3).

The K/Rb ratios, while rather variable, fall in the fields for granulites from Tarney and Windley (1977) (Figure 10.6) with one low exception. Their data displays a well established trend which is not followed even by the xenolithic granulites of Griffin et al. (1979). Rb/Sr ratios are  $< 0.1$  (Figure 10.7) and similar to those of most other granulites. Tarney and Windley conclude that these ratios result from the removal of K and Rb during granulite facies metamorphism although the metamorphism alone is not enough but requires a fluid capable of removing Rb. The generally high Ba/Rb ratios in the present study agree with the further observation of Tarney and Windley (1977) that granulites have  $Ba/Rb \sim 60$  and amphibolites  $Ba/Rb \sim 10$ . Since Ba remains fairly constant this is also inferred to imply Rb depletion.

These trace element characteristics are taken to confirm the granulite character of these rocks. However, the REE patterns (Figures 10.4 and 10.5) are more difficult to interpret. These xenolithic granulite REE patterns are very similar to those of Rogers (1977) showing LREE enrichment ( $La_N/Yb_N = 6-12$ ) and variable Eu anomalies. Non-xenolithic granulites from other areas (Tarney and Windley, 1977) which are interpreted as of lower crustal origin, also show LREE enrichment although at generally higher  $\epsilon_{REE}$ . Eu anomalies

are not common except in anorthosites. The present data are more in accord with the views of Taylor and McLennan (1979) with the reservation that these rocks may not be of lower crustal origin (see following section); they propose an andesite model for crustal growth and that therefore lower crustal rocks should have REE patterns with weak LREE enrichment and positive Eu anomalies to balance the more strongly LREE enriched upper crustal (sedimentary) rocks. The mean pattern for the whole crust is andesitic. Conversely Tarney and Windley (1977) consider the possibility that the complementary rocks to balance the upper crustal REE patterns may now reside in the upper mantle. Evidence for LREE enriched upper mantle REE patterns (Rogers, 1979) does not at this stage support such a hypothesis. A further conclusion, that the HREE depleted granulites were in equilibrium with eclogite when these patterns were generated, does not seem to accord with the chemistry of the present samples. Further the sample with the smallest Eu anomaly is the most siliceous and possibly is a metasediment. As such it might be expected to possess a negative Eu anomaly. The metasedimentary character of some of these xenoliths and the similarity of REE patterns to those of Rogers (1977) suggests that some other mechanism should be invoked to explain the patterns. At present the model of Taylor and McLennan (1979) seems the more plausible. Collerson and Fryer (1978) discuss the possibility of REE depletion as a result of complexing with volatiles (notable  $\text{CO}_2$ ). They conclude that the HREE may be preferentially removed in a volatile complex, thus giving rise to LREE enriched granulite REE patterns. If Eu were excluded from these volatile complexes, this might prove an effective mechanism for causing variable depletion of  $\Sigma$ REE with the most depleted rocks displaying the largest positive Eu anomalies (cf. Rogers, 1977).

TABLE 10.5: Granulite Phase Chemistry

	NLO52										NLO65									
	GT	PL	BI	GT		Cpx		Opx Adjacent	PL		Core	Cpx	Opx	PL		Core	Cpx	Opx	BI	
				Core	Rim	Core	Rim		Core	Rim				Core	Rim				Core	Rim
SiO <sub>2</sub>	38.57	61.74	37.65	40.09	53.53	53.16	53.05	53.16	62.79	53.16	53.05	53.16	63.16	62.79	53.16	53.05	53.16	38.52	38.52	
TiO <sub>2</sub>	N.D.	N.D.	4.03	N.D.	0.39	0.40	0.37	N.D.	N.D.	N.D.	0.37	N.D.	N.D.	N.D.	N.D.	0.37	N.D.	5.72	5.74	
Al <sub>2</sub> O <sub>3</sub>	21.37	24.75	15.28	22.35	3.82	3.50	3.75	1.93	23.80	1.93	3.75	1.93	23.28	23.80	1.93	3.75	1.93	14.26	13.92	
Cr <sub>2</sub> O <sub>3</sub>	N.D.	N.D.	N.D.	N.D.	N.D.	N.D.	N.D.	N.D.	N.D.	N.D.	N.D.	N.D.	N.D.	N.D.	N.D.	N.D.	N.D.	N.D.	N.D.	
Fe <sub>2</sub> O <sub>3</sub>	N.D.	N.D.	N.D.	N.D.	N.D.	N.D.	N.D.	N.D.	N.D.	N.D.	N.D.	N.D.	N.D.	N.D.	N.D.	N.D.	N.D.	N.D.	N.D.	
FeO	28.54	N.D.	16.79	25.26	7.51	7.32	7.87	22.59	0.12	22.59	7.87	22.59	0.11	0.12	22.59	7.87	22.59	11.58	11.36	
MnO	1.77	N.D.	N.D.	0.37	N.D.	N.D.	N.D.	N.D.	N.D.	N.D.	N.D.	N.D.	N.D.	N.D.	N.D.	N.D.	N.D.	N.D.	N.D.	
MgO	4.22	N.D.	12.27	8.44	13.14	13.70	12.84	23.19	5.09	23.19	12.84	23.19	4.98	5.09	23.19	12.84	23.19	16.65	16.79	
CaO	7.53	6.06	1.10	6.25	21.72	21.72	21.32	0.35	8.59	0.35	21.32	0.35	8.23	8.59	0.35	21.32	0.35	N.D.	N.D.	
Na <sub>2</sub> O	N.D.	7.83	N.D.	N.D.	1.34	1.40	1.34	N.D.	N.D.	1.34	1.34	N.D.	0.96	0.61	N.D.	1.34	N.D.	9.93	9.98	
K <sub>2</sub> O	N.D.	0.27	9.40	N.D.	N.D.	N.D.	N.D.	N.D.	N.D.	N.D.	N.D.	N.D.	N.D.	N.D.	N.D.	N.D.	N.D.	N.D.	N.D.	
P <sub>2</sub> O <sub>5</sub>	N.D.	N.D.	N.D.	N.D.	N.D.	N.D.	N.D.	N.D.	N.D.	N.D.	N.D.	N.D.	N.D.	N.D.	N.D.	N.D.	N.D.	N.D.	N.D.	
Cl <sub>2</sub>	N.D.	N.D.	0.6	N.D.	N.D.	N.D.	N.D.	N.D.	N.D.	N.D.	N.D.	N.D.	N.D.	N.D.	N.D.	N.D.	N.D.	0.15	0.15	
Total	102.00	100.62	96.58	102.76	101.44	101.21	100.51	101.22	101.00	101.22	100.51	101.22	100.70	101.00	101.22	100.51	101.22	96.82	96.45	
Si	2.99	10.89	5.86	3.00	1.95	1.94	1.95	1.95	11.05	1.95	1.95	1.95	11.14	11.05	1.95	1.95	1.95	5.84	5.86	
Ti	1.95	5.14	0.47	1.97	0.01	0.01	0.01	0.01	4.94	0.01	0.01	0.01	4.84	4.94	0.01	0.01	0.01	0.65	0.66	
Al	1.85		2.80	1.58	0.16	0.15	0.16	0.08	0.24	0.08	0.16	0.08	0.02	0.24	0.08	0.16	0.08	2.55	2.50	
Cr	0.11		2.18	0.02	0.23	0.22	0.23	0.69	0.02	0.23	0.23	0.69	0.02	0.02	0.23	0.23	0.69	1.47	1.45	
Fe <sup>3+</sup>	0.49		2.84	0.96	0.71	0.75	0.71	1.27	0.96	0.71	0.71	1.27	0.94	0.96	0.71	0.71	1.27	3.76	3.81	
Fe <sup>2+</sup>	0.63	1.15	0.18	0.46	0.85	0.85	0.85	0.01	0.46	0.85	0.85	0.01	0.94	0.46	0.85	0.85	0.01	1.92	1.94	
Mn		2.68			0.10	0.10	0.10			0.10	0.10		2.82	0.14	0.10	0.10		0.04	0.04	
Mg		0.06	1.87															0.04	0.04	
Ca			0.02															0.04	0.04	
Na																		0.04	0.04	
K																		0.04	0.04	
P																		0.04	0.04	
Cl																		0.04	0.04	
Total	8.02	19.92	16.22	8.02	4.01	4.02	4.00	4.00	20.04	4.01	4.00	4.00	19.98	20.04	4.00	4.00	4.00	16.23	16.25	
Mg/(Mg+Fe)	0.21		0.57	0.37	0.76	0.77	0.74	0.65	0.74	0.76	0.77	0.74		0.74	0.74	0.74	0.65	0.72	0.72	
Ca/(Ca+Mg)					0.54	0.53	0.55	0.5	0.55	0.54	0.53	0.55		0.55	0.55	0.55	0.5	0.72	0.72	
Ca	21.2		15.1	16.6	47.5	46.7	47.2	64.1	47.2	47.5	46.7	47.2		47.2	47.2	47.2	64.1	47.2	47.2	
Mg	16.5		31.6	31.1	39.7	41.2	39.3	34.8	39.3	39.7	41.2	39.3		39.3	39.3	39.3	34.8	39.3	39.3	
Fe	62.3		53.3	52.3	12.8	12.1	13.5		13.5	12.8	12.1	13.5		13.5	13.5	13.5		13.5	13.5	
An#		30.0							24.7				25.0	24.7					24.7	

TABLE 10:5 (cont..)

	NL110										NL423						BD1852			
	GT		CPX		PL		GT	CPX	PL	MGss	ILss	Core	Rim	Core	Rim	CPX	OPX			
	Core	Rim	Core	Rim	Core	Rim														
SiO <sub>2</sub>	39.08	39.39	51.92	52.45	59.98	60.13	38.56	52.66	61.48	0.30	0.35	38.70	38.80	52.70	51.76					
TiO <sub>2</sub>	N.D.	N.D.	0.53	0.22	N.D.	N.D.	N.D.	0.31	N.D.	10.61	32.15			0.17						
Al <sub>2</sub> O <sub>3</sub>	22.19	22.51	3.23	2.60	24.78	25.09	21.54	3.04	23.84	1.11	0.39	21.08	21.46	3.56	1.57					
Cr <sub>2</sub> O <sub>3</sub>	N.D.	N.D.	N.D.	0.12	N.D.	N.D.	N.D.	0.15	N.D.	N.D.	0.13	0.12								
Fe <sub>2</sub> O <sub>3</sub>	N.D.	N.D.	N.D.	N.D.	N.D.	N.D.	N.D.	N.D.	N.D.	46.24	38.82									
FeO	25.20	25.83	8.41	6.78	N.D.	N.D.	27.37	9.95	N.D.	40.62	28.42	26.77	26.88	8.54	24.37					
MnO	0.54	0.49	0.11	N.D.	N.D.	N.D.	0.85	N.D.	N.D.	N.D.	N.D.	0.63	0.54		0.15					
MgO	7.23	7.41	12.76	12.53	N.D.	N.D.	6.42	12.69	N.D.	N.D.	N.d.	7.17	7.36	12.68	21.54					
CaO	6.83	6.85	22.08	23.00	6.65	6.68	6.86	20.53	5.49	0.43	0.52	5.85	5.72	20.12	0.83					
Na <sub>2</sub> O	N.D.	N.D.	-	1.05	7.34	7.03	N.D.	1.45	8.16	N.D.	N.D.			1.94						
K <sub>2</sub> O	N.D.	N.D.	N.D.	N.D.	0.44	0.39	N.D.	N.D.	0.51	N.D.	N.D.									
P <sub>2</sub> O <sub>5</sub>	N.D.	N.D.	N.D.	N.D.	N.D.	N.D.	N.D.	N.D.	N.D.	N.D.	N.D.									
Cl <sub>2</sub> O	N.D.	N.D.	N.D.	N.D.	N.D.	N.D.	N.D.	N.D.	N.D.	N.D.	N.D.									
NiO				0.14																
Total	101.07	102.48	99.04	98.89	99.19	99.32	101.60	100.78	99.48	99.32	100.78	100.32	100.74	99.70	100.21					
Si	2.99	2.97	1.95	1.97	10.76	10.76	2.97	1.95	10.98	0.01	0.01	3.00	2.99	2.01	1.94					
Ti			0.02	0.01				0.01		0.30	0.61			0.01						
Al	2.00	2.00	0.14	0.12	5.24	5.29	1.96	0.13	5.02	0.05	0.01	1.93	1.95	0.08	0.07					
Cr				0.00				0.00			0.00	0.01								
Fe <sup>3+</sup>	1.61	1.63	0.26	0.21			1.76	0.31		1.32	0.74	1.74	1.73	0.27	0.77					
Fe <sup>2+</sup>	0.04	0.03	0.00				0.06			1.29	0.60	0.04	0.04							
Mn	0.82	0.83	0.71	0.70			0.74	0.70		0.02	0.02	0.85	0.85	0.72	1.21					
Mg	0.56	0.55	0.89	0.92	1.28	1.28	0.57	0.82	1.05			0.48	0.47	0.82	0.03					
Ca				0.08	2.56	2.44		0.10	2.82					0.07						
Na					0.10	0.09			0.12											
K																				
P																				
Cl																				
Total	8.02	8.01	3.97	4.01	19.94	19.86	8.06	4.02	19.99	2.99	1.99	8.05	8.03	3.98	4.02					
Mg/(Mg+Fe)	0.34	0.34	0.73	0.77			0.49	0.69				0.33	0.32	0.73	0.61					
Ca/(Ca+Mg)			0.56	0.57				0.54						0.53						
Ca	18.5	18.2	47.8	50.3			18.1	44.7				15.6	15.4	45.3	1.5					
Mg	27.2	27.3	38.2	38.3			23.6	38.4				27.7	27.9	39.8	60.2					
Fe	54.3	54.5	14.0	11.5	33.4	34.4	58.3	16.9	27.1			56.7	56.7	14.9	38.3					

TABLE 10.5 (cont.)

	BD1852				BD1865				BD1867/A					
	PL	IL	MG <sub>ss</sub>	GT Core	CPX		IL <sub>ss</sub>	GT		CPX		Core	PL Rim	
					Core	Rim		Core	Rim	Core	Rim			
SiO <sub>2</sub>	63.04	0.20	0.44	38.82	38.29	52.01	52.98	0.25	40.96	40.30	50.77	52.46	59.50	58.13
TiO <sub>2</sub>	N.D.	30.26	11.14			0.28		51.61			0.73	0.48		
Al <sub>2</sub> O <sub>3</sub>	22.76	0.30	1.99	21.66	21.30	2.78	1.86		22.83	22.61	6.51	4.62	25.68	25.26
Cr <sub>2</sub> O <sub>3</sub>	N.D.	0.18												
Fe <sub>2</sub> O <sub>3</sub>	N.D.	41.72	43.66	27.35	27.78	9.82	8.64	2.13	18.50	18.19	5.19	4.02		
FeO	N.D.	25.15	40.74	0.67	0.71			44.12	0.40	0.34				
MnO	N.D.	1.29	0.78	5.48	5.11	12.25	13.03	1.45	12.46	12.02	13.13	14.24	7.25	7.83
MgO	3.97			7.24	7.07	21.41	22.98		6.32	6.96	21.44	22.44	7.12	5.75
CaO	9.11					0.74	0.88				1.14	1.09	0.53	1.14
Na <sub>2</sub> O	0.57													
K <sub>2</sub> O	N.D.													
P <sub>2</sub> O <sub>5</sub>	N.D.													
Cl <sub>2</sub>	N.D.													
ZnO			0.21											
Total	99.46	99.10	98.96	101.22	100.26	99.34	100.37	99.56	101.47	100.42	98.91	99.35	100.08	98.11
Si	11.22	0.01	0.02	3.00	3.00	1.99	1.97	0.01	3.01	3.00	1.88	1.93	10.60	10.59
Ti		0.58	0.32			0.01		0.97			0.02	0.01		
Al	4.77	0.01	0.09	1.97	1.97	0.06	0.08		1.98	1.98	0.28	0.20	5.40	5.42
Cr		0.00												
Fe <sup>3+</sup>		0.81	1.24	1.77	1.82	0.31	0.27	0.04	1.14	1.13	0.16	0.12		
Fe <sup>2+</sup>		0.54	1.29	0.04	0.05			0.93	0.03	0.02				
Mn				0.63	0.60	0.70	0.72	0.05	1.36	1.33	0.72	0.78		
Mg		0.05	0.04	0.60	0.59	0.88	0.92		0.50	0.55	0.85	0.88	1.38	1.53
Ca	0.75					0.03	0.06				0.08	0.08	2.46	2.03
Na	3.14												0.12	0.26
K	0.13													
P														
Cl			0.00											
Zn														
Total	19.99	2.00	3.00	8.01	8.03	3.98	4.02	2.00	8.02	8.01	3.99	4.10	19.96	19.83
Mg/(Mg+Fe)				0.26	0.25	0.69	0.73		0.54	0.54	0.82	0.86		
Ca/(Ca+Mg)						0.56	0.56				0.54	0.53		
Ca				20.0	19.6	46.6	48.1		16.5	18.2	49.0	49.4		
Mg				21.0	19.9	37.0	37.7		45.1	43.8	41.7	43.7		
Fe				59.0	60.5	16.4	14.1		38.4	37.9	9.3	6.9		
An%	19.3												36.0	42.9



BD1867/D										BD1867/E									
	Core	PL	AM	BI	AP	IL <sub>ss</sub>	RU	Core	GT	CPX	PL	Core	AM	MG <sub>ss</sub>					
		Rim						Core	Core	Core		Core	Core	Rim					
SiO <sub>2</sub>	62.90	62.73	41.81	37.29		0.24	0.21	38.33	39.44	52.02	62.33	41.79	41.74	0.32					
TiO <sub>2</sub>			2.36	5.85		43.85	96.91			0.28		1.98	1.97	1.07					
Al <sub>2</sub> O <sub>3</sub>	22.47	22.74	12.74	13.51		0.28	0.30	21.09	21.64	3.39	23.61	12.32	12.24	1.65					
Cr <sub>2</sub> O <sub>3</sub>						16.27				0.13				0.11					
Fe <sub>2</sub> O <sub>3</sub>						36.85								64.63					
FeO			14.13	14.75	0.15			26.70	27.26	10.75	0.16	14.39	14.97	30.98					
MnO								0.48	0.49	N.D.									
MgO			11.59	14.12		1.50		6.44	6.35	11.59		12.27	12.26	0.82					
CaO	3.72	3.64	10.61		54.90	0.10		6.10	6.64	20.33	5.20	11.14	11.03						
Na <sub>2</sub> O	9.63	9.46	2.50							1.57	7.85	2.56	1.78						
K <sub>2</sub> O	0.62	0.60	2.08	9.21							0.68	1.45	1.34	0.09					
P <sub>2</sub> O <sub>5</sub>			0.28	0.27	41.31														
Cl <sub>2</sub>					0.36														
NiO														0.21					
Total	99.42	99.19	98.10	95.00	96.70	99.09	97.42	99.14	101.82	100.06	99.83	97.88	97.33	99.88					
Si	11.25	11.10	6.12	5.85		0.01		3.01	3.02	1.95	11.07	6.24	6.26	0.01					
Ti			0.27	0.69		0.83				0.01		0.22	0.22	0.03					
Al	4.74	4.79	2.24	2.50		0.01		1.95	1.95	0.15	4.94	2.17	2.17	0.07					
Cr										0.00				0.00					
Fe <sup>3+</sup>			1.77	1.94		0.31		1.75	1.74	0.34	0.02	1.80	1.88	0.98					
Fe <sup>2+</sup>						0.78		0.03	0.03										
Mn			2.58	3.30		0.06		0.75	0.72	0.65		2.73	2.74	0.05					
Mg	0.71	0.69	1.70					0.51	0.54	0.82	0.99	1.78	1.77						
Ca	3.34	3.32	0.72							0.11	2.70	0.74	0.52						
Na	0.04	0.04	0.40	1.84							0.16	0.28	0.26	0.00					
K			0.02	0.02															
P																			
Cl																			
Ni														0.01					
Total	20.08	19.94	15.94	16.14		2.00		8.00	8.00	4.03	19.88	16.16	15.82	2.99					
Mg/(Mg+Fe)			0.59	0.55				0.30	0.29	0.66		0.60	0.59						
Ca/(Ca+Mg)								16.8	17.9	0.56									
Ca								24.7	23.8	45.3									
Mg								58.5	58.3	35.9									
Fe										18.7									
An	17.5	17.2									26.8								





### Phase Chemistry

Minerals were analysed by P. Jackson at Edinburgh University, using a Cambridge Instruments Microscan V modified with a Link Systems on-line computer for rapid energy dispersive system analyses. Accelerating voltages were 20 Kv and specimen currents 0.06  $\mu$  amps. No recalculations for  $\text{Fe}^{3+}$  were made because the above system does not allow for accurate sodium analysis at the low concentration levels found in these samples. This has a profound effect on the validity of any thermodynamic calculations and must be borne in mind by the reader when making comparisons with the work of Griffin et al. (1979). The temperature and pressures reported here are possibly high by  $\sim 10\%$  as a result, but this may be within the limits of analytical uncertainty. Mineral analyses are presented in Table 10.5.

Clinopyroxene: The clinopyroxenes plot close to the diopside-hedenbergite join in the Ca-Mg-Fe ternary plot (Figure 10.8). FeO varies 5-10 wt.% and  $\text{TiO}_2$  is always  $< 0.8$  wt.%. In contrast with the granulites found in other Lesotho kimberlites (Rogers and Nixon, 1975; Griffin et al. 1979) these clinopyroxenes have a low jadeite and tschermakite content although Jd/Ts  $> 0.5$ .  $\text{Al}_2\text{O}_3$  varies 1.8-6.5 wt.% and  $\text{Na}_2\text{O}$  0.75-2.1 wt.%. There is a crude correlation of Jd/Ts ratio in the clinopyroxenes with the albite content of coexisting plagioclase (Figure 10.9a). Determination of the acmite component would probably improve this correlation.

All the clinopyroxenes show minor zoning notably with  $\text{Mg}/(\text{Mg} + \text{Fe})$  decreasing towards the rims. Jadeite content also often decreases slightly towards the rim, but the converse is sometimes seen. Griffin et al. (1979) noted jadeite depletion in the spongy rims (described above) but the absence of such rims from the vast majority of both granulite and peridotite clinopyroxenes from Letseng suggests that a process other than 'metasomatism and

decompression' (Griffin et al. 1979) was responsible for their formation. Incipient partial melting is a possibility, as has been suggested for peridotite pyroxenes (cf. Carswell, 1975).

Orthopyroxene: The orthopyroxenes show low CaO and  $Al_2O_3$  contents consistent with their metamorphic equilibration. The typical granulite hypersthene character (weak pink to pale green pleochroism) observed in thin section is confirmed by the chemistry (Figure 10.8).

Garnets: The pyrope-grossular-almandine garnets show a wide range in composition (Figure 10.8) which is essentially related to changing Fe/Mg ratio as a consequence of variations in bulk composition and equilibration conditions. On the basis of CaO content two groups may be recognised. A main group, coexisting with pyroxene, contains about 6.5 wt.% CaO on average; and a smaller group represented in the garnet-kyanite-plagioclase rocks with considerably less grossularite component. X-Ray, R.I. and density data for E6 (Nixon, 1960), a garnet-kyanite rock, suggest negligible CaO in garnet from this rock.

Both groups of garnet are also present in the kimberlite as xenocrysts. Figure 5.4 shows analyses of garnet xenocrysts. Orange, pale orange and pink garnets appear to match the above two groups.

A sympathetic reverse zoning to that seen in the clinopyroxenes is apparent although not so obvious. These rim compositions were measured on adjacent grains and must be inferred to reflect changing element partitioning in adjustment to new P-T conditions.

Feldspars: Plagioclase compositions range from  $An_{17}$ - $An_{51}$  but group around  $An_{25}$ - $An_{35}$ .  $K_2O$  contents are low and usually <1 wt.%. Zoning is common (although not microscopically visible) and usually reverse with An enriched rims. Some normal zoning is also found.

Micas and Amphiboles: Micas are biotites and phlogopites with remarkably similar chemistry except for varying Fe/Mg ratios. The Fe/Mg variation may reflect different bulk rock compositions or equilibration conditions; the linear correlation of Mg/Fe ratios of the micas with the Mg/Fe ratio of coexisting clinopyroxene or garnet suggests the former.

Amphiboles are pargasitic hornblendes and ferroan pargasitic hornblendes (terminology of Leake, 1978) in which the Mg/(Mg + Fe) ratio generally correlates positively with this ratio in coexisting clinopyroxene or garnet (Figure 10.9b), again, as with the micas, reflecting varying bulk compositions. Amphibole in BD1867/D is considerably enriched in Fe relative to coexisting garnet. The clinopyroxene-rimmed nature of this amphibole suggests mineral disequilibrium; this sample and BD1867/L containing abundant poikilitic amphibole, do not follow the linear correlation of Mg/(Mg + Fe) with coexisting garnet (Figure 10.9b) displayed by rocks with only minor (<1%) amphibole. As these different rocks have equilibrated under similar P-T conditions (see following section) the non-linearity of the correlation of Mg/(Mg + Fe) for the two samples mentioned is inferred to imply chemical disequilibrium.

Ilmenite and Magnetite: Where analyses of opaque phases have been made, it is apparent that the association rutile-(ilmenite-haematite)ss occurs but that (magnetite-ülvospinel)ss does not coexist with any other oxide. Ilmenite also appears alone as discrete grains in some granulites. Magnetite grains contain exsolution lamellae of (ilmenite-haematite)ss. These features are shown in Figure 10.10 with tie lines connecting coexisting phases and exsolution lamellae.

This exsolution feature cannot be used to estimate the primary metamorphic temperature (Buddington and Lindsley, 1963) because the experimental data on which this geothermometer is based requires 'granule exsolution' of

the phases. The ilmenite lamellae may relate to later cooling events and are of little value in geothermometric calculations (Rumble, 1976). The mineral assemblages are compatible with high grade metamorphism and low  $f_{O_2}$  conditions.

In Figure 10.10 the magnetite host to the ilmenite lamellae do not plot on the magnetite-ülvospinel join. This feature in other rocks has been attributed by Lindsley (1976) to late stage oxidation of titanomagnetite to titanhaematite.

#### Estimates of Equilibration P/T Conditions

The following estimates are rather crude and should only be taken as a rough guide to the pressure/temperature regime from which these rocks may be derived. There are several reasons for this lack of precision. First, as mentioned above, these analyses were solid-state detector analyses which give rapid but low accuracy results; in particular sodium analyses may lack precision. In some instances clinopyroxenes apparently contain no  $Na_2O$  despite other parts of the same grains recording  $>1$  wt.%  $Na_2O$ .  $TiO_2$  is also often below the detection limits for this system. Second, there is little agreement between results obtained from calculations by different methods, however the recent empirical correction for Ca in the garnet-clinopyroxene system (Ellis and Green, 1979) has greatly improved this correspondence. Third, calculations on most of the rocks using the solubility of jadeite in clinopyroxene coexisting with albite (Currie and Curtis, 1976) can only yield a minimum pressure in the absence of coexisting quartz.

The most important of these problems concerns the  $Na_2O$  determination; the allocation of Al to jadeite is critically dependent on the prior estimate of  $Fe^{3+}$  and acmite component. Without this calculation the Fe/Mg partitioning between garnet and clinopyroxene will shift to lower  $K_d$  values

TABLE 10.6: Granulite Equilibrium P/T Estimates

Sample	Kd (Gt/Cpx)	RG & CC		EG & CC		RG & W		EG & W		Wells & W	
		T°C	P.Kb	T°C	P.Kb	T°C	P.Kb	T°C	P.Kb	T°C	P.Kb
NL065	5.21	678	3.7	605	2.7	711	8.1	614	3.4	794	12.2
NL110	5.29	<600	<0								
NL423	5.37	673	3.8	635	3.2						
BD1852	5.46	677	5.0	609	4.1	698	8.0	609	3.8	758	~11
BD1865	6.34										
BD1867/A	3.77	780	5.8	712	5.1						
BD1867/C	4.55	753	9.1	757	8.2						
BD1867/D	5.21	707	7.6	666	6.9						
BD1867/E	4.46	744	7.2	674	6.1						
BD1867/L	5.29	<600	<0								

Geothermometers: RG = Raheim and Green (1974)  
 EG = Ellis and Green (1979)  
 Wells = Wells (1977)

Geobarometers: CC = Currie and Curtis (1976)  
 W = Wood (1974)

implying higher temperatures. As the pressure calculations are critically dependent on the estimated temperature these will also be high. In addition if no acmite component is calculated the resultant high jadeite will imply higher pressure. The absence of  $TiO_2$  from some of the clinopyroxenes probably does not seriously affect the results but is another bar to an accurate ferric recalculation.

In comparison with studies of other Lesotho granulites (Rogers and Nixon, 1975; Jackson and Harte, 1977; Griffin et al, 1979) the Letseng granulites demonstrate two very marked differences. Firstly, the  $K_d$  (Gt/Cpx) for Fe/Mg partitioning is higher than that shown by either Rogers and Nixon (1975) or Jackson and Harte (1977), neither of whom performed a ferric recalculation. The similar values of Griffin et al. (1979) are the results of this recalculation which tends to increase  $K_d$  (Gt/Cpx). Secondly the jadeite content of the Letseng granulites is lower (< 10%) than any of the other three studies (10-30%) although Griffin et al. (197) have recorded some lower jadeite values. It is concluded that this Letseng suite of granulites have equilibrated to lower temperatures and pressures than the generally more basic granulites from other Lesotho kimberlites.

The Fe/Mg partitioning between garnet and clinopyroxene (Figure 10.11) demonstrates closely similar  $K_d$  values (Table 10.6) for various bulk compositions. This implies a small range in equilibration temperatures. This Fe/Mg partitioning has been calibrated by Raheim and Green (1974) as a geothermometer at known pressures. At an assumed pressure of 10 Kb, estimated temperatures for the Letseng granulites are 670-810°C for adjacent garnet and clinopyroxene core compositions. Note that the adjacent rims have almost invariably equilibrated at lower temperature (higher  $K_d$ ).

Another approach is that of Currie and Curtis (1976) who have recalibrated the geobarometer of Kushiro (1969) for the reaction:



In the absence of quartz, Griffin et al. (1979) suggest this method will give a minimum pressure. They further suggest the inaccuracy of this method in rocks with calcic plagioclase ( $> \text{An}_{35}$ ) or showing disequilibrium. Used in conjunction with the above geothermometer this geobarometer shows a wide scatter of results for the Letseng rocks (Table 10.6). Temperature only varies  $670^{\circ}\text{C}$ - $780^{\circ}\text{C}$  but pressure varies 3.7-9.1 Kb. Two rocks gave negative P and only one of these anomalous results could be attributed to disequilibrium (BD1867/L). The quartz bearing assemblage NLO65 gave the lowest positive P. These unreliable results may be partly attributed to analytical inaccuracies although recalculation of  $\text{Fe}^{3+}$  would move the values to lower jadeite contents and hence lower P. It is also possible that the overall lower jadeite contents lead to a systematic error and low P values.

Wood (1974) has proposed a geobarometer based on the coexistence of aluminous orthopyroxene and garnet. Used in conjunction with the geothermometer above, this method yields temperatures of  $700$ - $710^{\circ}\text{C}$  at 8 Kb for the only two orthopyroxene bearing rocks analysed. These calculations show very poor agreement with the Currie and Curtis values for the same rock but are similar to some other rocks of more basic composition, e.g. BD1867/D. However, these results should also be viewed with some caution: BD1852 contains orthopyroxene which may require  $\text{Fe}^{3+}$  for stoichiometric balance. As this ferric iron would need to be considered as Fe tschermakite molecule some uncertainty surrounds this calculation.

Ellis and Green (1979) have made an empirical correction to the Råheim and Green geothermometer to account for non-ideal Ca-Mg substitutions in the garnet and clinopyroxene. Used in conjunction with the two geobarometers, described above, this geothermometer effects a considerable improvement in the correspondence of the calculated pressures and temperatures (Table 10.6). The range of temperatures and pressures using the Currie and

Curtis geobarometer remains the same but the absolute values are reduced by 0-70°C and 1 Kb (600-760°C and 2.7-8.2 Kb). These values would seem to allow much more confidence in the results obtained, although the previously described problems still require that caution be exercised in their interpretation.

A further approach might be to use the two pyroxene geothermometer of Wood and Banno (1973) recalibrated by Wells (1977). However, used in conjunction with the geobarometer of Wood (1974) for the two orthopyroxene bearing rocks analysed, this method yields both temperatures and pressures which appear too high on geological grounds. However, as this geothermometer has been calibrated for various compositions in a multicomponent system ( $X_{\text{Opx}}^{\text{Fe}} = 0-1.0$ ,  $\text{Al}_2\text{O}_3^{\text{Cpx}} = 0-10 \text{ wt.}\%$ ) but in the temperature range 800-1700°C it is probable that the calibration is inaccurate for rocks equilibrated at lower temperatures.

The above discussion demonstrates the difficulty of assigning firm estimates to the equilibration temperatures and pressures of these rocks. Compared to the other granulite xenolith suites (ibid) the important feature of these rocks is that they have apparently equilibrated at lower pressure (and perhaps lower temperatures). Approximate limits to their equilibration might be 600-750°C and 3-8 Kb; this accords well with the experimental results of Rogers (1977) but the temperatures are slightly higher than the results of Griffin et al. (1979). This could correspond to metamorphism on a geothermal gradient of 25-30°C/Km (cf. Clifford, 1974; Tarney and Windley, 1977) which accords with the late Archaean geotherms of O'Hara (1977) and Lambert (1976). The model of Griffin et al. (1979) of granulite facies metamorphism as a result of high heat flow at the culmination of the Karoo volcanic episode and during kimberlite intrusion is unnecessary. Indeed the annealed textures may be attributed to high grade metamorphism in a thermal dome such as that proposed by Joubert (1971) for Namaqualand.



In view of the Precambrian age obtained for granulite xenoliths from Lesotho kimberlites (Davis, 1977) this latter explanation is favoured. The lower temperatures recorded by mineral rim compositions (higher Kd) and the disequilibrium assemblages demonstrating increased  $P_{H_2O}$  may have resulted at the culmination of such an event.

### Summary

- (1) Xenolithic granulites from Letseng are mainly composed of the assemblage garnet-clinopyroxene-plagioclase. Other rocks are garnet pyroxenites and kyanite bearing garnet-plagioclase rocks. Rutile, magnetite and ilmenite are common accessory minerals.
- (2) The assemblage garnet-clinopyroxene replaces orthopyroxene-anorthite. Disequilibrium is also illustrated by poikilitic amphibole.
- (3) Bulk rock chemistry embraces a wide range of compositions including basaltic and gabbroic but also highlights the siliceous intermediate compositions of possible metasedimentary rocks.
- (4) Trace element abundances and ratios are compatible with granulite facies metamorphism. REE patterns are LREE enriched with variable Eu anomalies. The patterns may accord with an andesitic crust model or REE depletion during metamorphism.
- (5) Clinopyroxenes are diopsides with only low (< 10%) jadeite and tschermakite molecules. Orthopyroxenes are aluminous hypersthene. Garnets are pyrope-grossular-almandine; and plagioclase is oligoclase-andesine ( $An_{25}-An_{35}$ ).
- (6) The Fe/Mg partitioning between coexisting garnet and clinopyroxene reflects equilibration under similar temperature (and pressure) conditions.

(7) Estimates of equilibration T and P are poorly constrained, but Kd (Gt/Cpx) and Jd% shows equilibration at lower T and P to other Lesotho xenolithic granulites. Conditions of metamorphism may be 600-750°C and 3-8 Kb.

(8) These estimates agree with metamorphism on a late Archaean geothermal gradient of 25-35°C/Km. It is not necessary to invoke late Karoo high heat flow to explain the metamorphism.

Plate 10.1: Slightly altered scapolite in granoblastic texture with garnet (high relief mineral with kelyphite rim), clinopyroxene (small grey grains showing cleavage) and plagioclase. BD1867/A. Scapolite is outlined in black. Bar scale 0.5mm.

Plate 10.2: 'Spongy' rims to clinopyroxene in garnet clinopyroxenite. Garnet is outlined in black. Dark mineral is rutile. NL554. Bar scale 0.5mm.

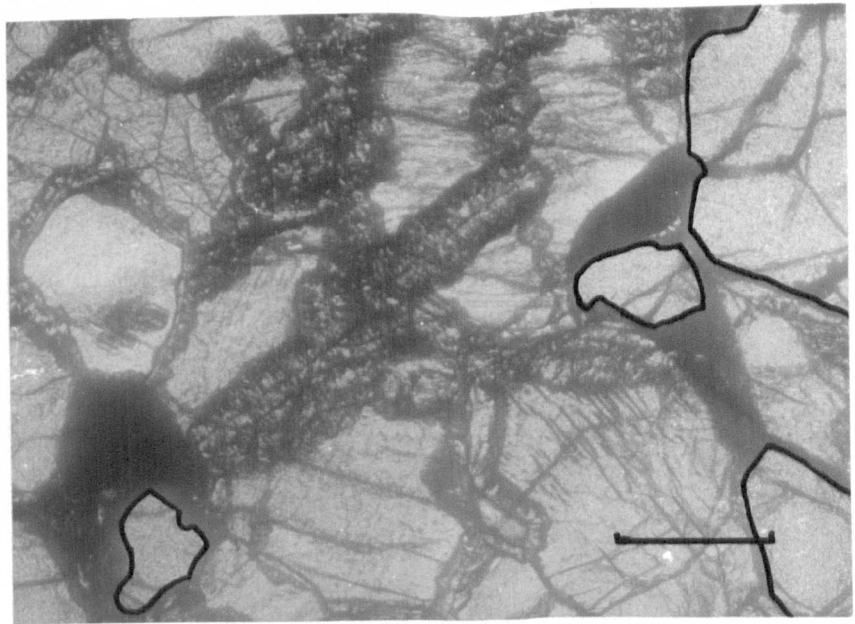
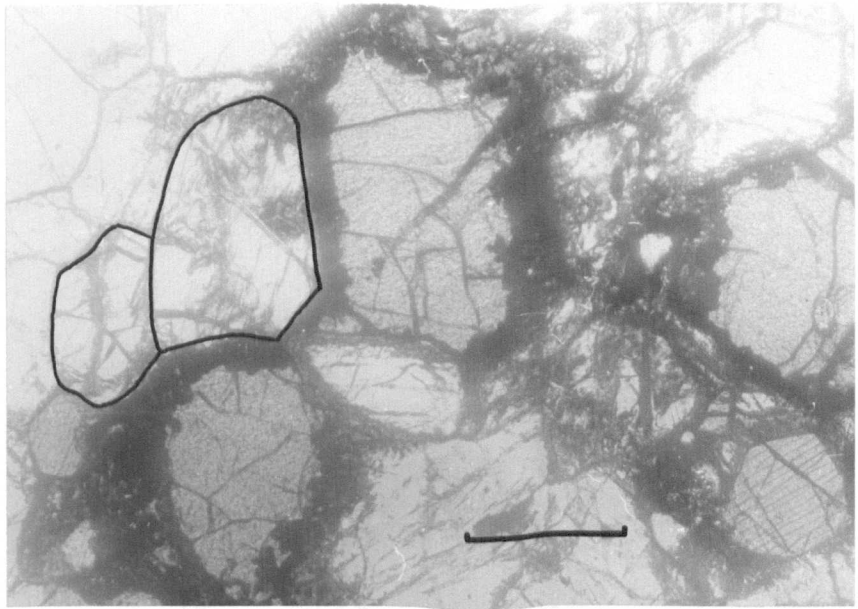


Plate 10.3: Orthopyroxene remnant as core to clinopyroxene in garnet granulite. The two pyroxenes are in crystallographic continuity as indicated by the cleavage. NL065. Bar scale 0.5mm. Crossed polars.

Plate 10.4: Orthopyroxene(OP) replaced by clinopyroxene(CP) in garnet granulite. The two pyroxenes are in crystallographic continuity as indicated by the cleavage. BD1852. Bar scale 0.5mm. Crossed polars.

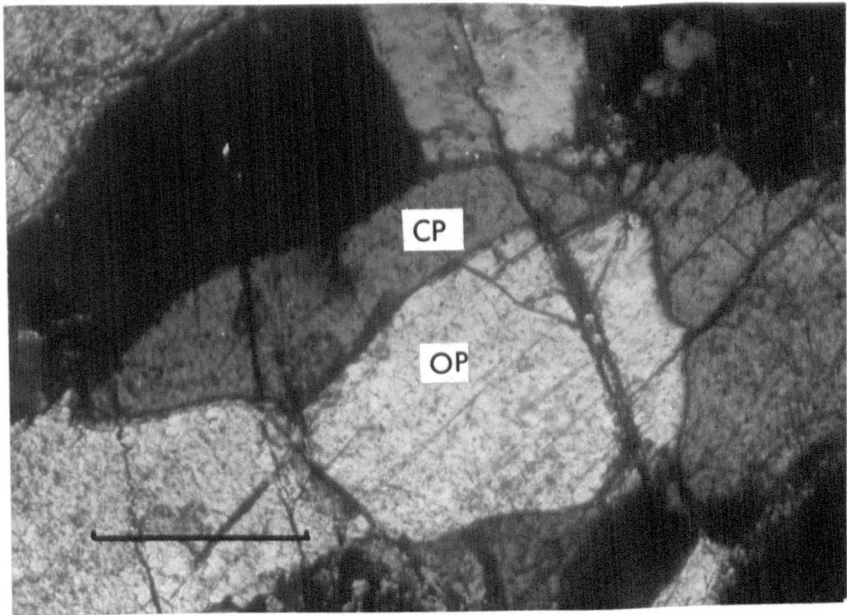
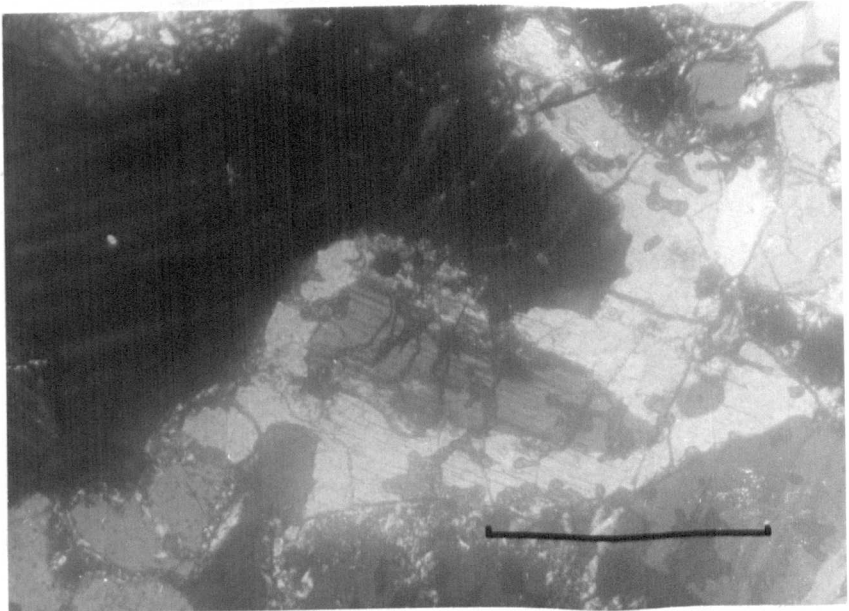


Figure 10.1: Plot of the modal variation in the granulite xenoliths in the system plagioclase-garnet-clinopyroxene. Closed circles: this study. Circled dots: Griffin et al (1979). Encircled points in this study contain orthopyroxene. Inclined crosses indicate the presence of amphibole. Vertical crosses indicate the presence of biotite. Tie lines connect modal variants in banded rocks.

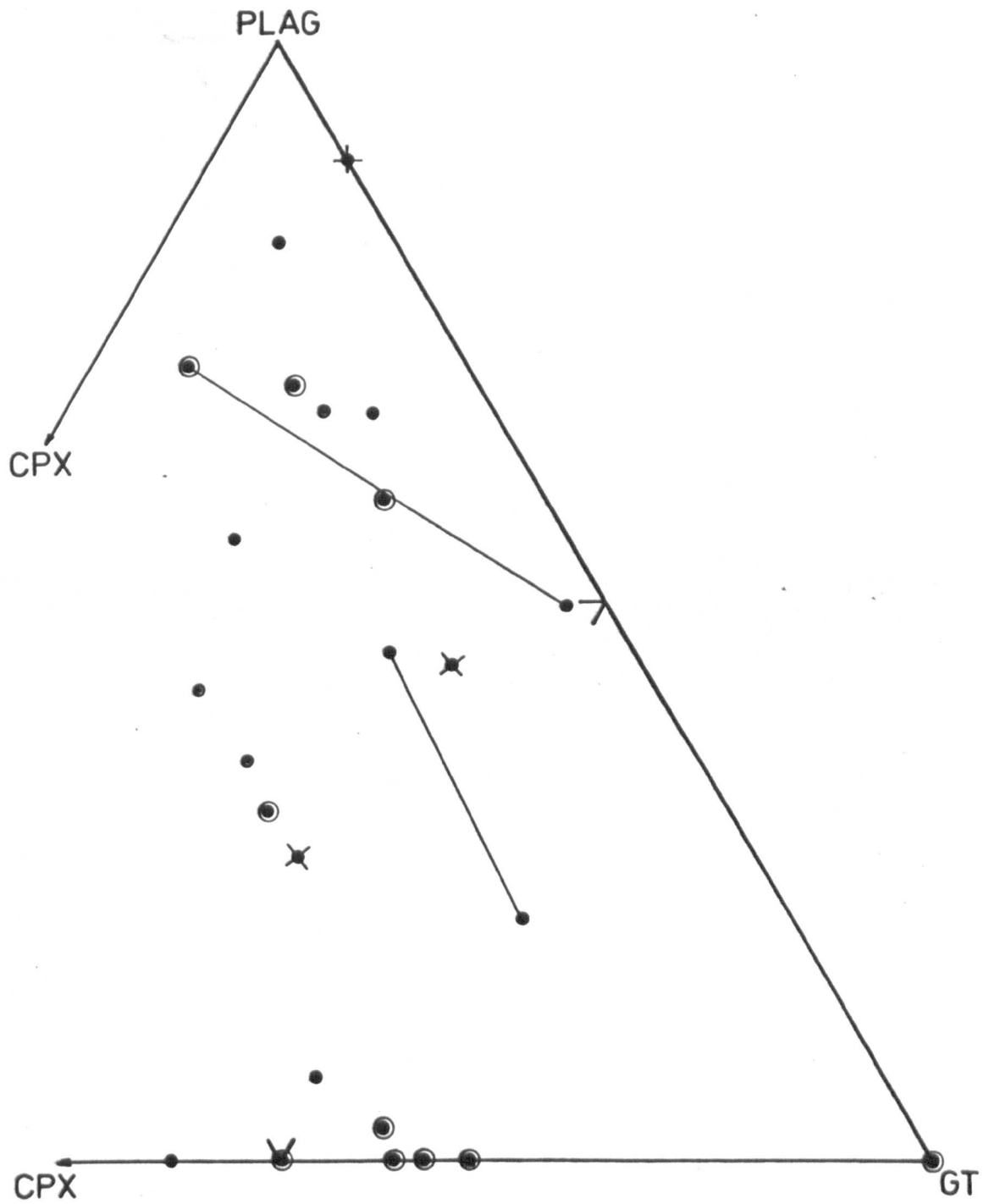




Figure 10.2: A - C - F plot for granulite whole rock analyses  
(uncorrected for minor CO<sub>2</sub>).

Closed circles: this study.

Open circle: Griffin et al (1979).

N.B. Garnet-kyanite-plagioclase rocks (not plotted) suggest  
possible metapelites.

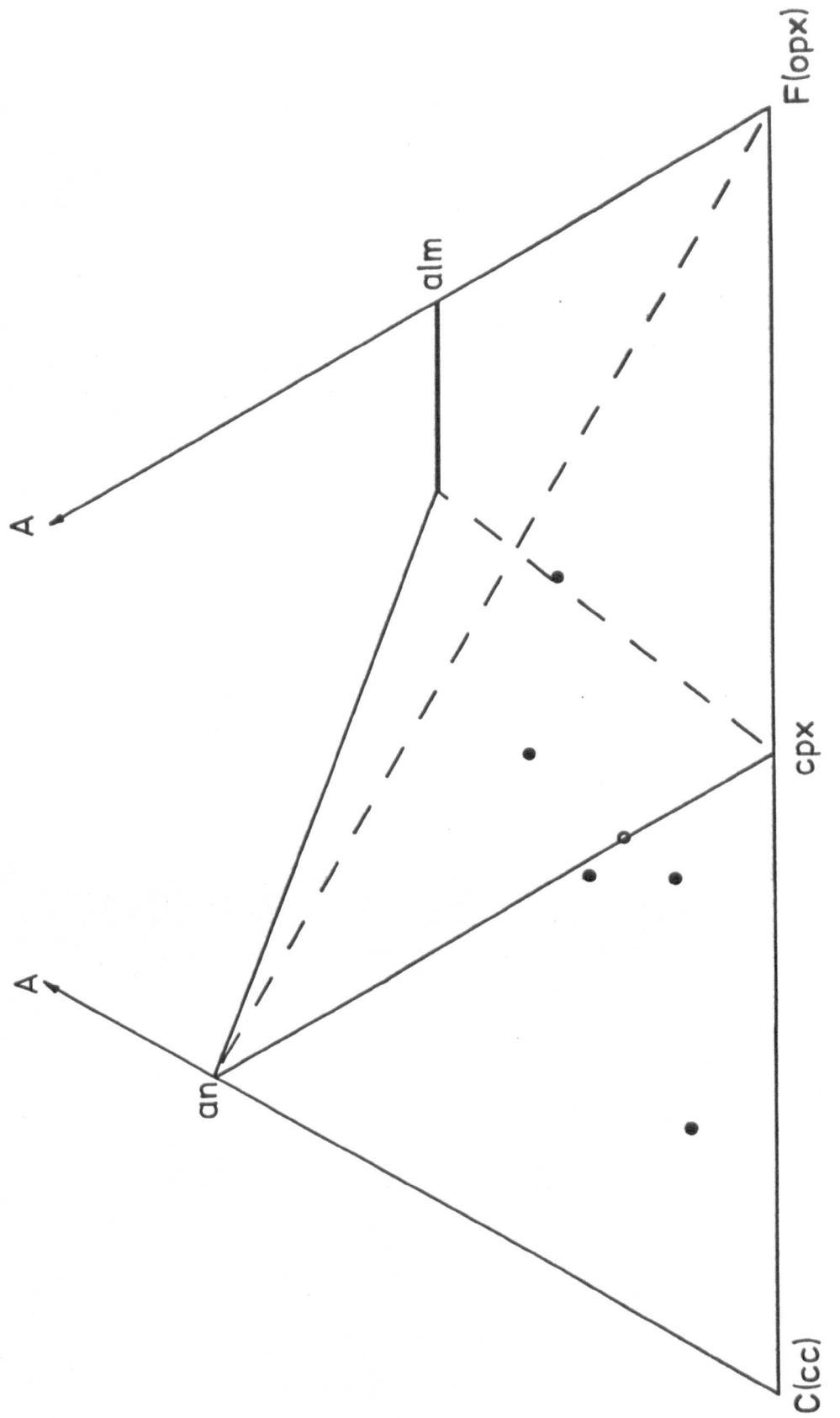


Figure 10.3a: A - F - M plot for granulite whole rock analyses.  
Broad line is differentiation trend for Skaergaard gabbros  
and granophyres (Turner & Verhoogen 1960 p.295).

Figure 10.3b: % normative feldspar+nepheline v. % normative  
pyroxene+olivine for granulite xenoliths.  
Symbols as for figure 10.2.  
Dashed line separates the fields of plagioclase-bearing  
and plagioclase-free rocks (Griffin et al 1979).

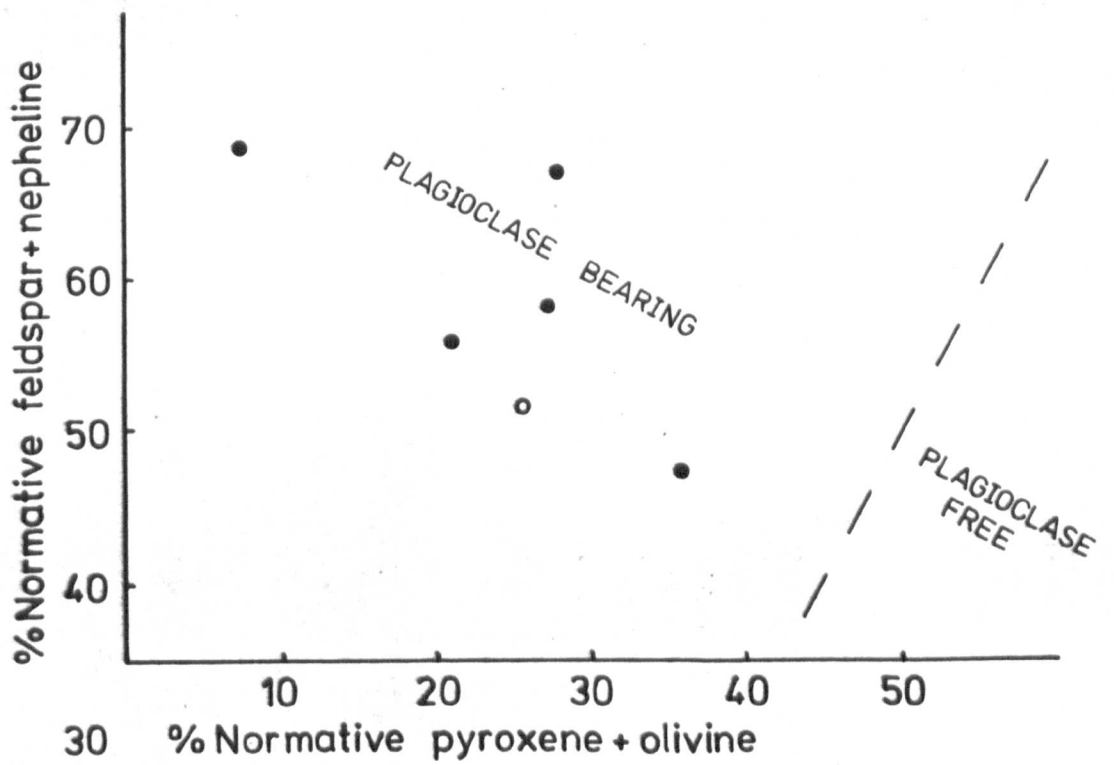
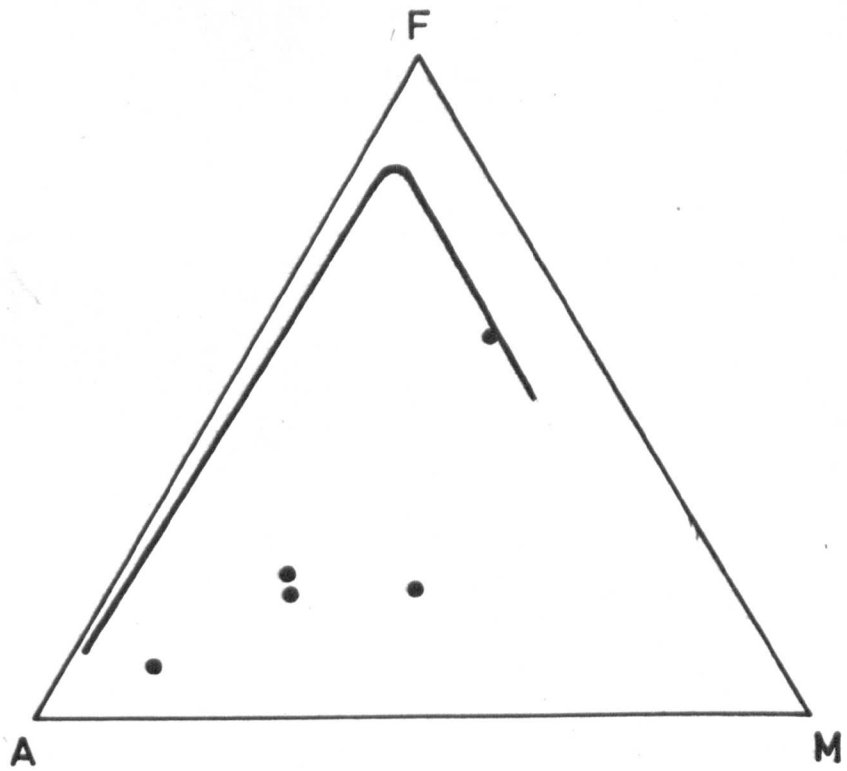
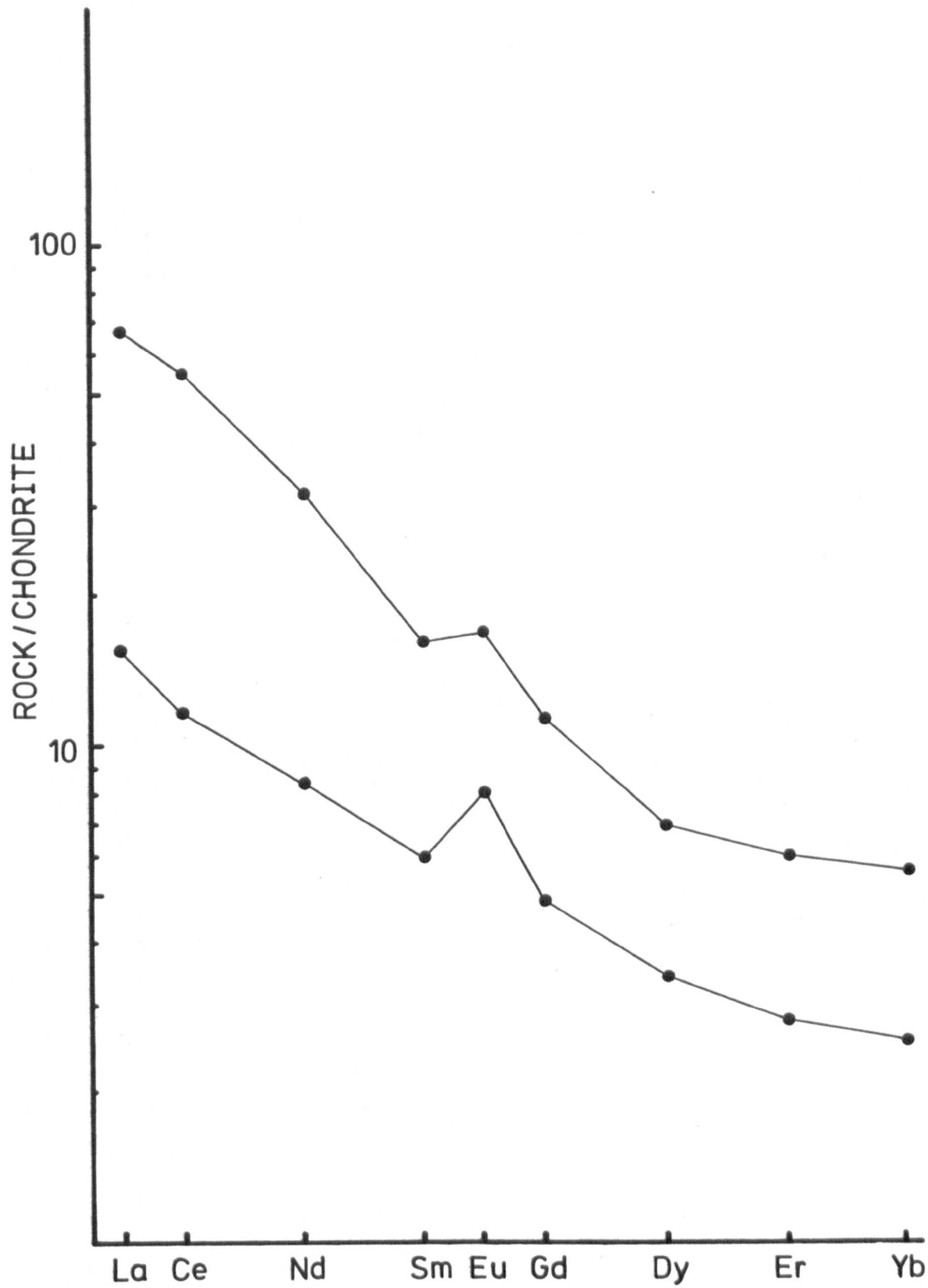


Figure 10.4: Chondrite normalised REE abundances for granulite xenoliths.

REE abundances measured by isotope dilution.

Chondrite values from Nakamura (1974).



**Figure 10.5: Chondrite normalised REE abundances for granulite xenoliths.**

**REE abundances measured by XRF analysis.**

**Chondrite values from Nakamura (1974).**

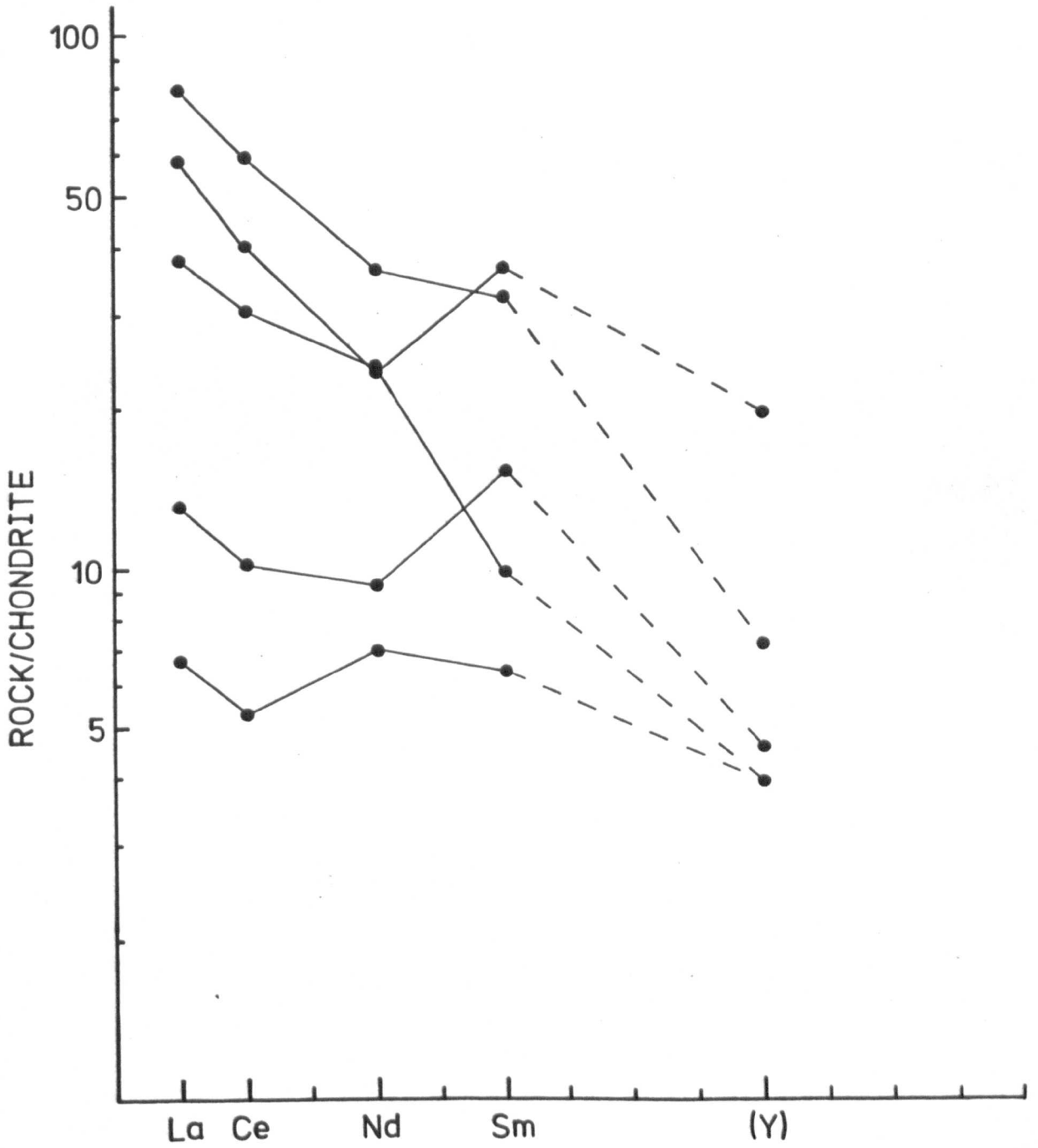




Figure 10.6: Plot of K v. Rb ppm for granulite whole rock samples.

Closed circles: this study.

Open circle: Griffin et al (1979).

Dotted line: field of Polish granulites.

Short dashed line: field of Lewisian granulites.

Long dashed line: field of E. Greenland granulites.

Granulite fields from Tarney & Windley (1977).

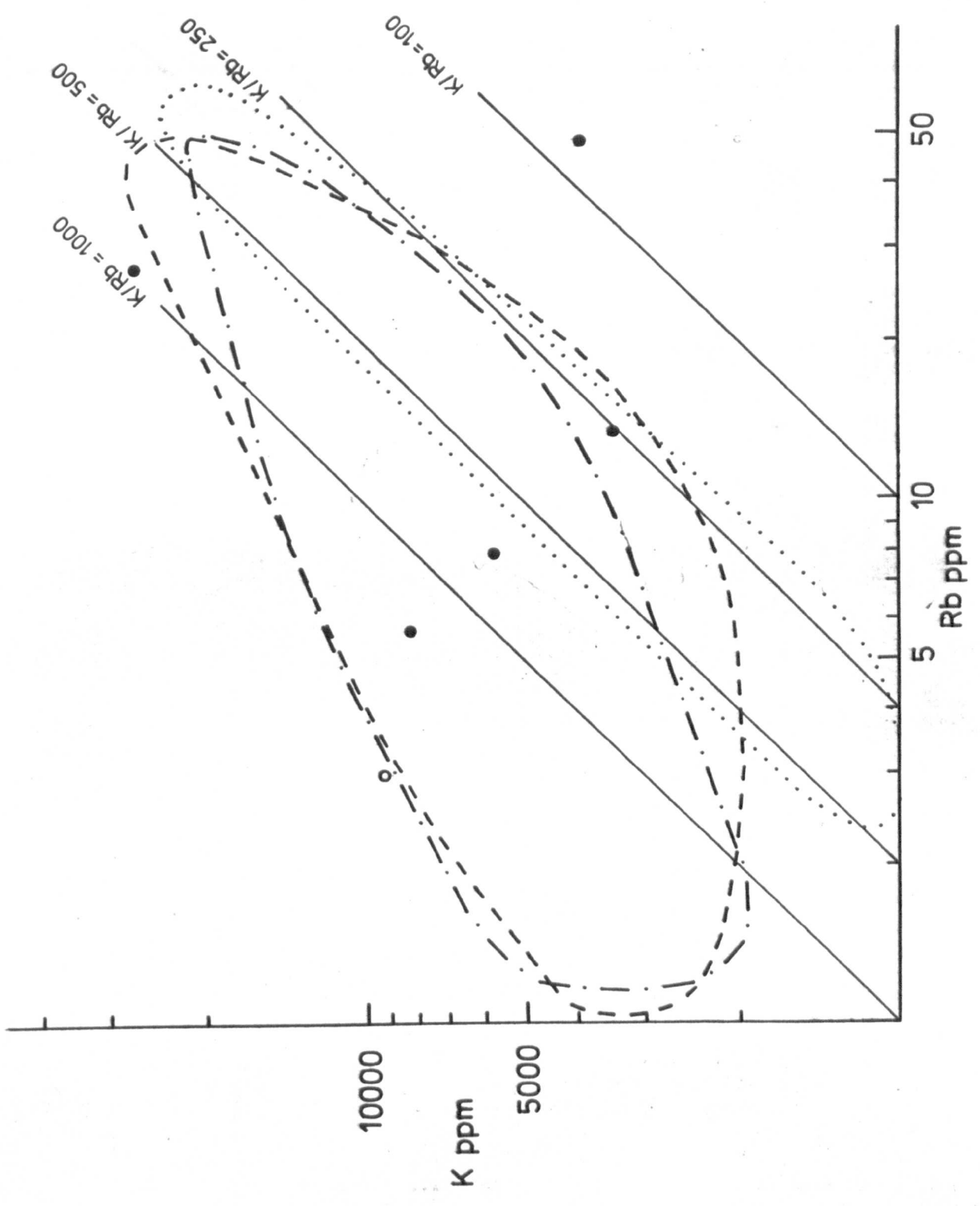


Figure 10.7: Plot of Rb v. Sr for granulite whole rock samples.

Symbols as for figure 10.6.

Dashed line: field of Lewisian granulites.

Dotted line: field of Polish granulites.

Granulite fields from Tarney & Windley (1977).

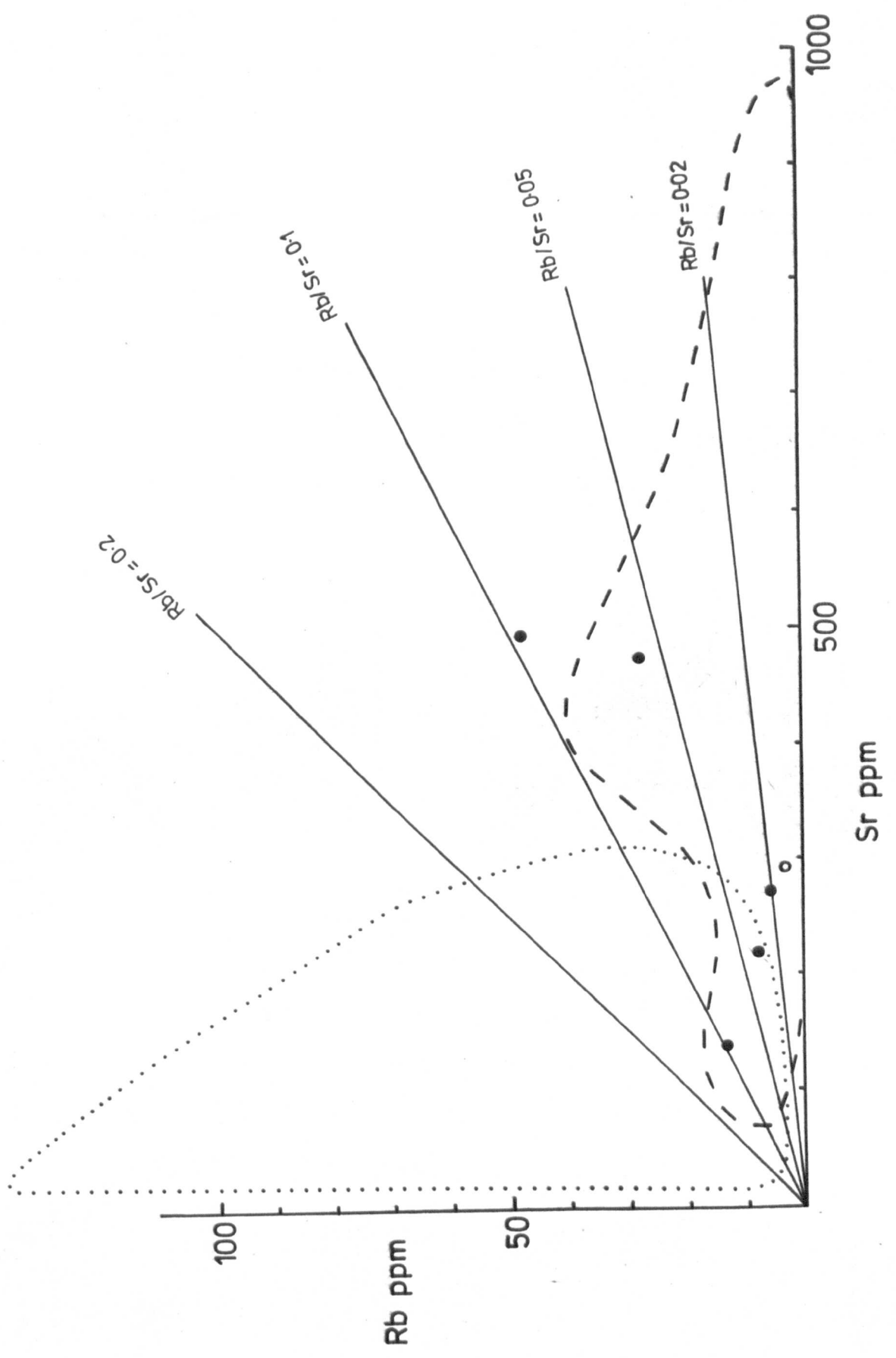


Figure 10.8: Ca - Mg - Fe plot of garnets and pyroxenes from granulite xenoliths.

Tielines connect the compositions of coexisting cores.

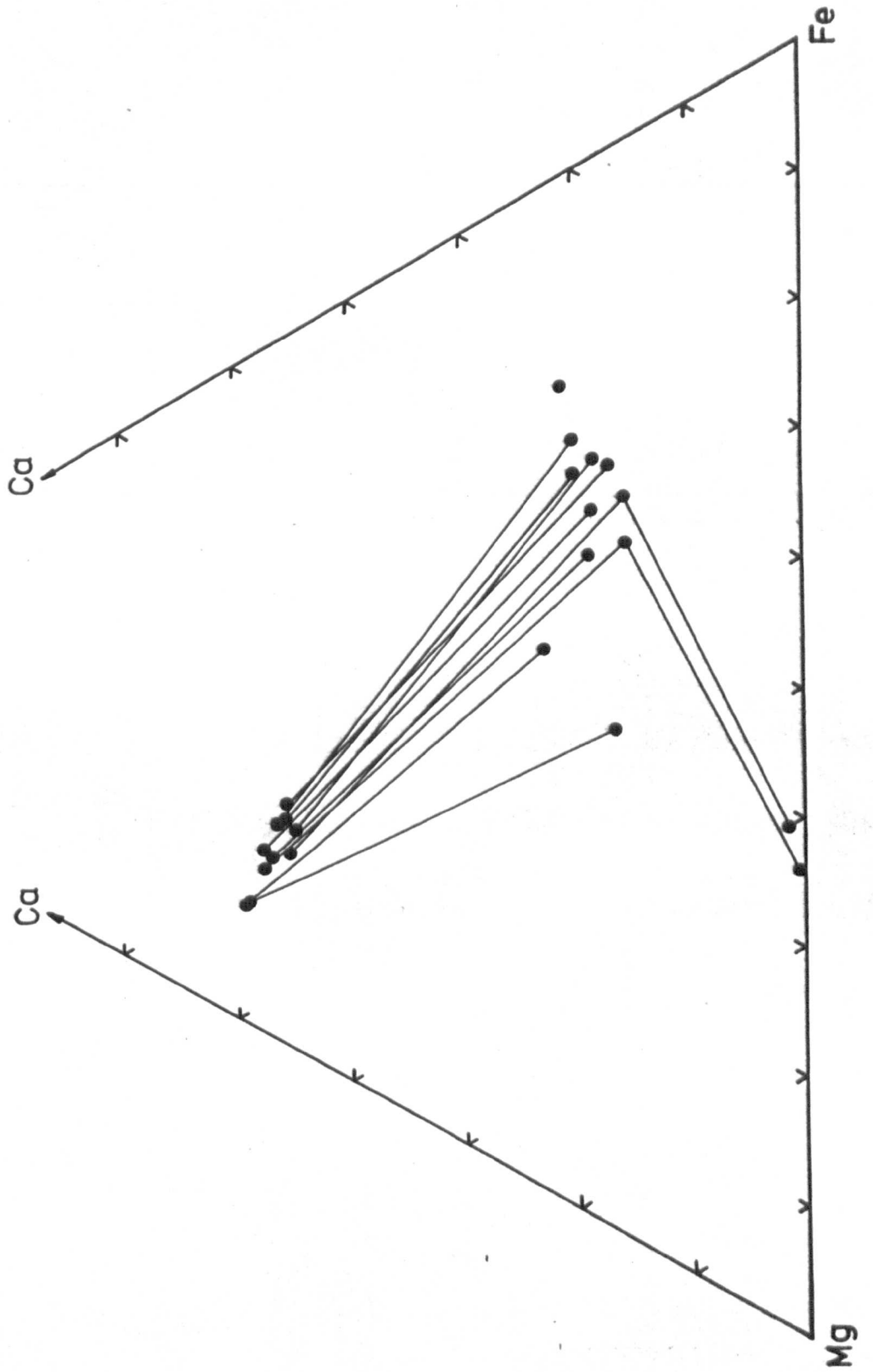


Figure 10.9a: %An in plagioclase v.  $Jd/(Jd+Ts)$  in coexisting clinopyroxene from granulites.

Jd=jadeite.

Ts=tschermakite.

Figure 10.9b:  $Mg/(Mg+Fe)$  for coexisting amphibole(AM) and garnet(GT) from granulites.

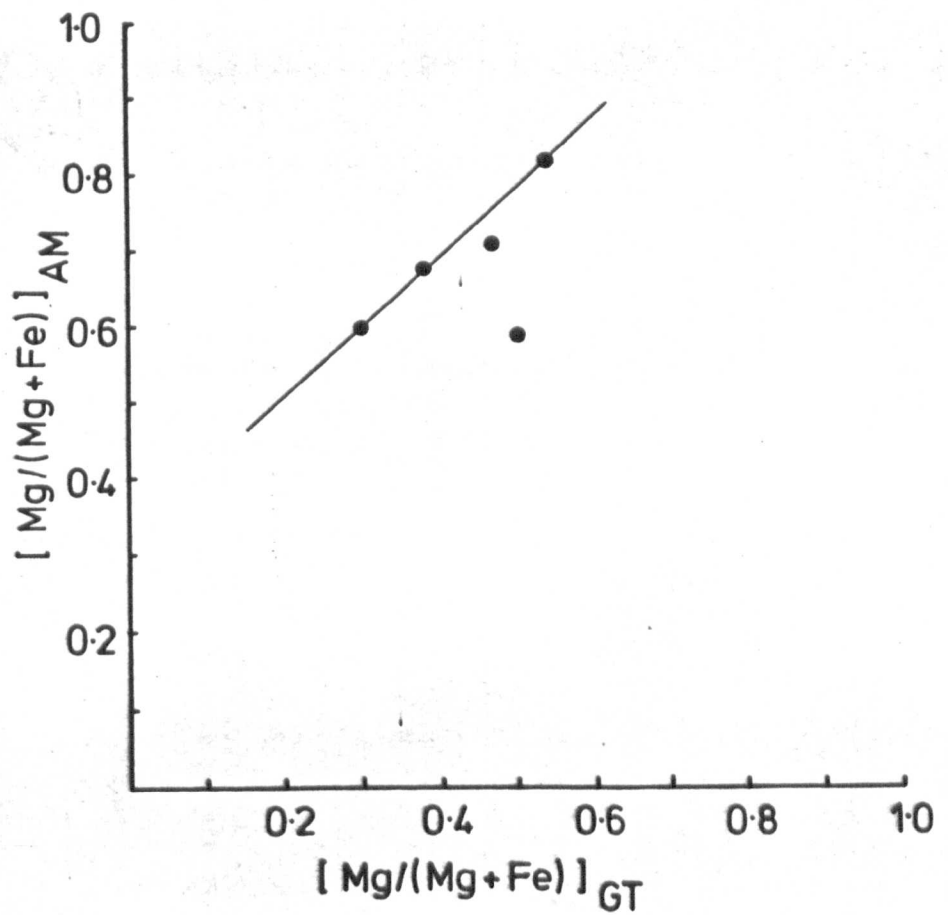
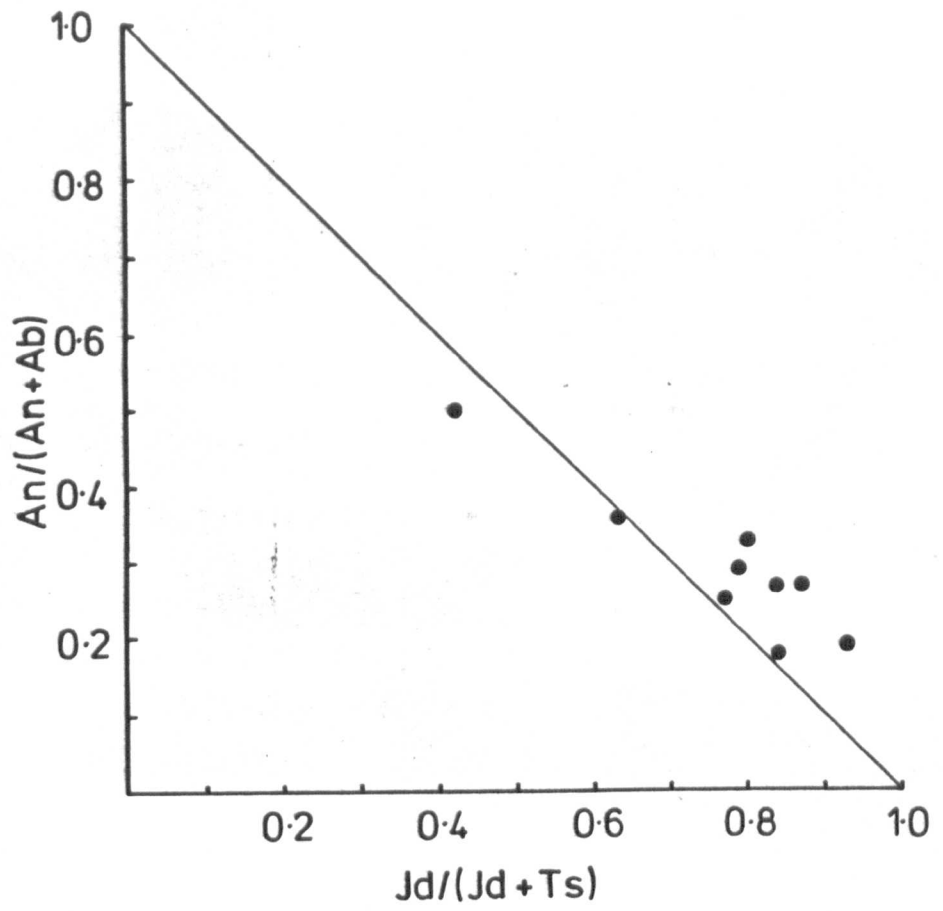




Figure 10.10:  $\text{TiO}_2 - \text{FeO} - \text{Fe}_2\text{O}_3$  plot of compositions of rutile, ilmenite, and titanomagnetite (with ilmenite exsolution) from granulites.

Tie lines from  $\text{TiO}_2$  to the join  $\text{FeTiO}_3 - \text{Fe}_2\text{O}_3$  are for coexisting rutile and ilmenite.

Tie lines from the join  $\text{FeTiO}_3 - \text{Fe}_2\text{O}_3$  to near the join  $\text{Fe}_2\text{TiO}_4 - \text{Fe}_3\text{O}_4$  connect the compositions of ilmenite exsolution lamellae in titanomagnetite.

The dashed tie line connects compositions of coexisting titanomagnetites.

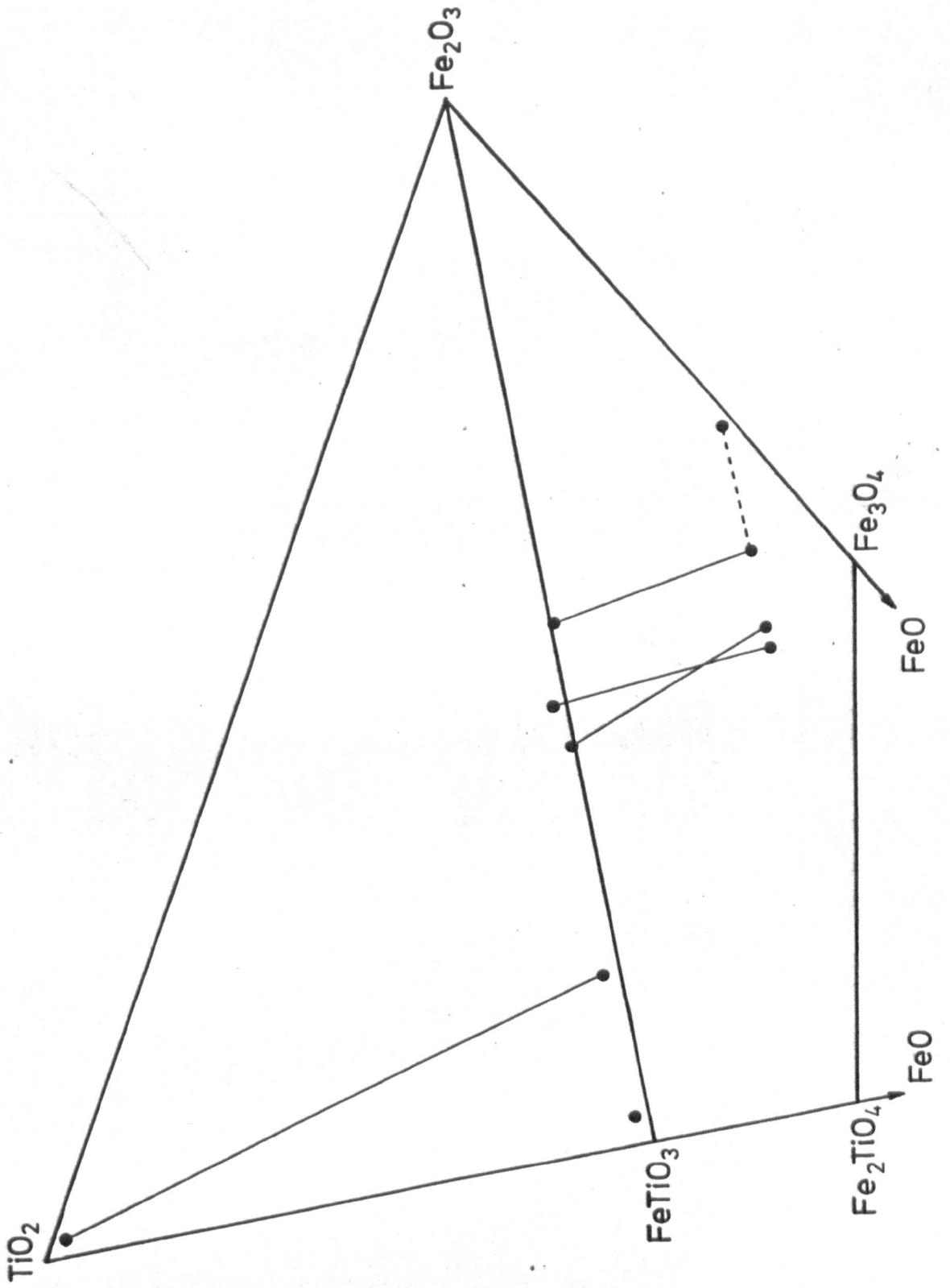
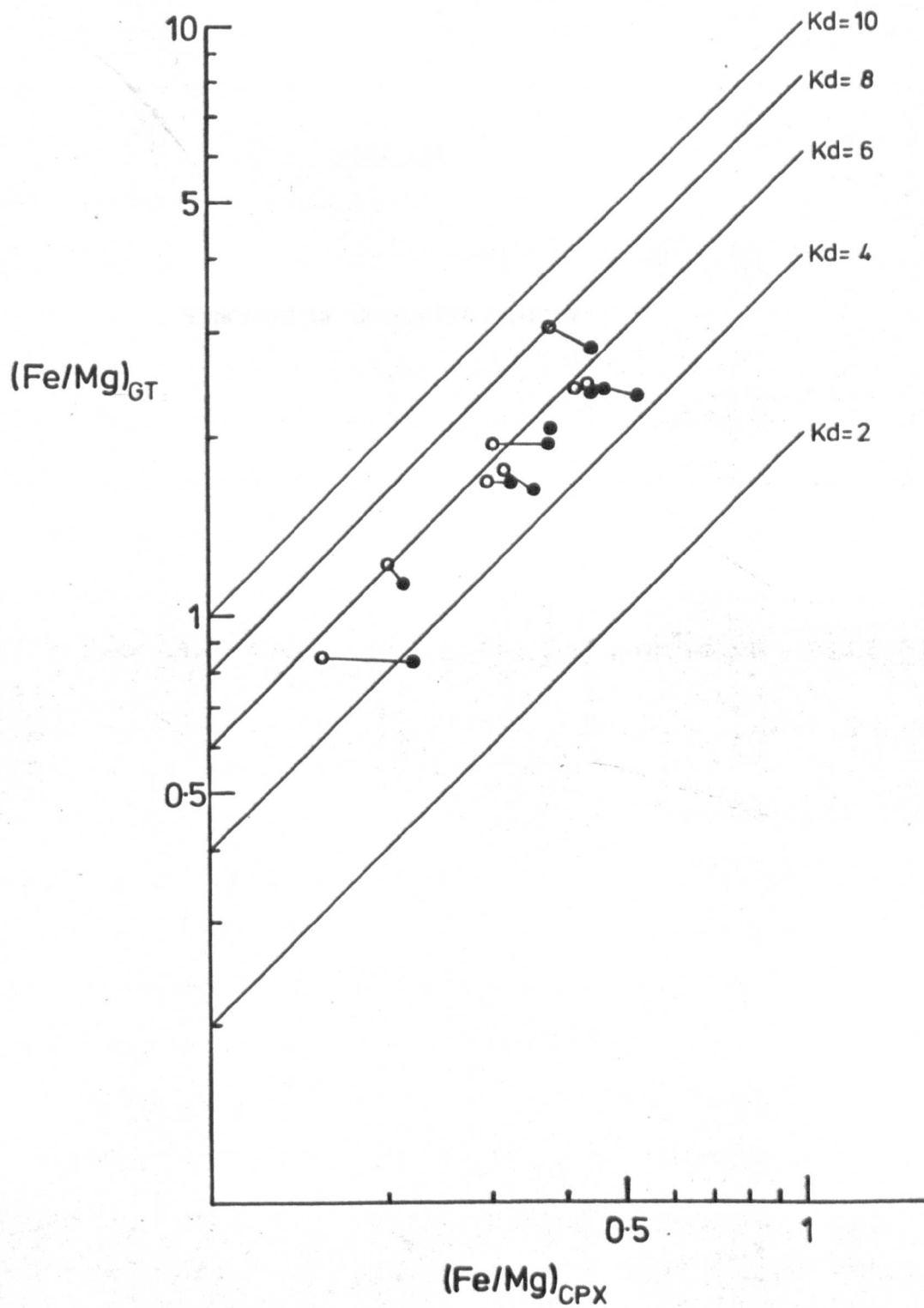


Figure 10.11: Plot of  $(\text{Fe}/\text{Mg})_{\text{GT}}$  v.  $(\text{Fe}/\text{Mg})_{\text{CPX}}$  for coexisting garnet and clinopyroxene from granulites.  
Closed circles: adjacent core compositions.  
Open circles: adjacent rim compositions.  
Tie lines connect the plots for core and rim in the same rock.  
Lines of constant  $K_d$  are shown for reference.  
$$K_d = (\text{Fe}/\text{Mg})_{\text{GT}} / (\text{Fe}/\text{Mg})_{\text{CPX}}$$



PART III

SYNOPSIS OF GEOLOGICAL HISTORY

CHAPTER 11

Synopsis of Geological History

1. The Genesis of the Kimberlite

Dawson (1971, 1972) reviewed the then current theories of kimberlite genesis. These included the 'residual' hypothesis (e.g. O'Hara and Yoder, 1967; Gupta and Yagi, 1979); the 'zone-refining' hypothesis (Harris and Middlemost, 1970), and the 'incipient melting hypothesis' (Dawson, op.cit.) The 'residual' hypothesis sought to explain kimberlite genesis by a process of eclogite fractionation from an upper mantle melt. The residual liquid was believed to be potentially kimberlitic. The hypothesis does not in itself explain the high concentrations of  $K_2O$ ,  $TiO_2$ ,  $CO_2$ ,  $P_2O_5$  and  $H_2O$ , nor indeed of the incompatible elements. The supposed 'cognate' eclogite xenoliths have much lower initial  $^{87}Sr/^{86}Sr$  ratios than the parent peridotite (Barrett, 1975) and are much older than the host kimberlite in some cases (e.g. Roberts Victor eclogite: 2500 m.y. (Kramers, 1979)). Such evidence seems to preclude a simple genetic link between these three rock types.

The 'zone-refining' hypothesis invokes the progressive concentration of residual elements in an ascending upper mantle melt. Dawson (op.cit.) has indicated several major objections to this essentially theoretical hypothesis: it ignores the presence of mantle derived xenolithic material; there is no resemblance to kimberlite major element chemistry; it is at variance with strontium isotopic data; and it does not accord with the rarity of kimberlite.

The 'incipient melting' hypothesis invokes partial melting of a high Ti phlogopite bearing peridotite parent and is in accord with more recent experimental studies which have examined melting in the system Peridotite- $CO_2-H_2O$  (e.g. Boettcher et al., 1965; Wyllie, 1977, 1979, 1980; Egger and

and Wendlandt, 1979). One major problem with this theory is the rarity of carbonate as a primary phase in mantle derived xenolithic material. Primary phlogopite is now a well established upper mantle phase (see Chapter 6), but it should be noted that the present study concurs with the observation of Boyd and Nixon (1975) to the extent that phlogopite-bearing nodules do not seem to derive from the higher temperature and pressure regime where melting must have commenced. This is also in agreement with the phase relations shown by Wyllie (1980).

In Chapter 4 I examined the REE abundances of various Letseng kimberlite samples and discussed the merits of these LREE enriched patterns being generated by eclogite fractionation or partial melting processes. The evidence however, is equivocal in isolation from other lines of reasoning. One such line is the examination of the strontium and neodymium isotopic composition of the rocks. The conclusions of this study presented in Chapter 4 are that the kimberlite may be generated by a small amount of partial melting of peridotitic material. It also shows that the source regions of kimberlites, like those of oceanic volcanic rocks, is of heterogeneous but near chondritic composition. The Letseng kimberlites derive from slightly depleted source regions but De Paolo (1978) has shown that some kimberlites derive from enriched sources. The similarity in isotopic character between kimberlites and oceanic rocks has also been confirmed in the U/Pb system (Kramers, 1977).

Wyllie and Juang (1976) concluded that kimberlitic magmas rising adiabatically must evolve  $\text{CO}_2$  at depths of 100-80 kms. If the overlying rock can be breached this may facilitate the explosive eruption of kimberlite and allow the intrusion of successive kimberlite pulses as described by Wyllie (1980).

The evidence of the peridotite xenoliths at Letseng shows that the kimberlite magma originated at some depth in excess of 150 km (see Chapter 9)

In addition the remarkable differences in the diamond populations from the two pipes (Harris et al. 1979) suggests that separate source regions were tapped. The chemical differences noted in Chapter 3 may also reflect on the source region but the possible differences in megacryst abundances (see Chapter 5) may account for this chemical separation as a result of crystal fractionation. There is no evidence to suggest whether these differences reflect lateral or vertical inhomogeneities in the mantle, but the very close proximity of the two pipes, relative to their depth of origin seems to indicate the latter. This might imply a measurable time separation between the emplacement of the two pipes which unfortunately has not been tested in this study.

Carbonatites also show the same isotopic relations to kimberlites and oceanic rocks, but one must be careful not to conclude that these rocks necessarily have a common genesis. Each may derive from a similar part of the upper mantle, but they follow very different evolution paths thereafter. Carbonatites in particular have often been linked as co-magmatic with kimberlite especially as these latter rocks are seen to differentiate to carbonate-rich residua (Dawson and Hawthorne, 1973; Robinson, 1975; Mitchell, 1979).

## 2. The Ascent of the Kimberlites

The underlying cause for the beginning of partial melting remains unknown. Perhaps it was a density inversion as suggested by Green and Gueguen (1974). The model of Wyllie (1980) explains this inversion as arising from partial melting induced by the upward migration of volatiles from below 260 km depth. As soon as melting occurs there will be adiabatic expansion and upward movement into a proto-diapir. With a continuing temperature differential between the diapir and the surrounding rock, natural buoyancy will carry the diapir ever upwards. The effect of this



movement and expansion on the surrounding mantle must be to displace the near horizontal steady-state isotherms towards lower pressures. In the subcontinental regions, where low geothermal gradients prevail, this displacement need not give rise to widespread melting as long as the movement remains within the solidus P/T field. However, given a large enough displacement towards lower pressure and enough time before incorporation in the kimberlite magma, it is possible for rocks equilibrated in the garnet peridotite stability field to transform to spinel peridotite. Such a transformation is recorded in all the Letseng garnet peridotites (see Chapters 6 and 7) although varying amounts of relict garnet are preserved.

Figure 11.1 shows a model cross-section of the upper mantle with the steady state isotherms of a continental geothermal gradient, disturbed by a small diapir. The model is very roughly to scale and the size of the diapir is inferred from the implied ~1% partial melting (Chapter 4). The isotherms record the minimum displacement required to move rocks from particular temperature/pressure regimes out of the garnet stability field (from MacGregor, 1974). The figure shows that for this minimum movement the higher temperature rocks require to move a greater vertical distance than the lower temperature rocks. Rocks from all levels may have moved similar distances, but if that had occurred one would expect the lower temperature rocks (which would have moved well into the spinel stability field) to exhibit more advanced garnet breakdown. This is not the case. I conclude that the higher temperature rocks have undergone greater vertical displacement and hence have become more attenuated and deformed than the lower temperature rocks. In this model, in contrast to that of Green and Gueguen (1974), none of the xenoliths are assumed to originate from within the diapir (although some xenocrysts may). The presence of low temperature deformed rocks is not incompatible with the model and the fact that some of these show disruption of the garnet distinguishes them

from the plastic flow fluidal textures seen in the higher temperature rocks. These low temperature LAD mosaic porphyroclastites may be similar to rocks at Bultfontein, South Africa (Dawson et al., 1975) which display deformation gradients from coarse to LAD within a single hand specimen. This style of deformation would appear to be more localised and may result from minor movement along the kimberlite conduit wall. Coarse textured rocks are not expected from the high temperature regions.

The relative size and numbers of xenoliths from the various depths also has a bearing on this discussion: in the Main pipe the great majority of garnet lherzolites derive from depths of about 110-100 km (33-36 Kbars) which when one also considers the prior movement out of the garnet stability field, is very close to the depth (100-80 km) from which explosive breakthrough may have occurred (see previous section). Xenoliths from other depths are relatively rare. The chromite bearing rocks are an exception but these rocks are presently assumed to derive from shallower levels. In the Satellite pipe the majority of garnet-bearing xenoliths are derived from much greater depths and the low temperature equivalents of the bulk of the Main pipe garnet peridotites are absent. If the Main pipe intrusion were older than that of the Satellite pipe it is possible to envisage this latter kimberlite utilising the pre-existing channelway. Because a passage had been cleared, more material from greater depth was able to move upward with less attenuation and hence less deformation (no fluidal textures in Satellite pipe xenoliths) before incorporation in the kimberlite. Wyllie (1980) questions whether progressively younger intrusions in the same kimberlite pipe include xenoliths from progressively greater depth. Letseng may provide the first evidence that such is the case, albeit only from adjacent pipes assumed to have used the same upper mantle conduit.

In Chapter 9 I discussed the effects of chemical disequilibrium on calculation of temperature and pressure. Consideration of the neoblast

compositions for high temperature rocks suggests these are adjusting to a temperature decrease. In contrast the low temperature deformed rocks have neoblasts indicating temperature increase. It is probable that a rising diapir will have an accompanying thermal aureole and the neoblast compositions in the low temperature rocks may reflect this localised heating. Alternatively, they may result from localised shear heating (Boyd, 1975). The neoblast compositions in the high temperature rocks however, seem to contradict this suggestion. In view of the deformation of these rocks, I believe the cooling effect of a much sharper local thermal gradient (bunching of isotherms) may be significant.

In Chapter 9 some peridotites were shown to display disequilibrium partitioning of certain critical elements between the coexisting phases. I concluded that these features resulted from partial re-equilibration to changed temperatures and pressures. These rocks in P-T space do not plot on the geotherm and are inferred to show part of the T/P trajectory from the steady-state situation existing before kimberlite genesis.

The small group of annealed spinel and garnet/spinel lherzolites from Letseng are interpreted to derive from normal garnet lherzolites (see Chapter 7). These specimens are believed to represent rocks which have undergone extremes of deformation followed by extensive annealing, during and after transformation from garnet to spinel facies. In the model (Figure 11.1) they may represent samples from the upper tip of the diapir where the isotherms are displaced sharply upwards to a point: deformation here would be expected to be most intense, and these specimens may have been carried further into the spinel-facies field. The fact that the estimated temperatures (Chapter 9) for these rocks is low means that the present texture and chemistry possibly does not relate to the present intrusion, but to an earlier pulse (represented

by kimberlite inclusions in diatreme facies rocks). It is not possible from the phase chemistry to determine where these rocks originated but the Fe-rich nature of some of them may imply a similarity to the higher temperature less depleted rocks. However, a low temperature origin cannot be ruled out.

Megacrysts of garnet, clinopyroxene, orthopyroxene, ilmenite and olivine are now believed to be the early phenocrysts of kimberlite crystallisation (Chapter 5). Of the opposing models describing their temperatures and pressures of crystallisation that of Gurney et al. (1979) involving a magma chamber of limited extent is the most compatible with my diapiric model. However they calculate that crystallisation has occurred at 45.3 Kbars which at Letseng would only allow crystallisation over the temperature range  $1400^{\circ}$ - $1250^{\circ}$ C before the geothermal gradient was reached. It has not been possible to calculate the pressures for minerals in the Letseng megacryst suite, but if the model of Gurney et al. (1979) is to be applicable it would appear these megacrysts must have crystallised at about 32 Kbars. This coincidentally is just deeper than the depth from which the majority of the Letseng Main pipe garnet lherzolites derive. The possibility that the geothermal gradient at Letseng is higher than at Monastery is not unreasonable in view of its proximity to the craton margin (Nixon, 1973) and the absence of ilmenite and ilmenite/silicate intergrowths indicates that the cooling episode has been interrupted at Letseng. This has important implications for the stability of the enclosed diamonds because the model shows that as soon as the diapir begins to rise the diamond stability field is breached (Figure 11.1). Unlike at Monastery, at no time thereafter does the Letseng kimberlite magma move back into this stability field. The primary crystal forms of diamonds are octahedra, cubes and macles, and degraded forms such as dodecahedra have been interpreted to result from resorption (Harris et al., 1979). These same authors have shown that Letseng diamonds

are characterised by the rarity of primary forms and are dominated by dodecahedral resorption forms. Whitelock (1973) gave a brief description of Monastery diamonds and the presence of octahedra seems much more common there. Interpreted in relation to resorption of diamond, the crystal forms seem to support the model for diapiric uprise and megacryst crystallisation outside the diamond stability field.

### 3. Emplacement of the Kimberlite

Cloos (1941) described the emplacement of the Swabian tuff cones by a process of fluidisation which has in recent years been applied to kimberlite diatremes (e.g. Dawson, 1971; Woolsey et al., 1975). The process is analogous to fluidisation as utilised in industrial applications (Reynolds, 1954). This involves the transport of mineral and rock fragments in a rapidly expanding gaseous medium which is believed to have developed from maximum depths of 2-3 km (Dawson, 1971). More recently Clement (1979) has described in great detail the structure of kimberlite pipes and concluded that fluidisation was relatively short-lived and may only develop from a depth of 200-300 metres.

Hawthorne (1975) extended the model of a kimberlite pipe to include the epiclastic (crater facies) kimberlites with the diatreme and hypabyssal facies varieties described by Dawson (1971). Clement (1979) has described in detail the characteristics of the pipe and the kimberlite in these three facies zones. He argued that explosive breakthrough may have occurred from very shallow depth. The proto-diatreme was then enlarged during a period of 'vapourisation and rapid adiabatic expansion' by a process of downward evolution. Hence he believes there is considerable overlap in the features typically attributed to each of these kimberlite facies zones. The presence of relatively high temperature microlitic diopside in segregation (= autolithic) textures is cited as evidence for the short duration of fluidisation.

In the Main pipe at Letseng the diatreme displays a wide range of kimberlite types, textures and intrusion features. The earliest kimberlites occurring only as inclusions in the autolithic kimberlite may represent crystallisation prior to explosive breakthrough and fluidisation. Their mineralogy (see Chapter 2) is compatible with crystallisation at moderate temperatures but low pressure as envisaged by Janse (1971) for the monticellite bearing rocks at Gross Brukkaros. Other rare kimberlite inclusions in this kimberlite indicate that some epiclastic rocks had been deposited prior to the emplacement of the presently exposed diatreme facies rocks.

The autolithic kimberlite is the major diatreme facies intrusion. I interpret that the emplacement during fluidisation was relatively slow with the widespread development of segregation textures. The upward movement was such that large and dense rocks and minerals were not carried very effectively: many of these inclusions moved downwards relative to the diatreme walls. I believe that large blocks of basalt, which foundered in this kimberlite (Chapter 1) during the diatreme formation may have sunk to quite deep levels and effectively choked the pipe causing a volatile build up. When the gas pressure had reached a certain level a rapid breakthrough back to surface occurred carrying with it the large foundered basalt blocks together with abundant mantle derived rocks and minerals not previously transported in any quantity by the autolithic kimberlite. This explosion breakthrough led to the emplacement of the garnetiferous kimberlite with its load of large, dense rocks and minerals. Necessarily if such a process occurred the intrusion rate would be fastest at the centre of the garnetiferous kimberlite: this seems to be confirmed by the zonation towards the centre of abundance, size and density of xenolithic material. The relative lack of microlitic diopside may result from the presumed more rapid quenching of this kimberlite.

Later pulses of kimberlite have crystallised without devolatilisation (K4 and K5) and are interpreted as hypabyssal facies varieties. Their presence at this relatively high level in the diatreme testifies to the extensive overlap of the facies zones.

The Satellite pipe has followed a similar early history with fluidised emplacement succeeding the crystallisation of high level monticellite-bearing kimberlite. Although the western contacts also indicate the foundering of large basalt blocks the pipe presumably did not become choked before the cessation of kimberlite magmatism. The enclosed diopside bearing kimberlite dyke may represent the uppermost limit of the hypabyssal facies in this pipe although its devolatilised character suggests a relationship rather closer to that of the diatreme facies rocks.

Early and late kimberlite dyke emplacement straddling the diatreme formation gives some indication of the chemical evolution of the parent magma as a result of increase  $f_{O_2}$  and fractionation towards carbonate rich compositions.

#### 4. Structure of the Sub-Letseng Crust and Upper Mantle

The contrasting conclusions of the studies of xenolith suites from Lesotho (Matsoku: Cox et al., 1973; Harte et al., 1975; Gurney et al., 1975; Thaba Putsoa: Boyd and Nixon, 1972, 1975; Nixon and Boyd, 1973) have led to considerable discussion about the structure of the upper mantle beneath Lesotho. Two essential differences are observed between rocks from these and other localities: first the Matsoku rocks are derived from a limited depth-interval in contrast to the wide range of depths interpreted for Thaba Putsoa xenoliths; second the Matsoku rocks show a wide range in composition which in the Thaba Putsoa suite is related to depth of origin.

The Matsoku suite has been interpreted as relating to some previous upper mantle igneous event unconnected with kimberlite generation. The

Thaba Putsoa suite has been interpreted to display an upper mantle chemical zoning resulting from progressively less depletion with depth.

The Letseng xenolith suites show some of the features of both these interpretations and I believe demonstrate that each can be accommodated in models of upper mantle stratigraphy. The Matsoku model is necessarily a local phenomenon but in view of the relatively short distance between Matsoku and Letseng (14 km) it is not surprising that some similar Fe rich rocks have been found at Letseng. In the Main pipe xenolith suite the majority of the garnet lherzolites derive from a similar temperature/depth regime as the Matsoku rocks. Although the majority of the Letseng rocks are considerably more depleted in fusible components (see Chapter 8) similar compositions trends are seen and rare Fe rich rocks are found. I believe that this group of rocks from the Letseng suite may be peripherally related to the Matsoku rocks.

Although these rocks form the bulk of the xenolith suite there are considerable numbers of samples derived from both shallower and deeper levels. Those from greater depths are similar to rocks in the Thaba Putsoa suite and indicate less depletion with depth, although bulk chemical data confirming this is rather poor. However, because the kimberlite itself derives from an undepleted (near chondritic) source region (Chapter 4) this proposed chemical stratigraphy is not surprising. Rocks from shallower levels contain chromite in addition to garnet and other rocks with chromite, but no garnet may also originate from the uppermost upper mantle (Boyd and Nixon, 1975).

The chemistry of xenoliths from the Precambrian Premier Mine kimberlite indicates that the deeper levels samples there were very similar to equivalent levels sampled beneath Lesotho over 1000 my later. Xenoliths from shallower levels however, are not as depleted as the equivalent Lesotho samples. The only major volcanic event to have affected



southern Africa during this 1000 my period was the outpouring of the Stormberg basalts (200 my B.P.) and the greater depletion of the mantle xenoliths in the Cretaceous kimberlites must be assumed to result from this event.

Not enough is known from this study to close the gap in lower-crustal/upper mantle stratigraphy because only the more intermediate/acid granulites were studied. This is not to imply that the more basic granulites originate from deeper levels but the intermediate granulites do not derive from the lowest lower crust. In any case there is no reason to believe that the mineral assemblages bear any relation to a Cretaceous geotherm beneath Lesotho. Carswell et al. (1979) have constructed a geotherm connecting the granulites and upper mantle peridotites from Pipe 200 in Lesotho. However, this curve cannot accommodate the high temperature rock from Letseng, Thaba Putsoa or anywhere else in Lesotho and these authors contention that the observed P/T relations may be telescoped is at variance with the results of this study, made using the identical geothermometer and geobarometer. What is interesting is that like Matsoku and Letseng the mantle at ~100 km beneath Pipe 200 has been sampled. This feature is not apparent in the studies of Nixon and Boyd as they do not indicate the relative abundances of the 'granular' and 'sheared' varieties.

Returning to the granulite problem, Carswell et al. (1979) have interpreted the granulite metamorphism in relation to some complex lower crustal processes involving anatexis, and emplacement of basic material by intrusion and abduction. While such processes may be involved, I believe they pay little attention to the known Precambrian age of two granulite xenoliths from Lesotho kimberlites (Davis, 1977) and place too much emphasis on the apparent absence of granulites from within the craton. I conclude that these rocks relate only to this Precambrian event and

are composed of metasedimentary and metaigneous rocks. Their plot in P/T space does not therefore relate to the Cretaceous geotherms plotted using peridotite xenolith suites. The true nature of the lowest lower crust remains an enigma.

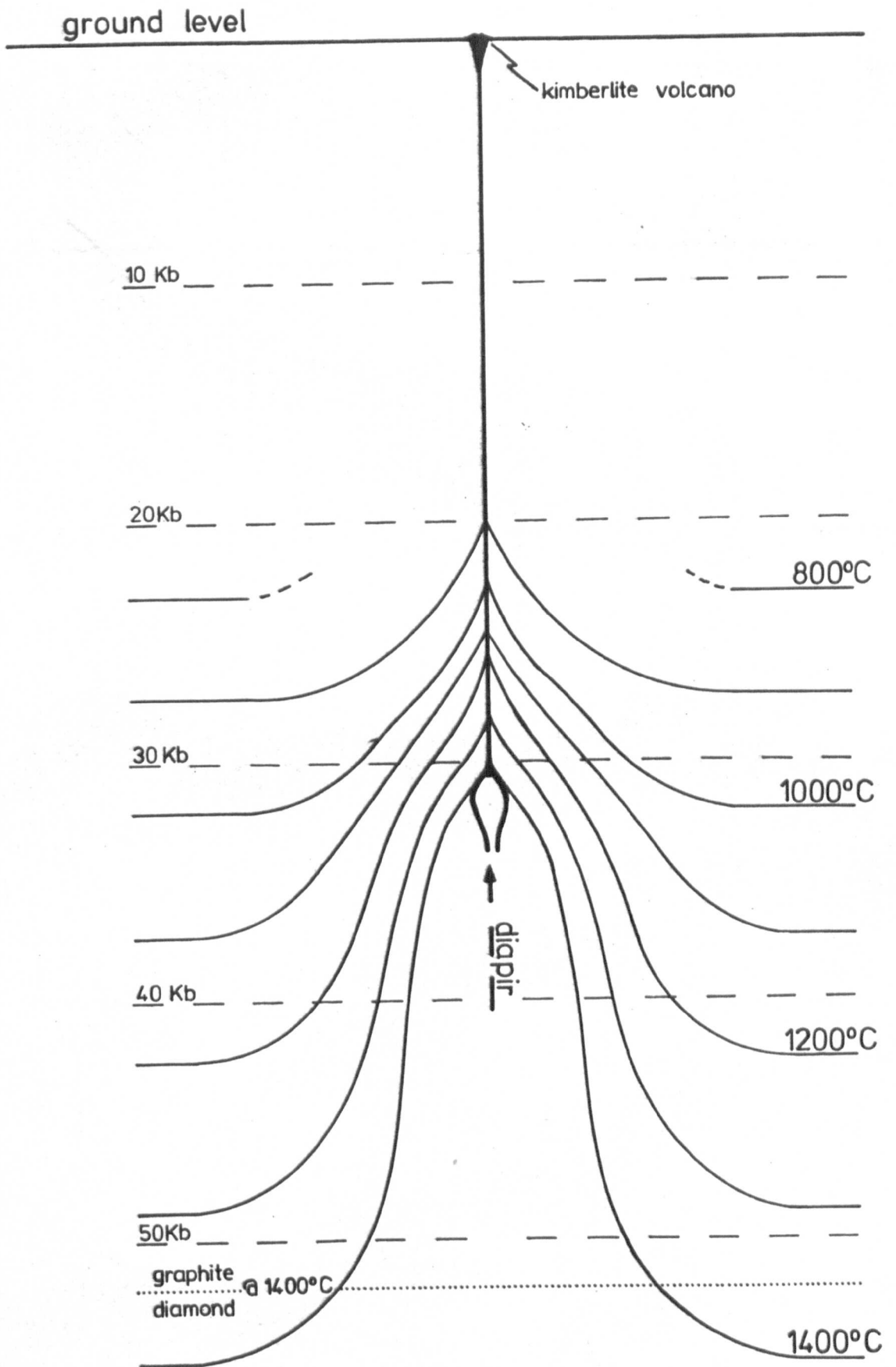
The nature and stratigraphy of the remainder of the crust sampled by the Letseng kimberlites is beyond the scope of this thesis, but is modelled in 'Lesotho Kimberlites' (1973).

**Figure 11.1: Model of kimberlite diapir.**

The model shows the steady state isotherms (solid lines) displaced by the diapiric uprise. The diagram shows the limiting condition for movement out of the garnet stability field (see text).

The isotherms and isobars (dashed lines) are plotted from the geotherm interpreted in figure 9.2.

The dotted line shows the graphite/diamond inversion curve at 1400°C .



REFERENCES

- ALLSOPP, H.L. and BARRETT, D.R., 1975. Rb-Sr age determinations on South African kimberlite pipes. *Phys. Chem. Earth, Oxford*, 9, 605-617.
- ALLSOPP, H.L., BURGER, A.J. and VAN ZYL, C., 1967. A minimum age for the Premier Kimberlite pipe yielded by biotite Rb-Sr measurements, with related galena isotopic data. *Earth Planet Sci. Lett.*, 3, 161-166.
- ALLSOPP, H.L. and KRAMERS, J.D., 1977. Rb-Sr and U-Pb age determinations on southern African kimberlite pipes. *Ext. Abstr. II, Int. Kimberlite Conf., Colorado*.
- ALLSOPP, H.L., KRAMERS, J.D., MILLER, J.A. and HUTCHINSON, G., 1979. A review of the application of the Rb-Sr, U-Pb and K-Ar methods to the dating of kimberlite pipes, with special reference to the occurrence of anomalously old ages. *Ext. Abstr. II, Kimberlite Symp., Cambridge*.
- BALDOCK, J.W., HEPWORTH, J.V. and MARENGWA, B.S., 1976. Gold, base metals, and diamonds in Botswana. *Econ. Geol.*, 71, 139-156.
- BARRETT, D.R., 1975. The genesis of kimberlites and associated rocks: Strontium isotopic evidence. *Phys. Chem. Earth, Oxford*, 9, 637-653.
- BARRETT, D.R. and BERG, G.W., 1975. Complementary petrographic and strontium isotope ratio studies of South African kimberlites. *Phys. Chem. Earth, Oxford*, 9, 619-635.
- BASU, A.R. and MACGREGOR, I.D., 1975. Chromite spinels from ultramafic xenoliths. *Geochim. Cosmochim. Acta*, 39, 937.
- BASU, A.R. and TATSUMOTO, M., 1979. Samarium-Neodymium systematics in kimberlites and in the minerals of garnet lherzolite inclusions. *Sci.*, 205, 398-401.
- BERG, G.W. and ALLSOPP, H.L., 1972. Low  $\text{Sr}^{87}/\text{Sr}^{86}$  ratios in fresh South African kimberlites. *Earth Planet Sci. Lett.* 16, 27-30.

- BISHOP, F.C., SMITH, J.V. and DAWSON, J.B., 1978. Na, K, P and Ti in garnet, pyroxene and olivine from peridotite and eclogite xenoliths from African kimberlites. *Lithos*, 11, 155-173.
- BLOOMER, A.G. and NIXON, P.H., 1973. The geology of the Letseng-la-Terae kimberlite pipes. In: Nixon, P.H. (Ed), Lesotho Kimberlites, 20-36. Maseru: Lesotho National Development Corporation.
- BOETTCHER, A.L., MYSEN, B.O. and MODRESKI, P.J., 1975. Phase relationships in natural and synthetic peridotite-H<sub>2</sub>O and peridotite-H<sub>2</sub>O-CO<sub>2</sub> systems at high pressures. *Phys. Chem. Earth* 9, 855-868.
- BOULLIER, A.M. and NICOLAS, A., 1973. Texture and fabric of peridotite nodules from kimberlite at Mothae, Thaba Putsoa and Kimberley. In: Nixon, P.H. (Ed), Lesotho Kimberlites, 57-66. Maseru: Lesotho National Development Corporation.
- BOULLIER, A.M. and NICOLAS, A., 1975. Classification of textures and fabrics of peridotite xenoliths from South African kimberlites. *Phys. Chem. Earth*, 9, 467-475.
- BOYD, F.R., 1973. A pyroxene geotherm. *Geochim. Cosmochim. Acta*, 37, 2533-2546.
- BOYD, F.R., 1973. Appendix of mineral analyses, by F.R. Boyd. In: Nixon, P.H. (Ed), Lesotho Kimberlites, 33-36. Maseru: Lesotho National Development Corporation.
- BOYD, F.R., 1975. Stress heating and compositional variations in enstatites from sheared lherzolites. *Ann. Rep. Dir. Geophys. Lab. Carnegie Inst.*, 74, 525-528.
- BOYD, F.R. and FINGER, L.W., 1975. Homogeneity of minerals in mantle rocks from Lesotho. *Ann. Rep. Dir. Geophys. Lab. Carnegie Inst.* 74, 519-525.
- BOYD, F.R. and NIXON, P.H., 1972. Ultramafic nodules from the Thaba Putsoa kimberlite pipe. *Ann. Rep. Dir. Geophys. Lab. Carnegie Inst.*, 71, 362-373.

- BOYD, F.R. and NIXON, P.H., 1975. Origins of the ultramafic nodules from some kimberlites of northern Lesotho and the Monastery Mine, South Africa. *Phys. Chem. Earth*, 9, 431-453.
- BOYD, F.R. and NIXON, P.H., 1978. Ultramafic nodules from the Kimberley pipes, South Africa. *Geochim. Cosmochim. Acta*, 42, 1367-1382.
- BROOKINS, D.G., 1967. The strontium geochemistry of carbonates in kimberlites and limestones from Riley County, Kansas. *Earth Planet Sci. Lett.*, 2, 235-240.
- BRUTON, E., 1979. Diamonds. 2nd Edition, NAG Press.
- BURKOV, V.V. and PODPORINA, Y.K., 1966. First data on rare earths in kimberlite. *Dokl Akad Nauk SSSR, Earth Sci. Sect.*, 171, 215-219.
- BURLEY, A.J. and GREENWOOD, P.G., 1972. Geophysical surveys over kimberlite pipes in Lesotho. *Geophys. Div. Rep. Inst. Geol. Sci.*, London.
- CARSWELL, D.A., 1975. Primary and secondary phlogopites and clinopyroxenes in garnet lherzolite xenoliths. *Phys. Chem. Earth*, 9, 417-429.
- CARSWELL, D.A., CLARKE, D.B. and MITCHELL, R.H., 1979. The petrology and geochemistry of ultramafic nodules from Pipe 200, northern Lesotho. In: Boyd, F.R. and Meyer, H.O.A. (Eds), *The Mantle Sample: Inclusions in Kimberlites and other Volcanics*, 127-144. American Geophysical Union, Washington.
- CARTER, S.R., EVENSEN, N.M., HAMILTON, P.J. and O'NIONS, R.K., 1978. Continental volcanics derived from enriched and depleted source regions: Nd and Sr isotope evidence. *Earth Planet Sci. Lett.*, 37, 401-408.
- CLIFFORD, T.N., 1974. Review of African granulites and related rocks. *Geol. Soc. Amer., Spec. Paper*, 156, 49 pp.
- CLIFFORD, T.N. and GASS, I.C., (Eds), 1970. *African Magmatism and Tectonics*. Oliver and Boyd, Edinburgh.
- CLOOS, H., 1941. Bau und Tätigkeit von Tuffschloten. Untersuchungen an dem Schwabischen Vulkan. *Geol. Rundsch.* 32, 709-800.

- COLLERSON, K.D. and FRYER, B.J., 1978. The role of fluids in the formation and subsequent development of early continental crust. *Contrib. Mineral Petrol.*, 67, 151-167.
- CORNELISSEN, A.K. and VERWOERD, W.J., 1975. The Bushmanland Kimberlites and related rocks. *Phys. Chem. Earth*, 9, 71-79.
- COX, K.G., 1969. Tectonics and vulcanism of the Karoo period and their bearing on the postulated fragmentation of Gondwanaland. In: Clifford, T.N. and Gass, I.G. (Eds), *African Magmatism and Tectonics*, 211-236. Oliver and Boyd: Edinburgh.
- COX, K.G., GURNEY, J.J. and HARTE, B., 1973. Xenoliths from the Matsoku pipe. In: Nixon, P.H. (Ed), *Lesotho Kimberlites*, 76-100. Maseru: Lesotho National Development Corporation.
- COX, K.G. and HORNING, G., 1966. The petrology of the Karoo basalts of Basutoland. *Amer. Mineral.* 51, 1414-1432.
- CURRIE, K.L. and CURTIS, L.W., 1976. An application of multicomponent solution theory to jadeitic pyroxenes. *J. Geol.*, 84, 179-194.
- DANCHIN, R.V., 1979. Mineral and bulk chemistry of garnet lherzolite and garnet harzburgite xenoliths from the Premier Mine, South Africa. In: Boyd, F.R. and Meyer, H.O.A. (Eds), *The Mantle Sample: Inclusions in Kimberlites and other Volcanics*, 104-126. American Geophysical Union, Washington.
- DANCHIN, R.V., FERGUSON, J., MACIVER, J.R. and NIXON, P.H., 1975. The composition of late stage kimberlite liquids as revealed by nucleated autoliths. *Phys. Chem. Earth*, 9, 235-245.
- DAVIS, B.T.C. and BOYD, F.R., 1966. The join  $MgSiO_3$ - $CaMgSi_2O_6$  at 30 Kb and its application to pyroxenes from kimberlites. *J. Geophys. Res.*, 71, 3567-3576.
- DAVIS, G.L., 1977. The ages and uranium contents from kimberlites and associated rocks. *Ext. Abstr. II. Int. Kimberlite Conf., Colorado.*



- DAWSON, J.B., 1960. A comparative study of the geology and petrography of the kimberlites of the Basutoland province. Unpub. Ph.D. Thesis, Univ. Leeds.
- DAWSON, J.B., 1962. Basutoland kimberlites. *Bull. Geol. Soc. Am.*, 73, 545-560.
- DAWSON, J.B., 1967. Geochemistry and origin of kimberlite. In: Wyllie, P.J. (Ed), *Ultramafic and Related Rocks*, 269-278. J. Wiley & Sons, New York.
- DAWSON, J.B., 1971. Advances in kimberlite geology. *Earth Sci. Rev.*, 7, 187-214.
- DAWSON, J.B., 1972. Kimberlites and their relation to the mantle. *Phil. Trans. R. Soc. Lond., Ser.A.*, 271, 297-311.
- DAWSON, J.B., 1977. Sub-cratonic crust and upper mantle models based on xenolith suites in kimberlite and nephelinitic diatremes. *J. Geol. Soc. Lond.*, 134, 173-184.
- DAWSON, J.B., GURNEY, J.J. and LAWLESS, P.J., 1975. Palaeogeothermal gradients derived from xenoliths in kimberlite. *Nature*, 257, 299-300.
- DAWSON, J.B. and HAWTHORNE, J.B., 1973. Magmatic sedimentation and carbonatitic differentiation in kimberlite sills at Benfontein, South Africa. *J. Geol. Soc. London*, 129, 61-85.
- DAWSON, J.B. and HAWTHORNE, J.B., 1970. Intrusion features of some hypabyssal South African kimberlites. *Bull. Volcanol.*, 34, 740.
- DAWSON, J.B. and SMITH, J.V., 1975. Chemistry and origin of phlogopite megacrysts in kimberlite. *Nature*, 253, 336-338.
- DAWSON, J.B. and SMITH, J.V., 1975. Chromite-silicate intergrowths in upper mantle peridotites. *Phys. Chem. Earth*, 9, 339-349.
- DAWSON, J.B. and SMITH, J.V., 1977. The MARID (mica-amphibole-rutile-ilmenite-diopside) suite of xenoliths in kimberlite. *Geochim. Cosmochim. Acta*, 41, 309-323.

- DAWSON, J.B., SMITH, J.V. and DELANEY, J.S., 1978. Multiple spinel-garnet peridotite transitions in the upper mantle: Evidence from a harzburgite xenolith. *Nature*, 273, 741-743.
- DAWSON, J.B. and STEPHENS, W.E., 1975. Statistical classification of garnets from kimberlite and associated xenoliths. *J. Geol.* 83, 589-607.
- DAWSON, J.B. and STEPHENS, W.E., 1976. Addendum: Statistical classification of garnets from kimberlite and associated xenoliths. *J. Geol.*, 84, 495-496.
- DEMPSTER, A.N. and RICHARD, R., 1973. Regional geology and structure. In: Nixon, P.H. (Ed), Lesotho Kimberlites, 1-19. Maseru: Lesotho National Development Corporation.
- DE PAOLO, D.J., 1978. Nd and Sr isotope systematics of younger continental igneous rocks. *US Geol. Surv. Open File Rep.*, 78-701, 91-93.
- DE PAOLO, D.J. and WASSERBURG, G.J., 1976. Nd isotopic variations and petrogenetic models. *Geophys. Res. Lett.*, 3, 249.
- DONALDSON, C.H., 1978. Petrology of the uppermost upper mantle deduced from spinel lherzolite and harzburgite nodules at Calton Hill, Derbyshire. *Contrib. Mineral Petrol.*, 65, 363-377.
- EDWARDS, C.B.E. and HOWKINS, J.B., 1966. Kimberlites in Tanganyika with special reference to the Mwadui occurrence. *Econ. Geol.* 61, 537-554.
- EGGLER, D.M., MCCALLUM, M.E. and SMITH, C.B., 1979. Megacryst assemblages in kimberlites from northern Colorado and southern Wyoming: Petrology, geothermometry-barometry, and areal distribution. In: Boyd, F.R. and Meyer, H.O.A. (Eds), The Mantle Sample: Inclusions in Kimberlites and other Volcanics, 213-226. American Geophysical Union, Washington.
- EGGLER, D.H. and WENDLANDT, R.F., 1979. Experimental studies on the relationship between kimberlite magmas and partial melting of peridotite. In: Boyd, F.R. and Meyer, H.O.A. (Eds), Kimberlites, Diatremes and Diamonds: Their Geology, Petrology and Geochemistry, 330-338. American Geophysical Union, Washington.

- ELLIS, D.J. and GREEN, D.H., 1979. An experimental study of the effect of Ca upon garnet-clinopyroxene Fe-Mg exchange equilibria. *Contrib. Mineral Petrol.*, 71, 13-22.
- EMELEUS, C.H. and ANDREWS, J.R., 1975. Mineralogy and petrology of kimberlite dyke and sheet intrusions and included peridotite xenoliths from south-west Greenland. *Phys. Chem. Earth.* 9, 179-198.
- FERGUSON, J., DANCHIN, R.V. and NIXON, P.H., 1973. Fertilisation associated with kimberlite magmas. In: Nixon, P.H. (Ed), Lesotho Kimberlites, 207-213. Maseru: Lesotho National Development Corporation.
- FERGUSON, J., DANCHIN, R.V. and NIXON, P.H., 1973. Petrochemistry of kimberlite autoliths. In: Nixon, P.H. (Ed), Lesotho Kimberlites, 285-293. Maseru: Lesotho National Development Corporation.
- FERGUSON, J., ELLIS, D.J. and ENGLAND, R.N., 1977. Unique spinel-garnet lherzolite inclusions in kimberlite from Australia. *Geology*, 5, 278-280.
- FESQ, H.W., BIBBY, D.M., ERASMUS, C.S., KABLE, E.J.D. and SELLSCHOP, J.P.F., 1975. A comparative trace element study of diamonds from Premier, Finsch and Jagersfontein mines, South Africa. *Phys. Chem. Earth, Oxford*, 9, 817-835.
- FESQ, H.W., KABLE, E.J.D. and GURNEY, J.J., 1975. Aspects of the geochemistry of kimberlites from the Premier mine, and other selected South African occurrences with particular reference to the rare earth elements. *Phys. Chem. Earth., Oxford*, 9, 687-707.
- FINGER, L.W., 1972. The uncertainty in the calculated ferric iron-content of a microprobe analysis. *Ann. Rep. Dir. Geophys. Lab, Carnegie Inst.*, 71, 600-603
- FITCH, F.J. and MILLER, J.A., 1971. Potassium-argon radioages of Karoo volcanic rocks from Lesotho. *Bull. Volcanol.* 35, 64-84.
- FREY, F.A., FERGUSON, J. and CHAPPELL, B.W., 1977. Petrogenesis of South African and Australian Kimberlitic suites. *Ext. Abstr. II. Int. Kimberlite Conf., Colorado.*

- FREY, F.A., HASKIN, L.A. and HASKIN, M.A., 1971. Rare earth abundances in some ultramafic rocks. *J. Geophys. Res.*, 76, 2057-2070.
- GREEN, H.W. and GUEGUEN, Y., 1974. Origin of kimberlite pipes by diapiric upwelling in the upper mantle. *Nature*, 249, 617-619.
- GREEN, D.H. and RINGWOOD, A.E., 1967. The stability fields of aluminous pyroxene peridotite and garnet peridotite and their relevance in upper mantle structures. *Earth Planet Sci. Lett.*, 3, 151-160.
- GRIFFIN, W.L., CARSWELL, D.A. and NIXON, P.H., 1979. Lower crustal granulites and eclogites from Lesotho, Southern Africa. In: Boyd, F.R. and Meyer, H.O.A. (Eds), *The Mantle Sample: Inclusions in Kimberlites and other Volcanics*, 59-86, American Geophysical Union, Washington.
- GUPTA, A.K. and YAGI, K., 1979. Experimental study on two picrites with reference to the genesis of kimberlite. In: Boyd, F.R. and Meyer, H.O.A. (Eds) *Kimberlites, Diatremes and Diamonds: Their Geology, Petrology and Geochemistry*, 339-345, American Geophysical Union, Washington.
- GURNEY, J.J. and BERG, G.W., 1969. Potassium, rubidium and caesium in South African kimberlites, and their peridotite nodules. In: *Upper Mantle Project*, 351-357, Geol. Soc. S. Africa, Spec. Pub. 2.
- GURNEY, J.J. and EBRAHIM, S., 1973. Chemical composition of Lesotho kimberlites, In: Nixon, P.H. (Ed) *Lesotho Kimberlites*, 280-284.
- Maseru: Lesotho National Development Corporation.
- GURNEY, J.J., HARRIS, J.W. and RICKARD, R.S., 1979. Inclusions in southern Africa diamonds and their relationship to the xenoliths. Ext. Abstr. II, Kimberlite Symp, Cambridge.
- GURNEY, J.J., HARTE, B. and COX, K.G., 1975. Mantle xenoliths in the Matsoku kimberlite pipe. *Phys. Chem. Earth*, 9, 507-523.
- GURNEY, J.J., JAKOB, W.R.O. and DAWSON, J.B., 1979. Megacrysts from the Monastery kimberlite pipe, South Africa. In: Boyd, F.R. and Meyer, H.O.A. (Eds) *The Mantle Sample: Inclusions in Kimberlites and other Volcanics*, 227-243, American Geophysical Union, Washington.

- GURNEY, J.J. and SWITZER, G.S., 1973. The discovery of garnets closely related to diamonds in the Finsch pipe, South Africa. *Contrib. Mineral. Petrol.*, 39, 103-116.
- HAGGERTY, S.E., 1975. The chemistry and genesis of opaque minerals in kimberlites. *Phys. Chem. Earth*, 9, 295-307.
- HAGGERTY, S.E., 1973. Spinel of unique composition associated with ilmenite reactions in the Liphobong kimberlite pipe, Lesotho. In: Nixon, P.H. (Ed), *Lesotho Kimberlites*, 149-158. Maseru: Lesotho National Development Corporation.
- HAMILTON, P.J., O'NIONS, R.K. and EVENSON, N.M., 1977. Sm-Nd dating of Archaean basic and ultrabasic volcanics. *Earth Planet Sci. Lett.*, 36, 263.
- HARRIS, J.W., 1973. Observations on Letseng-la-Terae diamonds. In: Nixon, P.H. (Ed) *Lesotho Kimberlites*, 37-38. Maseru: Lesotho National Development Corporation.
- HARRIS, J.W., HAWTHORNE, J.B. and OOSTERVELD, M.M., 1979. Regional and local variations in the characteristics of diamonds from some Southern Africa kimberlites. In: Boyd, F.R. and Meyer, H.O.A. (Eds) *Kimberlites, Diatremes and Diamonds: Their Geology, Petrology and Geochemistry*, 27-41, American Geophysical Union, Washington.
- HARRIS, P.G. and MIDDLEMOST, E.A.K., 1970. The evolution of kimberlites. *Lithos*, 3, 77-88.
- HARTE, B., 1977. Rock nomenclature with particular relation to deformation and recrystallisation textures in olivine bearing xenoliths. *J. Geol.* 85, 279-288.
- HARTE, B., 1978. Kimberlite nodules, upper mantle petrology and geotherms. *Phil. Trans. R. Soc. Lond., Ser.A*, 288, 487-500.
- HARTE, B., COX, K.G. and GURNEY, J.J., 1975. Petrography and geological history of upper mantle xenoliths from the Matsoku kimberlite pipe. *Phys. Chem. Earth.*, 9, 477-506.

- HASKIN, L.A., FREY, F.A., SCHMITT, R.F. and SMITH, R.H., 1966. Meteoritic, solar and terrestrial rare earth distributions. *Phys. Chem. Earth*, Oxford, 7, 167-321.
- HAUGHTON, S.H., 1969. Geological History of Southern Africa. Geol. Soc. S. Africa.
- HAWKESWORTH, C.J., NORRY, M.J., RODDICK, J.C. and BAKER, P.E., 1979.  $^{143}\text{Nd}/^{144}\text{Nd}$ ,  $^{87}\text{Sr}/^{86}\text{Sr}$  and incompatible element variations in calc-alkaline andesites and plateau lavas from South America. *Earth Planet. Sci. Lett.*, 42, 45-57.
- HAWTHORNE, J.B., 1975. Model of a kimberlite pipe. *Phys. Chem. Earth*, 9, 1-15.
- HOOKE, P.J., O'NIONS, R.K. and PANKHURST, R.J., 1975. Determination of rare earth elements in USGS standard rocks by mixed solvent ion exchange and mass spectrometric isotope dilution. *Chem. Geol.*, 16, 169-
- HORNUNG, G. and NIXON, P.H., 1973. Chemical variations in knorringite-rich garnets. In: Nixon, P.H. (Ed), Lesotho Kimberlites, 122-127. Maseru: Lesotho National Development Corporation.
- HOWELLS, S. and O'HARA, M.J., 1978. Low solubility of alumina in enstatite and uncertainties in estimated palaeogeotherms. *Phil. Trans. R. Soc. Lond., Ser.A.* 288, 471-486.
- HURLEY, P.M., 1967.  $^{87}\text{Rb}$ - $^{87}\text{Sr}$  relationships in the differentiation of the mantle. In: Wyllie, P.J. (Ed), Ultramafic and Related Rocks. John Wiley & Sons, New York.
- HUTCHISON, R. and DAWSON, J.B., 1970.  $^{87}\text{Rb}$ ,  $^{87}\text{Sr}/^{86}\text{Sr}$  in ultrabasic xenoliths and host rocks, Lashaine volcano, Tanzania. *Earth Planet. Sci. Lett.*, 9, 87-92.
- ILUPIN, I.P. and LUTZ, B.G., 1971. The chemical composition of kimberlite and questions on the origin of kimberlite magma. *Soretskaya Geol.*, 6, 61-73.

- JACKSON, P.M. and HARTE, B., 1977. The nature and conditions of formation of granulite facies xenoliths from the Matsoku kimberlite pipes, Lesotho. Ext. Abstr. II, Kimberlite Conf., Colorado.
- JANSE, A.J.A., 1971. Monticellite bearing porphyritic peridotite from Gross Brukkaros, South-West Africa. Geol. Soc. South Africa Trans., 74, 45-55.
- JENKINS, D.M. and NEWTON, R.C., 1979. Experimental determination of the spinel peridotite to garnet peridotite inversion at 900°C and 1000°C in the system CaO-MgO-Al<sub>2</sub>O<sub>3</sub>-SiO<sub>2</sub> and at 900°C with natural garnet and olivine. Contrib. Mineral. Petrol. 68, 407-418.
- JOUBERT, P., 1971. The regional tectonism of the gneisses of part of Namaqualand. Cape Town Univ., Dept. Geol., Chamber Mines Precambrian Res. Unit Bull., 10, 220.
- KRAMERS, J.D., 1977. Lead and strontium isotopes in Cretaceous kimberlites and mantle-derived xenoliths from Southern Africa. Earth Planet. Sci. Lett., 34, 419-431.
- KRAMERS, J.D., 1979. Lead, uranium, strontium, potassium and rubidium in inclusion-bearing diamonds and mantle derived xenoliths from Southern Africa. Earth Planet. Sci. Lett., 42, 58-70.
- KRAMERS, J.D., RODDICK, J.C.M., DAWSON, J.B. and BOYD, F.R., 1979. Pb, Sr, and Nd isotopic studies of xenoliths of the MARID suite and deep seated clinopyroxene megacrysts and their implications. Ext. Abstr. II, Kimberlite Symp, Cambridge.
- KRESTEN, P., 1973. Differential thermal analysis of kimberlites. In: Nixon, P.H. (Ed), Lesotho Kimberlites, 269-279. Maseru: Lesotho National Development Corporation.
- KRESTEN, P. and DEMPSTER, A.N., 1973. The geology of pipe 200 and the Malibamatso dyke swarm. In: Nixon, P.H. (Ed), Lesotho Kimberlites, 172-179. Maseru: Lesotho National Development Corporation.

- KRÖNER, A., 1977. The Precambrian geotectonic evolution of Africa: Plate accretion versus plate destruction. *Precambrian Res.*, 4, 163-213.
- KRUGER, F.J., 1978. A contribution to the petrology of kimberlites. Unpub. M.Sc. Thesis, Rhodes Univ., Grahamstown, South Africa.
- KRUGER, F.J., 1980. The occurrence of cebolite in kimberlite and included zeolitised crustal xenoliths. *Mineral. Mag.*, 43, 583-586.
- KUNO, H., 1967. Mafic and ultramafic nodules from Itinome-Gata, Japan. In: Wyllie, P.J. (Ed), Ultramafic and Related Rocks, 337-342. J. Wiley, New York.
- KUNO, H. and AOKI, K., 1970. Chemistry of ultramafic nodules and their bearing on the origin of basaltic magmas. *Phys. Earth Planet. Inter.*, 3, 273-301.
- KUSHIRO, I., 1969. Clinopyroxene solid solutions formed by reactions between diopside and plagioclase at high pressures. *Mineral. Soc. Amer.*, Spec. Paper 2, 179-191.
- LAMBERT, R. St. J., 1976. Archaean thermal regimes, crustal and upper mantle temperatures, and a progressive evolutionary model for the earth. In: Windley, B.F. (Ed), The Early History of the Earth, 351-360. Wiley, London.
- LEAKE, B.E., 1978. Nomenclature of amphiboles. *Mineral Mag.*, 42, 533-563.
- LINDSLEY, D.H., 1976. Experimental studies of oxide minerals. In: Rumble, D. (Ed), Oxide Minerals, Chapter 2. Mineral Soc. Amer. Washington.
- LINDSLEY, D.H. and DIXON, S.A., 1976. Diopside-enstatite equilibria at 850°C to 1400°C, 5 to 35 Kb. *Amer. Jour. Sci.* 276, 1285-1301.
- LOCK, N.P., 1974. Geological Report: Letseng-la-Terae. De Beers Consolidated Mines Ltd., (Internal Report).
- LOCK, N.P., 1975. Preliminary observations on points of differentiation of Letseng kimberlites. De Beers Consolidated Mines Ltd. (Internal Report).



- LOCK, N.P., 1976. The Letseng kimberlites. De Beers Consolidated Mines Ltd (Internal Report).
- LOCK, N.P. and DAWSON, J.B., 1980. Garnet-olivine reactions in the upper mantle: Evidence from peridotite xenoliths in the Letseng-la-Terae kimberlites, Lesotho. *Trans. R. Soc. Edinburgh, Earth Sci.*, 71, 47-53.
- MACGREGOR, I.D., 1965. Stability fields of spinel and garnet peridotite in the synthetic system  $MgO-CaO-Al_2O_3-SiO_2$ . *Annu.Rep. Dir. Geophys. Lab., Carnegie Inst.*, 64, 126-134.
- MACGREGOR, I.D., 1970. The effect of  $CaO$ ,  $Cr_2O_3$ ,  $Fe_2O_3$  and  $Al_2O_3$  on the stability of spinel and garnet peridotites. *Phys. Earth Planet Inter.* 3, 372-377.
- MACGREGOR, I.D., 1974. The system  $MgO-Al_2O_3-SiO_2$ : Solubility of  $Al_2O_3$  in enstatite for spinel and garnet peridotite compositions. *Amer. Mineral.*, 59, 110-119.
- MACGREGOR, I.D., 1975. Petrologic and thermal structure of the upper mantle beneath South Africa in the Cretaceous. *Phys. Chem. Earth.*, 9, 455-466.
- MCCALLISTER, R., 1979. The relationship between unmixing in subcalcic diopsides and the intrusion rate and P-T path of kimberlites. *Ext. Abstr. II, Kimberlite Symp, Cambridge.*
- MCCALLUM, M.E., 1976. An emplacement model to explain contrasting mineral assemblages in adjacent kimberlite pipes. *J. Geol.*, 84, 673-684.
- MENZIES, M. and RAMA MURTHY, V., 1980. Enriched mantle: Nd and Sr isotopes in diopsides from kimberlite nodules. *Nature*, 283, 634-636.
- MERCIER, J-C and CARTER, N.L., 1975. Pyroxene geotherms. *J. Geophys. Res.*, 80, 3349-3362.
- MERCIER, J-C and NICOLAS, A., 1975. Textures and fabrics of upper mantle peridotites as illustrated by xenoliths from basalts. *J. Petrol.*, 16, 454-487.

- MEYER, H.O.A. and SVISERO, D.P., 1975. Mineral inclusions in Brazilian diamonds. *Phys. Chem. Earth*, 9, 785-795.
- MITCHELL, R.H., 1970. Kimberlites and related rocks - A critical reappraisal. *J. Geol.*, 78, 686.
- MITCHELL, R.H., 1979. The alleged kimberlite-carbonatite relationship: Additional contrary mineralogical evidence. *Amer. Jour. Sci.*, 279, 570-589.
- MITCHELL, R.N. and BELL, K., 1976. Rare earth element geochemistry of potassic lavas from the Birunga and Toro-Ankole regions of Uganda, Africa. *Contrib. Mineral. Petrol.* 58, 293.
- MITCHELL, R.H. and BRUNFELT, A.O., 1975. Rare earth element geochemistry of kimberlite. *Phys. Chem. Earth, Oxford*, 9, 671-685.
- MITCHELL, R.H., CARSWELL, D.A. and BRUNFELT, A.O., 1973. Mineralogy and rare earth chemistry of an ilmenite-clinopyroxene xenolith from the Monastery Mine. In: Nixon, P.H. (Ed), Lesotho Kimberlites, 224-229. Maseru: Lesotho National Development Corporation.
- MITCHELL, R.H. and CROCKETT, J.H., 1971. The isotopic composition of strontium in some South African kimberlites. *Contrib. Mineral. Petrol.*, 30, 277-290.
- MORI, T. and GREEN, D.H., 1975. Pyroxenes in the system  $Mg_2Si_2O_6$ - $CaMgSi_2O_6$  at high pressures. *Earth Planet Sci. Lett.*, 26, 277-286.
- MORI, T. and GREEN, D.H., 1978. Laboratory duplication of phase equilibria observed in natural garnet lherzolites. *J. Geol.*, 86, 83-97.
- NAKAMURA, N., 1974. Determination of REE, Ba, Fe, Mg, Na and K in carbonaceous and ordinary chondrites. *Geochim. Cosmochim. Acta*, 38, 757-775.
- NIXON, P.H., 1960. A mineralogical and geochemical study of kimberlites and the associated xenoliths. Unpub. Ph.D. Thesis, Univ. Leeds.
- NIXON, P.H., 1973. Perspective. In: Nixon, P.H. (Ed), Lesotho Kimberlites, 300-311. Maseru: Lesotho National Development Corporation.

- NIXON, P.H. and BOYD, F.R., 1973. Petrogenesis of the granular and sheared ultrabasic nodule suite in kimberlite. In: Nixon, P.H. (Ed), Lesotho Kimberlites, 48-56. Maseru: Lesotho National Development Corporation.
- NIXON, P.H. and BOYD, F.R., 1973. The discrete nodule (megacryst) association in kimberlites from northern Lesotho. In: Nixon, P.H. (Ed), Lesotho Kimberlites, 67-75. Maseru: Lesotho National Development Corporation.
- NIXON, P.H., and BOYD, F.R., 1979. Garnet-bearing lherzolites and discrete nodule suites from the Malaita alnoite, Solomon Islands, S.W. Pacific, and their bearing on oceanic mantle composition and geotherm. In: Boyd, F.R. and Meyer, H.O.A. (Eds), The Mantle Sample: Inclusions in Kimberlites and other Volcanics, 400-423. American Geophysical Union, Washington.
- NIXON, P.H., VON KNORRING, O. and ROOKE, J.M., 1963. Kimberlites and associated inclusions of Basutoland: A mineralogical and geochemical study. *Am. Miner.*, 48, 1090-1132.
- NORRISH, K. and HUTTON, J.T., 1969. An accurate X-ray spectrographic method for the analysis of a wide range of geological samples. *Geochim. Cosmochim. Acta*, 33, 431-453.
- O'HARA, M.J., 1977. Thermal history of excavation of Archaean gneisses from the base of the continental crust. *J. Geol. Soc. London*, 134, 185-200.
- O'HARA, M.J., RICHARDSON, S.W. and WILSON, G., 1971. Garnet peridotite stability and occurrence in crust and mantle. *Contrib. Mineral. Petrol.*, 32, 48-68.
- O'HARA, M.J. and YODER, H.S., 1967. Formation and fractionation of basic magmas at high pressure. *Scott. Jour. Geol.*, 3, 67-117.
- O'NIONS, R.K., EVENSEN, N.M., HAMILTON, P.J. and CARTER, S.R., 1978. Melting of the mantle past and present: Isotope and trace element evidence. *Phil. Trans. R. Soc. London, A.*, 258, 547-559.

- O'NIONS, R.K., HAMILTON, P.J. and EVENSON, N.M., 1977. Variations in  $^{143}\text{Nd}/^{144}\text{Nd}$  and  $^{87}\text{Sr}/^{86}\text{Sr}$  ratios in oceanic basalts. *Earth Planet Sci. Lett.*, 34, 13-22.
- PANKHURST, R.J. and O'NIONS, R.K., 1973 Determination of Rb/Sr and  $^{87}\text{Sr}/^{86}\text{Sr}$  ratios of some standard rocks and evaluation of X-ray fluorescence spectrometry in Rb-Sr geochemistry. *Chem. Geol.*, 12, 127.
- PASTERIS, J.D., BOYD, F.R. and NIXON, P.H., 1979. The ilmenite association at the Frank Smith Mine, R.S.A. In: Boyd, F.R. and Meyer, H.O.A. (Eds), The Mantle Sample: Inclusions in Kimberlites and other Volcanics, 265-278. American Geophysical Union, Washington.
- PAUL, D.K., POTTS, P.J., GIBSON, I.L. and HARRIS, P.G., 1975. Rare earth abundances in Indian kimberlites. *Earth Planet Sci. Lett.*, 25, 151-158.
- PIKE, J.E.N. and SCHWARZMAN, E.C., 1977. Classification of textures in ultramafic xenoliths. *J. Geol.*, 85, 49-61.
- POWELL, J.L., HURLEY, P.M., and FAIRBAIRN, H.W., 1966. The strontium isotope composition and origin of carbonatites. In: Tuttle, O.F. and GITTINS, J. (Eds), Carbonatites, 365-378, Interscience.
- PRINZ, M., MANSON, D.V., HLAVA, P.F. and KEIL, K., 1975. Inclusions in diamonds: Garnet lherzolite and eclogite assemblages. *Phys. Chem. Earth*, 9, 797-815.
- RAHEIM, A. and GREEN, D.H., 1974. Experimental determination of the temperature and pressure dependence of the Fe-Mg partition coefficient for coexisting garnet and clinopyroxene. *Contrib. Mineral. Petrol.*, 48, 179-203.
- REID, A.M. and DAWSON, J.B., 1972. Olivine-garnet reaction in peridotites from Tanzania. *Lithos*, 5, 115-124.
- REYNOLDS, D.L., 1954. Fluidization as a geological process and its bearing on the problem of intrusive granite. *Amer. J. Sci.*, 252, 577-614.

- RICHARD, R., 1972. Final report of the photogeologist Diamond Exploration Project, Technical Report, No.2. Maseru: Department of Mines and Geology.
- RICHARD, P., SHIMIZU, N. and ALLEGRE, C., 1976.  $^{143}\text{Nd}/^{144}\text{Nd}$ , a natural tracer: An application to oceanic basalts. Earth Planet Sci. Lett., 31, 269.
- RINGWOOD, A.E., 1975. Composition and Petrology of the Earth's Mantle. McGraw-Hill, New York.
- ROBEY, J., 1979. Megacrysts from the Lekkerfontein kimberlite, north-central Cape, R.S.A. Ext. Abstr. II, Kimberlite Symp, Cambridge.
- ROBINSON, D.N., 1975. Magnetite-serpentine-calcite dykes at Permier Mine and aspects of their relationship to kimberlite and to carbonatite of alkali carbonatite complexes. Phys. Chem. Earth, 9, 61-70.
- ROGERS, N.W., 1977. Granulite xenoliths from Lesotho kimberlites and the composition of the lower continental crust. Nature, 270, 681-684.
- ROGERS, N.W., 1979. Trace elements in kimberlites and ultrabasic xenoliths. Ext. Abstr. II, Kimberlite Symp, Cambridge.
- ROGERS, N.W. and NIXON, P.H., 1975. Geochemistry of lower crustal granulite xenoliths from Lesotho kimberlites. 19th Ann. Rep. Res. Inst. Afr. Geol., Univ. Leeds, 38-41.
- ROLFE, D.G., 1973. The geology of the Kao kimberlite pipes. In: Nixon, P.H. (Ed), Lesotho Kimberlites, 101-106. Maseru: Lesotho National Development Corporation.
- RUMBLE, D., 1976. Oxides minerals in metamorphic rocks. In: Rumble, D. (Ed), Oxide Minerals, Chapter 3. Mineral Soc. Amer. Washington.
- RUSS, III, G.P., BURNETT, D.S., LINGENFELTER, R.E. and WASSERBURG, G.J., 1971. Neutron capture on  $^{149}\text{Sm}$  in Lunar samples. Earth Planet. Sci. Lett., 13, 53-60.

- SHEE, S.R. and GURNEY, J.J., 1979. The mineralogy of xenoliths from Orapa, Botswana. In: Boyd, F.R. and Meyer, H.O.A. (Eds), The Mantle Sample: Inclusions in Kimberlites and other Volcanics, 37-49. American Geophysical Union, Washington.
- SKINNER, E.M.W., 1976. Petrographic investigation. Satellite Pipe, Letseng-la-Terae. De Beers Consolidated Mines Ltd. (Unpublished Report).
- SKINNER, E.M.W., 1980. Petrographic examination of a relatively fresh inclusion of earlier generation kimberlite found in the K6 kimberlite, Letseng Main Pipe, Lesotho. De Beers Consolidated Mines Ltd. (Unpublished Report DBG/PI/80-2).
- SKINNER, E.M.W. and CLEMENT, C.R., 1979. Mineralogical classification of Southern African kimberlites. In: Boyd, F.R. and Meyer, H.O.A. (Eds) Kimberlites, Diatremes and Diamonds: Their Geology, Petrology and Geochemistry, 129-139. American Geophysical Union, Washington.
- SMITH, C.B., McCALLUM, M.E., COOPERSMITH, H.G. and EGGLE, D.H., 1979. Petrography, petrology and chemistry of kimberlite from the Colorado-Wyoming State Line, and Iron Mountain, Wyoming districts. Ext. Abstr. II, Int. Kimberlite Conf, Colorado.
- SMITH, D., 1977. The origin and interpretation of spinel-pyroxene clusters in peridotite. J. Geol. 85, 476-482.
- SMITH, J.V., BRENNESHOLTZ, R. and DAWSON, J.B., 1978. Chemistry of micas from kimberlites and xenoliths - I. Micaceous kimberlites. Geochim. Cosmochim. Acta, 42, 957-971.
- SMITH, J.V. and DAWSON, J.B., 1975. Chemistry of Ti-poor spinels, ilmenites and rutiles from peridotite and eclogite xenoliths. Phys. Chem. Earth, 9, 309-321.

- SMITH, J.V., HERVIG, R.L., ACKERMAN, D. and DAWSON, J.B., 1979. K, Rb and Ba in micas from kimberlite and peridotitic xenoliths and implications for origin of basaltic rocks. In: Boyd, F.R. and Meyer, H.O.A. (Eds) Kimberlites, Diatremes and Diamonds: Their Geology, Petrology and Geochemistry, 241-251. American Geophysical Union, Washington.
- SOBOLEV, N.V., LAVRENTEV, Yu G., POKHILENKO, N.P. and USOVA, L.V., 1973. Chrome-rich garnets from kimberlites of Yakutia and their paragenesis. Contrib. Mineral. Petrol., 40, 39-52.
- STEPHENS, W.E. and DAWSON, J.B., 1977. Statistical comparison between pyroxenes from kimberlites and their associated xenoliths. J. Geol., 85, 433-449.
- STOCKLEY, G.M., 1940. Geology of Basutoland. Geol. Mag., 77, 444-460.
- STOCKLEY, G.M., 1947. Report on the Geology of Basutoland. Maseru. Basutoland Government.
- TARNEY, J. and WINDLEY, B.F., 1977. Chemistry, thermal gradients and evolution of the lower continental crust. J. Geol. Soc. London, 134, 153-172.
- TARNEY, J. and WINDLEY, B.F., 1979. Continental growth, island arc accretion and the nature of the lower crust - A reply to S.R. Taylor and S.M. McLennan. J. Geol. Soc. London, 136, 501-504.
- TAYLOR, S.R. and McLENNAN, S.M., 1979. Discussion of 'Chemistry, thermal gradients and evolution of the lower continental crust', by J. Tarney and B.F. Windley. J. Geol. Soc. London, 136, 497-500.
- TURNER, F.J. and VERHOOGEN, J., 1960. Igneous and Metamorphic Petrology. McGraw Hill, New York.
- WAGNER, P.A., 1914. The Diamond Fields of Southern Africa. pp. 355. Struik, Cape Town.

- WEDEPOHL, K.H. and MURAMATSU, Y., 1979. The chemical composition of kimberlites compared with the average composition of three basaltic magma types. In: Boyd, F.R. and Meyer, H.O.A. (Eds), Kimberlites, Diatremes and Diamonds: Their Geology, Petrology and Geochemistry, 300-312. American Geophysical Union, Washington.
- WELLS, P.R.A., 1977. Pyroxene thermometry in simple and complex systems. *Contrib. Mineral. Petrol.*, 62, 129-139.
- WHITELOCK, T.K., 1973. The Monastery Mine kimberlite pipe. In Nixon, P.H. (Ed), Lesotho Kimberlites, 214-217. Lesotho National Development Corporation: Maseru.
- WHITELOCK, T.K., 1979. Letseng-la-Terai - the mine at the turn by the swamp on the roof of africa. *Optima*, 28, 120-136.
- WINKLER, H.G.F., 1967. Petrogenesis of metamorphic rocks. 2nd Edn. Berlin-Heidelberg - New York: Springer-Verlag.
- WOOD, B.J., 1974. Solubility of alumina in orthopyroxene coexisting with garnet. *Contrib. Mineral. Petrol.*, 46, 1-15.
- WOOD, B.J., 1977. The influence of  $\text{Cr}_2\text{O}_3$  on the relationship between spinel- and garnet-peridotites. *Ext. Abstr. II, Kimberlite Conf., Colorado*.
- WOOD, B.J. and BANNO, S., 1973. Garnet-orthopyroxene and orthopyroxene-clinopyroxene relationships in simple and complex systems. *Contrib. Mineral. Petrol.*, 42, 109-124.
- WYLLIE, P.J., 1977. Mantle fluid compositions buffered by carbonates in peridotite- $\text{CO}_2$ - $\text{H}_2\text{O}$ . *Jour. Geol.*, 85, 187-207.
- WYLLIE, P.J., 1979. Kimberlite magmas from the system peridotite- $\text{CO}_2$ - $\text{H}_2\text{O}$ . In: Boyd, F.R. and Meyer, H.O.A. (Eds) Kimberlites, Diatremes, and Diamonds: Their Geology, Petrology and Geochemistry, 319-329. American Geophysical Union, Washington.



WYLLIE, P.J., 1980. The origin of Kimberlite. Jour. Geophys.

Res. (in press).

WYLLIE, P.J. and HUANG, W.L., 1976. Carbonation and melting reactions in the system  $\text{CaO-MgO-SiO}_2\text{-CO}_2$  at mantle pressure with geophysical and petrological applications. Contrib. Mineral. Petrol., 54, 79-107.

## APPENDIX 1

### Underground Mapping Technique

Sample localities in the grid of underground tunnels in the main pipe were selected at 10 and 20 metre intervals (see Plate 1.7). At each locality a one metre square area of sidewall was thoroughly washed down.

In-situ observations included:

- (1) Estimation of the percentage abundance of the inclusion types ultra-basic, basement, sedimentary and lava (for +1 cm inclusions).
- (2) Observation and measurement of the size, alteration, shape, roundness and orientation of the ten largest inclusions of each type in the size ranges +10 cm and -10 +1 cm. Size was measured in centimetres. Alteration was recorded on a progressive scale 1-3. Shape was recorded according to the following coding:

1 = discoidal	2 = spheroidal
3 = rod	4 = bladed
5 = variform	

Roundness was recorded on a progressive scale of decreasing roundness 1-5 and orientation was measured in degrees from the vertical.

The rock 'classification' was that of C.R. Clement, but has since been superceded:

1 = kimberlite breccia
2 = basaltic kimberlite
3 = basaltic breccia kimberlite
4 = lamprophyric kimberlite

Hardness, weathering and alteration were each visually estimated on a progressive scale of 1-3.

Five hand specimen sized samples were taken at each locality for further study.

(3) The abundance of the kimberlitic minerals garnet and phlogopite were estimated on a progressive scale of 1-3 and the sizes (in mm) of the five largest measured.

(4) The roundness (see above) and the serpentinisation (on a scale 1-3) of olivine xenocrysts was recorded and the ten largest grains measured (in mm).

(5) Observations and measurements of the ten largest inclusions of each type were made as detailed above (except that no orientation could be measured).

Further measurements of mineral and inclusion abundances were made on polished slabs and in some cases point counting was carried out in thin section. These observations were all recorded on the accompanying (specimen) 'Letseng kimberlite description' form.





INCLUSIONS : LAVA

ABUNDANCE : UNDERGROUND + 1 cm  $\frac{23.6}{\dots}$  SLAB + 2 mm  $\frac{26.4}{\dots}$   
 THIN SECTION - 2mm ..... AVE.

410 cm (10 largest)	SIZE (cm)	24	10									17
	ALTERATION	2	2									2
	SHAPE	5	5									5
	ROUNDNESS	5	4									4.5
	ORIENTATION	36w	61w									
- 10 cm + 1 cm (10 largest)	SIZE (cm)	7	5	7	9	7	6	5	5	5	6	6.2
	ALTERATION	2	→									2
	SHAPE	5	4	5	5	4	5	5	5	5	5	5.0
	ROUNDNESS	4	4	4	5	4	4	3	3	3	3	3.7
	ORIENTATION	45W	98E	52W	58W	40W	49W	0	40W	19W	55W	
HAND SPECIMEN + 1 mm (10 largest)	SIZE (mm)	50	40	30	30	30	25	25	25	25	23	30.3
	ALTERATION	2	→									2
	SHAPE	5	5	5	5	2	5	5	2	2	5	5.2
	ROUNDNESS	3	3	3	3	2	3	4	3	3	3	3.0

Matrix 69.8 %  
 anthophyllite 0.0 %  
 garnet 0.5 %

## APPENDIX 2

### Brief Description of Thin Sections

#### Main Pipe Peridotites

- NLO01: Coarse textured garnet lherzolite, weakly deformed, some olivine neoblasts. Well developed garnet reaction corona. Secondary phlogopite.
- NLO03: Coarse textured garnet harzburgite, very weakly deformed. Moderately developed garnet reaction corona. Secondary phlogopite.
- NLO04: Coarse textured chromite harzburgite, very weakly deformed. Fingerprint spinel. Secondary phlogopite.
- NLO06: Coarse textured phlogopite garnet lherzolite, weakly deformed, some olivine neoblasts. Poorly developed garnet reaction corona. Secondary phlogopite.
- NLO07: Porphyroclastic textured phlogopite garnet lherzolite, strongly deformed, olivine, ortho- and clinopyroxene neoblasts. Garnet reaction near completion but obscured by secondary phlogopite (and clinopyroxene?)
- NLO08: Coarse textured chromite garnet harzburgite, very weakly deformed. Poorly developed garnet reaction corona. Secondary phlogopite.
- NLO09: Coarse textured phlogopite garnet lherzolite, weakly deformed, some olivine neoblasts. Moderately developed garnet reaction corona. Secondary phlogopite and clinopyroxene.
- NLO10: Coarse textured chromite harzburgite, weakly deformed, some olivine neoblasts. Secondary phlogopite.
- NLO11: Coarse textured phlogopite garnet lherzolite, very weakly deformed. Well developed garnet reaction corona. Secondary phlogopite.
- NLO12: Coarse textured garnet lherzolite, weakly deformed, rare orthopyroxene neoblasts. Moderately developed garnet reaction corona. Secondary phlogopite. N.B. Fe-rich assemblage.
- NLO13: Coarse textured garnet harzburgite, very weakly deformed. Poorly developed garnet reaction corona. Secondary phlogopite.

- NLO14: Coarse textured garnet harzburgite, weakly deformed, some olivine neoblasts. Poorly developed garnet reaction corona. Secondary phlogopite (and clinopyroxene?)
- NLO69: Coarse textured garnet harzburgite, weakly deformed, few olivine neoblasts. Poorly developed garnet reaction corona. Secondary phlogopite.
- NLO71: Coarse textured chromite harzburgite, weakly deformed, few olivine neoblasts.
- NLO72: Coarse textured garnet harzburgite, weakly deformed, few olivine neoblasts. Poorly developed garnet reaction corona. Secondary phlogopite.
- NLO73: Coarse textured garnet harzburgite, very weakly deformed. Well developed garnet reaction corona.
- NLO74: Coarse textured phlogopite garnet lherzolite, weakly deformed, few olivine neoblasts. Poorly developed garnet reaction corona. Secondary phlogopite.
- NLO75: Porphyroclastic textured garnet harzburgite, strongly deformed. Olivine and orthopyroxene neoblasts. Poorly developed garnet reaction corona. Secondary phlogopite.
- NLO76: Coarse textured garnet harzburgite, very weakly deformed. Poorly developed garnet reaction corona. Secondary phlogopite.
- NLO77: Coarse textured garnet lherzolite weakly deformed, few olivine neoblasts. Well developed garnet reaction corona. Secondary phlogopite. Pleochroic clinopyroxene.
- NLO80: Coarse textured garnet lherzolite, very weakly deformed. Well developed garnet reaction corona. Secondary phlogopite.
- NLO81: Coarse textured garnet lherzolite, very weakly deformed. Well developed garnet reaction corona.



- NLO82: Mosaic porphyroclastic (LAD) textured garnet harzburgite, very strongly deformed, olivine orthopyroxene and clinopyroxene neoblasts and disrupted garnet. Moderately developed garnet reaction corona. Secondary phlogopite. Kimberlite veinlet. Disrupted corona.
- NLO83: Coarse textured phlogopite garnet harzburgite, weakly deformed, olivine and orthopyroxene neoblasts. Well developed garnet reaction corona. Secondary phlogopite.
- NLO84: Coarse textured (garnet) lherzolite, undeformed. Garnet reaction complete. Secondary phlogopite. Melt (?) patches.
- NLO87: Phlogopite megacryst. Deformed single crystal.
- NL103: Coarse textured garnet harzburgite, very weakly deformed. Well developed garnet reaction corona. Secondary phlogopite.
- NL104: Coarse textured garnet lherzolite, weakly deformed, few olivine neoblasts. Well developed garnet reaction corona. Secondary phlogopite.
- NL105: Coarse textured chromite harzburgite, very weakly deformed. Possibly recovered granuloblastite.
- NL108: Texturally heterogeneous rock showing various aspects characteristic of coarse, porphyroclastic and granuloblastic textures. Garnet-Al spinel lherzolite. Narrow reaction corona to garnet. Kimberlite veinlet containing abundant phlogopite, euhedral and subhedral clinopyroxene and very small acicular clinopyroxene.
- NL113: Coarse textured garnet harzburgite, very weakly deformed. Moderately developed garnet reaction corona.
- NL115: Coarse textured garnet lherzolite, weakly deformed, few olivine neoblasts, tabular orthopyroxene. Well developed garnet reaction corona. Secondary phlogopite and clinopyroxene.
- NL117: Coarse textured chromite harzburgite very weakly deformed. Secondary phlogopite.

- NL124: Coarse textured chromite garnet lherzolite, weakly deformed, few olivine neoblasts. Garnet reaction complete. Secondary phlogopite.
- NL125: Coarse textured phlogopite garnet lherzolite. Undeformed. Moderately developed and garnet reaction corona. Secondary phlogopite.
- NL127: Coarse textured garnet lherzolite, very weakly deformed. Well developed garnet reaction corona. Secondary phlogopite and clinopyroxene.
- NL128: Coarse textured chromite garnet lherzolite, very weakly deformed. Poorly developed garnet reaction corona. Secondary phlogopite.
- NL130: Coarse textured phlogopite garnet lherzolite, weakly deformed. Moderately developed garnet reaction corona. Secondary phlogopite.
- NL137: Coarse textured chromite harzburgite, weakly deformed olivine.
- NL138: Coarse textured chromite harzburgite, weakly deformed olivine. Secondary phlogopite.
- NL141: Porphyroclastic textured garnet lherzolite, strongly deformed, olivine and orthopyroxene neoblasts. Well developed garnet reaction corona. Secondary phlogopite.
- NL142: Coarse textured phlogopite lherzolite, weakly deformed. Secondary phlogopite.
- NL143: Granuloblastic textured spinel harzburgite. Weakly deformed. Recovering to coarse texture.
- NL144: Coarse textured phlogopite garnet lherzolite, moderately deformed, few olivine neoblasts. Moderately developed garnet reaction corona. Secondary phlogopite.
- NL145: Coarse textured garnet lherzolite, weakly deformed. Well developed garnet reaction corona. Chrome-rich garnet. Secondary phlogopite.
- NL147: Coarse chromite harzburgite, weakly deformed. Secondary phlogopite.
- NL148: Granuloblastic spinel lherzolite, weakly deformed orthopyroxene. Strong tabular fabric.
- NL149: Coarse textured chromite harzburgite very weakly deformed. Secondary phlogopite.

- NL151: Porphyroclastic dunite. Coarse olivine strongly deformed, olivine neoblasts.
- NL152: Coarse textured phlogopite spinel (?) harzburgite, very weakly formed.
- NL153: Coarse textured phlogopite garnet lherzolite, very weakly deformed. Moderately developed garnet reaction corona. Secondary phlogopite.
- NL156: Coarse textured ilmenite (?) harzburgite, very weakly deformed.
- NL158: Coarse textured garnet lherzolite, very weakly deformed. Secondary phlogopite.
- NL163: Porphyroclastic textured garnet lherzolite, strongly deformed, olivine and orthopyroxene neoblasts. Garnet reaction almost complete. Secondary phlogopite.
- NL166: Coarse textured chromite garnet lherzolite, weakly deformed, few olivine neoblasts. Well developed garnet reaction corona. Secondary phlogopite and clinopyroxene.
- NL167: Coarse textured chromite garnet lherzolite, very weakly deformed. Poorly developed garnet reaction corona. Secondary phlogopite.
- NL169: Porphyroclastic textured garnet lherzolite, strongly deformed, olivine and orthopyroxene neoblasts. Secondary phlogopite.
- NL170: Fluidal mosaic porphyroclastic textured garnet lherzolite, very strongly deformed, olivine and orthopyroxene neoblasts. Poorly developed garnet reaction corona. Secondary phlogopite.
- NL171: Granuloblastic textured phlogopite spinel lherzolite. Some exsolution in clinopyroxene.
- NL173: Coarse textured phlogopite chromite harzburgite, very weakly deformed. Secondary phlogopite.
- NL176: Coarse textured chromite harzburgite, very weakly deformed. Some exsolution in clinopyroxene. Secondary phlogopite.
- NL180: Very coarse textured chromite dunite. Some secondary phlogopite.

- NL181: Coarse textured garnet harzburgite, weakly deformed, some olivine and orthopyroxene neoblasts. Well developed garnet reaction corona. Secondary phlogopite.
- NL184: Coarse textured chromite harzburgite, very weakly deformed. Secondary phlogopite.
- NL187: Coarse textured phlogopite garnet lherzolite, very weakly deformed. Poorly developed garnet reaction corona. Secondary mica. Relatively abundant calcite (probably secondary).
- NL189: Coarse textured phlogopite garnet harzburgite, weakly deformed, some olivine neoblasts. Well developed garnet reaction corona. Secondary phlogopite.
- NL195: Coarse textured garnet harzburgite, weakly deformed, some olivine neoblasts. Well developed garnet reaction corona. Secondary phlogopite and clinopyroxene.
- NL196: Coarse textured garnet harzburgite, very weakly deformed. Well developed garnet reaction corona. Secondary phlogopite.
- NL197: Coarse textured garnet lherzolite, very weakly deformed. Very well developed garnet reaction corona. Secondary clinopyroxene.
- NL200: Coarse textured chromite garnet harzburgite, weakly deformed, olivine neoblasts. Well developed garnet reaction corona. Secondary phlogopite and clinopyroxene.
- NL367: Porphyroclastic textured garnet lherzolite, moderately deformed, olivine neoblasts. Poorly developed garnet reaction corona. Secondary phlogopite.
- NL372: Coarse textured chromite lherzolite, very weakly deformed. Garnet reaction complete. Secondary phlogopite.
- NL373: Coarse textured chromite garnet harzburgite, moderately deformed, olivine and orthopyroxene neoblasts. Well developed garnet reaction corona. Secondary phlogopite.

- NL419: Coarse textured garnet lherzolite, very weakly deformed. Poorly developed garnet reaction corona. Secondary phlogopite.
- NL424: Coarse textured garnet lherzolite, very weakly deformed. Well developed garnet reaction corona.
- NL425: Coarse textured garnet lherzolite, very weakly deformed. Poorly developed garnet reaction corona. Secondary phlogopite.
- NL426: LAD mosaic porphyroclastic textured garnet lherzolite. Very strongly deformed, olivine, orthopyroxene and clinopyroxene neoblasts. Moderately developed garnet reaction corona. Disrupted garnet. Secondary phlogopite in kimberlite (?) veinlet.
- NL427: LAD mosaic porphyroclastic textured garnet lherzolite. Very strongly deformed, olivine, orthopyroxene and clinopyroxene neoblasts. Moderately developed reaction corona. Disrupted garnet. Secondary phlogopite.
- NL429: Coarse textured phlogopite garnet lherzolite, very weakly deformed. Poorly developed garnet reaction corona. Secondary phlogopite.
- NL430: Coarse textured spinel lherzolite, very weakly deformed. Exsolution in clinopyroxene. Recovering granuloblastite.
- NL431: Very coarse textured lherzolite, very weakly deformed. Garnet reaction complete. Secondary phlogopite and clinopyroxene.
- NL432: Coarse textured garnet lherzolite, very weakly deformed. Poorly developed garnet reaction corona. Secondary phlogopite.
- NL434: Coarse textured garnet lherzolite, very weakly deformed. Poorly developed garnet reaction corona. Secondary phlogopite.
- NL435: Coarse textured phlogopite garnet lherzolite, very weakly deformed. Well developed garnet reaction corona. Secondary phlogopite.
- NL436: Coarse textured chromite garnet lherzolite, very weakly deformed. Poorly developed garnet reaction corona. Secondary phlogopite. 'Spongy' clinopyroxene . Chromite inclusion in garnet.

- NL437: Coarse textured chromite harzburgite, weakly deformed. Secondary phlogopite. Recovered granulobastite (?).
- NL438: Coarse textured lherzolite, weakly deformed few olivine neoblasts. Abundant clinopyroxene(>10%).
- NL441: Porphyroclastic textured garnet lherzolite, strongly deformed, olivine and orthopyroxene neoblasts. Secondary phlogopite. Poorly developed garnet reaction corona.
- NL442: Coarse textured garnet harzburgite, weakly deformed, olivine and orthopyroxene neoblasts. Poorly developed garnet reaction corona. Secondary phlogopite.
- NL450: Coarse textured chromite lherzolite. Garnet reaction complete. Secondary phlogopite.
- NL451: Fluidal mosaic textured garnet harzburgite, very strongly deformed, abundant olivine and orthopyroxene neoblasts. Poorly developed garnet reaction corona. Secondary phlogopite.
- NL456: Coarse textured chromite harzburgite. Secondary phlogopite.
- NL461: Coarse textured chromite harzburgite, very weakly deformed. Secondary phlogopite and clinopyroxene together with acicular clinopyroxene in kimberlite (?) patches.
- NL466: Coarse textured chromite harzburgite. Garnet reaction complete.
- NL492: Coarse textured phlogopite garnet lherzolite, undeformed. Well developed garnet reaction corona. Secondary phlogopite.
- NL494: Fluidal mosaic porphyroclastic textured garnet lherzolite, very strongly deformed, olivine, orthopyroxene and clinopyroxene neoblasts abundant. Poorly developed garnet reaction corona.
- NL495: Fluidal mosaic porphyroclastic textured garnet lherzolite, very strongly deformed, olivine, orthopyroxene and clinopyroxene neoblasts abundant. Poorly developed garnet reaction corona. Secondary phlogopite.

- NL499: Porphyroclastic textured garnet lherzolite, strongly deformed, olivine, orthopyroxene and clinopyroxene neoblasts. Poorly developed garnet reaction corona.
- NL500: Granoblastic textured orthopyroxenite.
- NL518: Coarse textured pyroxenite. Clinopyroxene (and spinel) exsolution from orthopyroxene. Secondary phlogopite.
- NL519: Granuloblastic textured spinel lherzolite. Moderately deformed.
- NL521: Porphyroclastic textured garnet lherzolite, strongly deformed, olivine and orthopyroxene neoblasts abundant. Well developed garnet reaction corona. Garnet is unusually small and abundant.
- NL523: Coarse textured garnet lherzolite. Moderately developed garnet reaction corona. Secondary phlogopite.
- NL524: Coarse textured garnet lherzolite. Well developed garnet reaction corona. Secondary phlogopite.
- NL525: Garnet spinel lherzolite. Well developed garnet reaction corona. Abundant clinopyroxene. Texture is recovering to coarse. Spinel derived from reaction corona.
- NL527: Mosaic porphyroclastic textured garnet lherzolite, strongly deformed, olivine and orthopyroxene neoblasts. Moderately developed garnet reaction corona. Mosaic olivine recovering.
- NL528: Granuloblastic textured spinel garnet lherzolite. Contains 'pools' of reaction corona minerals and garnet showing remnant corona as well as discrete spinel grains.
- NL529: Orthopyroxene single crystal (>2 cm) with cross-cutting pyrope garnet veinlet.
- NL530: Porphyroclastic textured sub-calcic diopside megacryst.
- NL531: Coarse textured garnet clinopyroxenite. Poorly developed garnet reaction corona. Secondary phlogopite.

- NL535: Distinctive garnet clinopyroxenite (= eclogite ?). Rounded orange garnet in clinopyroxene single crystals (>1 cm). Garnets protrude from rounded surface.
- NL534: Coarse textured garnet lherzolite. Orthopyroxene and olivine crystals are unusually large. Clinopyroxene is weakly pleochroic, schiller structure and has a distribution suggestive of clinopyroxene rich band. Abundant secondary phlogopite (and clinopyroxene).
- NL535: Tabular granuloblastic textured spinel garnet lherzolite, weakly deformed, strong fabric. No remnant reaction corona on garnet of very irregular shape. Primary phlogopite and hornblende (?).
- NL537: Orthopyroxene single crystal (>2 cm) showing clinopyroxene exsolution.
- NL538: Coarse textured garnet clinopyroxenite. Distinct bright green garnet indicates chrome rich.
- BD1857: Coarse textured chromite lherzolite.
- BD1858: Mosaic porphyroclastic textured garnet harzburgite, strongly deformed olivine and orthopyroxene neoblasts. Well developed garnet reaction corona.
- BD1859: Coarse textured spinel lherzolite, weakly deformed. Recovering from granuloblastic texture.
- BD1860: Granuloblastic textured spinel harzburgite, very weakly deformed.
- BD1861: Coarse textured chromite harzburgite, very weakly deformed. Fingerprint spinel.
- BD1862: Coarse textured spinel lherzolite, very weakly deformed. Recovering from granuloblastic texture.
- BD1863: Coarse textured spinel lherzolite, very weakly deformed. Recovering from granuloblastic texture.
- BD1864: Coarse textured chromite harzburgite, very weakly deformed.



APPENDIX 3

Brief Description of Thin Sections

Satellite Pipe Peridotites

- NLO15: Coarse textured chromite lherzolite, very weakly deformed. Secondary phlogopite and clinopyroxene. Also acicular clinopyroxene in possible partial melt patches.
- NLO16: Coarse textured phlogopite chromite harzburgite, very weakly deformed. Secondary phlogopite.
- NLO17: Coarse textured chromite harzburgite, very weakly deformed. Clinopyroxene exsolution lamellae in orthopyroxene.
- NLO21: Mosaic porphyroclastic textured garnet lherzolite, strongly deformed olivine and orthopyroxene neoblasts. Well developed garnet reaction corona. 'Spongy' clinopyroxene.
- NLO22: Coarse textured chromite harzburgite moderately deformed, some olivine neoblasts. Secondary clinopyroxene.
- NLO23: Coarse textured dunite, very weakly deformed. Some chromite.
- NLO24: Coarse textured chromite lherzolite, very weakly deformed. Clinopyroxene exsolution lamellae in orthopyroxene.
- NLO25: Coarse textured chromite harzburgite, very weakly deformed.
- NLO26: Very coarse textured harzburgite, weakly deformed, some olivine neoblasts.
- NLO28: Porphyroclastic textured garnet lherzolite, strongly deformed, olivine and orthopyroxene neoblasts. Well developed garnet reaction corona. 'Spongy'clinopyroxene.
- NLO29: Coarse (recovered) textured spinel harzburgite, very weak deformation. Clinopyroxene exsolution lamellae in orthopyroxene.
- NLO38: Coarse textured garnet harzburgite, very weakly deformed. Well developed garnet reaction corona.
- NLO39: Porphyroclastic dunite.

- NOO45: Coarse textured chromite lherzolite, very weakly deformed.
- BD1869: Coarse textured chromite harzburgite, very weakly deformed.
- BD1870: Coarse textured chromite lherzolite. 'Spongy' clinopyroxene.
- BD1871: Coarse textured garnet lherzolite, very weakly deformed.
- Secondary phlogopite. Well developed garnet reaction corona.
- BD1872: Porphyroclastic textured garnet lherzolite, strongly deformed, olivine and orthopyroxene neoblasts. Well developed garnet reaction corona.
- BD1873: Porphyroclastic texture dunite.
- BD1874: Coarse textured chromite lherzolite, very weakly deformed. Fingerprint spinel.
- BD1875: Granuloblastic textured spinel lherzolite, very weakly deformed.
- BD1876: Coarse textured chromite harzburgite, very weakly deformed.
- BD1877: Coarse textured chromite harzburgite, very weakly deformed.
- BD1878: Granuloblastic textured spinel lherzolite, very weakly deformed.
- BD1879: Coarse textured chromite harzburgite, very weakly deformed.
- BD1880: Granuloblastic textured spinel lherzolite, very weakly deformed.
- BD1881: Coarse textured chromite harzburgite, very weakly deformed. Fingerprint spinel intergrown with amphibole (?).
- BD1884: Coarse textured chromite harzburgite, very weakly deformed. Fingerprint spinel.
- BD1885: Porphyroclastic textured dunite.
- BD1887: Porphyroclastic textured dunite.
- BD1892: Coarse textured chromite lherzolite, very weakly deformed. Secondary phlogopite.
- BD1893: Porphyroclastic textured garnet lherzolite, strongly deformed, olivine and orthopyroxene neoblasts. Poorly developed garnet reaction corona. 'Spongy' clinopyroxene.
- BD1894: Coarse textured garnet lherzolite, very weakly deformed. Poorly developed garnet reaction corona. 'Spongy' clinopyroxene.

- BD1895: Mosaic porphyroclastic textured garnet lherzolite, strongly deformed, olivine and orthopyroxene neoblasts. Very well developed garnet reaction corona. 'Spongy' clinopyroxene. Incipient melting (?) with acicular clinopyroxene.
- BD1896: Coarse textured garnet lherzolite, very weakly deformed. Well developed garnet reaction corona. Secondary phlogopite.
- BD1897: Porphyroclastic textured garnet lherzolite, strongly deformed, olivine and orthopyroxene neoblasts. Moderately developed garnet reaction corona.
- BD1902: Coarse textured chromite harzburgite, very weakly deformed.
- BD1908: Coarse textured garnet lherzolite, very weakly deformed. Well developed garnet reaction corona. Incipient melting (?) with acicular clinopyroxene.
- BD1909: Mosaic porphyroclastic textured garnet lherzolite, strongly deformed, olivine and orthopyroxene neoblasts. Moderately developed garnet reaction corona. 'Spongy' clinopyroxene.
- BD1912: Porphyroclastic textured garnet lherzolite, strongly deformed olivine and orthopyroxene neoblasts. Moderately developed garnet reaction corona.
- BD1913: Coarse textured chromite harzburgite, very weakly deformed.
- BD1914: Coarse textured garnet harzburgite, very weakly deformed. Moderately developed garnet reaction corona.
- BD1917: Coarse textured chromite harzburgite, very weakly deformed. Fingerprint spinel.
- BD1919: Coarse textured chromite harzburgite, very weakly deformed.
- BD1920: Coarse textured chromite lherzolite, very weakly deformed.

APPENDIX 4

Analyses of Minerals from Main Pipe Peridotites

Compositions were measured using a Cambridge Instruments Microscan V electron microprobe in the wavelength dispersive mode.

The ferric ( $\text{Fe}^{3+}$ ) component of the oxides analysed was estimated by the method of Finger (1972).

GT = Garnet  
OP = Orthopyroxene  
CP = Clinopyroxene  
OL = Olivine  
SP = Chromite/Spinel

NL001	GT	OP	CP	OL	NL006	GT	OP	CP	OL
SiO2	41.52	57.63	54.57	41.18		41.65	58.19	54.67	41.09
TiO2	0.07	0.06	0.10	0.03		0.08	0.01	0.05	0.00
Al2O3	18.91	0.80	2.54	0.03		19.25	0.72	1.75	0.05
Cr2O3	6.71	0.42	2.65	0.01		6.52	0.33	1.54	0.07
Fe2O3	0.00	0.00	0.00	0.00		0.00	0.00	0.00	0.00
FeO	6.40	4.36	2.12	7.12		6.83	4.67	2.33	7.72
MnO	0.39	0.12	0.10	0.10		0.41	0.12	0.07	0.10
MgO	20.42	35.85	16.23	51.62		19.63	35.77	17.15	51.24
CaO	5.70	0.45	19.00	0.03		6.45	0.48	20.34	0.04
Na2O	0.04	0.11	2.38	0.02		0.03	0.12	1.69	0.03
NiO	0.00	0.11	0.03	0.42		0.01	0.13	0.01	0.39
Total	100.15	99.91	99.73	100.56		100.87	100.54	99.61	100.74
Si	2.99	1.97	1.98	0.99		2.98	1.98	1.98	0.99
Ti	0.00	0.00	0.00	0.00		0.00	0.00	0.00	0.00
Al	1.60	0.03	0.11	0.00		1.63	0.03	0.07	0.00
Cr	0.38	0.01	0.08	0.00		0.37	0.01	0.04	0.00
Fe3	0.00	0.00	0.00	0.00		0.00	0.00	0.00	0.00
Fe2	0.39	0.13	0.06	0.14		0.41	0.13	0.07	0.16
Mn	0.02	0.00	0.00	0.00		0.02	0.00	0.00	0.00
Mg	2.19	1.83	0.88	1.86		2.10	1.82	0.93	1.84
Ca	0.44	0.02	0.74	0.00		0.50	0.02	0.79	0.00
Na	0.01	0.01	0.17	0.00		0.00	0.01	0.12	0.00
Ni	0.00	0.00	0.00	0.01		0.00	0.00	0.00	0.01
Total	8.02	4.01	4.01	3.01		8.02	4.00	4.01	3.01
Ca/(Ca+Mg)			0.457					0.460	
Mg/(Mg+Fe)	0.850	0.936	0.932	92.82		0.837	0.932	0.929	92.21
Cr/(Cr+Al)									
Ca#	14.43	0.84	39.89			16.35	0.88	41.39	
Mg#	71.96	92.16	47.39			69.17	91.66	48.55	
Fe#	12.66	6.30	3.47			13.51	6.72	3.70	

NLO07	GT	OP	CP	OL	NLO12	GT	OP	CP	OL
SiO2	41.41	57.58	54.27	41.17		42.03	57.47	54.99	40.77
TiO2	0.32	0.13	0.31	0.01		0.34	0.13	0.31	0.03
Al2O3	18.79	0.81	2.42	0.03		21.18	0.82	2.75	0.06
Cr2O3	6.39	0.46	3.13	0.03		2.77	0.22	1.32	0.00
Fe2O3	0.00	0.00	0.00	0.00		0.00	0.00	0.00	0.00
FeO	7.12	4.90	2.30	7.96		9.78	6.85	3.61	11.36
MnO	0.47	0.13	0.12	0.11		0.41	0.14	0.10	0.13
MgO	20.10	35.26	15.68	50.55		19.40	33.94	15.85	48.10
CaO	5.51	0.50	18.65	0.01		4.73	0.55	18.49	0.05
Na2O	0.08	0.16	2.55	0.02		0.07	0.18	2.41	0.04
NiO	0.00	0.13	0.04	0.38		0.04	0.14	0.08	0.52
Total	100.21	100.07	99.46	100.27		100.75	100.46	99.92	101.06
Si	2.99	1.98	1.98	1.00		3.00	1.98	1.99	1.00
Ti	0.02	0.00	0.01	0.00		0.02	0.00	0.01	0.00
Al	1.60	0.03	0.10	0.00		1.78	0.03	0.12	0.00
Cr	0.36	0.01	0.09	0.00		0.16	0.01	0.04	0.00
Fe3	0.00	0.00	0.00	0.00		0.00	0.00	0.00	0.00
Fe2	0.43	0.14	0.07	0.16		0.58	0.20	0.11	0.23
Mn	0.03	0.00	0.00	0.00		0.02	0.00	0.00	0.00
Mg	2.16	1.80	0.85	1.83		2.07	1.74	0.85	1.75
Ca	0.43	0.02	0.73	0.00		0.36	0.02	0.72	0.00
Na	0.01	0.01	0.18	0.00		0.01	0.01	0.17	0.00
Ni	0.00	0.00	0.00	0.01		0.00	0.00	0.00	0.01
Total	8.02	4.00	4.01	3.00		8.01	4.00	4.01	3.00
Ca/(Ca+Mg)			0.461					0.456	
Mg/(Mg+Fe)	0.834	0.928	0.924	%Fo 91.88		0.779	0.898	0.887	%Fo 88.30
Cr/(Cr+Al)									
Ca%	13.92	0.94	39.68			11.87	1.03	38.62	
Mg%	70.69	91.07	46.42			67.75	88.00	46.07	
Fe%	14.06	7.11	3.83			19.18	9.97	5.89	

NL103	GT	OP	CP	OP	NL104	GT	OP	CP	OL
SiO2	42.03	57.92	54.89	41.33		41.45	57.64	54.44	41.14
TiO2	0.00	0.00	0.00	0.01		0.07	0.02	0.08	0.00
Al2O3	19.75	0.80	2.27	0.05		19.15	0.77	2.42	0.10
Cr2O3	5.90	0.32	1.80	0.02		6.43	0.37	1.87	0.04
Fe2O3	0.00	0.00	0.00	0.00		0.00	0.00	0.00	0.00
FeO	6.63	4.49	2.27	7.41		6.92	4.78	2.33	7.70
MnO	0.38	0.10	0.08	0.10		0.41	0.10	0.10	0.12
MgO	20.10	35.63	16.79	51.28		19.67	35.62	16.55	50.79
CaO	6.08	0.51	19.70	0.01		6.01	0.49	19.46	0.04
Na2O	0.01	0.13	2.03	0.01		0.05	0.13	2.16	0.04
NiO	0.00	0.11	0.09	0.50		0.02	0.15	0.07	0.40
Total	100.88	100.01	99.93	100.71		100.17	100.07	99.49	100.36
Si	3.00	1.98	1.98	1.00		2.99	1.98	1.98	1.00
Ti	0.00	0.00	0.00	0.00		0.00	0.00	0.00	0.00
Al	1.66	0.03	0.10	0.00		1.63	0.03	0.10	0.00
Cr	0.33	0.01	0.05	0.00		0.37	0.01	0.05	0.00
Fe3	0.00	0.00	0.00	0.00		0.00	0.00	0.00	0.00
Fe2	0.40	0.13	0.07	0.15		0.42	0.14	0.07	0.16
Mn	0.02	0.00	0.00	0.00		0.03	0.00	0.00	0.00
Mn	2.13	1.82	0.90	1.84		2.11	1.82	0.90	1.83
Ca	0.46	0.02	0.76	0.00		0.46	0.02	0.76	0.00
Na	0.00	0.01	0.14	0.00		0.01	0.01	0.15	0.00
Ni	0.00	0.00	0.00	0.01		0.00	0.00	0.00	0.01
Total	8.01	4.00	4.01	3.00		8.01	4.01	4.02	3.00
Ca/(Ca+Mg)	0.844	0.934	0.929	%Fo		0.835	0.930	0.458	%Fo
Mg/(Mg+Fe)								0.927	92.16
Cf/(Cr+Al)									
Ca%	15.37	0.95	40.50			15.32	0.90	40.27	
Mg%	70.72	91.84	48.02			69.78	91.42	47.62	
Fe%	13.10	6.49	3.64			13.78	6.88	3.76	

NL128	GT	OP	CP	OL	SP	NL141	GT	OP	CP	OL
SiO2	42.04	57.73	54.44	41.22	0.00		42.01	57.36	59.19	41.24
TiO2	0.07	0.01	0.03	0.00	0.43		0.65	0.25	0.46	0.09
Al2O3	21.68	1.02	2.05	0.05	15.47		19.49	0.95	2.37	0.00
Cr2O3	3.17	0.35	1.33	0.00	42.40		4.88	0.44	2.00	0.05
Fe2O3	0.00	0.00	0.00	0.00	3.79		0.00	0.00	0.00	0.00
FeO	7.61	4.67	1.66	7.45	14.65		6.63	4.83	2.90	7.98
MnO	0.47	0.13	0.08	0.09	0.66		0.31	0.10	0.12	0.07
MgO	20.17	35.83	16.62	50.99	12.73		21.51	34.82	17.98	50.57
CaO	5.43	0.26	21.98	0.00	0.00		4.91	0.86	17.41	0.07
Na2O	0.01	0.08	1.42	0.01	0.00		0.10	0.27	1.87	0.04
NiO	0.01	0.12	0.04	0.44	0.14		0.03	0.12	0.05	0.41
Total	100.66	100.20	99.65	100.25	100.27		100.52	100.00	99.35	100.58
Si	2.99	1.97	1.98	1.00	0.00		2.99	1.97	1.97	1.00
Ti	0.00	0.00	0.00	0.00	0.01		0.03	0.01	0.01	0.00
Al	1.81	0.04	0.09	0.00	0.58		1.64	0.04	0.10	0.00
Cr	0.18	0.01	0.04	0.00	1.31		0.27	0.01	0.06	0.00
Fe <sup>3</sup>	0.00	0.00	0.00	0.00	0.09		0.00	0.00	0.00	0.00
Fe <sup>2</sup>	0.45	0.13	0.05	0.15	0.39		0.39	0.14	0.09	0.16
Mn	0.03	0.00	0.00	0.00	0.02		0.02	0.00	0.00	0.00
Mg	2.13	1.82	0.90	1.84	0.60		2.28	1.78	0.97	1.82
Ca	0.41	0.01	0.85	0.00	0.00		0.37	0.03	0.68	0.00
Na	0.00	0.01	0.10	0.00	0.00		0.01	0.02	0.13	0.00
Ni	0.00	0.00	0.00	0.01	0.00		0.00	0.00	0.00	0.01
Total	8.00	3.99	4.01	3.00	3.00		8.00	4.00	4.01	2.99
Ca/(Ca+Mg)			0.487						0.410	
Mg/(Mg+Fe)	0.825	0.932	0.947	%Fo	92.42		0.854	0.927	0.971	%Fo
Cr/(Cr+Al)					0.694					
Ca‡	13.65	0.49	47.32				12.20	1.63	38.88	
Mg‡	70.49	92.54	49.77				74.35	91.14	55.85	
Fe‡	15.86	6.97	2.92				13.45	7.24	5.27	





NL148	OP	CP	OL	SP	NL153	GT	OP	CP	OL
SiO2	54.95	53.03		0.00		42.37	56.79	53.81	41.42
TiO2	0.05	0.11		0.00		0.07	0.05	0.07	0.02
Al2O3	3.24	4.20		53.60		20.36	0.88	3.09	0.02
Cr2O3	0.30	0.73		14.04		5.83	0.50	3.66	0.02
Fe2O3	0.00	0.00		1.92		0.00	0.00	0.00	0.00
FeO	6.39	2.05		10.53		6.47	4.26	2.13	6.99
MnO	0.17	0.06		0.24		0.40	0.12	0.13	0.08
MgO	33.32	15.77		19.22		21.47	36.23	15.44	51.88
CaO	0.41	22.62		0.00		4.72	0.44	17.64	0.02
Na2O	0.03	1.15		0.00		0.06	0.19	3.13	0.04
NiO	0.10	0.03		0.31		0.03	0.14	0.06	0.38
Total	98.96	99.75		99.86		101.77	99.60	99.16	100.89
Si	1.92	1.93		0.00		2.98	1.96	1.96	1.00
Ti	0.00	0.00		0.00		0.00	0.00	0.00	0.00
Al	0.13	0.18		1.67		1.69	0.04	0.13	0.00
Cr	0.01	0.02		0.29		0.32	0.01	0.11	0.00
Fe3	0.00	0.00		0.04		0.00	0.00	0.00	0.00
Fe2	0.19	0.06		0.23		0.38	0.12	0.06	0.14
Mn	0.01	0.00		0.01		0.02	0.00	0.00	0.00
Mn	1.73	0.85		0.76		2.25	1.86	0.84	1.86
Ca	0.02	0.88		0.00		0.36	0.02	0.69	0.00
Na	0.00	0.08		0.00		0.01	0.01	0.22	0.00
Ni	0.00	0.00		0.01		0.00	0.00	0.00	0.01
Total	4.01	4.00		3.01		8.01	4.02	4.03	3.00
Ca/(Ca+Mg)		0.508						0.451	
Mg/(Mg+Fe)	0.903	0.932				0.855	0.938	0.928	%Fo 92.97
Cr/(Cr+Al)				0.149					
Ca%	0.79	48.96				11.77	0.80	37.87	
Mg%	89.34	47.48				74.51	92.14	46.09	
Fe%	9.87	3.57				12.61	6.08	3.57	

NL162	OP	CP	OL	SP	NL163	GT	OP	CP	OL
SiO2	55.98	53.41	0.00	0.00			57.65	54.22	41.28
TiO2	0.03	0.03	0.00	0.00			0.00	0.07	0.01
Al2O3	3.31	3.40	49.15	0.06			0.69	1.34	0.06
Cr2O3	0.39	0.73	19.95	0.00			0.33	1.62	0.00
Fe2O3	0.00	0.00	2.07	0.00			0.00	0.00	0.00
FeO	5.93	2.07	10.93	0.00			4.68	2.13	7.75
MnO	0.13	0.10	0.30	0.00			0.11	0.09	0.08
MgO	33.78	16.60	18.51	0.00			35.57	17.45	50.94
CaO	0.49	22.76	0.00	0.00			0.51	20.81	0.05
Na2O	0.01	0.71	0.02	0.00			0.07	1.26	0.05
NiO	0.09	0.03	0.23	0.00			0.12	0.09	0.44
Total	100.14	99.84	100.16				99.75	99.08	100.66
Si	1.93	1.94	0.00	0.00			1.98	1.98	1.00
Ti	0.00	0.00	0.00	0.00			0.00	0.00	0.00
Al	0.13	0.15	1.56	0.06			0.03	0.06	0.00
Cr	0.01	0.02	0.40	0.00			0.01	0.05	0.00
Fe3	0.00	0.00	0.04	0.00			0.00	0.00	0.00
Fe2	0.17	0.06	0.25	0.00			0.13	0.06	0.16
Mn	0.00	0.00	0.01	0.00			0.00	0.00	0.00
Mg	1.73	0.90	0.74	0.00			1.82	0.95	1.83
Ca	0.02	0.88	0.00	0.00			0.02	0.81	0.00
Na	0.00	0.05	0.00	0.00			0.00	0.09	0.00
Ni	0.00	0.00	0.00	0.00			0.00	0.00	0.01
Total	3.99	4.00	3.00				4.00	4.01	3.00
Ca/(Ca+Mg)		0.496					0.462		
Mg/(Mg+Fe)	0.910	0.935	0.206				0.931	0.936	92.13
Cr/(Cr+Al)									
Ca%	0.94	47.87					0.95	42.34	
Mg%	90.00	48.57					91.69	49.37	
Fe%	9.06	3.56					6.77	3.38	

NL166	GT	OP	CP	OL	NL169	GT	OP	CP	OL
SiO2	41.48	57.63	53.91	40.90		42.25	57.60	54.72	41.19
TiO2	0.13	0.09	0.28	0.03		0.36	0.14	0.36	0.01
Al2O3	20.62	0.88	2.66	0.02		20.39	0.96	2.15	0.08
Cr2O3	4.32	0.29	2.02	0.01		4.11	0.35	1.48	0.06
Fe2O3	0.00	0.00	0.00	0.00		0.00	0.00	0.00	0.00
FeO	8.12	4.78	1.97	8.21		6.14	4.59	2.71	7.64
MnO	0.53	0.11	0.09	0.09		0.30	0.12	0.09	0.10
MgO	19.67	35.58	15.71	50.61		21.98	35.14	18.34	51.07
CaO	5.47	0.27	20.29	0.01		4.85	0.93	17.98	0.06
Na2O	0.04	0.09	2.22	0.01		0.08	0.20	1.79	0.08
NiO	0.01	0.09	0.07	0.44		0.00	0.13	0.05	0.37
Total	100.37	99.83	99.22	100.33		100.45	100.14	99.69	100.66
Si	2.98	1.98	1.97	0.99		2.99	1.97	1.97	1.00
Ti	0.01	0.00	0.01	0.00		0.02	0.00	0.01	0.00
Al	1.74	0.04	0.11	0.00		1.70	0.04	0.09	0.00
Cr	0.24	0.01	0.06	0.00		0.23	0.01	0.04	0.00
Fe3	0.00	0.00	0.00	0.00		0.00	0.00	0.00	0.00
Fe2	0.49	0.14	0.06	0.17		0.36	0.13	0.08	0.15
Mn	0.03	0.00	0.00	0.00		0.02	0.00	0.00	0.00
Mg	2.10	1.82	0.85	1.83		2.32	1.79	0.99	1.84
Ca	0.42	0.01	0.79	0.00		0.37	0.03	0.69	0.00
Na	0.01	0.01	0.16	0.00		0.01	0.01	0.13	0.00
Ni	0.00	0.00	0.00	0.01		0.00	0.00	0.00	0.01
Total	8.02	4.00	4.02	3.01		8.03	4.01	4.01	3.00
Ca/(Ca+Mg)			0.481					0.413	
Mg/(Mg+Fe)		0.930	0.934	91.65		0.864	0.932	0.923	92.26
Cr/(Cr+Al)									
Ca%	13.79	0.51	42.44			11.94	1.72	36.72	
Mg%	68.98	91.96	45.70			75.31	90.60	52.10	
Fe%	15.98	6.93	3.22			11.81	6.64	4.33	

NL171	OP	CP	OL	SP	NL197	GT	OP	CP	OL
SiO2	55.64	52.77	40.86	0.00		41.73	58.35	55.22	41.49
TiO2	0.03	0.13	0.01	0.03		0.07	0.03	0.11	0.02
Al2O3	3.33	3.99	0.03	48.52		19.03	0.69	2.14	0.04
Cr2O3	0.42	0.92	0.03	19.24		5.03	0.26	1.70	0.02
Fe2O3	0.00	0.00	0.00	2.25		0.00	0.00	0.00	0.00
FeO	6.01	1.99	9.13	10.89		6.49	4.38	2.26	7.28
MnO	0.13	0.07	0.13	0.29		0.33	0.10	0.09	0.06
MgO	33.91	15.89	50.06	18.50		20.66	35.71	16.42	51.06
CaO	0.36	23.57	0.00	0.00		5.39	0.50	19.43	0.01
Na2O	0.05	0.80	0.02	0.00		0.04	0.16	2.20	0.03
NiO	0.11	0.04	0.40	0.22		0.00	0.09	0.09	0.44
Total	99.99	100.17	100.68	99.95		98.76	100.28	99.66	100.45
Si	1.92	1.92	0.99	0.00		3.03	1.99	2.00	1.00
Ti	0.00	0.00	0.00	0.00		0.00	0.00	0.00	0.00
Al	0.14	0.17	0.00	1.54		1.63	0.03	0.09	0.00
Cr	0.01	0.03	0.00	0.41		0.29	0.01	0.05	0.00
Fe3	0.00	0.00	0.00	0.05		0.00	0.00	0.00	0.00
Fe2	0.17	0.06	0.19	0.25		0.39	0.12	0.07	0.15
Mn	0.00	0.00	0.00	0.01		0.02	0.00	0.00	0.00
Mg	1.74	0.86	1.81	0.74		2.23	1.81	0.89	1.84
Ca	0.01	0.92	0.00	0.00		0.42	0.02	0.75	0.00
Na	0.00	0.06	0.00	0.00		0.01	0.01	0.15	0.00
Ni	0.00	0.00	0.01	0.00		0.00	0.00	0.00	0.01
Total	3.99	4.02	3.00	3.00		8.01	4.00	4.01	3.00
Ca/(Ca+Mg)		0.516						0.460	
Mg/(Mg+Fe)	0.910	0.934	%Fo	0.210		0.850	0.936	0.928	%Fo
Cr/(Cr+Al)			90.71						92.59
Ca%	0.68	49.85				13.64	0.93	40.35	
Mg%	90.16	46.74				72.71	91.95	47.44	
Fe%	9.16	3.40				12.82	6.33	3.67	

NL426	GT	OP	CP	OL	NL427	GT	OP	CP	OL
SiO2	42.05	57.52	54.49	41.09		41.70	57.66	54.47	40.84
TiO2	0.10	0.09	0.29	0.04		0.11	0.07	0.26	0.04
Al2O3	19.79	0.84	2.65	0.06		19.76	0.83	2.58	0.03
Cr2O3	5.47	0.36	2.08	0.03		5.48	0.32	1.98	0.02
Fe2O3	0.00	0.00	0.00	0.00		0.00	0.00	0.00	0.00
FeO	6.81	4.83	2.45	8.02		6.69	4.66	2.42	7.44
MnO	0.40	0.12	0.09	0.10		0.39	0.11	0.09	0.10
MgO	20.45	35.24	16.34	50.85		20.40	35.43	16.51	50.86
CaO	5.49	0.54	18.84	0.04		5.58	0.58	18.89	0.04
Na2O	0.07	0.16	2.18	0.05		0.05	0.16	2.22	0.03
NiO	0.02	0.12	0.05	0.44		0.00	0.14	0.11	0.44
Total	100.66	99.82	99.47	100.71		100.15	99.95	99.52	99.84
Si	3.00	1.98	1.98	0.99		2.99	1.98	1.98	0.99
Ti	0.01	0.00	0.01	0.00		0.01	0.00	0.01	0.00
Al	1.66	0.03	0.11	0.00		1.67	0.03	0.11	0.00
Cr	0.31	0.01	0.06	0.00		0.31	0.01	0.06	0.00
Fe3	0.00	0.00	0.00	0.00		0.00	0.00	0.00	0.00
Fe2	0.41	0.14	0.07	0.16		0.40	0.13	0.07	0.15
Mn	0.02	0.00	0.00	0.00		0.02	0.00	0.00	0.00
Mg	2.17	1.80	0.88	1.83		2.18	1.81	0.89	1.84
Ca	0.42	0.02	0.73	0.00		0.43	0.02	0.73	0.00
Na	0.01	0.01	0.15	0.00		0.01	0.01	0.16	0.00
Ni	0.00	0.00	0.00	0.01		0.00	0.00	0.00	0.00
Total	8.01	4.00	4.01	3.01		8.02	4.00	4.01	3.01
Ca/(Ca+Mg)			0.453					0.451	
Mg/(Mg+Fe)	0.843	0.929	0.922	91.86		0.845	0.931	0.924	92.41
Cr/(Cr+Al)									
Ca%	13.83	1.01	39.64			14.10	1.07	39.42	
Mg%	71.61	91.11	47.80			71.71	91.30	47.94	
Fe%	13.38	7.00	4.03			13.19	6.73	3.94	

NL426		GT	OP	CP	OL	NL427	GT	OP	CP	OL
SiO2	42.05	57.52	54.49	41.09			41.70	57.66	54.47	40.84
TiO2	0.10	0.09	0.29	0.04			0.11	0.07	0.26	0.04
Al2O3	19.79	0.84	2.65	0.06			19.76	0.83	2.58	0.03
Cr2O3	5.47	0.36	2.08	0.03			5.48	0.32	1.98	0.02
Fe2O3	0.00	0.00	0.00	0.00			0.00	0.00	0.00	0.00
FeO	6.81	4.83	2.45	8.02			6.69	4.66	2.42	7.44
MnO	0.40	0.12	0.09	0.10			0.39	0.11	0.09	0.10
MgO	20.45	35.24	16.34	50.85			20.40	35.43	16.51	50.86
CaO	5.49	0.54	18.84	0.04			5.58	0.58	18.89	0.04
Na2O	0.07	0.16	2.18	0.05			0.05	0.16	2.22	0.03
NiO	0.02	0.12	0.05	0.44			0.00	0.14	0.11	0.44
Total	100.66	99.82	99.47	100.71			100.15	99.95	99.52	99.84
Si	3.00	1.98	1.98	0.99			2.99	1.98	1.98	0.99
Ti	0.01	0.00	0.01	0.00			0.01	0.00	0.01	0.00
Al	1.66	0.03	0.11	0.00			1.67	0.03	0.11	0.00
Cr	0.31	0.01	0.06	0.00			0.31	0.01	0.06	0.00
Fe3	0.00	0.00	0.00	0.00			0.00	0.00	0.00	0.00
Fe2	0.41	0.14	0.07	0.16			0.40	0.13	0.07	0.15
Mn	0.02	0.00	0.00	0.00			0.02	0.00	0.00	0.00
Mg	2.17	1.80	0.88	1.83			2.18	1.81	0.89	1.84
Ca	0.42	0.02	0.73	0.00			0.43	0.02	0.73	0.00
Na	0.01	0.01	0.15	0.00			0.01	0.01	0.16	0.00
Ni	0.00	0.00	0.00	0.01			0.00	0.00	0.00	0.00
Total	8.01	4.00	4.01	3.01			8.02	4.00	4.01	3.01
Ca/(Ca+Mg)			0.453						0.451	
Mg/(Mg+Fe)		0.843	0.929	%Fo	91.86		0.845	0.931	0.924	%Fo
Cr/(Cr+Al)										
Ca%	13.83	1.01	39.64				14.10	1.07	39.42	
Mg%	71.61	91.11	47.80				71.71	91.30	47.94	
Fe%	13.38	7.00	4.03				13.19	6.73	3.94	

NL441	GT	OP	CP	OL	NL492	GT	OP	CP	OL
SiO2	41.63	57.84	54.46	41.25		41.98	57.55	54.36	41.05
TiO2	0.09	0.01	0.04	0.03		0.24	0.05	0.12	0.05
Al2O3	19.14	0.83	2.42	0.06		20.88	0.79	2.12	0.04
Cr2O3	6.47	0.39	2.48	0.01		3.84	0.23	1.37	0.04
Fe2O3	0.00	0.00	0.00	0.00		0.00	0.00	0.00	0.00
FeO	6.36	4.20	2.11	6.81		6.98	4.67	2.18	7.76
MnO	0.37	0.12	0.11	0.07		0.36	0.09	0.11	0.08
MgO	20.97	35.81	16.39	51.64		20.85	35.60	16.98	50.88
CaO	5.32	0.49	18.78	0.04		5.14	0.48	20.13	0.01
Na2O	0.03	0.14	2.33	0.03		0.08	0.11	1.71	0.01
NiO	0.00	0.09	0.06	0.44		0.02	0.10	0.01	0.40
Total	100.38	99.91	99.18	100.37		100.36	99.66	99.08	100.27
Si	2.98	1.98	1.98	1.00		2.99	1.98	1.98	1.00
Ti	0.00	0.00	0.00	0.00		0.01	0.00	0.00	0.00
Al	1.62	0.03	0.10	0.00		1.75	0.03	0.09	0.00
Cr	0.37	0.01	0.07	0.00		0.22	0.01	0.04	0.00
Fe3	0.00	0.00	0.00	0.00		0.00	0.00	0.00	0.00
Fe2	0.38	0.12	0.06	0.14		0.42	0.13	0.07	0.16
Mn	0.02	0.00	0.00	0.00		0.02	0.00	0.00	0.00
Mg	2.24	1.83	0.89	1.86		2.21	1.82	0.92	1.84
Ca	0.41	0.02	0.73	0.00		0.39	0.02	0.79	0.00
Na	0.00	0.01	0.16	0.00		0.01	0.01	0.12	0.00
Ni	0.00	0.00	0.00	0.01		0.00	0.00	0.00	0.01
Total	8.02	4.00	4.01	3.00		8.02	4.01	4.01	3.00
Ca/(Ca+Mg)			0.452					0.460	
Mg/(Mg+Fe)		0.938	0.933	93.11		0.842	0.931	0.933	92.12
Cr/(Cr+Al)									
Ca%	13.36	0.90	39.48			12.84	0.89	41.39	
Mg%	73.29	92.26	47.93			72.44	91.73	48.56	
Fe%	12.47	6.07	3.46			13.60	6.75	3.50	



NL494	GT	OP	CP	OL	NL495	GT	OP	CP	OL
SiO2	40.90	57.25	54.71	40.68		41.28	56.36	54.29	40.35
TiO2	0.07	0.01	0.03	0.03		0.93	0.20	0.36	0.03
Al2O3	16.19	0.94	0.85	0.05		17.92	0.99	2.29	0.05
Cr2O3	8.57	0.46	0.75	0.10		6.27	0.40	1.68	0.05
Fe2O3	0.00	0.00	0.00	0.00		0.00	0.00	0.00	0.00
FeO	5.76	5.22	3.25	8.71		7.15	5.55	3.18	8.81
MnO	0.37	0.15	0.14	0.12		0.34	0.12	0.11	0.10
MgO	17.59	34.32	21.05	50.07		20.46	34.22	18.00	49.97
CaO	6.69	1.59	18.25	0.07		5.64	0.74	17.19	0.05
Na2O	0.04	0.09	0.34	0.02		0.10	0.26	2.06	0.04
NiO	0.00	0.17	0.05	0.39		0.03	0.12	0.11	0.40
Total	96.18	100.18	99.42	100.25		100.12	98.96	99.27	99.85
Si	3.00	1.97	1.98	0.99		2.98	1.96	1.97	0.99
Ti	0.00	0.00	0.00	0.00		0.05	0.01	0.01	0.00
Al	1.41	0.04	0.04	0.00		1.53	0.04	0.10	0.00
Cr	0.49	0.01	0.02	0.00		0.36	0.01	0.05	0.00
Fe3	0.00	0.00	0.00	0.00		0.00	0.00	0.00	0.00
Fe2	0.40	0.15	0.10	0.18		0.43	0.16	0.10	0.18
Mn	0.02	0.00	0.00	0.00		0.02	0.00	0.00	0.00
Mg	2.18	1.76	1.13	1.82		2.20	1.78	0.97	1.82
Ca	0.52	0.06	0.71	0.00		0.44	0.03	0.67	0.00
Na	0.01	0.01	0.02	0.00		0.01	0.02	0.14	0.00
Ni	0.00	0.00	0.00	0.01		0.00	0.00	0.00	0.01
Total	8.05	4.01	4.00	3.01		8.01	4.01	4.01	3.00
Ca/(Ca+Mg)			0.384					0.407	
Mg/(Mg+Fe)		0.845	0.920	91.10		0.836	0.917	0.910	91.00
Cr/(Cr+Al)									
Ca%	16.57	2.95	35.91			14.13	1.40	38.36	
Mg%	69.69	88.74	57.61			71.23	90.20	55.89	
Fe%	12.80	7.57	5.00			14.64	8.39	5.75	

## APPENDIX 5

### Analyses of Minerals from Satellite Pipe Peridotites

Compositions were measured by EDS using the Cambridge University Miniscan. Sodium and aluminium were remeasured using a Cambridge Instruments Geoscan and the ZAF corrections recalculated using the new apparent element concentrations from these raw counts. A jadeite standard was used for both Na and Al. Aluminium was also monitored on a corundum standard.

GT = Garnet  
OP = Orthopyroxene  
CP = Clinopyroxene  
OL = Olivine

NLO21	GT	OP	CP	OL	NLO28	GT	OP	CP	OL
SiO2	42.58	57.79	55.30	41.19		42.19	57.05	54.82	41.06
TiO2	0.65	-	0.17	-		0.39	0.12	-	-
Al2O3	19.85	1.44	1.86	-		20.07	1.59	1.87	-
Cr2O3	3.59	0.34	1.07	-		3.10	0.22	0.90	-
FeO	6.91	5.50	3.74	9.05		6.85	5.30	3.66	9.08
MnO	0.22	0.11	0.15	0.10		0.25	0.12	0.13	0.13
MgO	21.75	33.75	20.25	49.91		21.71	33.36	20.21	49.72
CaO	4.82	1.40	15.33	0.09		4.63	1.40	15.18	0.09
Na2O	-	0.36	1.63	-		-	0.37	1.29	-
NiO	-	0.17	-	0.36		0.14	0.16	-	0.33
Total	100.37	100.86	99.50	100.70		99.33	99.69	98.06	100.41
Si	3.02	1.98	1.99	1.00		3.02	1.97	1.92	1.00
Ti	0.03	0.00	0.00	-		0.02	0.00	0.02	-
Al	1.66	0.06	0.08	-		1.70	0.06	0.24	-
Cr	0.20	0.01	0.03	-		0.18	0.01	0.04	-
Fe	0.41	0.16	0.11	0.18		0.41	0.15	0.08	0.19
Mn	0.01	0.00	0.00	0.00		0.02	0.00	0.00	0.00
Mg	2.30	1.72	1.09	1.81		2.32	1.72	0.75	1.80
Ca	0.37	0.05	0.59	0.00		0.36	0.05	0.77	0.00
Na	-	0.02	0.11	-		-	0.02	0.20	-
Ni	-	0.00	-	0.01		0.01	0.00	-	0.01
Total	8.00	4.00	4.00	3.00		8.04	3.98	4.02	3.00
Mg/(Mg+Fe)	0.849	0.916	0.906	%Fo		0.849	0.918	0.908	%Fo
Ca/(Ca+Mg)			0.352	91.0				0.351	91.7
Cr/(Cr+Al)									
Ca%	11.91	2.66	33.03			11.53	2.69	32.90	
Mg%	74.76	89.18	60.68			75.17	89.34	60.91	
Fe%	13.33	8.16	6.29			13.31	7.97	6.19	

NL503	GT	OP	CP	OL	BD1870/1	GT	OP	CP	OL
SiO <sub>2</sub>	43.37	58.30	55.82	41.90		41.90	57.50	54.24	40.95
TiO <sub>2</sub>	0.35	-	0.14	-		0.14	-	0.22	-
Al <sub>2</sub> O <sub>3</sub>	21.05	1.58	1.79	-		21.36	1.14	2.62	-
Cr <sub>2</sub> O <sub>3</sub>	2.80	0.30	1.06	-		2.94	0.24	1.66	-
FeO	6.62	5.33	3.51	8.83		8.76	5.48	2.11	8.93
MnO	0.22	0.17	-	0.10		0.38	0.13	-	0.14
MgO	22.29	34.09	20.66	50.61		19.38	35.10	15.68	50.12
CaO	4.70	1.38	16.16	0.11		5.12	0.20	20.70	-
Na <sub>2</sub> O	-	0.34	1.32	-		-	0.16	2.15	-
NiO	-	-	-	0.29		-	0.15	-	0.34
Total	101.40	101.49	100.46	101.84		99.98	100.10	99.38	100.48
Si	3.03	1.98	1.99	1.00		3.01	1.97	1.97	1.00
Ti	0.02	-	0.00	-		0.01	-	0.01	-
Al	1.73	0.06	0.08	-		1.81	0.05	0.11	-
Cr	0.15	0.01	0.03	-		0.17	0.01	0.05	-
Fe	0.39	0.15	0.10	0.18		0.53	0.16	0.06	0.18
Mn	0.01	0.00	-	0.00		0.02	0.00	-	0.00
Mg	2.32	1.72	1.10	1.81		2.07	1.80	0.85	1.82
Ca	0.35	0.05	0.62	0.00		0.39	0.01	0.81	-
Na	-	0.02	0.09	-		-	0.01	0.15	-
Ni	-	-	-	0.01		-	0.00	-	0.01
Total	8.00	3.99	4.01	3.00		8.01	4.01	4.01	3.01
Mg/(Mg+Fe)	0.857	0.919	0.913	%Fo		0.798	0.919	0.930	%Fo
Ca/(Ca+Mg)			0.360	91.1				0.487	90.9
Cr/(Cr+Al)									
Ca%	11.50	2.60	33.92			13.16	0.38	46.88	
Mg%	75.86	89.54	60.32			69.27	91.60	49.39	
Fe%	12.64	7.85	5.75			17.57	8.02	3.73	

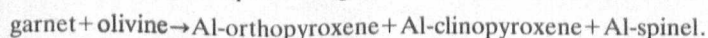
BD1894	GT	OP	CP	OL	BD1899	GT	OP	CP	OL	BD1910	GT	OP	CP	OL
SiO2	42.10	57.79	54.51	41.13		42.80	57.59	55.51	41.07		42.45	57.74	54.81	41.13
TiO2	0.15	-	0.23	-		0.15	-	-	-		-	0.15	0.32	-
Al2O3	21.00	1.33	2.68	-		20.25	1.28	1.10	-		20.02	1.08	1.95	-
Cr2O3	3.51	0.27	2.11	-		3.59	0.25	0.53	-		4.79	0.22	1.37	-
FeO	9.71	6.28	2.43	10.16		7.01	5.52	3.60	9.25		6.36	5.13	2.92	8.58
MnO	0.40	0.12	-	0.12		0.23	0.16	0.07	0.12		0.30	0.15	-	0.13
MgO	18.95	34.50	15.40	49.33		21.41	33.69	21.05	49.81		21.07	34.82	17.77	50.07
CaO	5.27	0.22	20.50	-		5.30	1.46	17.26	0.10		5.37	0.74	18.63	-
Na2O	-	0.10	2.34	-		-	0.14	0.75	-		-	0.30	1.91	-
NiO	-	0.12	-	0.34		-	0.14	-	0.37		-	0.24	-	0.35
Total	101.09	100.73	100.20	101.08		100.74	100.23	99.87	100.72		100.36	100.57	99.68	100.26
Si	3.01	1.98	1.96	1.00		3.03	1.98	1.99	1.00		3.02	1.97	1.98	1.00
Ti	0.01	-	0.01	-		0.01	-	-	-		-	0.00	0.01	-
Al	1.77	0.05	0.11	-		1.69	0.05	0.05	-		1.68	0.04	0.08	-
Cr	0.20	0.01	0.06	-		0.20	0.01	0.02	-		0.27	0.01	0.04	-
Fe	0.58	0.18	0.07	0.21		0.42	0.16	0.11	0.19		0.38	0.15	0.09	0.17
Mn	0.02	0.00	-	0.00		0.01	0.00	0.00	0.00		0.02	0.00	-	0.00
Mg	2.02	1.76	0.83	1.79		2.26	1.73	1.13	1.80		2.23	1.77	0.96	0.00
Ca	0.40	0.01	0.79	-		0.40	0.05	0.66	0.00		0.41	0.03	0.72	-
Na	-	0.01	0.16	-		-	0.01	0.05	-		-	0.02	0.13	-
Ni	-	0.00	-	0.01		-	0.00	-	0.01		-	0.01	-	0.00
Total	8.01	4.00	3.99	3.01		8.02	3.99	4.01	3.00		8.01	4.00	4.01	2.99
Mg/(Mg+Fe)	0.777	0.907	0.919	%Fo 89.7		0.845	0.916	0.912	%Fo 90.6		0.855	0.924	0.916	%Fo 91.2
Ca/(Ca+Mg)			0.489					0.371					0.430	
Cr/(Cr+Al)														
Ca%	13.44	0.42	46.79			13.07	2.77	34.97			13.55	1.39	40.83	
Mg%	67.23	90.35	48.88			73.44	89.04	59.33			73.93	91.08	54.17	
Fe%	19.33	9.23	4.33			13.49	8.19	5.69			12.52	7.53	4.99	

# Garnet-olivine reaction in the upper mantle: evidence from peridotite xenoliths in the Letseng-la-Terae kimberlites, Lesotho

N. P. Lock and J. B. Dawson

**ABSTRACT:** Garnet-bearing xenoliths from Letseng-la-Terae display a range of textures from coarse to granuloblastic. Equilibration temperatures and pressures of primary phases are in the ranges 950–1400°C and 27–50 kb, respectively. Deformed lherzolites equilibrated throughout this temperature range but coarse xenoliths are restricted to low temperature equilibration.

All garnets display coronas developed during the reaction:



In some rocks, reaction has completely eliminated garnet.

In rocks where garnet is disrupted, the corona minerals are strung out in the fluidal texture indicating that reaction occurred *before* deformation. Rocks transitional to, and of granuloblastic texture, contain garnet *and* aluminous spinel; in addition 'pools' of minerals originating by dynamic separation of corona fragments are observed.

Chemical comparison between the corona minerals and minerals in a garnet-spinel rock and two spinel granuloblastites, suggests that these spinel-bearing rocks may be derived from normal garnet peridotite by a complex sequence of reaction, followed by deformation, annealing and chemical homogenisation. The conclusion that reaction and deformation took place at high levels in the upper mantle is contrary to some earlier hypotheses of shearing within the low velocity zone in response to continental plate movement, but is consistent with mantle diapir models.

**KEY WORDS:** Lherzolite, corona, deformation, annealing, homogenisation, mantle, diapir.

The kimberlite pipes of Letseng-la-Terae, Lesotho (generally known as Letseng; lat. 29°00'S; long. 28°43'E), contain a variety of crustal and mantle-derived inclusions varying from granulites to peridotites (Bloomer & Nixon 1973). The peridotites are mainly garnet-bearing and belong to the common peridotite group as defined by Cox *et al.* (1973). The textures vary from coarse-grained equigranular through porphyroclastic to mosaic porphyroclastic (terminology of Harte 1977).

The olivines are high-magnesium varieties ranging from Fo<sub>88</sub> to Fo<sub>93</sub> in composition; the orthopyroxenes are mostly enstatites and titanian enstatites, the clinopyroxenes are diopside, chrome diopside and ureyitic diopside (classification of Stephens & Dawson 1977); and the garnets range from chrome pyrope to knorringitic uvarovite pyrope (classification of Dawson & Stephens 1976).

It is the purpose of this paper to describe, from amongst the Letseng peridotites suite, certain peridotites showing reaction rims indicative of transformation from garnet to spinel facies. This reaction has been studied in some detail for simple experimental systems (for summary see Ringwood 1975) and observed in nodules from basalts and other rocks (e.g. Kuno 1967; Reid & Dawson 1972) but the coronas in the Letseng rocks are better preserved than in any other peridotites hitherto described from kimberlite. Other peridotites are interpreted as having undergone a period of deformation following the formation of the reaction coronas and this has important implications as to the timing of deformation of

xenoliths in kimberlite, particularly in relation to the depth at which this deformation took place.

## 1. Formation of reaction coronas

Two particularly good examples, samples A and B were selected for study; B is a coarse garnet lherzolite, A has a porphyroclastic texture. Analyses of the primary phases and their structural formulae are given in Table 1. Analyses are of several grains within a single slide; no significant inter- or intra-grain variation was found. Compositions of the various phases are olivine Fo<sub>92</sub> and Fo<sub>93</sub> for A and B respectively; the orthopyroxenes are titanian enstatite and enstatites; clinopyroxenes are ureyitic diopside and chrome diopside; and the garnets titanian pyrope and chrome pyrope. The mineral compositions for B are similar to many other garnet lherzolites whereas the compositions of the phases in A are more similar to the so-called 'fertile' garnet lherzolites from Thaba Putsoa, Lesotho (Nixon & Boyd 1973). Calculated pressures and temperatures for equilibration of these two peridotites using the geothermometer of Wells (1977) and the geobarometer of Wood and Banno (1973) modified by Wood (1974) are 1325°C and 42 kb and 983°C and 33.5 kb for A and B respectively. These are within the range of temperatures (950–1400°C) and pressures (27 to 50 kb) for the Letseng peridotite suite as a whole (N.P. Lock *in preparation*).

Reaction coronas, which are extremely well developed on the garnets in these two samples, are very similar to those found in peridotites from the Lashaine volcano in northern



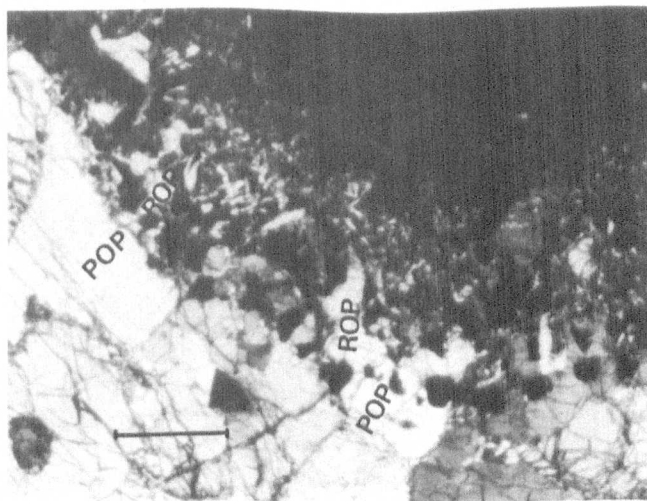
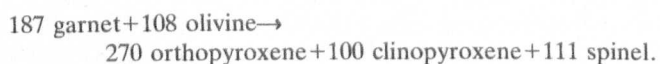
Tanzania (Reid & Dawson 1972) where there is a zonal development. Immediately adjacent to the garnet (zone 1) is a microcrystalline aggregate that was unresolvable under the microscope; this zone is succeeded outwards by a fine grain zone of acicular pyroxene and spinel, the grains being arranged approximately normal to the garnet margin (zone 2); this is succeeded by the outermost (zone 3) of relatively coarse phases containing equant spinel set in a matrix of orthopyroxene and clinopyroxene. These zoned coronas were found to be most commonly developed between olivine and garnet but also occur between garnet and orthopyroxene and garnet and clinopyroxene; where the primary phase involved in the reaction was pyroxene the reaction corona pyroxene has grown in optical continuity with the earlier primary pyroxene. The same general zonation holds true for the Letseng garnet peridotite coronas (Fig. 1). However, in some cases there is only a poor development of coronas, while in others it is extremely extensive and in a few cases reaction has gone to completion eliminating original garnet.

In many samples there is sporadic development of strongly pleochroic red-brown mica, of presumed secondary origin, which is replacing the reaction coronas; in certain cases the only reaction corona mineral left is the spinel which occurs as small inclusions within the replacing mica (Fig. 2). These textures serve as a link with the garnet kelyphite rinds which have been described in many garnet xenoliths from kimberlite (e.g. Carswell 1975).

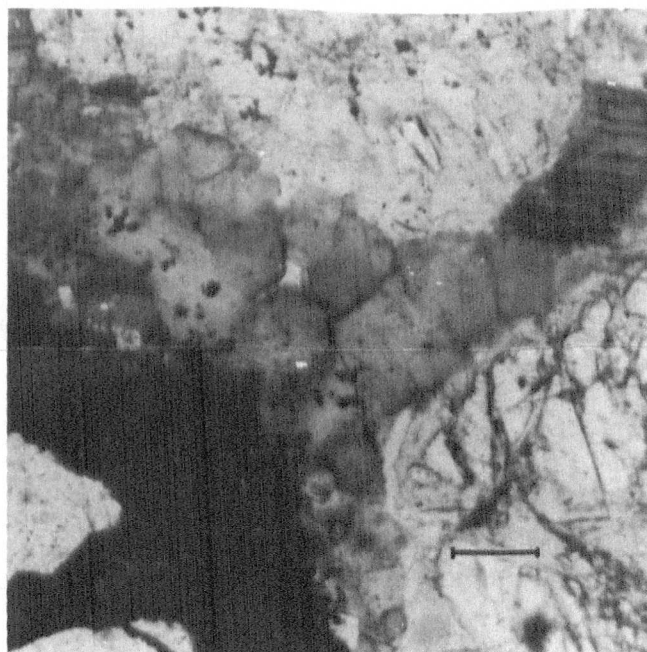
Electron microprobe analyses have been made on the phases in zone 3 of the coronas in samples A and B (Table 2). The reaction corona minerals are all characterised by being highly aluminous. The orthopyroxenes contain between 6 and 8.25%  $\text{Al}_2\text{O}_3$  and much of this  $\text{Al}_2\text{O}_3$  must be in four-fold co-ordination; nonetheless, on the basis of structural formulae, a considerable proportion of the alumina in the six-fold sites must in fact be regarded as magnesium tschermakite molecule. The clinopyroxenes likewise are highly aluminous and must contain calcium tschermakite molecule and, together with the orthopyroxenes, show an appreciable  $\text{Cr}_2\text{O}_3$  content. Both orthopyroxenes and clinopyroxenes show a very constant  $\text{Mg}/(\text{Mg}+\text{Fe})$  ratio of 0.89 to 0.91. The spinels are aluminous magnesian spinels unlike the chrome spinels which are found in the groundmass of many peridotite xenoliths (cf. Smith & Dawson 1975). In their high magnesian and high alumina content they resemble other spinels reported from reaction coronas around garnets in peridotites (e.g. Haggerty 1975; Reid & Dawson 1972).

As in the case of the Lashaine coronas, most of the chemical features of the pyroxenes are compatible with their being developed by reaction between garnet and olivine with their overall chemical composition being a reflection of the chemical gradient between garnet and olivine. An exception is an imbalance in the sodium and titanium contents of the corona pyroxenes. This is not matched by similar values in either parental garnet or olivine and our data would concur with the suggestion of Reid and Dawson (1972) that small quantities of sodium may have been introduced during an otherwise isochemical reaction.

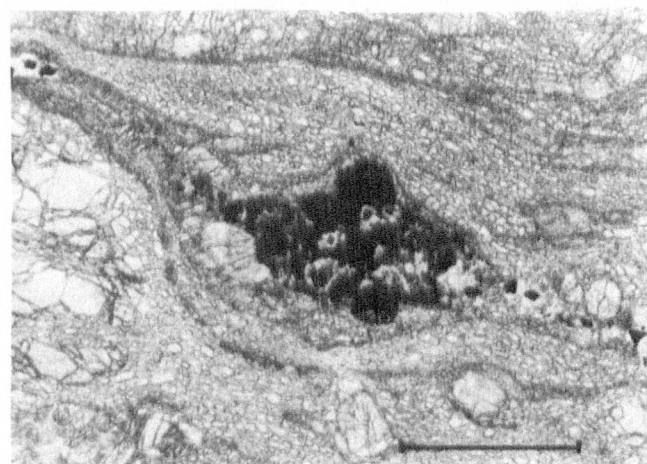
It should be noted that these two different samples show that different proportions of corona minerals developed; presumably as some reflection of difference in primary phase composition. For example, in the case of A (the more titanium- and iron-rich sample), a balanced equation for Si, Al, Cr, Mg and Ca, based on the structural formulae of the corona phases and primary phases, gives the reaction:



**Figure 1** Garnet reaction corona showing optical continuity of corona and primary orthopyroxene (specimen A); POP — primary orthopyroxene, ROP — corona orthopyroxene; crossed polars; bar scale 1 mm.

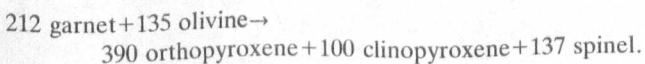


**Figure 2** Secondary phlogopite replacing corona minerals; garnet at bottom left with euhedral phlogopite at centre; plane polarised light; bar scale 0.1 mm.



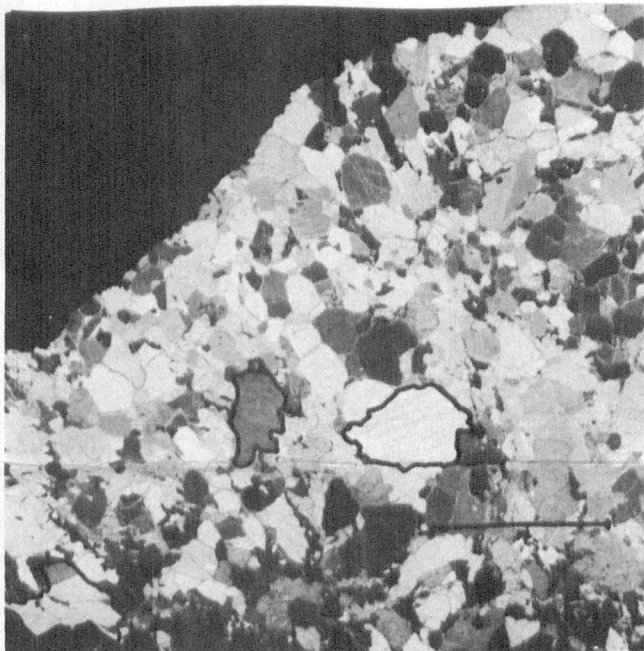
**Figure 3** Reaction corona spinel disrupted in fluidal mosaic porphyroclastic texture; plane polarised light; bar scale 1 mm.

By contrast, the corresponding reaction for B is:

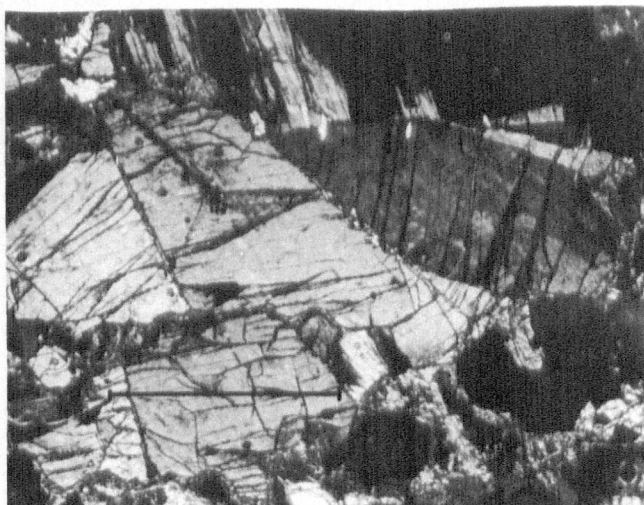


These reactions show that, compared with the Lashaine samples, the Letseng samples have more reaction corona clinopyroxene. A further difference between the Lashaine and Letseng samples is that whereas the pyroxenes of the Lashaine coronas attain values of 12–14%  $\text{Al}_2\text{O}_3$ , those at Letseng never exceed 10%  $\text{Al}_2\text{O}_3$ .

Theoretically the transition from a garnet lherzolite assemblage to the spinel lherzolite assemblage of the corona could take place by a rise in temperature to over 1300°C, by a drop in pressure, or a combination of the two (O'Hara *et al.* 1971).



**Figure 4a** Inequigranular texture of granoblastic aggregates and orthopyroxene porphyroclasts (specimen C); some porphyroclasts are outlined by a heavy line; small black grains are spinel; crossed polars; bar scale 5 mm.



**Figure 4b** Detail of orthopyroxene porphyroclast at bottom left of figure 4a; crossed polars; bar scale 1 mm.

## 2. Deformation of reaction coronas

Most reaction coronas show little evidence of deformation even where the primary assemblage has a mosaic porphyroclastic texture. Weak undulose extinction in the corona pyroxenes may be the result of volume expansion accompanying the reaction. Laminated and disrupted mosaic porphyroclastites, however, contain spinel grains that originate from the reaction corona and are strung out in the fluidal matrix between and beyond disrupted garnet grains (Fig. 3). Deformation is hence inferred to have post-dated the garnet breakdown in at least some of the Letseng peridotites.

The deformation cycles of Matsoku peridotites (Harte *et al.* 1975) is that of a granuloblastic texture derived by deformation of mosaic porphyroclastites. Letseng granuloblastites differ from those at Matsoku in two ways: the garnet displays a porphyroclastic habit and aluminous spinel is always present. Granuloblastites without garnet may be compared with the equigranular texture recorded by Mercier and Nicolas (1975) for peridotites in basalts and several textural and chemical features suggest that they were derived by further deformation of a rock such as that illustrated in Figure 3.

Another rock (C) exhibits an inequigranular texture (Fig. 4a) resulting from the association of granoblastic aggregates of orthopyroxene and olivine together with orthopyroxene porphyroclasts and represents a texture intermediate between mosaic and granuloblastic. One such porphyroclast showing misoriented segments (Fig. 4b) is interpreted as relict from a mosaic porphyroclastite. Garnet occurs as small (<5 mm) remnants with a microcrystalline corona of orthopyroxene, and brown aluminous spinel is abundant as intergranular and holly-leaf textured grains of up to 1 mm size. The olivine is of normal magnesian character ( $\text{Fo}_{94}$ ) and constant composition; clinopyroxene has a rather low FeO and  $\text{Na}_2\text{O}$  content (although within the Letseng peridotite range) but differs from most of the normal primary clinopyroxene in containing appreciable calcium tschermakite component; garnet is chrome pyrope. The spinel is highly aluminous and of very similar character to the reaction corona spinels previously described. The range in composition through the rock is similar to that shown by the corona spinels:  $\text{Mg}/(\text{Mg}+\text{Fe})$  varies antipathetically with  $\text{Cr}/(\text{Cr}+\text{Al})$  within fairly narrow limits (Table 1). Some slight zoning exists with alumina-enriched rims perhaps reflecting partial re-equilibration with orthopyroxene which shows a reversal of this zoning. Orthopyroxene shows a wide spread in composition.  $\text{Mg}/(\text{Mg}+\text{Fe})$  is remarkably constant but the alumina content varies between 1% and 3.5% and is as high as 9.9% in the orthopyroxene corona to the garnet. This alumina is largely as magnesium tschermakite component.

In exhibiting both textural and chemical disequilibrium this rock (C) is unlike any other found at Letseng. The texture is interpreted as transitional between mosaic porphyroclastic and granuloblastic, and the chemistry is inferred as resulting from the partial homogenisation and re-equilibration of an original garnet peridotite following extensive reaction between garnet and olivine, and subsequent deformation.

Several other similar specimens show varied amounts of small (<1 mm) irregular garnet grains in a typical granuloblastite (e.g. D Fig. 5). The garnets are partially or wholly surrounded by reaction coronas similar to those described above. Elsewhere in the rock 'pools' of reaction corona minerals including a greenish-coloured spinel occur with no apparent association with the garnet. Brown aluminous spinel is intergranular throughout the rock with no apparent association with either the garnet or the 'pools'. These rocks are also interpreted as texturally intermediate and the 'pools' of corona



minerals are taken as evidence of the derivation of these rocks by further deformation of mosaic porphyroclastites whose garnets have undergone considerable breakdown.

Some peridotite xenoliths (represented by specimen E Fig. 6) are tabular granuloblastites showing a very strong fabric and texturally very similar to other Letseng rocks in which garnet is not present (Fig. 7). Garnets are irregular in shape and large in size (up to 3 mm) and inferred to be porphyroclasts. There are only tiny remnants of a reaction corona partially surrounding the garnet. Brown aluminous spinel occurs as intergranular grains. These granuloblastic spinel peridotites show remarkably homogeneous mineral compositions through the rock (e.g. specimens F, G; Table 1). The olivine is magnesium-rich ( $Fe_{90}$ ) and similar to that in Letseng garnet peridotites; clinopyroxene is chrome diopside with a considerable calcium tschermakite component; orthopyroxene is a Cr-Al-enstatite with a moderate magnesium tschermakite component. The spinel is alumina- and magnesia-rich and identical in composition to those from the reaction coronas. A high degree of chemical homogeneity is shown by these specimens and estimates of equilibration temperatures using the method of Wells (1977), give 827°C for F and 712°C for G. The effect of solution of tschermakite molecule is uncertain but these temperatures may prove on the low side.

Both F and G and other similar rocks are interpreted as being derived by further deformation of mosaic porphyroclastites in which the garnet-olivine reaction has gone to

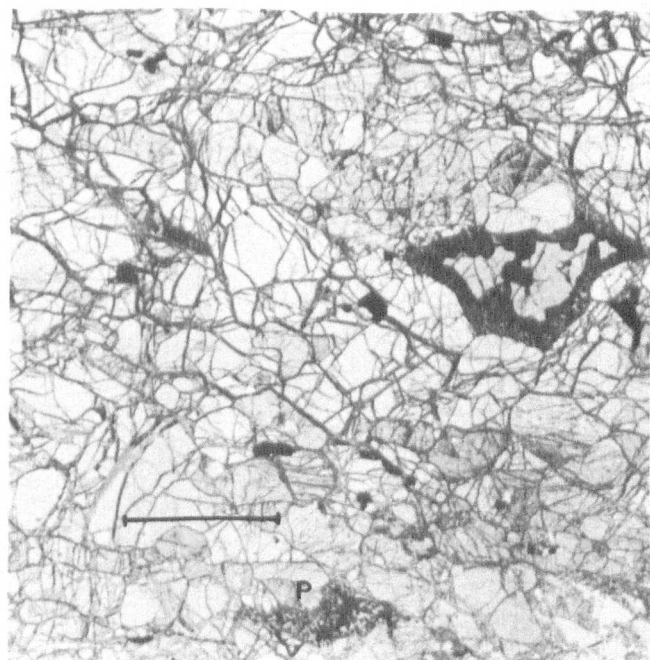


Figure 5 Garnet and aluminous spinel rock with 'pools' of corona minerals (specimen D); 'pools' are marked by P; black grains are spinel and garnet shows a typical corona; plane polarised light; bar scale 2 mm.

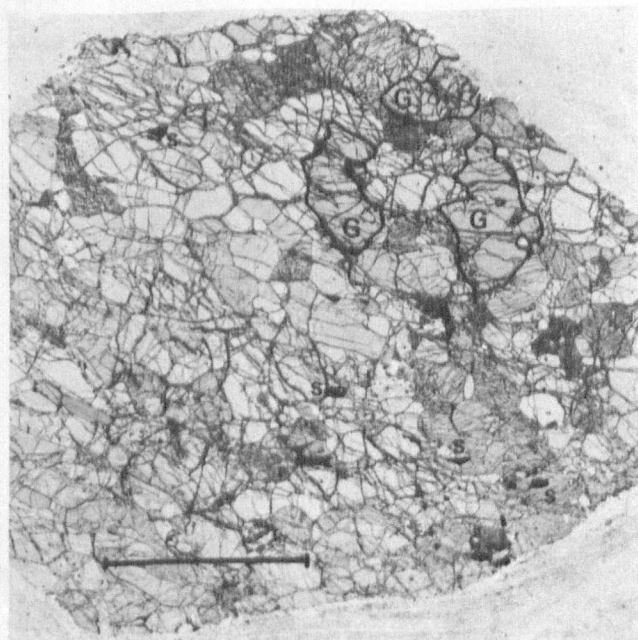
Table 1 Microprobe analyses and structural formulae of primary minerals in specimens A, B, C, F and G

Specimen	A				B				C				
	GT	OP	CP	OL	GT	OP	CP	OL	GT	OP	CORE	RIM	OP
SiO <sub>2</sub>	42.01	57.36	54.19	41.24	41.73	58.35	55.22	41.49	41.98	57.16	56.89	57.62	55.28
TiO <sub>2</sub>	0.65	0.25	0.46	0.09	0.07	0.03	0.11	0.02	—	—	—	—	—
Al <sub>2</sub> O <sub>3</sub>	19.49	0.95	2.37	0.06	19.03	0.69	2.14	0.04	22.39	1.48	2.39	2.10	3.58
Cr <sub>2</sub> O <sub>3</sub>	4.88	0.44	2.00	0.05	5.03	0.27	1.70	0.02	1.37	0.35	0.41	0.31	0.57
Fe <sub>2</sub> O <sub>3</sub>	—	—	—	—	—	—	—	—	—	—	—	—	—
FeO	6.63	4.83	2.90	7.98	6.49	4.38	2.26	7.28	7.62	4.24	4.39	3.88	4.09
MnO	0.31	0.10	0.12	0.07	0.33	0.10	0.09	0.06	0.52	—	—	—	—
MgO	21.51	34.82	17.98	50.57	20.66	35.71	16.42	51.06	19.55	36.25	35.78	35.57	34.70
CaO	4.91	0.86	17.41	0.07	5.39	0.50	19.43	0.02	5.94	0.20	0.22	0.16	0.18
Na <sub>2</sub> O	0.10	0.27	1.87	0.04	0.04	0.16	2.20	0.03	—	0.28	0.26	0.34	—
NiO	0.03	0.12	0.05	0.41	0.00	0.09	0.09	0.44	—	—	—	—	—
TOTAL	100.52	100.00	99.35	100.58	98.77	100.28	99.66	100.46	99.37	99.96	100.33	99.98	98.40
Si	2.99	1.97	1.97	1.00	3.03	1.99	2.00	1.00	3.01	1.96	1.94	1.96	1.92
Ti	0.03	0.01	0.01	0.00	0.00	0.00	0.00	0.00	—	—	—	—	—
Al	1.64	0.04	0.10	0.00	1.63	0.03	0.09	0.00	1.89	0.06	0.10	0.08	0.15
Cr	0.27	0.01	0.06	0.00	0.29	0.01	0.01	0.05	0.08	0.01	0.01	0.01	0.02
Fe <sup>3+</sup>	—	—	—	—	—	—	—	—	—	—	—	—	—
Fe <sup>2+</sup>	0.39	0.14	0.09	0.16	0.39	0.12	0.07	0.15	0.46	0.12	0.13	0.11	0.12
Mn	0.02	0.00	0.00	0.00	0.02	0.00	0.00	0.00	0.03	—	—	—	—
Mg	2.28	1.78	0.97	1.82	2.23	1.81	0.89	1.84	2.09	1.85	1.82	1.81	1.80
Ca	0.37	0.03	0.68	0.00	0.42	0.02	0.75	0.00	0.46	0.01	0.01	0.01	0.01
Na	0.01	0.02	0.13	0.00	0.01	0.01	0.15	0.00	—	0.02	0.02	0.02	—
Ni	0.00	0.00	0.00	0.01	0.00	0.00	0.00	0.01	—	—	—	—	—
TOTAL	8.00	4.00	4.01	2.99	8.02	3.99	4.00	3.00	8.01	4.03	4.02	4.00	4.00
O	12	6	6	4	12	6	6	4	12	6	6	6	6
Mg/(Mg+Fe)	0.85	0.93	0.92	0.92	0.85	0.94	0.93	0.93	0.82	0.94	0.94	0.94	0.94
Ca/(Ca+Mg)	—	—	0.41	—	—	0.01	0.46	—	—	—	—	—	—
Cr/(Cr+Al)	—	—	—	—	—	—	—	—	—	—	—	—	—
Wo	—	1.63	38.88	—	—	0.94	44.04	—	—	—	—	—	—
En	—	91.14	55.85	—	—	92.54	51.80	—	—	—	—	—	—
Fe	—	7.24	5.27	—	—	6.52	4.16	—	—	—	—	—	—

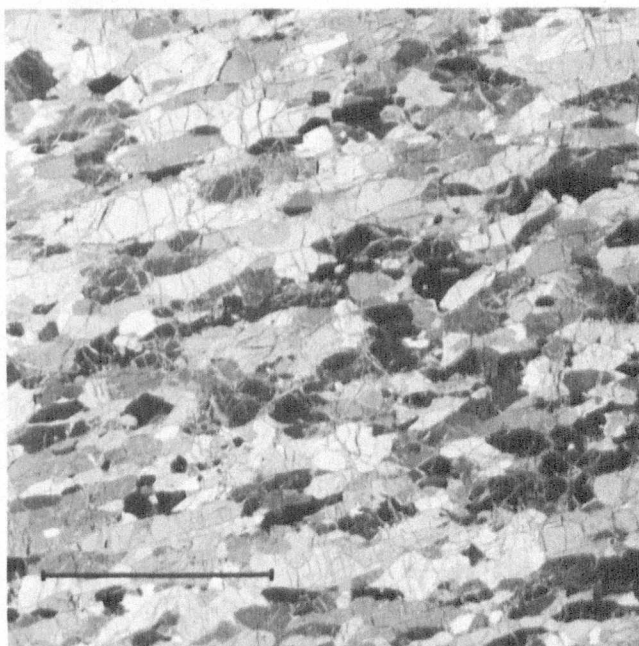
Key: GT—garnet; OP—orthopyroxene; CP—clinopyroxene; OL—olivine; SP—spinel

Specimens: A—NL 141; B—NL 197; C—NL 108; F—NL 148; G—NL 171

(NL numbers refer to the collection of the first author that is deposited in the Department of Geology, Sheffield University)



**Figure 6** Garnet and aluminous spinel granuloblastite showing a strong fabric (specimen E); porphyroclasts of garnet are marked G and outlined; black grains of spinel are marked S; plane polarised light; bar scale 5 mm.



**Figure 7** Aluminous spinel granuloblastite showing a very strong fabric; small black grains are spinel; crossed polars; bar scale 5 mm.

**Table 1** (continued)

Specimen	C						F			G			
	CP	OL	SP	CORE	RIM	SP	OP	CP	SP	OP	CP	OL	SP
SiO <sub>2</sub>	54.31	41.38	—	—	—	—	54.95	53.03	—	55.64	52.77	40.86	—
TiO <sub>2</sub>	—	—	—	—	—	—	0.05	0.11	0.03	0.03	0.13	0.01	0.03
Al <sub>2</sub> O <sub>3</sub>	2.15	—	43.56	45.25	47.25	49.91	3.24	4.20	53.60	3.33	3.99	0.03	48.52
Cr <sub>2</sub> O <sub>3</sub>	0.35	—	25.06	23.19	21.33	18.88	0.30	0.73	14.04	0.42	0.92	0.03	19.24
Fe <sub>2</sub> O <sub>3</sub>	—	—	—	—	—	—	—	—	1.42	—	—	—	1.65
FeO	1.07	5.84	9.64	9.39	9.13	8.30	6.39	2.05	10.30	6.01	1.99	9.13	10.62
MnO	—	—	—	—	—	—	6.17	0.06	0.24	0.13	0.07	0.13	0.29
MgO	17.30	51.84	19.33	19.76	19.90	20.91	33.32	15.77	19.22	33.92	15.89	50.06	18.50
CaO	24.04	—	—	—	—	—	0.41	22.62	—	0.36	23.57	0.00	—
Na <sub>2</sub> O	0.57	—	0.28	—	—	0.27	0.33	1.15	0.00	0.05	0.80	0.02	0.00
NiO	—	0.44	—	—	0.39	0.32	0.10	0.03	0.31	0.11	0.04	0.40	0.22
<b>TOTAL</b>	<b>99.79</b>	<b>99.37</b>	<b>97.87</b>	<b>97.57</b>	<b>98.00</b>	<b>98.67</b>	<b>98.96</b>	<b>99.75</b>	<b>99.16</b>	<b>100.00</b>	<b>100.17</b>	<b>100.67</b>	<b>99.07</b>
Si	1.97	1.00	—	—	—	—	1.92	1.93	—	1.92	1.92	0.99	—
Ti	—	—	—	—	—	—	0.00	0.00	0.00	0.00	0.00	0.00	0.00
Al	0.09	—	1.43	1.47	1.52	1.58	0.13	0.18	1.67	0.14	0.17	0.00	1.55
Cr	0.01	—	0.55	0.51	0.46	0.40	0.01	0.02	0.29	0.01	0.03	0.00	0.41
Fe <sup>3+</sup>	—	—	—	—	—	—	—	—	0.03	—	—	—	0.04
Fe <sup>2+</sup>	0.03	0.12	0.23	0.22	0.21	0.19	0.91	0.06	0.23	0.17	0.06	0.19	0.24
Mn	—	—	—	—	—	—	0.01	0.00	0.01	0.00	0.00	0.00	0.01
Mg	0.93	1.87	0.80	0.81	0.81	0.84	1.73	0.85	0.76	1.74	0.86	1.81	0.75
Ca	0.93	—	—	—	—	—	0.02	0.88	—	0.01	0.92	0.00	—
Na	0.04	—	0.02	—	—	0.02	0.00	0.08	0.00	0.00	0.06	0.00	0.00
Ni	—	0.01	—	—	0.01	0.01	0.00	0.00	0.01	0.00	0.00	0.01	0.00
<b>TOTAL</b>	<b>4.01</b>	<b>3.00</b>	<b>3.02</b>	<b>3.01</b>	<b>3.01</b>	<b>3.02</b>	<b>4.01</b>	<b>4.00</b>	<b>3.00</b>	<b>4.09</b>	<b>4.02</b>	<b>3.00</b>	<b>3.00</b>
O	6	4	4	4	4	4	6	6	4	6	6	4	4
Mg/(Mg+Fe)	0.97	0.94	0.78	0.79	0.80	0.82	0.90	0.93	0.77	0.91	0.93	0.91	0.75
Ca/(Ca+Mg)	0.50	—	—	—	—	—	0.01	0.51	—	0.01	0.52	—	—
Cr/(Cr+Al)	—	—	0.28	0.26	0.23	0.20	—	—	0.51	—	—	—	0.21
Wo	—	—	—	—	—	—	0.79	48.96	—	0.68	49.85	—	—
En	—	—	—	—	—	—	89.34	47.48	—	90.16	46.74	—	—
Fe	—	—	—	—	—	—	9.87	3.57	—	9.16	3.40	—	—

Key: GT—garnet; OP—orthopyroxene; CP—clinopyroxene; OL—olivine; SP—spinel

Specimens: A—NL 141; B—NL 197; C—NL 108; F—NL 148; G—NL 171

(NL numbers refer to the collection of the first author that is deposited in the Department of Geology, Sheffield University)

completion. Chemical homogenisation and re-equilibration is inferred to have accompanied the continued deformation.

A number of other samples containing brown aluminous spinel are considerably coarser grained than the normal granuloblastites and grain boundaries may also become rather ragged and interlocking, a characteristic of the normal coarse rocks. A notable feature of these more annealed rocks is the presence of spinel and clinopyroxene exsolution as tiny lamellae and blebs across kink boundaries, in the orthopyroxenes.

### 3. Discussion and conclusions

Peridotite xenoliths from Letseng show similar phase chemistry to those from other kimberlite pipes in Lesotho and in carbonatite from Tanzania, when showing evidence of only low to moderate deformation. However, when there is evidence of more intense deformation, the mineralogy is no longer straightforward and both garnet and aluminous spinel occur in rocks showing laminated and disrupted mosaic textures. Such rocks are unlike any previously described peridotites from kimberlite although coarse garnet-Cr/Al spinel lherzolites are known (e.g. Ferguson *et al.* 1977). Other granuloblastic spinel lherzolites are texturally similar to equigranular-textured peridotite xenoliths from basalt (Mercier & Nicolas 1975).

All the xenoliths show reaction between garnet and olivine representing a transition from garnet peridotite to spinel peridotite, the reaction having occasionally gone to completion. The extent of reaction bears no relation to the degree of deformation but the products of the reaction are shown to be deformed, at least in the more advanced stages of deformation. There is some indication that reaction continued during progressive deformation.

The mineral chemistry of the spinel-bearing rocks suggests their derivation from garnet peridotites by a process of reaction, deformation, homogenisation and re-equilibration. The reaction may have resulted from increase in temperature, decrease in pressure or a combination of the two as shown experimentally for simple systems (e.g. MacGregor 1965, 1970, 1974; Green & Ringwood 1967, and summarised by Jenkins & Newton 1979). Other studies of this phase transformation in natural systems (e.g. Kuno 1967, Reid & Dawson 1972; Smith 1977) have attributed the reaction to decrease in pressure and Kuno (1967) suggests this decrease was due to diapiric upwelling.

The deformation observed in kimberlite xenoliths has been variously attributed to large-scale shearing at the base of the lithosphere (Boyd & Nixon 1972; Nixon & Boyd 1973) and to more localised shearing within the kimberlite diapir envelope (Dawson *et al.* 1975; Harte *et al.* 1975). Calculations of equilibration temperatures and pressures of primary phases in

**Table 2** Analyses and structural formulae of corona minerals in specimens A, B and C

Specimen	A						B						C
	OP	±	CP	±	SP	±	OP	±	CP	±	SP	±	OP
Mineral													
Number of Analyses	8		5		9		5		5		5		1
SiO <sub>2</sub>	52.10	1.94	50.14	2.00	0.08	0.02	51.69	0.91	51.14	1.52	0.09	0.04	52.53
TiO <sub>2</sub>	0.46	0.10	1.49	0.45	0.69	0.12	0.08	0.01	0.17	0.05	0.07	0.02	—
Al <sub>2</sub> O <sub>3</sub>	7.52	2.24	8.25	1.88	50.23	1.69	7.77	0.90	6.23	1.81	49.76	1.30	8.72
Cr <sub>2</sub> O <sub>3</sub>	1.40	0.40	1.70	0.43	16.92	1.65	1.24	0.44	1.29	0.66	16.36	1.36	0.67
Fe <sub>2</sub> O <sub>3</sub>	—	—	—	—	3.48	—	—	—	—	—	2.51	—	—
FeO	6.15	0.52	4.30	0.45	8.26	0.50	6.52	0.13	3.82	0.25	9.48	0.55	7.35
MnO	0.27	0.06	0.22	0.05	0.28	0.03	0.38	0.01	0.33	0.30	0.36	0.02	0.43
MgO	30.36	1.43	19.53	2.58	20.62	0.40	29.81	0.60	17.75	1.73	19.13	0.40	29.18
CaO	1.44	0.17	14.02	1.76	0.01	0.01	1.39	0.30	17.21	0.82	0.04	0.02	2.20
Na <sub>2</sub> O	0.15	0.02	1.14	0.20	0.01	0.01	0.12	0.02	0.90	0.23	0.02	0.01	0.26
NiO	0.01	0.01	0.03	0.02	0.03	0.03	0.00	0.00	0.02	0.02	0.06	0.02	—
<b>TOTAL</b>	<b>99.86</b>		<b>100.81</b>		<b>100.61</b>		<b>99.00</b>		<b>98.84</b>		<b>97.88</b>		<b>101.34</b>
Si	1.82		1.79		0.00		1.82		1.87		0.00		1.81
Ti	0.01		0.04		0.01		0.00		0.00		0.00		—
Al	0.31		0.35		1.56		0.32		0.27		1.59		0.35
Cr	0.04		0.05		0.35		0.03		0.04		0.35		0.02
Fe <sup>3+</sup>	—		—		0.07		—		—		0.05		—
Fe <sup>2+</sup>	0.18		0.13		0.18		0.19		0.12		0.22		0.21
Mn	0.01		0.01		0.01		0.01		0.01		0.01		0.01
Mg	1.58		1.04		0.81		1.56		0.96		0.77		1.50
Ca	0.05		0.54		0.00		0.05		0.67		0.00		0.08
Na	0.01		0.08		0.00		0.01		0.06		0.00		0.02
Ni	0.00		0.00		0.00		0.00		0.00		0.00		—
<b>TOTAL</b>	<b>4.01</b>		<b>4.03</b>		<b>2.99</b>		<b>3.99</b>		<b>4.00</b>		<b>2.99</b>		<b>4.01</b>
O	6		6		4		6		6		4		6
Mg/(Mg+Fe)	0.90		0.89		0.81		0.89		0.89		0.77		0.88
Ca/(Ca+Mg)			0.34						0.41				
Cr/(Cr+Al)					0.18						0.18		
Wo	2.96		31.35				2.87		38.16				4.47
En	86.75		60.75				85.95		54.66				83.80
Fe	10.29		7.90				11.17		7.18				11.73

Key: OP—Orthopyroxene; CP—Clinopyroxene; SP—Spinel.  
Specimens: As in Table 1.

Letseng garnet lherzolites indicate that there is no simple correlation between depth of origin and degree of deformation, thus favouring the latter hypothesis. The deformation took place at relatively high levels in the mantle, well above the base of the lithosphere.

The following sequence of events is proposed to explain the textural and chemical features described above.

1. Equilibration of the peridotites to the prevailing P. T. environment in the garnet stability field.
2. Diapiric upwelling associated with kimberlite formation leading to movement of the peridotites out of the garnet stability field and consequent garnet breakdown.
3. Deformation of peridotite at the margin of the diapir envelope accompanying continuing garnet breakdown reaction.
4. Entrainment of peridotite in the kimberlite magma and rapid transport to the surface preserving, within the specimen suite as a whole, both the original high temperature and high pressure mineralogy together with the products of the later chemical and textural disequilibrium.

#### 4. Acknowledgements

Most of the specimens were collected by N. P. L. whilst in the employ of the Anglo American Corporation of S.A. Ltd, to whom gratitude is expressed for encouragement and permission to undertake this research. The study was carried out during the tenure of a Natural Environment Research Council research studentship at St Andrews and Sheffield Universities. Thanks are also due to the staff of the Departments of Geology at Edinburgh and Manchester Universities where microprobe analyses were made.

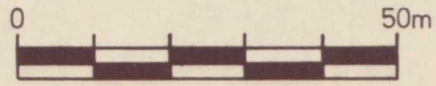
#### 5. References

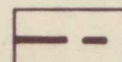
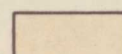
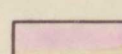
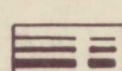
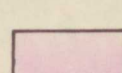
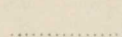
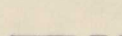



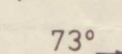
- Bloomer, A. G. & Nixon P. H. 1973. The geology of Letseng-la-Terae kimberlite pipes. In Nixon P. H. (ed.) *Lesotho Kimberlites*, 20–36. Maseru: Lesotho National Development Corporation.
- Boyd, F. R. & Nixon, P. H. 1972. Ultramafic nodules from the Thaba Putsoa kimberlite pipe. ANNU REP DIR GEOPHYS LAB CARNEGIE INST **71**, 362–73.
- Carswell, D. A. 1975. Primary and secondary phlogopites and clinopyroxenes in garnet lherzolite xenoliths. *PHYS CHEM EARTH OXFORD* **9**, 417–30.
- Cox, K. G., Gurney, J. J. & Harte, B. 1973. Xenoliths from the Matsoku pipe. In Nixon P. H. (ed.) *Lesotho Kimberlites*, 76–98. Maseru: Lesotho National Development Corporation.
- Dawson, J. B., Gurney, J. J. & Lawless, P. J. 1975. Palaeogeothermal gradients derived from xenoliths in kimberlite. *NATURE LONDON* **257**, 299–300.
- Dawson, J. B. & Stephens, W. E. 1976. Addendum: Statistical classification of garnets from kimberlite and associated xenoliths. *J GEOL* **84**, 495–6.
- Ferguson, J., Ellis, D. J. & England, R. N. 1977. Unique spinel-garnet lherzolite inclusions in kimberlite from Australia. *GEOLOGY* **5**, 278–80.
- Green, D. H. & Ringwood, A. E. 1967. The stability fields of aluminous pyroxene peridotite and garnet peridotite and their relevance in upper mantle structures. *EARTH PLANET SCI LETT* **3**, 151–60.
- Haggerty, S. E. 1975. The chemistry and genesis of opaque minerals in kimberlites. *PHYS CHEM EARTH OXFORD* **9**, 295–307.
- Harte, B. 1977. Rock nomenclature with particular relation to deformation and recrystallisation textures in olivine bearing xenoliths. *J GEOL* **85**, 279–88.
- Harte, B., Cox, K. G. & Gurney, J. J. 1975. Petrography and geological history of upper mantle xenoliths from the Matsoku kimberlite pipe. *PHYS CHEM EARTH OXFORD* **9**, 617–46.
- Jenkins, D. M. & Newton, R. C. 1979. Experimental determination of the spinel peridotite to garnet peridotite inversion at 900°C and 1000°C in the system CaO-MgO-Al<sub>2</sub>O<sub>3</sub>-SiO<sub>2</sub>, and at 900°C with natural garnet and olivine. *CONTRIB MINERAL PETROL* **68**, 407–18.
- Kuno, H. 1967. Mafic and ultramafic nodules from Itinome-Gata, Japan. In Wyllie P. J. (ed.) *Ultramafic and related rocks*, 337–42. New York: J. Wiley.
- MacGregor, I. D. 1965. Stability fields of spinel and garnet peridotite in the synthetic system MgO-CaO-Al<sub>2</sub>O<sub>3</sub>-SiO<sub>2</sub>. *ANNU REP DIR GEOPHYS LAB CARNEGIE INST* **64**, 126–34.
- MacGregor, I. D. 1970. The effect of CaO, Cr<sub>2</sub>O<sub>3</sub>, Fe<sub>2</sub>O<sub>3</sub> and Al<sub>2</sub>O<sub>3</sub> on the stability of spinel and garnet peridotites. *PHYS EARTH PLANET INTER* **3**, 372–7.
- MacGregor, I. D. 1974. The system MgO-Al<sub>2</sub>O<sub>3</sub>-SiO<sub>2</sub>: Solubility of Al<sub>2</sub>O<sub>3</sub> in enstatite for spinel and garnet peridotite compositions. *AM MINERAL* **59**, 110–9.
- Mercier, J. C. & Nicolas, A. 1975. Textures and fabrics of upper mantle peridotites as illustrated by xenoliths from basalts. *J. PETROL* **16**, 454–87.
- Nixon, P. H. & Boyd, F. R. 1973. Petrogenesis of the granular and sheared ultrabasic nodule suite in kimberlites. In Nixon, P. H. (ed.) *Lesotho Kimberlites*, 48–56. Maseru: Lesotho National Development Corporation.
- O'Hara, M. J., Richardson, S. W. & Wilson, G. 1971. Garnet peridotite stability and occurrence in crust and mantle. *CONTRIB MINERAL PETROL* **32**, 48–68.
- Reid, A. M. & Dawson, J. B. 1972. Olivine-garnet reaction in peridotites from Tanzania. *LITHOS* **5**, 115–24.
- Ringwood, A. E. 1975. *Composition and Petrology of the Earth's Mantle*. New York: McGraw-Hill.
- Smith, D. 1977. The origin and interpretation of spinel-pyroxene clusters in peridotite. *J GEOL* **85**, 476–82.
- Smith, J. V. & Dawson, J. B. 1975. Chemistry of Ti-poor spinels, ilmenites and rutiles from peridotite and eclogite xenoliths. *PHYS CHEM EARTH OXFORD* **9**, 309–22.
- Stephens, W. E. & Dawson, J. B. 1977. Statistical comparison between pyroxenes from kimberlites and their associated xenoliths. *J GEOL* **85**, 433–49.
- Wells, P. R. A. 1977. Pyroxene thermometry in simple and complex systems. *CONTRIB MINERAL PETROL* **62**, 129–39.
- Wood, B. J. 1974. The solubility of alumina in orthopyroxene coexisting with garnet. *CONTRIB MINERAL PETROL* **46**, 1–15.
- Wood, B. J. & Banno, S. 1973. Garnet-orthopyroxene and orthopyroxene-clinopyroxene relationships in simple and complex systems. *CONTRIB MINERAL PETROL* **42**, 109–42.

N. P. LOCK and J. B. DAWSON, Department of Geology, University of Sheffield, Sheffield S1 3JD, England.

Ms received 14 August 1979. Accepted for publication 24 October 1979.

LETSENG LA TERA  
 SATELLITE PIPE  
 55m Level  
 Scale 1:1000



-  Late kimberlite dyke(s)
-  Tuffisitic kimberlite breccia
-  Basalt/kimberlite breccia
-  Early kimberlite dykes
-  Basalt
-  Outline of kimberlite at surface
-  55m level kimberlite/wallrock contact
-  Kimberlite contacts
-  Kimberlite dykes
-  Outline of underground drives
-  Dip of pipe contact

X +5600m

X +5800m

Y +6000m

relatively more abundant  
ultramafic xenoliths

calcitic dykes  
vertical, strike 117°E

sharp contacts

dyke showing  
gradational  
contacts

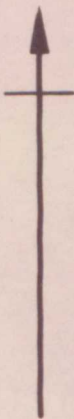
generally sharp but sometimes  
irregular contacts

to adit portal

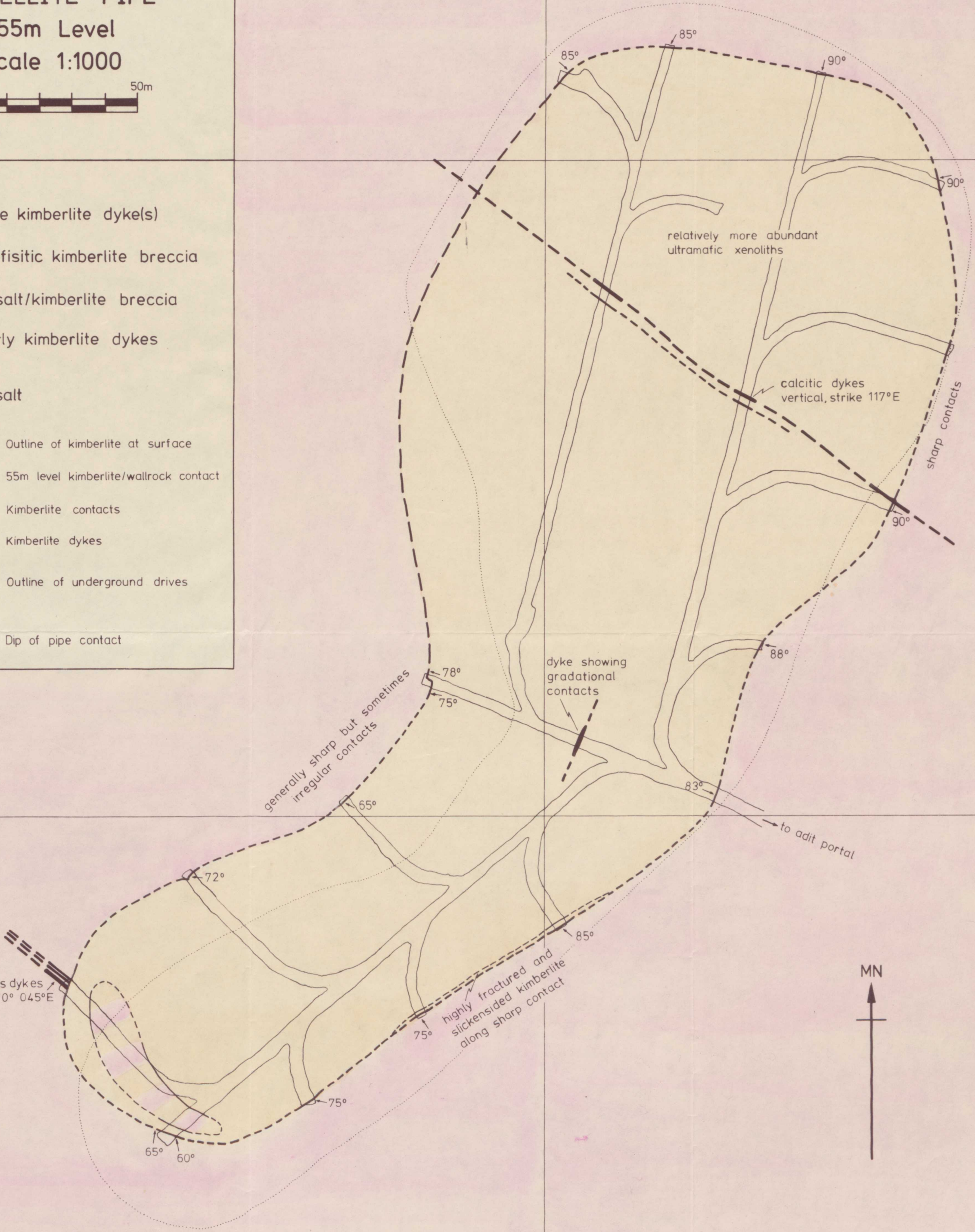
micaceous dykes  
dip 70° 045°E

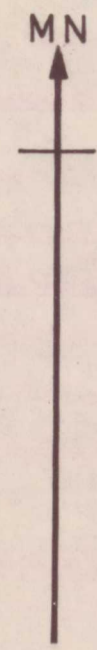
highly fractured and  
slickensided kimberlite  
along sharp contact

MN



trace of dyke exposed at surface



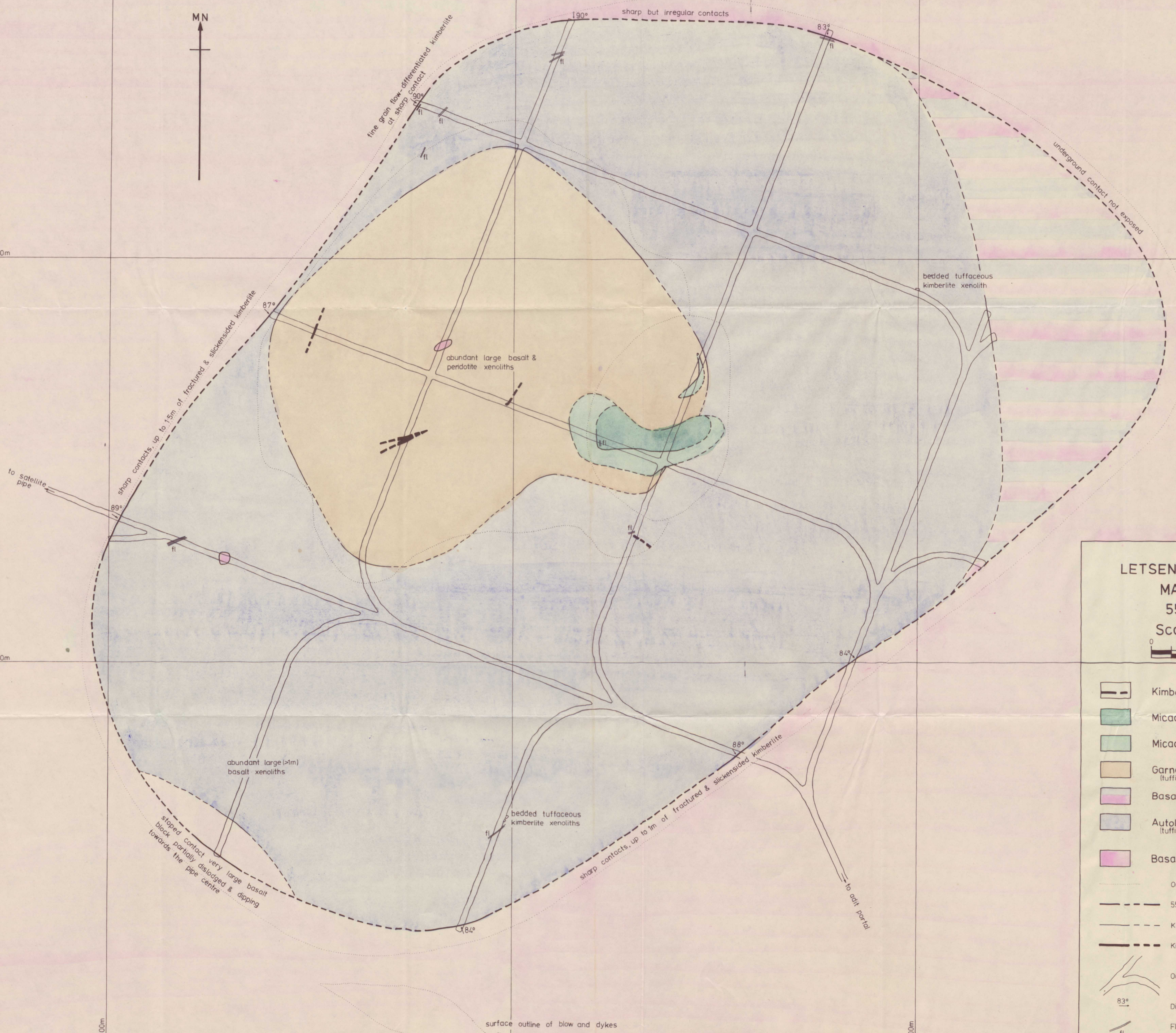


X +5800m

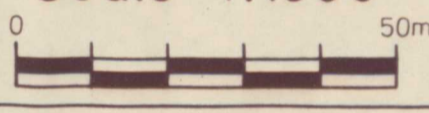
X +6000m

Y +5600m

Y +5200m



LETSENG LA TERA  
MAIN PIPE  
55m Level  
Scale 1:1000



- Kimberlite dykes
- Micaceous kimberlite
- Micaceous kimberlite (tuffitic kimberlite breccia)
- Garnetiferous kimberlite (tuffitic kimberlite breccia)
- Basalt/kimberlite breccia
- Autolithic kimberlite (tuffitic kimberlite breccia)
- Basalt
- Outline of kimberlite at surface
- 55m level kimberlite/wallrock contact
- Kimberlite contacts
- Kimberlite dykes
- Outline of underground drives
- Dip of pipe contact
- Flow textures